Series in BioEngineering

M. M. Kaila · Rakhi Kaila

Molecular Imaging of the Brain

Using Multi-Quantum Coherence and
Diagnostics of Brain Disorders

Springer

M. M. Kaila
School of Physics
University of New South Wales
Sydney, NSW
Australia

Rakhi Kaila
School of Medicine
University of New South Wales
Sydney, NSW
Australia

Printed on acid-free paper

Foreword for the First Part of the Book: 'Quantum What Quantum Tell Me More About It.......'

The routine MRI literature in the scientific world does not much emphasize MRI as a quantum coherence phenomena. The educational aspect of MRI does not depict well the multi-quantum part of the nuclear magnetic resonance (NMR). The nuclear multi-quantum aspect forms an integral part of the MQMRI (multi-quantum magnetic resonance imaging). The proper role of the word 'Nuclear' has been avoided in the RF radiation imaging literature. The imaging is basically referred to as the MRI instead of clearly mentioning the NMRI (nuclear magnetic resonance imaging). This is done so as not to scare the patients. It was felt in the past that patients may think that they are being exposed to dangerous nuclear radiations. MRI is as much an atomic as much a nuclear resonance phenomenon. The magnetic moment of protons in nuclei provide a rich source of information about the microscopic events happening in the brain, through spectroscopy as well as imaging. The multi-quantum aspect of spectroscopy in an ensemble of molecules like our brain is well advanced and the imaging aspect is fast progressing. The MRI technology developed tries to emulate the functional system operative in the brain. Nature has evolved the internal functional system operative in our body over millions of years. In MRI the investigation of the life functioning system is done in a gentle way using radio frequency (RF) radiation. MRI does not involve breaking the nuclei by using neutrons to produce fission of the nuclei which would then lead to the production of dangerous nuclear radiations destructive to our body. This misconception had arisen due to the lack of populous education about the basics of the science of MRI in particular, and also science as a whole. In fact, on a wider scale the basic infrastructure of education about science for the new generation of students is on the fast decline. Expansion in financial and bureaucratic fields like, accountancy, management, IT (information technology), etc., is fast on the rise.

One must not forget that science leads to creation of the necessary literacy about life itself on the one hand and develops practical inventions like the MRI

which is worth billion dollars of industry today on the other. The bureaucracy is destructive to the creation of knowledge-based economy. Propagating scientific knowledge is the only way to survive today. Society is heading toward ignorant misconceptions and neglect. What useful benefits of science the human civilization should adopt and leave others should be decided based on the proper education about the existing scientific balance that nature has created on earth. There is no other planet like earth in our universe. Better protect the one we have than trying to invent another which you cannot make use of. MRI can detect soft organic and inorganic matter in addition to the rigid, e.g., the calcite structure like bones in our body. It can thus be a very useful method of detection involving security procedures in the aviation industry. We are a scientific civilization. Using science to produce wealth is a constructive way of employing young minds. Just shouting about 'climate change' as a 'political word' of power is not going to produce anything. But starting education at the school level about the 'science of climate' and science as a whole will produce an appropriate scientific manpower for the future to take right decisions.

MRI is only one among many visible commercial products from science working in our day-to-day life. The scientific society we have developed ourselves into over the centuries cannot survive without science. There is no point in destroying the very foundation of humanity developed based on science. Nature itself has preferred science in its own evolution. Over time the present civilization has studied the secrets of nature, learnt them, and used them toward its own benefit. A freely available scientific-educational material produced by research and development work over the world would go a long way toward the education of humanity. The authors feel the work prepared here is a step in the right direction for the future generations. Pretending that we do not need science is a shear act of ignorance. Survival of the human race today is only on education about science. One should realize that plant and animal life is the science of atoms and molecules. Deep inside it is the quantum science that nature builds on. It is what the MQMRI is based on. This is very much a quantum (in fact multi-quantum) phenomena. It is better to understand the quantum science of our body than to ignore it. The conventional MRI uses quantum science as a wholesome, i.e., in a broader quantum perspective. Assuming molecules in our brain as an ensemble of independent spins is the crudest model of the brain and that is what the conventional MRI is about. It is natural for any technology to evolve starting from the simplest and the very fundamental basics. That is how the development of the MRI technology has evolved. The mind can only start from the simplest, and then work out the intricacies step-by-step. Nature itself has followed that in the evolution of life. The intricate discrete nature of atoms and molecules does not form the basis of imaging in the conventional MRI of today.

The technology of MRI employs the use of noninvasive RF radiation. This is in order to excite the nuclear and atomic magnets which are an integral part of the biological structure of our brain. RF radiation is chosen because we are interested in exciting atoms and molecules to their higher energy level. On returning back to their normal or say zero energy state the RF radiation is transmitted back. The

receiver which is tuned to this out-coming radiation registers the events happening in a local selected area under investigation. A point-by-point repetition over the whole brain and coordinating the events over the global brain produces the picture we are so familiar with. It is important to recognize here that the magnitude of the excitation energy involved here is of the order of a few meV. One should compare this with Mev (million electron volt) used in X-ray imaging. We live our day-to-day life on earth under the influence of the solar radiations with full electro-magnetic radiation spectrum and under the effects of the magnetic field of earth. Our life on earth exists in earth's magnetic field of around 1 micro Tesla. This is very small to think about having any dangerous effects on the human brain. But inside our brain things on a similar scale are happening. There is no research to suggest yet that this (Earth's) small magnetic field in any way controls the routine functions happening in our brain. But it is curious enough to find out what does. MRI just tries to emulate it through imaging.

It is important to recognize that a nucleus as a part of an atom or of a macromolecule produces a field of about 1 Tesla around it. But this is over a region of nm (nanometer) to micrometer scale. It decays fast over many molecular distances. But as the volume under consideration locally, becomes larger, the larger is the number of spins (remember a mole of a substance has 10^{23} spins) participating, in a particular activity. The result is that the effect of the decay of the field is not as fast as one would think. The distant spins as far as 1 micron to 1 mm distance can influence the local spins through a small distant dipole (spin)–dipole (spin) field indirectly created within by the applied external static magnetic field. In the MQMRI literature this new field is referred to as the distant dipole field (DDF). The distant spins produce a demagnetizing field at a point locally and generate the intermolecular multi-quantum phenomena. This is the basis of imaging in the newly emerging MQMRI. Whether the earth's magnetic field is already doing this in the brain is what we are trying to find out? Would not it be nice to know?

The natural dipole–dipole interactions (DDI) in the brain can be studied using the proton magnetic resonance spectroscopy imaging (PMRSI). It is one of the many techniques available. The PMRSI technique utilizes mainly the nucleus, i.e., the proton spin. The nucleus is part of the overall electron-atom-nucleus quantum structure present in the brain. In the conventional concept of imaging, e.g., the chemical shift imaging (CSI), the atomic spins polarized along the direction of the applied static magnetic field are being used as independent entities with no multi-quantum interaction between them to get the desired result. This is basically the macroscopic effect in the small regions (referred to as a voxel) of the order of mm^3 and above. But in order to see the intricate events happening in the brain in space and time over smaller distances, i.e., the atomic distances, one needs to understand the quantum interactions between atoms and molecules. The affective macromolecular distances, i.e., micron (10^{-6}m) to mm is the region of the 'multi-quantum magnetic resonance imaging (MQMRI) '.

What MQMRI means is that one takes into account the explicit quantum reactions between atoms and molecules as the source of the imaging, and the collected data is then more than just the broader imaging. This means getting close

to exactly what nature has created in our brain. That is what allows our body functions to continue on a moment-to-moment and day-to-day basis. We need to understand this nature's, atomic level incredible quantum phenomena happening in our brain to work out the right diagnostics and the treatment of diseases which our brain suffers in our lifetime. In order to master the intricate quantum science of life one needs to start from a standard textbook on quantum mechanics (QM). Also, the reader should refer to the recent research papers describing the science of life as the quantum science (QS). For the reader, however, is presented below a simplified conceptual picture. It explains the basics of the multiple quantum coherence (MQC). MQC exists between the molecules in our brain. It is a kind of interaction which allows various fundamental processes like metabolism, neuro-transmission, etc., to continue in our brain.

A: Single Quantum Coherence (SQC): (Conventional MRI)

The expression through illustration here is as if the whole brain has all the spins (tiny dipole magnets) pointing along the Z-direction, the direction along which the static magnetic field is applied. The spins are assumed to be identical in nature though they are not. This is a crudest possible model. But one should remember that in the first stage we image the identity of the spins through their being present in different environments. It is in space and time. The output signal is produced using RF radiation pulses. A 90° pulse is applied along the X-direction. It leads to a rotation of a fraction of the spins pointing toward the Y-direction. Because of the oscillatory (pulse) nature of the RF radiation applied the output signal is also an alternating current (A.C.) one. The signal is picked up as an output along the Y-direction by a copper coil or some other form of sensor. There is evolution of the spins after applying the RF radiation pulse in the X–Y plane. As time progresses evolution of spins leads to their dissociation as a group in the X–Y plane.
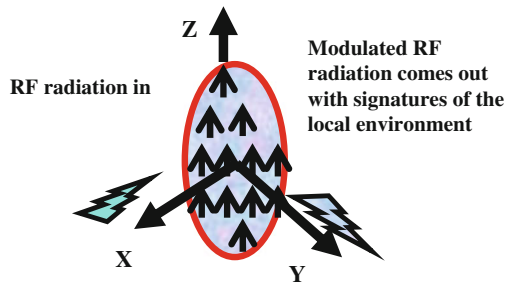
They are refocused by applying an inverting (180°) pulse inverting the spins toward the –Y direction in the X–Y plane. It allows longer times to measure and analyze them. This basically leads to mapping a specific (choosing a particular slice thickness in the Z-direction) X–Y plane. The relaxation time of the spins in

the X–Y plane is called the characteristic time, T_2 (transverse relaxation time) of decay. In a similar fashion the spins are reversed by applying 180° pulse reversing spins toward the −Z direction and the spins are allowed to relax back toward the +Z direction. This characteristic time of relaxation is called the T_1, the longitudinal relaxation time. Both T_1 and T_2 weighted data in space is used in producing the final image. Repetition voxel-by-voxel over the whole brain produces the global brain image. These are the basics of the conventional MRI technique. A technique using this principle in MRI is broadly referred to as the EPI (eco planar imaging) in MRI. Other concepts, e.g., correlating diffusion-based anisotropy of the spins, called tensor imaging, e.g., in a tumor situation are also prevalent in conventional MRI. Refer to Section 6, for details about T_1, T_2, and the k-space imaging concept used in MRI.

B: Double Quantum Coherence (DQC): (The MQMRI)

Input RF Radiation has resonance frequency, specific to the two spins, pointing in the same direction, in a bound state. It is called as the double quantum coherence

Output RF radiation, is modulated, by the simultaneous interaction, of the bound groups, of the two bound spins, pointing in the same direction.
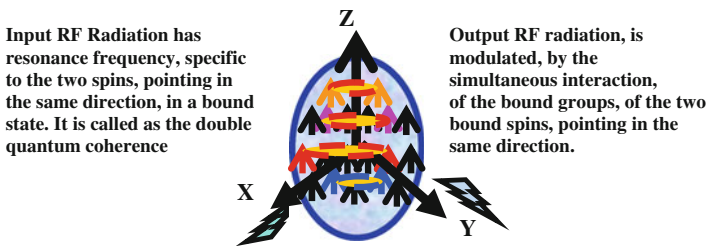
In this case the expression through illustration about two spins pointing in the same direction is considered as a bound group in action. Generally, nearby spins pointing in the same direction repel each other like two bar magnets with north–south poles pointing in the same direction. But there will be some spins further away pointing in the same direction where the magnetic influence of the spins will be attractive to each other. This in other words means quantum coherence (acting together for a specific activity say metabolism) in the quantum science language. This correlation or interaction of two parallel spins in a 'group of two' is called the double quantum coherence. This picture holds on a scale in the brain over distances of microns to mms. One needs to see the in-depth picture of this two-spin bound state resonance. In a selected region we have to go to distances of the order of a micron (10^{-6} m) and choose a resonance frequency corresponding to this group-of-two-bound spins pointing in the same direction for the regional analysis.

C: Zero Quantum Coherence (ZQC): (The MQMRI)

Input RF radiation is tuned in resonance to the bound-state of, the group of two spins, pointing in the opposite direction
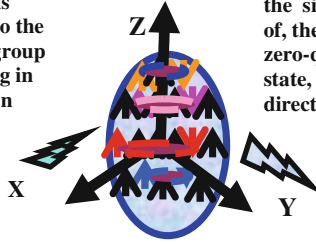
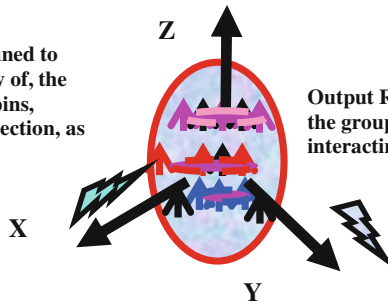**Output RF radiation, is modulated by the simultaneous quantum interactions of, the groups of the two-spins, in the zero-quantum state. The zero-quantum state, is due to, the two oppositely directed spins, bound together.**

This interaction group consists of two spins bound together with the spins pointing in the opposite direction to each other. The two nearby spins in an ensemble influence each other. One spin tends to reverse the direction of the other spin. This bound state is the lowest energy state for the two spins near (and far) to each other. The applied static magnetic field along the Z-direction tries to keep all the spins aligned along the Z-direction. The spins pointing in the Z-direction is the equilibrium energy state of the spins. This oppositely directed binding of the spins near and far is called the ZQC. This will have a unique resonance frequency. It can be excited by externally applying a suitable RF magnetic field like in the case of DQC to the brain. The quantum interactions allow the quantum chemistry of nuclei to be observed in space and time. Detection of the quantum interactions is very helpful to predict in early stages the onset of a tumor or a disorder in our brain. ZQC is magnetically neutral. It is insensitive to magnetic field inhomogeneities. It is considered to be a powerful quantum probing tool in the MRI.

D: Triple Quantum Coherence (TQC)

Input RF radiation is tuned to the resonance frequency of, the group of three bound spins, pointing in the same direction, as a single quantum state

Output RF radiation is modulated, by the group of three, simultaneously interacting spins, quantum state

One can involve more than two spins, e.g., three or even four spins in a bound group. The triple-bound state will have a quantum energy structure of its own.

Thus a unique resonance frequency of its own. One can excite the group of three bound-nuclei and study their interactions on a microscopic scale and predict which way the local quantum chemistry is heading and make an early detection of a cancer in the brain. One should remember that our brain is a heteronuclear (multiple species of nuclei) structure. Various nuclei present in a macromolecule as part of a tissue, fluids, etc., are performing their routine duties of metabolism, neurotransmission, etc. The influence of interaction extended can be visualized through analyzing the resonance of the TQC (triple quantum coherence) as a group in a subvoxel space in the brain. As a bound group of spins becomes larger one is approaching towards what the conventional imaging does. One may however be interested in the detailed chemistry of the participation of a regional group of nuclei. The chemical identity of nuclei due to their unique electronic structure provides a probe to understand in-depth the science of the brain. This opportunity is provided by the triple-quantum coherence imaging. The word coherence means in the literary sense acting together. In scientific knowledge it means exciting or stimulating simultaneously a group of atoms or nuclei which may be part of a macromolecule. We then find out what activity they are enhancing i.e. having a constructive interference within a specific period of time and the others they are suppressing (i.e. making a destructive interference). The unique resonance frequency of a macromolecule gets smeared out due to its constituent nuclei; the nuclei being of different identities. This group may be interacting with a neighboring group. The group–group interaction is through their common group-resonance (a wider band of frequencies). This gives rise to multiple quantum coherences. It now is a broader frequency RF band. The RF radiation can be chosen to include as many widely dispersed nuclei one is interested in.

The quantum mechanical imaging (QMI) approach in MRI is a fast advancing area and will one day be able to predict moment-to-moment events happening in the brain. It is common knowledge that the MRI has its origin in using the quantum behavior of the magnetic spins present in atoms and molecules. But the quantum nature of the MRI is evident explicitly only when one is dealing with ZQC, DQC, etc. The scientific literature in MRI loosely refers to molecular and atomic magnets as spins. They are atomic size dipole-magnets which are globally present in the brain and due to their random distribution overall neutralize themselves. Atoms and molecules, the constituent parts of the tissues, fluids including the blood cells, etc., are integral parts of the biological and medical activities happening in our brain, in equilibrium. The atomic spins are the natural result of the circular motion of the electrons around the nucleus in an atom. An electron by itself (due to intrinsic rotation about its own axis) makes an additional contribution of spin to that due to the electron's orbital motion around the nucleus. A nucleus also has its own magnetism. It arises from the circulating electrical currents of neutron and protons inside the nucleus.

The relative circular motion of the negative charge of the electron with respect to the positive charge of the nucleus produces locally a magnetic field of about 1 Tesla. The internal magnetic field is strong enough to create a local magnetism in the soft matter in the brain. The local magnetization created is called the

diamagnetism. The result is a local polarization. There is of the neighborly atomic and molecular spins some sort of local equilibrium due to this internal magnetic field. It controls the local events, e.g., metabolism, neurotransmission, etc. Nature has cleverly manipulated this order on its own. How clever? One may say that we are still today on the path of slow evolution of life. It is true to say that. Nature has passed on from generation to generation the secrets of survival of the human gene code and keeps on mutating it for survival in worse and worse scenario of diseases. It is for us to find out now 'how and why'. The internal magnetic field of 1 Tesla of a nucleus naturally present in our brain produces a local magnetic order of atoms and molecules in the brain on the micrometer scale. The MRI by its externally applied static magnetic field of around 3 Tesla and sometimes even higher (allowed within safe limits) extends the spatial order over larger spaces.

The MRI technology provides us with an easy tool to mimic nature's operation of the brain system. This can be skillfully observed by the modern day MRI technology. It is certainly a powerful tool to find out how our brain works. The natural internal static magnetic field creates a stable equilibrium of the spins over regions of the order of nanometers to micrometers to mms. The external magnetic field in the conventional MRI on the other hand produces rough regions of magnetic equilibrium from mms to cms. These are the regions of externally imposed diamagnetic equilibrium. This created diamagnetism in MRI, in the brain, is a natural consequence of the reaction of the atoms and molecules, to the applied static magnetic and the dynamic RF fields. The reaction to the applied field is to shield or say to save the brain from any damage. How clever of nature. The diamagnetism due to the internal nuclear magnetic field is basically neutralized locally as well as globally all over the brain. The application of the external magnetic field as is done in MRI mimics this invisible order over large volumes of order, say mm^3–cm^3 termed as voxels. After the application of the static magnetic field an RF electromagnetic field is subsequently applied to the brain to excite the magnetic spins to their higher order quantum states. The quantum correlations of the neighboring atoms and molecules provide the basis of the advanced technique of MQMRI (multi-quantum magnetic resonance imaging). This becomes a source of better resolution in imaging as compared to the currently prevalent techniques of chemical shift imaging (CSI), diffusion weighted imaging (DWI), etc. The intensity variation of the echoes received acts as the sources of the signatures of the activities in the brain in conventional imaging. In multi-QMRI it is the fine physical and chemical quantum reactions in space and time that is the source of imaging. In this way one is approaching the intricate situation present in the brain. A healthy brain works in a mysterious way. It can think, analyze, and control body functions in a judicious manner. But when diseased the functions of the brain are impaired and it cannot perform in its full analytical capacity. The idea behind writing this work is to implicate the basic principles of physics, chemistry, and mathematics (PCM) involved in the science of the human brain. MRI is a humble tool trying to solve the mysteries of nature. More often than not professionals and technical workers use MRI for analyzing human brain disorders.

MRI is a standard tool used in the diagnostics of tumors. Some workers in the field do not really have a strong enough background of the PCM principles used in producing an image. Hence, they are not able to make the best of the image produced. In this work effort is made to explain the concepts involved, through pictures, diagrams, etc. The mathematics involved is kept to a minimum. Some simple equations are included only as symbolic representations of the physical quantities involved. Although MRI is based on the physics of the quantum nature of soft matter a detailed relationship to quantum science is avoided to keep things simple. Quantum information science (QIS) is emerging as a discipline where detailed quantum mechanical mathematics is used to study quantum systems. This is not the aim here. Here, the goal is to lay down simple concepts of quantum physics and analyze their use in imaging the moment-to-moment activities in the brain, etc. So far the imaging has been based on manipulating the maximum magnitude possible of the signals received from the echoes produced by the RF radiation in the brain space.

A small region is chosen at a time for examination called as a voxel. In the present day EPI (echo planar imaging), the voxel is macroscopic in size of around mm^3–cm^3. Recently, there is a growing trend in going toward a microscopic level imaging. This means moving to narrower spacing of less than 1 mm^3 to even less than a micron volume (10^{-6} m^3). This brings us into a more rigorous territory of quantum science in operation. The theoretical quantum details are avoided in this work. Instead pictures and diagrams are used for the expression. The quantum-detailed imaging provides a much better resolution than the conventional, broad relaxation-time-based imaging. The MRI uses as a typical example a simple echo-planar imaging (EPI) method. It is a fast technique but lacks good resolution. Further developments in MRI depend on the continuous education of the professionals who develop it and others who want to use it. This work has a simplified approach to attract medical professionals to make better use of the science of imaging in the diagnostic decision-making process. This work is also aimed at achieving a much wider circulation of the understanding of the basics of MRI and its application in turn through the enchanting knowledge of the science of the human brain.

Preface for First Part of the Book

Humans on earth out of curiosity have developed powerful telescopes to look into the structure of the universe around us. We are striving to look for signs of life whether in the galaxy in which we live or in other galaxies. Are we so special? Is there need to be looking for our image billions and billions of kilometers away? As a matter of curiosity and knowledge there is such a need. The dynamics of the motions of the stars, planets, etc., is explained by Newton's gravitational laws and is a well-established science in theory and experiment. There is another aspect of science. We have several elements in the earth's crust, e.g., iron, copper, calcium, sodium, potassium, silicon, etc. Some of these elements, e.g., sodium, potassium, chlorine, in the form of some compounds, etc., form an essential part of the survival of life, plant, or animal. We should look deep inside the atomic structure of the elements and of the molecules they form, e.g., the water molecule H_2O, the essential ingredient for our survival. The dynamics of the electrons, protons, nuclei in our body is as intriguing as puzzling. For example, the electrons stay in stable orbits around the nuclei. It is no different from, say, the planet earth going around our Sun. One needs to go to nanometer distances (10^{-9}) deep from the surface of a macromolecule to work out the amazing science inside the atoms and molecules. This branch of science which deals with the deep down discrete structure of matter, i.e., atoms and molecules, is called quantum science.

Quantum science also has its laws in nature worked out though not in as clear a way as the gravitational ones. In a practical use, e.g., in our brain one can see quantum laws of dynamics as clearly brought out through MRI. They are related to simple concepts in physics. The quantum magnetic resonance used in Magnetic resonance imaging (MRI) is a typical example. As a machine, MRI is seen very prevalent in hospitals, medical centers, universities, etc., as a part of our health system. We can hardly miss to look at it through a diagnostic picture to find what has gone wrong in our body when we fall sick. Multi-quantum spectroscopy which reveals the multi-quantum structure of atoms and molecules is century old. It is now being applied to in vivo brain imaging over the past of couple of decades. It acts as a complement to find out the concentration and specific functional role of various chemicals present in our brain. Multi-quantum coherence imaging (MQCI)

does both (spectroscopy and imaging) together in an integrated form. This book which has purely educational aim behind it tries to put together quantum science and the imaging of the brain together. For some readers, e.g., for clinicians to learn quantum science in-depth can be a difficult task. This book has avoided the phenomenological development of the physics, chemistry, and mathematics (PCM) that form a detailed exposure of brain imaging. The approach taken here instead, is to let the reader learn through practical visualization of the concepts in action.

Preface for the Second Part of the Book

Nature has evolved though essential elements like oxygen, hydrogen, nitrogen, iron, zinc, etc., via their inorganic and organic compounds, e.g., NaCl, H_2O, KCL, F_eO, etc. There are various organic matter macromolecules encompassing the basic isotopes, e.g., ^1H, ^{13}C, ^{23}Na, ^{35}Cl, ^{31}P, ^{39}K, ^{57}Fe, etc., which have regulated the animal and plant life evolved over millions of years on the earth. Deep down in life which evolves all the time are tiny building blocks, atoms, and molecules, which conglomerate to form bigger molecules, the macromolecules, the tissue, and ultimately the body. Atoms, when looked into deeply, have a nucleus with a positive charge at the center surrounded by negatively charged electrons. The magnitude of the positive charge at the center of the nucleus (basically due to the protons) is equal to the negative charge of the surrounding electrons. This keeps the atoms and the molecules electrically neutral as it should. One should remember that there are always some ionized free radicals present in our body. The electrons in atomic and molecular situations are not stationary but orbit around the nucleus and stay in a number of stationary orbits so as not to collapse into the nucleus. The orbital motion of an electron around the nucleus generates an electric current. This electric current when multiplied by the area of the orbit of the electron is called the magnetic dipole (in analogy with the earth's giant, the north–south pole dipole-magnet) moment. The tiny atomic dipole magnets in our body coordinate with other atoms to form bigger molecular magnets. The molecules expand their electron correlations with their surrounding molecules to form cohesive charge and spin configured macromolecules. The macromolecules which form the essential part of the dynamics of life in the human body (and even in the plants and animals) retain the feature of the magnetic (over a large molecular space) dipole character. These macromolecules are tens and hundreds of nano (10^{-9}) m in size and control the dynamics of the life of all living creatures.

One needs to remember that orbital motion of electrons (and of protons and neutrons inside the nucleus) generates a basic physical quantity in motion dynamics, the angular momentum locally in macromolecules in our body. This local basic physical quantity, the macromolecular angular momentum, becomes the source of all the activities coordinated in the brain. The dipole magnetic

moment is a naturally associated part of the angular momentum. Unfortunately, angular momentum in the molecular situation cannot be measured in the laboratory. But fortunately, nature is kind to let us find the secrets of life through the molecular dipole magnetic moment associated with the annular momentum. Nature's secret is that the magnetic dipole moment creates electrical signals which we measure and help to create the MRI we know. How lucky are we? We are at the center of a vast universe which is formed of atoms and molecules. The atoms and molecules have evolved over millions of years in such a way as to create the most intelligent form of life on earth. Intelligence does not progress without a healthy scientific environment and the interaction of the body and mind with the universe which surrounds us. The magnetic resonance (MR) phenomena observed through MRI in our body is like many other resonance phenomenae observed in nature. These can be seen all around us and are used in many technologies, e.g., Radio and TV broadcast, Lasers, etc. The development of MR into a practical MRI machine we are so familiar with now has been the result of more than half a century of research and development efforts. It is now not only a routine health care technology in hospitals and medical centers but is also a valuable noninvasive tool of research and education about the science of the human body. Sodium is an important element and there are several others found in almost every organ of the human body involved in the functioning of organs on a moment and day-to-day basis.

Sodium nuclear magnetic resonance imaging (SNMRI) is now being used in the area of diagnostics of diseases of several organs of the body, e.g., the brain, liver, heart, kidney, etc. In the present day MRI we have the single-quantum (conventional) MRI technology approach. It is a routine versatile technological tool in the diagnostics of the human brain disorders. It is important to point out here that the single quantum basically means that we assign a single resultant spin covering all the spins of the group of molecules in a voxel (a small volume) under measurement. The dispersion in the output signal observed in time and space is the result of the various dynamic activities in the brain. These are measured by various techniques, e.g., the blood oxygen level dependence MRI, called the fMRI (functional MRI), SNMRI, etc.

The multi-quantum means the subvoxel molecular level structure dynamics. It does not form part of the present (conventional) MRI technology. MRI enables scientific research follow-up through monitoring the effects of a treatment therapy. During the practice of following this research scientists discover new and better treatments for a disorder. A useful secretive knowledge gathered through the MRI about our brain creates literacy about our brain and how it works. In essence, in the conventional MRI, which we have at present one is looking for the spin (tiny atomic and molecular magnets) interactions over the wider average volume (mm^3–cm^3) as the medium in which they reside and move. This medium provides the environment of generation of the spin electrical signals. Through the brain medium of tissues, fluids, etc., spins perform dynamic activities, e.g., metabolism, communication, etc. In the conventional MRI model we assume spins behave like an averaged entity over a selected volume. Over the voxel-to-voxel situation they are

magnetic entities with little multi-quantum interactions with other molecular spins. Their imaging identity is through their interaction with the environment in which they respond to the applied static magnetic field and the radio frequency (RF) radiation that is applied.

The physical and chemical multi-quantum interactions on a molecular level between spins are of little consideration in the conventional MRI. The result is more like mapping rather than a picture of the precise dynamical events happening in the brain. This is the limit (called as single quantum) on which the conventional MRI has been founded. In-depth MRI would allow one to understand the basic science of the human brain. Sodium and potassium are very basic elements involved in life controlling the familiar sodium–potassium pump in our body. They perform essential energy transport and metabolic functions for the natural life-running mechanisms in the body. Typically in the brain, e.g., in the ischemic situation, it is known that the healthy natural sodium concentration inside the cell membrane is disturbed. There is extra uptake of sodium ions in the cell inside a tissue than the healthy normal balance requires. The life giving sodium–potassium equilibrium pump then does not perform in a normal healthy manner, anymore. The brain becomes disordered and the person ends up with a stroke. Normally, sodium is in a bound state inside the cell; it is not a free, nucleus. It is a part of the macromolecule structure inside the cell. On the other hand, outside the cell there is sodium in a free state as part of the fluids, e.g., blood and other fluids around the cell. In an MRI situation sodium nuclei are exposed to a relatively strong static magnetic field (around say 3 T).

The direction along which this static magnetic field is applied is referred to as the z-direction in the MRI literature. This is along the axis of the direct current (DC) carrying coil that produces the static magnetic field inside which the human body is placed for imaging. A much weaker (milli-Tesla) radio frequency (RF) electro-magnetic field is subsequently applied in different X–Y directions in the Z-planes to cover 3D space of the organ under investigation. The purpose of the RF field is to project the spins in different directions with respect to the main static magnetic field and excite them to their higher energy states. The sodium nuclei in a selected small volume (the voxel) on de-excitation reradiates back the RF radiation carrying the signatures of the local events in the voxel. In the diseased state of a tissue, modified activities are happening inside and outside the tissue as compared to a healthy body. The changed interactions between the sodium nuclear magnetic dipole and the electrical quadrupole (charge) moment inside and around the cell act as a barometer of the diseased dynamic state of the tissue. Inside the cell, normally one observes two types of relaxation mechanisms, the fast and the slow. This is during the de-excitation of the spins. We now have the two characteristic relaxation times, the fast and the slow, for examination. In MRI, the fast and the slow T_1 and T_2 relaxation times become the source of imaging in a stroke situation. These two relaxation times routinely form the weighting parameters in the imaging produced in the conventional MRI. In the particular case of sodium imaging we look for the interactions between the electric (charge) quadrupole character of the sodium ion (Na^+) and the fluctuating electric field created by the

variable nuclear ion concentration around it. Each relaxation time has a fast and a slow component.

The observed behavior of spins is now a nature of the perturbed abnormal charge distribution inside and outside the cell. It can be compared to the case of a healthy normal brain and use it as a diagnostic tool, for the disease. In essence the changed T_1 and T_2 relaxation times in a voxel are used as the source of conventional sodium MRI. MQ-MRI will take it to the molecular level. It is important to remind the reader here that in the sodium MRI (S-MRI) we are after the result of interaction between the electric quadruple sodium nucleus and the surrounding electric field gradient. But the external static magnetic field applied in the Z-direction is still the key in the investigation process. The magnetic dipole of the sodium nucleus points in that direction and is the source of a standard reference for the analysis.

One should note that inside the cell the sodium nucleus is in the bound state within a macromolecule of the tissue. The quantum correlations among the spins of various nuclei are very strong. The quantum science principles guide, that inside the cell the spin relaxation mechanism, should be bi-exponential, that is there will be two distinct decay rates for the relaxation times. It arises due to the sodium nuclei being in a bound state in macromolecule inside the cell. The bound nuclei interact with the free sodium nuclei surrounding the cell. There is a charge concentration gradient due to sodium ions inside the cell and the surrounding area in which the cell is present. This gradient is non-uniform in its character. Sodium nuclei have electric quadrupole (four poles, two positive, and two negative) moment character. This is in addition to the nuclear magnetic dipole character which is inherently present in the sodium nucleus. The electric field gradient (due to the varying sodium concentration) from inside to outside of the cell is asymmetric and thermally dynamic in character. The electric field gradient fluctuations trigger electric quadrupole–magnetic dipole interaction among the nuclei. This produces a split of the magnetic state $I = 3/2$ of the sodium nucleus into the four degenerate levels, $-3/2$, $-1/2$, $+1/2$, and $+3/2$. The result is a mixture of two prominent fast and slow decay rates in response to the electro-magnetic RF radiation.

Outside the cell the free nature of the sodium nuclei still allows a unique single exponential decay. Thus the sodium nuclei inside and outside the cell with a separating membrane in-between behave in different manners when exposed to RF field. The longitudinal (T_1) and transverse (T_2) relaxation times of the sodium nuclei inside and outside the cell become a source of differential chemistry in space and time for imaging. The conventional single-quantum MRI in use has been developed over half a century now. It is implicitly expressed as being single quantum in the MRI literature. Why it is called as single quantum is that it is assumed that all nuclei have the same identity as a single magnetic dipole and do not interact coherently between each other quantum-mechanically during the process of imaging. One needs to see the underlying microscopic events in detail. Microscopically the interactions are very far from the single-quantum type. The multi-quantum MRI now is felt as a basic necessity. It has found way to success

very recently. This approach allows the molecular level physics and chemistry among the nuclei as the source of imaging. Any organ of the body say e.g. human brain is a heterogeneous ensemble of very many species of nuclei among the macromolecules. These, macromolecules are surrounded by other macromolecules; several types of fluids with complex chemistry of their own in a dynamic state.

We know that the atomic chemical elements when in a free state in nature have their characteristic signature called as the electronic-quantum energy structure. In a confined state like the soft condensed matter in our body the discrete atomic and molecular, quantum energy structure is modulated by the region where they are present and the functions they perform as a group. The individual discrete single atom electronic quantum structure inside a macromolecule environment is part of a wider discrete macromolecular quantum structure. This is spread over all in space and time. A macromolecule has its characteristic charge and retains it through equilibrium with neighbors in a unique discrete energy structure of its own. At the cell level there is a much broader quantum character in space and time as an ensemble. The smearing electron clouds in-between among the macromolecules provide the conventional region of chemical shift mapping. The molecular magnetic dipole-dipole interaction provide the source of a reference axis in MRI.

In the imaging the sodium quadrupole characteristics are depicted with respect to the fixed Z-axis of the magnetic dipole spins produced by the application of the applied static magnetic field in the Z-direction. As one goes deeper to the nuclear level of the macromolecules the quantum correlations among the nuclei reveal the real quantum chemistry events happening in micro-space-and-time imaging domain. Multi-quantum sodium imaging is a step in the forward direction. It will develop quantum coherence imaging (QCI) through the understanding of the nano-molecular science phenomena. Unfortunately the magnitude of the electrical signals created at the electric-quadrupole, nano-quantum coherence level, are much weaker in magnitude as compared to the case of mm^3–cm^3, volume, generating, the single quantum signal. The magnetic field in-homogeneities due both to static and the RF fields add to the complications of the multi-quantum MRI (MQMRI). We are trying to observe in the MQMRI much weaker multi-quantum coherence imaging signals. This book presents a first hand picture of the research and development efforts in progress to date in the newly emerging field of the multi-quantum, sodium, electric-quadrupole, magnetic-dipole imaging.

Acknowledgments

Special Tribute

Dr. Madan Kaila pays gratitude to his late father Dr. (medicine) Mulkh Raj Kaila, his late brother, Dr. (Geophysics) Krishan Lal Kaila and late mother Smt. Pushpa Wanti Kaila all from Lahore. Madan's mother Pushpa passed away last year (08/01/2011) in Delhi. It was Mrs. Pushpa Kaila, Dr. Mulkh and Krishan, Kaila's persistent desire towards higher education of Madan like that of his brothers and sisters in the family. This was despite the unfortunate division of India as a result of freedom in 1947 from the British Empire. It led to the mass exodus of the millions of people from their homes and loss of millions of lives. This has been forgotten so easily. It did not happen long ago. Madan is only one of the many million victims as refugees who had to move to the India in search of the restart of new life from the ground zero. Millions who survived as displaced people moved to near by Jammu and Kashmir (J & K) for restart of their life in 1947. Mysteriously they were uprooted again a few months after the Independence Day. They were told to leave as UNO will decide who can live there. They have not decided as yet it is more than 60 years now. Madan's mother like some others were born in Kashmir but most other families (like ours) were not. Only those who were born in J & K could live there, this was declared, by the Indian Government. It will take generations for the refugees created then and their descendents to re-establish their normal life in India, or elsewhere. The new rulers of India want to remain ignorant about it. In fact they prefer to stay ignorant to avoid the embarrassment and continue abuse of the benefits of the so called freedom as it lasts. This book has been written especially as a great tribute to Madan's mother, Pushpa, whose portrait is included below as a special mark of respect being most loving and extraordinary caring mother despite all odds.

Mrs. Pushpin Want Kaila,
born 1916 (Sopar-Kashmir),
moved after marriage in 1935
to Lahore-Punjab then to
Jammu after independence in
1947, then to Delhi in 1947,
she died in Delhi in January
2011.

Our Mysterious Mind

Mind is a mysterious hunter.

  It haunts the brain to manipulate what it wants.

  Mind has the desire to know how the brain functions.

  It strives to know what the science is behind. Why it is so efficient and so perfect?

  The brain science has the secrets of the life encompassing events like,

  the metabolism, neurotransmission-inhibition, etc.,

  It would be nice to see in real time and non-invasively,

  how the brain achieves what it does

Our brain is a miracle science machine. It performs functions of controlling our body movements through neuron communication in a split second. It also regulates its own temperature and that of the body. An overheating of the brain due to too much stress or a disease can lead to death. There are activities like metabolism, neurotransmission, etc. happening in the brain on moment to moment basis trying to keep our body active and to the required level to perform cognitive tasks. It is done through a network of macromolecules and the electrical interconnections spread over the brain. The macromolecules maintain interface in-between themselves and with the bigger surrounding systems including, e.g. tissues, membranes, fluids in motion, blood circulation, etc. The macromolecules are of tens and hundreds of nanometers in size and collaborate with their neighbors for various dynamic activities. The electrons, nuclei (consisting of protons plus neutrons) are essential constituent parts of the chemicals present in the brain. Some of the chemical elements e.g. hydrogen (part of water), sodium, potassium, iron, carbon, etc., provide to the macromolecules in our brain an electric quadrupole charge (two positive and two negative poles) structure and a magnetic (dipole) character. These characteristics can be observed through MRI indirectly over volumes of sizes $(10^{-6}\text{m})^3$ to mm^3. The microscopic, spin (tiny molecular magnets) dynamics inside the brain relates more to the sub-voxel ($<\text{mm}^3$) structure rather than the mm^3 to the cm^3 size volumes. The larger volumes ($\sim\text{cm}^3$) are refereed to as voxels in the conventional (single quantum) MRI (magnetic resonance imaging).

For a single voxel selected for imaging we measure the total effect of the spins as an overall average effect. That is why it is called as the single-quantum (assuming atoms within macromolecules have single identical structure) MRI. The spins (tiny molecular magnets) add up to a macro-overall effect within the medium in which they are present. The scanning of the molecular spins in voxels in a planar X–Y projection (for a selected thickness DZ) provides an average X–Y mapping of the brain for the selection. One can expend the whole Z-axis (in small DZ steps) to obtain three dimensional image of the brain. This is briefly the conventional MRI. The macromolecular-spins act as the source of electrical signals in space and time when irradiated with the RF (radio frequency radiation) in the presence of a static magnetic field in the brain. The electrical and magnetic effects of heterogeneous species of nuclei in a voxel get smeared out with little details disclosed about the atomic and molecular level quantum interactions. This however can be discerned in a multi-quantum MRI (MQ-MRI) approach. MQ-MRI is performed basically in response to a strong ($\sim$3 T) static magnetic field applied in a chosen (referred to as the Z-direction) as in the conventional MRI. But this is followed by suitably designed magnetic field gradient pulses applied, in the X, Y, Z directions.

The field gradients provide localization of spins in space and time at the microscopic level. The RF (radio frequency) pulses of radiation applied as usual in the perpendicular direction then provide the electrical signals required for imaging and analysis. Measuring output from a sub-voxel level structure can allow the electric and magnetic dynamic activities at the multi-quantum interaction energy level in the brain to be born out. This is the basis of the new approach, i.e. imaging at the muli-quantum coherence level. The conventional MRI works on the smeared out (broader average) macro-space electric and magnetic dynamic activities through the surrounding, electron cloud regions spread over large distances. The multi-quantum interactions in-between the molecules are lost in the conventional MRI. Thus the in depth knowledge of the electric and magnetic dynamics of the brain does not form the part of the conventional MRI. There is a need now for a molecular level quantum approach to our brain. This is the approach of the quantum way. Actually it means the multi-quantum way.

At the molecular level deep down the electric and magnetic dynamic activities in the brain need to be thoroughly understood. Some nuclei e.g. the sodium, potassium, etc., have non spherically symmetric charge distribution due to the asymmetry in the arrangement of the electron charges in the atoms and the protons charges in the nucleus. It leads effectively to a quadrupole (four poles, two positive and two negative) character of the charge distribution around the nuclei. The quadrupole charge asymmetry is expressed through interaction with electric field gradient normally present in a situation like a tissue and the trans-membrane space around it. Some nuclei have magnetic dipole character, e.g. the hydrogen ^{1}H (single proton in the nucleus and an electron orbiting around it) atom. Hydrogen is present in the water molecule the source of life regulation in our body. The water molecule has an electric dipole. In an electric dipole structure the centre of positive nuclear charge

symmetry and the negative electron charge symmetry are separated by a small distance. Here there are two poles, one positive and one negative. The dipole characteristic of a molecule however produces little change in the MRI situation.

There are some nuclei in our body which have both magnetic dipole and the electric quadrupole character. They have very important role to play in the functioning of the body and the brain. These typical nuclei are e.g. the sodium and the potassium. They exhibit unique electric and magnetic character.

One can make use of the sodium (quadrupole) nucleus as a probe of investigation and that is what we do in the sodium MRI (SMRI). The idea is to track the life maintaining metabolic dynamic events happening in our brain. This sure is a very difficult task. However this task has been made relatively simpler by using, the conventional MRI technology to start with. The oriented magnetic spins in the Z-direction created by the application of the static magnetic field provide the internal magnetic reference direction to the asymmetric electric field surrounding it. We study the hyperfine magnetic energy spectrum of the magnetic dipole nucleus (e.g. the ^{23}Na), resulting from interaction with local conditions e.g., the ischemia. In a disturbed local chemical equilibrium i.e. a disorder there is shift in the magnetic energy structure of the sodium due to the coordination of asymmetric quadrupole moment of the nuclear charge and the electric field gradient present locally. One should remember the multi-quantum environment can only be seen in the sub-voxel structure. The RF spectrum emitted would in this case hold signatures of very many nuclei involved at the multi-quantum level coherence. Consider as an example a specific brain disorder condition i.e. the Alzheimer disease (AD). Here replacement of Zn (Zinc) by the Fe (iron) nucleus locally is considered as the chemical disorder responsible for the AD.

It may be possible in the future that we can make use of the quadrupole nucleus Zn as a viable probe to understand as to how the AD. works. This book is not written as a normal routine text book. It exposes the recent developments in the field of MRI and are presented through practical illustrations and yet linked to the basic concepts involved. It is hoped the material covered will be useful to the medical professionals (MPs) in their efforts to make a scientific diagnostics of the brain disorders and tumors easier. One should realize that it is not an easy task to write a book on MRI exclusively for the MPs (medical professionals). An author will find it not an easy task to exclude some reference to the physics, chemistry, and mathematic (PCM) in some form or the other. Brief exposure to the PCM of the MRI appears from time to time in the book. The MPs can skip those references if desired and use illustrations as a guide to understand the basic concepts. But a simultaneous exposure to the PCM introduces to them as an encouragement to understand the connection to the quantification procedures of the PCM required in the MRI diagnostics. As the awareness among the MPs about the value of the MRI tool in the field of medicine improves it would be possible in future for them to use MRI in a more effective manner in their work. At the same time the PCM experts have to be on the look out how to simplify the PCM of MRI and write in the form of an introductory text book

specifically useful for the MPs. The present book is addressed to a wide variety of audience. The audience spectrum spans from the academics and the technical staff working in the field of medicine to the medical scientists and the PCM professionals, engaged in research and to the teachers, educationists, etc.

A Brief Note to the Reader About the Complete Book (Parts I and II)

The book consists of two Parts. The part I is initially devoted towards the basic concepts of the conventional (single quantum) MRI techniques. It is supplemented by the basic knowledge required to understand multi-quantum MRI (MQ-MRI). Practical illustrations are included both on recent developments in conventional MRI and the MQ-MRI. This is to illustrate the connection between theoretical concepts and their scope in the clinical applications. The Part II initially sets out the basic details about quadrupole charge distribution present in certain nuclei and their importance about the functions they perform in our brain. Some simplified final mathematical expressions are included to illustrate facts about the basic concepts of the quantum level interactions between magnetic dipole and the electric quadrupole behavior of useful nuclei present in the brain. Selected practical illustrations, from research and clinical practices are included to illustrate the newly emerging ideas and techniques. The reader should note that the two parts of the book are written with no interdependence. One can read them quite independently. They are very much standing aloe in character in the book.

The Glossary of Terms List at the end of the two parts of the book is a comprehensive and general in nature. It corresponds to the important terms that appeared in the present book and the previous Book 'Quantum Magnetic Resonance Imaging Diagnostics of Human Brain Disorders' recently published by the authors. This book was published by the publisher, Elsevier, in the year, 2010/ISBN:978-0-12-384711-9. It can be browsed at http://www.elsevier.com. The organization of this already published book was as follows. Chapter 1: 'Bio-medical Quantum Computer' Chap. 2: 'Magnetic Resonance Imaging of the Human Brain'. Chapter 3: 'Magnetic Resonance Imaging Diagnostics of Human Brain Disorders'. In addition the reader's attention is directed to the following. The first part of the present book is written to present to the reader a simplified version of the molecular spin dynamics and the basics of the imaging techniques prevalent in the world of modern MRI (magnetic resonance imaging). Phenomenological, mathematical formalism, is avoided. Some helpful guidance is included through

appendices at the end of the first part of the book for those readers interested to venture into details of theoretical concepts involved in the molecular spin dynamics and the imaging. Further some selected clinical illustrations will help a reader to learn without having to go through theoretical details about the application of spin dynamics to the imaging including the multi-quantum coherence imaging (MQCI). The second part of the book is particularly devoted to the applications of the electrical quadrupolar nuclei in imaging.

There is asymmetrical electron charge distribution in some nuclei which gives them an electric quadrupole character. Sodium is good example in this respect and is commonly used as a source of imaging in MRI. It brings out information about the disturbed metabolism in a diseased state in a tissue. Use of multi-quantum techniques of imaging provides a more precise diagnostic tool about tumors and disorders in the brain. In addition the second part of the book includes specially selected illustrations on quadrupole nuclei to help a reader learn by reading through practical clinical applications of sodium MRI. Appendices included in the second part of the book at the end will help those readers who want to know and learn more about the basics and the newly emerging sodium multi-quantum imaging and the disorder diagnostics for the brain. In the end we expect the reader to appreciate that the MRI is not just a routine imaging technology, like the X-ray technology. It provides image of the atoms, molecules, and macromolecules while they are performing their normal moment to moment functions in the brain. This is done non-invasively. Now we are after a clear picture about the molecular level science happening in the brain and in real time. The main theme behind witting this work is the exposition of the applications of MQCI using quadrupolar nuclei e.g. Sodium, Potassium, etc. This has been done in reference to the diagnostics of the brain disorders. Bu as it is closely linked with the magnetic-dipole nuclei. Some technical illustrations exclusively on magnetic dipole nuclei, e.g., the 13-Carbon, 31-phophorous, etc., are also included. It is not necessary and not even possible for every reader to learn MRI science from the roots, e.g., by going through a phenomenological treatment in every step. There are the PCM professionals however who create and recreate new concepts to expand the use of the MRI machine. They are supported by the electrical and mechanical engineers who finally finish the product. The end users the professionals working in the field of medicine help redesign the tool through the deficiencies they experience and the benefits they want to enjoy in their routine use of MRI.

M. M. Kaila
Rakhi Kaila

A Special Note for the Reader About First Part of the Book

Human mind is always curious to know the unknown.

How much does the mind know about the brain?

It is a curiosity for the mind to find out

The aim behind writing this work is purely an educational one. It is to establish a sound simple understandable basis for the unknown science of the brain and its various moment to moment functions, in-operation. There are several technologies in use, e.g. the nuclear medicine, computer tomography, etc., to diagnose tumors in the brain and provide a suitable treatment. Each technology in some form or the other complements and supplements the knowledge about the brain science. This work restricts itself in scope towards the use of the nuclear magnetic resonance (NMR) phenomena. NMR uses RF (radio frequency) radiation to stimulate molecules in the brain and uses very small amount of RF energy. One should note that the RF radiation is a very small part (frequency band) of the nature's overall electromagnetic radiation spectrum in which we live in. The RF band is towards the lowest energy scale of the electromagnetic radiation spectrum. The energy involved is around the mev (milli electron volt) scale and is very safe to use. One should compare this energy with the Mev (million electron volt) used in the X-ray imaging. In the brain it is the energy transition and transport among the macro-molecules which in some form or the other are part of various activities measured in MRI.

The molecules are excited from their natural ground state to an excited state by the RF radiation. The de-excitation of the molecules back to their previous state sends out information (through the re-radiated RF radiation) about the distributed activities happening in space and time in the brain.

The brain is a confined multinuclear-ensemble comprising electrons, atoms, molecules, etc., in a bound cooperative arrangement. They are present among

tissues, fluids, etc., in a static and dynamic, electronic-quantum-exchange-equilibrium. Quantum science is about a century old, now and has its own well established rules of operation. It is known that the matter including the soft organic matter which our body is made of follows the quantum science rules. The most fundamental of these rules is that the electrons in atoms exist in stationary quantized energy states around the nucleus. They move up and down the energy states in quantum jumps rather then in a continuous manner. This behavior in principle remains the same as the atoms group together to form a molecule and the molecules in turn form the macro-molecules. There is a cooperative jump in the macro-molecular situation. That is where the concept of quantum and the multi-quantum interactions among molecules originates. The quantum science of the group of molecules has been well worked out for various naturally occurring or laboratory produced molecules.

The field of spectroscopy of molecules e.g. optical, infrared, radio-frequency, etc., is well established, and over the last century has developed a good enough knowledge about the variety of molecules as for as one can think of. Then what is holding us to find out what is so peculiar about our brain? The reader should note that the terms spin, dipole magnetic moment, angular momentum, etc are very common to observe in the MRI literature. At the core of MRI lies the structure of the atomic disc like magnetic-dipole (north–south poles). It arises due to the circulating electrical current created by the orbiting electron around the nucleus. The atomic electric current (i) and the orbital area of the electron A when multiplied together becomes the atomic magnetic moment and is expressed in the units of amperes-m^2. As we are dealing with rotational motion of the electrons the angular momentum rather than liner momentum becomes an intrinsic physical property to deal with. The quantum interactions between atoms, molecules, etc., exchange angular momentum following some selection rules. These rules basically control, the conservation of the angular momentum as the molecules interact. It provides the basis and the source of understanding the quantum interaction between molecules. The angular momentum of nearby nuclei, atoms and molecules interact and produce a resultant refereed to as the J.

It is common to see J as the source of imaging and is referred to as the J-coupled imaging. It is a scientist's curiosity to find out whether nature is manipulating in the brain the quantum interactions we already know of, e.g. the spin (intrinsic electron rotation)-orbit (electron orbit around the nucleus) interactions within an atom. We know there are interactions among molecules through metabolism, neurotransmission, etc., as the source of the functions of the brain. The MRI (magnetic resonance imaging) is just an imitation tool to unravel those mysteries of the brain. It uses the output due to the safe RF radiation's induced quantum-interactions within the brain, to find out, the secrets of the brain. This information is recorded over a small volume called as the voxel. It is repeated and collated over the whole brain to produce an image overall. The atoms, nuclei, molecules, fluids are the building blocks of the various scientific processes in the brain. The molecules are in operation all the time in our brain. At the atomic and molecular level the information gathered through the new emerging approach i.e.

the multi-quantum magnetic resonance imaging (MQMRI), is very crucial. The MQMRI enables a much deeper understanding of the metabolic, neurotransmission, etc activities, happening in the brain. The presentation of this work at the moment is considered very timely for the benefit of the scientific community overall and the medical professionals in particular. The reader may find some of the information in its form of presentation as repetitive in nature over some sections of the work. It is with a purpose. The authors feel that exposing the same information but in different illustrative forms make the educational-level of the understanding of the brain science more effective and much better.

This work is not intended to be a routine exclusive text book in MRI and or its applications to the neuroscience. Several text books have been written in the field. The approach adopted here is a quite a different one. Here learning is encouraged through the results of the research and development efforts in progress in the world at present. The aim behind writing this work is to bring to light as to how the quantum science works within the human brain. The MRI with recent developments towards the micron (10^{-6} m) dimension imaging will provide just the right technology to expand knowledge about the brain science. The ability to find out the chemistry and physics of the metabolic events happening in the brain at atomic and molecular level can be very rewarding in the development of the knowledge about the functioning of our brain. It is now the right time to make use of the multi-quantum resonance coherence (MQC) aspect of the MRI. Our brain is a highly dynamic ensemble of the molecules of the multi-nuclear species. Multi-quantum interactions are thus natural. Unraveling the multi-quantum scientific processes in operation in our brain is the theme behind writing this work. The approach, using practical illustrations rather than the phenomenological presentation is specifically taken up in writing this work.

The new development in progress is referred to as the MQMRI. It provides the appropriate technology to unravel the secrets of the brain science. The term MQMRI has been recently introduced by the authors in the MRI literature of the brain science. The authors here make specific efforts in propagating knowledge and the renewal of ideas and education for the medical science community. The knowledge required to understand the information compiled here does not necessarily require a higher level knowledge about the field of quantum mechanics (QM). What is learnt at the school level about the electron-atomic orbits and the internal structure (protons and neutrons) of the individual nuclei would be adequate. One should remember that the periodic table of elements was classified and based on the individual orbital electronic structure of each element. This knowledge was developed further through the studies of the spectroscopy of each individual element. One can always refer to the available standard tables in the handbook of chemistry and physics for details. But when the elements are confined in a region like our brain their individual properties are not very individual. They are modulated according to the environment where they are present and are affected also by the mobility of the fluids in which they are functioning.

The MRI depicts the events happening in the brain in space and time in the form of a picture. Multi-QMRI goes a step further. It brings out the quantum

coherence interactions happening between atoms and molecules. This becomes the real time and space picture of the brain. The intention behind writing this work is to induce education among the medical professionals to be able to see the benefits of using atomic and molecular level events happening as part of the MRI. These events are e.g., metabolism, neurotransmission, neuroinhibition, etc. They are happening in our brain, moment to moment, in time and space. The MRI will hopefully lead to a way for early detection of the brain disorders and tumors. The understanding of the quantum chemistry of the events happening in a localized region around 1 micron to mm in scale in the brain is paramount in finding about the metabolic and other functional events happening locally and globally in the brain. Quantum coherence science of imaging is still in its infancy and there will be a long way to achieve a state of perfection. Quantum science is a science of atoms and molecules. The MRI in its present form is based on macro-quantum phenomena. This approach is on a macro-level, i.e., mm to cm scale regions. The conventional MRI technology uses a large ensemble of spins in a macroscopic volume, of mm^3–cm^3 referred to as voxel. The intricate science of the atoms and molecules happening in the brain is the internal dynamics at the molecular level. It is at its most natural level i.e. the atomic and molecular level. We need to be exploring the events happening in space of microns (10^{-6} m) to mm and time of micro (10^{-9}) to milli (10^{-3}) s.

The MRI technology of today can be improved and in fact is under development to learn about the quantum science of the brain. This will one day lead to the design and construction of a 'wonder quantum machine' dealing with the brain at its most natural level i.e. the nano meter (nm) level. The term spin is vaguely used in the MRI medical literature. Its origin lies in the intrinsic behavior of electrons spinning around the nucleus and also around its own axis. The electron being a negatively charged particle generates electric current by virtue of its orbital motion around the nucleus. An electric current in circular motion generates a magnet with its north and south poles directed in opposite directions through the centre of the electron orbit. This is no different from a familiar bar magnet we learnt about at the school stage of our education. The difference is only in the size and shape of the magnet. In the present context the magnet is on an atomic scale in dimension and the shape is a disc like rather than a bar like. The form of magnetism which is instantly created by the MRI machine by the application of RF radiation is called as the diamagnetism and is at the core of the technique used in MRI. Taking MRI to the atomic and molecular level is the approach under development behind the MQMRI technology. Diamagnetism is instantly created in atoms and molecules by the externally applied magnetic fields in MRI.

All inventions start with a curiosity. It is inherent nature of all humans to be curious to find out as to how nature works. Human brain is the question in mind at the moment. NMR study started as a curiosity tool to study diamagnetism in various nuclei during the 1950s, of the last century. That curiosity study soon led to the discovery that the protons and neutrons inside the nucleus also contribute magnetism of their own, although of a much weaker magnitude, as compared to the atomic one. Proton magnetic resonance spectroscopy (PMRS) is now an

integral part of the MRI diagnostics of the human brain disorders. Spectroscopy of individual atoms as independent naturally existing elements in nature was worked out more than a century ago. It led to the standard sound footing of the arrangement of the elements we are familiar today in the form of 'the 'Periodic Table of the Elements'. In an ensemble of elements as in our body especially the brain, the energy spectrum of each element, changes due to the proximity and the interactions with its neighbors. One should remember that they are not only part of the macromolecules present in various tissue structures but are also part of the mobile fluids in the brain. The sodium–potassium pump through the membrane of a tissue and the blood circulation in the body are only typical examples of the wondrous curiosity of the existence of our very life.

In this first part of the book the sections 1 and 2 are devoted to help those readers who do not have a good enough background of atomic physics. It should enable them to gain first hand knowledge about the basic principles involved behind the basics of the MRI. We have atomic size magnets performing routine functions in the brain through interactions. A parallel is drawn between the gravitational spinning top in which most people are familiar with and the electron precession in the atomic precessing top case. It makes it easier this way to explain the meaning of the precessional resonance frequency in the atomic case. The reader is reminded that MRI basically works on the precessional resonance frequency generated electrical signal produced by the incident RF radiation. Its space and time variation throughout the brain is at the root of the imaging. A brief explanation of the commonly used echo-planar imaging technique is included in the first section. The section 2 is particularly devoted to the basics of the multi-quantum MRI. The meaning of the microscopic quantum model of the brain is developed in length and width in the section two. A rough model picture of the brain used in conventional MRI is included to see the comparison between the two models of the brain.

The spin–orbit interactions in the context of a single atom and how they are translated to a multi-particle system, in a voxel situation are explained using pictorial representations. How magnetic field gradients applied in different directions to an ensemble of spins encode phase (time) of the signals is explained through, the illustrative line pictures drawn. The explanations in this work are mainly made based on the pictures and diagrams to visualize the concepts without the need to go into the rigorous mathematics. One is advised to refer to the references [1–9] in particular for further reading about the basics to enable gain more insight. It would enable one to understand the detailed quantitative details of the concepts involved. Though the work is written with medical professionals as the target there will be some physics, chemistry and mathematics (PCM) experts who will also like to venture in the field of QMRI and be more useful to the medical community in particular. One particular form of the venture can be like the one we have taken up here i.e. writing an educational work; presenting a simplified picture of the MQMRI. This work is not written as a phenomenological based text book. It is rather an exposition of the recent research and development efforts in the field of MRI and integrating it with the basic concepts involved.

Establishing the connection between the quantum science of the brain and the MRI technology is the aim behind writing this work.

The section 3 has some practical illustrations where one can see the application of MRI in selected areas of clinical medicine. Some practical cases on multi-particle angular momentum J, imaging and spectroscopy are included to highlight how the information gathered is used to diagnose neurodegenerative brain disorders. The illustrations are selected from the conventional MRI and the MQMR developments. References [1-36] overall listed towards the end of this work would be helpful in general support of the learning process about the basics of the diagnostics and the science of MRI. Sections 4 and 5 go into some details about the simple introductory mathematics of spins dynamics under the influence of applied static magnetic field and the RF radiation field. The section 4 in particular deals with the spin dynamic in the form of simplified mathematical expressions. The representation of spins using matrices and their operation is explained. The connection between matrix representation spin space and multi-quantum coherence imaging is included.

The section 5 is particularly devoted to the density matrix concept in reference to a simple two-spin system. A reader who is not interested in the mathematical aspect of the spin dynamics in our brain can instead learn about the function of the spins through the practical illustrations both conventional and quantum included in the section three instead. The idea of including simplified mathematics is to encourage simultaneous exposure to both theoretical and practical aspects of the imaging. Section 6 is devoted to a simplified picture of the k-space imaging. The k-space basically is wave number (k) space, because; $k = 1/k$. Here k is the wavelength of the RF radiation used in the MRI. Although wave phenomena is a part of learning in the science curriculum at High School and first year science degree programs at the university level a rigorous mathematical approach is avoided except for the major physics degree programs. The section 7 is devoted to new developments in the area of MRI i.e. the Multi-QMRI. This is done through explanation of the basic quantum science concepts involved in MQMRI and the learning process is enhanced via illustrations from recent practical efforts carried on world wide. Section 8 is added as a summary and conclusion about the work. The medical professionals have a chance through this work to enhance their knowledge without going into the detailed mathematics. They are motivated though to learn at an advanced level through the guidance and the references provided in section 9. On the whole the work provides an overall exposure to the field of MRI and its applications in the area of clinical medicine in the human brain. Appendices A and B are added at the end to include additional diagrams and figures as a helpful illustrative learning material for the reader.

The reader is reminded that the broader perspective of this work is a comparison of the conventional MRI with the multi-quantum MRI (MQMRI). Although MRI itself is based on quantum phenomena but it is only recently that the term MQMRI has prominently started appearing in the MRI literature. The reason for this is that in the conventional MRI it was only a single quantum (no multi-quantum interactions between spins included) spins phenomena that was

used. The spins were given identity through the unique characteristic they gather due to their presence in different environments. This approach continued over several decades without any reference to the possible multi-quantum effects. The multi-quantum effects were seen present here and there in imaging but were not properly recognized. They were considered as a kind of field induction disturbances to the imaging. It became norm to say the technology as MRI without referring to it as a single quantum technology in all situations. But in recent research efforts at the molecular level the MQMRI has changed the situation. There is now need to separate MRI from the MQMRI. MQMRI is specific to treating spins as individuals with their unique atomic and molecular level electronic and nuclear structures. We have used references [1–9] as the basis for the exposition of the basics of the conventional MRI. On the other hand the references [10–36] mainly form the basis through some selected illustrations for explanation of the differences between MRI and MQMRI. This is done with minimum involvement of mathematics as the basis of interpretations. The reader will find that some guidance has been provided in the appendices A and B for those with mathematical bent of mind to adventure into the field of MQMRI further.

A Special Note to the Reader for the Second Part of the Book

The aim behind writing this book is purely an educational one. It is to disseminate the newly emerging knowledge about the science of the human brain. The work would be particularly useful to those who work in the field of clinical medicine and have a strong desire to learn more about the basics of the MRI and its use it in the diagnostics and the treatment of the human brain disorders. A path is set in this work to expose to the medical professionals (MPs) the importance of, the basic quantum science happening in our brain. The style in which this book has been written is not that of a routine text book type. Several text books in the field of MRI have been written and are available in the market. This book is different one. In this work we try to simplify the knowledge about the basic concepts of the magnetic dipole and the electric quadrupole interactions with the environment in which they are present. The quantum concepts have formed the basis of NMR spectroscopy over several decades. But the use of molecular level quantum interactions to develop new techniques of imaging and diagnostics of diseases is a new venture. The selection of the references [1–61] provide the reader with a good and a wide balance between the basics of the Muti-Quantum MRI (MQMRI) and the new research efforts in place.

New developments are taking place round the clock in the conventional sodium MRI as well as in the Sodium-Multi-Quantum MRI (SMQ-MRI). Over the last decade or so there is emphasis in research and development efforts for improvements in the area of MRI-diagnostics of human brain disorders. In specific the idea is to be able to use and understand sodium, potassium, etc elements and their unique quadrupole charge distribution inside a cell. It is crucial to understand the intra-extra cellular charge transport equilibrium dynamics. MQ-MRI approach will enable us to quantify the flow of ions in and out of the cell after the cell has been damaged in a disordered situation e.g. the stroke. In the second, part of the book there are five major sections. The section one expands on the basic science of the electric-quadrupole moment nuclei in the context of the MRI. We use in the section the mathematical expressions for electric dipole and electric

quadrupole as developed for a free space for explaining various concepts involved in the electric quadrupole-magnetic dipole MRI. This section lays down the basic concepts of the electric-dipole, electric-quadrupole and magnetic dipole moments of the atoms and the molecules. The basic theoretical concepts can be seen expanded in the section 1.1. The development in the section 1.1 is subsequently applied to the real atomic and nuclear cases in the section 1.2.

In a human body situation a nuclear electric-quadrupole moment e.g. that of sodium will reside in a naturally occurring non uniform charge distribution in a tissue in a specific region of the body say e.g. a tissue in the brain. A simplified approach to the learning process as is done in this book is in lieu of the full mathematical formulation. It is about simplifying the concepts behind the electric dipole, electric quadrupole and the magnetic dipole properties of the macromolecules present, in the brain situation. Full mathematical formalism about electric dipole and quadrupole moments in a free space can be commonly seen in an undergraduate text book of physics. The exact phenomenological PCM of the dynamics of the electric-magnetic interactions in the brain is beyond the scope of this book. The idea here is to expose the reader to the basic concepts as they are seen in the analysis of clinical applications of the MRI. The knowledge, disseminated is not developed in a sequential phenomenological order in this book. This would require large amount of space and time. A reader particularly interested about detailed basics is advised to learn from a basic text book on physics and chemistry in this matter. Here the idea is rather to expose broadly the applications of the basics. The appendices A and B added at the end of the book will be useful to those readers who are interested in finding more details about the basic concepts and the mathematical formalism involved. Here the section 1 of the 2nd part of the book expends on the simplified basics of the dipole and electric quadrupole moments and their interaction with a magnetic dipole in the real MRI situation.

The brief exposure of the basics in the 1.1 and 1.2 section is followed by the section 1.3. In this section are presented practical quantum structure details about the quadrupole spin 3/2 system. In the section 1.4 some actual selected practical quantum spectroscopy and imaging situations are presented as the illustrations. This is to enable visualize and perceive how electric-magnetic interactions in the brain can produce useful pictures for a diagnostic purpose. In particular the quantum approach where the central theme of the book lies, imaging benefits at the molecular level are exposed. The section 2 covers much wider aspect of the sodium, potassium imaging concepts. Theoretical concept of density matrix is simplified and its relevance in application to the spin 3/2 electric quadrupole-magnetic dipole system is highlighted. Some practical conventional and quantum imaging systems are included for illustration in this section. The sections summarize the quantum-sodium approach to the imaging in the human and animal model. The section three covers wide spectrum of clinical and research illustrations from the recent development efforts in progress world wide. This section includes illustrations from the cases of, various organs of the body both in the human and the animal models to introduce to the reader the important various techniques emerging.

Section four summarizes what is broadly covered in the second part of the book and includes illustrations about the basic concepts covered in the book. Further directions along which the future of MRI lies is summarized in this section. This is done so in reference to the basics of the unique bi-exponential relaxation behavior of the electrical signals arising out of the quantum energy structure of the macromolecules in the cell. This aspect is emphasized to encourage developments of various new horizons, in the offing in the area of Sodium-MQMR. The section 5 covers conclusion about the newly emerging Multi-quantum Sodium-MRI. A list of references is provided in section 6 which also formed in some form or the other the source of the educational material compiled in the book. The book has included an important additional reading section at the end. This is the section of appendices, A, B and A1. It presents an assortment of topics and their brief assessment covering different aspects of sodium-quantum, and multi-quantum techniques in general. The idea is to allow the reader become aware of the many newly emerging techniques and their applications in the MRI and the basics in the diagnostics and treatment of diseases. It also exposes summary of some of the phenomenological PCM involved which can be useful in further development of the field of the sodium MRI (SMRI).

The appendices added it is believed will help those readers with an adventurous bent of mind in the areas of PCM and will lead to further development of the applications in the field of MRI. A person need to learn from many different text books and the research articles in journals about the research and developments that are taking place to see the diverse knowledge emerging. This process is an essential part of advancement in the field of SMRI. This book presents the basic knowledge required in an abridged guiding manner in one place to different types of readers. In specific it presents a simplified educational exposure of the recent developments in the area of quantum sodium magnetic resonance imaging (QSMRI) techniques. This is the underlying theme of work in this book. It is believed that it will provide a rich source of education about the past and present developments in the field of MRI to a wide variety of readers. This includes specialists in neuroscience, clinical doctors, PCM experts, bio-scientists, medical scientists, etc. The presentation of the Appendices has been selected with a summary from a variety of theoretical and experimental research done past and present both in conventional and multi-quantum MRI. It should provide the reader with a comprehensive guide about further reading in the area of sodium MRI.

An Overview of the Second Part of the Book

We are a technological society. There has been research and development world wide in science, and, education about science, for more than a century, now. It has been through the PCM (physics, chemistry and mathematics) education that has resulted in to economo-technologies on which the present human civilization survives. With the culture of PCM on the fast decline the new techno-disasters emerging, e.g., the fuel emissions in the atmosphere, oil spills in the oceans, unsafe nuclear waste dumps, floods, bushfires, volcanic eruptions, tsunami, climate change, etc., will soon become un-manageable risks. The maintenance of PCM educational culture starting from the secondary and pursued in tertiary education system in the society and its application to all forms of life on earth is worth the preparedness for the risks, we face in the future. It is essential to preserve the safety and predict the risks involved to us all. Health and security of human body and mind is a barometer of the quality of the environment we live in. What price if we have to monitor the well being of the environment and the life on earth. This book highlights about the education of the newly developing principles in the field of science the multi-quantum magnetic resonance imaging (MQMRI). Its application can be seen world wide to the human body in general and to the science of the human brain in particular.

The book briefly covers how in a non-invasive manner one can diagnose diseases in human body and look after our health in a systematic scientific manner. The human body is nothing short of a miracle scientific machine. Leaving, to let the body function as it can and treat with pills to feel better when sick is simply an act of ignorance. There is now happening in-depth research and advancement although in very limited locations around the world in the 'Molecular Level Insight' in to our body. This is being done via research in the area MQMRI. It includes the nano-molecular level research in imaging and its applications to the area of neuroscience. The book presents a simplified educational exposure to cover the audience as wide as possible. The way this book has been prepared is unique. It is not prepared in a normal routine text book manner. The idea is to stimulate, invite participation, learn and perpetuate, the knowledge, about the basics of MRI and its new developments, among medical professionals (MPs), neuroscientists,

PCM experts, etc. We are sure there will be some enthusiastic minds who will like to carry this venture a step further for the benefit of the future generations. The enthusiastic curious minds are invited to participate and make the knowledge advance further and help to make it available within the reach of everybody.

Contents

Abstract for the First Part of the Book

This work is written to help scientific, technical, and medical professionals involved in the area of human brain science to gain a firsthand knowledge in the field. The scope of the work is restricted to the knowledge gathered through the technology of MRI. Professionals working in the areas of physics, chemistry, and mathematics (PCM) can also gain preliminary insight into the area of brain science and apply themselves to further enhance the field. PCM experts who are normally involved in their own areas of interest will find this work very stimulating to explore this new area of science. Some brain science practical illustrations are included in the work for their benefit. The technology of the MRI commonly used today in the study of brain science is highly developed and is a noninvasive tool. It is through the eyes of MRI that brain science has advanced considerably over the last decade or so. This work is broadly divided into nine sections. The first section is the introduction. This section covers the microscopic and macroscopic character of the brain modeled on the basics of the spin character of an electron orbiting around the nuclei in atoms. The spins of the molecules and the spin character of the nuclei are also included. Through these spins one finds out the secret behavior of the macromolecules which help to carry on the moment-to-moment metabolic neurotransmission, etc., activities in the brain. The rotational motion of the electrons around the nucleus forms the basics of the natural magnetism called the diamagnetism. This magnetism remains globally neutral in the brain due to its random distribution in space and time. In order to understand the process of diamagnetism we have tried to draw an analogy between a simple gravitational spinning **Top** and atomic spinning **Top**. The motion of a simple spinning top used by school kids for fun is illustrated through a diagram in terms of the gravitational forces involved. The meaning of the precession of the angular momentum vector around the vertical gravitational axis is explained. An analogy between the gravitational spinning **Top** and the atomic magnetic spinning **Top** is drawn using figures and diagrams as the source of depicting the concepts involved. The meaning and magnitude of the frequency of oscillation of the atomic spin (dipole magnetic moment vector) precession as compared to the gravitational case is

elucidated in the first section. The most fundamental technique of MRI, the echo planar imaging (EPI), is briefly covered in this section. Section two of the work is devoted to the concept of the angular momentum of the orbiting electrons around the nucleus and the dipole magnetic moment which is created due to this motion. The quantum nature of the angular momentum and of the associated dipole magnetic moment is broadly explained in the second section. The internal quantum science of the brain is elaborated in section 2 through diagrams. The idea is brought out that the human brain has its own magnetic order. A group of nuclei collectively create an internal magnetic field of the order of 1 Tesla at a point. This field rapidly falls off from a point in the brain. It creates a polarized volume around it where spins (the dipole magnetic moments) are aligned along this field. This region is of microscopic dimensions on the scale of micrometers. The internal nuclear field is strong enough to create interactions between electronic, atomic, and nuclear dipole moments. In this work, the treatment of the orbiting electrons around the nucleus for simplicity reasons is treated in detail. The nuclear and the molecular structure in principle follow the same building blocks. In fact, there are four basic angular momentums involved in atoms. These are due to the electron rotating around its own axis, the electron rotating around the nucleus, and the angular momentum corresponding to the circulating protons and neutrons inside the nucleus. A resultant angular momentum $\mathbf{J}$ due to all these (due to orbital electron spin and nuclear spin) is created by an internal nuclear magnetic field. The internal magnetic field encourages interactions, among atoms and molecules and the environment in which they are present. The measurement of the magnetic moment associated with this internal (intrinsic) total angular momentum is the one that one should be after. But the scale (<micrometer) on which it is felt makes it un-measurable in any sensible way by any present day available technology. The precessional motion of the dipole magnetic moments around an externally applied magnetic field >1 Tesla along the Z-direction in the brain creates aligned magnetic spins at every point in the brain. Their average effect over a small volume ($\sim$mm^3) is measured. By applying small RF (radio frequency) fields along X and Y directions the signals are projected on the X–Y plane. The frequency of the RF field applied is chosen so as to modulate the precession of the spins with respect to the internal activities in the brain. This is done over a small selected volume called the voxel over a selected thickness of an X–Y plane. Then a global image of the brain is constructed from the collected data. This is basically what the MRI technology does. Behind the MRI picture produced is a valuable information stored in a disk in the computer detailing the possible events happening in the brain in real time. One measures the electrical signal that is created by the pre-cessional motion of the dipole magnetic moments which closely follows the angular momentum. The information about the angular momentum is derived from the behavior of the magnetic moment. The recently developed use of quantum-correlations among dipole moments as a new technique of imaging is explained in this work. On a timescale of ms (millisecond) to microsecond (μs) there are quantum chemistry reactions happening in the brain. This is the timescale of the excitation and de-excitation of molecules and their interactions with their

neighbors. This information is carried on by the RF radiation which acts as a carrier back to the sensor placed around the brain which records the message. Section 3 includes illustrations from both the conventional and the newly emerging quantum imaging techniques. Sections 4 and 5 are basically included to encourage PCM experts to be aware of the fact that the field of the brain science is new and an opportunity exists to get involved in simplification of the physics and mathematics involved to help benefit the medical professionals. Section 6 should be very helpful to clinical doctors involved in the analysis of MRI pictures and their interpretation toward diagnostics of human brain disorders. It includes through diagrams a description of the meaning of the T_1 (conceptually called the longitudinal or the spin-lattice (the brain)) relaxation time and the T_2 (conceptually called the transverse or the spin–spin relaxation time). The concept of k-(the wave number) space is highlighted and its basics are explained in Section 6. Section 7 is devoted to the newly emerging quantum concepts of imaging and their applications to the human brain science; it is done through practical illustrations. Section 8 is devoted to the summary and conclusion. A brief picture is presented about the overall organization used in the assembly of the work. In Section 9 a list of references is included for the readers to initiate a further detailed study. Appendices A and B are added at the end for readers who want to learn more about the PCM of the spin dynamics in the brain.

Part I
Brain Spin Dynamics and the Multi-Quantum Magnetic Resonance Imaging

Chapter 1
Introduction

1.1 The Science of the Macroscopic World Around Us

The human brain has evolved over many millenniums. But over the last three centuries or so the analytical power of mind has accelerated many fold and at a much faster rate. There is a gradual increase in the desire to understand the science of the human mind and of the brain. The brain science in action we need to know has to be experienced at the miniaturized the atomic and molecular level. Newton around three centuries ago was amazed to see that an apple from a tree falls to the ground and not the other way around. Our earth is like a sphere hanging (due to gravitational forces among our star the Sun and other planets revolving round it) in space. All points on earth are equally exposed to the space around it and yet the apple is attracted toward the earth. This is despite apple's density is higher than the density of air space surrounding it. This thought about the act of science was just a curiosity in Newton's mind. Science is curiosity and curiosity is science. The science in its mathematical analytical aspect was little developed in Newton's time. Soon the art of thinking became the art of scientific creation. The science became a tool, of production of technologies those followed. It changed the humanity forever. This was the beginning of the discovery of the forces of gravity which keep the sun, earth, moon, the galaxies, etc. in a dynamic equilibrium. In fact the universe we live in makes the human mind create science all the time.

The mathematical techniques e.g., the calculus, algebra, trigonometry, coordinate geometry, etc. then evolved to quantify the dynamics of planetary motion. It created the technology of aviation industry, space travel and created many other inventions we take for granted. The technologies that have evolved over the last century have created wonderful applications in our, day today life. To mention a few are aviation, satellite communication, microwaves as source of energy in household cooking, mobile phones, TV, etc. Mind imagines out of curiosity sometimes impossible but wonderful things. In today's environment of economics human mind is restricted to limit its scope of thinking. This is to limit imagination now. It is to fit according to the

survival in the materialistic world we live in. The scope of the thinking today is restricted to the art of money making as the main priority. Money drives science and the science is restricted in its horizon to simply making more money. So the scope of science is not unlimited now in the environment we live. The Newtonian's art of thinking was free and, unlimited. It was on finding the secrets about the universe around us. The science and, the technology that developed then was about the dynamics of large physical bodies like planets, aeroplanes, cars, etc. The society today cannot live without the technologies that have been developed. Think of the indoor and outdoor comforts we enjoy in our day to day life. They are not the results of restricted art of thinking. So far the major developments that have taken place are about the macroscopic world which we can see, and feel around us. But there is another world the microscopic world. This is the world of ensemble of nano-scale atoms and molecules which make the world of living beings e.g., our body.

The science of the dynamic functions of the atoms and molecules happening in a living body keeps a living being going. The nature has worked out the art of the control of life quite well. Science has yet to work out many mysteries. Even god likes to keep many secrets for a scientist to find out. The activities of atoms and molecules on a nano scale in our body cannot be seen by a naked eye. To view their behavior in small volumes we use sophisticated tools, like the electron microscope, atomic force microscopy, magnetic resonance imaging (MRI) etc. They are expensive tools. But they expose the secrets of nature which would not be known otherwise. The wealth they generate e.g., a good health system, industries, etc., more than compensate, the cost of the art of the creativity of the human mind. Human mind has the power of the art of thinking to inherit the science of the universe we live in. The microscopic secrets of the human brain science are not externally visible. They are the invisible, science of the nature. To work them out would be a science of our survival.

1.2 The Internal Science of the Microscopic Brain

The human body is made of the microscopic world of the atoms, molecules, electrons, etc. These tiny particles control the day to day and moment to moment functions of our brain, mind, and the body. The dynamics (Figs. 1.1 and 1.2) of these particles is processed in our brain without us knowing how it works. How does the molecular dynamics coordinates about what is happening in our brain? It also controls the other parts of the body? There comes the art of thinking. In today's science we call it as art of modeling about the unknown things. In this work an effort is made to expose the art of imaging the activities happening in the human brain. The technology we have at present about the magnetic resonance imaging (MRI) is called as the conventional MRI. It started about half a century ago as a curiosity tool to understand the phenomena of nuclear magnetic resonance (NMR) in solids and liquids. But as the time progressed, it slowly found its way into applications in imaging in plants, animals and the humans. Human brain is made of soft matter

including tissues, molecules, electrons, atoms, nuclei, etc. The electrons with their negative charge are orbiting the nuclei due to coulomb attraction from the nucleus with its positive charge. Due to the quantum mechanical art of nature an electron can only stay in a fixed quantized stationary orbit. The outer slightly loosely bound electrons around the nucleus and the coordinated geometry of the atoms and molecules establishes the chemistry of events happening in the brain.

Electrons simultaneously can be part of many molecules in a region. There is like a smeared out cloud of the electrons shrouding the much deeper secrets of the nuclei. MRI through the magnetic spins of the electrons, atoms and molecules spread locally over a small region called as a voxel images a small region in time. Scanning the small regions (voxels) one at a time in a sequential order over the whole brain by the use of RF radiation and collating them one can develop a planar image of the whole brain. This is a broad the simplest and the crudest mode of imaging. It is referred to as the chemical shift imaging (CSI). The electrons buried deep inside the atoms, molecules, in tissues are stable and are not electrically active. They however provide the necessary background in controlling the science of the brain over all. Near the surface of the macromolecules, charges form the basic equilibrium structure of a tissue. The charges create a collective reactive protected equilibrium for the brain. The equilibrium among the molecules is over distances varying from nanometers (nm) to millimeters (mm) to centimeters (cm). The common molecular electron charges have a magnetism associated with them. It is loosely called as the spin magnetism.

Inside each molecule the atoms act like small disc shaped magnets of the size of around nm. The rotation of the electrons around it own axis plus around the nuclear axis constitutes the total magnetism of the atom. The atoms add up to produce the resultant magnetic moment for the molecule. It is the overall effect over many tens and hundreds of nm that is the key to the performance of the brain. There is some kind of local magnetic order in the brain in the short range. The human brain is overall electrically and magnetically neutral. But over small regions say hundreds of nm there is an effective local magnetic field at any point created by the local group of nuclei. This magnetic field can be of the order of 1 Tesla (somewhat lesser due to the medium of the brain). It polarizes the region around it into a magnetic order along its direction. Every small (around a micron wide) region all over the brain has an independent magnetic order of its own. But these orders are randomly distributed with an overall effect being zero. There is interaction or say communication between all these small regions to make the moment to moment activities e.g., neurotransmission, metabolism, etc. to continue. The surrounding mobile fluids like water, blood, etc. keep the overall all activities of the brain and the body alive and thus keep us going. The overall simplified picture of the brain has in fact to be quantified to enable understand the functions of the brain. It amounts to understanding the order–disorder processes on nm and ns (nanosecond) scales. This is an impossible situation. There now comes the art of thinking.

One needs to make a machine which can probe the secret dynamics of the brain. The new machine will have to do quantum imaging with minimum disturbance to

the brain. The present MRI machine strives to achieve wonderful things. But it still has long way to go. The more the knowledge is disseminated about MRI in a simplified manner to the masses the better is the chance for its further development. This is the aim behind this exposition. MRI allows us to work out the dynamics of the invisible processes happening in the brain by using non-invasive RF (radio frequency) electromagnetic radiation. The MRI technology tries to simulate an order of its own in the brain by external means. It mimics a probe by external means to find out the local magnetic order in the brain created by nature. The external means stimulate the local order and it is measurable in the laboratory with minimum disturbance to the internal order. Since the internal order is on a nm scale, simulating a superficial internal situation in the brain, in the laboratory, can be a formidable task. The MRI machine tries to achieve a close to the real situation in the brain. A static magnetic field larger than 1 Tesla is first applied through the skull. This direction in the MRI literature is referred to as the Z-direction. What this field does is that all the tiny magnets i.e., the spins bound to the molecules, tissues, and the free ions as part of the moving fluids etc. are oriented magnetically along the Z-direction. The RF radiation applied in the perpendicular direction to the static field allows to manipulate the spins in space and time for imaging.

1.3 The Nature's Invisible Science of Magnetic Order in the Brain

There is some kind of regional as well as overall magnetic order in the brain. It is experienced through a local distribution in the size and the extent of the arrangement of the spins. This order produced is static as well as dynamic. It changes over space as well as time. This is because the atoms, molecules, tissues, fluids, etc. are reactive and interact with each other. The dynamics of the atoms and molecules is governed by the rules of quantum science. In quantum science the statics and the dynamics of the atoms and molecules is a totally different matter. The tiny molecules not only move in space and time but also react chemically with each other. They also communicate electronically with each other and also exchange a few quantum's of energy in the process. These objects are guided by the rules of quantum mechanics (QM). This is in contrast to the dynamics of the larger bodies like the aeroplanes, space shuttle, etc. The large body's dynamics is a continuous one and is controlled by the Newtonian Mechanics (NM). The reactions between atoms and molecules take place in a discrete manner rather than in continuous manner. What it means is that when the amount and direction of interaction is just right a quantum or two of energy is exchanged and so is the information for a particular activity. The most fundamental (smallest) quantum of energy is expressed as $\hbar\omega$. The $\hbar$ is the familiar angular Planck's constant $\grave{O} = h/2\pi$ of electromagnetic radiation and ω is the angular frequency of the RF radiation. RF energy is in a narrow band selected in MRI. It is out of the much
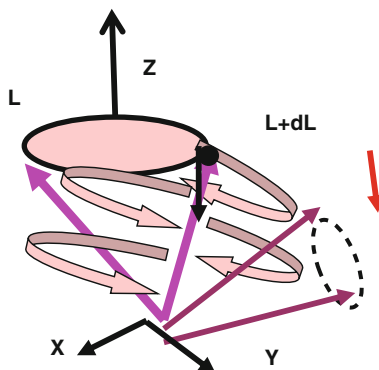
Fig. 1.1 The Gravitational spinning Top (GST). Suppose that the toy GST is set into circular motion as the kids do by wrapping around a string around the rim of the top, pulling the string, and let the Top go landing on the ground vertically. Initially the Top rotates around the vertical axis. There is an initial angular momentum of magnitude L of the Top along Z-axis and acting through the centre of the Top. It is produced by rotational motion about the vertical Z-axis. Soon the angular momentum L changes to, $L' = L + dL$ with its direction slightly away from the vertical axis. This change is produced by the force the Top's weight mg (m is the mass of the Top and g the acceleration due to gravity) as if there were a torque at a point on the periphery around the X-axis. The Top is slightly tilted from the vertical axis. This makes a change in the magnitude and direction of the angular momentum L initially pointing in the Z-direction, by dL, towards Y-direction. There is thus now an additional rotational component (around X-axis) on the Top, L' being side-way from the Z-axis. This additional component rotation of the tip of the top is as if to rotate the Top around the X-axis and let it fall ultimately towards the Y-axis. The motion at an instant of time is now more complex. There are now two types of motions. The top is still executing circular motion instantly around its new axis with angular momentum axis, L'. But the Top, as a whole body, also starts rotating around the Z-axis. The tip of L' is now executing circular motion with larger and larger radius in time around the Z-axis. The Top eventually, falls towards the ground

wider spectrum of the total electromagnetic (EM) radiation spectrum. This is called as the RF band of the EM radiation. The band is selected because the reactions between atoms and molecules in our body take place in this band of energy.

The MRI machine uses RF radiation for its operation. The RF radiation extends over frequencies in the MHz ($\sim 10^6$ Hz) range and in wavelength over the meters range. To probe the brain the RF radiation is applied in a perpendicular direction to the applied static field. This direction is referred to as the X-direction (refer to Fig. 1.1). The RF field is applied in pulses in time in the X-direction so as to project the spins in the X–Y plane. In the time in between the pulses called as the evolution time the spins decay and produce electrical signals in the X–Y plane. The spins are used to collect the naturally happening events in the brain in a controlled manner. The signals collected carry the signatures of the locally happening events. This information is collected by a receiver as a field induction decay. There is an asymmetric distribution of the field induction decay with a particular characteristic time. The characteristic decay time of spins in the X–Y

plane is called as the transverse relaxation time T_2. This becomes the source of the so called T_2, weighted image. Alternately the spins can be projected from +Z to −Z direction by applying the $18\bar{0}$ RF pulse along the X-direction. The decay of the electrical signals induced by the spins in this case can be measured as the spins move from −Z towards the +Z direction. The inversion of spins method collects information about the decay time which is called as the longitudinal relaxation time T_1 and is present in the X–Z and Y–Z planes.

The asymmetry due to chemical and physical events happening, in the X–Z and Y–Z planes becomes the source of image called as the T_1 weighted image. The broader T_1 and T_2 weighted imaging restricted to mm^3 to cm^3 voxels with little insight into atomic and molecular level intricacies is the major source of information in the conventional MRI. The modulations of the incident RF radiation received back as echoes over selected voxels in a sequence all over the brain are later coordinated in a computer program and produced as an image. The data collected provides a detailed bank of the scan of the events over space and time. One can analyze data much further rather than just looking it as source of an image to understand the human brain science deep to the roots. The nano science of the brain is a quantum one. One needs to slowly approach the quantum chemistry of the natural events and image them. The emphasis as multi-quantum magnetic resonance imaging (MQMRI) rather than just MRI in this work has two prong purpose. Firstly it helps advance imaging on the real natural scale that is the nano scale. Secondly it induces education about quantum science over a much wider population. So far it has remained within the domain of physics, chemistry and mathematics (PCM) experts. Further it has only been a part of the university level education so far. It did not form secondary school level part of the education system. This is the status all over the world today. It is high time for a change. The UNESCO (United Nations Educational Scientific and Cultural Organization) owes this initiative to the education system on an international scale.

1.4 The Familiar Gravitational Spinning Top and the Not so Familiar Atomic Magnetic Spinning Top

1.4.1 The Gravitational Spinning Top (GST, The Gyro)

It would be very instructive to understand the dynamics of the familiar toy spinning Top which basically represents a Gyro used in satellites in space. It is used for fixing the direction of the axis of the satellite towards the centre of the earth. The basic principle involved in the rotation of the familiar gravitational spinning (GST) is similar to that of an electron orbit around the nucleus i.e., the atomic spinning top (AST). In AST the electron motion around the nucleus is such that the electron stays in stable orbit around the nucleus and does not collapse into the nucleus. On the principles of the quantum mechanics (QM) one would expect that there are
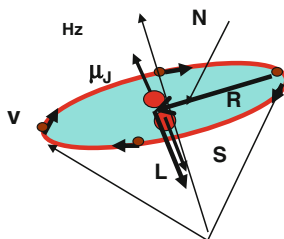
Fig. 1.2 The Gyro Magnetic Ratio (GMR) is the ratio of the μ_J = the total dipole magnetic moment to the resultant angular momentum, J and is, GMR = μ_J/J, J = L+S+... Here μ_J = i A, i = electrical current created by the orbital motion of the electron of charge, e, around the nucleus and i = ev; A = area of the orbit = πr^2; L = angular momentum = mvr, pointing perpendicular to the plane of the orbit and acting through the centre of the circle; m = mass of the electron; v = tangential velocity; r = radius of the orbit; μ_J/J = e$\hbar$/2m = (e/2m)/$\hbar$ = $\mu_b/\hbar$ (the atomic orbital case only); μ_b = (e$\hbar$/2m) = Atomic Bohr Magneton = 0.927 æ 10^{-23} amperes meter^2 (Am^2) = the fundamental unit of the dipole magnetic moment. The electron orbiting around the nucleus generates an angular momentum L. It is directed in a direction perpendicular to the plane of the obits and acts through the centre of the orbit

n electron orbits around the nucleus and are quantized i.e., the area of the orbits would have quantized values in terms of the area of the closest orbit (A) expressed as $A_n = 1A, 2A, 3A, \ldots$,etc. In the atom there is a precise balance between coulomb attraction on the orbiting electron due to the positive charge of the nucleus at the centre and the repulsive centripetal force. The balance is a quantum one that is the radius of the orbit changes in quantum numbers, n = 1, 2, 3, $\ldots$, etc. and not in continuous manner. Nature has cleverly produced the quantization of the angular momentum of the electron in orbits around the nucleus. These orbits have stationary energy states. Why has this happened? Is quantization the nature's science? In fact this is the science of the basis of the quantized nature of atomic orbits and the possible inter-molecular interactions in an ensemble like the brain.

It is not the right place to go into the quantum science of the atoms and molecules in detail. An undergraduate or perhaps a secondary school text book in physics may be very helpful to gain some conceptual insight. The Figs. 1.1 and 1.2 are included as a pictorial illustration about GST and AST respectively. The illustrations draw an analogy between rotational motion of the familiar gravitational spinning Top and the motion of the electron orbiting around the nucleus. The simplified comparison depicted is purely on the educational concept involved and not an exact quantitative estimate of the physical quantities involved.

In summary the initial rotational motion of the Top along the Z-axis is soon taken over by the torque due to the weight milligram (mg) (arising due to frictional forces, m being the mass of the GST) till it falls to the ground. But in-between the Top is still executing a circular motion around its own axis which gets weaker and weaker with time till the whole thing comes to a sudden halt. This is as if one motion (pointing towards the ground) takes over the other (trying to keep rotation as whole around the Z-axis) as time progresses. Imagine there were no frictional

force (between the bottom tip of the GST and the ground, air, etc.). Will the Top keep on rotting around the Z-axis? The second slower motion of the Top as a whole around the Z-axis is called as the precession. The change in L is due to mg (the weight of the GST) is in the direction outward, from the Z-axis. The magnitude of L around the Top's own axis in fact reduces as its initial angular velocity, $\omega = v/r$ (v the tangential velocity around the rim if the GST and r its radius), gradually reduces. The rotational speed of the Top around its own axis gradually slows down due to frictional forces e.g., air, contact at the floor, etc. Momentarily the tip of the Top is in the new position, with changed angular momentum L′. The result is that while the Top is spinning around its own axis with new frequency say ω′ it is as well rotating around as a whole around the Z-axis.

This additional rotation around Z-axis is with a different frequency, Ω. This is the precessional frequency. Gradually the Top increases its tilt from the Z-axis till it falls to the ground. The precession frequency is controlled by the gravity and is given as $\Omega = (mgr/L)$, g = the acceleration due to gravity. The force (weight) mg acts and produces a torque around X-axis. The precession frequency, Ω, is different from the angular frequency of rotation of the Top, ω. The angular acceleration of any point on the rim of the Top is towards the centre of the plane of Top. It is, $\alpha = v^2/r = r\omega^2$. Here v = the tangential velocity at a point on the rim of the Top and $\omega=$ the angular velocity towards the centre of the circle of the top and r is the radius of the Top. One should note that the precessional frequency Ω is a result of the twist produced by the weight mg of the top around the point distant r from the point where the new centre of gravity of the top lies.

The precessional frequency Ω of the tip starts as small value increase gradually and suddenly comes to zero as the Top hits the ground. One can find that $\Omega = (mgr/L) = g/v$ initially. The change in angular momentum is the product of the linear momentum mv at a point on the rim of the Top multiplied with twist say R around the X-axis and is dL = mvR (note R increases with time). The g has constant enough value on the surface of the earth therefore the only variable left is v. But v = Rω (the twist circle around X-axis). The change in initial angular velocity ω with time controls the precessional frequency Ω. The ω gets slower and slower with time and Ω gets faster and faster with time till it suddenly comes to zero as the Top hits the ground. The two processes compensate each other controlled by the frictional forces. Now think of the case of an electron orbiting around the nucleus. Why does it go on executing that motion forever? What are the forces responsible for it? Are there any frictional forces involved in the AST?

1.4.2 The Atomic Precessing Top: Case of Single Electron Orbiting Around Nucleus in an Atom

One should note that although the AST and the GST conceptually behave the same way the forces responsible for the precessional motion are different in the two cases. In the atomic case it is the quantum energy structure of orbital motion of an electron

around the nucleus which is under consideration. In an ensemble of atoms and molecules like in our brain it is the angular momentum of a bunch of spins (tiny molecular magnets) say in a voxel, that spin around the applied static magnetic field, H_z, applied in the Z-direction, that is important. There is an associated magnetic dipole magnetic moment for the orbital electron pointing in the opposite direction to the angular momentum. The result is due to the negative charge of the electron. Similar kind of things are happening inside the nucleus due to protons and neutrons. The frequency of precession of an electron or a proton is given as

$$\Omega = g_1(\mu_b/h)H_z$$

Here, μ_b, is the magnetic moment of the disc shaped magnet created by the orbital motion of the electron, around the nucleus, h, the Planck's constant, and g_l, the spectroscopic splitting factor. This factor allows to predict (calculate) various modulations in Ω which arise in an ensemble like the brain due to the interactions between the electron angular momentum (intrinsic S around its own axis), atomic orbital (L), the nuclear (I) and the intermolecular, etc. The value of g_l is 1 for the orbital case that is if we only have spin due to the orbital motion of the electron around the nucleus and nothing else. It becomes 2 for the pure (intrinsic) electron precession, spin S, around its own axis and is represented by symbol g_s. Thus in the electron intrinsic (around its own axis) case only one can write, $g_1 = g_s = 2$. Spin S (electron) and orbital (atomic) angular momentum in fact interact and produce a resultant J. Each orbital energy spectral line thus will be split into two due to g_s. Please see Fig. 2.3 for details about spin–orbit (SO) interactions. The precessional frequency of an atom or a nucleus is the source of resonance for the applied RF radiation for imaging. One should note it is the applied static magnetic field which produces planar quantization that leads to a concrete measurable result. Without this field the spins are randomly distributed and cancel each other.

In order to see a good example as to how the angular momentum operates one should consider the case of a helicopter. Normally the motion of the helicopter is vertically upward while its blades rotate in a plane perpendicular to the vertical axis, i.e., in the plane of the ground. When the helicopter wants to move sideways it simply twists the axis of rotation sideways. The angular momentum then points in the side direction of the helicopter. The helicopter thus flies side way. The laws of circular motion are analogous to that of the laws of motion of a body moving in a straight line. The linear motion generates a linear momentum, $p = mv$, in the direction of motion. Here, m, is the particle's mass and v is its liner velocity. In a linear motion the force acts in the direction of the motion. In a circular motion of the electron there is a force that acts in turning the electron at every moment. This force is at right angle to the momentary linear motion at a point. The applied force acts in changing the direction of motion and not the distance from the centre (i.e., the radius R). The distance is fixed and is equal to the radius of the circle R traced. The angular momentum at a point in the circle can be worked out from the momentary linear momentum at a point. The circular motion is a result of a kind of angular force which turns the object at constant angular rate $\omega = v/R$. Here ω is the turning velocity at any instant of time t, and at any point, on the circle, and is

constant. The rotational force is the result of a torque $\tau = FR$ at a point as if trying to produce a couple or a twist at the point around the centre of the circle.

The angular momentum can be written as $L = pR = mvR = mR^2w = I\omega$. It is analogous to the linear momentum equation, $p = mv$. In rotational motion, $I = mR^2$, takes the place of mass m. I is called as the moment of inertia of the object around the centre of rotation. The direction of the angular momentum L is perpendicular to the plane of the orbit. The angular momentum is taken as acting through the centre of the orbit. Thus L plays the same role in rotational motion as does the linear momentum p in a linear motion. In rotation the speed of rotation, ω, is the rate of change of angle θ with time i.e., $\omega = d\theta/dt$. In linear motion the distance l changes with time t and we deal with linear velocity $v = dl/dt$. The linear force is given by $F = ma$, a being the linear acceleration; $a = dv/dt$. In a rotating electron we deal with a torque τ. It changes the angle θ with time. It is equal to the rate of change of angular momentum with time and is written as $\tau = dI/dt = d(I\omega)/dt = I(d\omega/dt) = I\alpha$, assuming that I is constant in time. Here, α, is now the angular acceleration rather than the liner acceleration for a straight line motion. Thus in rotational motion the liner force equation, $F = ma$, is replaced by an analogous torque equation $\tau = I\alpha$.

One should remember that the above quantum model of an atom and the associated magnetic moment is an intrinsic behavior. The simplest example of an atomic magnetic dipole moment is a hydrogen atom. It has a single orbiting electron and there is only one proton in the nucleus. In an ensemble like the human brain there is large number of atoms and molecules and of different species. One calls this kind of ensemble as a multi-nuclear ensemble. The concept of magnetic moment still remains valid. The atoms within a molecule arrange themselves due to various binding forces so that the molecule has a resultant magnetic moment and an associated resultant angular momentum. There would be various groups of molecules called as macro-molecules who would do the same thing. So long there is no external force applied to atoms and molecules, their random motions at a point will all cancel each other's magnetic moment in the brain. The net result is that the brain is magnetically neutral overall as it should be. However when the brain ensemble is placed in a static magnetic H_z, directed along a specific direction, let us call it the Z-direction, the magnetic moments, due to the atoms and molecules tend to align themselves along the magnetic field direction as this would be the lowest state of energy for the spin system.

It is timely to point out here that these magnetic moments are loosely referred to as the spins in the MRI literature. It would be an ideal situation to expect the spins to be hanging in space all perfectly aligned along the Z-direction. The spins experience lot of disturbance e.g., due to temperature oscillations, interactions with their neighbors, etc. So there is tendency for them to drift away from the Z-direction. These disturbances can be random in nature. But the presence of the magnetic field keeps control of the situation. It produces an order of its own. The spins (as a group over a small region) precess around the applied magnetic field with a characteristic frequency called as the resonance frequency and at a characteristic flip angle wrt
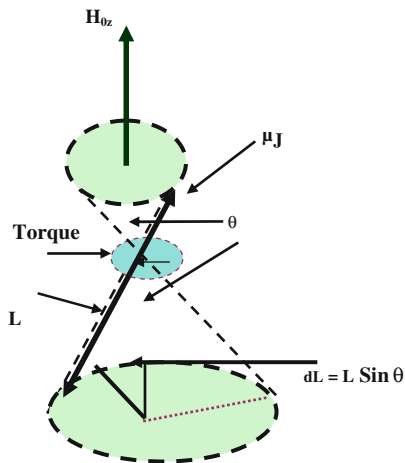
Fig. 1.3 The above diagram depicts a configuration of the dipole moment (μ_J), orbital angular momentum (L) and the magnetic Field (H_{0z}) in space. The angular momentum L and the magnetic moment μ_J are shown in the figure as pointing diametrically opposite to each other. The reason is that the electron is a negatively charged particle thus positive electrical current created is opposite to the direction of the motion of the electron. The angular momentum on the other hand is a property of the rotation of the particle irrespective of it charge

(with respect to) the static magnetic field applied. By applying now RF radiation at an angle (normally $9\bar{0}$) to the static field and choosing its amplitude suitably one can pick different species of nuclei in space and time and study them as one wishes. This in a nut shell what MRI is about. Figure 1.3 is a simple illustration for the case as if it were a single spin. After the RF radiation is applied in pulses to the brain during the quiescent (pulse free period) period the spins will naturally relax back to their original direction and produce a characteristic electrical signal which becomes the source of imaging in space and time.

There is a Torque $\tau = \mu_1 \times H_{OZ} = (g_1\mu_b/\hbar)(L \times H_{OZ})$, on the electron (the magnetic moment) in orbit. One should remember that symbol æ means a cross product between two vectors L and H_{oz}. The result would be equal to $LH_{oz}\sin\theta$. Here θ is the angle between the two vectors. The result of the cross product of two vectors produces is a third vector which is present in a third direction perpendicular to both the individual vectors while its magnitude is equal to the product of the two vectors multiplied by the sin of the angle between the two vectors. The torque gives rise to a change dL in the angular momentum in time dt. According to the Newton's Law one can write $dL/dt = \tau$. But the change dL causes L to precess through an angle $\theta = \Omega dt$. Here Ω is the precessional angular velocity. From the Fig. 1.3, $dL = L\sin\theta(\Omega dt)$. One can rearrange such that $L\sin\theta\Omega = dL/dt = \tau = (g_1\mu_b/\hbar)LH_{OZ}\sin\theta$. Thus one works out the frequency of precession of the electron, $\Omega = g_1(\mu_b/\hbar). H_{zo}$ Here a factor g_l has been inserted in the magnetic moment equation. It is to emphasize that here we have considered the electron's atomic orbital angular momentum L only. There is also the electron's intrinsic angular

momentum associated with rotation about its on axis. Here g_l is introduced as the spectroscopic splitting factor corresponding to the orbital motion only.

The reason of inclusion of the factor g_l, in the equation above, becomes clear, as below. One has to add to the orbital spin (angular momentum) of the electron L, the intrinsic spin (angular momentum) of the electron (due to rotation about its on axis), S. In pure orbital case $g_l = 1$. In actual practice one need to consider the total angular momentum $J = L + S$, where S is the spin angular momentum of the electron around its own axis. So in the total case one will replace, g_l by $g_l = g_l + g_s$. In the presence of an applied (or the internal) static magnetic field H_{z0}, along say the Z-direction, the spin angular momentum S can have only two value $S_z = \pm(1/2)\hbar$, where $\hbar$ is the angular Planck's constant. Otherwise it would tend to follow the general quantum law, $S = \sqrt{s(s + 1)}\hbar$, with multiple directions of orientation for the spin in space. Here s is called as the spin quantum numbers with possible values as 0,1, 2,…. Similarly, without the magnetic field internal or external L can have the quantized values, $L = \sqrt{l(l + 1)}\hbar$. Here l is the orbital quantum number = 0, 1, 2,…. With the static magnetic field (internal or external) in the Z-direction L is replaced by $L_Z = I_z\hbar$. Now $I_Z = 0, \pm1, \pm2, \ldots$.

The importance of the splitting factor g lies in the fact that for the MRI active elements, e.g., Fe, Na, K, etc., present in the brain environment in the presence of the internal magnetic field of 1 Tesla the dipole magnetic moments have a defined multiplet quantum structure locally. The localized macromolecules however are randomly oriented in space. In the presence of the applied static magnetic field in the Z-direction the angular momentum components within the macromolecules and macromolecule-to-macromolecule point in the Z-direction both for the atoms and the electrons. Over all they will combine according to the quantum selection rules. By applying RF radiation field along x and y directions in MRI we simply are trying to unravel the multiple spectroscopy of the elements. The magnetic resonance spectroscopy enables one to work out the relative concentrations of the metabolites and the metabolic science of the brain. One should remember the purpose of MRI is to probe the internal difficult to observe molecular spin structure by creating its own measurable macro-spin structure in the brain.

1.4.3 Multi Electron Orbital Energy Levels in an Atom and Muti-Electron Interactions Within an Atom

The energy of the electron around the nucleus is quantized in, n, orbits as $E_n \sim (-KZ^2/n^2)$. Here K is constant comprising the fundamental constants, the electron charge e, its mass m, Panck's constant h etc. Z is the atomic number of an element. The integers $n = 1, 2, 3, \ldots$ are the principal orbital quantum numbers. An electron can stay in one of these stationary orbits and n = 1 is the ground state. The electron in the orbit can be disturbed by external means e.g., by a pulse of an RF radiation. It can go to next higher level up, but comes down to its ground state in a microsecond time by emitting back the radiation. For the element hydrogen

which is the simplest and first in the periodic table of elements, $Z = 1$ and $E_n \sim (-13.6/n^2)$. For $n = 1$, on gets, $E_1 = 13.6$ eV. This is the maximum binding energy of the electron to the nucleus for the hydrogen atom. The negative sign is significance of the fact that the electron is bound to the nucleus and E_n is the binding (potential) energy of the electron in the orbit around the nucleus. One need to supply this much energy to remove the electron from the nucleus and the electron then becomes free of the nucleus. Then the hydrogen atom is said to be ionized and becomes positively charged free radical. In other elements more and more electrons are present and are distributed in higher and higher orbits. As the atomic number Z of elements increases extra electrons are accommodated in higher orbits, $n = 2, 3, \ldots,$ etc., following certain quantum selection rules. Electrons in higher orbits are not as strongly bound to the nucleus as in first orbit e.g., in the hydrogen case. How many electrons will stay in a particular orbit, n, is a matter that begins the journey of the science into the quantum nature of the matter. The angular momentum associated with each main orbit n breaks each main orbit n into subshells. An electron is a charged particle and also has a magnetic moment associated to it due to its rotation. Two or say even number of electrons with oppositely directed magnetic moments spins can be accommodated together in one subshell (s, p, d, f,…,etc.) of a main orbit. Parallel magnetic moments repel each other so they cannot be in the same level. This is called as the Pauli's exclusion principle. The last (unneutralized) odd electron in the outermost orbit is the one influenced by the RF radiation and counts towards imaging.

Each main orbit n has a further subshell structure. The angular momentum L of the rotating electrons can only have quantized levels. The subshell quantum numbers corresponding to L are l (quantum number) = 0, 1, 2,…. The quantum structure of L is expressed as $L = \sqrt{I(I+1)}\hbar$ in space when no static magnetic field is applied. Here $\hbar$ is the angular Planck' constant. The subshells due to l are referred to in spectroscopy as, s, p, d, f,…, etc. corresponding to the quantum numbers $I = 0, 1, 2, \ldots$. The progressing capacity of accommodation of the electrons in the subshells is given by $2(2l + 1) = 2, 6, 10, \ldots,$ corresponding to $I = 0, 1, 2, \ldots$. These are the standard, s, p, d, f… spectroscopy levels that accommodate 2, 6, 10, 14 etc. electrons. Any principal orbit n allows more than one subshell to be accommodated without changing the energy of the main orbit. This is referred to as the degeneracy. It is the degeneracy of the orbit n. It arises due to the degeneracy of the angular momentum in each main orbit. Any atomic element X in the periodic table is represented as ^AX_z. Here Z is the atomic number and A the atomic mass of an element.

For the typical cases of the $^{23}Na_{11}$ (sodium atom) and the $^{39}K_{19}$ (potassuim atom) the arrangement of electrons in the subshells $I = 0, 1, 2, \ldots$ is as follows. Na (11): $1s^2 2s^2 2p^6 3s^1$; K(19): $1S^2 2S^2 2p^6 3s^2 3p^6 3d^1$. They are part of the alkali metal group with single electron in the outermost shell. They are very reactive and form stable compounds with halides, e.g., Cl, Fl, etc. The stable compounds that exist in nature are e.g., NaCl, Kcl, etc. This information would be useful later in the work in the Na–K pump, the pump of life in the brain. Detailed quantum mechanical theory shows that there is a substructure for l within the same n. This finer

structure comes from the fact that l has a sub-quantized space according to another quantum number m_l, which can only have values $m_l = -1, -1+ 1, \ldots 0, +1 \ldots + 1 - 1, + 1$. It is called as the magnetic quantum number. There is highest and lowest limit on m_l, according to $m_l = \pm 1$.. This limit comes from the internal electric (coulomb) field symmetry and asymmetry associated with the coulomb force field exerted by the positive charge of the nucleus on the electron and the spatial arrangement of the orbit of the electrons around the nucleus.

The spatial arrangement of the subshell structure is worked out by the technique of the possible spatial symmetrical electron eigen (energy) wave functions. This is done keeping in view the principle of the conservation of angular momentum and the electron charge distribution around the nucleus. The eigen functions represent various selected quantum probabilities. It is for the same energy E_n, corresponding to the same principal quantum number n but with different l and m_l quantum numbers. This work is not the right place to go into further details for which a reader should consult a standard text book on quantum physics [1–3]. When atoms are not isolated single entities but are part of an ensemble then the environment in which they are present puts natural limitations, on their quantum energy structure. The brain is a very good example of such an ensemble. Here electrons, atoms, molecules, tissues, fluids, etc. produce a natural limitation on the quantum energy structure over small regions. In fact the nucleus of an element has its own magnetic field of magnitude around 1 Tesla and produces an equilibrium arrangement around it over some distance. In MRI we apply externally a magnetic field of around 3 Tesla along Z-direction. The internal quantum energy structure degeneracy of molecules in a local region is thus lifted. The orbital magnetic quantum number would then according to the values $m_l = 0, \pm 1(-1, 0, +1), \pm 2(-2, -1, 0, +1, +2), \ldots$, etc., depict in the MR image a detailed quantum structure. One should remember that an electron has its own spinning behaviour around its own axis. Due to this spinning behavior of an electron while still in an atomic orbit each subshell l is further degenerated by the intrinsic electron spin angular momentum, $S = \pm 1/2.\hbar$. It's quantum numbers are $m_s = -1/2$ and $+1/2$. Thus there will be further fine structure in the form of doublets to each magnetic quantum number multiplet. All the fine structure revelations can be part of the final scan of the brain produced. The detailed quantum coherence (interactions between various nuclei) image would be the ultimate but close to the real time image.

MRI still has long way to go to fine details. As a very simplified mathematical expression for the quantum energy structure for an atom one can write the main orbital quantum number, $n = [1+\{l\}+(m_l + m_s)]$. Here number 1 has been added in the beginning so that when $l = 0, m_l = 0, m_s = 0$; then, $n = 1$, and E_n has its maximum negative value. This circumvents the otherwise mathematical (uncertainty) problem. The problems is that for $\{l\} + (m_l + m_s) = 0, n = 0, E_n = \infty$ (infinity) an indeterminate value. Thus the minimum value for n is 1 and not 0. One should note that the periodic table of elements is classified according to the quantum nature of the orbital electronic configuration. The detailed description of that text can be seen in the elementary books of physics and chemistry. Below we

are summarizing the main basic features in the context of our brain. In an ensemble of atoms and molecules like that of our brain the system behaves collectively over small regions of volumes locally. Those who are interested in learning details about the secretive nature of the quantum science are referred to the references listed at the end of this work. In this work only an induction and a guidance at the ground level is presented. For simplicity we will first consider a single isolated atom. In a single isolated atom in space the spin (electron) angular momentum S and the orbital angular momentum L of each atom combine to produce a resulatnt $J = L \pm S$. This is called as the spin orbit interaction. The vector J is quantized in space as $J = (\sqrt{j(j + 1)})\hbar$.

In the presence of a static magnetic field H in the Z-direction we only consider the Z-component, $J_Z = m_j \hbar$. The quantum numbers allowed for m_j are $- j, = j + 1, ..., + j - 1, +j$, with $2j + 1$ values. This energy of interaction called as the spin-orbit (S-L) interaction energy corresponds to a single atom case and is proportional to the factor $\sim [j(j + 1) - l(l + 1) - s(s + 1)]$. Here j is the quantum number corresponding to the total angular momentum J, l is the quantum number corresponding to the atomic angular momentum L an s is the quantum number corresponding to the electron spin angular momentum S. The picture becomes very complicated when there are very many atoms interacting in a macromolecule situation. There are two rough sketches (Figs. 1.4a and b) shown depicting how the various angular momentum components combine to produce a resultant angular momentum J' in a multi-particle macro-molecule–macromolecule system. The associated multi-partcle resultant angular momentum and the magnetic moment vector (sarising out of the angular momentum) can be approximately represented similarly to the macromelecular-macromolecular interacting system in the brain, as shown, in the Fig. 1.4a.

In a single atom situation say for example a free hydrogen atom spin (electron angular momentum around its own axis)-orbit (electron angular momentum around the nucleus) interaction energy can be expressed as $\Delta E = LS = LS \cos \theta$. The expression on the right is called as the dot product of the two vectors, i.e., the orbital angular momentum L and the spin (electron rotation around its own axis) S. Here θ is the angle between the two vectors. This interaction arises due to the fact that nucleus of the atom exerts a magnetic field of around 1 Tesla on the electron in an atom if the atom were alone in a free space. In an ensemble like the brain the magnitude of the field will be smaller due to the medium present around atoms md molecules. This diagrammatic (Fig. 1.4a) representation is only an approximate one as if there were only two macromolecules in a voxel in the brain. This is very far from reality. There will be many such macromolecules participating in interactions in a voxel. A macromolecule is a multi-electron system due to many atoms bound together as large group. The diagram is drawn purely to illustrate the concepts involved. Please refer to the Fig. 1.4 for detailed angular momentum, J, structure in a macromolecule. One should realize that the dipole magnetic moment in a static magnetic field Hz produces an interaction energy with the field, of $\Delta E = \mu H$. Here μ corresponds to the multi-particle system diamagnetic moment. The final result is $\Delta E = \left(g_j'\right)\mu_j'Hm_j'$. Here g_J' is the spectroscopic splitting factor,
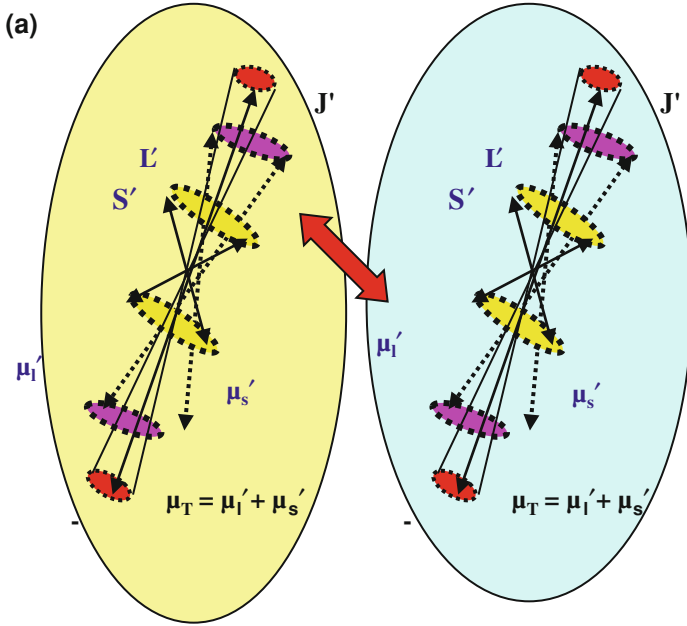
Fig. 1.4 **a** The diagram is representative of the multiparticle macromolecule to macromolecule J′ coupling (interaction) in a situation like the brain ensemble. Two giant neighboring macromolecules shown interact locally in the brain and produce a resultant effect. One can write the total angular momentum when added together as, J′ = L′ + S′ in a multi-partice system. **b** Although brain looks like a disordered structure mechanically yet there is a certain short range electrical-magnetic order among macromolecules to perform routine duties through electrical networks in some sensible manner. (i) Imagines an overall regular macromolecular order in a sub-voxel structure. This is a modeled rough conceptual picture of the repeated micro-magnetic-order among molecules created in a small space. The order is around a giant nucleus of a group of molecules in a small space. The local order inside each macromolecule is produced by an internal (intrinsic) magnetic field of around 1 T (actually much smaller in the brain situation) due to the orbiting charge of the electrons around the giant nucleus. This is a result due to a a single representative giant nucleus at the centre of a macromolecule and a cloud of electrons orbiting around the giant nucleus

μ_J′ is the dipole magnetic moment and m_j′ is the multiparticle (within a macro-molecule) magnetic quantum number $\Delta m_j' = 0, \pm 1$, transitions allowed).

The factor 'g_J'' controls the splitting of the energy levels of a macromolecule. It is given as g_J′ (total) $= [1 + \{j'(j' + 1) + s'(s' + 1) - l'(l' + 1)\}/2j'(j' + 1)]$. One can see that $g_J' = 1 =$ orbital alone splitting factor, when $S' = 0$, so $j = 1$. On the other hand $g_J' = 2 = g_s$, when $l = 0$, so $j' = s'$. These are the two extreme splitting cases that is no splitting (purely orbital angular momentum) and the doublet (purely spin angular momentum). The reader should note that the factor 'g_J''also appears in the ratio of the magnetic moment to the angular momentum i.e., $\mu_J'/'J' = g_J'(\mu_b)/\hbar$. This ratio is called as the gyromagnetic ratio (GMR). The factor 'g_J'' is like a variable factor that controls the ratio of the total
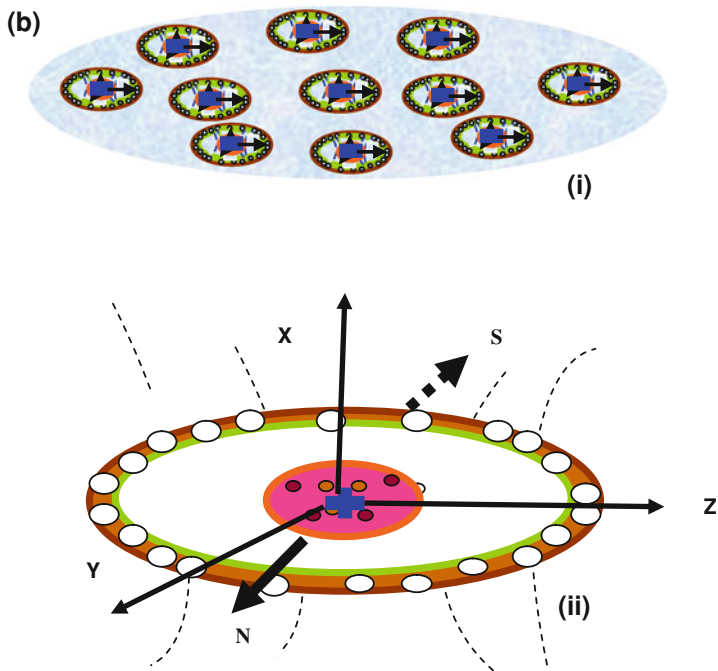
Fig. 1.4 (continued)

(macromolecule) magnetic dipole moment $\mu_J{}'$ to the total (macromolecule) angular momentum J'. The GMR has unique value for every nucleus and is expressed in units of radians per second (or cycles per second) per Tesla (the unit of the magnetic field). For a fixed external magnetic field applied it will have a constant value. One can find the values for the magnetic dipole elements μ for important chemical elements, present in our body which form the source of MRI. They are usually listed in a text book of physics e.g., [4] or an MRI text book. It would be interesting to mention here the magnitude of various physical quantities involved in the above simplified mathematical expression for GMR.

The quantity $\mu_b = (e\hbar/2m_e)$ is called as the Bohr magneton. It is a standard physical constant and its value $= 0.927 \times 110^{-23}$ amp-m^2. The unit amp-m^2 can be alternately expressed as Joles/Tesla (J/T). The $\hbar$ is angular Planck's constant and $= 1.055 \times 10^{-34}$ Js, m_e is the electron mass $= 9.10910^{-31}$ kg, and e is the electron charge $= 1.602 \times 10^{-29}$ coulomb. The Bohr magneton μ_b is basically the intrinsic magnetic moment of the electron. For a nucleus we have the corresponding magnetic moment called as the nuclear magnetron. But it is thousand times smaller as the mass of the nucleus is thousand times larger than that of an electron. One can calculate spin-orbit interaction energy ΔE, for a, carbon, ^{12}catom (6 electrons in various orbits, 6 protons and 6 neutrons in the nucleus) with 2p3s electron orbit configuration. It can be considered as a local atomic multi-

electron system. In this case one finds $g'_J = 3/2$. On substitution in ΔE the magnitudes of the various physical quantities one gets for a magnetic field of H = 0.1 Tesla, $\Delta E = \pm 8.7 \times 10^{-6}$ eV. Compare this energy with the X-ray energy of 1×10^6eV used in X-ray imaging. That is why MRI is called as a non-invasive technique. The coupled order produced locally by macromolecules is randomly distributed in the global brain. This happens through macromolecules distributed all over the brain. Random distribution of the spins in the molecules makes sure that the brain is magnetically neutral overall. But locally the magnetic order does control the functions of the brain e.g., metabolism, neurotransmission, etc. In the Fig. 1.4b the order is depicted as if there is a local order and is uniformly distributed over the brain with macromolecules-block-by-block. Actually the order is nowhere near this. It is haphazard or say random in nature.

A group of molecules in a macromolecule in a tissue like situation behaves as if there were a concentrated positive charge at the centre due to a giant nucleus and a group of collective bound electrons in a collective orbit. Different voxels in reality would have a resultant magnetic order pointing in different directions yet coordinated in some manner with other voxels. Figure 4b (ii) Depicts a conceptual single macromolecular magnetic structure. The electrons of the group distribute their charge so as to neutralize the central resultant positive charge. The solid thick arrows represent north and south poles of the macro-molecular magnet corresponding to a group of molecules. The dotted lines represent magnetic lines of force emanating from a single macromolecular dipole magnet. These magnetic lines of force of one macromolecule interact with that of the neighboring macromolecule and become the source of an ordered electrical communication system of the brain.

The Figs. 1.4a and 1.4b represent a rough overall as if dynamic (time and space) imaginary model picture of the regionalization of the magnetic order present in our brain. One should remember that this geometrically regular picture is oversimplified and is only to help understand dynamic internal electronic brain structure in a simple manner which otherwise is more complex and has a very intricate structure. All the locally ordered spin regions in practice would be randomly distributed and thus the overall magnetic field will be zero keeping the brain magnetically neutral. Imagine what would happen if it did not? The word random is imagined for the model sake. It is doing inside whatever it does in a perfectly ordered manner. Unfortunately we are not advanced enough to unscramble that order which is much more mysterious than we know. It is important to point here that the brain is organized into small pockets of regions as we know from the well understood the medical brain structure. Various regions perform different functions e.g., vision, hearing, cognitive tasks, etc. and these are coordinated in a split second by some kind of central processing unit (CPU) to perform a coordinated action.

We yet know very little about the brain CPU. MRI tries to emulate the real system in the brain by one of its own which is periodic in time and space so that we can make some sense out of it. What a periodic system in time space means is that MRI selects a small voxel in the brain at one time. It gets all the dynamic information in time-space from this voxel and stores it in the computer. Then it

goes to the next voxel and then to the next in a sequential order along the X-direction. At the end we move a step down in the Y-direction and exhaust all the voxels again in the the X-direction. This process is repeated all over the brain till all the X–Y planes for each Z-plane are exhausted. So we can see that MRI has created an order of its own to collate the look like systematic (voxel by voxel) information out of the brain which really does not have any real systematic physical periodic structure at all. The reader is reminded that our brain works more like a parallel magnetic-spin-electrical signal coordinated quantum parallel computer than like the well known a sequential-signal-operated electronic CPU of the desk-top computer. The reader is referred to recently published the first chapter the "Biomedical Quantum Computer" in the book "Quntum Magnetic Resonce Imaging Diagnostics of The Human Barin Disorders" by the Elsevier Publisshers/ 2010.ISBN: 978-0-12-384711-9/http://www.elsevier.com/books/authors/kaila, for details about the information on a "quntum-computer".

1.4.4 The Nuclear (Protons and Neutrons) Angular Momentum, the Nuclear Magnetic Moment and Interactions with the Atomic Ones

The nucleus has protons and neutrons called as nucleons in its core. The nucleons have magnetic moments and angular mometa properties like those of electrons and atoms. In fact the two systems i.e. atomic and nuclear interact and form the basis of imaging in more than one way in MRI to analyze the brain science. A dominant exmple of intercations is called as the strong nuclear jj-coupling referred to as the J-copling. The orbiting electrons around nucleus experience an internal magnetic field around the nucleus. The nuclear dipole magnets due to the protons and neutrons interact with this field and split the atomic energy levels further than those observed due to the electron spin and the orbital atomic angular momentum in an atom. This leads to the hyperfine splitting of the atomic energy levels. This hyper-fine energy splitting is proportional to the factor $\sim \mu_N [(f(f + 1) - i(i + 1) - j(j + 1)]$. Here μ_N = the nuclear magnetic moment, j = the quantum numbers specifying the magnitude of the atom's total electronic and atomic angular momentum, i = the total nuclear angular momentum and f = the grand total angular momentum. The nuclear angular momentum behaves analogous to the atomic case. It is written as $I = \sqrt{(i(i + 1)\hbar)}$. One can see that there is a close relationship between the electron-atomic and nuclear-atomic interactions. Which system will dominate in real situation depends upon internal and external factors. The externally applied magnetic field is an external factor. The internal magnetic field is the internal factor.

Nature has cleverly manipulated an internal magnetic order in the brain. This is due to internal regional magnetic field around 1 Tesla. The internal field is random in nature. It is distributed with modulations of regional interactions over space and

time. Overall the brain is magnetically neutral. It is electrically neutral as well. It should be so otherwise? The MRI with its external magnetic field, static and the dynamic (RF pulses), tries to mimic an internal order and explores the secrets of the brain science in the laboratory. One should remember that in an atom's case in a multi-electron system we add $L's$ ($L' = L_1 + L_2 + \ldots$) and $S's$($S' = S_1 + S_2 + \ldots$) first to form total $J' = L' + S'$. In the strong nuclear involvement we add each L and S first individually, to make $J_1 = L_1 + S_1$, etc., and then add all the J's (J_1, J_2, …) to produce the resultant $J' = J_1 + J_2, \ldots$ The weaker atomic coupling is called as the L-S couplig and the stronger nuclear one the J–J coupling. This procedure is followed because in the nuclear case spin–orbit (S-L) interaction is much stronger than in atomic case with little spin-orbit (S-L) coupling interaction. Now we can see that the analysis of the ensemble of atoms and molecules in the brain is no simple matter. But the things are not so bleak. There is no chaos after all.

We should realize nature is very kind to us. It all depends how much we know about it. The nature has worked out all very well. It allows the interactions between atoms, molecules, nuclei, etc. according to some selection rules. In the case of atomic electrons the selection rules are summarized as follows. Only those energy transitions are allowed where, $\Delta s\prime = 0, \Delta l = 0, \pm 1, \Delta j\prime = 0, \pm 1$. The nuclear magnetic moment is much smaller than that of the electron. This is because the nucleus is composed of protons and neutrons, having nearly the same mass, but they are thousand times heavier than an electron. The magnetic moment of all the neutrons and protons do not just add up in total. There is a pairing mechanism as in the atomic case. The opposing ones in a pair cancel out and make a bound pair. Only the odd ones left out make the resultant magnetic moment. The magnetic moment of a proton is given as $\mu_p = (e\hbar /2M_P) \sim 10^{-3}\mu_b$. Most of the protons and neutrons pair themselves in the nucleus and the resultant magnetic moment is zero.

There are nuclei with even mass number A (sum of the number of the protons and neutrons). But the number of neutrons or protons can be both even and odd to add up to even A. The situations are not equivalent in the proton–proton, proton–neutron and neutron–neutron pairing. These forces me not have the same magnitude. The nuclear forces are much stronger and very short range as compared with the coulomb interactions in the atomic case. It is seen by experiments that the nuclear magnetic moment is positive-parallel (to the applied static magnetic field) in some cases and negative-anti-parallel in others. Nuclei, with both atomic mass number A and the atomic number Z (protons) even the total (protons + neutrons) magnetic moment is zero $(i = 0)$. For even A nuclei with N and Z odd the value of j and the parity (the exchange force due to exchange of two particles in their space coordinates) can be a contributing factor for each of the two odd nucleons. One can set limits (selection rules) on the nuclear spin and say that it must have an integral value. There are only a few odd number-nucleons (=protons + neutrons) referred to in the periodic table of elements.

In order to know what selection rules the nature follows in a complex ensemble like the brain one need to perform experiments. MRI provides a practical tool to work out the selection rules in a multi-nuclear ensemble. The nuclear energy levels

have capacity to accommodate protons and or neutrons according to the rule, $(2j + 1) = 2, 4, 6, 8, \ldots$. This structure is in line with magnetic Z-quantum number, of j. This quantum number can have the values, as $m_j = 1/2, 3/2, 5/2, \ldots$. In dealing with the dynamics of the electrons, atoms and molecules, nuclei in an ensemble like the human brain it is the exchange of energy and the communication among them that controls the dynamics of the various functions of the brain. This exchange of energy involves interaction through exchange of angular momentum of the particles and the parity (symmetry-asymmetry) in the environment in which they are present. It is very fortunate that the nature has chosen the system of interacting atoms and molecules to be a quantum one. The result is a discrete-quantum one and can be worked out from the quantum selection rules. The conservation of angular momentum and the quantum selection rules are easy to work out in an ensemble of an ideal homo-nuclear environment. It behaves like a collective system just replicating the one atom case into a multi-electron system.

In a real complex ensemble of heteronuclear nuclei like the brain we have a much more involved situation. But, nature has surprisingly played its dominating role again. It restricts the selection rules basically following the conservation of the angular momentum but in a much broader perspective. It is now spread over larger volumes with wider variety of particles participating. The MRI technology which has taken nearly half a century to evolve is only a humble tool to find out the secrets of the brain science. It would also be interesting to find out as to why the human brain has evolved to the level of intelligence we have today while the animal brain has stayed so unintelligent. One should not forget that life is made of atoms and molecules animal or human. Evolutionary changes on earth may be one reason. It is important to know the "reasons for the change" along with the change itself. When you know the reason you would also know how to predict the change e.g., malfunction of the brain exhibited as a tumor. This basically boils down to the education about the brain functions among the younger generation and about the brain science in general. This written work taken up by the authors here is an effort to educate medical professionals about the science of the brain. Hopefully this will equip them better professionals in the medical field.

1.4.5 The Precession of the Magnetic Moment μ of a Single Electron in an Atom, in an Externally Applied Magnetic Field

The case of a single electron-single atom is the easiest one. It is the case of a hydrogen atom. As one adds more and more electrons in the atom one is progressing towarsds higher and higher atomic number (Z), elements, e.g., He, Na, K, Ca, Fe. The multi-electron system in an atom is not as complex as one may think. Normally it is only the odd numbered electron in the outer most orbit due to their unpaired magnetic moments that counts. Inner stable electrons are not chemically active and are not part of the intrinsic electron angular momentum S and the orbital
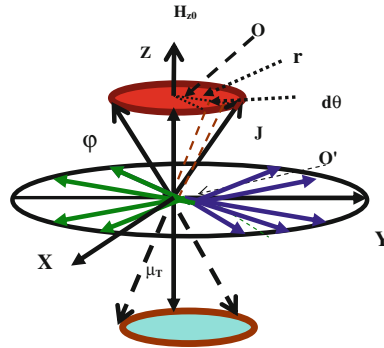
Fig. 1.5 The above diagram is a rough picture of the result of application of a static magnetic field H_{z0} along the Z-direction. The RF radiation electromagnetic field is applied in X or Y-direction to a (in fact a group of) precessing electron spin. The representation remains more or less in principle the same for a collective system say e.g., a molecular system like in the brain. Part of the spins precessing along the Z-direction are projected in the X–Y plane for measurement of the electrical signal created by them. A 90 RF pulse along X-direction rotates some spins in the Y-direction. A 90 RF pulse along Y-direction rotates some spins in the X-direction. Let us leave for the curious mind to try to find out as to why and how it happens. The Sect. 2.8 further on deals with an overall quantum picture of the brain. Without the application of an external static magnetic field the magnetic spins are randomly oriented in space except for a regional intrinsic local order over a short space

angular momentum L. The electron atom interactions are called as the spin–orbit or S-L interactions and are the roots to the behavior of magnetic moments or spins. In an ensemble like the brain one is dealing with multi-atom, multi-molecule, and hetero-nuclear system. The basic picture of the spins still remains the same. In a complex system like the brain there are interactions among the molecules in a small region. This small region behaves like an equivalent-single-atom system. As the region becomes larger in size the broader selection rules of the angular momentum modulate the local order. Nature finds easier paths where the conservation of the changed angular momentum e.g., $\Delta L = \ldots \pm 3, \pm 2, \pm 1, 0$ is still observed. In fact there is an internal magnetic field over a small region in the brain, created by the atom (nucleus) itself. This restricts a local order among the spins in the brain. The magnitude of this field can be very close to one Tesla. This order is very local and extends over short distances say ten to hundreds of nm. In the presence of the external static magnetic field there are quantum paths balanced out to produce a broader order over larger distances of the order of a 1 mm. How and why all this happens?

In the presence of the applied static magnetic field Hz_0 the tip of the spin (represented like an arrow) is circulating randomly. This precession is at an angle φ to the Z-axis in a cone shaped behavior (Fig. 1.5). The angle φ can be varied by the applied RF field. The precessional motion of the spin magnetic moment μ is similar to the gravitational Top but not exactly the same. In atomic Top the position of the tip of the spin occupies quantized oriented energy positions, $= \mu Hz_0 \cos\phi$, ϕ is the flip angle that can be changed from 0 to π by suitably

choosing the direction and the magnitude of the application of the RF radiation. In the above equation μ is the magnetic moment of a spin. The applied magnetic field allows the spin to keep on precessing around the field Hz_0. Spins can be excited to different energy levels (precessions) by using RF radiation. The radiation received back is used to produce an image. The description below depicts in summary the behavior of a spin under applied fields.

An electron has its intrinsic spin angular momentum S, of its own. $S = \sqrt{(s(s+1)}$ ℏ. Its Z-component is, $S_z = \pm(1/2)$ ℏ, ℏ is the angular Planck's. The quantum number, s = 0, 1. The orbital angular momentum, $L = [\sqrt{\{I(I+1)\}}]$ ℏ. Its Z-component, $L_z = I_z$ ℏ. The orbital angular momentum quantum number can only have values, l = 0, 1, 2, …. The Z-component orbital quantum number can only have the values $l_z = -l… + 1$, the (2l+1) values. The orbital angular momentum L is generated by an electron in an atomic orbit. One need to add to L the electron spin angular momentum S, due to the electron's rotation about its own axis to give the resultant angular momentum J = L + S. Now J is given as, $J = [\sqrt{\{j(j+1)\}}$ ℏ]. Its Z-component is, $J_z = m_z$ℏ, $m_z = … - j… + j$, (2j + 1) values. Here j = $l - 1/2, l + 1/2, l = 1, 2, …$. We know, $L = l\Omega = \{mr^2(\Omega)\}$, I = the moment of inertia of the rotating electron, around the axis of rotation. Ω = precession frequency of angular momentum J around Z. Also Ω = (g_l, u_b ℏ) Hz_0. Here g_l = the orbital spectroscopic splitting factor. In the case of the total J, $g_J = g_l + g_s$. In the orbital case alone g_l= 1 and for the electron intrinsic spin alone, g_s = 2.

The total, g_J is given as $g_J = [1 + \{j(j+1) + s(s+1) - l(l+1)\}/\{2j(j+1)\}]$. The fundamental unit of the magnetic moment is written as, μ_b = (e ℏ /$2m_e$.$2m_e$) = the atomic Bohr magnetron. On substituting the fundamental constants, e = 1.602×10^{-19} coulomb, the electron charge, ℏ = $(6.626/2\pi) = 1.055) \times 10^{-34}$ Js, the angular Planck's constant, one gets μ_b = 9.27×10^{-24} amp-m² or Joules/Tesla. The orbital atomic magnetic moment of the electron, μ_l = iA = ($g_l\mu_b$/ ℏ)L. Here i = the electrical current generated by the electron in the orbit. The resultant angular momentum J also gives rise to a resultant magnetic moment μ_J. The magnetic moment is in direction opposite to L for an electron. When there is spin orbit interaction one has J = L + S. An RF pulse can be applied along the X-direction to rotate the angular momentum L and consequently the spin and then allow it to relax. During this time the magnetic moment interacts with the environment and sends back an echo to the receiver. The variation in space and time of the echo received becomes a source of the imaging of the events in the brain.

1.4.6 The Conventional MRI: Echo Planar Imaging

The Radio frequency (RF) spectrum of electromagnetic radiation has low energy of around 10^{-6} eV (μeV) and occupies a very narrow part of the much wider spectrum of the electromagnetic radiation band. The X-ray band on the other hand is towards the much higher energy scale. It has a high energy around the 10^6 eV (MeV) mark.

The frequency is around 10^{20} Hz. The RF radiation has wavelength is on the scale of a meter. The frequency is around 10^6 Hz (MHz). Atoms and molecules in the brain exchange energy in the milli (10^{-3}) to μ (10^{-6}) eV range. RF radiation is the right and the safest radiation to study the science of the brain. In order to produce image of an object one need to make a graphical projection of the spatial distribution of one or more of its physical and or chemical properties. One uses interaction of a radiation field with the object to achieve that. In a field like e.g., the electron microscopy the wavelength of the waves should be very close to the size of the smallest feature to be imaged. This is because the phenomena used there is the diffraction of the radiation via the electron waves. That way the smallest region of interest can easily be resolved. The radiation the one used in MRI is the RF electromagnetic radiation. Here the phenomena used is a different one.

The diffraction approach is not possible in the brain situation not directly any way. Firstly the structures of interest are not regular and secondly the different sections are performing different activities. The events are time dependent as well. The dynamics of the brain involves e.g., metabolism, neuronal communication, etc. It is found fruitful to induce interactions among atoms, molecules etc. locally using RF radiation and collect the response. Then scan over the whole brain and thus collect the complete data. This data can be digitized and produces as an image of the brain. The image is only a summarized and a stationary state representation of the brain. The dynamics can be worked out from the complete stored data. The local interactions produced by the incident RF radiation create the echo-electrical-signals from the spins. In order to produce a 3D image echo signals are manipulated by rotation of spins into different planes and directions. Spins are tiny atomic and molecular magnets and produce electrical signals as they move and vibrate under the influence of the applied RF radiation pulses. This is superimposed on the equilibrium created by the static magnetic field. The intelligence of the echo planar imaging (EPI) technique is this that the structural and time dependent variations in a small selected region (called as the voxel) are transformed by the two applied fields a static magnetic field and a RF magnetic field into measured electrical signals. The information is collected and imaged by the MRI machine. It is done with little disturbance to the moment-to-moment functions of the brain.

The above conventional approach in MRI can be further improved for a better resolution on an atomic scale by using quantum interactions among the molecules as the basis of the imaging. The major content of the soft tissues in the brain is the water (H_2O) and is tainted with important functional chemical elements e.g., the potassium (K), sodium (Na), iron, and others. The hydrogen nucleus in the water molecule has a single proton. One normally carries out spectroscopy results of a voxel at the same time as the EPI. The technique used is called as the proton magnetic resonance spectroscopy (PMRS). The macromolecules in a small region have a resultant quantum correlated spectroscopy. It is of great value in the diagnostics of the tumors in the brain. The spectroscopy provides whole host of vital additional information of great value not only in the diagnostics of the disorders but also for the development of the brain science. One of the techniques prevalent in MRI is the PMRS (proton magnetic resonance spectroscopy).
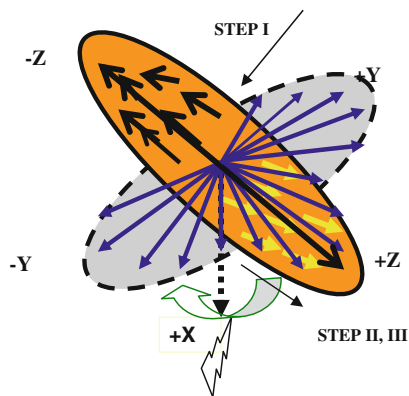
Fig. 1.6 A static Z-directed magnetic field creates (STEP I) longitudinal magnetization of spins along the +Z-direction. Y–Z are in the plane of the paper. X-is perpendicular to the plane of the paper. STEP II. A 180° pulse rotates the spins about the +X-axis towards the –Z-direction. After the inversion time TI the spins try to relax back towards the +Z-direction. The relaxation in the Y–Z plane is called as the T_1 relaxation. STEP III. A subsequent 90° pulse along X-direction rotates and groups the spins along $-Y$ or +Ydirection depending upon whether the spins were still in the –Z-direction or they have moved towards +Z-direction. The spins then relax back along the +Z-direction from either $-Y$ or +Y-direction, this time taking longer route (Z-Y–Z). This provides better measure of the T_1 relaxation time of the spins. The longitudinal magnetization relaxes as $M_z \sim M_0[e^{(-TI/T)}]$. Here Ti = the inversion time, T_1 = the longitudinal relaxation time, M_0 is the maximum magnetization (magnetic moment per unit volume) and Mz is the magnetization at ant any time. T_1 is also referred to as the spin–lattice relaxation (interaction) time

Spectroscopy, e.g., utilizing phosphorous is also used. The multi-quantum magnetic resonance imaging (MQMRI) will form a theme discussion in this work and is illustrated by practical examples. It is worth mentioning here that the spectroscopy of the individual (free) elements is well known and tabulated in the handbook of chemistry and physics available in most of the science libraries in the world. When the elements are present in a confined environment in space like the brain the spectroscopy one is talking about is the spectroscopy of the biological macro-molecules in the brain modulated by real time dynamics of the chemical elements.

The Imaging of the Brain: T_1 Weighted Image (Steps I, II, III)

Refer Fig. 1.6

The Imaging of the Brain: **T_2 Weighted Image (Steps I, II, III)**

In the T_2 imaging technique the emphasis is on the interaction among the spins themselves rather than between the spins and the lattice (the brain). The reader should note reference to the direction of rotation of the spins here around a particular axis say x or y in the Figs. 1.6 and 1.7 as a positive or negative has been
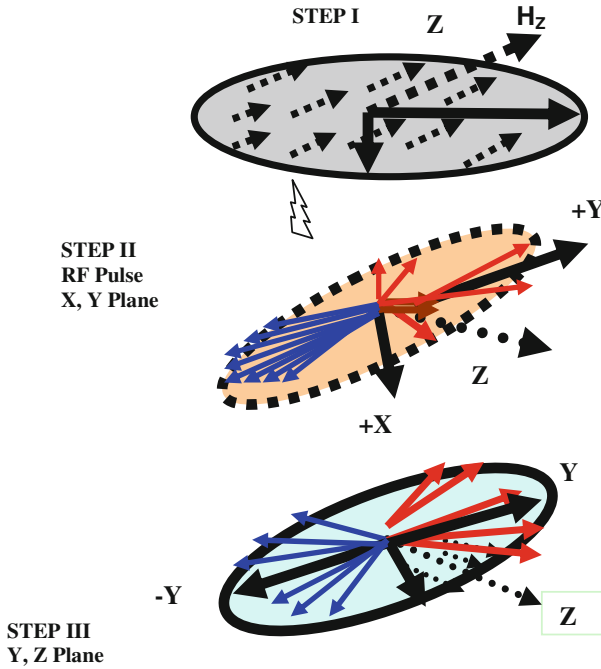
Fig. 1.7 Step I. Magnetic field H_z is applied along the Z-direction. Spins are in a static equilibrium in that direction. Z-is perpendicular to the plane of the paper. X–Y are in the plane of the paper. Step II. Oscillatory (pulsed) RF magnetic field is applied along X-direction using the 90° RF pulse. It directs and bunches the spins along the +Y-direction. Soon they start dissipating away from the +Y-direction. Step III. A 180° pulse along +X-direction reverses the spins from the +X, +Y quadrant to-X –Y quadrant. The spins still continue moving away from the +Y (but bunching towards – Y) direction in the –X -Y quadrant. They look now bunching closer towards –Y direction. Very soon spins start dispersing away from the –Y direction towards the +Y directions, and so on. As the spins bunch and de-bunch in the X–Y plane the electrical signals induced due to spin–spin interactions are collected. The time to relax in-between (+Y to −Y) is called as the T_2 (the transverse) relaxation time. The T_2 weighted signals are mapped and the brain is imaged. This is called as the T_2 weighted Image. The T_2 signal decays as $M_y \sim M_0 [e^{-(TE/T2)}]$. TE is the echo time of the spins. It is also referred to as the spin–spin interaction relaxation time. The X, Y axis are in the plane of the paper and Z is perpendicular to the plane of the paper

stated purely from the point of view of the basic concepts involved. The exact + or − sense of rotation of spins depends upon a standard convention chosen. It is not considered necessary here to go into those kind of details. The reader is advised that information presented in this section can be further supplemented by going through the information in the appendices A and B presented at the end of this part of the book. The text part of the Fig. 1.7 summarizes the technical steps involved in obtaining a T_2-weighted image.

References

1. Goswami, A.: Quantum Mechanics. Wm. C. Brown Publishers, DubuqueI A., (recent edition)
2. Giancoli, D.C.: Physics for scientists and engineers. Prentice Hall, NJ (recent edition)
3. Kaila, M., Kaila, R.: Quantum magnetic resonance imaging diagnostics of human brain disorders. http://www.Elsevier.com/book/kaila ISBN: 978-0-12-384711-9/2010
4. Eisberg, R., Resnick R.: Quantum physics of atoms, molecules, solids and particles. Wiley & Sons, NY (recent edition)

Chapter 2
Simplistic Theory of the Functions of the Ensemble of the Electrons, Atoms, Molecules, Nuclei, in the Brain

2.1 Simple Macroscopic Brain Model

One should realize that the quantum science is not as much a common knowledge as the Newtonian Science is. It thus becomes a formidable task, to propagate further about the new developments in the brain science. The neuroscience audience who this work should attract the most would normally have little and basically no exposure to the basics of the quantum physic so deeply rooted in the dynamics of the atoms, molecules, tissues, etc., in the brain. However an effort at grass roots level is made in this work in that direction. To keep it simple explanation is made by reference to diagrams drawn. It is a rough spin model picture of the brain MRI that is exposed here. It is as if it were a collection of ordered spins in an ensemble of molecules in the direction of the static magnetic field naturally present around the nucleus. Spins in molecules are surrounded by smeared out orbital electron cloud of the molecules, fluids, tissue, etc. There are as many electrons in the orbital state as there are the protons in the nuclei in a small region consisting of several molecules.

An approximate spin model picture is illustrated here globally (Fig. 2.1) over the brain. The brain on the whole is electrically neutral as if it were a single atom. From this rudimentary equivalent over simplified picture to progress further towards reality one has to add regional perturbations in space and time. These are due to the local fine structure of individual atoms, molecules, tissues, fluids, etc., and the functions they perform. Then it will take the knowledge about brain science a step closer to the otherwise a very complex picture. In the regional areas there are various forces e.g. coulomb, nuclear, quantum, etc., which control the regional behavior in carrying out moment to moment brain functions. In a broad sense there is an overall system within the brain that looks after the intricate and wider functions of the brain. Figure 2.1 is a broad pictorial representation of the spin model of the brain. This is as if the orbiting electrons in molecules are circulating in copper coils and influence neighbors through self and mutual electrical induction.

(a)

(b)

Electrical current enerated   **Magnetic field enerated**

(c)
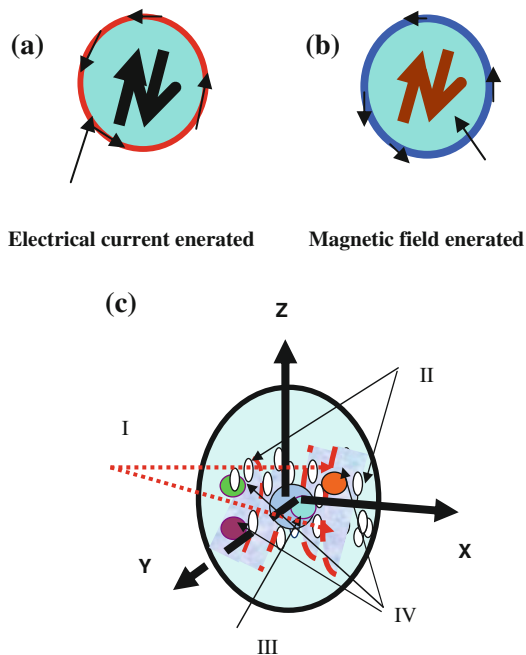
Fig. 2.1 **a** Electric current generated around the copper coil due to alternating magnetic field at the centre. **b** Alternating magnetic field generated at the centre of the coil due to alternating current flowing around the copper coil. **a–c** In this Figure is shown a pictorial depiction of an over simplified model of the brain. One can visualize a group of molecules (or macromolecules) in the brain under RF radiation behaving like copper coils carrying oscillating electrical current. This will lead to a generation of oscillating magnetic field through and around the molecules. The electromagnetic field created due to the RF radiation excitation encourages interaction between molecular dipole magnets. **a**, **b** Simple analogy to an experiment which can be conducted in a laboratory. It is a rough picture of a representation of the famous more than a century old copper coil experiment, by Hertz, the physicist, after whose name the unit of frequency of radiation Hz was adopted. **c** An approximate picture of a regional local order assumed present in pockets, in the brain, created by the internal magnetic field of around 1 Tesla, due to a group of nuclei, at a point. Small elliptical spots shown are examples of the several local micro-order regions in space. There is also an order on the global scale but is a weak one

The order can be regional as well as long range one. In the long (but on macro-molecular scale) range orbiting electrons are shown as a smeared out cloud as if they were a part of single giant molecule with single giant nucleus. But on this order is superimposed a regional (and long range) quantum-order due to quantum correlations between atoms and molecules. This order can be measured through multi-quantum coherence imaging from small voxels of 1 micron^3 to 1 mm^3 size. One can also mathematically model and get computational results and compare it with experiment. Both approaches where they will meet ultimately, to an agreement, will lead to the understanding of, the real, the unknown brain science. Thus there are four parts of the model of the brain as follows. I The effective internal

surrounding magnetic field lines of force are imagined as if the whole brain were made of several macromolecular dipole magnet grouped with N–S poles. They interact quantum mechanically to produce long range orders. II The electrons as if belonging to a group of molecules as a unit surrounding the central positive nuclear charge of protons. III The filled ellipses represent sort of scattered short range ordered macromolecules submerged in the surrounding electron cloud depicted by unfilled circles. IV The giant nucleus of a local order is as if belonging to a group of macro-molecules as a unit in a local volume say a voxel.

The spatial density, $\rho(x, y, z)$ variation of the spins can be worked out from the measured k space (k_x, k_y, k_z) intensity distribution in the MRI. The wave number in k-space, is given as, $k = 1/\lambda$, λ being the wavelength of the RF radiation. The measured k-space intensity variation (converted into the x-y-z space picture produced) has one to one correspondence to the spatial variation of spins density in the real (x, y, z) space in the brain. The density of spins (their number per unit volume) is related to the magnetic moment per unit volume created by the spins at a point. Due to the multinuclear structure of the brain the spin density sharply varies from point to point. The procedure of the transformation of the data form the k-space to the real space is a standard procedure well established in the conventional MRI. It is called as Fourier Transform Technique (FTT). It is a simple physics principle in electricity that an alternating current through a copper coil (Fig. 2.1a) induces an alternating magnetic field at the centre of the coil. This alternating magnetic field at the centre also influences a current in the same coil. This is called as the self induction. Similarly in a reverse manner an alternating magnetic field at the centre of a coil generates an alternating current through the coil and the generated current influences the magnetic field at the centre. Also a current in one coil induces a current in the neighboring coil which also generates a magnetic field at the centre of the second coil. This is called as the mutual induction. Atoms and molecules in our brain are a sort of copper coils with circulating electrons around the nucleus. The atomic orbits act like copper coils. The single electron in the outermost orbit of an atom is called as the valence electron. It has an intrinsic magnetic moment called as spin $Sz = \pm 1/2\hbar$. This is added to the atomic magnetic moment produced by the circulating electron in the orbit of an atom. One should remember that it is the valence electron in an atom that is the reactive one and creates interaction with its neighbors through its charge and spin. The Na–K pump which is the source of life in our brain is typical example of interest in this book. On the long range the influence on the neighbors in the short range is smeared out. This is what we get in conventional MRI. In the short range the quantum nature of the atom and the molecules can be seen. This is what QMRI is about.

In the real situation like the human brain in a small region of it referred to as a voxel the atoms and molecules overlap and the electron cloud charge spreads over a smeared out region. The shared electrons in a voxel represent signatures of the local interactions between the molecules, atoms, nuclei, as if there were a single large molecule and many electrons were bound to it due to the coupling between the electron spins. The overlapping electrons become a sort of shadow of the

chemical structure in the local region. In the small region which may be spheri-
cally symmetric in regard to the distribution of spins the spin effects over-all
cancel out. Thus there is no structural abnormality shown in the image of the
region. The brain is thus a normal healthy one. If there is an asymmetry at a point
due to say a tumor the symmetry is broken down and the spins appear as an
outstanding spot in the MRI scan of the brain. This would be the most rudimentary
form of image and is called as the chemical shift imaging (CSI). In this conven-
tional MRI an RF pulse is applied along the X and Y directions perpendicular to
the applied static magnetic field which is in the Z direction. A macroscopic
average three dimensional spin asymmetry of the region can be projected as a
planar asymmetry on the X–Y plane. In this plane the atomic spins evolve in time
by interactions among themselves and the environment. The dynamics of the spins
can be mapped in macro space and time to produce images of the local molecular
events. One can venture now with the multi-quantum coherence technology newly
emerging to explore spin dynamics in a multi-quantum regime. It is possible to
look for quantum correlations among spins as a source of imaging rather than just
be satisfied with the conventional topological echo planar imaging (EPI).

2.2 The Relationship Between the Angular Momentum L of the Orbiting Electron Around the Nucleus and the Associated Magnetic Moment μ_L

2.2.1 The Induced Electrical Signals Created by the Incident RF Radiation

An electron spins around its axis and thus has an intrinsic angular momentum
referred to by symbol S. But the electron also orbits around the nucleus and thus
there is an orbital momentum for the electron associated with the atom. It is
referred to by the symbol L. Normally in an ensemble like human brain the
intrinsic electron and atomic angular momentum are randomly oriented in space.
They cancel themselves on a macroscopic scale. But on a microscopic scale the
internal magnetic field of a group of nuclei makes the two types of angular
momentum add up to produces a resultant $J = L + S$. It is called as the spin-orbit
interaction. This is the result referring to a single electron and an atom in isolation
with no atom to atom interactions (correlations). But in an ensemble like the brain
there are around 10^{23} (Avogadro number) nuclei including different species in a
mole of the soft matter. Most of the spins in the absence of an applied (or internal)
magnetic field cancel out in a small region say a voxel used for examination. In the
presence of a magnetic field the spins have all their L′(multi-particle) and S′(multi-
particle)s added up to produce a resultant $J' = L' + S'$.

Since an electron is a charged particle its rotation produces an electric current
over the nano size area traced by it. This orbital motion of an electron in an orbit in

the atom makes an atom a nano-magnet. There is an intrinsic relationship between angular momentum and the tiny magnet generated due to it. The product of the electric current i generated by the electron and the area of the orbit traced A is called as the magnetic dipole moment μ_l (=iA). In a very small volume of the order of tens and hundreds of nano meter^3 the local nuclear magnetic field induces a resultant orientational force on magnetic moment μ_J as if trying to align the tiny magnet, along its own direction. The situation however enhances in the presence of an external applied magnetic field Hz_0.

In an externally applied field all the spins order themselves with their resultant magnetic moment tending to be pointing in the Hz_0 direction. The disturbance due to the local environment in which the spins are present however tend to disorient spins from the externally applied field direction and try to return them to their natural random behavior. The result is a compromise i.e. μ_J (the resultant magnetic moment corresponding to the total angular momentum **J**) rotates around the static magnetic field. The spin vector corresponding to it moves in a cone around the field. A single rotating vector around the static magnetic field Hz_0 is a representative of many spins grouped together as a bunch. Individual spins corresponding to different species of nuclei will rotate at different flip angles. But it is very hard to observe them on individual basis experimentally. It is the group effect that is observed.

One chooses to use a band of frequency of RF radiation to observe a small group of spins at a time. The tip of the spin (of a group corresponding to say a macromolecule) may be located anywhere at any moment in space and time. The angular momentum controls the position of the magnetic moment at any time. The angular momentum however can not be measured in a laboratory. The magnetic moment as a group representation can however be measured. On the scale of micrometer to mm to cm a large electrical signal is generated by the RF radiation. This signal created by the application of RF (radio frequency) radiation due to the magnetic spins vibration produces an electrical signal. An average magnetic moment per unit volume over a region is called as the magnetization of the soft matter. It is not constant over different points in space and its susceptibility to external RF radiation also varies in space and time. In fact this is what provides the secrets of the human brain science.

2.2.2 The Magnitude and the Quantum Nature of the Atomic Magnetic Moment

The angular momentum and the associated magnetic moment of the electrons and atoms are quantized. This means they can only occupy fixed quantum energy levels. In the process of transition above and down in the energy levels the energy is absorbed and re-radiated in quantum jumps, $\Delta J = 0, \pm 1, \pm 2, \ldots$ The angular momentum J and the magnetic moment μ_J are oppositely directed for an electron
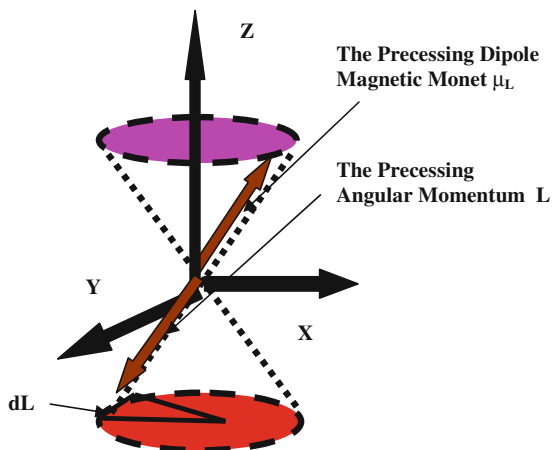
Fig. 2.2 The static magnetic field H_0 is applied along the Z-direction through the skull of the brain under scan. An electron being a charged particle produces an electric current in the orbit around the atom. This electric current say i when multiplied by the area A generated by the orbit is equal to the term called as the orbital dipole magnetic, $\mu_L = iA$, of the atom. Normally μ_L is randomly oriented at any point in space and time in the absence of the field H_o. So the resultant effect overall is zero. H_o is perpendicular to the X–Y plane of the orbit and remains situated at the centre of the orbit

in an atom. Application at an angle θ of the RF pulse to the static field produces a rotation of spins by an angle θ from the static field. Normally $\theta = 90°$ is used to rotate spin from Z-direction to say X or Y direction. These pulses are called as 90° pulses. The static field exerts a torque τ on the spins. The torque is on the plane of an atomic orbit and it tries to orient the plane perpendicular to the static field and consequently keeps the spins in its own direction. RF pulse oscillations make the spins vibrate. Their vibration produces an electrical signal which is measured. By choosing suitable magnitude direction and frequency of the RF radiation applied the study of the quantum nature of the spins helps bring out the quantum secrets of the brain from the real time quantum images produced. Figure 2.2 is an approximate pictorial depiction of the macroscopic relationship between L and μ_L, in the presence of on externally applied magnetic field applied in the Z-direction.

The angular momentum vector L of the orbiting electron that produces the magnetic moment is not static in space along the Z-direction. It is under precession at an angle θ to the static magnetic field. This happens because though the spins are under force to remain oriented in the Z-direction the local activities, e.g. metabolism, neurotransmission, etc., try to keep the spins oriented, away from the Z-axis. This results in an equilibrium i.e. the precession of the spins at an angle θ to the Z-axis. The length of the vector of the angular momentum L i.e. its magnitude remains fixed for a particular frequency of resonance and amplitude of the RF radiation. However as a result of the precession in space its direction is changing at the rate of a fixed angular frequency. Due to the quantum nature of the

angular momentum a fixed quantum of energy is supplied by H_0, i.e. $E = \mu_L H_0 \cos\theta$. Here θ is the angle between μ_L and H_0. L remains quantized in space. But it rotates around H_0 in random fashion i.e. it can be anywhere in X–Y plane at any time. It can change its values up and down in quantum jumps. The magnitude of the jump is $L_z = \hbar m_z$, where m_z is the magnetic quantum number with values, $\pm(0, 1, 2, \ldots)$ and $\hbar$ is the angular Planck constant. The tip of L moves in a circle generating a cone around H_0. This angular momentum cone generated is shown in the lower part of the diagram (Fig. 2.2). Since the magnetic moment is oppositely directed to the angular momentum due to the negative charge of the electron the corresponding cone generated by the magnetic moment is shown in the upper part of the diagram (Fig. 2.2).

The rotation of the angular momentum L in a circle is due to the precession of the magnetic moment μ_l. The precession frequency is referred to by the symbol Ω. The orbital magnetic moment of the electron is given as $\mu_l = g_l (\mu_b L/\hbar)$. It is coupled to the angular momentum and rotates at the same frequency. The precessional frequency Ω of the spin magnetic moment μ_l is given as $\Omega = g_l (\mu_b H_0/\hbar)$. g_l = orbital spectroscopy splitting factor. $\mu_b = (e\hbar/2m_e) = 0.927 \ae 10^{-23}$ amp-m^2 (or Joules/Tesla) is the fundamental unit of the dipole magnetic moment μ_l, m_e being the mass of the electron and e its charge. In a multi-particle system one deals with total spectroscopy splitting factor g_J. An electron in an atomic orbit is also rotating around its own axis. It is called as the intrinsic angular momentum (spin) of the electron S. In the presence of the field H_0 there is the resultant angular momentum $J = L + S$ of the atom which one need to consider. The brain ensemble is a hetero-nuclear one. In a small volume one need to take some kind of an average of the magnetic moments and also in regard to the resultant angular momentum J. The ratio of the magnetic moment to the angular momentum is called as the gyro-magnetic ration GMR. The GMR = $(\mu_J/J) = g_J (\mu_b/\hbar)$. Here μ_b is the fundamental unit of the magnetic moment and $\hbar$ provides the fundamental unit of energy (has units of joules second) and is called as the Planck's constant of the RF radiation, g_l is the resultant spectroscopic splitting factor. This ratio has very important place in the MRI literature. There are many species (hetero-nuclear situation) of nuclei in a small selected volume in the brain. For examination one needs to take into account the resultant effect of all the local interactions among the nuclei. It is a common practice now to take spectroscopy of a small region of say mm^3 – cm^3 dimension as part of MRI. This small volume is referred to as a voxel in the medical MRI literature.

Spectroscopy is very helpful in determination of the distribution in space of the relative and absolute metabolic concentration in the brain. The spectroscopy also helps in the diagnostics of the brain tumors. The precessional frequency of the magnetic spins around H_0 is $\Omega = g_J (\mu_b H_0/\hbar)$. Here g_J is the spectroscopy splitting factor that determines the splitting of the energy levels in a voxel and is a measure of the distribution of the metabolite concentrations. In Fig. 2.2 there is only a rough depiction of the precession of the diamagnetic dipole moment. The μ_l shown is representative of a single electron or a proton. In fact it can very well be the resultant of several neighboring electrons and protons. Furthermore in a small selected region i.e. a voxel in the brain for imaging the outer orbital electrons in
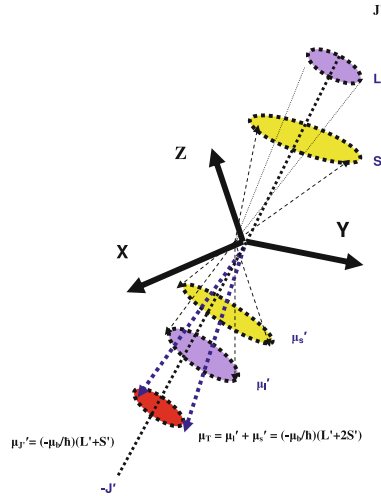
Fig. 2.3 Above is a picture representation of how the multi-electron intrinsic spin angular momentum $S' = \pm 1/2\hbar$ and the multi-atomic angular momentum L' are oriented and add together in space in a multi-particle system. The resultant produced is modulated due to the interactions e. g. metabolism, neuronal synapses etc. events in-between the molecules. This is induced due to the presence of the internal the nature's magnetic field in the brain. In each little volume (voxel) in the brain there is a resultant angular momentum J' due to all the local spins present. Because of the local nuclear magnetic field spins try to align themselves along the local Z-direction the internal local direction of the local order. One should remember that the local order direction being called as z-direction is purely arbitrary. This is just to keep analogy with the real laboratory MRI situation where the Z-direction is taken as the direction along which the static magnetic field is applied

the neighboring molecules and the protons in the nuclei will all couple together to produces a resultant angular momentum $J = L + S$. Here L precisely could be the resultant of angular momentum of atomic angular momentum and that of the nuclear one. The over all S would be the intrinsic angular momentum of outermost orbital electrons in the neighboring molecules. In larger size voxels diffusion dynamics of the molecules modulates the received signal.

It is part of the space and time functional dependence of the fluids e.g. blood circulation on the angular momentum J. A typical example where the spin dynamics can be seen in action is the BOLD (blood oxygen level dependent)-MRI. One should always remember that it is not the angular momentum J that is a measurable quantity. Instead it is the changes associated with the precession frequency of the magnetic moment and the phase (time of arrival of signals) due to varying angles between spins created by the RF radiation that is measured. Finally the received modulated radiation is the consequence of the variations of the magnetic dipole moment which oscillates because of the precession of the angular momentum J. According to the simple physics principles of dynamic electricity an oscillating magnet in space produces electrical signals around it. Its space and time variation detected by the sensor forms the image.

2.3 The Multi-Particle Angular Momentum Has a Resultant Due to the Internal Nuclear Magnetic Field of ~1 Tesla

In a multi-particle system the internal magnetic field due to various nuclei (generated due to relative motion of electron and nucleus) in macromolecule situation adds up to a resultant, locally, and tends to orient the neighboring spins around it along its own-order-Z-direction. The angular momentum of a spin (the atomic magnet) is given as $L = I\omega$. Here I is the moment of inertia of rotation of an electron around its axis of rotation and ω is the frequency of rotation due to the electron rotation around the nucleus. In a voxel L's and S's are the resultant due to various atoms, molecules, etc., given as $L' = L_1 + L_1 + \ldots$; $S' = S_1 + S_1 + \ldots$. The resultants (Fig. 2.3) consist of the components of the angular momentum of the neighboring interacting particles. Then due to the internal magnetic field, L's an S's, add up to produce a resultant $J' = L' + S'$, and thus a local order is produced. Spin-Orbit (L-S) interaction breaks the degeneracy of the doublet quantum state of S ($\pm 1/2\,\hbar$). It makes instead, $J' = L' + 2S'$. The resultant magnetic moment μ_J' is thus not exactly oppositely directed to J'. This offset is suppressed in MRI by the externally applied static magnetic field. Figure 2.3 depicts Z as the internal magnetic field direction and shows how the internal order along J' is created locally.

In MRI the brain's internal order is suppressed by the external static magnetic field which is applied in the laboratory in the Z-direction. A suitable sequence of RF pulses is applied along X and Y directions, to excite the spins for imaging. The $J' = L' + S'$ interaction is commonly used in chemical shift imaging in the conventional MRI. The quantum energy correlation between nuclei in molecules on the other hand is excited by the magnetic field gradient-pulsed radiation and the correlations can be imaged. The quantum order can be detected on a micron to mm region scale. This is what makes the QMRI (quantum magnetic resonance imaging). In QMRI also the spins are projected to new positions in the X, Y plane as in conventional MRI. One tries to produce gradient echoes using the incident gradient RF pulses and is analyzed through the received signals. Specifically in QMRI we are particularly looking for multi-quantum correlations between molecules. This is different from just an average overall resultant of local environmental effects due to the molecules in a voxel. The spins vibrate due to the incident RF radiation gradient magnetic field pulses and produce the electrical signals.

In QMRI the gradient magnetic field pulses are applied in different directions to reinforce quantum correlation among multinuclear molecules. Further the signals in particular due to the quantum interactions are measured. In between the pulses the spins undergo a relaxation back to their original equilibrium position with quantum correlation relaxation times. As in the conventional MRI there are two main types of relaxations. One is called as the longitudinal relaxation. This characteristic time is also referred to as spin–lattice relaxation time T_1. T_1 basically originates from spins rotated or deflected away from +Z direction by the incident RF radiation; eventually they try to comeback to the +Z-direction. The second type of relaxation is called as the transverse relaxation. The characteristic
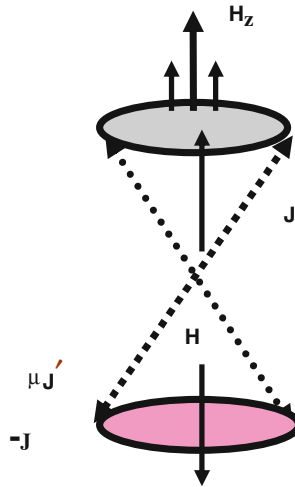
Fig. 2.4 In the presence of an externally applied field H_Z, the internal magnetic moment μ_J' is suppressed and only the externally (in the laboratory) created μ_{Hz} survives and is measured. For the particular case of a single electron (e.g. electron in Hydrogen atom) the intrinsic electron spin S will produce for the energy level of the atom a doublet split ($g_s = 2$) as shown. In a multi-atom molecule, multiple splitting will be observed that will include the effect of the angular momentum quantum numbers $l = 0, 1, 2...$ in each main orbit $n = 1, 2, ...$

time of this relaxation is called as T_2. In this relaxation the spins are kept in the X–Y plane while evolving. They are initially focused in +Y direction. Then they are reversed in the plane along the −Y direction. The repeated reversal generates gradient echoes and thus the electrical signals are measured. This relaxation is also called as the spin–spin relaxation.

There can be interactions in-between the voxels too. The process is a resultant effect overall over large (mm^3 to cm^3) volumes. The overlapping resultant orbital angular momentum is $L'' = L_1' + L_2' + ...$, over all particles and the overlapping spin angular momentum is $S'' = S'1 + S_2' + ...$, over all particles. The overall resultant is $J'' = L'' + S''$ ...over all particles. Because the electron-spin angular momentum S has duplicity ($S_z = \pm 1/2\ \hbar$), actually speaking,, we have, $J'' = L'' + 2S''$. The spin–orbit (L''–S'') interaction, does not allow μ_J'' to be exactly aligned in opposition to the J''. The overlapping space in between the voxels becomes the source of continuity in the overall global image of the brain. Internally the magnetic moment does not follow the same precessional rule as does the angular momentum. What exactly happens in the brain is not exactly the same thing what we can measure in laboratory. The magnetic moment is supposed to be an exact replica of the angular momentum but it is not.

One should note in passing here that the conventional MRI does not take much notice of the intermolecular quantum level interactions. They are treated as if they were scalar J-couplings producing the average effect in imaging. In QMRI the quantum interactions are encouraged by applying suitable magnetic field gradients of the order of mT/m (milli Tesla per meter) in x, y, z-directions. These gradients

tend to concentrate molecular spins in one direction more than the other, thus producing localization of the molecules in a desired quantum state. The concept of the two relaxation times and the echo still remains the same as in the conventional MRI. But the reason for relaxation is different for the QMRI. Here one selects zero quantum coherence (ZQC), double quantum coherence (DQC), etc., as the source of analysis in a particular voxel.

2.4 Application of an External Static Magnetic Field H_z Along the Z-direction Suppresses the Random Internal Magnetic Order

There is no technology yet which can work out the arrangement of internal magnetic field around a nucleus and it influence on nature's intricacies of the brain functions. MRI tries to impose an order of its own on the brain and find out whatever it can. Figure 2.4 shows a rough depiction of an average measurable magnetic moment μ_H, created by the external static field applied in the z-direction.

The multi-nuclear ensemble like the brain produces a complex spectrum. It can be a rich source of information gathering about a tumor in the brain. Over a small region when there is no externally applied magnetic field the internal magnetic field creates an order of its own. Due to the degeneracy of $g_s = 2$, of the electron's intrinsic angular momentum, $S_z = \pm 1/2\hbar$, the multi-particle resultant is $J' = L' + 2S'$ and not $J' = L' + S'$. On should note the coupling between S' and μ_S' is twice as much stronger than the coupling between L' and μ_L'. Thus the magnetic moment μ_J' does not follow $J' = L' + S'$ but instead follows $J'' = L' + 2S'$. Accordingly the total magnetic moment, $\mu_T' = \mu_L' + \mu_S'$ is not exactly oppositely directed to J' i.e. it is not along $-J'$. By applying an external field H_Z the above offset between the total multi-particle angular momentum J' and the total magnetic moment μ_J' is removed. They then follow each other and make the analysis simpler. The Z component of the total magnetic moment μ_H on the application of the RF radiation can now be easily manipulated with little modulations from the internal nuclear magnetic field.

The quantum correlations between the spins within a voxel become a source of detailed spectroscopy. The quantum numbers according to the main orbital n are, $n = 0, 1, 2, \ldots$. For each main total quantum number n there are the familiar spectroscopic sub shells, s. p. d, ... corresponding to the orbital quantum numbers $l = 0, 1, 2, 3 \ldots$. The angular momentum sub-shells accommodate the number of electrons as, $n_l = 2, 6, 10,..$ according to $2(2l + 1) \ldots$ in each sub-shell. For the total spectroscopic effect of the electrons, protons, nuclei, etc. the total spectroscopic splitting factor due to all the interactions, $g_J\mu_L' = g_l\mu_L' + g_s\mu_L'$, will be used. In the simplest case like that of a Hydrogen atom as an illustration there will be a doublet split of the single energy level of an electron in the orbit. This is the ideal lowest level splitting. This doublet split will be present in the each orbit n for different levels corresponding to different sub-shells in any other tom.

Z

Uniform static magnetic field H_Z
along the z-direction, indicated by
uniform spacing of magnetic
lines of force

X-gradient field
direction cretes non-
uniform magnetic lines
of force along
x-direction

The force exerted on the spins in the X-
direction is $F_x = (\partial H_Z/\partial x)(\mu_{HZ})$. μ_{HZ} is
the static spin dipole magnetic moment,
e.g. of a molecule, created in
the Z-direction

X

Y
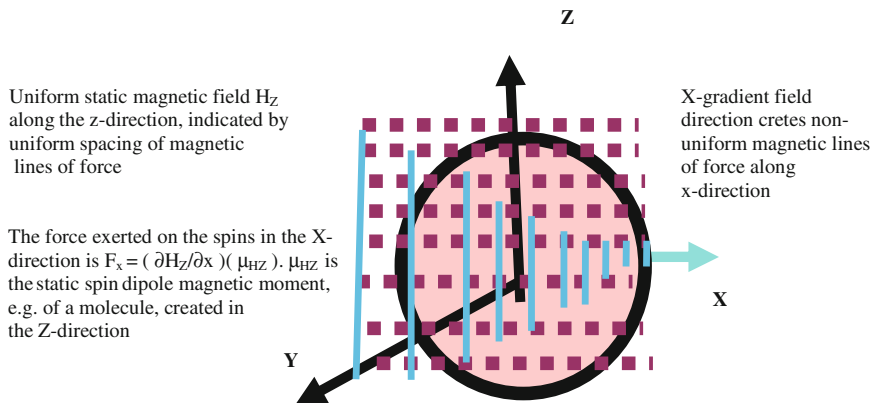
Fig. 2.5 In this figure a uniform static magnetic filed is shown applied in the Z-direction. A static magnetic field gradient is also shown applied in the X-direction. Uniform spacing of the magnetic lines of force (*dotted lines*) in space along the Z-direction (X–Z plane) is representative of the uniform magnetic field along the Z-direction. On the other hand a non-uniform spacing of the magnetic lines of force (concentrating in the +X direction and dilating in the −X direction) represents the presence of the gradient field in the +X direction. In a gradient magnetic field spins are focused in the direction of the gradient. This is the result of a force $F_x = (\partial H_Z/\partial x)(\mu_{HZ})$ on the spins, superimposed on the strong static magnetic field (representing uniform spacing of spins in the X–Z plane) applied in the Z-direction. It is as if trying to divert a fraction of the total number of Z-directed spins, into the X direction. The result is a translational motion of the spins in the direction of the x-gradient

The total quantum number can be written as n = 1 + l + s where the spin quantum number, **s**, of the electron produces doublet of its own. This is referred to as the multiplet-structure in spectroscopy due the l sub-shells and the s-degeneracy. The internal atomic-nuclear magnetic field produces dynamic interactions among the atoms and molecules due to the various brain activities happening all the time. The overall resultant multi-particle-effect will thus further split the sub-shells. This is called as the hyperfine-splitting. Thus a detailed spectroscopy will show the signatures of, what exactly is happening in a small volume called as the voxel. This information is commonly collected by using the technique called as the proton magnetic resonance spectroscopy (PMRS). For a voxel PMRS is done at the same time when the image scan is performed. In the single particle spin only case the spectroscopic splitting factor, is referred to by the symbol, g_s. This will be the case e.g. for the electron in the simplest atom. This is the case of the Hydrogen atom. Here the gyromagnetic ratio (GMR) is given by, $g = g_s = 2$. This is an ideal situation when there are no interactions among the atoms and molecules as if they are isolated atoms with no interactions.

2.5 Effect of the Application of a Magnetic Field Gradient: Illustration of the Effect on a Single Spin (Orbiting Electron in an Atom)

A uniform static magnetic field applied in space at any moment of time directed say in the Z direction orients atomic spins in that direction. Now suppose we superimpose a gradient field of relatively small magnitude on the uniform field in another selected say X direction. This gradient exerts a directed force on the resultant magnetic moment $\mu_j = \mu_l + \mu_s$ over a small volume in the X direction. This is as if trying to make a linear displacement of a group of spins in the X direction. By changing the sign of the gradient i.e. applying it in the opposite direction the force will be exerted in the opposite direction. If one makes the applied gradient field vibratory (or pulsed gradient) in time with positive and negative amplitudes included the spins in the localized volume will vibrate and produce electrical signals. This is due to the vibrating magnetic field produced by the oscillating gradient pulse. Electrical signals can be generated in a plane perpendicular to the direction of the vibration of the spins (in a selected slice ΔZ, in the z-direction) i.e. in the Y–Z plane. A sensor can then detect the signals for mapping of the brain. These signals will have all the information about the molecules and the nuclei as to what activities they are performing. This will be in reference to a particular instant, in space and time. This information is collected and stored during a scan of the brain (Fig. 2.5).

Quick reversal of the gradient in space and time forward (+x) and backward (−x) by means of an RF gradient pulse will produce echoes with electrical signals representative of the signatures of the dynamic events happening in the brain. One can use the directed gradient pulse simultaneously or one at a time in all the three x, y, and z directions. We can thus build a three dimensional dynamics of the brain in space and time. One can think as if a three dimensional virtual RF wave diffraction grating has been created in the brain. An optical grating is fairly well known. It is a structure with fine line grooves on a glass plate made in one direction. The width and spacing of the lines is very close to the wavelength of optical light.

When light is incident on the optical grating it produces a diffracted spectrum of the light into various components (colors) i.e. in wavelengths, orders, etc., on a screen. The above analogy may not be a perfect one but similar things are happening in both situations. In MRI we are creating in the time–space a dynamic RF grating. In an optical grating one uses a coherent source of light to produce the spectrum from static grating. In the brain application of the frequency selected RF gradient pulses in different directions becomes a source of detailed imaging of the artifacts and of the modulated spectroscopy observed. This is as if a three dimensional virtual diffraction grating has been created in the brain in the time–space.

The artificially created grating by MRI provides an ordered structure in time. It is required for an ordered collection of signals. But one should remember that our brain physically is a microscopic order (remember on a macroscopic scale we

are able to make imaged portions according to the functions of the various regions)
and is not an ordered structure like a crystal. That is what distinguishes the brain
from easily discernable three dimensional diffraction gratin we are so accustomed
to, e.g. in X-ray and electron diffraction in solids (crystals). The spatial
non-uniformity in our brain is transformed into a uniform and periodic time space
by using carefully designed structure of RF pulses. The reader is reminded that the
above effort trying to describe the microscopic MRI analysis of the brain in words
is not an exact description that could have been created by including some
mathematical equations. Then unfortunately the book will go more in the direction
of the PCM experts version. Some compromise has been struck here to make
things simpler. A reader interested in a detailed mathematical treatment should
refer to a normal text book in MRI.

2.6 The Quantum Model of the Brain

One can think as a first level of physical impression of the quantum brain as made of
several macromolecules arranged in a random manner locally. Suppose each
macromolecule has a central processing unit (CPU) like the desk top electronic
computer we are so familiar with an equivalent giant nucleus. There are peripherals
in the macromolecule. These are the quantum spin-correlations. They comprise
electron–electron correlations e.g. the chemical shift, multi-quantum correlations,
etc., etc. Wide spread are the correlations for the resultant multi-particle angular
momentum L' and the spin S' producing $J' = L' + S'$, i.e. the J-coupling and similarly
others. Aside the couplings on a macroscopic scale created by spin–orbit
interactions there can be pure quantum coherence couplings at the nm to micron
scale level. These are generated by the demagnetizing field created by the distant
dipole spins. This field can activate coherence between spins pointing in the same
direction or in the opposite direction. These coherences lead to multi-quantum
effects. There can be zero and double quantum coherences in addition to the single
quantum coherences which are easily observed.

   The coordinated macro-molecules in the brain in a small volume can be thought
as if jointly having a giant nucleus at the center with several protons and neutrons
in it. There is a group of, correlated electrons orbiting around a group of nuclei in a
macromolecule. A nucleus intrinsically has a magnetic field of its own which
varies in direction and magnitude over small distances. This creates a magnetic
order over distances of nano-meters to micrometers and to millimeters. This order
influences the activities of the electrons, atoms and molecules. Under the influence
of the nuclear magnetic field atoms and molecules are busy in carrying out
communication and regional activities e.g. metabolism, electrical communication,
etc. The energy transfer between the metabolic and other connected activities is
quantized. The energy is passed on as bundles called as quantum of energy rather
than transferred in a continuous manner.
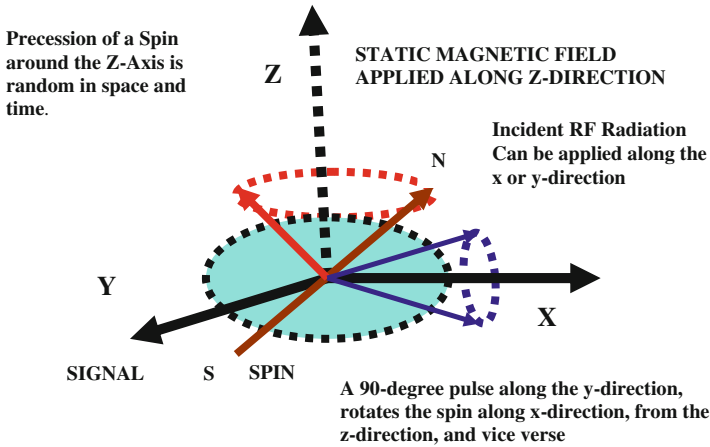
Fig. 2.6 Certain selected number of spins with average natural resonance frequency ω_0 and phase (time in reference to some standard reference) are projected in the x (or y)-direction by a 90° pulse applied in the y (or x-direction), with a selected frequency profile (content). A bundle of the 'coherent superposition' of states of close by independent spins is called as the single quantum coherence. Spin is observable as the field induction decay along the chosen X, Y, Z-directions. Spins precess about the static magnetic field with random phase (position) in time due to the strong static magnetic field along the Z-direction. This means the tip of the spins can be anywhere any time in the circle of precession

This is as if we are having switching electrical networks within our brain allowing transmission of signals in one direction with an inhibition in another or the reverse direction. Neuroscientists are well versant with inhibitory events in the brain protecting it from damage, e.g. abuse of drugs, alcohol, etc.

With the RF field on resonance applied along the say y-axis the spins temporarily precess around the x-axis. The induced magnetization consequently is left aligned along the x-axis and is measured. Once the RF field is turned off the spins are again quantized along the static field along Z (Fig. 2.6). Ideally there should be equal number of spins with their Z-components of angular momentum towards and against the Z-field when no RF radiation is applied. The representation as a circulating cone for the projected average spin in the X-direction is a purely qualitative impression of the spread of the frequencies and flip angles the spins may have. In fact most of the population of the spins is along the –Z axis being the lower energy state. A small fraction of the 10^{23} (present in a mole) but still a large number in the absolute sense is till pointing in the +Z direction. The RF field transfers a small fraction of the population of spins directed along the +Z-direction towards x and y-directions by the application of 90° pulses. A single pulse is sufficient to create single-quantum coherences on which basically the conventional MRI is based. But in order to have multiple-quantum coherences a second and third 90° pulse is required. Multiple sequences of pulses can be so designed as to create interferences between single quantum coherences to produce double quantum
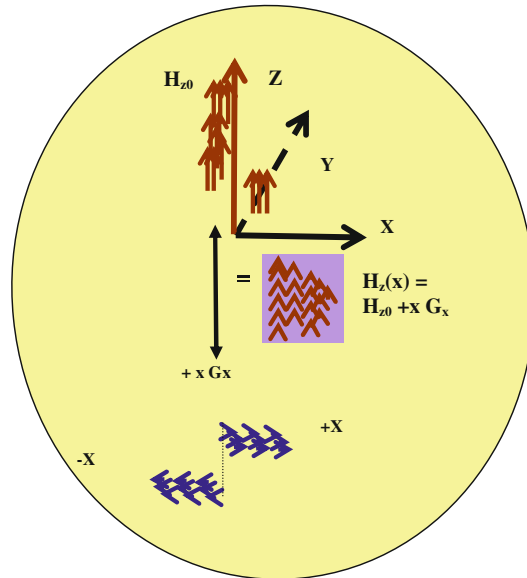
Fig. 2.7 This figure makes a pictorial depiction of the effect of the X-field gradient in the X–Z plane on the spins directed along the +z-direction. Magnetic Field Gradients in X, Y, Z directions can be used to induce quantum correlations in the brain in space and time thus creating the scenario for QMRI. In the above situation the gradiated spins along the +x direction are shown added at point x to the uniformly spaced z-oriented spins. The final result of addition is shown on the right hand side of the figure. One can notice in the Figure a uniformly distributed spins along the z-direction. A bunch of spins are created in the voxel pointing along the z-direction but are non uniformly spaced along the X-direction. A gradient of magnetic field along the +x direction is applied to a small selected volume. It produces focused spins along +x direction. Same will hold when gradient is applied along the-X direction

coherences and triple, etc. coherences. In order to sustain multi-quantum coherences (MQCs) in time a phase cycling process is repeated in time. This means repeated cycle of 90° pulses along X, −X, Y, −Y is applied to reinforce MQCs.

2.7 Quantum Magnetic Resonance Imaging in Brain

The phenomena of interference of waves in one, two or three dimensions in a medium are well known. An application of magnetic field gradients pulses in the X, Y, Z directions can effectively simulate this phenomena in the brain. It can provide frequency selection and interaction of the spins with modulations of the brain activities in space and time. This can consequently be imaged. The following diagrams (Figs. 2.7 and 2.8) illustrate how the QMRI can be realize.

By applying the magnetic field gradient pulses in three directions one can collect information in space and time from the re-radiated back RF radiation. The signatures
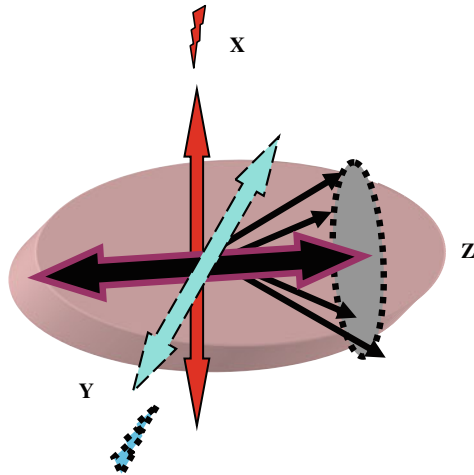
Fig. 2.8 This figure depicts an illustration of application of magnetic field gradients which can be applied in the X, Y, directions. The static magnetic field is applied along the z-direction. This arrangement allows a desired space and time modulation of spins in the brain to be measured. The selected (resonance frequency) RF radiation application allows to choose the spins of hetero-nuclear components. The procedure has to be quantum mechanically manipulated to allow imaging in the X–Y–Z planes. It amounts to a pulsating spin model corresponding to macromolecule in the Brain. One should remember the global brain picture would be an ideally replica of the macromolecule model with added modulations of spins in space and time. One follows voxel by voxel scan to obtain a coordinated and continuous picture through computer programs. Gradient pulses here are shown applied along x and y, directions here

of the events happening at the level of quantum coherence can be detected by a receiver. One should realize that the picture depicts as if the RF gradient pulses are being applied globally over the brain. In fact one would choose a small volume around 1 mm^3 size called as the voxel for analysis at a time. The chance of observing quantum correlations is much greater on distance scale of 1 μm (10^{-6}m) to 1 mm than on scale of mms–cms. An overall global picture of the brain is shown in the Fig. 2.8. It is to emphasize as if brain were a three dimensions RF diffraction grating. In fact what happens in MRI is not exactly a normal wave diffraction phenomenon. The re-radiated RF radiation is channeled out in different quantum channels referred to in the literature as CTPs. In a small volume (<1 mm^3) the atoms and molecules behave as if they were a single large molecule. The macromolecule acts with a common structure of spin-orbit and other quantum interactions. A simplified pictorial representation of the as if, RF radiation diffraction model, of the brain is represented in book (Fig. 2.8).
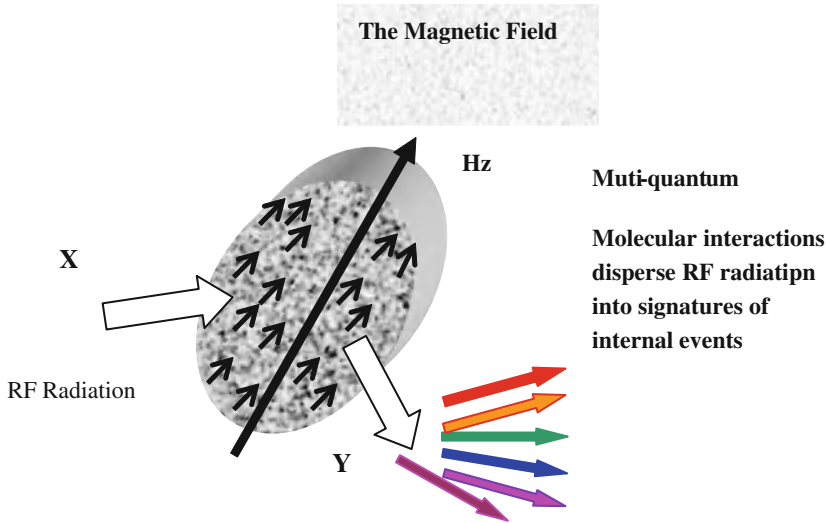
Fig. 2.9 The model presented here for illustration sake is as if the brain were a wave dispersive medium (e.g. an optical prism). The Figure is a rough illustrative dispersive model of the brain. Low energy radiation (radio-waves) is incident on the brain. The in-going and the out-coming radiation here is an invisible (RF) radiation. However the brain is a much more complex medium rather than just being a dispersive medium. It has intricate contagious spread of the various artifacts. There are real time events happening inside. The situation is much more complex and is in real time. Incident RF radiation excites the macromolecules present in the heterogeneous (species) medium of the brain. The magnetic field H_z applied along the z-direction aligns spins in macromolecules in the brain in the z-direction. A macromolecules group of spins disperses the RF radiation as if it were diffracted in different orders (frequencies and wavelengths) of spectrum representative of the various events happening

2.8 How QMRI Can Be Produced

2.8.1 A Rough Radiation Dispersive Medium Model of the Brain

One can start with a very simple interpretation of the model of the brain. Figure 2.9 presents a rudimentary pictorial representation of it. There is an ordered group of spins created by the Z-directed external static magnetic field along the Z-direction. These spins act as if they are behaving like lines as in an optical diffraction grating. In fact more exactly they are like atomic discs. They can be a source of diffraction for the RF radiation. One can derive a simplified model picture by analogy to the rainbow scene observed in nature about the dispersion of light. We may say the spins are like tiny rain drops of water hanging in the air in the sky after the rain. When the sun shines on them we see the beautiful rainbow. The sun light goes through the rain drops and is dispersed into beautiful rainbow with seven visible natural colors of different wavelengths. Each color corresponding to a specific

wavelength and is dispersed in space according to the dispersion produced in the water droplet. In fact if the sky were a diffraction media rather than the dispersive one would see very sharp line spectrum instead of the usual fussy rainbow. The spectrum would be discrete and sharp in contrast as well. Also one would see many more wavelengths not visible in rainbow. Situation with RF radiation is quite a different one particularly in reference to interaction with our brain. Firstly its an invisible radiation. Secondly our brain is complex structure. It has tissues, water, membranes, arteries, veins, etc. White light can not pass through the brain as it is opaque to it. The RF radiation also can not pass through the brain. But RF radiation can excite the local spins of atoms, molecules etc., to their higher energy states.

The ordered spins in the brain are taken as representative model of the soft matter of the brain in the presence of the applied static magnetic field. For simplicity sake we can imagine as if the spins were sitting, in a kind of variable dispersive medium. The RF radiation when incident on the brain gets dispersed by the spins with information from the dispersive medium that is present in the brain. Mere dispersion of radiation and its detection in different directions however does not serve much purpose as a model. The model has to be a bit more comprehensive commensurate with the more complex problems of the brain. We are interested in moment to moment and point to point modulations of the spins by the local events. We have to be able to record the local events through the received back electrical signals generated by the spins. The spin–spin quantum interactions are missing in the dispersion model (closer to the conventional MRI) of the brain. The RF radiation signals generated are invisible (dark light) to a naked eye. The reradiated RF radiation output from the spins is measured in MRI. They have a region to region information from the protons (e.g. water molecules), blood oxygen level dependent (BOLD) movements, metabolic activities between molecules and tissues, neuro-transmission, etc. The measurement of the dispersed RF radiation by virtue of the presence of spins in a dispersive medium is the approach taken in the conventional MRI. One may say that conventional MRI in a simple expression (in common persons' language) detects dispersed RF radiation from spins associated with different artifacts of the brain which when collated in space and time is reconstructed into a real picture. But the individual components of information collected do not include quantum-coherent interactions among the spins. The mutual interaction of spins in conventional MR is as result of the medium in which they reside and move. Below is a rough pictorial presentation in terms of the oversimplified dispersive model of the brain.

Our brain is a strongly interacting quantum-molecular medium. If the incident radiation were only visible white (optical) light the output from the imagined optical brain prism one may imagine would be something akin to seven rainbow colors. The brain has a dispersive (fluids, artifacts, etc.) medium. In MRI we use the invisible RF radiation. The spins in the brain are in fact part of the dispersive medium in which they are present. The method of dispersion in MRI is the absorption of the RF radiation by the molecules, tissues, fluids, etc. and re-radiated back with modulation in amplitude frequency and phase from the local medium. One may think of RF radiation used in MRI for simplicity sake illustrated above as if it were going through some kind of dispersive biological prism. But the brain is
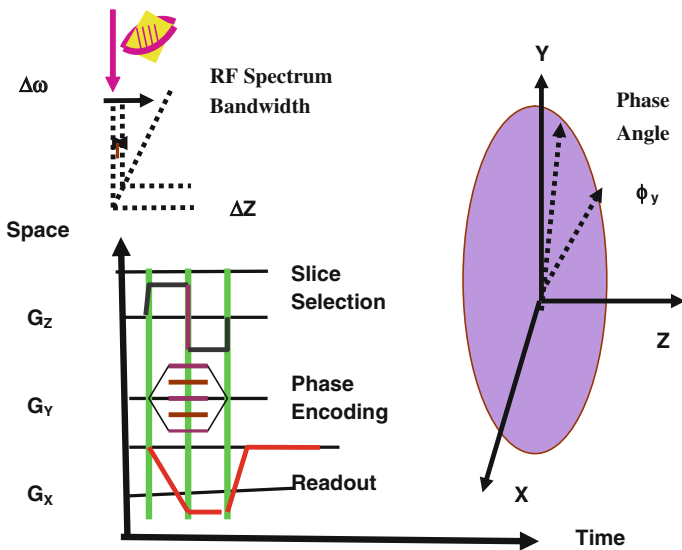
Fig. 2.10 It is a pictorial representation of the basic pulse sequence technique of imaging of the brain. A series of magnetic field gradient pulses with positive and negative components are used along X, Y, Z directions. One can follow the pulses in a sequential structure with a typical arrangement as shown. But in a commercial situation different machines would have their own specific routines to follow. Hz is the static magnetic field applied in the Z-direction. Y-gradient is the phase encoding gradient. The phase angle is $\varphi_y = \gamma \, y \, G_y \, t_y$. Here γ is called as the gyro-magnetic ratio = the ratio of the magnetic moment μ to the angular momentum L, G_y is the field gradient in the Y-direction, y is a coordinate point in the Y-direction and t_y is any instant of time. The X-Gradient, G_x is then applied in the X direction to select the output. The resonance frequency selection along X at a position x is $\omega(x) = \omega_0 + \gamma \times Gx$

not as simple as the optical type dispersive medium. It is a complex biological structure. The brain consists of atoms, molecules, tissues, fluids, etc. It makes it internally an irregular medium. One can say it is somewhat a spheroid shaped complex biological medium. In the presence of a static magnetic field applied in z direction to the brain and the RF electromagnetic field applied in the x direction one observes in the y direction like a diffracted RF beam of radiation. This modulated beam of RF radiation brings out what is happening in the brain over space and time. This is converted into a map of the brain. In a nut shell one can say if one wants to know about the detailed intricate-dynamic-quantum mechanical structure of the brain just the single quantum conventional MRI technology we have at present is not adequate.

2.8.1.1 A Basic Quantum Imaging Technique

The use of magnetic field gradients along the three x, y, z directions can be exploited to stimulate RF electronic excitations of the macromolecules in the brain
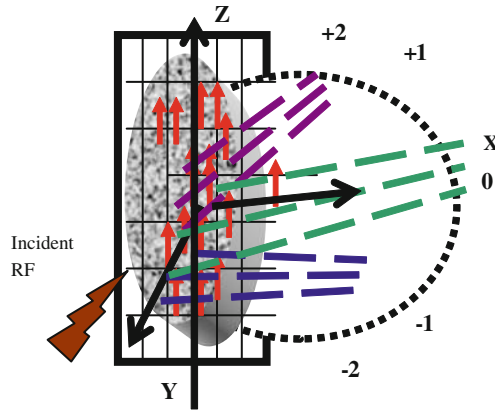
Fig. 2.11 The above pictorial representation depicts a more refined (from the macroscopic medium -dispersive) model of the brain. It is as if the brain were a three dimensional diffraction gratin. This model in fact is seen very close to reality. On the left hand side (LHS) is shown round about a three dimensional ellipse (representing the brain) with arrangement of spins pointing in the Z-direction created by the static magnetic field applied in the Z-direction. Suppose now a small gradient magnetic field is superimposed on this order in the X-direction. The result will be a fraction of the spins will be moved in the X-direction. If the gradient is in the form of pulsed gradient, echoes will be generated, by the vibrating spins. These spins will tend to dissipate in the X–Y plane. A phase (angle with respect to Y-axis) reversal by 180 pulse is applied around the X-axis. The spins now flip to −Y axis first bunch together towards −Y and then start dissipating towards + Y axis. This bunching and de-bunching (phase recycling) is repeated in-between a time (called as the relaxation time T_2) several times. It provides the amplified signal required for the Quantum MRI (QMRI)

and build a multi-quantum imaging. Figure 2.10 provides a round about illustration giving a brief description of the simple three basic steps involved in quantum imaging. First a slice selection (the X–Y plane) is done in the brain space along the Z-direction. Then the spins are then projected on the X–Y plane using a 90° pulse. The maximum amplitude signal arrived due to the spins in the X–Y plane is recorded at an angle φ (=0 initially) along the Y-axis (X–Y plane) like a reference point. In subsequent phase encoding steps (Y-direction) the strength of the Y-magnetic field gradient (phase) gradient is gradually increased. This enables more and more participation of the regional (X–Y plane) molecules. A readout gradient in X-direction then makes selection of the signal in a particular bandwidth and is recorded. The three steps are repeated in succession over a period of time called as the repetition time (TR). Each time a new slice selection (X–Y plane) is made the procedure is repeated. This procedure enables systematic data information being collected about the events happening in all the X–Y planes progressing gradually in the Z-direction and finally recorded. It is later converted into a global image of the brain. Figure 2.10 is only an over-simplified pictorial representation of the steps one carries out in succession and thus builds up the data. The data is used to make a picture using a standard mathematical package

e.g. Mathematica, Matlab, etc. The reader is referred to further sections for some more details about imaging. One should refer to a standard text book on MRI for exact techniques followed in the imaging. This book is more on conceptual physical principles of multi-quantum imaging rather than on imaging technology itself.

2.8.1.2 The Quantum Approach to Imaging

Today we are in the process of refining MRI further i.e. designing the QMRI machine. In the presence of a magnetic field gradient applied in a narrow region along a chosen direction the output RF radiation will have in its components different orders of coherence-of-interaction between spins, in the dispersed state. These components are the natural result of different quantum orders of coherences between spins. The multiple orders of coherence originate from the fact that a bunch of spins is excited into different levels of energy within a macromolecular structure or due to interaction in-between the macro-molecules. The spins can correlate to each other in many different ways. The spins may be pointing in opposite ($\pm Z$) directions i.e. correlation corresponding to spins being anti-parallel. This is the lowest level bound state of energy. These correlations give rise to ZOC. But there can be spins in correlation a distance apart pointing in the same direction. These correlations give rise to DQC. There can be multiple coherences as well.

Multiple coherences of higher orders are difficult to observe. One normally observes coherences in lower orders, i.e. $+2$, $+1$, 0, -1, -2, etc. The digits 2, 1 and 0 correspond to double, single and zero quantum level coherences. These coherence arise due to the distant dipole field (DDF) created among spins in the otherwise uniform applied magnetic field in the z-direction. The selection of the quantum orders in the brain takes place in the presence of RF radiation by natural selection of the principle of the conservation of the angular momentum. Both positive and negative coherence transfer paths (CTPs) are possible but in the end it is the -1 (single quantum coherence) which is detected. Others are not directly observable. One can illustrate as a typical example shown below that our brain has the capacity to perform multiple quantum coherences. The digit 2 chosen is purely incidental. Each of these coherences may be a part of some collective activity e.g. the metabolism, etc. Having correlated the event the brain then dissipates along five different channels the messages collating different actions.

The use of the phenomena of dispersion of light in a prism or say in a rainbow as analogy discussed before was purely an over-simplification in a layman's language. That was a rough illustration for the sake of analogy and simplicity without involving a detailed PCM (physics, chemistry and mathematics) of the phenomena involved. But in the real brain there are several complex correlations of activities happening. MRI is yet a humble tool to see the distinct out puts of the several electronic happening simultaneously. It does not bring out an exact scientific truth underneath which is much more complex. It is not possible to design an MRI machine which in one go can be perfect to the finest details. One should not forget it has taken more than half a century to create the MRI machine

(a)

(b)
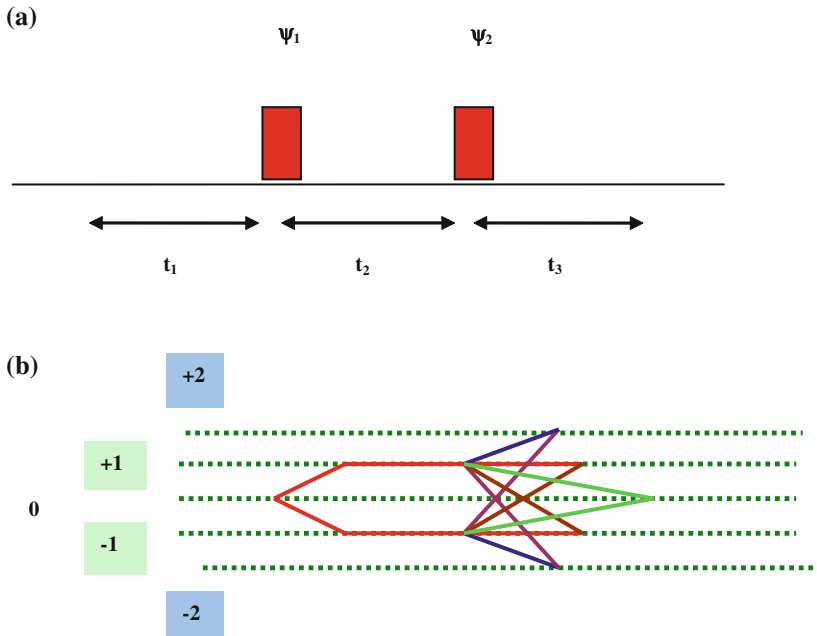
Fig. 2.12   a The ψ_1, ψ_2, phase angle (in the X–Y plane) pulses, are applied along the X-direction in succession. Normally the 90 angle (rotation along X or Y) pulses are used, and the time intervals t_1, t_2, t_3 in between the pulses, are allowed, and then repeated. The intervals can be variable or kept constant. The duration of the pulses, is normally kept fixed, $=\tau$ seconds. **b** The number of pulses applied depends upon the number of CTPs desired. Normally the number of pulses used is one higher than the quantum coherence order required

which we have today. It is a common knowledge that an optical prism disperses white light into seven rainbow colors. But in MRI we use RF (radio frequency) radiation which is invisible to eye and the brain is not an optical prism either. In MRI RF radiation impinges on the brain. The brain is first polarized with spins pointing in the z-direction by the applied static magnetic field.

The RF radiation excites hetero-nuclear species of atoms and molecules to higher energy states. These molecules when they come back to their ground state emit back the RF radiation. This re-emitted radiation is a random mixture of various frequencies and phases (emitted at different times). In order to get useful information out of this radiation one needs to reinforce certain signals and eliminate others. The gradient echo technique selects the required constructive interference of the important events and destroys others. One can apply oscillatory magnetic field gradients along the x, y, z directions. In general the x, y, z magnetic pulsed field gradients make the molecular spins to vibrate about their mean position and different species isolate themselves from each other in response in space and time. The receiver of the signal classifies the incoming signal into different categories according to their magnetic moments and thus a quantum

image of the brain is formed in space and time. Figure 2.11 is a rough pictorial diffraction model representation of the brain as if it were a three dimensional diffraction grating but not in the real x, y, z space but in the time–space for the spins.

In between the pulses there will be time for the spins to interact and create quantum correlations between them. Correlation between spins aligned in opposite directions leads to 'zero quantum coherence (ZQC)'. Correlation between spins pointing in the same direction separated due to magnetic repulsion over a distance leads to 'double quantum coherence (DQC)'. ZQCs and DQCs provide imaging signals which are smaller in intensity than the SQC (single quantum coherence) signals used in the conventional MRI but provide better resolution in the image. A single quantum coherence assumes that all the spins have the same identity over large volumes in the brain. But this is very far from reality and that is where QMRIsteps into unravel the true mystery of the brain.

2.8.2 A Pulse Sequence Used to Explore Quantum Model of the Brain

The following is a typical pictorial illustration of the use of pulses to explore the secret of our brain. It is used as a routine technique and allows creation of many coherence paths possible for the quantum correlations under the applied RF radiation in the brain. But the quantum science of correlations among the atoms and molecules allows only a few selected correlation paths in preference to others. The selection comes from the overall conservation of the angular momentum in a selected region in space and time. The paths carry information due to the metabolic and other events happening in the brain. Figure 2.12 is a pictorial representation of the arrangement of two pulses used in a typical experiment and the resulting quantum coherences possible. One can select the coherence one is interested in and eliminate the others.

The reader is advised that the support information presented in the Appendices A and B at the end of the book will be very helpful in enhancing knowledge about the various concepts involved in the modern day MRI. The appendices provide greater insights in brief about the technical aspects which otherwise for details on need to look into a routine text book on MRI.

Chapter 3
Practical Illustrations

3.1 Conventional MRI Techniques

3.1.1 T_1 and T_2 Weighted Images: Wilson Disease

The neurodegenerative Wilson disease (NWD) [1] is a genetic disease. It is caused by mutations in the P-type ATPase. The defect leads to abnormal copper transport and metabolism in mitochondria and causes apoptotic and necrotic cell death due to oxidative damage after excess accumulation of intercellular copper. MRI shows T_2 hyper intense lesions involving mostly the putamina and less frequently the thalamic brain stem cerebellar dentate regions and cerebral white matter. The diffusion weighted imaging (DWI) and proton magnetic resonance spectroscopy (PMRS) are very useful techniques to shed light on the pathogenesis of NWD by inspecting the microscopic water diffusion and cellular metabolism in vivo. The T_1-weighted imaging (T_1WI) shows low signal intensity and markedly high intensity on T_2-weighted imaging (T_2WI) on asymmetrical basal ganglionic lesions. Moreover there is seen increased intensity on T_2WI, of the occipital, periventricular and subcortical white matter bilaterally without mass effect, suggestive of demyelination. Single voxel PMRS with voxel placed in the right putaminal lesion shows a low N-acetylaspartate/creatine ratio and a high lactate/Cr ratio, in contrast to those of bilateral occipital lobes. It is seen that impairment of copper transport across membranes leads to accumulation of copper in the liver, brain, cornea and kidney, and causes toxicity to those regions.

The damaged copper transport secondarily causes a low serum ceruloplasmin level. The lesions tend to be bilateral and often symmetrical and may involve gray and white matter. The putamen, caudate nucleus, global pallidus, claustrum, thalamus, cortical, subcortical regions, mesencephalon, pons, vermis and dentate nucleus, are all targets of injury. One finds in WD the gene defect (P-ATPase) affects the function of cytochrome C oxidase at the level of the mitochondria. Cytochrome C oxidase (COX-complex IV) requires copper to function. In the

absence of functional copper there may be COX deficiency with resultant elevation of lactate. The presence of the lactate accumulation in the edematous putaminal lesion suggest failure of aerobic respiration of the brain cells and the start of apoptosis. The MR image findings of bilateral putaminal necrosis at an acute stage can be a savior for the patient. Figure 3.1a is a rough picture of the regions of the brain on a global scale. Figure 3.1b [1] shows how measurement of relaxation Time T_2 is achieved. In the X-Y plane Fig. 3.2 [1] presents clinical results for Wilson disease in a particular case.

3.1.2 J-Resolved 2D-Spectroscopy Imaging: Metabolite Concentrations

GABA (gamma-amino butyric acid) is the primary inhibitory neurotransmitter in the brain. It is of considerable interest in many neuropsychiatric and neurological disorders [2]. It exists in low concentration, in vivo, ~ 1 μM/cc. GABA has a complicated multi-resonance spectrum that is overlapped by the dominant creatine (Cr), n-acetyl-aspartate (NAA) and glutamine/glutamate (Glx) resonances. Linear interaction like the chemical shift is averaged out during echo time TE. The decay of the transverse magnetization is solely due to T_2 relaxation neglecting effects due to spin diffusion and chemical exchange. Bilinear interaction i.e. J-coupling is unaffected by the refocusing pulse leading to the J-modulation of the magnetization during TE (echo time). The second dimension in 2D J-resolved spectra has information only about the J-interaction. The location of cross-peaks due to each coupled spin-pair yields the magnitude of the J-coupling. Due to strong coupling, improper refocusing of chemical shifts, leads to additional cross-peaks. It is seen that the 2D-J-resolved MRSI (two dimensional J-resolved magnetic resonance imaging) is sensitive to detect physiological differences in the living brain. Elevated grey matter GABA concentration makes physiological sense since ~ 75 % of all synapses are GABA-ergic. One can isolate and focus GABA measurement to specific tissue-type.

MRS (magnetic resonance spectroscopy) studies can now interrogate the complex biochemical interactions relating GABA activity and also that of the other amino acid-metabolites with bioenergcis and membrane metabolism detected with phosphorous (^{31}P) MRS. It is not clear how macromolecules and other close proximity metabolites differ between grey and white matter. The tissue-specific concentration differences are still very much unaddressed. It is an issue of particular importance since it is known that a prominent macromolecule resonance exists at 3.00 ppm with cross peaks at 7.8 Hz. Two other noteworthy metabolites that have chemical shifts and J-resolved cross peaks in close proximity to GABA are aspartate and glutathione. Aspartate has a resonance at 2.80 ppm with 9.1 Hz J-coupling whereas glutathione has components at 2.93 and 2.97 ppm with 4.7 and 14.1 Hz J-coupling, respectively. Owing to the closely matched J-coupling but relatively distant chemical shift the contribution from aspartate to J-resolved
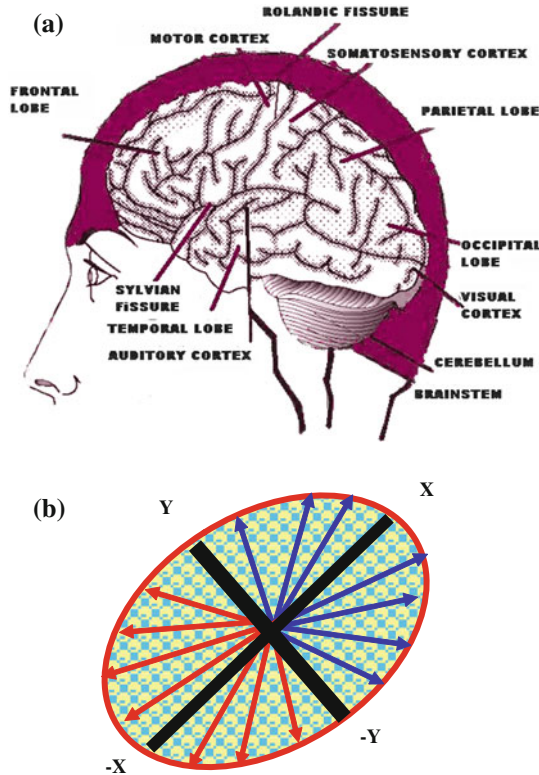
Fig. 3.1 **a** Human brain seen from the left side. Some of the important structural landmarks and special areas of the cerebral cortex are indicated. **b** A rough sketch of the projection of the spins in the X-Y plane is shown above. By applying static magnetic field along Z-direction spins are initially oriented along Z-direction. Later these spins are projected on the X-Y plane by applying 90^0 RF pulse along the X or Y-direction. The spins dissociate and re-associate (converge) in the X-Y plane; the time in between is recorded as the T_2 relaxation time. Spins can externally be reversed by application of 180^0 (reversal pulse) with respect to the X or Y-axis,. Then their relaxation in the X-Z or Y-Z plane cane be measured. This is called as the T_1 relaxation time

GABA peak is more influenced by T_2 as opposed to glutathione which is removed enough in its J constant but directly overlapping in its chemical shift that a possible contribution may exist (Figs. 3.2, 3.3 [2]).

3.1.3 Huntington's Disease: 3 T (Tesla) MRI (T_1 and T_2 Protocols)

One of the autosomal dominant neurodegenerative brain disorder is the Huntington's disease (HD) [3]. HD originates from CAG repeat expansion in HTT the
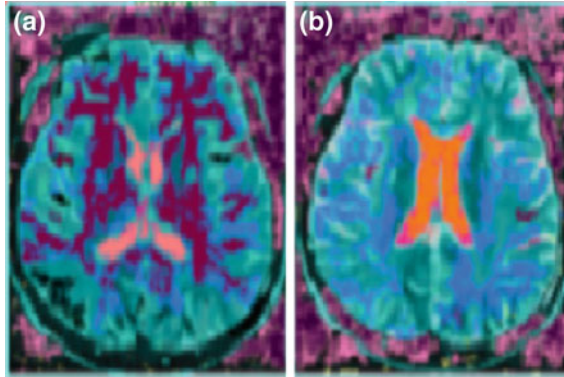
Fig. 3.2 **a** An MR study, **b** six months later, showed collapse of the bilateral putamina and the diffuse white matter hyper intensity over the bilateral cerebral hemispheres on T_2WI (T_2-Traansverse relaxation time weighted image). A diseased (Wilson disease) brain. The conventional imaging

gene that encodes Huntington which is on chromosome 4HD is characteristic of a triad of signs: progressive motor dysfunction, cognitive decline and psychiatric disturbance. The formal diagnosis of HD is made on the basis of motor signs. The concept of 'motor onset' or 'phenoconversion' is defined as the unambiguous presence of an otherwise unexplained movement disorder. This does not however account for the many individuals who show cognitive or behavioral disturbances several years before the onset of motor systems. In HD (Fig. 3.4 [3]) one aims to exploit the certainty of disease manifestation to ascertain the biomarkers and endpoints to test therapeutic interventions early in the disease. The MRI technique used was that of the conventional T_1 and T_2 weighted images with a 3 T (Tesla) scanner. One experiences a shrinkage of the caudate nuclei and expansion of the CSF spaces in participants in the study.

Automated volume of the striatum, caudate nuclei, and putamen are seen significantly reduced compared with controls. Semi-automated whole brain measures show a stepwise decline. It is seen there are progressive abnormalities in both the grey and white matter. The MRI indicates that abnormalities occur before diagnosis in the absence of overt motor signals in the grey and white matter and involve both cortical and subcortical regions. One finds that that neuronal dysfunction occurs many years before the development of motor signs that are diagnostic of HD. Highly sensitive MRI readouts include 3T neuroimaging, quantitative motor and cognitive assessments and emphasize the multi-system nature of the abnormalities. The predictability of the HD makes it the most governable of the neurodegenerative diseases from the standpoint of early intervention. Below is included a useful practical illustration for educational purpose.
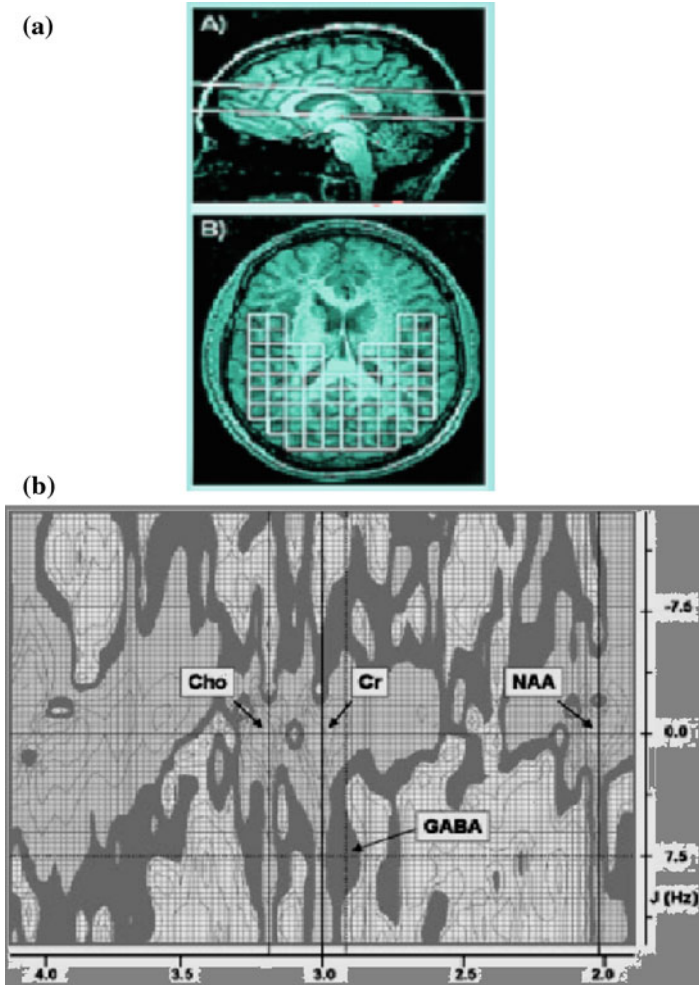
Fig. 3.3 **a** Sagittal image at 4T depicting the placement of the 30 mm thick magnetic resonance spectroscopy slab. **b** Oblique T1-weighted image. It shows sampled 2D-JMRSI (J-coupled magnetic resonance spectroscopic imaging) voxels used to derive *grey* and *white* matter estimates of brain GABA concentration. **C** 2D plot of J-resolved spectrum from a voxel in the human brain. The main resonance lines of Choline, Creatine and NAA are clearly visible. The J-resolved GABA resonance at 2.95 ppm exists at the intersection of the J = 7.5 Hz and 2.95 ppm lines

3.1.4 Sodium Long Component

T_2^* mapping

It is a common knowledge now that it is very important to have reliable information about the cellular and metabolic integrity of the brain. The presence of the nuclei, e.g. Na, K, etc. in the tissue-brain system, control the energetics and the

dynamics of the local brain spin system [4]. Information collected in MRI about sodium ion concentration in the brain-tissue system provides an initial knowledge base for the pathologic conditions such as tumors and acute cerebral ischemia. Sometimes in MRI literature T_2^* instead of T_2 is referred. Basically the two time are the same except that T_2^* is made free of the unwanted effects of in homogeneity e.g. due magnetic field. The T_2^* of concern here is in the regions of interest These are cerebrospinal fluid (CSF) at the level of the lateral ventricles, thalamus, putamen and occipital and frontal gray matter, splenium of the corpus callosum and periventricular, occipital, frontal and cerebellar white matter. In vivo T_1-weighted anatomic images together with corresponding sodium images and T_2^*-decay parametric maps as an illustration are shown in Fig. 3.4 [4]. The T_2^* values are seen to vary considerably between CSF and the grey and white matter. Since signal due to quadrupolar splitting from sodium ions in dilute water solutions is removed by motion averaging, Na CSF transverse relaxation rate (T_2^*) should be similar to that of the saline.

The similarity of T_2^* values for the grey and white matter suggest that the sodium ion environment in these two tissue types is similar despite the differences in the sodium concentrations. This problem can be alleviated using instead the quantum magnetic resonance imaging (QMRI). It is seen that the correlation time of the random sodium ion motion is much smaller compared to the time scale defined by the Larmor frequency. The study of T_2^* values through conventional MRI at he moment is of great help in mapping of the brain. It provides diagnostic potential in pathological conditions such as the brain tumors, head trauma and multiple sclerosis (MS). Sodium ion due to its non-centro symmetric charge distribution produces electric quadrupole effect and interaction with the magnetic dipole. Measurement of this interaction through triple quantum coherence technique can form a source of exact quantification in variation of sodium ion concentration through various tissues. See Sect. 7.2.2 for another a practical illustration. Figure 3.5 [4] is a typical practical illustration on conventional Na MRI.

3.1.5 Water Diffusion in Human White Matter: Ischemic Stroke

In a normal healthy brain the orientation of the magnetic spins present in a small volume (voxel) are magnetically isotropic. The spins are randomly oriented in all possible directions and overall annul each other. Application of a static magnetic field in a chosen direction referred to as z direction in MRI makes them align along that direction in the voxel chosen. Subsequent application of RF (radio frequency) radiation along say x direction will produce signals along y direction. If the voxel chosen is a diseased part of the brain the echo of the radiation received back will have the overriding response due to an anisotropy created by the disease. The received signals will deliver information about the behavior of spins compared to
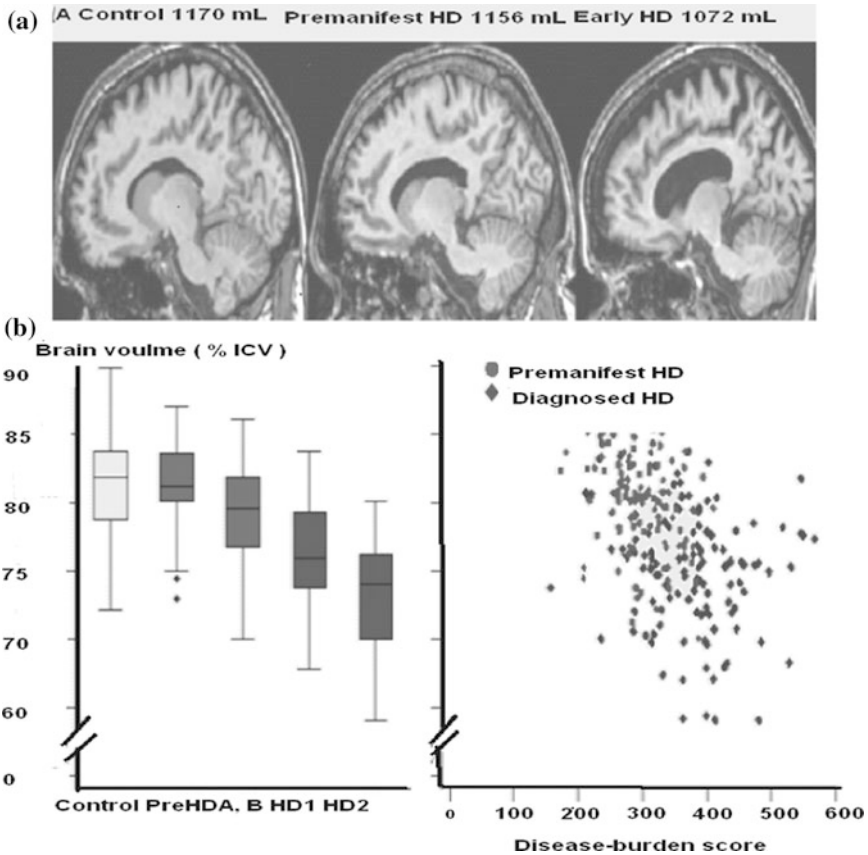
Fig. 3.4 Whole brain and regional atrophy in the controls premanifest and early Huntington's disease groups. **a** 3T volumetric MRI scan in a 50-year-old control a 55-year-old individual with pre HD and a 49-year-old with early Huntington's disease. Brain volumes are corrected for intracranial volume. **b** *Left* Y-axis: Brain volume (% ICV), X-axis: Control, PreHD-A, PreHD-B, HD1, HD2. *Right* Y-axis: *Filled circle*, Premanifest HD, *filled diamond*, diagnosed HD, X-axis: Disease-burden score. Brain volume as a percentage of intracranial volume (ICV) across all groups (*horizontal lines* are median; b*oxes*, upper and lower quartiles; *bars* are range; *dots* are outliers) and scatter plot of brain volume as a percentage of intracranial volume against disease burden. **c** Cortical thinning in the Huntington's disease groups compared with controls. The top panel shows statistical maps corrected with the false discovery rate; magnitude maps are shown below. All results are adjusted for age and sex. *ICV* intracranial volume. *LH* left hemisphere, *RH* right hemisphere

that of a healthy person where spins were involved in the normal functions of the brain. One can perform evaluation of ischemic stroke [5] using knowledge about temporal anisotropy progress of the water molecules diffusion in the brain. The apparent diffusion coefficient (ADC) is used as the physical parameter towards the means of evaluation of the status of the stroke. The unit of measurement of the
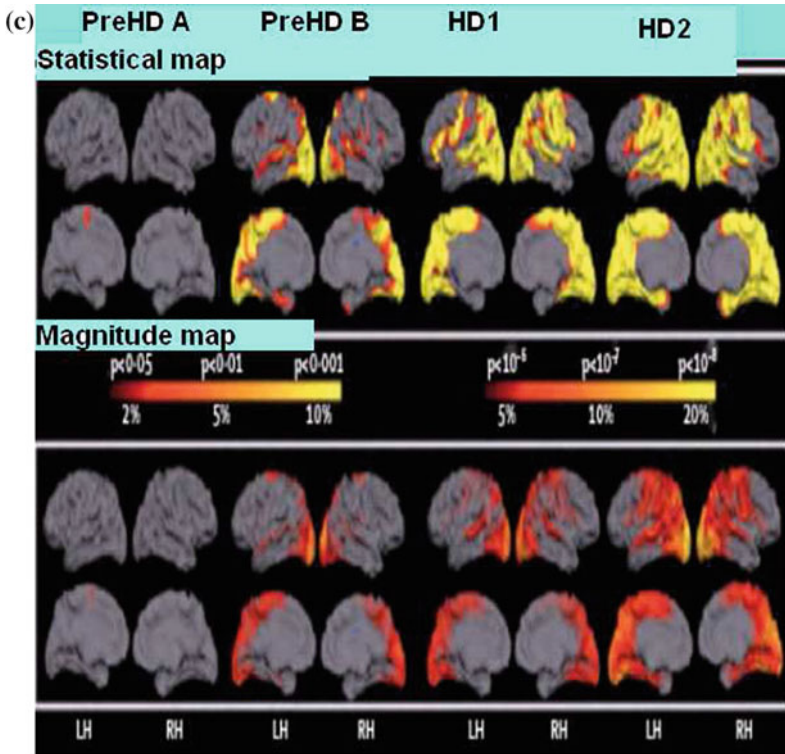
Fig. 3.4 continued

ADC is unit area of water diffusion/milli seconds i.e. $(\mu m)^2/ms$. Diffusion weighted imaging (DWI) using MRI provides a standard technique for this purpose. It is seen that there is decline in diffusion isotropy from a few hours after stroke onset. In the same time period there is gradual increase in signal intensity on T_2-weighted images in ischemic lesions. This is attributed to vasogenic edema, membrane degradation, and cell lysis. In the x-y plane the abnormal area of the brain has structural elongated axis in a particular direction. It effectively produces variations with major component changes. This requires description with components more than just in the x-y directions. The intensity variations study in MRI is then refereed to as Tensor imaging. It means anisotropy in intensity due to water diffusion is then considered in more possible directions.

One can quantify temporal evolution of water ADC ∥ (apparent diffusion coefficient parallel), and ADC ⊥ (apparent coefficient perpendicular) for the human white matter tract following ischemia. A prompt reduction of the ADC in ischemic tissue results in hyper-intensity in DW (diffusion weighted) images. One can evaluate the DWI data to develop a model of nerve tissue that incorporates cytotoxic and vasogenic edema (changes in volume of intra and extra-cellular spaces). A restricted study on ischemic lesions involving the posterior limb of the
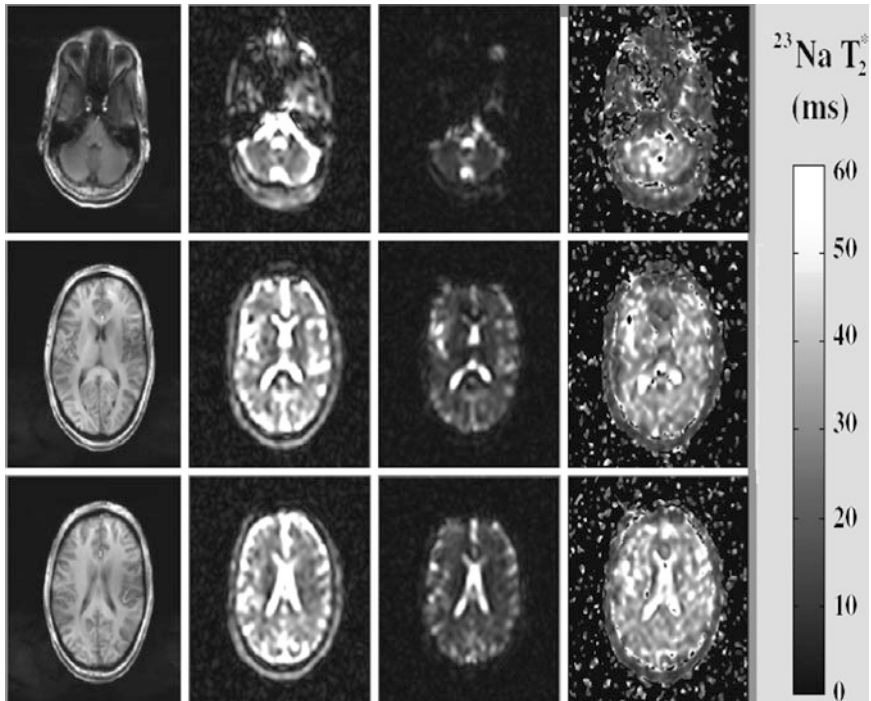
Fig. 3.5 T_1-weighted axial brain images (8 mm thick) from a healthy volunteer at 7 T (*left column*), single-quantum (T_2) sodium images of the corresponding slices at TE - 12 ms and TE -37 ms (*center columns*), and T^*_2 parametric map of the selected brain slices (*right column*). The short TE images were acquired once, while the long TE images were averaged three times, yielding total acquisition time of 63 min

internal capsule (PLIC) provides a suitable path of accuracy in a true model development. DWI is performed with motion probing gradients (MPGs) in three orthogonal directions or in six directions for diffusion tensor imaging (DTI). DW images are obtained using single shot spin echo echo planar imaging (EPI) in three orthogonal (one oriented perpendicular to the imaging plane) or six noncollinear MPG directions. Echo-planar images without MPG (T_2 weighted images) were acquired simultaneously. The imaging section of DTI is perpendicular to the long axis of the magnet bore and that of DWI is nearly parallel to the anterior commissure-posterior commissure plane. The registered DW images in three orthogonal MPG directions is summed into an isotropic DW image. A set of six ADC maps per section (DTI set) is produced from the registered DW images for six MPG directions, and the corresponding T_2 weighted images. From the DTI set, maps of eigenvalues of the diffusion tensor, an <ADC> (averaged across patients) map, and a color coded map, depicting the direction of the first eigenvector, were generated (see Fig. 3.6 [5]).
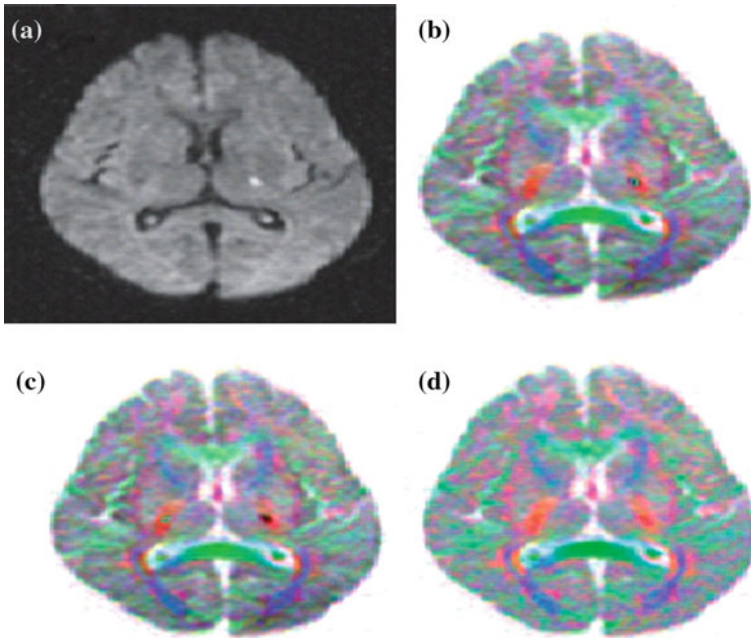
Fig. 3.6 Isotropic diffusion-weighted image (**a**) shows hyperintense lesion in the left posterior limb of the internal capsule (PLIC). On color-coded images (**b**, **c**), PLICs appear in *red*. Regions of interest (ROIs) in the *left* (**b**) and *right* PLIC (**c**) are depicted as *small cyan ellipses*. Although the color in the lesion on color-coded images (**b**) and (**c**) can not be seen clearly, adjustment of the brightness enables us to see the color in the lesion (**d**)

3.1.6 Neuromelanin in the Substantia Nigra Pars Compacta (SNc) and Locus Coeruleus (LC)-MRI-3D Gradient Echo: Magnetization Transfer Contrast (MTC)

In this MRI technique one makes use of the two proton conditions in vivo. The free-pool and the bound-pool. In the free-pool, the protons are mobile in free bulk water and have a relatively long T_2. In the bound pool, the restricted protons are bound in proteins, macromolecules and cellular membrane and have a very short T_2. In conventional MRI the bound pool is invisible. There is relationship between the free-pool and the restricted protons. It is called as a cross relaxation or an exchange mechanism. MTC uses off-resonance radio frequency (RF) pulse to saturate protons in the bound pool selectively [6]. There is the transfer of magnetization from the bound to the free pool. One finds a decrease of the signal in the area of the free pool. In tissue containing large number of macromolecules the MR signal is reduced. The SNc contains dopaminergic neurons and the LC nonradrenergic neurons. Neuromelanin is a byproduct of the synthesis of monoamine neurotransmitters such as noradrenalin and dopamine. Neuromelanin has the

general characteristic of cutaneous melanin. It is seen that the use of 3D-GRE (gradient echo) with SORS-STC (slice selective off resonance-saturation transfer contrast) identifies neuromelanin-generated contrast in the SNc and LC at 1.5 T. In clinical use of neuromelanin-contrast imaging one sees reduced neuromelanin levels in the SNc and LC in Parkinson's disease using a 3 T MR imaging scanner (see Fig. 3.7 [6]).

3.1.7 Metabolite Proton Mapping, Advanced Model: Neurologic Diseases

It has been found that the biochemical, morphologic and the functional similarities between the human brain and its non human counterpart primate (Rhesus Macaqque) has led to the extensive use of the latter as an advanced model. In the study [7] molecular environment requires knowledge of the longitudinal (T_1) and transverse (T_2) relaxation times. Alternatively one need to minimize their influence with long repetition time $>>T_2$ and short TE $\ll T_2$. The ability to find true metabolite levels from mere changes in relaxation times (quantification accuracy) depends on the knowledge of T_2. Unlike the human diseases where the effects of metabolites on T_2 are yet unknown, animals used in the study are the healthy ones, and provide a good benchmark. It is necessary to establish the base line T_2 values in order to correct for their weighting. In order to achieve as above one obtains the T_2s of NAA, Cho, and Cr at 3 T. A strong 18 mT/m Hadamard slice select magnetic field gradient helps to reduce the chemical shift displacement between NAA and Cho. Six different structures, caudate, thalamus, putamen, and cingulated gyrus in gray matter (GM) are of interest. Figure 3.8 [7] is a helpful illustration in this area of interest.

3.1.8 J-Resolved Proton MRS Spectra, Neuro-Biological and Neuro-Psychiatric Disorders, Amino Acids: Glutamate (Glu) and Glutamine (Gln)

It is known spectroscopically in a broad sense that Glu and Gln have a singlet at 2.35 and 3.75 ppm respectively. This may be optimally so for the Glu at 2.35 ppm arising from the ${}^4CH_2$ spin group. The Gln peak on the other hand has lower concentration and has overlap from residual of both myo-inositol and Glu. The J-coupled spectrum [8] of these amino acids in vivo provides a good resolution. The data analysis uses LCModel (linear combination model) combined with theoretical simulations.
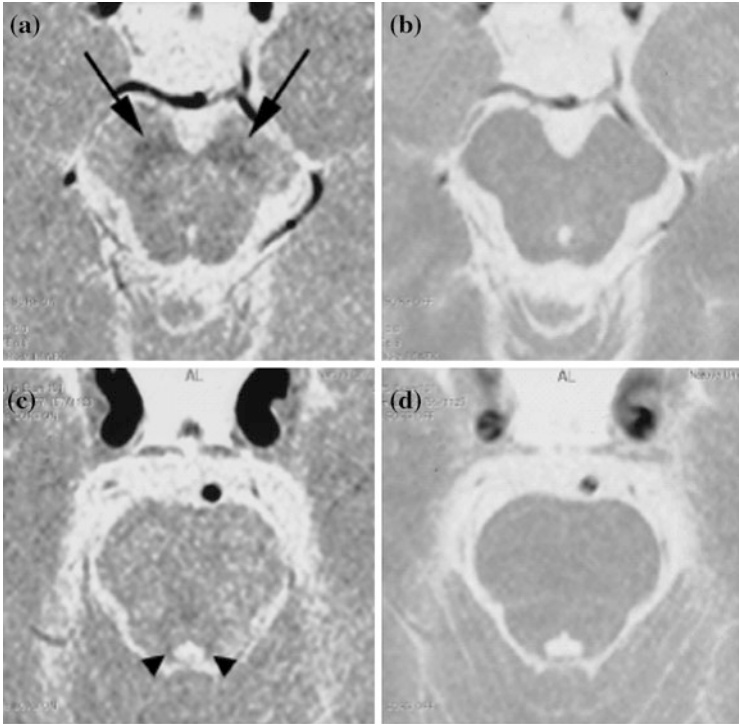
Fig. 3.7 A 23 year old-male volunteer. Representative images of the susbtantia nigra pars compacta (SNc) and locus coeruleus (LC). SNc was evaluated at the level of the mid brain (**a**, **b**). LC was evaluated at the level of the pons (**c**, **d**). Neuromelanin in the SNc (*arrows*) and LC (*arrow heads*) was "apparently visible" with slice-selective off-resonance sinc pulse-saturation transfer contrast (SQRS-STC) (**a**, **c**). Neuromelanin in the SNc and LC was "apparently NOT visible" without SORS-STC (**b**, **d**)

Analysis is done using GAMMA (general approach to magnetic resonance mathematical analysis) computer package. A single voxel ($2.5 \times 2.5 \times 2.5 \text{ cm}^3$) is placed in the parie-to-occipital cortex (POC) along the midline.

One performs optimization of the tip angle and the water suppression using the WET(water suppression enhanced through T_1) technique, the 2D-JPRESS (J-resolved point resolved spectroscopy) collected TE-stepped spectra. It provides a J-resolved bandwidth of 50 Hz. It can adequately resolve the following metabolites of interest. Aspartate (Asp), Choline (Cho), GABA, Glu, Gln, Glutathione (GSH), Glycine (Gly), Myo-inositol, N-acetylaspartate (NAA), N-acetylaspatylglutamate (NAAG), Creatine (Cr), Phosphocreatine (PCr), Scyllo-inositol (scy), Taurine (Tau), and Lactate (Lac). Figure 3.9 is an illustration, comprising the proton MRS (magnetic resonance spectroscopy) results [8].
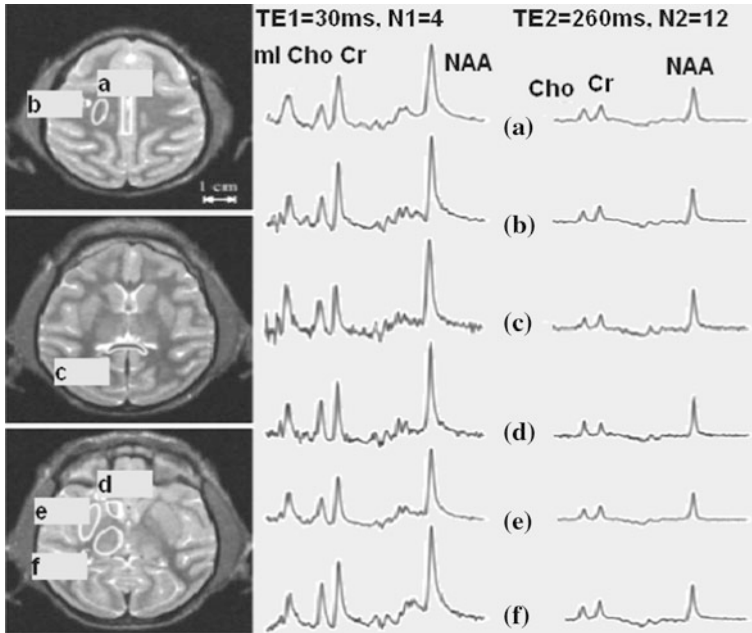
Fig. 3.8 *Left*: Axial T$_2$-weighted images showing the regions where the voxels' T$_2$s were averaged (*solid lines*). In GM: cingulate gyrus (**a**), caudate (**d**), putamen (**e**), and thalamus (**f**); and in the WM: **b** centrum semiovale, **c** splenium of the corpus callosum. *Right*: Real part of the averaged spectra from the corresponding regions at both TEs (*black lines*) with the model functions used for T$_2$ estimation superimposed (*gray lines*) on common 3.8–1.8 ppm and vertical scales. Note the quality of the fit at either TE, the improved SNR of regional averages versus voxel spectra and the T$_2$ weighting between the two TEs, underscoring the need for T$_2$ values for accurate quantification

3.2 Quantum Techniques

3.2.1 Intermolecular Double-Quantum Coherence Imaging (iDQCI) in Human Brain

There is seen a drastic improvement in contrast of images in MRI technology when one uses MQC (multiple quantum coherence) as the basis for image formation. It is now well established that there is a connection between the magnetization field, created by distant spins locally and the intermolecular dipole–dipole coupling. The residual dipolar couplings between distant spins are responsible for the dipolar demagnetization field, and give rise to the intermolecular MQCs [9]. The phenomena are due to the demagnetization field produced as a result of the spatial modulation of the nuclear magnetization arising in the sample. This happens following a second RF pulse in the CRAZED [correlation spectroscopy (COSY) sequence revamped by asymmetric z gradient echo detection] mode. One can use zero-quantum coherence (ZQC) for imaging. ZQC is insensitive to the magnetic
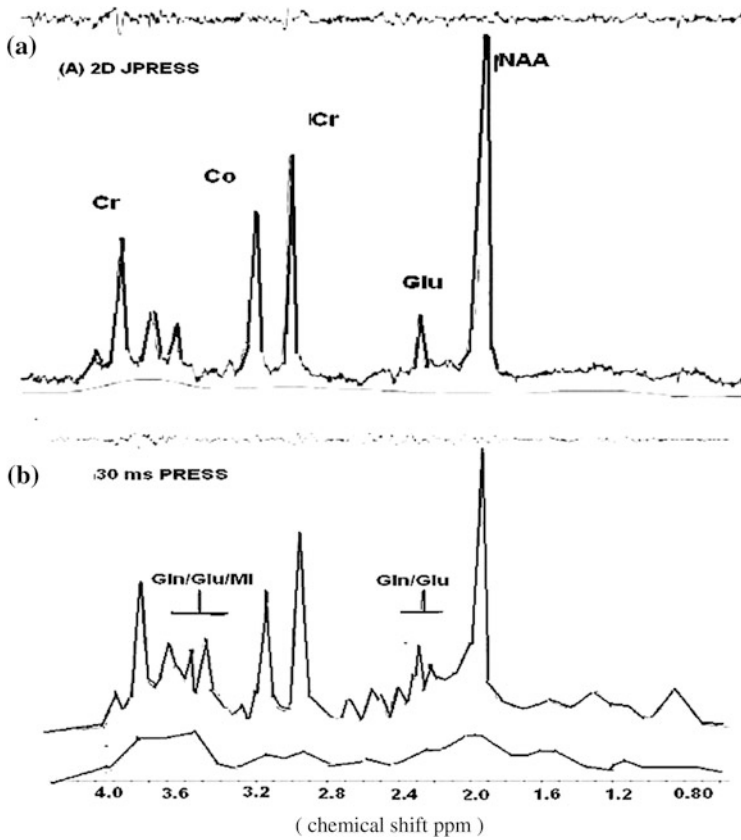
Fig. 3.9 2D-J-PRESS (point resolved spectroscopy) (**a**) and 30 ms PRESS (**b**) spectra shown with LC Model fits, residuals and baselines from the same scan for comparison. The 2D-JPRESS spectrum is from the central (J = 0.0 Hz) extraction. All spectra are displayed without any time-filtering and represent 13 min of signal averaging

field in-homogeneity and has a higher signal/noise ratio than other MQCs. In fact ZQC, DQC and triple quantum coherences (TQC), are in use not only for imaging but also for evaluating the change in the metabolite concentration in tumors.

One should remember that the conventional MRI technology is based on single quantum coherence (SQC) echo imaging. The imaging is basically on the global scale. In conventional MRI it is assumed in the brain all the spins are identical. In that case the spins are treated as if they have no identity of their own. The only identity they portray is the environment in which they are present. That is how they help to image the local artifacts. MQCs are different. The ZQC correlates spins pointing in opposite directions (as a bound state) over a region. The distant spins also contribute. Similarly there is correlation among two spins pointing in the same direction. They create DQC (double quantum coherence) and the three spins pointing in the same direction create TQC (triple quantum coherence).

A knowledge gathered from the MQCs about the quantum chemistry of events happening in space and time in a region is invaluable in detailed (molecular level) diagnostics of a tumor. DQC and ZQC are twins among possible MQCs for images of a multi-spin system. The choice of DQC or ZQC is based on convenience and the need for a specific imaging in interest. It is seen that DQC imaging is sensitive to the double-quantum transverse relaxation time T_{2DQ}. One can use a whole body 1.5 T scanner to obtain MQC imaging. It is believed that DQC signal provides a new form of contrast for MRI. Figure 3.10 [9] is an illustration on DQC. The illustration shows the potential of iMQC (intermolecular quantum coherence) imaging for probing trabecular bone structure. It is at a spatial resolution that simultaneously permits direct visualization and quantification of trabecular network architecture. In this manner the observed signal modulations as a function of correlation distance can be compared with actual structural parameters. Unlike in structured phantoms the structural heterogeneity inherent to trabecular bone is likely to smear out the diffraction like signal behavior. Diffraction can be observed in studies of structured materials.

The iDQC (intermolecular double quantum coherence) images, of bone specimens acquired at various correlation distances are shown in Fig. 3.10. It is noted that the image contrast is a function of correlation distance (distance between two double quantum correlated spins). This behavior depends on local trabecular architecture. An edge attenuation etc is observed at the largest correlation distance. Signal loss occurs at the boundary between bone and water causing the trabecular elements to appear thicker than in the SQC image.

3.2.2 Quantum Functional MRI (Q-fMRI): Intermolecular Multi-Quantum Coherence Imaging (iMQC)

Conventional BOLD (blood oxygen level dependent) fMRI (functional magnetic resonance imaging) technique measures susceptibility (magnetic moment per unit volume) variations over each voxel. One can directly observe only single-quantum MRI. MQCs can only be observed indirectly. The fMRI technique uses the BOLD effect. This arises from the localized changes in the concentration, of the strongly paramagnetic deoxyhemoglobin in the brain. It is coupled to the alterations in neuronal activity. Blood flow increases within seconds near the site of activation and overcompensates for the increased metabolic demand. This results in decreased deoxy and increased diamagnetic oxy-hemoglobin contents. The ensuing changes in susceptibility gradients across capillaries and venous blood flow result in an increase of the apparent relaxation T_2^* of the spins.

One can have a T_2^* weighted image showing neuronal activation through the secondary effect of blood oxygenation as an increase in signal intensity. This conventional approach is not very intense on contrast in imaging. On the other hand one can use iMQCs (intermolecular quantum coherences) with much better
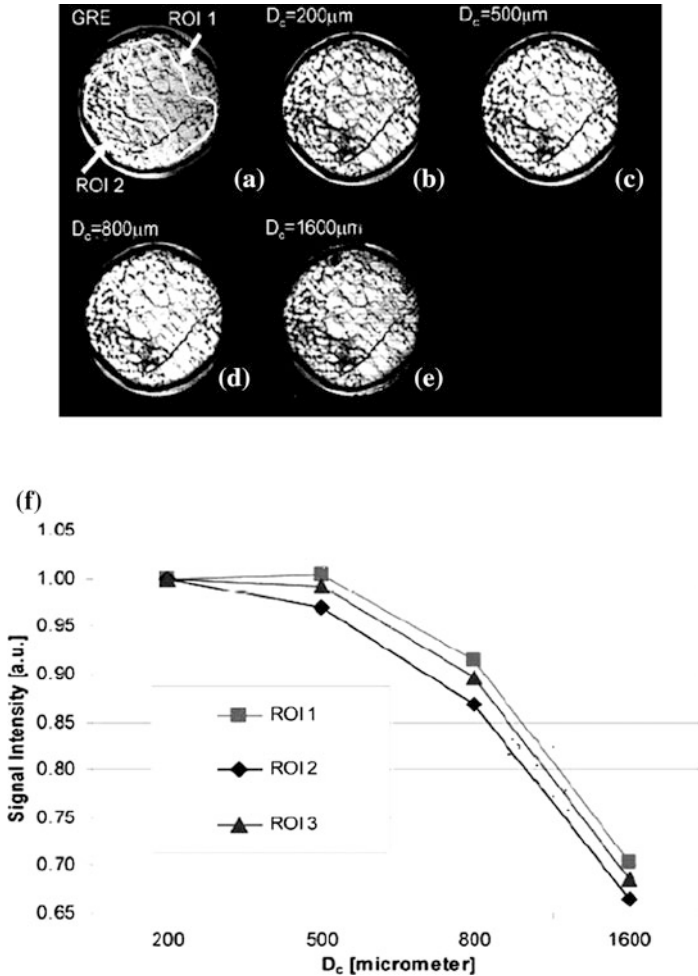
Fig. 3.10 a A gradient-echo reference image (pixel size, $156 \times 156 \ \mu m^2$, $1 \ \mu m = 10^{-6} m$) of the trabecular bone specimen. **b–e** iDQC images of trabecular bone acquired at various correlation distances. **f** Plot of iDQC signal intensity versus correlation distance for the ROIs indicated as in (**a**). Also included as well is the average from the entire section (labeled ROI 3). The weak modulations observed in (**e**) are caused by leakage signals at the large correlation distance selected

results in contrast in the images. The MQCs [10] have a better sensitivity to susceptibility gradients. They are more specific to the site of activation. As an example iZQC (intermolecular zero quantum coherence) evolves at the difference of the single quantum frequencies of the two spins involved. Therefore the ZQC intensity is a function of the distribution of the susceptibility gradients. The BOLD signal on the other hand is a function of the average strength of those gradients within a voxel.
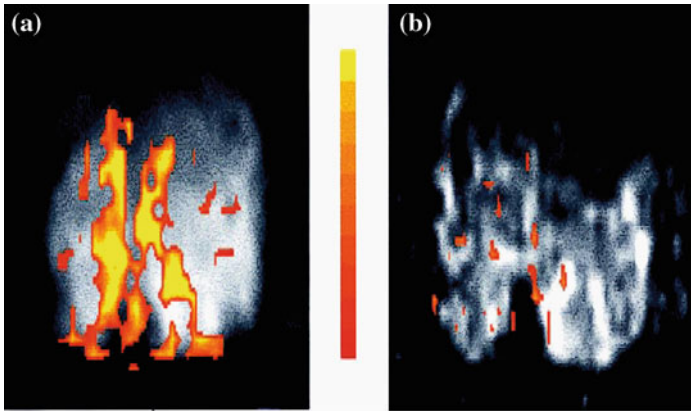
Fig. 3.11 **a** GE (gradient echo)-EPI (echo planar imaging) BOLD map. **b** iDQC (intermolecular double quantum coherence) image on a background iDQC contrast

The choice of correlation distance can be controlled by the strength of the RF magnetic field gradient. It gives an additional degree of freedom to optimize contrast. The conventional MRI does not possess this. The susceptibility gradients due to deoxyhemoglobin arise from blood vessels. It ranges from the blood vessels densely distributed capillaries, etc., to low density large veins. The iMQCs offer the possibility of altering the distance scale over which the dipole-couplings lead to observable signal and hence the sensitivity to blood vessels, of different sizes. The illustration in Fig. 3.11 [10] shows a conventional GE-EPI (gradient echo–echo planar imaging) in gray scale. Superimposed on it is the corresponding BOLD activation map. On the right is shown an iDQC image. It is in gray scale with the iDQC activation map superimposed. The anatomic contrast is fundamentally different between the two images. The iDQC map is considerably more sparse and the foci of activation are only partially overlapping. It is observed that iDQC contrast is also sensitive to the changes subsequent to neuronal activation. It is now established that iMQCs method yields signal changes in the brain that are coupled to alterations in neuronal activity.

Note that the anatomic contrast is fundamentally different between the two images. The iDQC map is considered more sparse. In this case the foci activation are only partially overlapping.

3.2.3 Triple Quantum Sodium MRI: Non-Human Primate Focal Brain Ischemia

In healthy brain cells a number of physiological functions happen due to a large sodium concentration gradient across their membranes. The gradient is maintained by the basic sodium–potassium-ATPase. This is the basic ion pump that splits

adenosine triphosphate (ATP) to pump Na^+ out of the cell and K^+ into the cell. Ischemia in acute stroke situation results in disturbed energy metabolism and consequently an unbalanced sodium out of the cell. Though both the intercellular sodium concentration (ISC) and the total tissue sodium concentration (TSC) increase in ischemia the increase in ISC occurs earlier. QMRI provides a suitable tool to allow an early detection of acute stroke. One uses anisotropic relaxation time based technique; the multi-quantum (MQ) filtering, in the QMRI. The sodium nucleus exhibits changed relaxation times (T_1 and T_2) in the intra and extra-cellular parts.

It is seen that in biological tissues the MQ sodium NMR (nuclear magnetic resonance) signal comes primarily from the intracellular space. This is as opposed to the total TSC as measured in the conventional single quantum (SQ) sodium MRI. The Triple quantum (TQ) sodium MRI can be successfully used [11] in vivo in visualizing the increase in ISC that occurs in the brain ischemia. Figure 3.12 [11] is presented an illustration in nonhuman primate model-pig tail monkey (Macaca nemestrina) for the induced focal brain ischemia using the endovascular method.

3.2.4 Selective Multiple Quantum Coherence (Sel-MQC) Technique: Fadu Tumor Located on the Leg of the Mouse

This technique is valuable when information about a specific metabolite (e.g. lactate) is required. As an example in extracranial tumor tissues the Lac (lactate)-CH_3 resonance (at 1.33 ppm) has been filtered from the overlapping methylene groups of the mobile lipids. Normally one applies a slice selective pulse and two or three-dimensional phase encoding gradients before signal acquisition. In Sel-MQC one accelerates the experiment by using a read magnetic field gradient during the signal acquisition [12]. When metabolites are imaged in vivo the principle point of comparison is the sensitivity of the applied fast sequence compared to the conventional chemical shift imaging (CSI). The Sel-MQC editing using magnetic field gradients for the coherence pathway selection is expected to completely suppress signal from water resonance. In conventional MRI (CSI) technique when the experiment is accelerated to reduce overall time the residual water signal causes artifacts in the metabolic image.

In Sel-MQC one separates water and lipids simultaneously. This requires at least two experiments with a defined phase shift and afterwards apply a phase (time)-sensitive reconstruction to the data. Multiple echoes of the Sel-MQC edited metabolite group can be acquired without **J** (electron spin angular momentum **S** and atomic spin angular **L** interaction)-modulation. This is achieved through frequency selective refocusing to further accelerate the measurement or to measure the apparent transverse relaxation time T_2. Figure 3.13 [12] depicts a practical illustration of the imaging in vivo for a tumor. It is done using the Sel-MQC-edited
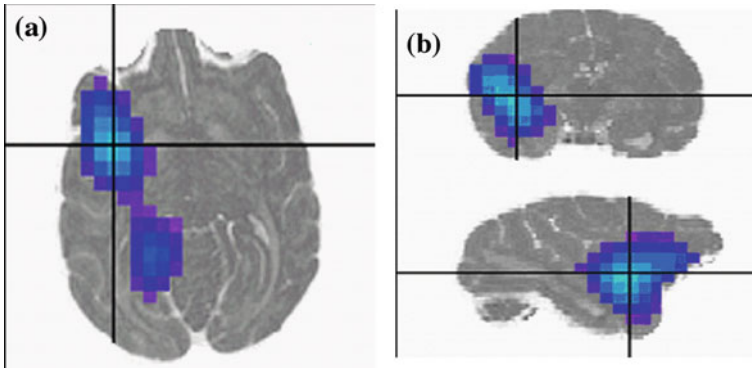
Fig. 3.12 Skull-stripped axial (**a**), coronal (**b**), and sagittal (**c**) sections through the hyperintense region in the right MCA (middle cerebral artery) territory for the 3-hr time point TQ sodium image (contra-lateral signal are shown) co-registered with the SPGR (spoiled gradient) proton MRI data set (*grayscale*). The *"cross-hair" lines* on each section indicate the relative location of the other two perpendicular sections. The two regions of increased TQ signal intensity, can be seen on the axial section (**a**)
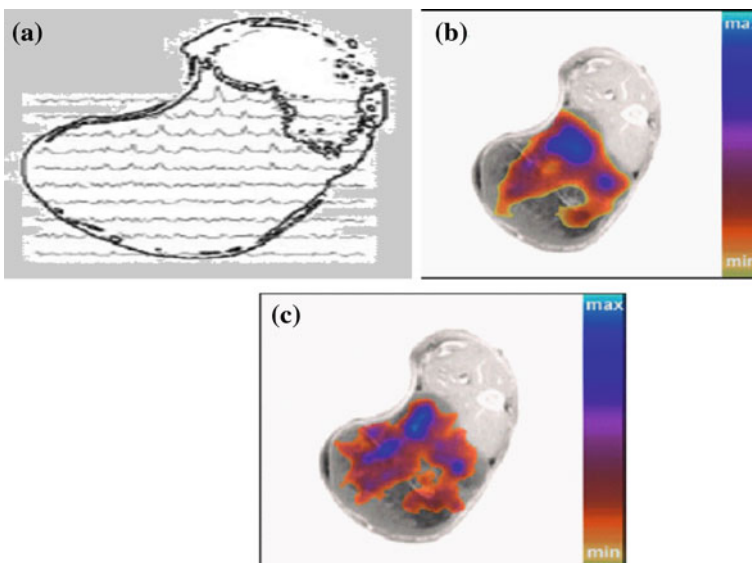
Fig. 3.13 In vivo measurements. Images of a FADU tumor located on the leg of the mouse can be seen with different Sel-MQC-edited Lac overlays. **a** A spectral map of the edited Lac CH_3 group acquired with the classic 2D phase-encoding method (SE-CSI) is laid over the tumor and leg contours. **b** The corresponding interpolated Lac distribution. **c** The interpolated Lac image acquired with the SEGRAD (spin echo gradient) method in the same total measurement time is shown. The total time of both experiments was 10 min 48 s

signal, with two different acquisition schemes. One can see a spectral overlay of the Sel-MQC on the tumor/leg contours. The Lac distribution using the classic 2D phase encoding is shown. There the interpolated Lac metabolite is laid over an image of the tumor located on the mouse leg. The T^*_2 effective value of the resonance relaxation is 13.3 ms is shown. The interpolated result of the SE-GRAD (spin echo-gradient) is also displayed.

References

1. Juan, C.-J., Chen, C.-Y., Liu, Y.-J., Chung, H.-W., Chin, S.-C., Hsueh, C.-J., Chu, H., Zimmerman, R.A.: Acute putaminal necrosis and white matter demyelination in a child with subnormal copper metabolism in Wilson D: MR imaging and spectroscopic findings. Neuroradiology **47**, 401–405 (2005)
2. Jensen, J.E, deB Frederick, B., Renshaw, P.F.: Grey and white matter GABA level differences in the human brain using two-dimensional, J-resolved spectroscopic imaging. NMR Biomed. **18**, 570 (2005)
3. Tabrizi, S.J., Langbehn, D.R., Leavitt, B.R., Roos, R.A.C., Durr, A., Craufurd, A., Kennard, C., Hicks, S.L., Fox, N.C., Scahill, R.I., Borowsky, B., Tobin, A.J., Rosas, H.D., Johnson, H., Reilmann, R., Landwehrmeyer, B., Stout, J.C.: Biological and clinical manifestations of Huntington's disease in the longitudinal TRACK-HD study: cross-sectional analysis of baseline data. Lancet Neurol. **8**, 791–801 (2009)
4. Fleysher, L., Oesingmann, N., Stoeckel, B., Grossman, R.I.: Sodium long-component T2* mapping in human brain at 7 Tesla. Matilde Inglese, Magn. Reson. Med. **62**, 1338–1341 (2009)
5. Stroke, I., Tamura, H., Kurihara, N., Machida, Y., Nishino, A., Shimosegawa, E.: How does water diffusion in human white matter change. Magn. Reson. Med. Sci. **8**, 121–134 (2009)
6. Nakane, T., Nihashi, T., Kaewl, H., Naganawa, S.: Visualization of neuromelanin in the substantia nigra and locus ceruleus at 1.5 T using a 3D-gradient echo sequence with magnetiztion transfer contras. Magn. Reson. Med. Sci. **7**, 205–210 (2008)
7. Liu, S., Gonen, O., Fleysher, R., Fleysher, L., Babb, J.S., Soher, B.J., Joo, C.-G., Ratai, E.-M., Gonzalez, R.G.: Metabolite proton T2 mapping in the healthy Rhesus Macaque brain. Magn. Reosn. Med. **62**, 1292–1299 (2009)
8. Jensen, J.E., Licata, S.C., Öngür, D., Friedman, S.D., Prescot, A.P., Henry, M.E., Renshaw, P.F.: Quantification of J-resolved proton spectra in two-dimensions with LCModel using GAMMA-simulated basis sets at 4 Tesla. NMR Biomed. **22**, 762–769 (2009)
9. Chin, C.-L., Tang, X., Bouchard, L.S., Saha, P.K., Warren, W.S., Wehrli, F.W.: Isolating quantum coherences in structural imaging using intermolecular double quantum coherences. J. Magn. Reson. **165**, 309 (2003)
10. Richter, W., Richter, M., Warren, W.S., Merkle, H., Andersen, P., Adriany, G., Ugurbil, K.:Functional magnetic resonance imaging with intermolecular mutiple-quantum Coherences. Magn. Reson. Im. **18**, 489 (2000)
11. LaVerde, G., Nemoto, E., Jungreis, G.A., Tanase, C., Boada, F.E.:Serial triple quantum sodium MRI during non-human primate focal brain ischemia. Magn. Reson. Med. **57**, 201–205 (2007)
12. Melkus, G., Mörchel, P., Behr, V.C., Kotas, M., Flentje, M., Jakob, P.M.: Sensitive J-coupled metabolite mapping using Sel-MQC with selective multi-spin-echo readout. Magn. Reson. Med. **62**, 880–887 (2009)

Chapter 4
Quantum Spin Dynamics and the MRI

4.1 The Basics

There are no short cuts to science and development. The quantum nature of matter is learnt through the basics of the quantum mechanics (QM). Quantum science education unfortunately at present does not form part of the curriculum at secondary level of education. It is the situation all over the world. Learning QM is no more difficult than learning the Newtonian Mechanics (NM). In NM we are dealing with large rigid bodies; the dynamics is macroscopic in nature and the object's position, velocity, acceleration etc. can be accurately determined. Further in NM the large objects e.g. planets do not react chemically. The only interaction they have is through the gravitational forces and is very weak. It has little affect on the human life visually to any degree of significance known. Planets in our solar system interact through gravitational forces among each other and with the sun in space and time and keep their dynamics of motion in equilibrium. The forces which make them move and remain in balance are well understood. The motion of the moon under the influence of gravitational forces around earth does however control to some extent the tidal effects and probably the climate on earth as well.

The situation in QM is quite different in many ways but similar in some manner. The electrons orbit around the nucleus very much like in the planetary motion. But the forces involved are of coulomb (charge-interaction) type and much stronger in nature. In an ensemble like the brain they interact chemically through charge transfer, energy transfer, spin transfer, etc. But the dynamics (interactions between them) of the atoms, molecules etc. involved is quantized. What it means is the interactions are a result of exchange of charge, spin, etc. happening in jumps of pockets called as quantum. In quantum dynamics (QD) only some selected values of energy transfer as quantum jumps are allowed. These are based on the laws of the conservation of the angular momentum of the orbiting electron, in an atom. In an ensemble like the brain interactions with the neighboring and distant spins (atomic and molecular magnets) is involved. This is what

quantum dynamics is about. The reader is referred to an introductory textbook on quantum physics for more insight into the wonders of the quantum science.

In QD the position, momentum, energy, etc. are not continuous variables. Their values are quantized i.e. they change in fixed quantum jumps. The energy of confinement of the ensemble of molecules is, called as the Hamiltonian of the system and is quantized i.e. it can only change in small quantum jumps. There are energy transitions between different quantum energy levels of the molecules. Also there are quantum correlations between different molecules. The chemical shift due to the varied surrounding electronic environment, J-coupling due to the interaction of the spin (magnetic moment) and angular momentum, etc. are the variable parameters. The position, momentum, energy, etc. in quantum science (QS) like in NM are the tools of the study of the dynamics of spins. Here the position, energy and momentum are, in their order of magnitude scales very microscopic in magnitude, e.g. the distances between molecules are around nm to micrometer scale. The coordinates in space i.e. position and momentum, behave like mathematical operators rather than being continuous analytical (e.g. x, y, z) variables. They operate on an ensemble of atoms, molecules etc. and bring out concrete results. For example, an operator can rotate spins and determine their evolution with time in an ensemble of the molecules. The dynamics of the spins in an ensemble like the brain is dealt in a space of matrices called as the Hilbert space. The size of the space is variable and is given by $(2)^N \times (2)^N$. Here N is the number of spins and the digit 2 corresponds to the, up and down, two states, of the magnetic spin. For a single spin (N = 1) case the space is of 4 matrices with each matrix having two rows and two columns. In the case of two spin (N = 2) system there will be 16 matrices of size 4×4 and so on.

The matrix operators are the basis of the spin dynamics in the brain ensemble. In order to predict the dynamics of the atoms, molecules etc. one uses the mechanics of the matrices. The behavior of the spins can be mapped by using spin matrices as variables in space and time and solving appropriate equations of dynamics of the matrices. In QM, the operators (energy momentum, etc.) do not commute. This means as an example for the position (operator q) and momentum (operator p), in NM, $qp - pq = 0$. But in QM, $qp - pq \neq 0$, instead $qp - pq = i\hbar$. The letter i represents a complex number $i = \pm\sqrt{-1}$. Here $\hbar = h/2\pi$ and h, is the familiar angular Planck's constant of the electromagnetic radiation. Those readers who are not familiar, with this complex number need not really bother about it. They only need to remember that this complex number makes the mathematics of the interaction of waves with matter easy to deal with. It is seen that matrices satisfy the same non commutative character as do q and p and other operators in QM. Thus matrices can be used to handle the operators in quantum mechanics. Alternatively one can write the familiar Schrödinger wave equation each time for a system and solve it. This equation is easy to solve for a single atom e.g. hydrogen, helium or a homonuclear ensemble of atoms. For a complicated system like the brain filled with hetero-nuclear species solving Schrödinger wave

equation is an impossible task. But matrix mechanics (MM) does allow a reasonable approach and the computer programs are available now to produce prior information and a model image of the brain.

4.2 Multi-Dimensional Spin Space and the MRI

The Biological spin systems have been created in nature for some reason. The reason is to sustain life. They (the animal model) shed some important conclusions to explore the model of the human brain. In order to learn first hand about the role of magnetic spins in the evolution of life on earth it is easier to start with some real life illustrations. The spins can be produced and used in a laboratory environment and that is what MRI is about. The virtues of the use of spins as scientific model to predict outcomes in the natural life becomes clear through the following arguments. In a laboratory one can produce a biological quantum computer. Here use can be made of the spin's up and down the two logic states of the spins. These arise out of the electron's intrinsic magnetic moment. It also has coupling with atomic and nuclear spin states. This coupling referred to as the J-coupling can be used to connect the two logic states reversibly by applying an RF radiation pulse in a suitable chosen system. One can build the q-bits (termed this way in contrast to the term 'bit' used in an electronic computer) and the required quantum logic gates to develop a quantum computer.

There can be a large number of spins ($\sim 10^{23}$) in a small volume e.g. in 1 mol of a liquid. The enormous power of the quantum computer is thus clear. The dimension of the space required where the spins will work is very large. Manipulation is easy if all the spins are identical. In a natural situation there can be a multinuclear environment e.g. the one we have in our brain. In that case the spins are not-equivalent. The problem is much more complex than imagined. The matrix coordinate space (called as the Hilbert space) provides a good solution to this problem. If all the spins are equivalent, i.e. taken from the same kind of molecules (species) in an ensemble the system is considered as pure. They only need repetition of some basis coordinate basis. Identical spins in a liquid system are a good source to develop a quantum computer. The molecules and atoms are very fluid in their nature in an environment like our brain. They can easily tumble, translate, etc. in space.

It does not take an Einstein to understand that our brain is a biological quantum (parallel) computer. In order to make one in a solid-state situation in a laboratory we can use a pure crystalline environment. Crystals have atoms arranged symmetrically throughout e.g. in a Silicon crystal. The crystalline environment for every atom is identical throughout. What happens to one atom is representative of the whole crystal. The spin scale can be multiplied easily but only mathematically yet. In actual practice the solid state quantum computer is riddled with unsurmountable problems. The situation of manipulating spins can be much more advantageous in an ensemble consisting of identical molecules in a liquid state e.g.

a selected suitable chemical solution. MRI provides a good insight into the design of a suitable quantum computer which will work at room temperature. In the liquid state every effective single spin of a molecule (if it has multi-spin character) has a unique character. This character is easily preserved throughout when identical molecules form a concentrated liquid chemical solution.

Each atom (spin) in the molecule has a unique position in its bonding with its neighbors. In a solution the molecules repeat themselves in their coordinated arrangement. The arrangement can be identical and repetitive. This single-molecule spin character can be retained in the solution throughout. A single equivalent spin in a molecule is the unique representation of the whole molecule and thus can be for the whole solution. The number of spins in a molecule can be the core order developed for use in the liquid solution. Their large number can be used to process large amounts of data. There is certainly advantage in using liquid-state rather than the solid-state as the molecules can easily translate, rotate etc. in space in a fluid environment.

The rotation degree of freedom is easily available to the spins in liquid state crystals. This is not the case in the solid-state where the atoms are rigidly fixed in space. They are limited in interactions in space with their neighbors. The reader is referred to the Ref. [1] for details. If the molecular structure is repeated over the whole liquid solution the ensemble is in its purest form and the q-bit manipulation is easy as the molecules are identical. This perfectly ideal system is easy to obtain in a laboratory but not seen in real biological systems. There can be more than one in-equivalent spins present in one molecule and in the whole system. In fact in MRI we do not need pure ensemble. The situation in MRI is very ordered for spins. The variations due to the interactions within the molecules and between the molecules over the different regions of the brain is the source of the image produced. The variations created by the nature are just the ones we are looking for in MRI. Are the spin variations in space and time control the cognitive activities of the brain?

The two states up and down of a single spin or many spins in a matrix mathematical space can be represented by a column matrix with its elements arranged vertically. This is like a vector in NM with three components x, y, z of say position in space arranged as a vector column or a tenor. In MRI the spin vector is restricted in motion up and down along the z-direction. To produce image from selected regions in space the spin vector is projected into $x - y$ plane (in a slice thickness ΔZ, along z-direction) to allow interactions with differing environments in different directions. This adds a three dimensional character to the image. In the ensemble of N spins the matrix space required to describe the system is, $2^N \times 2^N$ wide. The digit 2 represents the two states of the spin. For single (or many with perfect identity) spin, N = 1, we have a matrix of size 2×2 (two rows and two columns) representing the two states $\alpha, -\alpha$, as the diagonal elements of the matrix the off diagonal elements being zero.

In the case of two spins there are four (N = 2) states possible i.e. $\alpha\alpha, -\beta\beta$ states up and down and the two-exchange pairs states, $\alpha\beta, -\beta\alpha$ states. These form the 4 diagonal elements of the 4×4 matrix. The off-diagonal elements in the matrix represent time evolution of the events in the brain. One can develop higher and higher orders of the matrices representing larger and larger number of spins in a

system. The matrices can be multiplied, divided, factorized, etc. as the ordinary numbers but with their own set of laws and rules analogous to having rules in he NM. Computer programs are available now which can handle large matrices. One can obtain a model image of the brain with little knowledge of the matrix mechanics. The user only needs to input the values and character of the spins of the elements involved in a computer program. It is simple art of usual data punching in an electronic computer. The matrix mechanics (MM) is no more difficult than its counterpart the tensor mechanics in the NM. It is only a question of exposition and the basic academic training at an early stage i.e. at the secondary education stage. This will remove the fear and create appreciations of the benefits of the quantum science in the later professional life, particularly in the field of medicine. A reader who would be interested in learning details about the spin dynamics of the atoms and molecules is referred to the set of Appendices B, added, towards the end of the book.

4.3 Complimentary Nature of MRI and Quantum Computer (QCr)

In the quantum computing arena spins are used to store and transfer the information through reversible logical gates (note in electronic desktop computer the gates are irreversible-the signals goes only in one direction in sequential order). The quantum gates are unitary transformations performed using the operators of the type $e^{-iHt/\hbar}$ and $e^{iHt/\hbar}$. They include the energy Hamiltonian operator H (energy becomes an operator in QM) and the time t, i, is the complex number $= \sqrt{-1}$. The quantum computation using NMR is very advantageous and useful educational tool in the field of quantum information science (QIS). In the purest form spins can be grouped together and their coupling e.g. the J-coupling (spin orbit interaction) can be used to perform Boolean algebra operations e.g. the AND, OR, or the universal NAND gate s as required in the presently available electronic computer. It is done in NMR by remotely applied RF field pulses. A liquid state quantum computer if developed would operate at room temperature. This is an advantage clearly possible in the liquid state QCr over the solid-state computer. The spins in an ensemble of molecules can be used to build a quantum computer (QCr) with very large number of bits $\sim 10^{23}$ (in a mole). One is cautioned here that an ideal condition of collective coherent participation among spins is a prerequisite to design a QCr.

A carefully organized experimental set up is required. QCr large scaling is not possible in the EC (electronic computer). A QCr would act in parallel simultaneously to all the inputs from all the spins. It will also produce parallel outputs simultaneously thus producing a fast and a large volume information processor. It would be better than the central processing unit (CPU) of the present day desktop computer. The progress in this direction has been very slow. The use of the liquid

state NMR (LS-NMR) technology has been able to demonstrate operations up to 10 qbits. In quantum computer (QCr) one is after designing the purest state in the form of a molecular solution. Then one performs the logical operation of the signals via the universal quantum gate (called as the CNOT gate in the quantum computing). The gates provide the connections and the operations between different molecules in an ensemble. The connections are the unitary transforms producing identical superposition of states. These sub states can be states of the same energy but with different physical identities e.g. the different angular momentum states. The angular momentum can not be measured. But the interaction of the angular momentum states through the associated magnetic moment changes can be measured. This is exhibited as an electrical signal due to the magnetic moment associated with each angular momentum state.

The choice of J-coupling present in a molecule is a useful part of the manufacture of the quantum gates. The human brain is an ensemble of the spins in its most impurest form. The hetero-nuclear spins ensemble in the brain would require for mathematical analysis construction of spin-matrices of higher and higher orders. To simplify the matter the higher order matrices can be broken down into smaller and smaller order matrices which are of purer and purer spin-coherences. One builds purer coherences by distilling in steps through quantum correlations. Experimentally this is done by applying RF radiation signals in carefully selected planes rotating spins along certain angles etc. and processing, the signals received. The quantum imager and the QCr (quantum computer) act complementary to each other. Research in one area will help the research in the other. The knowledge developed in one area will complement the development in the other. The smaller the voxel chosen in the brain more likely it will be a pure spin zone and thus closer to a QCr. Thus a tiny volume of the brain can be treated as a small quantum computer and can work in isolation. But is that the way our brain works? As the selected volume increases the spins in neighboring areas would destroy the QCr character. This is where the bottleneck comes. The bigger the volume becomes closer it is to the imaging situation and that is the transition towards the imaging arena.

The progress in the NMR-QCr will add to further understanding of the quantum correlation imaging in the brain. May be the answer to the unknown question i.e. as to whether the human brain is a 'quantum computer or not' lies in the two complimentary directions of research. One thing is sure our brain does not take sequential messages as does the present day electronic computer. All the information received from different sensual organs of the body, e.g. eye, touch, etc., is processed simultaneously for an immediate reaction. Our brain is very vast in the distribution of the heterogeneity of the species of the spins. There are the varied metabolic concentrations over different regions of the brain. Also there are varied neuronal transmissions of the metabolic activities etc. In order to produce the human brain activities in the form of an image in real time is a formidable task. The proper interpretation of the image needs some threshold of the knowledge involved. It is not easy to treat all the diversities of the fields involved in a place like this. The shape of a simplified work like the present one is an oversimplified

version of the MRI of the brain. An approach is adopted here so as to make the work understandable by a much wider audience with little background in the PCM (physics, chemistry and mathematics) areas. The academic experience, knowledge etc. presented in this work however enables one to make a beginning in the right direction. The scope of this particular venture is not just restricted to the MRI of the brain. The authors want to create a base of knowledge about quantum correlations among nuclei and their use in exploring the brain science.

4.4 Multiple Quantum Coherences and Imaging

Over the last two decades or so physicists, chemists and mathematicians (PCMs) have enlightened the field of MRI to a stage much higher up. Simple diffusion of molecules within a particular voxel at a point more or less allows, all the spins in the molecules to come to a local equilibrium over a short period of time. This is as regards to their orientations around the static magnetic field applied along the z-direction. It characterizes the T_1 weighted image. But their projection in the transverse $x-y$ planes tries to pick up the results of asymmetric interactions with local environment which forms the basis of the T_2 weighted image. This is the conventional MRI. In between the application of the transverse RF pulses there is the simple field induction decay (FID) with a characteristic transverse relaxation time e.g. the T_2. The FIDs are weighted by anisotropic diffusion, blood flow (f-MRI) etc. to produce the structural and functional images. But the recent developments have taken the imaging technology a step further. Locally spins align themselves in an environment of chemical shift, scalar (J) coupling, and enhance quantum coherences among the neighbors. The use of quantum coherences among the molecules is the area of the quantum magnetic resonance imaging (QMRI). The distant spins within and outside the boundaries of a selected voxel for imaging produce locally on a selected spin a demagnetization field. The cut-off distance as to how far the distant spins affect locally is not so clearly manifested by the interactions. These cross-interactions created by the distant dipole magnets create quantum correlations for the spins. These correlations can be of zero quantum coherence (ZQC)-two spins antiparallel, double quantum coherence (DQC)-two spins parallel type and may be of even of higher orders (much larger number of spins with common a quantum order aligned together). To add further complications the brain actually has hetero-nuclear ensemble of spins.

A group of macro-molecules in the brain at a point would create a local quantum order of their own. They would allow collective quantum coherence transfer pathways (CTPs) for the energy and the information transfer. The coherences with the help of J (total angular momentum) couplings can be converted by the choice of suitable RF pulse sequence to the observable single quantum coherence (SQC) signals. Images based on multiple coherences as opposed to the diffusion weighted images would include the effects due to chemical changes, metabolite concentration variations, etc. This would be in space

and time. In these images contrast rather than high intensity is the aim. Variations on the scale of 1 μm (10^{-6} m) to 1 mm can be recorded. Thus a real time–space chemical change imaging diagnostics become possible. These advances have been presented through illustrations in this work with a minimum possible exposure to the mathematics involved. No effort is made to go into the mathematical phenomenology of the images. A simple visual exposure to new kind of images with physical concepts explained as is done in here can be very educational for the doctors and others. In MRI, recently the focus is on, how to produce an image which can provide additional information on the chemistry of events happening in a voxel. Learning QIS (quantum information science) can be very helpful part in learning about QMRI. One need not be an expert in quantum mechanics (QM) to learn the benefits of the use of NMR in imaging. One uses rotations, inversions, flipping, etc. of the spins to different angles on different planes to get as much information as possible about the environment in which the spins are interacting, and the quantum correlations among them.

4.5 The Matrix Concept: The Imaging of the Brain

4.5.1 The Single Spin-Identical Spins Ensemble: Fundamental Spin Representation

The experimental MRI involves the following basic steps. First is the excitation of the selected regions (voxels) in the brain containing a limited group of spins. It is done by a $90^{°}$ shaped (allows a band of frequencies to be picked up) pulses applied along the x-direction. This is to project the initially directed spins along the z-direction due to the static magnetic field applied along z-direction on to the x − y plane. In between $180^{°}$ pulse can be applied to reverse the direction of the spins to allow more time to decay and relax for the spin. The process helps to select or annul a specific kind of imaging e.g. the J-coupled imaging in preference to an another say the chemical shift imaging, etc. The J-coupling, will reveal the characteristics e.g. the local interactions i.e. the metabolic events etc. The whole brain voxel by voxel is then scanned to obtain whole brain imaging data. This is then converted into a whole brain image using a standard computer program. The diagnostics of the brain tumors through the MRI of the abnormal regions of the brain and comparing with the image that of a healthy person is then carried out. Achieving a quality in the diagnostics can be the most important factor for a clinical doctor. An appreciation of the basic phenomena involved which led to a tumor would naturally enhance the quality of diagnostics. The exposition for the reader through concepts and techniques which went into the production of the images would stimulate the curiosity to learn more and make the diagnostics a better one. As is said something comes out of something and nothing comes out of nothing. The something-MRI has come out of the minds of many dedicated

scientists, who have created the simple basic MRI machine. To learn about the quantification methods on which the imaging and consequently the diagnostics are based is a different matter.

   This work is not really the place to go into details of all the basics involved. One should refer to a standard text book on MRI, for details. An electron has a spin (magnetic moment) of $(1/2)\hbar$. This $(1/2)\hbar$ is the result of its intrinsic angular momentum associated with the electron. A single electron spin when polarized (oriented in one preferred direction say z) in a static magnetic field (along z) can occupy two energy states $+(1/2)\hbar$ (up state) and $(-1/2)\hbar$ (down state). In order to convert a particular spot in the brain into its observable signature in an image one measures the average magnetization (magnetic moments of the electrons, atoms and nuclei per unit volume) and its interaction to the applied RF field in a local region. The molecular interactions as electrical signals are collected over a short period of time and the average behavior, of the magnetic moments appears, as an output in the receiver. One needs to know about the variations in resultant intensity and the resolution in the image at a particular point in space and time. It depicts e.g. the chemical environment and various physical couplings of the coherences involved. There is need to relate the signal to some basic quantified event. This quantification is done through the use of matrix representation of the spins and their time evolution operations. Standard user friendly computer programs are available to make the matter simple for those who are interested to learn further.

4.5.2 Quantification of Image Intensity and Contrast: The Spin Matrices

We are familiar with vectors in the Cartesian, x, y, z space. In MRI the things area a bit different. In the spins world we have tiny (microscopic particles) magnets which are interacting with each other. The vast degrees of freedom which an ensemble of spins has needs to be broken down to the simplest i.e. the lowest possible level. This is the basis of the four 2×2 matrices called as Pauli's spin matrices. They create a space analogous to the familiar, x, y, z, t space, which is the normal Cartesian space. The matrices have their own set of rules to analyze in their operations and manipulations. It is known that it is much easier to handle wave-matter interaction phenomena through the use of the complex exponential function $e^{i\theta}$ rather than representing them as sine and cosine waves. One needs to refer to the area of complex trigonometry for details. It may simply be helpful here to explain the simple purpose of the complex number $i = \pm\sqrt{-1}$. One can represent a composite cosine and sine wave as an exponential, $e^{i\theta} = \cos\theta + i\sin\theta$. The, $e^{i\theta}$, exponential frequently appears, in the construction and manipulation of the wave phenomena, whether classical or quantum. The coherences of the spins which is used to produce the image can be analyzed in terms of their matrix representation. The phenomena of interference i.e. adding and subtracting of
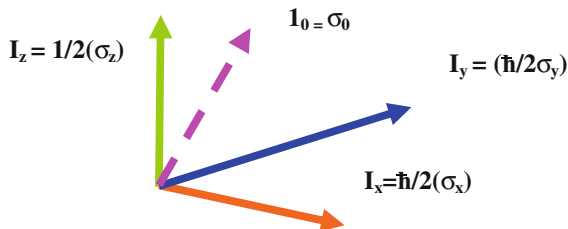
Fig. 4.1 There are four basic single-spin, Pauli-Spin Matrices. One can think for the sake of analogy like the Cartesian space (x, y, z, t) that there is a basis of the four lowest level matrix space spanned by the 2 × 2, σ_x, σ_y, σ_z, σ_0, matrices. The rest of the system is built on it. This is called as the Hilbert space. The next dimension would be of sixteen 4 × 4 matrices. Basically one can reduce, the larger number of higher order spins to effectively a two spins system. The matrix I_0 is called as the unitary matrix

waves becomes much easier to handle by the use of the function $e^{i\theta}$. Similar to the Cartesian basis the basis selected in QM is the basis of the 3, x, y, z spin-matrices and the fourth identity or the unit ($\sigma_0 = I$) matrix. Figure 4.1 is a pictorial representation of the matrices in space.

$$\sigma_x = \begin{pmatrix} 0 & 1 \\ 1 & 0 \end{pmatrix}; \ \sigma_y = \begin{pmatrix} 0 & -i \\ i & 0 \end{pmatrix}; \ \sigma_z \begin{pmatrix} 1 & 0 \\ 0 & -1 \end{pmatrix}; \ \sigma_0 = \begin{pmatrix} 1 & 0 \\ 0 & 1 \end{pmatrix}$$

The x, y, z matrices can be regarded as, the x, y, z components of a spin. The matrices have to be multiplied by the electron spin $\hbar/2$ for an absolute magnitude. In an experimental situation the projection of the spins (from the static z-direction) on to the x, y plane is performed by applying RF (oscillating) pulses in the x and or y-directions. The measurement is performed in the x, y-directions by the receiver for the induced (produced by the RF x, y-directed pulse) signal. It has the information about the behavior of the local spins. That is what produces the imaging by scanning in the x − y plane and taking planar slices in the z-direction. It thus helps to produce the three dimensional image. One should note that the y-matrix has a multiplier $i = \sqrt{-1}$ to the matrix. We should remember that the full spin space is of a much higher order. Like the Cartesian space (x, y, z, t) the spin space has its own fundamental rules of multiplication, division, etc. The quantity which one ultimately measures is the x − y component of the z-oriented magnetic moment per unit volume, M_z. It is given as $M_{x-y} = N_0\gamma\hbar (M_x + i M_y)$. M_x and M_y are the components in the x − y plane. Here γ is the gyromagnetic ratio, and N_0 is the average density of the spins in thermal equilibrium.

The two-valued ness ($\pm 1/2)\hbar$ of the electron spin S is due to its intrinsic angular momentum with rotation being viewed either clockwise or anticlockwise. Since the multiplicity is 2 one can associate an electron with the spectroscopic splitting factor, $g_s = 2$. Each one of the energy level is associated the spin as $(1/2)\hbar$. In the case of an atom the ratio of the orbital magnetic moment (μ_l) created by the orbital motion of electron, around the nucleus to the orbital angular momentum (L) has a

unique importance in MRI. This ratio is expressed as g_l ($\mu_b/\hbar$). The proportionality constant g_l (also called as the orbital spectroscopic splitting factor) is1 if there, is no spin S (due to the electron spin angular momentum around its own axis) and no orbit (L−S), interaction. Here μ_b is the fundamental unit, called as, the Bohr magneton, and $\mu_b = e\hbar/2m_e$, where m is the mass, e, the charge of the electron, and $\hbar$, the angular Planck's constant. For the electron spin alone, this proportionality factor g_s is 2.

The ratio, (μ_l/L) is called as the gyromagnetic ratio γ and $\gamma = 2$ for the electron spin alone. The electron spin has double the magnetism of orbital motion. For protons $\gamma \approx 5.58$ and the magnetic moment is $\mu_p = \gamma$ ($e\hbar/4m_p$) ≈ 2.79 nuclear magneton. Here m_p is proton mass and the nuclear magneton $=(e\hbar/4m_p)$. The simplest ensemble of spins is formed by single type of spins. It is the simplest possible case of single spins. It forms the most fundamental basis set. The ensemble of spins in the brain is a multi-nuclear one. One uses small voxels at a time for simplicity. The electron, atomic and nuclear spins all interact to produce a complex spectrum of events. But MRI has the capacity to sort all out using small steps at a time. The 2-spin formalism can be built from the one spin basis set. This will lead to the 4×4 matrices and there will be 16 different matrices (see Appendix B6). A heteronuclear ensemble like our brain has to be analyzed by handling large number of spins using a much higher order of matrices. A large matrix is very difficult to handle. But there is no reason to despair. One would realize that the various forms of interactions (chemical, J-, dipole–dipole, etc.) decompose the dimensionality to a much lower level. It is seen that it is possible to learn almost everything through the 2-spin formalism. Please see the Appendices B for a guide on the mathematical formalism.

Reference

1. Kaila, M., Kaila, R.: Quantum Magnetic Resonance Imaging Diagnostics of Human Brain Disorders http://www.Elsevier.com/book/kaila ISBN: 978-0-12-384711-9/2010

Chapter 5
The Density Matrix Concept

5.1 The Single Spin (Identical Spins Ensemble)

One naturally asks a question what is this density matrix and why do we need it. The answer is that the density matrix (DM) is a physical representation of an ensemble of atoms, molecules in a matrix format, whose elements tell us at any point in space and time what is the status of the spins and the spin system as a whole. In the absence of any external field the spins distribute themselves in a random manner in the brain. The net magnetism is thus zero. The magnitude of the magnetization (magnetic moment per unit volume) at any point in space and time is not constant in an ensemble like the brain. It is measured through the number of spins per unit volume N_0. One basically measures the susceptibility variation which is the same thing as the magnetization variation in space and time in the MRI mapping of the brain. The spin distribution overall can be assumed to be in equilibrium (though not uniform in space) in an ensemble like our brain. The equilibrium is due to the internal fields e.g. the magnetic fields of the nuclei, various metabolic activities etc.

In order to find about the behavior of the equilibrium and the associated activities (which basically what the MRI does) we first create a superficial equilibrium of our own by orienting all the spins (free and bound) along z-direction by a static magnetic field H_z. Then one uses RF radiation to interact with the ensemble i.e. the brain. In an ideal situation one would expect half of the population of spins would be along +z and the other half along –z direction. In a sense it is quite like tossing a coin and expecting that it would either be head or tail, since the probability for either (head or tail) is 1/2. But the real situation is quite different. There are many disturbances. We have temperature variations, spin interactions between electrons, atoms, etc., all over the brain. If you take a mole of the brain there are $\sim 10^{23}$ spins. But only a small fraction, **p**, of the 10^{23} spins will be oriented along the field. Let us say there is a uniform background distribution of spin density (the number of spins per unit volume) over the brain. For simplicity it

is convenient to call uniform density the background of spins as $\mathbf{N_0}$ and call the z-oriented ordered fractional concentration as $\mathbf{p}$.

One can write the value of the ordered population at a temperature T as, $\mathbf{p} = \mathbf{N_0}$ $\mathbf{(\hbar\gamma H_Z I_z)/(kT)}$. Here γ is the overall average gyromagnetic ratio (note there are many species of nuclei, n_i, in the brain; one should take into account some kind of average of γ as $\gamma = \Sigma_i\gamma_i/n_i$). The other parameters in $\mathbf{p}$ are, $\hbar =$ the Planck's constant, H_Z the static magnetic field, $k =$ the Boltzmann constant and $T =$ the temperature of the ensemble. It is more convenient to normalize $\mathbf{p}$ as a fraction between 0 and 1. So we take $N_0 = 1$ and remember that in the final result we have to multiply the result of $\mathbf{p}$ with $\mathbf{N_0}$ to get the absolute value of $\mathbf{p}$. The $\mathbf{p}$ thus just represents a fractional number i.e. the ratio of the magnetic spin energy ($\hbar\gamma H_z I_z$) with respect to the thermal energy kT. One can say $\mathbf{p}$ is the fraction of the spins contributing finally to the signal collected. I_z is the z-component of the spin with values $(1/2)\hbar$ and $(-1/2)\hbar$. The reason why the matrix of the spin ensemble is called as the density matrix is clear now.

It gives the density of the population of spins in the various energy states and their evolution in time. It is possible to separate spins into sub-systems (groups) of 1-spin, 2-spin etc., by using magnetic field gradients in space and time in the brain. The density matrix of an ensemble is an arrangement of coefficients (representing fractions of spins) as elements in the matrix structure format. In its the simplest form a single-type spin ensemble (identical spins) is represented by a 2×2 density matrix. In the next level up i.e. in a 2-spin system by a 4×4 density matrix and so on. The density matrix has information about the time evolution of the spins and can be broken down into components along the y-axis along which direction the signal is measured. Without the application of the z-field the diagonal elements of the matrix under equilibrium (static magnetic field) have a uniform population density representation in up and down states of the spins. The net magnetization is thus zero.

After application of the static magnetic field a preferred z-oriented redistribution takes place. There is an excess fractional population $\mathbf{p} = \mathbf{(\gamma\hbar H I_z)/kT}$ in the z-oriented state (Fig. 5.1). One can predict the behavior of spins through the process of breaking down the density matrix into a measurable configuration. In an experiment one applies RF pulses along x and y-directions to get the desired result. Theoretically this is achieved by applying rotational and time evolution operations to the density matrix. Usually one performs 90° angle rotations in a sequence to the density matrix. This methodology helps in designing experiments requiring suitable rotational and time evolution RF pulse sequences. One can use a computer simulation program predicting the configuration of the sequence of pulses required for a desired result. In this section below is summarized in a simple language (the matrix representation) of the NMR phenomena. This is done in the perspective of an ensemble of electrons, atoms, molecules and the artifacts which bind (the close system) them in a brain scenario. The simplification done is to make it easier for a reader to understand the terminologies of the matrix mechanics. It can be particularly helpful to those involved in the area of the clinical medicine, radiology, etc.
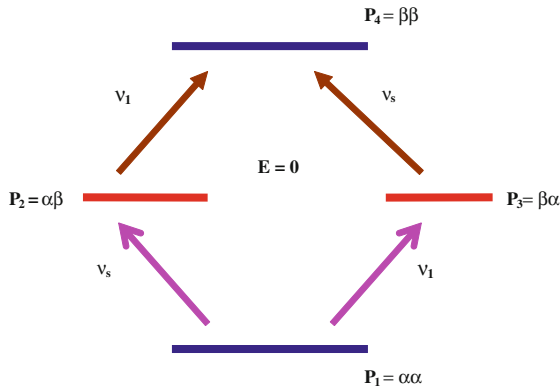
Fig. 5.1 A pictorial exposition of the density matrix of the 2-spin system (4 × 4 matrix). Here it is shown energy level diagram of a non-identical two α, β-Spin 1/2 System. The populations of the four levels are P_1, P_2, P_3, P_4 and are assumed to be all equal i.e., $p = N_0\hbar\gamma B/kT$. N_0 density of spins per mole, $\hbar$ Planck's constant, γ gyromagnetic ratio, H applied static magnetic field, k Boltzmann constant and T The temperature of the ensemble. The population of all the levels, p, is expressed wrt to P_2. It is taken as the reference level. Ideally without an external disturbance the population of all the levels should be equal, that is 1/4th of the total, 1. But on application of the static magnetic field, the population of P_1 is lowered by 1/4 and that of P_4 increased by the same amount, conserving the total population, as one

In a computer simulation packages now available the standard MRI technical terms involved simply act as input data into the computer program which basically can perform predictions about imaging in a specific situation. There is a need to quantify the diagnostics, of the cancerous chemical reactions that take place at a particular spot. This work will help familiarize the medical professionals about the various technical terms in common use in the field of MRI. Learning the basic quantum physics can be very rewarding. Just using an image as T_1 or T_2 weighted or J and chemical shit imaging is not enough. One need to understand the concepts involved behind the various technical terms in the various techniques of imaging. A good example of a technique is the COSY (correlation spectroscopy). There are many basic physics concepts involved in MRI. Avoiding understanding the concepts behind the techniques leads to a partially fulfilled progress of the field of MRI overall. It also leads to an under utilization of the vast ocean of intellectual abilities which all human being have. Participation by all kinds of professionals will make the field more professional and easily communicable to each other. A single spin system would give two energy states, and two spin system four energy states. In component (matrix) form the density matrix for 1-spin system can be written as (see Fig. 5.1).

$$\rho = 1/2 \begin{pmatrix} 1 + p/2 & 0 \\ 0 & 1 - p/2 \end{pmatrix} = 1/2 \begin{pmatrix} 1 & 0 \\ 0 & 1 \end{pmatrix} + (p)1/4 \begin{pmatrix} p & \\ & -p \end{pmatrix}$$

$$= p/4 \begin{pmatrix} 1 & 0 \\ 0 & -1 \end{pmatrix} = p/4(\sigma_z)$$

The first matrix in the addition is the identity matrix $\mathbf{1}$(or σ_0) and will not change in time evolution and is therefore discarded. One should note here that the diagonal elements in the final matrix add up to zero. You have to separate them out to measure otherwise the resultant signal received, would be zero. Experimentally separating spins for measurement is done by rotating (projecting) them on to the x-y plane by applying a 90° pulse. In between, the 180° pulses can be applied along the x-direction enabling reinforcement of the spins. This enables finally measurement in the y-direction due to the induced signal in the receiver coil. In a modeling situation one need to actually perform rotation and time evolution operations mathematically to work out an expected result. One can in effect utilize a prior knowledge of the density matrix in a particular situation creating a model image of the brain. This is done using an available standard computational program.

5.2 Two Spin System: The Density Matrix

The exposition in this work intends to simplify the knowledge about the spin dynamics involved in real time images. This work helps to the least to gather basic knowledge about the science behind and the technology involved in MRI. The study of non identical 2-spin case is considered as fundamental in understanding the more complex multinuclear systems. A sequence of RF excitation waves can be represented by the wave function ψ_i. The imaging process involves spins rotated through various angles, $\theta = \gamma H_1 t$. The symbol γ represents the gyromagnetic ratio. H_1 is the amplitude of the RF wave and t an instant of time. The phases φ of the incident waves can be chosen to be $\varphi = 0$ (along +x), $\pi/2$ (along +y), $3\pi/2$ (along –x), etc. These phases can be reinforced (repeated) to enhance certain kinds of coherences and eliminate others. One can draw an analogy of the matrices, to the components of a vector in a the Cartesian space. The sum of the interference of waves, in an echo experiment, can be written as, $\psi_i = \Sigma_{j,\,i}\, c_j^{*} c_i\, \psi_i$. Two symbols i and j are used to include various permutations of coupling between different degrees of freedom e.g. the chemical shift, j-coupling, etc. The, echo waves received, in MRI, would have the changes in the coefficients c_j's in time.

In the case of several spins the coefficients c_j's would have a structure of a single column matrix, with information from various interactions. One needs to form a new set of coefficients, c_j^{*}, from this set, which when is multiplied by this set, one by one, is orthogonal and orthonormal, to it. Those readers who do not have the mathematics background to understand this, suffices it may, to say that,

$\sum_{ij} C_i\, C_j^* = 1$ if i = j, (the orthogonal condition), = 0 (orthonormality condition).The coefficients C_i^*, thus constructed from C_i, form the so called, the Hermitian row matrix; the single row of components. The meaning of C_i^* is that it is Hermitian conjugate of C_i. Technically it is obtained by, changing rows into columns and columns into rows and, i into −i, and −i into i, in each element. One can write the vector representation of the magnetization in the z-direction, in the 2-spin case as

$$M_z = N_0\gamma\hbar[\text{row vectors } c_i^*, c_2^*, c_3^*, c_4^*].I_z.[\text{columnvectors } c_1, c_2, c_3, c_4]$$

In the case considered here $\mathbf{I_z}$ is the z-spin matrix for the 2-spins case, i.e. a 4×4 matrix. This matrix would have only 16 elements (rows and columns) in total. The result of the product of the above three matrices (from right to left, row by column) can be written as $M_z = (N_0\gamma\hbar\, I_z^{nn})\, C_n^* C_n$. Here $C_n^* C_n$ is defined as the density matrix, $\mathbf{I_z^{nn}}$. It is a square matrix of size 4×4, with 16 elements as I_z^{11}, I_z^{12}, $I_z^{13}\, I_z^{14}, I_z^{21}, I_z^{31},..I^{41}\, I_z^{44}$ etc. A 4×4 matrix would have four 2×2 blocks in it. There will be two diagonal and two reverse diagonal blocks. The 2×2 blocks matrices, within the 4×4 matrix, is the same as the fundamental 2×2 Pauli single-spin matrices. This approach of construction, allows to keep the 4×4 matrix orthogonalized and normalized. All the changes that occur in the system in time, as a result of the precession, relaxation, J-coupling, etc. are pursued through the density matrix. There is one to one correspondence between what evolves in the density matrix, in time, and what is observed, in the laboratory. The changes in the image can be predicted through the analysis of the density matrix by performing the operations of rotation, time evolution, etc. The advantage of the density matrix approach is that one can find the magnitude of a desired quantity i.e. the magnetization M_y at any instant of time.

One evaluates the trace relation $M_y = (N_0\gamma\hbar)\, [\text{Tr}\{(M_x + i\, M_y)\{\{\boldsymbol{\rho}\}]$ at any instant of time. Here the symbol Tr means the sum of the diagonal elements, of the product of the two matrices, $\{(M_x + iM_y)\}$ and $\boldsymbol{\rho}$, the density matrix. We are at a stage in the field of MRI today where all the algebra of one and two-spin matrices has actually been tabulated. The exposition in the present work creates just awareness as to what goes on behind the MRI scene. Computer modeling of the MRI of the brain familiarizes one, with the knowledge of the input data format required, for a particular computer program, to compare with the actual image obtained. The brain is a hetero-nuclear ensemble of atoms, nuclei, etc. This is what makes the MRI of the human brain, so difficult but, so intriguing at the same time. Higher order matrices can be broken down into smaller dimensions. This is done keeping in mind as to what type of imaging one is interested in i.e. J-coupling, multi-quantum coherence etc. The reader is referred to Appendices B, for details on dynamics of one spin and two spin systems, including some practical illustrations. One can find there, more about the rotation and time evolution operations and the density matrix. A summary of the mathematical steps included should be helpful to some readers.

Chapter 6
The Imaging

6.1 T_1 and T_2 Weighted Images

In the presence of an external static magnetic field H_0 say applied in the Z-direction the isolated non-interacting (no quantum correlation) spins will try to align themselves along the field. The spins do not stay stationary along the Z-direction. Instead they precess (rotate) randomly at a resonance frequency of ω_0 around the field H_0. Here $\omega_0 = \gamma\, H_0$, γ being the gyromagnetic ratio (GMR) $= (\mu_b/\hbar)$, $\hbar$ is the angular Planck's constant and μ_b is the fundamental dipole magnetic moment of an atom called as the Bohr magneton. The frequency ω_0 is referred to as the Larmor frequency. Now if an additional RF electromagnetic field say H_1 in the form of a pulse is applied along a perpendicular direction to H_0, say in the X-direction the angle of precession around the Z-direction of the spins acquires new angle $\alpha = (\gamma H_1\, \tau)$. This angle α is called as the flip angle and the time τ is called as the pulse time. This simplified picture is true if the applied RF signal has a single frequency and is in exact resonance with the natural frequency of vibration of a single spin i.e. the Larmor frequency. But the pulse has a bandwidth of frequencies Ω_i. Further a single spin is not in vacuum and is surrounded by many others of varied nuclear structure. The angle α should thus be $\alpha = (\Omega_i - \omega_0)\,\tau$, different angle for each frequency. In fact it should be $\alpha = (\Omega_i - \omega_0)\, T$, where T is the time when signal is measured and the time $T \gg \tau$. The response of the pulse is measured as a decay of the maximum amplitude with time. The rate of decay will be different in different directions. In the X–Z and Y–Z planes it is taken as T_1 and in X–Y plane it is T_2. The mapping of the anisotropic structure of T_1 and T_2 in different directions (X, Y, Z) leads to T_1 and T_2 weighted images.

6.2 The k (Wave Number)-Space Imaging

Once the scanning process is over, one has to convert the data obtained in the k (wave number) space to the real (x, y, z) space. The T_1 and T_2 weighting image, and many other methods, are commonly used techniques, in MRI. The spins have to be selected by their frequency band content, where there resonance frequency lies. Frequency content of each of the species of nuclei is different. The spectroscopic content of the different species in the X, Y, Z directions, can be measured. The frequency selection enables content resolution of the various species in the image. In order to depict sensitivity and resolution in an image one uses the Fourier Transform (FT) imaging technique. In this method one uses the spectrum collected, due to the response to a series of RF pulses of duration τ and, a time T in-between the pulses. Repeating τ and T one can collects data for different frequency bands of interest and over various intervals of time. One needs to reduce the total data collection time, and perform T_1 and T_2, measurements, and minimizes time of exposure to the patient.

A compromise between total time spent with the patient and the quality of image has to be found. The frequency Ω of precession of the spins around Z-axis in time space is related to its time period T_p as, $\Omega(t) = 2\pi/T_p$. One needs to transform what happens in the wave number k space, i.e. the space where all the data is collected, to the real space (Fig. 6.1) in the brain, i.e. the X, Y, Z, space where the events are actually happening. The real space is the space excited by the RF radiation i.e. the brain space. The k-space (Fig. 6.2) originates from wave number $k = 1/\lambda$, that is the reciprocal of the wavelength of the RF radiation. One normally uses, $k_\theta = 2\pi/\lambda$, k_θ being the angular wave number. The velocity of propagation of the RF radiation in vacuum (in the brain it will be reduced due to the medium present in the brain) is given as $c = f \lambda$. Here $f = \Omega(t)/2\pi$ and $\lambda = 2\pi/k_\theta$ are the linear frequency and the linear wavelength of the RF radiation.

The Fig. 6.1 gives a rough picture of how the k-space imaging is performed. The k-space is divided into fine intervals Δk_x and Δk_y. These intervals are part of the overall k-space. The RF radiation transforms the static equilibrium system of spins in the z-direction, into a dynamic equilibrium of spins, in the X–Y plane. The spins during their relaxation period, try to come back to their original equilibrium state. During this interval, they emit radiation, with signatures of the local region, under examination. This is what is recorded in the MRI machine. The Fourier Transform Technique (FTT) converts the response measured in k-space to an image in the brain space. This work is not really a place for going into details about the FTT. Some further helpful reading guide is included towards the end, in the list of references.

In the Fig. 6.2, $T_x = N\Delta t$ becomes the total time of scan in the voxel space, $\Delta x \Delta y$. This process is repeated for the whole plane X–Y, and subsequently again, for each next ΔZ, till the whole brain space is covered. It results in a total scan time of T. One should note that the k-space is basically the space of the RF radiation. By changing its frequency content, one is changing the extent of the k-space of
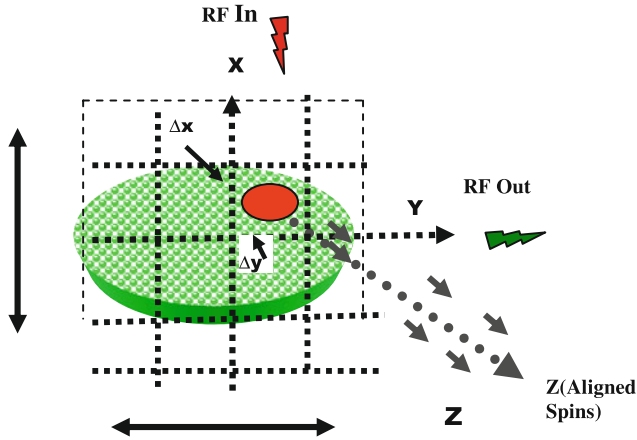
Fig. 6.1 The object is shown as an ellipses in the X–Y, plane in the brain. The k_x and k_y will be the coordinate axes in k-space (see Fig. 6.2) corresponding to the x and y in the real space. In the k-space, the signals received from the real space i.e. the brain space (x, y, z) are recorded by the sensor. In order to obtain an MRI picture, first a slice ΔZ thick, along the Z-direction is selected, by application of a magnetic field gradient in the Z-direction. Each Z-such slice will have information from an X, Y plane. The signals from each small interval Δx, Δy in the brain space, in a plane, X, Y are recorded by the sensor. By incrementing space, in Δx and Δy steps, each time, signals are recorded, through the RF pulse irradiation. The repetition of the procedure, along the whole z-direction, ultimately covers the whole brain, in three dimensions

The k-Space
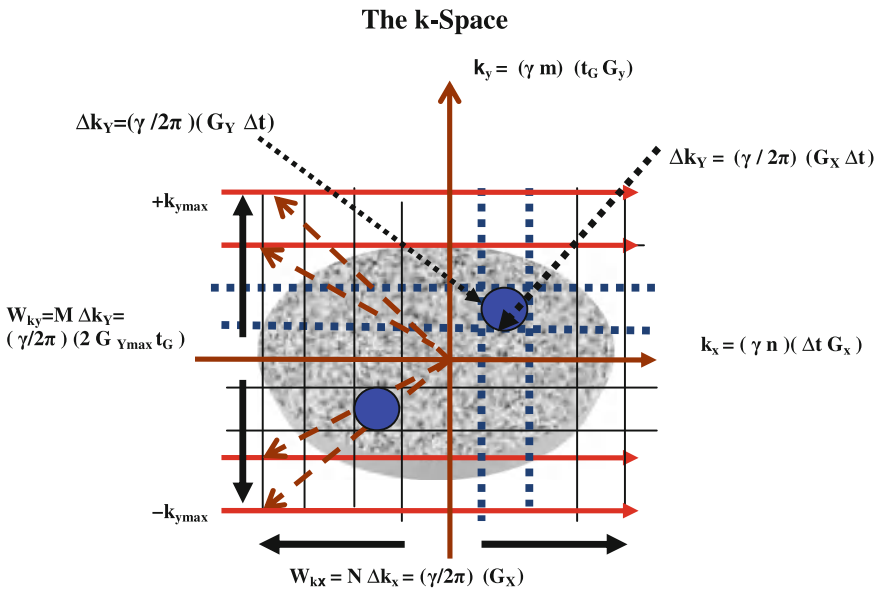
Fig. 6.2 The received echo signals are in small k-space intervals $\Delta k_x = (\gamma/2\pi)(G_X\Delta t)$ and $\Delta k_Y = (\gamma/2\pi)(G_Y t_G)$. The gradient field in the real space, in the X-direction and in the Y-direction, are increased in small equal steps. Steps in the y-direction, are m times, m = 1….M; M, being an integer. Similarly the steps in the x-direction, are n times, n = 1….N; N, being an integer. This will generate a matrix data of size M æ N. Normally M = N = 256 points

interest. One has to include all the possible precessional frequencies, corresponding to a selected voxel. The procedure is then repeated for the next voxel. The image of the brain is then created by use of a mathematical computer package, for the standard FTT. One should realize that in each new little time step, Δt, in the X-direction, the scan picks up a new group of frequencies $\Delta\omega_X = \omega_x - \omega_0 = (\Delta x)(\delta\omega/\delta x)$. Here $(\delta\omega/\delta x) = \gamma[\delta H_0/\delta x]$, H_0 being the static magnetic field applied along the Z-direction and γ is the gyromagnetic ratio (GMR). The gradient in the Y-direction adds to this, a band of frequencies $\Delta\omega_Y = \omega - \omega_0 = (\Delta y)(\delta\omega/\delta y)$. Here $(\delta\omega/\delta y) = \gamma[\delta H_0/\delta y]$. One should note that the GMR is not a constant, instead it varies from point to point in the brain space. The gradient fields applied in the X, Y, Z directions, allow various nuclear species, being detected and imaged.

6.3 Collection of Data in k-Space and Transforming it to Obtain Image in Real (x, y, z) Space

When M frequency-encoded FIDs (field induction decays) are obtained each one experiences a different value of the phase-encoding gradient amplitude. One obtains data for both positive and negative amplitudes. The signal for a slice in a normal to z-plane, i.e., the x–y plane, and recorded in time (frequency) space, can be written as.

$$S^m(t) = \left[\left(\int\limits_{-\infty}^{\infty}\int \rho(x, y)e^{-i\gamma(xG_xt + y_m{}^{mGyt})}\ dx\ dy\right)\right]e^{-i}\omega t$$

The data is converted into digital, brain space (x, y) data, as follows. The data acquired during frequency x-gradient activation are sampled. It is memorized in a matrix format. The size of the matrix is M æ N points. Here N is the number of samples along the reading gradient. M is the number of times the phase y-gradient is activated. If each FID is sampled and Δt is the sampling time interval, the demodulated signal would be as follows.

$$S^m(n, m) = \left[\int\limits_{-\infty}^{+\infty}\int \rho(x, y)\ e^{-i\gamma(xG_xn\Delta t + y_mGyt)}dx\ dy\right]$$
$$0 \leq n \leq N, - M/2 + 1 \leq m \leq M/2$$

One obtains a data matrix of M æ N points, usually a 256 æ 256 matrix. In reference to the Book Fig. 6.2, explanation through the following terms should be helpful. Δk_x, Δk_y = k-space interval steps sizes in the x, y directions; $W_{k, y}$ = the maximum frequencies that contain the object information; Δt = the readout sampling time interval T_x = the readout gradient time; Δy = the phase encoding

gradient step size G_{ymax} = the phase gradient maximum amplitude. In order to create MRI picture in real space one need to sample the two-dimensional k-space with sufficient density of Δk_x, Δk_y intervals over a specified extent W_{kx}, W_{ky}. The extent of the acquisition in k-space (also called as the Fourier space) makes the high spatial frequency content, and hence the spatial resolution. The spatial resolution Δx and Δy and the field of view (FOV) can be roughly defined as follows. $[FOV]_x = 1/\Delta k_x$; $\Delta x = [1/W_{kx}]$, $[FOV]_y = 1/\Delta k_y$; $\Delta y = 1/W_{ky}]$. The above simple mathematical relations pertain to a simple pulse sequence and a homogenous sample. In actual practice the mathematical analysis is more complex. The reader is referred to a standard text e.g. Ref. [1] listed at the end of this section. Under the general heading of MRI one would use lot of common features, based on RF pulse shapes and repetitions. There are lots of variations added, to the above simple pictorial representation, to produce a desired image.

One need to get familiar with, e.g., gradient echo, spin-echo, inversion recovery, data acquisition, image reconstruction velocity, etc. We comes across, a number of rapid imaging techniques, that could be grouped as, echo planar imaging (EPI), spiral imaging, parallel imaging, etc. It is important to note that the k-space sampling method may not be homogenous. It can include a partial k-space filling instead of full k-space filling. There is one feature that distinguishes all the imaging methods and that is, how quickly one can acquire data, for an image, and how easily the method can be extended, to generate higher spatial resolution. The simple method described above is rather slow (Book Fig. 6.2). Here only one line in k-space is acquired for each repetition time (TR). The EPI method is routinely used and is fast method. But it has a limited resolution. One would notice a single RF pulse is all that is needed to produce sufficient data for an image. This is called as single shot imaging technique. It is very popular in conventional functional MRI (fMRI). But there are limitations as to how fast the gradients can be changed and how good a resolution can be achieved.

Reference

1. Landini, L., Positano, V., Santarelli, M.F. (eds.): Advanced Image Processing in Magnetic Resonance Imaging. CRC Press, Taylor & Francis Group, FL., USA (2005)

Chapter 7
Future Horizons of the Brain Science

7.1 The Molecular Level Science of the Brain

MRI is a valuable tool to explore and understand the human brain science. It provides a scientist with a bundle of knowledge about the static and dynamic status of the brain. The information collected can be due to the collective echoes from a region on a mms to cms scale due to the incident RF radiation. There is a broadly referred to in MRI the technique of echo planar imaging (EPI). The technique analyzes echo signals received back by an RF receiver in space an time. In its simplest form it treats all the spins as identical. One collects the variant signals from the brain by virtue of the spins being present in a gradual change of their environment. The imaging with treatment of the spins as being identical is referred to as the single quantum magnetic resonance imaging (SQ-MRI). Recently NMR (nuclear magnetic resonance) has entered into the field of medical imaging. Over the years reference to MRI as single quantum MRI was dropped. It has been simply called as the MRI. In the last decade the discovery of the multi-quantum spin–spin interactions and their use in imaging, has changed the situation [1–26]. The imaging can be the result of quantum coherent interactions between individual macromolecules and also within the molecule itself. The heteronuclear atoms and molecules retain their individual identities due to their individual electronic orbits structure as well as their nuclear structure. The dynamics of the electrons around the nucleus and of the protons and the neutrons inside the nucleus is a quantum one. What it means is that when the atoms and molecules are excited by the RF radiation the electrons, protons and neutrons occupy only quantized higher energy states due to the absorbed extra energy. They interact quantum mechanically to create local coherence transfer pathways (CTPs) and present information in a coherent manner.

The atoms and molecules normally occupy the ground state when not irradiated. When irradiated they occupy the excited states. The states are the positions of their stable angular momentum by virtue of their rotational motion in the orbits. During the relaxation period in between the RF pulses on de-excitation of the atoms and

molecules the RF radiation emitted has the signatures of the events of the quantum interactions between the atoms and the molecules and the environment around them in space and time. This spin dynamics of the atoms and molecules will be on the scale of micrometers to mms dimension regions and will involve quantum physics and chemistry on the atomic and molecular levels. In order to analyze events on the quantum scale one need to know the mathematics of matrix mechanics and the associated spin dynamics (Appendices B). Spins cover multi-nuclear atoms and molecules. One need to learn application of the spins to the molecular dynamics in the brain. It basically needs a coverage within the science frame work of the quantum mechanics (QM). This however does not fall within the scope of this work. We need to learn systematic application of the QM to the brain science. It basically means the matrix mechanics (MM) approach of the QM, to the spin dynamics of the brain. Thus one need to get familiar with basic physics of the QM. A reader is referred to a standard text on QM for that purpose. In the Appendices B at the end of this work a summary in a descriptive manner is however presented. It should be helpful. It also provides a guidance for further reading.

Our brain is a complex chemical machine which uses metabolic, neurotransmission, etc events to control the moment to moment functions of the body. It is a formidable task, to have a simpler exposition for a wider audience of the quantum science involved. One need to learn the science of the atoms, molecules, nuclei in an ensemble like the human brain. MRI is safe to use and exploits the basic principles of quantum physics in imaging. In retrospective it provides an experimental evidence of the quantum science in action in the brain. This work encourages through a much simpler visual and textual presentation the readers like the clinical doctors, other medical professionals, e.g., the neurologists, radiologists, etc, to become continuous learners. It creates a new vision for them in the diagnostics of the brain disorders. Unfortunately it is not possible to take the aim of the exposition very far in a work like this. The effort has been kept, to only the level of the conceptual basis with explanations through pictures, diagrams, analogies, etc, as the procedure of education. Use of physics, chemistry and mathematic (PCM) knowledge required to quantify techniques, procedures, results, etc. has been kept to minimum. It can be quite a difficult task to quantify brain science without exposing the basics of the quantum physics. MRI allows us to find out the overall picture of the events happening in the brain. It may be a very useful to some with specialization directions in which they work. The common platform, of different professionals, thinking alike, is not easy to create, in an exposition like the one in this work. But it does bring the difficult problem to a step closer to the establishment of a solution.

It is not easy for an individual to be a neurologist and understand the physics of neuroscience at the same time. Even a physicist who may have intense training in QM may need help in the use of a suitable computer mathematical package to unravel the mysteries of the brain science. The computer packages available are based on, e.g. Mathematica, Matlab, etc, programs, to solve complex quantum matrix equations. The need for interdependence is natural in today's vast scientific world. Specializations advance by continuous education in a broader perspective. All the humans are born thinkers in their own imaginary world. But the common

scientific efforts bring them close to a common practical thinking. The technologies like the MRI do create a common platform for the scientific professionals to advance themselves and work together. But to improve the mental health system on an organized scale deeper research and development efforts and better education and understanding, of the field of neuroscience is required. It is right to say that science advances technology and technology advances science. Sometimes when you are exposed to a visual picture of a scientific advancement, even if, exposed as a piece of art, it may induce in you, a new thinking, in a new creative scientific horizon. This may result in a new direction one had not imagined before. In other instances when you are trying to imagine in your brain how to build something new to be able to put into practice a visual exposure can trigger the means to implement an appropriate machine. This may be something un-achievable otherwise. Nature has done its job in running life on earth marvelously well, for millions of years. We can help maintain it to a decent level by finding out how the nature works. Nature does not take permission from the humans to evolve. It is controlled by the science of evolution of the cooperative (coherent) behavior of the atoms and molecules. Why a molecule e.g. water, is a more stable structure than, the hydrogen molecule?

7.2 Quantum Horizons of the Brain

7.2.1 Multi-Quantum Coherence in MR, FADU Tumor (A Primary Hypopharyngeal Tumor Grade 4)

It is routinely required in NMR to separate signal of a desired metabolite from the overlapping ones which may not be very important in a specific imaging task. A new class of filters called as the multi-quantum coherence (MQC) filters recently are under development [21] world wide. They use magnetic field gradients to excite by frequency selection (Sel-MQC) of a particular molecule of interest and suppress others e.g. molecules of water. A typical case is in an extracranial tissue; the Lac (lactate) CH_3 resonance (1.33 ppm) is filtered from the overlapping methylene groups of mobile lipids. In order to image a cancerous part of a tissue one needs to perform localization of the tumor in the x, y, z space by the MRI technology. We perform two separate experiments. One is the classical spin echo-chemical shift imaging (SE-CSI) and the other is the quantum SE (spin echo)-GRAD (magnetic field gradient) experiment. The Sel-MQC editing performs its function to edit the Lac resonance and image its distribution in the tumor. The frequency selective refocusing of the Lac CH_3 causes the signal to be unaffected by the j-modulation (used in classical MRI). The classical SE (spin echo)-CSI (chemical; shift imaging) mapping has a higher sensitivity. This can be maintained during Sel-MQC imaging. One can add a read magnetic field gradient (Sel-MQC edited metabolite) for spatial acceleration (acquisition time-T_{AQ}) in the imaging process. Measurement of the apparent (effective value due to various in

homogeneities) T_2 relaxation time after the MQC filtering can be used to quantify the edited metabolite. It can also be used to characterize different tissues.

7.2.2 Sodium (Na) Double Quantum Filter: Spinal Disc Degeneration

It is seen that Na-NMR spectroscopy provides a useful technique [21] to understand the degenerative state of the inter-vertebral disc tissue. The spinal disc is composed of two regions. The outer ligamentous and the fibrocartilaginous regions. They are referred to as annulus fibrosus. The inner gelatinous region is called as the nucleus pulposus. The disc tissue is primarily composed of proteoglycan aggrecan, collagen I and II fibrils and the water. Sodium ions are an integral component of the disc matrix. They are present to balance the negative charge on the sulfated glycosaminoglucan chains of the proteoglycans. The sodium concentration within a healthy disc is around 335 mM. It is more than twice as high as in the extracellular fluid. Aging and degeneration are accompanied by the loss of proteoglycan. This leads to a diminished ability of the disc to maintain hydration under load, and retain sodium ions. A local asymmetric sodium ion distribution, can present an electric quadrupole (four poles) behavior, in addition to the normal, familiar dipole magnet character, found as e.g., in an hydrogen atom. The none uniform distribution of the charge concentration, of the Na^+ ions, in a region, due to, a tissue deformity, lead to an electric quadrupole-magnetic dipole interaction, for the Na charge distribution. This is in addition to the normal magnetic dipole spectrum. In the presence, of the static magnetic field H_z, the spin of the sodium atom, will exhibit four energy states, corresponding to the 4 possible magnetic spin values, it can have. These four projected values in the static magnetic field are, $S_z = -3/2, -1/2, +1/2, +3/2$. The DQFMA (double quantum filter magnetic anisotropy) spectroscopy of sodium ions in the disc degenerated environment, can reveal basic information about, the biophysical and bio-chemical structure of, the damaged tissue.

When a sample in vivo is exposed to an RF radiation with a suitable chosen bandwidth the spins will evolve with a characteristic build up time (τ, along X-axis, see Fig. 7.1). This is controlled by the quadrupole coupling constant C_Q. The signal components will decay with different relaxation times T_2. Figure 7.1 [21] is an illustration of a DQF (double quantum filter) spectra, line shapes and intensities, resulting from non-vanishing quadrupole couplings. It is seen in experiment that there are at least three discrete type of environments or compartments in the spinal disc. These are, one isotropic, and two anisotropic, contributing to the sodium lineshapes. These compartments show different dynamic behavior of the sodium ions, characterized by C_Q and T_{2f} (fast) and T_{2S} (slow) characteristic transverse relaxation times.

The diffraction of waves due to X-rays, electrons, photons, neutrons, etc are well known phenomena. Studies of crystal structures by X-ray diffraction,
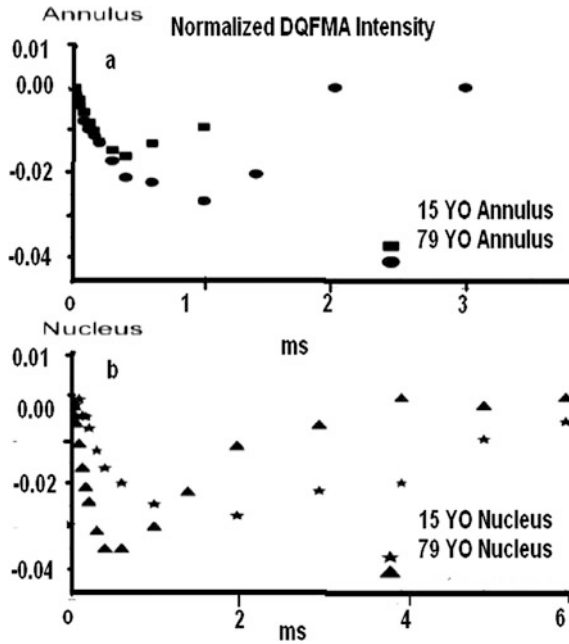
Fig. 7.1 The signal intensity at the center of the Na DQFMA spectra as a function of τ (X-axis) value. The normalized intensities are given as the fraction of the signal intensity compared to the single-pulse experiment. Legends: X-axis/Build up time (τ). **a** Y-axis: Double Quantum Filter Magnetic Anisotropy (DQMFMA) Intensity. X-axis: τ (ms). Examples: 15 Year Old Annulus, 70 Year Old Annulus **a** Example: Double Quantum Filter Magnetic Anisotropy (DQFMA), Intensity, X-axis: τ (ms);15 Year Old Nucleus; 70 Year Old Nucleus **b**

biological structures by electron microscope, etc, are clearly visible world wide, as commercial enterprises, created by the science of waves. These techniques, make use of, the diffraction of waves, from some kind of regularity, or periodicity, in the structure of the lattice, of a crystal, molecule, etc.

The brain is a complex system, with no periodic spatial order having a mixture of soft tissues, fluids, free chemical radicals, etc, etc, and are not static, but in fact, are performing coordinated actions in time. On the small spatial scale, there is some order, between hetero-nuclear interactions and the interaction with the environment, in which they are present. On the global space scale, in the brain on the other hand there is little, spatial periodic order but there is temporal order the secrets of which are not fully known. The temporal order, in activities from different regions of the brain is what MRI is trying to figure out. At the moment it rather makes use of them to produce a simple image. The brain and therefore the body without temporal order could not function as a wholesome structure controlling various functions of the body. That is where the MRI performs its miracle. The MRI converts the not so apparent spatial order in the brain into a reasonably good periodic structure of its own, in time–space. This virtual order is sometimes refereed to as phase space. One

can collect the signals arriving from a chaotic space in the brain in some form of ordered data, in k-space. One should remember we create a spatial order of our own (means the MIR clinical examination) in the brain by applying a fairly strong static magnet field. The field is applied along a chosen direction called as the z-direction. This is the order of the magnetic spins of the atoms and molecules trying to align themselves along the applied static magnetic field.

The atoms and molecules both static and mobile which form an integral part of the functioning tissues, fluids, etc, provide the dipole magnets which become the pawns, to create the required manipulation for an image. In multi-quantum, inter-molecular coherence imaging (MQ-iMCI) we are trying to make so to say the diffraction science of waves to work for us in the brain situation but in an indirect manner. The waves used in this instance are the radio waves. Firstly we create a static order on the spins present in our brain by the static magnetic field applied. This creates an order locally as well as globally. The local order will modulate the global order. The spins though aligned along the direction of the applied static magnetic field in fact precess around the field at a frequency characteristic of the electronic structure of the atoms and molecules in which they are present. This precessional frequency of the spins (dipole magnets), in the MRI literature is called as the Larmor frequency. The RF radiation is applied in a perpendicular direction, to the static magnetic field say the x- direction to a small volume called as voxel. It excites the spins to higher energy states. The spins are part of the local bunch of atoms and molecules, being in higher energy states create situation for multi-quantum coherences. On de-excitation the out coming signal in the y-direction in a way represents diffracted RF by the created order of the spins. This is the so called, diffracted beam, of the RF radiation. It contains information about the temporal coherence (events happening together) locally. On the global scale image of the brain the local events will act as a local modulation. This clever science of the collection of the invisible information about the events happening in the brain may seem miracle for some. In fact it is a simple matter of converting intuition and curiosity into a practical outcome with no danger (non-invasive) to the body.

One can say that the brain is a chaotic mixture of atoms, molecules, fluids, etc doing haphazard and random things. But deep down it is not. Brain has an inbuilt local static magnetic field of 1 Tesla, on atomic and molecular scale (nano meter to micron). It is strong enough to create a local order of its own. This order will be in interaction with a similar neighboring order and so on all over the brain. But the coherence gets weaker and weaker as the volume selected becomes larger and larger. Detection of these weaker signals is what QMRI is about. QMRI will have information at the atomic and molecular level. This way the contrast in the image produced will get better. The image will then reveal the quantum chemistry of events happening in the brain. This means the QMRI is like getting close to the knitty gritty of the brain. In other words we are getting close to the wonders of the nature. One can say the closer we are to the nature the closer we can get, to the understanding of the nature's forces, keeping the life on earth going. Thus, increasing literacy about science in the society is the key to the survival of the mankind. In order to translate the QMRI science into a commercial enterprise one

needs to really quantify all aspects of the QMRI. This can be done by the well established discipline of the QM.

This written work in its scope does not really go that far. But brief exposures as in this work may be helpful. Suppose there is an ensemble of a gas of ions, positive and negative in a container. It is referred to as plasma in the physics world. Now one applies a combination of DC (direct current) and AC (alternating current) magnetic field to the ensemble. One sees some kind of periodic order created among the ions of the gas. This order is in the shape of a helix like structure and is periodic (sinusoidal) in spatial character. A typical example where this kind of structure can be seen is a plasma nuclear reactor trying to convert fusion energy of nuclei into useful heat energy. Plasma gas is a familiar phenomena in stars. Stars (e.g. our Sun) are, a plasma state of gaseous ions. But there the large gravity effect due to the large collective mass of ions keeps them together despite the interacting charges and the electrical currents and magnetic fields present. That is not what is happening, in our brain. Gravitational forces are of little significance in the brain. But one must remember laws of physics are universal in their nature whether it is gaseous medium, liquid or semisolid semi-fluid structure we have in the brain. It is only a matter of reinventing them in an environment of one's choice, e.g. here we are interested in the brain.

One applies magnetic field gradients to the created ordered spins, in the brain. Gradient basically means magnetic filed is not constant in a region instead it increases or decreases linearly in any one direction, among the x, y, z directions. The gradient magnetic fields produce a focused directional force on the molecules and a helix like order in a chosen direction on the spins. One can make the spins vibrate for the sake of imaging. On making the magnetic field gradient oscillate say between +x and −x directions will apply force in the shape of periodic pulses on the molecules. This will naturally make spins to create echo like electrical signals. A gradient can be made frequency selective over a narrow bandwidth. This way one can choose a desired group of nuclei of different species for a desired action. The product $\gamma H_z = \Delta\omega$, provides the much desired band of frequencies to choose from the static order though the characteristic gyromagnetic ratio γ of the nuclei. One applies magnetic field gradients $G_{x,\,y,\,z}$ along the three orthogonal (x, y, z) directions of the order of mT/m (milli Tesla per meter). The, magnetic field, gradients applied as pulses of duration T to the brain lead to the creation of a three dimensional tunable dynamic (space and time) periodic helix like structure overall.

The adjustable pitch or the period of the helix is given as $d = [2\pi/(\gamma GT)]$. In three dimensions it becomes a virtue of the sort of tunable diffraction of the RF radiation, applied to the brain. This artificially created magnetic helix periodic structure among the spins is the source of much desired but indirectly created diffraction for the RF radiation. The frequency band $\Delta\omega$ created by H_z, can be fine tuned to a small chosen group of nuclei through their γ values and the coherence distance d. Normally diffraction means bending of waves around objects of the size of the wavelength of the radiation. We can not do that in the brain. The molecules will vibrate with the energy received and lead to over heating locally. That would be a disaster. It is not the MRI-diffraction scenario for imaging here.

The molecules here go to the higher orbital quantum state with the energy absorbed and in a microsecond come back to the ground state where they were before with no energy left in the system. In a way the brain is a 100 % efficient machine but in a temporal world. Repetition in a local real physical space can create the un-required heating. The clever MRI does not do that. Also here is a limit on the scan time. There are safety radiological standards in place to be observed. In MRI RF radiation excites locally a group of atoms and molecules and the group reradiates back as a modulated radiation.

The meaning of diffraction here is a bit more complex. The static magnetic field creates superficially a z-directed periodic line-like mesh of spins. This can be divided into finer three dimensional frequency band series of periodic boxes in time space by the field gradients. On the other hand the pitch of the helix like structure created in the brain can be fine tuned to the local internal structure of the brain by adjusting the strength of the magnetic field gradient G and or the duration of the gradient field pulse T. The meaning of the multi-quantum coherences is now taking some shape. It is linked to the coherence distance between groups of atoms and molecules. The coherence means how these groups act together towards a required result. It can be a metabolic activity to perform a certain function of the brain. If there is spherical symmetry in the local structure in a localized region then there is identical diffusion of spins in all directions resulting in no intensity variation in the region as a group. This is neutralization i.e. cancellation of the spins happening on a micron scale in a local region. One should realize that the distribution of local internal magnetic field created by the local nuclei and that of the spins and modulated by the external static magnetic is not uniform throughout. Some distant dipole-atomic magnets will try to demagnetize a local dipole. This is called as the distant dipole–dipole interaction. This induced local magnetic field from a distant spin is called as the distant dipole field (DDF).

The DDF interaction can extend from 1 μm (10^{-6} m) to a mm. In quantum coherence imaging (QMI) these distant spin interactions form the source of imaging. The two spin (oppositely directed) dipolar interactions i.e. the iZQC (intermolecular zero quantum coherence) and the two spin (pointing in the same direction) iDQC (intermolecular double quantum coherence) have repeatedly appeared in the recent MRI literature. The application of higher orders e.g. triple quantum is fast emerging in MQMRI. The demagnetization time τ_d due to one spin on the other can be roughly expressed as $\tau_d \sim [(1/(\gamma\mu_0 M_0)]$. Here μ_0 is the vacuum magnetic permeability of the medium and M_0 is the static magnetization (magnetic moment per unit volume) produced by the applied static magnetic field. τ_d is approximately 250 ms for pure water at the human physiological temperature of 310K. Figure 7.2 [14] is given as an illustration, how the design of a suitable structure of the sequence of pulses can be used to produce the multi-quantum coherences in QMRI. The area of the gradient pulses can be changed in the ratio nGT:1, to create multi (n)-quantum coherences.
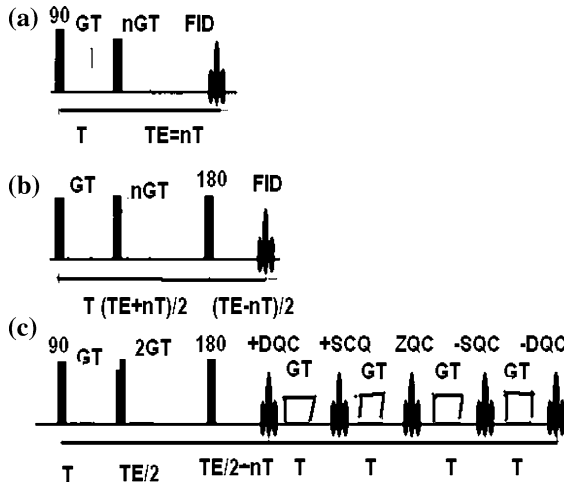
Fig. 7.2 Sequences for acquiring iMQC signal. **a** Original n-quantum CRAZED (correlation spectroscopy revamped by asymmetric z-gradient echo detection) sequence. The 1: n gradient pulse ratio saves coherences that evolve as n-quantum during the time T, and +1-quantum during TE. This echoes any inhomogeneous broadening at TE = nT. The optimum value of TE for maximum signal is approximately T_2 (the transverse relaxation time), but this implies that the delay T should be long enough for the n-quantum coherences to undergo significant dephasing. **b** Addition of a 180 pulse during TE allows TE $\sim T_2$ and T $\ll T_2$, which enhances the signal. Note that the echo appears $n\tau$ early (for a positive n). **c** The MultiCRAZED (multiple correlation spectroscopy revamped by asymmetric z-gradient echo detection) sequence takes advantage of the difference in echo timing to acquire multiple echoes, at full intensity. The +SQC (+1 or single-quantum coherence) and -SQC images have primarily conventional contrast; the +DQC (+2-quantum), ZQC (zero-quantum) and -DQC (-2-quantum) coherences have contrast from sub-voxel variations, in the magnetization density or resonance frequency

7.2.3 Double Quantum Coherence

It is well known that diffusion weighted imaging (DWI) plays a very vital role in the field of brain science and diagnostic of brain disorders. In biological tissues diffusion may be more accelerated in one direction than the other. In cerebral tissues white matter contains fibrous components where diffusion of water molecules across fibers is much more restricted than along the fibers. Thus the diffusion becomes anisotropic. It means that the diffusion coefficient is dependent on the direction of the applied field gradient. This leads to the technique of diffusion tensor imaging. One can use residual intermolecular dipole couplings between distant spins. It gives rise to double and zero quantum coherences [24]. This is created in the brain by using a correlation magnetic field gradient with amplitude that breaks down the magnetic isotropy of a local region in the brain. So the intrinsic dipole–dipole interactions give rise to a refocusing in a sample. The intensity encountered in DQC is much smaller than in SQC (single quantum
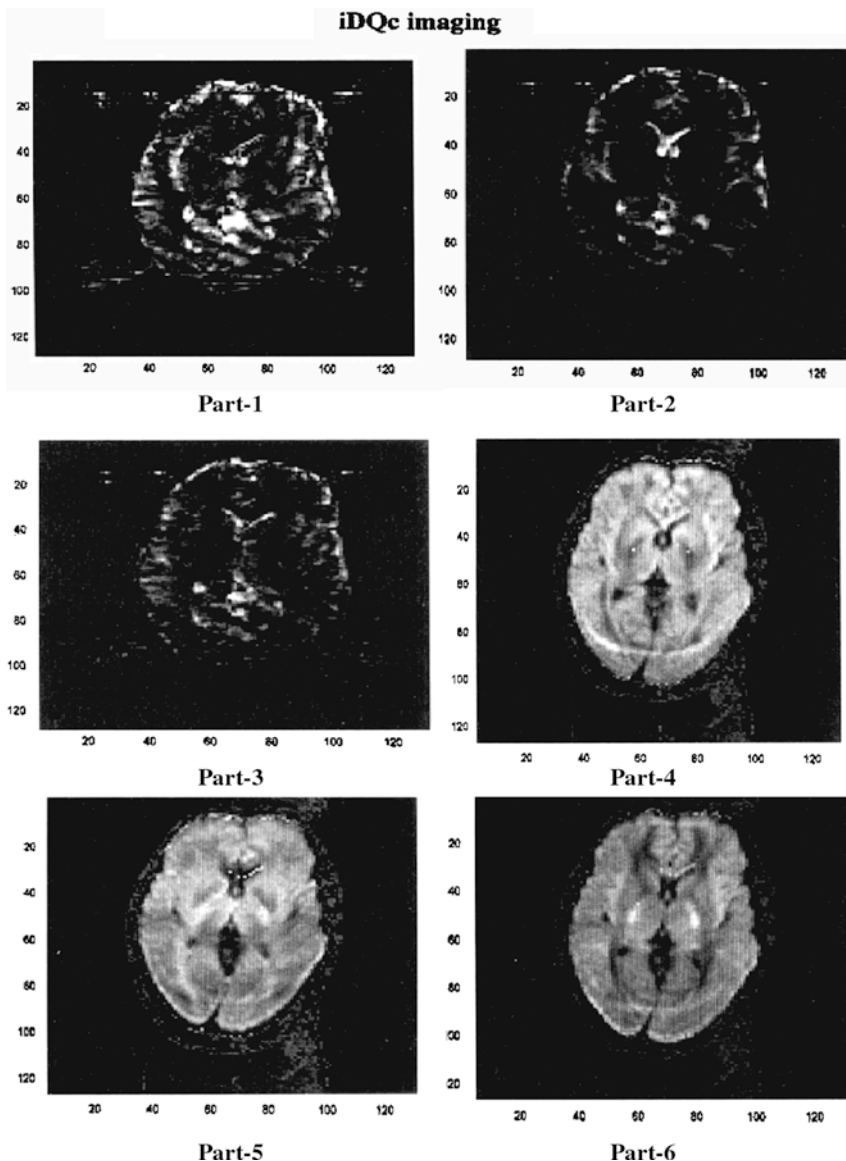
Fig. 7.3 iDQC and diffusion weighted images obtained at a particular correlation gradient and a diffusion gradient respectively along x. y, z directions. The correlation distance was selected equal to 140 µm. One should note that there is a little discernible difference in the pictures within the same kind i.e., the iDQC or the DWI, along X, Y, Z direction. But there is drastic difference between the two types. The quantum imaging technology is not yet advanced enough to bring out the differences, to a visible extent when one makes an overall broader (global brain) presentation. Gradient Z-direction/iDQC imaging, Gradient X-direction/iDQC imaging, Gradient Y-direction/iDQC imaging, gradient Z direction/diffusion weighted imaging, gradient X direction/diffusion weighted imaging, gradient Y direction/diffusion weighted imaging

coherence and ZQC (zero quantum coherence). These lower order coherences therefore have to be eliminated. Suitable phase cycling techniques are chosen to achieve this. The correlation distance between distant d_c between spins can be chosen by using suitable magnitude of the magnetic field gradient and the time during which the gradient pulse is applied. The illustration in Fig. 7.3 [24] shows a comparison of the technique of the diffusion gradient and the quantum correlation gradient. The gradient is shown along the x, y, z directions chosen in the Fig. 7.3.

The iDQC images show a different contrast with respect to the conventional DWI. One finds that iDQC signal varies with magnetic filed correlation gradient. The DWI is the result of apparent diffusion coefficient (ADC), presenting a perspective vision of much larger structure thus poorer contrast. iDQC on the other hand is controlled by the residual dipolar interaction on a molecular level allowing to work out the actual quantum chemistry of events happening in the region. In an approximate manner one can write the fine tuned magnetization M produced over the selected volume as $M \sim \gamma \hbar (N/V)[2\, \tau_d /(t_2 \Delta_s)]$. Here N = the number of spins in volume V, τ_d = the demagnetization time = $1/(\gamma\, \mu_0\, M_0)$, γ = the gyromagnetic ratio, μ_0 = the magnetic permeability in vacuum, M_0 = the magnetization (magnetic moment per unit volume) in equilibrium (in the static magnetic field), Δ_s = the direction of the applied magnetic field gradient wrt (with respect to) to the static magnetic field H_z., t_2 = the delay time between the second 90° RF pulse and the refocusing time of the signal. In the iDQC images the lateral ventricles are clearly delineated as are the subarachnoid spaces. Varying the spatial direction of the correlation gradients results in different visualizations of micro-brain structures including the internal capsule genu and splenium of the corpus and the optic nerves. Below are the practical illustrations.

7.2.4 Zero Quantum Coherence

It is now well known that an initial RF pulse (with flip angle say $\alpha = 90^{\circ}$) can create two-spin intermolecular double-quantum coherences (iDQC) and the zero quantum coherences (iZQC) [25] as well as the conventionally one-spin one-quantum coherences and even the higher order coherences. A strong magnetic correlation gradient eliminates all but the iZQCs. During the delay τ_{zq} after the first pulse the iZQCs terms evolve at the difference between the resonance off-sets (reflecting magnetic field or susceptibility differences over that distance) of the two spins say i and j. A second slice selective RF pulse of variable flip angle β ($\pi/4$, $3\pi4$) is applied after the delay τ_{zq}. The approximate relation for the magnetization produced for the ZQC can be written as $M_{ZQ} \sim M_0\, \Delta_s\, \beta\, (TE/\tau_d)$; Δ_s = direction of the gradient field wrt (with respect to) the main static field along the z-direction, = $[3\, (s.z)^2 - 1]/2$, τ_d = the delay time = $(\gamma\, \mu_0\, M_0)^{-1}$; M_0 = the magnetization at a point due to the static field; γ = the gyromagnetic ratio; μ_0 = magnetic permeability in vacuum.
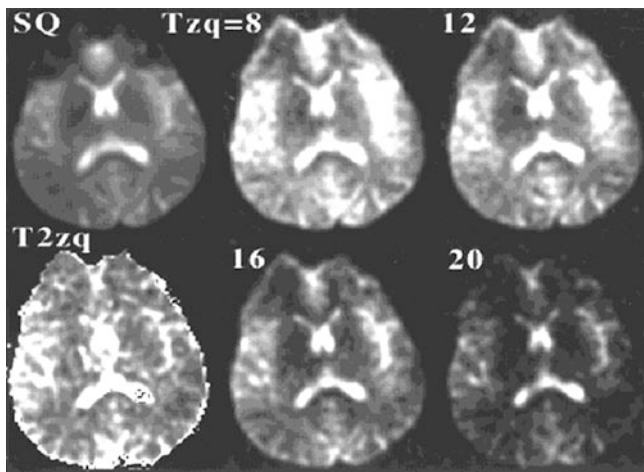
Fig. 7.4 Conventional spin-echo EPI image (*top left*) is compared to four different iZQC images using spin-echo EPI (*right*). The iZQC intensity and contrast are different from any conventional image, particularly in regions with large susceptibility variations. For short values of τ_{zq}, the iZQC has a magnetization squared weighting. The figure at the bottom left shows a "map" of iZQC relaxation times by pixel (white, 60 ms, black, 10 ms). Other imaging parameters include FOV = 24 × 24 cm, matrix size 128 × 64, slice thickness of 10 mm, TE 60 ms, and TR = 4 s

Single quantum coherences (SQCs) generated by the first pulse are completely dephased by the correlation gradient and are undetectable. It is now known that intermolecular multi-quantum coherence signals come primarily from spins separated by a distance d = $\pi/\gamma GT$—half a cycle of the magnetization helix, generated by the correlation gradient. This distance, d, is dictated by the strength of the correlation gradient and is much smaller than a conventional voxel size. Thus as opposed to conventional imaging where the spin signal is a simple direct average of the signal from all the spins in voxel iZQC imaging reflects subvoxel structure. Thus the image contrast is affected by the local susceptibility variations rather than by the macroscopic static field inhomogeneity. It is thus possible to develop clinically useful imaging protocols in an early diagnostics of brain tumors, by iZQC (see Fig. 7.4 [25]).

7.2.5 Selective Multi-Quantum Coherence Imaging Using Chemical Shift Imaging Sequence: Clinically Detected Lactate Methyl Resonance

Lactate is the product of anaerobic glucose metabolism. Normally it is only produced in small quantities in vivo in limited cell types under certain conditions. But in many disease states and under certain physiological conditions increased lactate
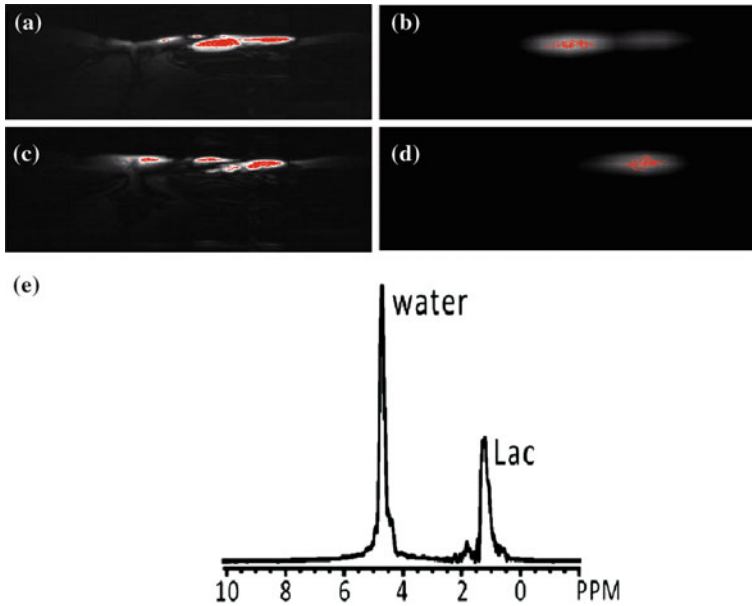
Fig. 7.5 HDMD (Hadamard slice selection technique)- Sel-MQC (selective multiple-quantum coherence)-CSI (chemical shift imaging) lactate images from an NHL patient. **a, c:** T_2-weighted (conventional MRI) images; **b** and **d** are the corresponding HDMD Sel-MQC-CSI lactate images from a 34-year-old female, diffuse large B cell, non-Hodgkin's lymphoma patient, with a tumor in the inguinal node, of the upper right thigh. In the T_2-weighted axial images **a, c** two nodes of 25 mm × 25 mm × 40 mm and 20 mm × 15 mm × 35 mm were observed. The two slice lactate images **b, d** match well with the slices from T_2-weighted images. **e** A magnitude spectrum from a voxel of tumor in **b**. The peak centered at 1.3 ppm is considered to be lactate (Lac, with minimal lipid contamination), with residual water (4.7 ppm) included. This water can be completely removed by adding WET pre-pulses, but has not been large enough to cause errors due to receiver saturation

is observed. The selective homo-nuclear multi-quantum coherence (MQC) technique [18] offers a new method for distinguishing lipid and lactate resonances. Lactate production is enhanced in mitochondrial diseases especially in the brain and the muscle. It is seen in vivo there is a difficulty in separating the overlapping Ch$_3$ resonance of lipids from the methyl resonance of the lactate at 1.3 ppm. The DQ (double quantum)-ZQ (zero quantum) transition produces echo, which is relatively insensitive to motion and is faster in acquisition and is used in this technique. In this methodology it is possible to track lactate response for treatment. One can by MQC imaging and spectroscopy correlate lactate with response to therapy in NHL (Non-Hodgkin' Lymphomas) patients. Figure 7.5 [18] is a practical illustration of the usefulness of this new technique.
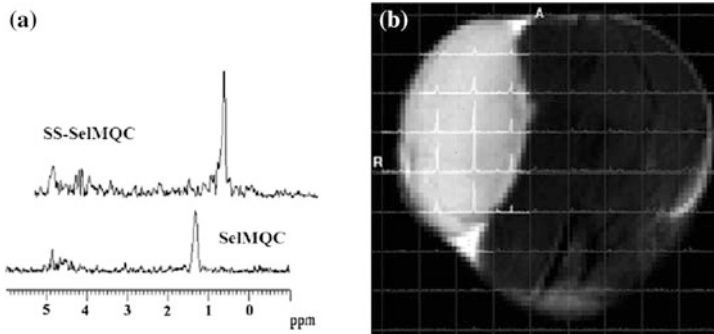
Fig. 7.6 a Stacked plot of experimental 1D localized 1H (proton) lactate spectrum obtained from in vivo R3327-AT tumor (volume = 857 mm^3) using SS-Sel-MQC and Sel-MQC. **b** 2D Lactate CSI from sagittal 5 mm thick slice using SS-Sel-MQC. CSI data is overlaid on T$_2$-contrast MR image. Chemical shift scale displayed over the tumor is between 2.5–0.5 ppm. Measured line widths of Lac signal were 27 Hz, 25 Hz using Sel-MQC and SS-Sel-MQC sequences. Number of scans = 8, TR = 2 s, and total acquisition time 1 h 15 min

7.2.6 Spectroscopic Lactate to Lipid Signal Enhancement: Spectral Selective (SS)-Elective MQ (Multi-Quantum) Coherences (SS-Sel MQC)-Dunning R3327-AT Prostate Cancer Cells

It is observed that the detection of lactate in a tumor tissue as a potential biomarker is difficult due to the presence of the co-resonating lipids. We know that PMRS (proton magnetic resonance spectroscopy) can be used for biochemical measure of the metabolism. This can be used to distinguish healthy tissue from tumor tissue. It can then be correlated to metabolic abnormalities. The tumors are known to be hetero-genious. The multi-voxel MRSI (magnetic resonance spectroscopic imaging) is a routine tool to investigate therapy response [18]. It provides guidance to optimization to individual treatment. It can be based on various metabolic levels or concentrations in a voxel. This may be used in significance towards an aggressive tumor. Lactate (Lac) reflects elevated tumor glycosis and or poor tissue perfusion. Lac is the end product of glycolysis and the methyl resonance peak is typically a doublet situated at 1.3 ppm. In the conventional imaging techniques such as PRESS (point resolved spectroscopy) and STEAM (stimulated echo acquisition mode) it is very difficult to isolate Lac from Lipids. The spectral editing techniques such as spin-echo (SE) difference spectroscopy and multi-quantum (MQ) coherence are seen as better alternatives. The J-difference spectroscopy detects Lac quite well but Lipids cause artifacts resulting from subject motion. MQ filters eliminate these kind of disturbance by a single-shot acquisition. But the MQ coherences exhibit signal contamination from residual lipid MQ coherences. The Sel-MQC technique avoids excitation of lipid MQ coherences. But residual lipid
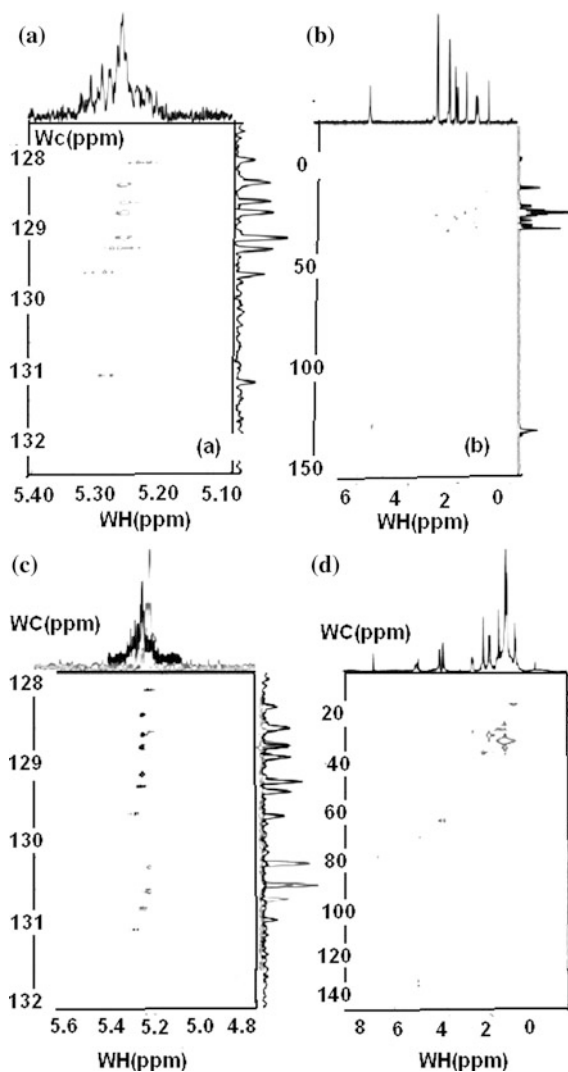
Fig. 7.7 a Selective HSQC (hetero-nuclear single-quantum coherence) spectrum of arachidonic acid showing the eight ^{13}C resonances clearly resolved. **b** The corresponding conventional HSQC spectrum collected with the sequence of pulse used. It shows the limited resolution of the diagnostic, vinyl resonances, which are not resolved. **c** An overlay of individually collected spectra of the fatty acids, oleic, linoleic, linolenic and arachidonic, showing that, even in a mixture, at least one or two resonances can be identified as belonging to a particular fatty acid. Spectra such as these would be expected from biological samples containing mixtures of such compounds. **d** A conventional HSQC spectrum of a liver extract sample showing limited resolution of the target metabolites but that the ^{13}C resonance from the methine group of the glycerol backbone resonates, well away from the vinyl resonances of fatty acids, and is thus not detected in the final spectrum

resonances is still a problem. The SS-Sel-MQC technique using Lac detection in non-localized and slice-localization versions with complete removal of lipid and water resonances is a step further. Figure 7.6 [18] presents an illustration of the application of the technique.

7.2.7 Single-Quantum Coherence Spectroscopy, Alteration in Fatty Acyl Group Composition-Unsaturated Fatty Acidic: Association with Brain Cancer

It is now known that in oncology one deals with specific markers characterizing tumor-genesis [22]. As an example choline phospholipids metabolism is implicated in the brain cancer. The fatty acid species, each contain unsaturated bonds (a vinyl moiety) but can be difficult to isolate by NMR. This is because the chemical environment of the vinyl groups in these molecules are similar. Studies have shown that the concentration of compounds containing one or more double bonds is significantly increased in a cancerous situation. It is seen by taking ratio of the area under the bis-allyl and vinyl peaks it is possible to see a shift towards fewer double bonds, with age and tumor genesis. But there is a limitation in disseminating species from the vinyl resonances (~ 5.3 ppm). One can in this situation use selective spectroscopy combined with in-line digital processing of the free induction decay (FID). This can be restricted to a narrow, selective bandwidth of spins. It leads to increased spectral resolution.

The vinyl group can be treated as a simple two coupled I (^{13}C), S (^{1}H), spin system. In this circumstance a suitable hetero-nuclear single quantum coherence (HSQC) pulse sequence becomes a useful tool.

This requires a proton detection experiment. It includes an INPET (initial insensitive nuclei enhanced polarization transfer) period for polarization transfer from ^{1}H(proton) to ^{13}C. This is followed by a back-transfer via inverse INEPT.

The larger chemical-shift range of the ^{13}C resonance allows a collection of spectra with increased resolution. But there is a disadvantage. There is low natural abundance of ^{13}C isotopes (~ 1 %) and it also has low gyromagnetic ratio. It contributes to poor detection sensitivity. But this is compensated by the fact that signals from ^{1}H are detected with HSQC spectroscopy. In HSQC spectroscopy, the INEPT transfer requires the inversion of the attached spins. This is to refocus the scalar coupling evolution. When inverting spins, it is useful to achieve high sensitivity, across an effective spectral bandwidth. High sensitivity can be produced, without affecting resonance, outside a chosen spectral bandwidth. Also a rotation can be achieved adiabatically in the true sense. It contributes to the robustness of the technique. In case a sensitivity enhancement is not used, a coherence selective gradient, can be applied. This is done immediately after the t_1 (first pulse) evolution. The decoding gradient is then applied immediately after the last pulse in the sequence. The resonance frequency of ^{13}C of the vinyl group is ~ 9640 Hz. The

proton frequency is ∼1974 Hz. It is found that the fatty acid moieties are expected to arise from side chains of the glycol backbone of the phospholipid found in cellular membrane and intra-stitial and inter-stitial fluid of the cells. Below is practical illustration of the new development (Fig. 7.7).

References

1. Mellon, E.A., Lee, S.-C., Pickup, S., kim, S., Goldstein, S.C., Floyd, T.F., Poptani, H., E.J., Delikatny, Reddy, R., Glickson, J. D.: Detection of lactate with a hadamard slice selected, selective multiple quantum coherence, chemical shift imaging sequence (hdmd-sel-csi) on a clinical mri scanner: application to tumors and muscle. Magn. Reson. Med. **62**, 1404–1413 (2009)

2. Zhong, J., Chen, Z., Kwok, E.: In vivo intermolecular double-quantum imaging on a clinical 1.5 t scanner. Magn. Reson. Med. **43**, 335, (2000)

3. Jensen, J.E., Frederick, B.deB., Renshaw, P. F.: Grey and white matter GABA level differences in the human brain using two-dimensional, J-resolved spectroscopic imaging. NMR Biomed. **18**, 570 (2005)

4. Juan, C.-J., Chen, C.-Y., Liu, Y.-J., Chung, H.-W., Chin, S.-C., Hsueh, C.-J., Chu, H., Zimmerman, R.A.: Acute putaminal necrosis and white matter demyelination in a child with subnormal copper Metabolism in Wilson D: MR imaging and spectroscopic findings, Neuroradiology, **47**, 401–405 (2005)

5. Richter, W., Richter, M., Warren, W.S., Merkle, H., Andersen, P., Adriany, G., Ugurbil, K.: Functional magnetic resonance imaging with intermolecular mutiple-quantum Coherences. Mangn. Reson. Im. **18**, 489 (2000)

6. Hämäläinen, M., Hari, R., llmoniemi, R. J., Knuutila, J., Lounasmaa O.V.: Magneto encephalography-theory, instrumentation, and applications to non-invasive studies of the working human Brain, Rev. Mod. Phys. **65**, 413 (1993)

7. Tabrizi, S.J., Langbehn, D.R., Leavitt, B.R., Roos, R.A.C., Durr, A., Craufurd, D., Kennard, C., Hicks, S.L., Fox, N.C., Scahill, R.I., Borowsky, B., Tobin, A.J., Diana Rosas, H., Johnson, H., Reilmann, R., Landwehrmeyer, B., Stout J.C.: Biological and clinical manifestations of Huntington's disease in the longitudinal TRACK-HD study: cross-sectional analysis of baseline data, Lancet. Neurol. **8**, 791–801 (2009)

8. Fleysher, L., Oesingmann, N., Stoeckel, B., Grossman, R.I., Inglese, M.: Sodium Long-component T2* Mapping in Human Brain at 7 Tesla, Magn. Reson. Med. **62**, 1338–1341 (2009)

9. Tamura, H., Kurihara, N., Machida, Y., Nishino, A., Shimosegawa, E.: How does water diffusion in human white matter change following ischemic stroke, Magn. Reson. Med. Sci. **8**, 121–134 (2009)

10. LaVerde, G., Nemoto, E., Jungreis, G.A., Tanase, C., Boada F.E.: Serial triple quantum sodium MRI during non-human primate focal brain ischemia. Magn. Reson. Med. **57**, 201–205 (2007)

11. Nakane, T., Nihashi, T., Kaewl, H., Naganawa, S.: Visualization of neuromelanin in the substantia nigra and locus ceruleus at 1.5T Using a 3D-gradient echo sequence with magnetiztion Transfer Contrast. Magn. Reson. Med. Sci. **7**, 205–210 (2008)

12. Melkus, G., Morchel, P., Behr, V.C., Kotas, M., Flentje, M., Jakob, P.M.: Sensitive J-coupled Metabolite Mapping Using Sel-MQC With Selective Multi-Spin-Echo Readout. Magn. Reson. Med. **62**, 880–887 (2009)

13. Chin, C.-L., Tang, X.i., Bouchard, L.S., Saha, P.K., Warren, W.S., Wehrli F.W., Isolating quantum coherences in structural imaging using intermolecular double quantum coherences. J. Magn. Reson. **165**, 309 (2003)

14. Tang, X., Ong, H., Shannon, K., Warren, W.S.: Simultaneous acquisition of multiple orders of intermolecular multiple-quantum coherence images, Magn. Reson. Im. **21**, 1141–1149 (2003)

15. Tang, X.-P., Chin, C.L., Bouchard, L. S., Wehrli, F. W., Warren, W.S.: Observing Bragg-like diffraction via multiple coupled nuclear spins, Phys. Lett. A, **326**, 114 (2004)

16. Liu, S., Gonen, O., Fleysher, R., Fleysher, L., Babb, J.S., Soher, B.J., Joo, C.-G., Ratai, E.-M., Gonzalez R. G.: Metabolite proton T2 mapping in the healthy Rhesus Macaque brain. Magn. Reosn. Med. **62**, 1292–1299 (2009)

17. Eric Jensen, J., Licata, S.C., öngür, D., Friedman, S.D., Prescot, A.P., Henry, M.E., Renshaw, P.F.: Quantification of J-resolved proton spectra in two-dimensions with LCModel using GAMMA-simulated basis sets at 4 Tesla, NMR Biomed. **22**, 762–769 (2009)

18. Tahkur, S. B., Yalingar, J., Koutcher, J. A.: In vivo lactate signal enhancement using binomial spectral-selective pulses in selective MQ coherence (SS-SelMQC) spectroscopy, Magn. Reson. Med. **62**, 591–598 (2009)

19. Lewis, I.A., Schommer , S.C., Markley, J.L.: γ NMR: open source software for identifying and quantifying metabolites in NMR spectra, Magn. Reson. Chem. **47**, S123 (2009)

20. Kirsch, S., Bachert, P.: Visualization of the distant dipolar field: a numerical study, Concpts. Mag. Reson. **34**A, 357–364 (2009)

21. Ooms, K.J., canella, M., vega, A.J., Marcolongo, M., Polenova, T.: The application of 23Na double-quantum Filter (DQF) NMR spectroscopy for the study of spinal disc degeneration, Magn. Reson. Med. **60**, 246–252 (2008)

22. Tesiram, Y.A., Saunders, D., Rheal A.: Towner. chemical specification by selective heteronucler single-quantum coherence spectroscopy: determination of double-bond quantity in unsaturated fatty acid compounds, NMR Biomed. **21**, 345–346 (2008)

23. Cho, J.-H., Ahn, S., Lee, C., Hong, K.S., Chung, K.c., Chang, S.-K., Cheong, C., Warren, W.S.: Magnetic resonance microscopic imaging based on high-order intermolecular multiple-quantum coherences, Magn. Reosn. Im. **25**, 626–633 (2007)

24. Fasano, F., Capuani, S., Hagberg, G.E., Branca, T., Indovina, I. Castriota-Scanderberg, A., Maraviglia, B.: Intermolecular double quantum coherences (iDQc) and diffusion weighted imaging (DWI) of the human brain at 1.5 T, Magn. Reson. Im. **21**, 1151–1157 (2003)

25. Rizi, R.R., Ahn, S., Alsop, D.C., Roe, S.G., Mescher, M., Richter, W., Schnnall, M.D., Leigh, J.S., Warren W.S.: Intermolecular zero-quantum coherence imaging of the human brain, Magn. Reson. Med. **43**, 627–632 (2000)

26. Bodenhausen, G., Kogler, H., Ernst, R.R.: Selection of coherence transfer pathways in NMR pulse experiments, J. Magn. Reson. **58**, 370 (1984)

Chapter 8
Summary and Conclusion

Is our brain a coordinated spin (tiny molecular magnet)-ensemble, quantum computer? Answer to this question lies in the fact as to how much do we know about the physics, chemistry and mathematics (PCM) that is happening in our brain. MRI does provide some clues to this aspect of our brain. As one goes to smaller and smaller (sub-voxel) volumes (micron to nm scale) of the brain i.e. approaching molecular quantum science in the brain we are in fact trying to get an answer to the question. MRI picture of the brain at Sub-voxel level can be predicted using the quantum mathematics of the spins (e.g. ^{B}H, ^{31}P, ^{13}C, etc. nuclei) in a real ensemble like our brain. This has been and being done to get multi-quantum coherence images in MRI. Where MRI becomes quantum computing rather than just imaging is the place where one can visualize design of a quantum computer in the laboratory situation. MRI liquid state technology provides a chance to make a quantum computer at room temperature. This is in contrast to the solid-state technology where milli Kelvin (10^{-3} K) order of temperatures are being used to achieve the same. Those readers who are interested in learning details of the spin dynamics happening in our brain using the spin density matrix approach have the option in pursuing their interest through the preliminary spin matrix basics presented in the appendices, B, at the end of the first part of the book.

The quantum science (QS) of the brain needs to be developed right from the grass roots. It would be an ideal thing to build it as a formal source of learning for medical professionals. The newly emerging QMRI (muti-quantum magnetic resonance imaging) technology is based on QS. It is not easy to present that kind of knowledge via a work like this. What this work has done is, that it has made a beginning. It is hoped that later this will be followed by a more comprehensive work. It would be worth taking up the venture of writing a text book in this field at the undergraduate level and even at the secondary level of education. This would require tremendous amount of time and resources at one's disposal. It is not easy to obtain that unfortunately in the present state of environment of the science. The status of science and opportunities to participate in the research and development in the field of QMRI and neuroscience is very limited for scientists at large. It is available only at limited number of places in the world and to limited number of people, unfortunately. Availability of wider research participation in the field is

only a part of the problem. Transmission of the newly emerging knowledge by research, to a wider community is very crucial and quicker the better. This aspect is not easy to fulfill. As the gap between the known and the unknown, keeps on becoming wider the chance of catching up becomes even slower.

The spread of the basic science education right from the secondary and later at tertiary level remains on decline. It further exacerbates the problem. One should note that the ability to learn the quantum science (QS) is easy to create when started at an early level of education. Learning about quantum science is no more difficult than any other area of basic education e.g. physics, mathematics and chemistry (PCM). It is only a matter of starting early. One can learn QS without going through detailed treatment, based on complex differential equations. Learning QS through quantum algebra, as an alternative approach, is available. Formal courses and text books are widely in circulation. They need simplification which is not difficult to achieve. One should realize that it is no more difficult learning quantum algebra than the classical algebra, already taught at the schools. It is a matter of introducing QS in the secondary school and then pursuing it earnestly at the tertiary level of education like any other discipline of science.

Learning QS is important for the future generations. It is intimately connected to the science of life. This awareness is missing in the present system of education in science world wide. As Newtonian Mechanics (NM) is the science of the dynamics of large rigid bodies QS is the science of the dynamics of the atoms and molecules. The large bodies e.g. the planets are in equilibrium and their dynamics is controlled through gravitational forces. On the other the plant and animal life has a confined ensemble of atoms and molecules performing function of day to day life. A typical example is the human body. Our body functions through quantum science. A young mind would certainly be curious to find out how his or her body works. It would be wise to introduce human physiology as part of science curriculum at the school level as soon as possible. Learning about one's own body is no burden on young minds. Who wouldn't want to? Learning about quantum algebra is as easy as learning about the numerology. Here the numbers are replaced by matrices. Matrices have their own rules of addition, multiplication, division, etc.

The elements of the matrices are functions representing some activity in the brain, in space and time. Computer mathematical softwares are now available to handle operation of matrices. In the present day of computers being available in every household it is time to raise the intellectual level of individual minds to a higher level the level of quantum science. The Chaps. 1 and 2 in this work were devoted to the simple basics of the reasons behind diamagnetism generated in an ensemble like our brain constituting electrons, atoms, macromolecules, tissues, fluids, etc. When the atoms and molecules are in free space there is no magnetic interaction between them. When they are brought together in a confined space then interactions between them is natural. Nature has evolved the molecular structure the way it is in our brain over millions of years and is to perform routine functions of life. The interaction between atomic and molecules is through their basic intrinsic diamagnetic character. This is basically the result of the angular momentum associated with the atoms and molecules. The angular momentum

associated with the electrons is represented by the mathematical symbol **S** and that of the atoms and molecules by the symbol L. Even protons and neutrons inside the nucleus contribute angular momentum of their own. When the molecules are close to each other they add and subtract their angular momentum with certain allowed quantum values, as J = L ± S. They can not arbitrarily take up any values. They have to observe the laws of conservation of angular momentum.

The resultant angular momentum **J** obviously describes the chemical interaction between molecules. In conventional techniques of the MRI one uses larger scale dynamic (chemical) interactions between neighboring molecules as the source of imaging. It is referred to as chemical shift imaging (CSI). The distant spins (including as part of macro-molecules) can also produce a local interaction for a single or a group of spins. This distant dipole field (DDF) produces more intricate results. This is like producing a fine structure at a point. This becomes the source of quantum coherence imaging referred to as the QMRI. Chap. 3 included in this work illustrated practical observations from clinical medicine and research and development efforts in progress in the MRI. One can see in the Chap. 3 a comparison between the achievements based on conventional MRI and the MQMRI. Recent achievements reported in research and development in MRI have been simplified in expression in this work. We have translated them into a simpler language of science making it understandable by a much wider scientific community. This is to make it useful for medical professionals to comprehend the real physical and chemical events happening, at a spot in the picture produced by MRI. Q (multi) MRI will provide a doctor more than just what the technology of MRI picture shows. Q(multi) MRI knowledge will equip a professional to see a tumor at early stages rather than waiting till a clear abnormal spot appears in the picture. Chaps. 4 and 5, covered some preliminary information on the quantum algebra of QMRI and its relevance to the various interactions between molecules. It is worth finding out as to how it becomes the source of imaging. Chap. 6 covered the basic concepts of the k-space imaging and the Chap. 7 presented some practical illustration in QMRI.

Appendices A and B at the end have been provided for the readers to see the connection between properties of spins and their representations as matrices, for quantitative estimates, of desired results. The simplest basis of 4, 2×2 matrices, for a single spins, is no different than having ten digits 0–9. In digits world multiplying on orders of ten one gets 10, 100, 10 000, etc. The numbers are just numbers, but matrices represent more than just numbers. The rules of matrix operations involve, rotation, inversion, evolution of spins in time, etc. For a learner in medical profession, computer packages are now available, with little effort required to learn about the algebra of the matrices. The matrices are just symbolic representation of the operations to be performed on spins to get a desired result. One need not learn manually, how to use them. User friendly computer programs can be created for the medical professionals without having to learn the details.

After the RF radiation is used to excite the spins they are allowed to relax to their equilibrium position. Their relaxation characteristics are monitored through the two main relaxation times i.e. T_1 (spin–lattice relaxation) and T_2 (spin–spin

relaxation). T_1 and T_2 weightings are among the many sources of the techniques, used in imaging, in space and time in conventional MRI. In the conventional MRI, the T_1 and T_2 are treated as if the spins are relaxing in space in longitudinal (X–Z, Y–Z space) and transverse (X–Y) space respectively, but in a much broader perspective. The atomic and molecular intricacies do not form part of the image. The Q(multi) MRI takes the spin relaxation to a whole new dimension. Here quantum correlations between molecules, becomes the source of relaxations of spins, which is very discrete i.e. quantum in character. The record of events happening not only at ms (10^{-3}), but to μs (10^{-6}) and even smaller level, thus become possible. This is as if getting close to the transition time of the energy levels of the molecules, and to the metabolism, neurro-transmission, etc. In the real pictorial depiction of the MRI, one should realize that the information received in the sensor has originated from the real space Δx, Δy, in the brain. But the receiver senses it in the wave number, Δk_x, Δk_y space.

The wave number k space is simply constructed from the inverse of the wavelength λ, of the RF radiation. The wave number k is related to the wavelength as, $k = 1/\lambda$. While the relaxation is in progress, the sensor samples the RF radiation information, in small steps of time, and k. Chap. 6 was included to help the reader, through pictures and diagrams, to get simple explanation of the technique of the k-space imaging. An incident RF signal has a specific amplitude and a bandwidth in its frequency content. The signal on return (echo signal) from a small area in the brain, contains modulated signal, with information on resonance frequency, from a group of molecules and the amplitude, also gets modulated. This information is in terms of the wave number k and the frequency ω. The amplitude variation is converted into intensity variation over real space and ultimately forms the k-basis of the image produced. At a point in space the signal intensity would depend upon tissue parameters, such as spin density ρ, relaxation time times T_1 and T_2, the scanner parameters such as echo time (TE), repetition time TR, etc. The spin density function $\rho(x, y)$ is basically an unknown parameter, and varies over space in the x–y plane, in the brain. This can be indirectly worked out from the received data in k-space.

The k-space scanning in its simplest form can be done by choosing a line from lowest $-k_x$, incrementing it by Δk_y in the y-direction, and repeating along the next k_x line, till the maximum, up to $+k_x$ is exhausted (refer Chap. 6 for details). This process of going along all the k_x lines, and incrementing steps, along y, till one has exhausted all the lines from $-k_x$ to $+k_x$, is very time consuming. The k-imaging technique has been illustrated in this work, as merely a conceptual educational exposure, about the k-space imaging. Better techniques have been developed over the last two decades. Figures 6.1 and 6.2 in Chap. 6, presented a simple pictorial depiction of the steps involved in k-space imaging. This k-space technique is the most fundamental one and is used in the echo planning imaging (EPI) technology. In order to have a more detailed exposure, the reader is referred to the Ref. [1]. Over the decades lots of variations of the technique of imaging have been developed. One such technique is the spiral k-space imaging, instead of the rectangular one, discussed in Chap. 6. Now there is a new trend in the imaging

area. In a new approach the effort is, not to make use of, the full k-space and instead use it partially. The partial space is created by using only part of real x–y space. One example in this direction is the parallel imaging. In this case a series of sensors with variable sensitivity to the received radiation, in space, are used, as compensation for the missing k-space. This helps to increase the speed, as well as the contrast, of the imaging. Appendix A is added, in this work, in particular, for those readers who would like to know more about, the basic physics concepts, involved in MRI.

One can in advance predict through available mathematical techniques, computer programs, etc., the details about the information, which can be collected, by the receiver, and relate it to what is inside the brain. This is the area of computer simulation in MRI. It is based on the already well developed formalism of quantum science or to be more specific, the quantum mechanics (QM). QM handles, QS (quantum science) by the 'density matrix' and the 'product operator' mathematical formalism. Only a very brief exposure is provided here to the QS involved. For details the reader is provided with references for further reading. Appendix B, in particular, is added, to lay out the basics, of the spin dynamics involved, in MRI. Detailed mathematical treatment would be out of place for a work like this. This would not interest the medical professionals particularly. But there are 'computer software packages' available through which one can perform computer simulations without knowing the detailed formal mathematics involved.

Before closing the authors would like to remind the reader that nature likes order. The order may be complex. Nevertheless it is an order. Without order the universe can not function. If the humans could. find as to how and why that order exists there may be no need to live in misconceptions and ignorance. Human brain has gone through million of years of evolution. The brain is most advanced and highly functional in humans among the animal kingdom. In its own language the nature created a perfect scientific machine. The MRI machine is not able to fully unscramble the intricate scientific order nature has created, in our brain. New development in MRI i.e. the Q(multi)MRI approach to produce intricate images and the real time data that can be collected can lead to evidence as to how the human brain works. It is a basic desire by humans to know the diseases we suffer from and how we can detect them at early stages of life. This basic desire is translated by human curiosity to find how the MRI machine can be improved to meet our needs. It is not like making a new car or a new aero plane. It is designing a machine capable of unraveling the life itself and how it functions. The basic question of 'how and why' is the basic quest of 'human curiosity'. One should not forget what status the MRI machine is today is nothing else but the fruit of 'curiosity research' which was to conduct research for the unknown. But that was the way about half century ago. That kind of research is considered as taboo today or say unnecessary. The driving force behind improving the MRI machine is the curiosity to find the secrets about how our brain works and why it works the way it does. Without this motivation there will be no awakening as to why to create the required knowledge and then how to use it in the benefit of humanity.

Is this a curiosity to find out why we are humans (advanced species in the animal kingdom) or to find why humans are curious (the basic human nature)? The mathematical and computer programs available today have considerably reduced the expenses involved in today's experimental curiosity research. If one could one would rather avoid 'experimental curiosity research'. Would one avoid 'theoretical curiosity research'. Perhaps no as it does not need an expensive experimental laboratory. Is theoretical research cheaper? The theoretical laboratory in the human mind can not really work out the real situation in mind about which we hardly know any thing. In a way mathematical modeling is also a curiosity research. The available powerful computers today allow complex mathematical problems to be solved with great success. But the imaginary parameters used to solve a problem are only imaginary. One still needs to carryout phantom and in vivo experiments to know the reality about the brain. The reader is referred to a useful illustration as an example on a theoretical curiosity research. It is presented, in the appendix A [2]. The theoretical computations have been carried about the interaction between distant spins due to distant dipole field at a point in water in a spherical sample (a symmetric model) with symmetric distribution of spins and the anisotropic cylindrical (asymmetric model) samples. Ideally the observed result on magnetization in a sphere should be zero as all spins being randomly oriented cancel out. But as one imposes an asymmetry on spins by applying a magnetic field gradient in a specific direction the observed results are quite staggering in a sphere.

Our brain is an asymmetric structure by nature. Spins in every little corner of the brain demonstrate different behavior under the applied RF radiation. The applied magnetic field gradients in vivo in the brain interrogate the metabolic activities which can be observed in imaging. This practical knowledge thus accumulated will help in turn to improve the model of the brain. This back and forth process will go on till the realty is known. Is this a curiosity research? Is it necessary? Perhaps more necessary than to pretend to the use the superficial word 'climate change' on which humans have no control except their proper behavior towards what the nature has created. The MRI machine in its present technological form is very huge in its mechanical structure. One of the contributing factors is the large magnetic field required. Large magnetic field requires large electrical currents to go through the electrically conducting coils. The coils are not ordinary copper coils. They have to carry large electric currents, more than hundred amperes or so. They have to be superconducting coils. These superconducting coils have to be immersed in liquid Helium (boiling point 4 K) to keep them close to their superconducting transition temperatures of around 20 K. These are called as the low temperature superconductors (LTSCs). Liquid helium cooling system is expensive to maintain and adds to the physical vastness of the machine. Recent scientific breakthrough has developed high temperature superconductors (HTSCs) which can be operated at the boiling point of liquid nitrogen i.e. the 77K mark. This discovery was the result of experimental curiosity research. The theory later followed to explain the observed experimental results. This is a clear demonstration (not a first time one) that theoretical techniques are not yet advanced

enough to able to predict a real situation without the help of an experiment. Research and development efforts yet have not been able to make flexible coils out of these materials. Sensors using HTSCs however have been developed to detect weak electromagnetic signals [3]. These can form in future convenient (operated at 77 K) sensors for the newly emerging parallel imaging technique. This will reduce dependence on the huge infrastructure of MRI.

References

1. Landini, L., Positano, V., Santarelli, M. F. (eds.): Advanced Image Processing in Magnetic Resonance Imaging, CRC Press, Taylor & Francis Group, Florida (2005)
2. Kirsch, S. Peter Bachert, P.: Visualization of the distant dipolar field: A numerical study. Concpts. Mag. Reson. **34A**, 357–364 (2009)
3. Kaila, M. M.: Hot electron non equilibrium high temperature superconductor thz radiation sensing and the integrated electron cooling, 1st Chapter in Book, New Topics In Superconductivity Research, Nova Science Publishers, Inc., New York, (2006) ISBN 1-59454-985-0

Part II
Sodium Multi-Quantum Magnetic Resonance Imaging Diagnostics of Brain Tumors and Disorders

Chapter 9
Introduction

9.1 The Natural Magnetic Materials and the Human Body

Nature has played a very clever role in the evolution of higher life forms such as animal and human. There are many chemical elements which are involved as integrated part of enzymes and proteins in electron charge and energy transport in our body. They are at the centre of action and are directly engaged in biological actions of life. The physiological processes in our body takes place using major simple ions e.g., Na^+, K^+, Mg^{2+}, Ca^{2+}, Cl^-, etc. These act through being in a bound state of a tissue and or of the free state in the mainstream of the fluids present in our body system. An optimum dynamic balance of the concentration of the ions in the tissue-cell-fluid pump is worked out by the life maintaining mechanisms. We need to understand the physics, chemistry and mathematics (PCM) of the electronic charge and the energy transfer of the life giving processes happening in our body. The PCM processes evolved by nature give us a healthy normal active life. Any abuse from the nature's chosen dynamic balance leads to diseases and ultimately death. It is thus time to learn in detail about the basics dynamics of the life maintaining processes happening in our body.

9.1.1 Nuclear Magnetic Resonance: Imaging (NMRI) and Spectroscopy

A scientist predicts the secrets of the natural dynamic processes happening in our body through mathematical modeling. He or she then looks for its experimental verification in clinical situation through the use of the technological wonder, the MRI (magnetic resonance imaging), machine. This is done in vivo situation of an organ of the body as well as using the phantom laboratory experiments simulating

a real life situation. A disagreement between what is observed and what is modeled is translated into a better physical and chemical model for further experimentation. This iterative process followed by a scientist leads to not only better understanding of the human body but also paves the way for the design of a better MRI machine. The nuclear magnetic resonance (NMR) phenomena was at the root of the curiosity research more than half a century ago. It has now resulted into the commercial MRI machine we have today. Over the last decade or so there is now demand on the technology to use multi-quantum dipole magnetic spin processes toward imaging rather than just the prevalent single-quantum spin processes. The multi-quantum processes happen in the molecular nm (nano meter) level and represent true natural character of events in progress in our body. The triple-quantum (coherent quantum spin action of three spins identical or of different species pointing in the same direction near and far) sodium imaging in vivo of the human brain is a typical example among the research and development efforts in progress in the direction of multi-quantum MRI (MQMRI).

NMR spectroscopy of elements in human body is now routinely used as a diagnostic tool. It is to make in depth analysis in particular in vivo in an ensemble of nuclear spins in a particular organ of the human body. The basics of the cooperative (multiple-species) electronic quantum structure of the elements in an ensemble like our body needs to be understood from the grass roots. This knowledge can then be used to derive the metabolic synaptic etc. activities of the chemical elements in our body in time and space.

Slowly NMR spectroscopy has found integration with the in vivo imaging in MRI. One should remember that the quantum spectroscopy of each element helped classify the chemical elements as arranged in, '**The Periodic Table of The Elements**' (please see Appendix A1 for the place of the useful magnetic dipole and electrical quadrupole nuclei in the Periodic Table). It is interesting to mention that the **Periodic Table of Elements** was completely worked out more than century ago based on the quantum energy structure of each element. Behind this classification in detail is the arrangement of electrons in orbits around the nucleus and that of the protons and neutrons inside the nucleus. The, individual orbit-electron-atom arrangement in an element makes the unique place for each element in the '**Periodic Table**' and controls its chemical and physical properties. The standard quantum electronic structure of each individual element worked out through spectroscopy can be accessed in a 'Handbook of Chemistry And Physics' and in routine text books of chemistry and physics available in a university science library throughout the world. But when the chemical elements are part of an ensemble e.g. macromolecules in our body the spectroscopy takes up a totally different horizon. The curiosity then asks the following questions. How do the chemical elements manipulate life? Why they are the architecture of the ensemble like our body is? Why and how do they acquire a typical macromolecular structure so important to our daily life?

The human civilization at large need to engage in research and development efforts to find out the answers to the above questions. MRI being a non invasive technology provides an appropriate tool for this purpose. It is important to note as

follows. If the knowledge developed remains as the privileged property among the higher elite levels of the scientific community e.g. in the universities, research institutions, private companies etc. and is not passed on to the mass education e.g. the secondary school level the gap between the known and the unknown will eventually become insurmountable. If there are no minds to know more then we are left with obsolete machines doing routine jobs with limited future. Think of the coming generations. What are they going to do? There is wilderness of technology available to society in different fields e.g., tele-communication, imaging technology, etc., etc. today. But how to use a technology appropriately, efficiently and rediscover and improve it on a continuous scientific basis seems of little concern to our leaders. This book has been written to pave the way to stimulate the reduction of the gap of illiteracy between science and technology. There is need starting from the production and use of technology to the education as to how to use efficiently and why and where to use it. There can be a healthy supply of common-minded decision making leaders only if three is an education about science of the masses at the secondary school level of education. This unfortunately in fact is on fast decline world wide. Sports, recreation, selfish bureaucratic financial manipulations, media, etc., etc., have taken over the science of reason and the intuition in today's life.

Life today is under too much complex stress created by bureaucratic constraints. There is no basic freedom to be just you. Now let us try to analyze what is the chemistry of the human body in the light of the magnetic materials present in the body. It is seen that among all the elements in a biological system like ours there are some potentially valuable magnetic isotopes. We have a small group of dipole magnetic nuclei, ^{1}H, ^{2}H, ^{13}c, ^{15}N, ^{19}F and ^{31}P (the superscript shown in each element is the mass number of the element approximately equal to the total number of the protons and the neutrons in the nucleus as the mass equivalent number) present in our body. One may ask a question at this point why nature has chosen only some particular elements and not others as a source of life progression? One can find out a scientific reason for that. But at the moment we have no choice but to leave it just as a secret of the nature. The above listed elements intrinsically at the lowest level of quantum energy (the ground state) have an atomic moment (expressed in symbol as μ_L) and a nuclear magnetic (expressed in symbol as moment μ_N) moment. Both types of magnetic moments are identical in their behavior but they differ in the size of their magnitudes and the strength of the forces involved. The dipole magnetic moment is expressed in terms of the angular momentum which generates it. In the lowest state, the nuclear magnetic dipole moment is symbolically expressed in the two lowest (higher states are possible) possible quantum states as $I = \pm 1/2$. This is only a simplified qualitative quantum symbolic expression. In magnitude a fundamental physical constant will be multiplied to it to get an exact magnitude. In the case of a nucleus this constant is called as the nuclear magneton and in the atomic case the Bohr magneton. We know in the case of an tom that an electron is bound to the atom and performs an orbital motion around the nucleus. This is the origin of the atomic magnetic moment. In addition an electron also spins around its own axis. In a physical meaning of the quantum language the electron spin (the angular momentum

around its own axis) has two simplest possible quantum values S = ±(1/2). The electrons angular momentum around the nucleus, L, is expressed through the quantum number l = ±1 in the lowest state. It can have higher quantum values, ±2, ±3,…etc. The reader is reminded that the above simplified quantum structure for the angular momentum is only obtained by application of a static magnetic field in a chosen direction called as the z- direction. This is the result of the planar atomic orbit quantization the magnetic field creates.

The idea is that when we rotate the spins from z-direction (by the application of RF pulses) into the x–y plane they can have higher possible quantum states of, ±2, ±3, …etc., by absorbing the applied RF radiation. In an ensemble like our brain the atoms combine to form molecules and the molecules combine to form macromolecules. The angular momentum (also loosely refereed to as spin) of the electrons, atoms, and molecules all add up to produce a resultant. If there were no quantum interactions among molecules the respective angular momenta just add up as scalar quantities. But more often than not the molecules do interact as that is the source of continuation of the life in our brain. Thus the molecular quantum coherence (interaction) imaging (MQMRI) needs to be the tool of technology of the future MRI. We are hopefully progressing in that direction now. The reader is reminded that in the MRI literature the symbolic mathematical equations about the magnetic dipole moment, angular momentum, quantum numbers etc. may look identical in their appearance. In true sense they may represent different magnitudes, different meanings, etc. The ratio of the dipole magnetic moment to the angular momentum is referred to as the gyromagnetic ratio (GMR). This is the link between the dipole magnetic moment and the angular momentum which generates it. Unfortunately we can not measure in the laboratory the angular momentum directly. The measurement of the magnetic moment in the MRI situation provides an indirect measurement of the angular momentum of atoms and nuclei in an imaging situation.

The vibrations of magnetic moments produced by the incident RF radiation becomes the source of the varied electrical signal across the brain. The Planck's content $\hbar$ is multiplied with the frequency (resonance) of the radiation i.e. the radio frequency (RF) radiation to get the energy absorbed in the MRI processes. The RF radiation is in the 100 MHz (megahertz, i.e., $\sim 10^8$ Hz) in the MRI perspective. RF radiation is used to excite an electron in its orbit. It provides the energy of the transition between two consecutive quantum states of the magnetic moment of the atom. In the MRI literature the mathematical expression, I = ±1/2 is normally retained (for the magnetic moment and the angular momentum) and multiplication by $\hbar$ is left out for simplicity. The angular Planck's constant in magnitude is given as $\hbar = 1.055 \times 10^{-34}$ Js (joules second) = 0.6582×10^{-15} eVs (electron volt second). The conversion from Js unit to the eV unit is given by 1 eV = 1.602×10^{-19} J. The energy of electron transition to a next higher energy state is given as, E = $\hbar f \sim 10^{-27}$ J or $\sim 10^{-7}$ eV. This should give the reader a rough idea about the order of energies involved in MRI. We only have here µeV (micro electron volt) range of energies. The energies involved are very small and are of little danger to the body. Thus one can see the grounds of MRI as a non-invasive technology. One

should remember that quantum energy structure of an electron in an orbit around the nucleus is not unique to electrons only. The protons and neutrons inside the nucleus have an analogous quantum energy structure. In a small volume of our body atomic and nuclear processes are in interaction with each other to produce an overall effect. One, should, compare the energies involved in MRI to the X-ray imaging. In X-ray imaging we have energy $\sim 10^6$ eV i.e. the Mev (mega electron volt) range. This can be very dangerous to the human body in particular the brain.

One should note the intrinsic electron spin originates from the intrinsic circular motion of the single electron around its own axis. But an electron is also in an orbit around the nucleus. The electron spin (rotation) around the nucleus creates an orbital magnetic moment of $\mu_l = (g_l)(\mu_b)(m_l)L$, where g_l is called as the spectroscopic splitting (degeneracy) factor, μ_b (called as the Bohr Magneton) = $[(e\hbar/(2m_e)] = 0.927 \times 10^{-23}$ amp-m^2 the fundamental (the smallest unit) magnetic moment, e = the electron charge = 1.602×10^{-19} C and m_l = orbital magnetic quantum number and L the orbital angular momentum.. The magnetic quantum number m_l has the possible quantum states (numbers) = $0, \pm 1, \pm 2, \pm 3, \ldots$, in a static magnetic field applied in the z-direction. In addition to the electron orbiting the nucleus the protons and the neutrons are also in circular motion inside the nucleus. They have identical quantum spin structure. One can say a small volume (called as voxel in MRI literature) in our brain is a typical ensemble of the electrons, nuclei, atoms, molecules. They are present within a complex inter and intra macromolecular structure of tissues, fluids, etc. This is a micro representation of the brain. In the brain when a voxel (a small volume) is subjected to an external static magnetic field (say in the z-direction) the spins (atomic and molecular magnets) in the fluids and in the stationary soft matter reorganize themselves into an ordered resultant quantized mixture of energy states. The spins now have the electrons, atoms and molecules with their magnetic axis aligned along the externally applied magnetic field. One should note without the static magnetic field applied the spins are randomly oriented and the total magnetism in a small volume (voxel), may be zero. But this ideal situation is possible only provided the volume is biologically isotropic in space an time.

In a real life situation in our brain the spins do not diffuse (translate, rotate, etc.) fast enough and far enough to neutralize each other. The anisotropic medium in-between deflects them from their course of action i.e. the tendency to neutralize each other. Consequently a small resultant magnetism is produced in a voxel. It is measured through a physical quantity called as the magnetic moment per unit volume or the susceptibility. Anisotropic diffusion of spins along different directions becomes the source of imaging referred to as the diffusion tensor imaging. There are many characteristic parameters for obtaining image in conventional MRI. The commonly in use are the anisotropic relaxation of longitudinal (T_1) and transverse (T_2) relaxation times of spins on irradiation of spins in a voxel with RF radiation. One should realize that the magnetic axis of the tiny atomic dipole-magnet is perpendicular to the orbital plane of the electrons around the nucleus. However these axes are randomly oriented in pace. The application of the static magnetic field along the z-direction simplifies the chaotic 3-dimensional random system into a simpler easier to handle planar quantum system in the X–Y pane.

One may ask a question then how the nature lets the chaotic network of molecules make the brain think and manipulate action in such an orderly fashion. The answer to that question is not so straightforward. We know that the orbital motion of electrons in an atom in a free space from simple physics principles would lead to creation of an internal magnetic field on the electron of around 1 T.

In a condensed matter space like our brain with medium of various fluids the field will be somewhat less due to the dielectric properties of the medium where charge motion takes place. The electrons, atoms, molecules are part of macromolecules. The macromolecules farther form a cohesive group of the size of nms (nano meters) to microns size are part of mutual interactions. The effective internal magnetic field in space can be considered as large when a large group of molecules are involved. This field is what provides an odder locally to let the molecules perform their function in a coherent orderly manner. One need to explore the order in the brain on the nm scale with little disturbance to the inside order from outside. That technology yet does not exist. The MQ-MRI (multi-quantum magnetic resonance imaging) is a step in that direction. The present MRI technology only humbly tries to unscramble the naturally present order in the brain system. Inside there is a complicated electric–magnetic system that is operative in our brain. We externally manipulate the internal system through the applied static magnetic field of around 3 T and the RF radiation to make some sense. But this has to be done in such way as not to disturb or alter the internal brain order. We are in a dilemma. Aren't we?

In MRI the RF radiation is applied along the three orthogonal directions (x, y, z) to the brain system. It excites the planar quantum (called as the quantization) system to higher magnetic quantum energy states. The higher energy states naturally come back to their original ground state in a microsecond. A series of RF pulses are used to excite a voxel. The quantized system (created by virtue of the applied static magnetic field) releases back the extra energy absorbed from the applied RF radiation. The out coming radiation carries with it the signatures of the physical and chemical events happening in space and time in the brain. The returned electrical signals are then converted into the shape of a picture which we call the MRI. The structure of the brain system depicted in the MRI picture can be translated to the real time bio-medical quantum mechanical events happening in the brain. For a detailed quantum mechanical treatment of an ensemble of atoms and molecules the reader should refer to a standard text in physics. The references [1–4] should prove helpful to the reader in this matter.

One should always remember that the spin (the magnetic dipole character) of an atom and of a nucleus arises due to the circulation of the electrical charges i.e. due to the electrons in an atom and the protons and neutrons in the nucleus respectively. The circular motion of electrons in atoms functionally is very much like the linear motion of the electrons when an electrical current flows through a copper wire when subjected to a potential difference between the two ends of the copper wire. In the linear motion it is the linear momentum which is important. In a circular copper coil geometry where the electric current is produced around the coil there is a magnetic field produced at the centre directed along the axis of the

coil. The magnetic field reverses with the reversal of the direction of the electrical current. In the atomic and nuclear case we are encountering rotational motion and it is angular momentum that steals the show. In the atomic situation an electron could be circulating clockwise or anticlockwise and thus the degeneracy is ± 1; the spin in turn is written as, numbers I = 1/2 or $-1/2$. As earlier pointed out in exact physical magnitude it should be written as $\pm 1/2$ $\hbar$. Here $\hbar$, the Planck's fundament quantum (quantity) and is the source of the fundamental quantum of energy. The magnetic dipole elements present in our body are the basic source of imaging labels in the MRI. It is important to point out here that the electrical charges in our body play a very important role in the moment to moment happening the physiological functions in our body.

9.1.2 The Nuclear Quadrupole Charge State in a Biological Medium Like Our Brain

There are some elements in our body system e.g. sodium, potassium, etc., which perform the important metabolic function in the natural system of life. This function depends on the electric charge distribution within a macromolecule and interaction with its neighbors. Simple free atoms like H, N, etc. possess a centrally symmetric charge distribution. What it means is that the centre of the spherical negative electron charge distribution around the nucleus and that of the plosive charge distribution inside the nucleus are coincident. Thus symmetrically for the total atom the total charge at the internal centre of symmetry of the atom is zero. But this simple situation may not hold for some molecular and a macromolecular situation. There the resultant charge distribution may not have a centre of symmetry. The positive and negative charge centers of the system may be displaced by a small displacement d of around a 100–1,000 nm (nano meter) in scale. In case of two charges, q (one positive and one negative) having one dimensional symmetry (+ and $-$) separated by a distance d the electric dipole moment is written in magnitude as p = qd. Its direction is taken from negative to positive charge. In a molecular situation generally it is the volume of the molecule that is important.

If the charge distribution is spherically symmetric (but the positive and negative caters displaced) the dipole moment is expressed as, $p = \varepsilon_o \alpha E_o$. Here α is the polarizability of the molecules, ε_o is a constant determined by the dielectric (electrically insulating property of the medium in which the molecule is present) constant and $\alpha = 4\pi a^3$, where a is an effective radius of the molecule (assuming as if it were a sphere), and E_o, is the local electric field, crated by the separation of + and $-$ charges. Thus the polarizability of a molecule to acquire a dipole character depends on its volume. However there can be situations where the centre of positive and negative charges are coincident but the charge distribution itself is not spherically symmetric. It is seen that in those cases the nuclear charge distribution adopts an oblate (flattened at the poles) or a prolate (elongated at the poles) charge distribution leading to nuclear quadrupole moments of negative and positive sign

respectively. In the presence of an external axially symmetric electric field gradient it is seen that the quadrupole moment, causes a precession of the angular momentum and splitting of the nuclear spin (dipole magnetic) levels. This can happen even in the absence of an applied magnetic field. This is the effect observed in nuclei with spin I ≥ 1.

Unfortunately the concentration in the brain of quadrupole nuclei is too low. It produces a very week electrical signal in MRI. In MQ-MRI the signal produced is even weaker. There lies the challenge to the Sodium Multi-Quantum MRI in particular and the electric–magnetic analysis of the events happening in our brain. There are chemical elements of interest in the human body science which are electric–magnetic in character. These are nuclei with spin I > 1/2. The scientific meaning of spin >1 is that these nuclei also possess, an electric quadrupole moment in addition to the magnetic dipole moment. The readers who are interested in looking at detailed practical examples of quadrupole nuclei in action are referred to the Appendices A, B and A1. The Appendix are included for those readers who wish to have some familiarity with the phenomenological mathematics of the interactions between electric field gradient in which a quadrupolar nucleus is present and the magnetic dipole moment which controls the direction of these interactions. It is shown how these interactions lead to the splitting of the central core I = ±1/2 spin structure into the detailed, −3/2, −1/2, +1/2, +3/2, structure. The Figs. 79 and 80 (Appendix B1), demonstrate details about the new emerging spectroscopic details in the electric quadrupolar and dipolar magnetic scenario which can be observed by the RF spectrometer. In a multi-quantum sodium imaging approach one would be looking how to translate the microscopic detail into an imaging structure. One should note that the positive and negative electrical charges behave in nature quite differently than the two magnetic poles (north (N)–south(S)) of a magnet. We know electrical charges (+ an −) can exist independently. But the two N–S poles of a magnet can not be separated. They always exist in nature together. It is a dual magnetic character. i.e. a magnetic dipole. Electrical charges are the basic routes of communication of signal in human body. They are also the basic carriers of energy from one point to the another e.g. the metabolism. When a positive and a negative charge are bound together say e.g. in a molecule like water we call it as an electric dipole. But in a macromolecular situation e.g. tissues in our body there can be four charges (two positive and two negative) in a bound state. They are called as electric quadrupoles.

Why nature has given the freedom to electric charges (+ and −) to have multipole character and as well to exist independently and not to the magnetic poles (N–S)? There are many unanswered questions in the maintenance of life which nature has created. To find a real answer one need to have a strong desire to go and find out why? This will mount to carry out a curiosity (basics) driven research. But there will be some unwanted cost involved in it. The second answer is to say that nature wanted it like that. This easy way out is much cheaper. There is a saying in Australia why fix something if it ain't broken. What it means is why worry about something that does not affect us. It is not surprising that more often than not ignorance is the preferred path chosen today. Unfortunately one needs not only

financial resources (plenty available in many nations) but also the will power (not so easily available) to do the required scientific research. One need to involve many on a wider intellectual scale to find out why electrical charges and magnetic dipoles do what they do in our brain. At the moment we are busy in simpler alternatives i.e. the sports, entertainment, etc., etc. These are the much easier outlets for the young minds and are so good economic engines. It is cheaper to stay ignorant about what goes inside our body and mind. Why worry about what happens in the future. The future will take care of itself. The oil spills in oceans, the fuel emissions in air, climate change (if there is something like that), etc., etc., need not bother us; they will take care of themselves. Leave with nature to work out.

9.1.3 Nuclear Quadrupole Materials

One may ask why not use electrical quadrupole nuclei which are much larger in number in our body, than the magnetic dipole nuclei which are so few in our body. Moreover quadruple nuclei are more intimately linked to the moment to moment and detailed spatial activities than are the magnetic dipole nuclei. The answer is that 1/2 spin nuclei exhibit a pure dipole magnetic character and are much easier to handle. The conventional MRI technology has used magnetic dipole nuclei over decades quite well. It is important to note that 75 % of NMR-active nuclei are quadrupolar and of these the vast majority are multiple half (3/2, 5/2,) and integer (0, 1, 2,) spins. Even if there are a number of convenient 1/2 spin nuclei available we can not hope to obtain a full structural picture inside our brain if we ignore all the atomic species that have quadrupolar nuclei. Many otherwise useful spin-1/2 nuclei have inconveniently, low natural abundance. For example ^{13}C (magnetic dipole) has 1.1 % natural abundance (see Appendix 24 in this regard) and ^{15}N (magnetic dipole) has 0.037 % natural abundance. If one were to study the structure of a naturally occurring solid protein one has the option of using the low-abundance nuclei or the ^1H if one restricts to using spin-1/2 nuclei. One could in fact use the ^{14}N (100 % abundance) quadrupolar (I = 1) nuclei. NMR studies of quadrupolar nuclei can provide valuable biochemical information. Using NMR of quadrupolar nuclei one can identify and characterize cation or anion binding sites on biological macromolecules or molecular aggregates. It is possible to follow how these binding sites become modified in the course of a biochemical reaction of transformation. NMR allows to determine metal ion populations of individual binding sites of a multiple protein.

The relaxation of quadrupolar nuclei are usually determined by their interaction with fluctuating electrical field gradients at the site of the nucleus. NMR can provide insight into ion binding to highly charged molecular aggregates or poly-electrolytes. It is seen that if we exclude the most commonly used magnetic nuclei (e.g. hydrogen/proton in water) then NMR sensitivity observed is too low. It can be even lower than the lowest known. The lowest known is that experienced for the ^{13}C nuclei (see Appendix 14.3.24) which are normally avoided in MRI. The low

sensitivity is in reference to the six essential element nuclei: ^{33}S, ^{43}Ca, ^{53}Cr, ^{57}Fe and ^{67}Zn. The I = 1/2, nuclei are generally considered to be much easier to handle than nuclei with I = 3/2 which possess electric quadrupole moment. However in biological systems the prospects of studying I = 1/2 nucleus like ^{57}Fe (see Appendices A22 and A23, in relation to the Alzheimer disease) is limited. One should realize that diamagnetism (magnetic dipoles) is instantly created when a magnetic field is applied as a shield (reaction) to the applied field. On the other hand paramagnetism is a permanent feature naturally preset in a molecule. Some molecules are natural magnets (paramagnets). The applied field only tries to align them in its own direction. The occurrence of paramagnetic relaxation will also add to difficulty of observing I > 1/2 nuclei like ^{63}Cu, ^{65}Cu in Cu_2^+ complexes, etc. For quadrupolar nuclei (I > 1/2) evaluation of the experimental situation is more complicated than for I = 1/2 nuclei.

There is occurrence of the non-exponential relaxation (refer to Appendix A3, A17, A26 and A27 for some Na and K examples) of the atomic and nuclear excitations of the quadrupolar nuclei by the RF pulses. It is seen that the second order dynamic frequency shifts (offsets of the resonance frequency in time) are some of the problems (see Appendix A2 for the basics involved) which need further insight. Quadrupole relaxation is caused by the interaction of a nuclear electric quadrupole moment with fluctuating electric field gradient at the place of the nucleus. Electric field gradients are system dependent properties and may be regarded as either intramolecular or intermolecular in origin. The aim behind writing this book is not to create just another text book in the field of MRI. The idea is to make the medical professionals (MPs) aware of what goes behind making an MRI picture and how well they can make use of it in the diagnostics of human brain disorders. The education about sodium imaging using multi-quantum coherences at the molecular level is the main theme of the book. This awareness is carried out by including practical illustrations from recent clinical studies.

The explanation of the connections to the basics of the fundamental quantum chemistry involved among the macromolecules is included as part of the illustrations. Detailed mathematical and phenomenological treatment is avoided. We have given some glimpses of the practical approach used in the book through demonstration of practical examples. A typical example of an illustration is a study of an ischemic tissue in the brain. It sets an example of the basics involved for a reader. An accurate concentration gradient of sodium and potassium ions across a membrane between tissue and the free surrounding ion environment is maintained by a healthy tissue in a specific pattern by natural forces. In an ischemic situation this gradient is disturbed. It leads to an unpredictable and erratic electric field gradient around the tissue. The result is that the I = 3/2 quadrupole (electric)-magnetic (dipole) moment character of the nucleus breaks (the degenerate spectral energy level character) into multiple (four possible) spectroscopic transitions (14.3.32–14.3.34 for mathematical details). These transitions carry with them the information about the abnormal behavior of the region of interest (ROI).

A scientist uses his or her professional, physics, chemistry and mathematics (PCM) skills to design,a suitable RF (radio frequency) pulse structure to excite the molecules in a ROI (region of interest). Then one develops suitable parameters of detection in the MRI machine to produce results to the desired level of perfection. This finally leads to the MRI picture we see. Efforts are made in this book for the reader to enable to learn about all the methodologies that have evolved involved in as simple a manner as possible. Though the book is aimed at improving continuous education of the clinical doctors through presentation of illustrations of conceptual pictures, etc., other professionals working in the field of medicine and science will find it equally interesting. The PCM education experts are now exposed to new challenges ahead. They have to simplify the research and development results created by the MRI researchers. PCM professionals have on their hand a duty to develop simplified versions of the MRI literature essential for the future user generations. There is a decline in education at the grass roots level about science among the much wider community today. One will always see further developments in the MRI technology. Coming generations will face a missing gap to handle further advancements.

There will be a limited supply of scientific manpower world wide very soon to handle the disasters both due to natural causes and the technology created. Oil spills in the ocean and the fuel emission in the air, etc., are here to stay. Are we developing suitable and enough, the scientific know how, the intellectual human resources to be able to handle the inevitable, the much worse disasters bound to come? This book is written specifically to enhance knowledge of the medical professionals working in the field of the applications of MRI to the area of medicine. The technology of MRI offers opportunities to visually see the events happening in real time, e.g. in a tumor in the brain. The standard techniques employing chemical shift imaging in a broader voxel (mm^3 to cm^3) using echo planar imaging (EPI) is common place in the routine MRI diagnostics of the brain disorders.

There is a recent change in approach in the MRI technology to use micron μ $(10^{-6}$ m$)^3$ to mm^3 size volumes for closer scrutiny of the events happening in space and time e.g. in a tumor. This is called as the quantum (more precisely the multi-quantum) magnetic resonance imaging i.e. the MQMRI. The reason why it is called as the MQMRI is that now one is looking at the atomic and molecular level the details of the multi-quantum interactions between atoms in molecule and the molecular–molecular interactions on a finer scale (<mm) of imaging. The quantum structure of events happening is truly revealed in MQMRI while in the conventional MRI it gets smeared out. The conventional MRI treats the magnetic spins of the electron-atom system as a single quantum system. What it means is that the atomic magnetic moments are assumed all identical in a voxel. The variable response to the applied static magnetic field applied along the z-direction and the RF (radio frequency) magnetic field applied in the x–y directions is due mainly to the different dispersive character of the spins because of the specific medium in which they reside. The fine atomic-nuclear quantum structure possessed by the tissue does not come into the picture.

In order to work out the real chemistry of the region discrete quantum level signal from a narrow region should form part of the detailed imaging. We want the book not to become too diverse in its character. The scope of the book is directed towards quantum coherence imaging and its applications to understand the human brain science. The development of the book surrounds imaging as the nucleus. The associated knowledge of the PCM required is provided in as simplified manner as possible as an induction to the reader to be able to make a better use of the MRI picture. The nuclear magnetic resonance imaging (NMRI) is basically in conceptual matter very identical to the atomic case. The major difference is the magnitude of the nuclear dipole-magnetic moment is about thousand times smaller than the atomic one. This is because a neutron or a proton is thousand times heavier that the electron. But there are some other subtle differences. The authors feel that this is not the right place to go into the details about atomic and nuclear physics involved behind the MQMRI. The reader is referred to a standard text book in this matter. But a summarized account forms part of this book in the following sections.

9.1.4 Human Brain: An Ensemble of Heterogeneous Spins Atomic and Nuclear

Our brain is a complex structure of atoms, molecules, macromolecules, etc. An atom has a fundamental magnetic dipole moment generated due to the valence (outermost) electron in orbit around the nucleus. Identically a nucleus also exhibits a resultant magnetic moment due to the circulating neutron and proton electric currents inside the nucleus. There is also a magnetic moment associated with the intrinsic electron rotation about its own axis. Fundamental to all these components of dipole magnets is the angular momentum of rotation. In the case of an electron its angular momentum is represented by the quantum selection rule, $S = \pm(1/2)\hbar$. In an atom, S, combines with the angular momentum due to an electron in an orbit, L, to produce the resultant angular momentum, $J = L \pm S$. L can have simplified quantum states of 0, ± 1, ± 2 in the presences of an applied static magnetic field in the z-direction. But S has only two quantum state $\pm 1/2$. The corresponding resultant J magnetic moment will also have a well defined quantum structure depending upon the quantum selection rules due to spin (electron)–orbit (atom) interaction within an atom. In an ensemble of atoms, molecules, etc., a multi-particle resultant quantum structure will be established with its own set of selection rules. The nucleus has a well established magnetic order of its own. A nucleus is buried deep inside the atom and relatively free from the atomic perturbations. The situation is quite similar but quite different in the magnitude of the magnetism and its quantum structure. In the nuclear case we have a different spin structure of the magnetic states. We can have 1/2, 3/2, 5/2,.. etc., states. We can also have integer values 1, 2, 3, …. What multiple quantized states, for the overall atomic-molecular magnetic system can have is decided by the overall quantum selection rules.

An interested reader for a detailed account need to refer to a standard text book in physics, e.g., [2], in this matter. Only the final results will form part of discussion here. A nucleus can have higher diamagnetic quantum energy states, e.g. $\pm 3/2$, $\pm 5/2$, etc. due to the peculiar charge distribution (e.g. the quadrupole charge distribution) around the centre of the nucleus. Nuclear magnetic moment is also a magnetic moment arisen analogous to the atomic one. A nucleus can have magnetic moment = 0, 1/2, 1, 3/2 ….The origin of the magnetic dipole moments for a nucleus has, protons and neutrons circulating currents, inside the nucleus. It is similar to the atomic case. The exact explanation of the mechanism of the processes involved in detail is beyond the scope of this book. A brief summary as follows should prove useful for the reader. The reader is reminded that the importance of the knowledge about the overall macromolecular quantum structure is the key factor that controls the imaging structure in a voxel. The, contagious data recorded from voxel to voxel allows the overall picture of the brain, produced. We wish to point out here that not all the electrons in orbit in an atom contribute towards atomic magnetic moment. It is only the odd numbered electron in the outermost orbit usually called as the valence electron that makes a debut. This is also chemically the most active electron and is responsible for creating binding between atoms to produce molecules and macromolecules. The inner-orbit electrons cancel their magnetic moment as pairs up and down. The situation in the nuclear case is similar. Here the odd numbered (unpaired) neutrons and protons produce the nuclear magnetic dipole moment. Also one should note that not all the chemical elements in the periodic table have a dipole-magnetic moment and not all diamagnetic-quadrupole nuclei are present in our body health system. Why is it so?

A nucleus has a complex structure made of neutrons and protons. The total magnetic moment is the combined effect of intrinsic magnetic dipole moments of neutrons and protons. The magnetic moments of most nuclei have been accurately determined in the laboratory (see Appendices A1) for nuclei important to human body. It is done by measuring the hyperfine splitting in the spectroscopy of an atom-nucleus system due to the hidden degeneracy present. This degeneracy in the, nuclear-atomic system dipole magnetic moment arises as a result of an internal magnetic field exerted on the electrons by the nucleus. The magnitude of this interaction between the atomic electrons and the nucleus is expressed in the form of an interaction energy ΔE. Its value depends, upon the orientation of the nuclear dipole magnetic moments in the presence of the internal magnetic field. It can in a descriptive manner be written as $\Delta E_N \sim C_N[f_{GT}(f_{GT} + 1) - i_N(i_N + 1) - j_A(j_A + 1)]$. Here the symbols j_A, i_N, and f_{GT} have their importance as follows. j_A = the quantum numbers in regard to the magnitude of the atom's total electronic (electron plus atomic orbital) angular momentum; i_N = the quantum number corresponding to the total nuclear angular momentum; f_{GT} = the quantum number obtained as result of the resultant, worked out from the atomic and the nuclear quantum numbers. Here C_N is a constant which is proportional to the magnitude of the nuclear magnetic dipole moment.

We feel the presentation of knowledge through mathematical symbols, should prove very effective. It is easy to remember something new if it is associated with, a

symbol, a process or a result. By measurements experimentally it has been verified that for all nuclei the most fundamental dipole magnetic nuclear magnetic moment is given as $\mu_N = (e\hbar/2M_P) = 5.05 \times 10^{-27}$ amp-m^2. Here e is the electron (or proton) charge, $\hbar$ is the Planck's (angular) constant and M_P = the mass of the proton. All the quantitative nuclear magnetic moments are expressed as an integral multiplication of it. This fundamental (nuclear) dipole magnetic moment in the physics world, is referred to, as the nuclear magneton. The magnitude of nuclear magnetic moment in each case, is worked out, by experiments through, measurement, of the nuclear hyperfine splitting of the magnetic dipole energy levels. The sign of μ_N can be positive in some cases and negative in others. It is found that for the nuclei with both atomic mass number A (total mass equivalent number of the neutrons and protons) and the atomic number Z (equal to the total number of protons in the nucleus or the total number of electrons in the orbit of an atom), being even, $\mu_N = 0$. The total nuclear angular momentum quantum number i_N, sometimes referred to as the nuclear spin can be obtained from an experiment simply by counting the number of energy levels of hyperfine splitting multiplet. If the multiplet is associated with a value of j_N, larger than i_N, then f_N can assume $(2i_N + 1)$ different values. It results into $(2 i_N + 1)$ different energy levels. It is also found that, i_N is an integer, for nuclei of even A, with $i_N = 0$, if Z is also even. But i_N is a half integer for nuclei of odd A.

The magnitude, I, of the total nuclear angular momentum is given in terms of i_N as, $I = \sqrt{[i_N(i_N + 1)]}\hbar$, i_N, bring the quantum number corresponding to the total nuclear angular momentum. The total angular momentum of a nucleus arises from the intrinsic spin angular momentum of its protons and neutrons, and also from the orbital angular momentum due to the motion of these particles within the nucleus. It is also important to point out here that in the nuclear case the word spin frequently refers to the total angular momentum of a nucleus in contrast to the atomic case. In the atomic world the word spin refers to the intrinsic spin angular momentum of the electron. We wish to say here that the reader who is not able to comprehend the simple descriptive mathematics as presented here need not really bother about it. The, presentation is purely to perceive a connection between what is observed and why it is observed in an MRI picture. It is done in round about quantitative but yet in a descriptive manner. The above logical deductions for the nuclear case have in fact been made in analogy with the case of electron spin and the atomic orbital angular momentum and have been verified experimentally. It is, considered appropriate here to shed some more light as below on the atomic case itself. In the atomic case there are two types of spins. One is the intrinsic spin of the electron around its own axis, referred to in the MRI literature by the symbol S. The other is the orbital angular momentum of the electron motion around the nucleus. It is referred to by the symbol L. Each of these are randomly oriented in space except for a small order created by the internal nuclear magnetic field present in the ensemble. This field is naturally present around a nucleus. It is local in nature in a confined environment like our brain as a result of ensemble of group of atoms, molecules, etc.

The multi-particle electron spin resultant is expressed as, $S' = \sqrt{[s'(s' + 1)]}\hbar$ and the atomic angular momentum as, $L' = \sqrt{[l'(l' + 1)]}\hbar$. These magnitudes in real atom situations, e.g. Hydrogen, Potassium, etc., have been worked out through the

rules of quantum mechanics (QM) and experiments. This book is not the right place to go into details of the quantum mechanical selection rules. The reader is referred to a standard text book in physics, e.g. [1–3]. It, should suffice here to include description as a helpful conceptual matter for a reader as follows. We, should remember that in an enclosed space like our brain the atoms and molecules are free to participate, coherently, in any function or activity in the brain. They behave collectively in a small volume say a voxel. Thus it is a multi-particle system in operation. But to have a coherence in space and time a regional force is required. This regional force, is provided by the electron-nuclear, electric–magnetic field, provided by the bound, electron and nucleus, system. In the absence of an external magnetic field a quantum number say, l', can have values, $\sqrt{l'(l'+1)}$, in space. This is the three dimensional quantization with very-many possible orientations for the spins. One can see that, l' an s' are the quantum numbers with permitted integer values 0, 1, 2, ….

The three dimensional projection with various components in space is reduced to a two dimensional structure on the application of the external, static magnetic filed. This is to reduce, the number of possible components. However a quantum number say for example, l', would be restricted to values $l_z' = 0, \pm 1, \pm 2$, etc. in the presence of, an externally applied static magnetic field H_z. This is the simplicity achieved in the situation. A factor of the type, $\sqrt{l'(l'+1)}$, $l' = 0, 1, 2, …$, often appears before the magnitude of any angular momentum. It specifies in free space the quantized angular (oriented) positions of the individual angular momentum. Its direction, is perpendicular, to the plane of the rotational orbit, and acting, through the centre, of the orbit e.g. in an atom. S' and L' are the angular momentum in reference to the multi-electron and multi-particle system. This is the situation we have in our brain. These further combine, to produce a resultant, $J' = L' + S'$. The J' logically is expressed as, $J' = \sqrt{[j'(j'+1)]}\hbar$. Here j' are represented as quantum numbers 0, 1, 2, … for the resultant local (say a macromolecule) system. In a magnetic field however it takes up the simplified values $J_z' = m_z \hbar$, $\hbar$, being the angular Planck constant, and $m_z = 0, \pm 1, \pm 2, …$etc. The reader is reminded, that the L–S (the two angular momentum) coupling, which results into the resultant J, makes the basis of J-coupled imaging, in a real MRI situation. In the atomic case the L–S (often referred to as the spin–orbit interaction) results into a spectrum of energy levels given as, $\Delta E = (\mu_b B g m_z')$. Here μ_b is the fundamental dipole magnetic moment[2] due to an electron in an atom, given as $\mu_b = (e\hbar/2m_e)$. The symbol e = the electrons' charge, $= 1.6 \times 10^{-19}$ C, $\hbar$ = the familiar angular ($\hbar = h/2\pi$) Planck's constant, $= 1.055 \times 10^{-24}$ J/s, and m_e is the electron mass, $= 9.109 \times 10^{-31}$ kg. Upon substitution, one gets $\mu_b = 0.927 \times 10^{-23}$ amp-m^2. It is often referred to as the atomic Bohr magneton. The symbol B (the symbol B and H are interchangeably used in the MRI literature) is the static magnetic field. Internally, some B, is naturally present, around a nucleus, in a natural ensemble, like our brain.

It is interesting to note this internal magnetic field is expected to be of the order of 1 T, in free space. One should compare it with 3 T magnetic field normally used in MRI machine. This internal magnetic field which the nature has created locally around a nucleus (or macromolecule collectively) in our brain is capable of

creating a local order. The natural local magnetic order though experimentally very difficult to observe creates the local network of electrical circuits used by the brain to carry on communications between different channels of the brain, e.g. metabolism, functionally mediated blood flow, etc., etc. The reader is reminded that in MRI we just suppress the local order and superimpose an order of our own by applying a much stronger (3–7 T) static magnetic field B externally. We can work out very well the intricacies of the static order we have imposed in the brain. Further, the excitation of the molecules by an external RF (radio frequency) field leads to the generation of the electrical signals we receive back. It give us all the information about what is happening, in the brain in a selected region during a particular interval of time. The reader may have realized that we have not yet completely defined the symbol g which appears in the interaction energy between the magnetic dipole and he applied field B. Mathematically it can be written as, $g = [1 + (\{j'(j' + 1)\}\} + \{s'(s' + 1)\}\} - \{l'(l' + 1)\}\})/2\{j'(j' + 1)\}]$.

In the presence of the external or internal magnetic field the J′, L′, S′ have two-dimensional space quantization (orientation in space). It is controlled such that instead of the j′, l′, s′, following the quantum numbers, 0, 1, 2,…, they reduce to their, z-component values only. These are called as the magnetic quantum numbers as, $m_z = 0, \pm 1, \pm 2, \pm,\ldots$Now the general J′, L′, S′ take on specific z-resolved, magnitudes as, $J' = m_{jz} J_z$, $L' = m_{lz} J_z$ and $S' = m_{sz} J_z$, respectively. The reader is reminded here that for the sake of simplicity the z-components (sometime refereed to as the azimuthal quantum numbers), m_{lz}, m_{sz} and m_{jz} are referred to as if having the allowed same integer values. In a real situation they will follow different specific selection rules, in different situations. The reader is reminded that symbols with the superscript are for the multi-electron system. The symbols without mean the case of a single particle. The exact spectrum energy structure for any atom can be built from an observed experimental spectroscopy, with appropriate selection rules [2]. A simplest illustration as an example is, $\Delta s' = 0$, $\Delta_{l'} = 0, \pm 1$, $\Delta_{j'} = 0, \pm 1$ (but not j′ = 0 to j′ = 0). The symbol Δ means a change in quantum number in a transition from one energy state to another. These, are only, illustrative values, to impress upon the reader the type and the complexity of the conceptual matter, involved. A detailed knowledge [2] is required for the actual situations. Before, proceeding further it is important to mention as follows. If education about simple quantum mechanical concepts for a learning purpose is introduced as part of education curriculum at the secondary school education system then it will become easy for the professionals to assimilate new developments later, in their life.

9.1.5 Anisotropic Nuclear Charge Distribution and Its Intrinsic Consequences

An atom has a cloud of negatively charged electrons surrounding the positively charged nucleus. Taking everything to be spherically symmetric with the nucleus at the centre and the centre of gravity of the total + charge coincident with that of

the total − charge the whole atom would spatially and electrically be neutral at the centre. But in some situations the centre of gravity of the negative charge around the nucleus may not be coincident with the centre of the positive charge at the centre of the nucleus. In such circumstances the atom is said to behave as an electric dipole. The hydrogen molecule in this circumstance presents a good example. Also when charges are present as an ensemble like in the case of macro-molecules in a tissue the charges try to associate themselves in a minimum energy configuration as surface charges rather than line charges (electric dipoles). The result is the formation of higher order poles. Electric quadrupole structure is often observed in many molecules. The result is that the nuclei do not just have $\pm 1/2$ $\hbar$ magnetic dipole energy states. The presence of quadrupole nuclear charges around can excite the nuclear magnetic dipole states to higher energy states, $\pm 3/2$ h, $\pm 5/2$ h, etc. The nuclei within a molecular structure can have more complex charge distribution structure, e.g. an ellipsoidal distribution of electrical charges in space. This deviation of charge distribution in a nucleus from perfect spherical symmetry has some natural consequences.

It is observed that the doublet magnetic dipole magnetic structure may have a further finer structure. This is contributed by the electric quadrupole charge structure. The new structure is partly a result of electric charge interaction between an ellipsoidal nuclear charge distribution and the internal (intrinsic) electric field present around the atom. The overall orientation of the quadrupole electric field in space is controlled by the orientation of the nuclear magnetic dipole moment which is controlled by the magnetic field internal (naturally present in the brain) or external. The observed departure of the nuclear charge distribution from spherical symmetry is specified by the nuclear electric quadrupole moment q. For $q > 0$, the ellipsoidal charge distribution, is elongated, in the direction of, its symmetry axis. The elongation increases as the q becomes more positive. For $q < 0$, the ellipsoidal charge distribution is flattened in the direction of the symmetry axis. The flattening increase, as q becomes more negative. For nuclei with spin $i \geq 1$, the hyperfine splitting, measurements show that there are cases with electric quadrupole moment $q > 0$ as well as with $q < 0$. For nuclei with dipole magnetic moment, $i = 0$ or $i = 1/2$, the measurements always yield $q = 0$; that is no departure from spherical charge shape are observed for such nuclei.

One should realize that a nucleus seems to have spherical charge distributions shape if it has zero nuclear spin. In this case it does not have any particular orientation in space since there is no total angular momentum vector that must maintain a fixed component in some direction. The nucleus can be thought of assuming in very rapid succession all possible orientations in space. Even if it is actually non spherical in shape one may not see this in the hyperfine splitting measurements. Hyperfine splitting and most other observable effects depend on the time average of the nuclear shape. To put it in another way most measurements, simply do not have the time resolution required to detect the instantaneous nuclear shape. But measurements involving nuclear reactions do. In fact it is seen that many nuclei with nuclear spin, $i = 0$ actually are nonspherical although this can not be seen by hyperfine splitting. More complicated symmetry arguments prove that

nuclei must also be observed to be spherical in hyperfine splitting and other time-averaged measurements if they have nuclear spin 1/2. The largest values of q are found for the nuclei in the region of the rare earth elements. In the most extreme case the largest dimensions of the ellipsoidal charge distribution is along the direction of the symmetry axis and it exceeds the smallest dimension by about 30 %. But for typical nuclei with $i \geq 1$, the difference in the largest and the smallest dimensions of the ellipsoid is only a few percent. So for most purposes it is a good approximation to assume that typical nuclei are spherical particularly since more than half of all the nuclei have $i = 0$ and so they appear in most circumstances to be precise spherical.

We have discussed above that the electric quadrupole moment q is a measure of the departure of spherical symmetry of the nuclear charge distribution as observed in measurements. An example is hyperfine splitting which is sensitive to the time average of this departure. The exact definition of the electric quadrupole moment is $q = \int \rho[3z^2 - (x^2 + y^2 + z^2)]d\tau$. Here ρ is the time averaged nuclear charge density in units of proton charges. The three-dimensional integral is taken over the nuclear volume with small volume $d\tau$, taken as initial, small volume, element. One should note that q (charge) is equal to Z, the number of protons in the nucleus, multiplied by the average over ρ, of the difference between three times the square of the z coordinate, and the sum of the squares of all the coordinates, x, y, z. That is $q = Z[3 <z^2> - (<x^2> + <y^2> + <z^2>)]$. One can see then, that $q = 0$, if the time averaged nuclear charge density ρ is spherically symmetrical, since in that case, $x^2 = y^2 = z^2$. If ρ is not spherically symmetric, it must at least have an axis of symmetry, along the direction, about which, the total angular momentum, of the nucleus, randomly processes, as time passes. In typical cases, the time averaged charge density, is an ellipsoid, with a symmetry axis, in ellipsoid direction. In the above equation the symmetry axis is taken as the z-axis. The equation demonstrates that for $q > 0$, ρ is elongated in the z-direction since then, $[<z^2>] > [<x^2> + <y^2>]$. On the other hand when $q < 0$ ρ is flattened in the z-direction so that, $[<z^2>] < [<x^2>] + [<y^2>]$.

The basics about the electric dipole moment, electric quadrupole moment and the interaction with magnetic dipole moment is of fundamental importance to the metabolic and other electrical activities in the brain function. The mathematics involved is kept to its simplest possible level in this book. Please see references [1–5] as a guide for further reading. Other references listed at the end of the book form the source of some practical illustrations included in the book.

The authors feel that the exposition of the concepts involved in sodium magnetic resonance imaging (MRI) are easier to explain through figures, diagrams, practical illustrations, etc. rather than going through phenomenological aspect of the field. The phenomenological approach involves development of rigorous mathematical equations which may be of little interest to the medical professionals (MPs). In the normal (magnetic effects alone) MRI images the effects of the interactions of the magnetic dipole moment (loosely called as spin) with the applied static field and the RF radiation. The spins also interact with the environment in brain where the nuclei are present and function. A full scan of the brain

produces a map of the brain which when compared with that of a healthy brain gives information about a tumor if present. This information may be incomplete in its use towards the knowledge about the abnormal chemical reactions that may have taken place at the diseased spot of the brain. In order to fully understand the events happening, in space and time e.g. a metabolic equilibrium between a tissues and the fluid around it a much better technology is required. We know the ions e. g., Na^+ (sodium), K^+ (potassium), cl^- (chlorine), etc., in the bound state with the macromolecules inside the tissue and in the free state around, form a very essential part of the dynamics of the basic life we live on moment to moment basis. Any impairment in the normal functions of nuclei, molecules, etc. in our brain can lead to a disease and eventually death. Over the last two decades or so MRI has changed its course towards acquiring more detailed information on a molecular scale spatially and temporally. In this respect the use of in vivo spectroscopy due to the interactions between electric quadrupole moments of the nuclei and the magnetic dipole moments is gaining momentum. This book aims in writing information about the new technologies emerging in as simple manner as possible. First of all a brief description of the basic concepts behind technical terms e.g. the electric potential, electric dipole moment electric quadrupole moment etc. is considered important. This is done in the following section.

9.2 Electrostatic Charges: Statics and Dynamics

9.2.1 Single Point Charges: Electric Potential and Electric Field in Free Space

9.2.1.1 Force of Attraction and Repulsion Between Charges

If there are two point charges q_1 (positive) and q_2 (negative) separated by a distance r, in the fee space, there will be a force of attraction F between them, given as

$$F = (1/4\pi\varepsilon_0)(q_1 q_2 / r^2)$$

Here ε_0 is called as the permittivity of free space, and $(1/4\pi\varepsilon_0) = 9.00 \times 10^9$ Nm^2/C^2. (Newton meter square/Coulomb square).

9.2.1.2 Electric Field E at A Point

Let us now call the second charge as a unit charge $q_2 = 1$. Then we call the force experienced by the second (unit) charge located at a point r due to the first charge as the electric field or the electric intensity at r. The electric filed or intensity is given as

$$E = (1/4\pi\varepsilon_0)(q/r^2)(\text{calling } q_1 \text{ as } q).$$

If the test charge is at infinity the force experienced by the test charge is zero. Important point to note here is that the force varies as $1/r^{-2}$ with distance.

9.2.1.3 Electrical Potential at a Point

Suppose now that the unit positive charge is brought from infinity closer to the charge q. Some work has to be done, to achieve this, as the charge q will repel the other charge, with greater and greater force, as it approaches the charge q. In other words, in order to place another (say positive at the moment) charge close to the positive charge q, an external force, has to be applied. This is to overcome repulsion from the charge q. The amount of work done or say energy stored in doing so, to place an additional (single unit charge) charge, at a position, say r_a, is called as the potential energy, stored in the charge, at that point. One can calculate, it, from the work integral, $W = \int F dr = \int (1/4\pi\varepsilon_0) (q/r^2) dr = (1/4\pi\varepsilon_0)(q/r)$ (neglecting the negative sign for simplicity and remembering the second charge is a unit charge). This work, or energy, is called as the potential, at the point r_a, with respect to (wrt) the position of the first charge. The final result can be written as (see Fig. 9.1)

$$V_a = (1/4\pi\varepsilon_0)(q/r_a).$$

Similarly to place a second unit charge at the position r_b, the potential energy stored at that position in the second unit charge would be

$$V_b = (1/4\pi\varepsilon_0)(q/r_b)$$

9.2.1.4 Differential Electric Potential at a Point

The difference in potential energy (normally referred to as the potential) between the two points is written as

$$V_{ba} = V_b - V_a = q(1/4\pi\varepsilon_0)\left[(1/r_b) - (1/r_a)\right]$$

If the second charge is of unit magnitude and is at infinity, one can write, in general, the potential at point r as

$$V = (1/4\pi\varepsilon_0)[q/r]$$

One should realize that the electric field E at a point, due to a charge q, is the force experienced by a unit charge, at that point. One can make an alternative interpretation of E as follows. If the unit positive charge is moved through a distance d, say from r_b to r_a, closer to the positive charge q, the amount of work required would be

$$V_{ba} = V_b - V_a = Ed: E = (V_{ba}/d) = [(V_b - V_a)/d]$$

Here E is called as the electric field or intensity. Thus one can also define, the electric field, in a region, as the potential difference, divided by the distance of separation, of the two charges.

These basic concepts, of charge, potential, electric field etc., in free space, are the essential physical quantities, to understand. As, one, goes, to a real situation, e.g. a tissue, with charged macromolecules, inside, the analysis becomes more complex. The tissue, has a charge distribution at its surface, pertaining to the atomic (electron) and nuclear (proton) charges within the macromolecule. What has been said above, about two positive charges, holds also, when one charge is positive and the other is negative. Then, the force, between the charges, is that of attraction. In that case one need to apply an external force, to keep the charges, apart, so that the negative charge, does not collapse into the positive charge.

This, again, requires some work, to be done. One should remember, that in an atom, electron orbits, around the positive charge. What keeps the positive and negative charges apart here. Why doe the electron does not collapse, into the nucleus? Can we really see that it is true, that that electron is orbiting, around the nucleus? We let you keep guessing. In a general situation, like our brain, there may be a volume of a space, which encloses several charges, e.g., a tissue in our brain does so. One should remember a charge inside a volume induces an opposite charges on the surface of the volume (say a tissue) that encloses it. So in a real situation one would be dealing with surface charges instead, of the point charges, inside the surface. One should remember any selected small volume in our body, will be electrically neutral. It holds for our body at any particular instant of time. It is felt important here, to mention about, an impotent law, the Gauss's law of surface charges. The law states that (in free space)

$$\oint E.dA = Q/\varepsilon_0$$

What it means is that the electric field E at various points on the surface of a tissue may nor be constant. There will be a variable surface charge distribution (charge per unit area) point to point on the surface. Thus one need to perform, a surface integration (this is the easier way, if the surface charge varies continuously in analytical manner, otherwise one need to perform summation point by point), over all the surface areas to get the total charge. The final result should be equal to the right hand side (RHS) of the above equation. In a real situation like the brain however, one need to replace ε_0, by the permittivity of the medium, in which the charges are present. In the simplest case of a charge q placed at the centre of a sphere of radius r, E is constant at any point on the surface of the sphere. One can work this out from the above equation, $E = (1/4\pi\varepsilon_0)(4\pi\ r^2)(q/r^2) = (q/\varepsilon_0)$, because the dA on integration becomes the surface area of the sphere = A, and is = $4\pi r^2$. Thus $\oint E.dA = q/\varepsilon_0$. The real brain situation is not as easy as that.

The above description, for, a charged sphere, is an oversimplification. It is, just, for the visualization purpose, only, about the basic concepts involved. Our brain is a very complex biological structure with charge behavior changing, from point to point in an unpredictable manner and in time. In the real life situation, i.e. in a

body organ, the physics, chemistry and mathematics (PCM) involved, becomes very complicated. We will not venture here to formulate a phenomenological PCM development, of the brain science. Nonetheless, some mathematical equations, will be exemplified, in the book, in order to appraise the reader, about the physical and chemical concepts, and the technical terms involved, in describing a particular MRI (PCM) situation.

9.2.2 Electric Dipole Moment

9.2.2.1 Electric Potential at a general Point P in Empty Space Around an Electric Dipole: Polar Coordinates

An, electric dipole is defined as a bound state of two point charges of opposite signs +q and –q and separated by a distance l (see Fig. 9.2). The mathematical definition for an electric dipole moment, is, $p = q \, l$. In space around it this electric dipole will produce an electric field at point P, and is measured, by putting a test unit (1 C) of positive charge at the point p. When one adds the repulsive and attractive forces experienced by the test positive charge at the point P and divides the resultant force by the test charge (which in our case is unity) one gets the electric field at the point P. For simplicity one can fist calculate electric potential at a point using the potential approach, as follows

$$V = (1/4\pi\varepsilon_0)(q/r) + (1/4\pi\varepsilon_0)(-q/(r + \Delta r))$$
$$= (q/4\pi\varepsilon_0)[1/r - 1/(r + \Delta r)]$$
$$= (q/4\pi\varepsilon_0)[\Delta r/r(r + \Delta r)]$$
$$= (1/4\pi\varepsilon_0)[p \cos\theta/r^3]$$

Here one takes $\Delta r = l \cos\theta$, $r + \Delta r \approx r$, and $p = l \, \Delta r$ as the dipole moment, and the approximation, $r \gg l$, has also been made. Now, one can differentiated the

Fig. 9.2 A pictorial representation of electric potential V at a point P due to an electric dipole moment $V = (1/4\pi\varepsilon_0) [p \cos\theta/r^2]$
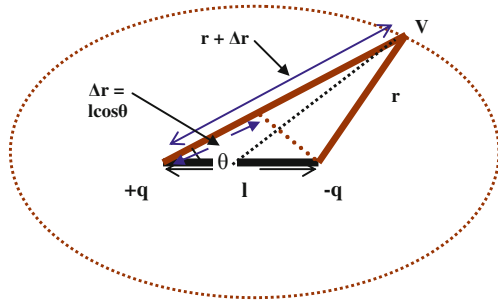
above V, expression with respect to r $(E = -dV/dr)$, and get the electric field at the point r, as follows.

$$E = (-dV/dr) = (1/4\pi\varepsilon_0)\left[p \cos\theta/r^3\right]$$

In the Figs. 9.2 and 9.3 is presented a pictorial representation of the points and distances involved and the electric field produced respectively around an electric dipole.

In an alternative approach one can deduce the electric field due to a dipole at a point using the definition of the electric field, instead of the route of the electric potential, as follows. In Cartesian coordinates at the middle point (Fig. 1.3) perpendicular to the dipole moment (axis), one can write

$$E(x, y) = E_+ + E_- = 2E_+ = (as, E_+ = E) \text{ or}$$
$$E = 2E_+ \cos\theta = (1/2\pi\varepsilon_0)[q/(r^2 + l^2/4)][(l/2)/\{(r^2 + l^2/4)^{1/2}\}] \text{ or}$$
note here, $E = [1/(4\pi\varepsilon_0)/r^2]$, $\cos\theta = [(l/2)/[\{r^2 + l^2/4\}^{1/2}]$
$$= (1/4\pi\varepsilon_0)[p/\{(r^2 + l^2/4)^{3/2}\}](as \ p = ql) \text{ or}$$
$$E \approx (1/4\pi\varepsilon_0)[p/r^3] \text{ for } r \gg l(a \text{ far away point}), \text{ and}$$
$$E_{(0,y)} = (1/4\pi\varepsilon_0)[p/(r^2 + l^2/4)]^{3/2}$$
$$\approx (1/4\pi\varepsilon_0)[p/r^3](\text{for } r \gg l)$$

One can calculate as shown above the electric field, around an electric dipole in Cartesian coordinates, E(x, y), or in polar coordinates, E(r, θ).

A vectorial representation, of the electric field E, produced by the dipole at a point P, is shown in Fig. 9.3. In a free space i.e. vacuum, E would be constant along the circumference of a circle. One should notice, that as one goes away from the centre, the electric field, falls off as $\sim 1/r^3$, in magnitude, for a dipole. This is an ideal model for the effects of a dipole charge present at a point in the surrounding space. In the real space e.g. a cell in the brain tissue the nuclear charge is surrounded by soft condensed matter, fluids, etc. The medium will affect the electric field experienced at a point on the surface of the cell. The cell has a net nuclear positive charge on the surface due to the $^{23}Na^+$ nuclei, inside. The positive charge
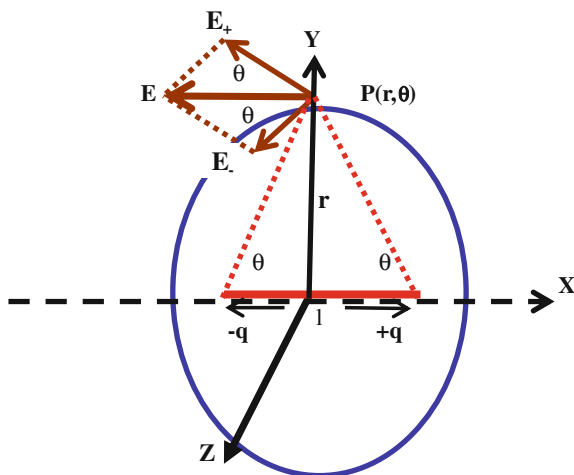
Fig. 9.3 A rough sketch, of the Cartesian (x, y, z) and polar (r, θ) coordinate system, involved, to calculate electric field at a point in a plane, for an electric dipole. The reader, should, realize in a real situation dipole would not be like a straight line (single dimension) structure. It could be due to charge distributed on the surface of a small volume, with three dimensional character. In a voxel used for imaging, there can be, charge distribution in an asymmetric shape leading to a dipole or even a quadrupole (4 poles character). The dipole character has no contribution in MRI situation. It is the quadrupole which makes the most contribution

of the sodium nucleus is due to electrically un-neutralized protons inside the nucleus. The $^{23}Na^+$ nucleus, present in the cell, is ionized, meaning, it has lost an electron. On the surface of the tissue which encloses, the positive nuclear charge due to several nuclei there is induced a negative charge due to many nuclei thus creating, a dipole character. The surface charge distribution would normally be non-uniform. There can be very many different species of dipoles due to the various chemical nuclei, present in the space, inside a small volume, in the brain. Their interactions produces a resultant electric field at a point in space. The dipoles are not static in time. Various, charge exchange activities, in the intra-cellular, and extra-cellular space, produce dynamic effects, in the space. In fact, the dipoles behave, in associations, and produced, electric-quadrupolar units.

This dynamic behavior of charges in space can be converted into an image. It is done through the electrical signals, quadrupoles produce, by interaction with magnetic dipoles, in space and time. The Fig. 9.3, depicts an ideal situation, around an electric dipole, in free space. In order, to comprehend, the phenomenological physics, of the electric charges, in a complicated situation like the brain, a reader is advised, to refer to, a standard undergraduate physics text in physics or biophysics, and the research and development efforts [4–61], that have taken place over more than half a century, in the area of MRI. For medical professionals (MPs) particularly the clinical doctors this may amount to an impossible task to learn. This book has not been written as a routine text book or a phenomenological resource as to how to apply, the text book physics content to a complicated
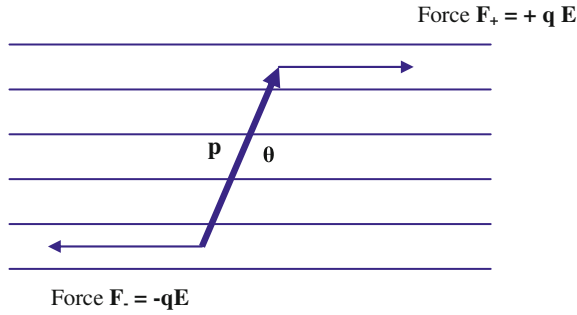
Force $\mathbf{F}_+ = + q\,\mathbf{E}$

Force $\mathbf{F}_- = \mathbf{-qE}$

Fig. 9.4   An electric dipole p, in a uniform electric filed E, experiences a torque $\tau = pxE$. Here, τ is a vector equal to the cross product of the two vectors p and E. In magnitude the vector τ, is given as $\tau = (pE)\sin\theta$. In direction it is directed perpendicular to the plane of the paper. In or out of the paper is decided by making a rotation like a screw from the first vector p to the second vector E or otherwise. The right handed screw will advance (rotating p to E) in the direction of the torque which in this situation means pointing inside the paper

structure like brain. It is more like a continuous education resource for MPs, medical scientists, etc., engaged in research and applications. Here learning is encouraged through visualization of the MRI pictures and technical information produced, for a specific body organ, e.g. The brain. Trying to correlate research results, to the basic physic and chemistry involved, in space and time in the brain, in as simplified manner, as possible, is the theme behind writing this book. It is hoped, this would, help clinician, to learn and be able to, make a scientific diagnostics, in a diseased cell state situation, in an organ, e.g., the human brain.

Now, we will briefly explain as to what happens when a simple dipole is present in an electric field surrounding it. In the presence of a uniform electric field (it can be naturally created by say concentration gradient due to ion charges in the brain situation), a dipole will experience (see Fig. 9.4) a torque, $\tau = pxE = pE\sin\theta$ (the axis of rotation is perpendicular to the plane of the paper). The effect of the torque is, so that dipole becomes parallel to E. The maximum torque is exerted when $\theta = 90°$. If the electric field is not uniform there will be an additional net translational force acting on the dipole in a particular direction. This will be in the increasing direction of the electric field gradient. A simple picture of the rotation of a dipole in presence of a uniform electric field is presented in the Fig. 1.4. The work is done on the dipole, by the electric field, changing the potential energy, of the dipole as, $U \sim p.E = pE\cos\theta$. Here θ is the angle between the vectors p and E, and it is called as the dot product of the two vectors p and E. We get $U = 0$ when p is perpendicular to E ($\theta = 9°$). If the electric field, in which the dipole is present, has a gradient dE/dx in the x direction, then the d dipole will experience a translational force $F = [(p.dE/dx = p(-\partial^2 V/\partial^2 x)]$, in the x direction. We wish to say here, that in this section we wish to briefly present the physics of the electric dipoles and quadrupoles in as descriptive manner as possible. The simple equations included should in fact help rather than hinder the learning process for those who want to go a step further to learn more. The quadrupole charge effects matter

Fig. 9.5 An example of a simplified model configuration for an electric quadrupole. The two negative charges add together at a point, as −2Q, flanked by, a unit charge +Q on either side

E

r

-2O

+O ━━━━━━━━ ┊ ━━━━━━━━ +O

⟵ l/2 ⟶   ⟵ l/2 ⟶
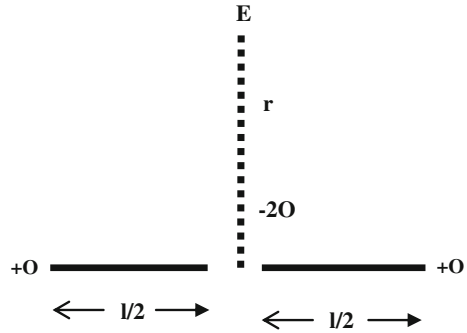
the most in the MRI situation. Simple mathematical equations in the quadrupole case of charges are interpreted in the next section.

9.2.3 Electric Quadrupole Moment

In a real life situation like in our body a small volume of a tissue would have a non-uniform distribution of charges on its surface. It could be the result of non-centro-symmetric volume distribution of positive and negative charges. The centers of symmetry, of the charges, can be more than two, e.g. four. In that case, one need to, deal with a quadrupole (four pole) electric moment. The simplest arrangements of charges one can think of to produce an electric quadrupole moment is shown, in the Fig. 9.5. One can say as if, there are two dipoles placed end to end, with their negative charges, say overlapping. This means there is −2Q charge placed at the centre flanked by the +Q charge on either side. One can calculate the electric potential V_{QP} due to this simple charge distribution, like the one, we did, for an electric dipole. The geometric configuration of the charges is shown in Fig. 9.5. The mathematical expression for the potential due to this simple electric quadrupole at a point r, can be written as

$$V = (1/4\pi\varepsilon_0)\left[(2Ql^2)/r^3\right] \text{ or}$$
$$= (1/4\pi\varepsilon_0)[(p_{QP})/r^3]$$

The above expression represents potential at a point due to a simple quadrupole moment. The quantity $2Ql^2$ is called as the quadrupole moment. In order to obtain the electric field at a point r (in the r direction) due to this potential, one simply performs, a differential, in the r-direction, giving

$$E = -(dV/dx) = (3/4\pi\varepsilon_0)\left[(2Ql^2)/r^4\right] \text{ or}$$
$$= -(3/4\pi\varepsilon_0)\left[(p_{QP})/r^4\right].$$
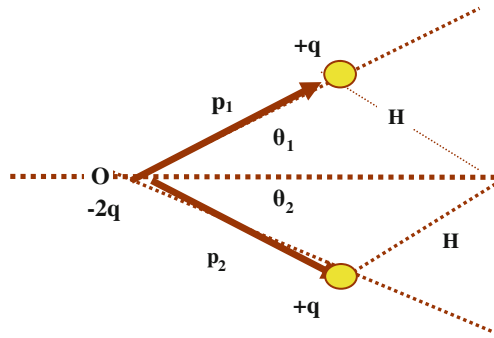
Fig. 9.6 Practical example of a water molecule with two dipoles p_1(O–H), p_2(O–H) at an angle θ, with respect to a horizontal axis. The total angle between the two dipoles in magnitude is, $\theta_1 + \theta_2 = 104°$. The potential at a distant point r ≫ l (l = the length of each dipole) in this case would sum as due to two dipole vectors p_1 and p_2. Thus V = $[(1/4\pi\varepsilon_0)$ (p cos $\theta/r^2)]$, p = p_1 + p_2 (as vectors). The two dipoles interact most strongly when they are directly lined up

On looking at this expression one should note that in the case of a quadrupole moment the electric field decreases as r^{-4}, as compared to, r^{-3}, in the case of a dipole. So it decreases much faster.

It is important, to point pout here that in a real life situation as in our brain in a small volume there will be many dipoles and quadrupoles preset close to each other. There will naturally, be some interaction between them as groups. Their interaction will add locally some extra energy in the region. The interaction will not be as point charges, but as groups of dipoles and even as quadrupoles. It is more of a text book work to cite some practical examples about calculation of interaction energy between dipoles and quadrupoles. The reader is referred to the introductory undergraduate text in physics, e.g. [1–4]. The reader is reminded that the text book level concepts have to be applied to a real life situation [5–61] to get the specific results. This is not within the scope of this book. Here we are only interested in presenting the conceptual matter involved in context of the MRI. There is an another simple example of a simple configuration for the electric quadrupole. One can have two dipoles with dipole moments p_1 and p_2, in line with each other separated by a distance r. At r (distance from both the poles) ≫ l, l being the length of the dipole, the potential (interaction) energy, of one, in the presence, of the other, is given as

$$U = \left(1/2\pi\varepsilon_0\right)(p_1\ p_2)/r^3$$

On the other hand if the two dipoles are oriented at angles θ_1 and θ_2 respectively with respect to the horizontal axis then the interaction energy can be written as

$$U = (1/4\pi\varepsilon_0)\{(p_1\ p_2)/r^3\}[\cos(\theta_1 - \theta_2) - 3\cos\theta_1\cos\theta_2]$$

It would be interesting here to get an idea about the magnitude of interaction energy involved in a real practical example. We know that the two strands of a DNA molecule are held together, by electrostatic forces between them. DNA is the

natural genetic material present in the human and other biological cells. The interaction energy between the dipole C = O (on a thymine molecule) and the dipole H–N (on an adenine molecule) is = −0. 13 eV. The symbol eV means electron Volt. It is the fundamental unit, of energy. What it mean is that it is the energy acquired by an electron when it is moved through a potential difference of one Volt. The, negative sign means that the binding energy is negative. Thus a work is required to be done to separate the molecules. We can see our body is a scientific machine doing scientific things without we even knowing it. Perhaps nature (may be god) is also a scientist. We should recreate ourselves in his/her image.

9.2.4 Atomic and Nuclear Magnetic Dipole Moment

9.2.4.1 The Atomic Magnetic Moment

The concept of the atomic magnetic dipole moment arises due to the orbital motion of the electrons around the nucleus. For those readers who are not familiar with, the meaning of the precession of, an atomic magnetic spin, around the applied static magnetic field, are reminded of the familiar 'Gravitational Spinning Top (GST)' which they may have played with in the school when they were teenagers. The picture is more or less the same. Let us call what we see in the MRI situation, as the 'Atomic Spinning Top (AST)'. The major difference between the two, is that GST is controlled, by the gravitational forces, whereas the AST is controlled by, the intrinsic centripetal and the attractive electrostatic, forces, between electron and the nucleus, in an atom. The atomic magnet is a tiny (nm in size) disc shaped magnet very much like the familiar, bar magnet. In GST the top rotates around the gravitational axis through its centre which in fact passes through the centre of the earth. This is to keep the GST vertical. It is due to the gravitational pull of the earth on the GST. The GST slows down due to the friction and ultimately falls to the ground. But one can see while it is falling down it is still rotating around its own axis and at the same time it rotates as a whole, around the vertical axis.

The tilted vertical axis of rotation in GST is close to circular in motion around the original gravitational axis but the orbital speed is fast decreasing and at the same time the falling speed is fast increasing. The GST does not stay stationary due to the frictional forces of the ground and the air in which it moves. In the AST case the magic is done by the static magnetic field applied. The spins (atomic magnets) tend to align themselves along the field. Thermal and other local activities distract the spin from perfect alignment. The applied magnetic field tries to oppose this distraction and tends to realign the spin, along itself. A balance is struck between the two forces. But the tip of the spin can not hang in the air along one direction and stay static. There is equal probability for it to be anywhere. The result is that it processes around the magnetic axis and we do not know where it is at any moment, in time. We say the tip of the spin (which in fact is opposite to the direction of the rotational angular momentum) processes around the externally

applied static magnet field axis with certain angular frequency. This is called as the precessional frequency.

The reader is reminded that to have an exact conceptual picture of the **GST** or the **AST** one need to go into the mathematics of the balance of forces and actually draw pictures by an exact analytical approach based on the mathematical equations. The reader, needs to go to a secondary school or an under graduate tertiary education level physics text book to have an exact visualization effects of the dynamics of the **GST** and the **AST**. The authors of this book feel this will take up an unnecessary volume of the book. We have written this book with an aim to cover latest developments in the field of MRI and where it will go in the future rather than the basic physics of it. In passing it is important to point out that it is the mathematics of the whole process and the association of what pictures we derive from it that makes a permanent impression in the learners mind as to what is happening. We need to ask the following question to ourselves. Is our secondary and tertiary education system in science equipped well enough to meet the technical challenges of the future. Just shouting about the slogans 'climate charge', 'fuel emission', 'oil spills', 'insecurity', etc. etc. and be happy about the glory of the words for sure will not take the world anywhere better. Simple common sense tells it. Unfortunately the common sense is not very common today to see what is happening around us. The, angular momentum J and the associated magnetic moment μ_J of the electrons orbiting around the nucleus is quantized. This means they can only occupy fixed quantum energy levels. In the process of a transition above and down in the orbital energy levels the energy is absorbed and re-radiated according to quantum jumps of angular momentum and energy. The transitions follows e.g., the quantum rules $\Delta J = 0, \pm 1, \pm 2, \ldots$etc. Here $J = L + S$ basically is the resultant due to spin-orbits interaction in an atom and ΔJ is the change in a transition from on atomic orbit to the other. In, a, multi-particle situation J is replaced by J' accordingly.

The angular momentum, J and the associated magnetic dipole moment, μ_J, are oppositely directed for an electron orbiting around the nucleus. One, normally applies an RF pulse at an angle 90° to the static magnetic field. It is possible to produce a rotation of the spin (magnetic dipole) by an angle θ away from the static magnetic field. Normally $\theta = 90°$ is used to rotate the spin from z-direction in say x or y direction. These pulses are called as 90° pulses and the angle of rotation the flip angle normally is 90°. The flip angle θ in any direction can be manipulated for specific purposes. The static magnetic field exerts a torque τ on the plane of an electron orbit. The torque on the plane of the orbit acts in such a way as to keep the atomic orbit plane (x–y) perpendicular to the static field. This consequently amounts to keeping the atomic spin moment along the direction of the static magnetic field. By choosing a suitable magnitude direction and the frequency of the RF radiation applied the study of the quantum nature of the spin helps bring out the quantum secrets of the brain from the real time quantum images produced.

The Fig. 9.7 is an approximate pictorial depiction of the precession of the vectors of the angular momentum L, and the dipole magnetic moment, μ_L, for a single electron in an orbit around the nucleus. One should remember in an actual situation like our brain there will be many nuclei participating locally as well as
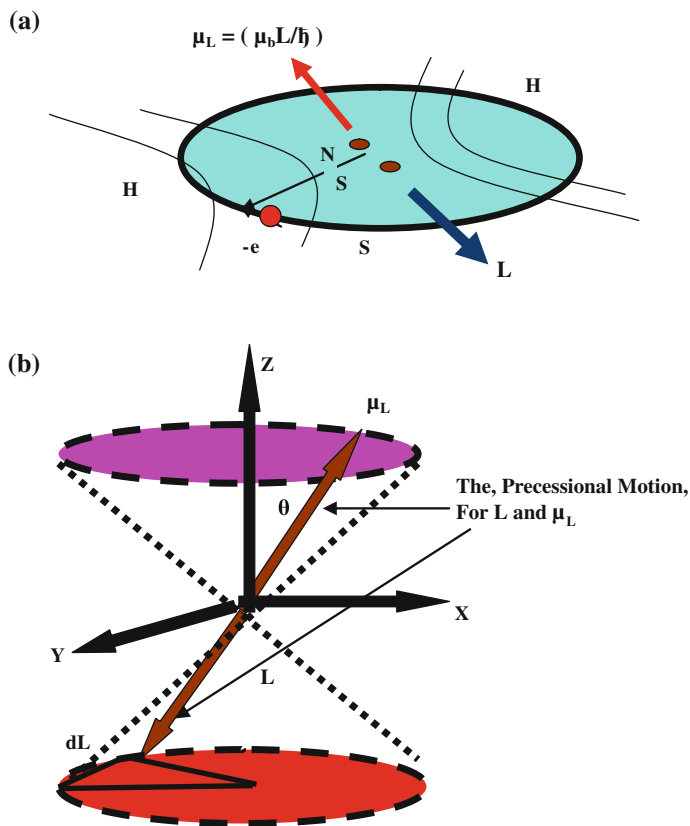
Fig. 9.7 a The electron orbit around a nucleus and the associated magnetic dipole moment μ_L, the angular momentum L, and the magnetic field lines in space for the case of a single atom are hewn. **b** The precessional motion of the angular momentum L and the orbital magnetic dipole moment around the applied static magnetic field are pictorially depicted. The static magnetic field H_0 is applied along, the Z-direction through the skull of the brain under scan. An electron being a charged particle generates an electric current in the orbit around the nucleus. This electric current say i, when multiplied by the area A generated by the orbit is equal to the term called, as the, orbital dipole magnetic, $\mu_L = iA$, of the atom. The μ_L, corresponding to different spins (nuclei and atoms) are randomly oriented in space and time when there is no applied static magnetic field along the z-direction. So, the resultant effect overall is zero. However when, H_o is applied perpendicular to the X–Y plane it behaves as if H_o acts through the centre of the orbit. The angular momentum vector L of the orbiting electron produces the magnetic moment. It is not static in space along the, z-direction. It is under the process of precession (rotation) at an angle θ tracing a cone around the static magnetic field

globally in similar as well diverse activities. Thus the above description is only a close approximation of the overall situation. We give here a simple pictorial depiction of the above description of the magnetic moment annular momentum etc., in the context of the MRI.

The precession of the electron around the static magnetic field H_0 happens because though the spins are under force to remain oriented in the z-direction the local temporal activities e.g. metabolism, neurotransmission, temperature disturbance etc. try to keep the spins oriented away from the z-axis. This results in an equilibrium i.e. the precession of the spins at an angle θ to the z-axis. The length of the vector the angular momentum, L, i.e. its magnitude remains fixed at a particular frequency of resonance as result of the applied RF radiation. The RF pulses only make it go faster due to the electromagnetic energy absorbed. However as a result of the precession in space its direction is changing, at the rate of a fixed angular frequency. Due to the quantum nature of the angular momentum a fixed quantum of energy is supplied by H_0, i.e. $E = \mu_L H_0 \cos\theta$. Here θ is the angle between μ_L and H_0. L remains quantized in space. But it rotates around H_0, in random fashion such that it can be anywhere in X–Y plane at any time. It can only change its values by going up and down (two possible state for the spin) in quantum jumps. The magnitude of the quantum jump in angular momentum is $L = m_z L_z$ where m_z is the magnetic quantum number with values, $\pm(0, 1, 2, \ldots)$. The angular momentum cone generated is shown in the lower part of the Fig. 9.7b. Since, the magnetic moment is oppositely directed to the angular momentum due to the negative charge of the electron the corresponding cone generated by magnetic moment is shown in the upper part of the diagram. The rotation of the angular momentum L in a circle is connected to the precession of the magnetic moment μ_l. The precession frequency is referred to as the Larmor frequency and is represented by the symbol Ω.

The orbital magnetic moment of the electron is given as $\mu_l = g_l (\mu_b L/\hbar)$. It is connected to the angular momentum, and rotates at the Larmor frequency. The precessional frequency Ω of the spin magnetic moment μ_l is given as $\Omega = g_l (\mu_b H_0/\hbar)$. Here g_l = orbital spectroscopy splitting factor. We have $\mu_b = (e\hbar/2m_e) = 0.927 \times 10^{-23}$ amp-m^2 factor g_J. An electron in an atomic orbit is also rotating around its own axis. It is called as the intrinsic angular momentum (spin) of the electron, = S. In the presence of the field H_0, there is the resultant angular momentum $J = L + S$, of the atom, which one needs to consider. The brain ensemble is a hetero-nuclear one. In a small volume one need to take, some kind of an average, of the magnetic moments, and also the same in regard to the resultant angular momentum J. The ratio of the magnetic moment to the angular momentum is called as the gyro-magnetic ration **GMR**. The **GMR** = $(\mu_J/J) = g_J (\mu_b/\hbar)$. Here μ_b is the fundamental unit of the magnetic moment and $\hbar$ provides the fundamental unit of energy and is called as the angular Planck's constant of the RF radiation; g_l is the resultant, spectroscopic splitting factor. This ratio has very important place, in the MRI literature. There are many species (hetero-nuclear situation) of nuclei, in a small selected volume.

For, imaging, one need to take into account, the resultant effect of all the local interactions, among the atoms and the nuclei. It is a common practice, now, to take spectroscopy of a small region of say mm^3 to cm^3 dimension as part of the MRI. This small volume is referred to as a voxel in, the, medical MRI literature. The spectroscopy is very helpful in determination of the distribution in space of the relative and absolute metabolic concentration in the brain. The spectroscopy helps

in the diagnosis of the brain tumors. The, precessional frequency, of the resultant (orbital plus that of electron intrinsic), atomic magnetic spins, around H_0 is given as, $\Omega = g_J (\mu_b H_0/\hbar)$. Now g_J is the resultant spectroscopy splitting factor that determines the splitting of the energy levels in a voxel and can be used as a measure of the distribution of the metabolite concentrations.

In the Fig. 9.7 there is only a rough depiction of the precession of the dia-magnetic dipole moment. The μ_l shown is representative of a single electron or a proton (in the nucleus). In fact it can very well be, the resultant, of several neighboring, electrons and protons, as a group. A nucleus also has angular momentum properties, analogous, to the atoms. In a small selected region i.e. a voxel in the brain, for imaging, the outer orbital atomic electrons in the neigh-boring molecules, and the protons (and the neutrons), in the nuclei, will all couple together, to produces a resultant angular momentum $J = L + S$. Here, J, would, be the resultant of angular momentum of atomic angular momentum and that of the nuclei. One, should, note, however, that the nuclear magnetic dipole moment is much smaller in magnitude, than, the atomic one. The, mass, of the protons and neutrons is thousand times, more than the electrons, so their magnetic moment, is thousand times smaller. However nuclear forces are much stronger resulting into much stronger L–S interactions. It is important to point out here that S would be the intrinsic angular momentum of outermost orbit electrons, participating in interactions, among the neighboring molecules. The inner orbits atoms do not provide chemically active electrons. Their spins are internally neutralized.

In larger size voxels the diffusion dynamics of the molecules modulates the received signal. The received signal is part of the space and time functional dependence of the dynamics of the fluids e.g. blood circulation, metabolism, etc. The message is conveyed through the functional interactions in the brain of the resultant angular momentum J of a group of molecules. A typical example where the spin dynamics can be seen in action is the **BOLD** (blood oxygen level dependent)-**MRI**. One should always remember that it is not the angular momentum J, that is a measurable quantity instead it is the changes associated with the precession frequency, of the magnetic moment, and the phases (time of arrival of signals), that is measurable. There are varying angles between spins oriented by the local activities and picked up by the applied RF radiation. The received signal helps to measure the local activities through a variable response with time. Returned back modulated radiation has the signatures of the variations of the magnetic dipole moments. The observed effect is through the precessional oscil-lations. The change is because of the variation in the precession of the angular momentum J. According to the simple physics principles of the dynamic electricity an oscillating magnet in space produces electrical signals around it. Its space and time variation detected by the sensor forms the image.

There is a multi-particle system that is experienced in real situation in the brain. Our brain is a heterogeneous system of various nuclear species. It is good to remind here that due to that the relative motion of electrons with respect to the nucleus, there is created a local magnetic filed in the neighborhood of an atom. It is called as a natural internal magnetic field. This internal magnetic field due to

various nuclei, adds up to a resultant, locally, (the magnitude of this field can be around 1 T, in fact slightly less due to the medium of the brain) and tends to orient the spins, along its own z-direction. The angular momentum of a spin (the atomic magnet) is given as $L = I \omega$. Here I is the moment of inertia of rotation of an electron, around the axis of rotation, and ω is the frequency of rotation, due to the electron rotation, around the nucleus. In a voxel, L's and S's are the resultant, due to various atoms, molecules, etc., given as $L' = L_1 + L_1 + ...; S' = S_1 + S_1 + ...$ The resultant J consists of the components of the angular momentum of the neighboring interacting particles. Then due to the internal magnetic field, L's and S's, add up, to produce a resultant $J' = L' + S'$, and thus a local order is produced. There is a magnetic interaction between the atomic angular momentum L' and the electron's intrinsic angular momentum S'. This Spin-Orbit (L–S) interaction breaks, the degeneracy of the double quantum state of S' into ($\pm 1/2$ ℏ). It makes instead, $J' = L' + 2S'$. The resultant magnetic moment $\mu_{J'}$ now, is not exactly, oppositely directed to J'. This offset is suppressed in MRI by the externally applied static magnetic field. The Fig. 9.8, depicts, Z, as the internal magnetic field direction, and shows, how the internal order along J', is created, locally.

In MQMRI the spins are projected to new positions in the X, Y plane as in conventional MRI. But the electrical signals are produced by the magnetic field-gradient, excited echoes. The process is done using the incident gradient field RF pulses and the response is analyzed through a respectively tuned receiver. But specifically in MQMRI we are particularly looking for multi-quantum correlations between molecules, rather than just the local, non-quantum, environmental, interactions, within, the molecules. The spins vibrate due to the incident RF radiation, gradient magnetic field pulses and produce the desired electrical signals. In the MQMRI the gradient magnetic field pulses are applied in different directions (phase cycling) to reinforce quantum correlation among multinuclear molecules. Furthermore the signals in particular due to the multi-quantum interactions are selectively measured. In between the pulses the spins undergo a relaxation back to their original equilibrium position with quantum correlation relaxation times. As in the conventional MRI there are two main types of relaxations. One is called as the longitudinal relaxation. Its characteristic time is referred to as spin–lattice relaxation time T_1. T_1 basically originates from spins projected in the –Z direction (possibly returning through Y-direction) trying to comeback to the +Z-direction. The other type of relaxation is called as the transverse relaxation. This characteristic time of this relaxation is called as T_2. In this relaxation, the spins are kept in the X–Y plane while evolving. They are initially focused in +Y direction. Then they are reversed in the plane along the –Y direction. The repeated reversal generates gradient echoes, and thus the electrical signals are measured. This relaxation is also called as the spin–spin relaxation.

One measures in MQMRI multi-quantum interactions within and in-between the voxels but the voxel size is ≤1 mm. The process is a resultant effect overall. The resultant orbital angular momentum is $L' = L'_1 + L'_2 + ...$all particles and the total spin angular momentum is $S' = S'_1 + S'_2 + ...$, all particles. The resultant is $J' = L' + S'$ …all particles. Because the electron-spin angular momentum S has duplicity ($S_z = \pm 1/2$ ℏ), actually speaking, $J'' = L' + 2S'$. The spin–orbit (L'–S')
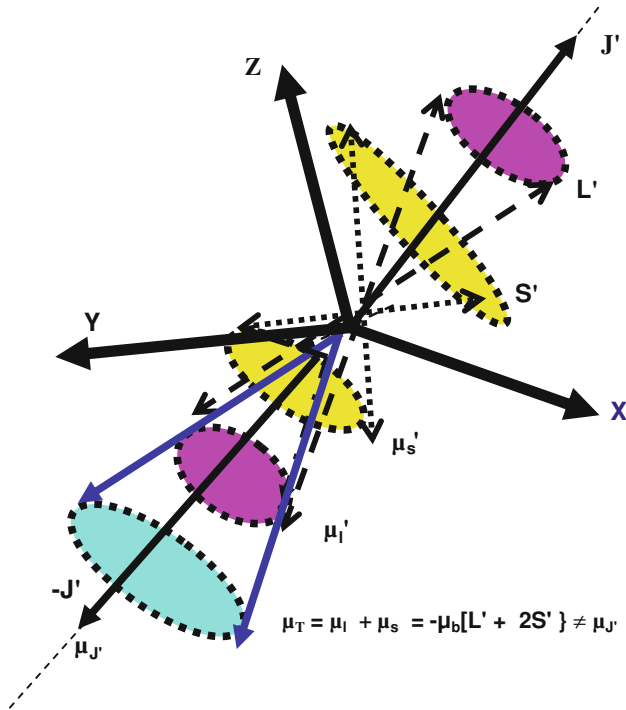
Fig. 9.8 Above is a picture representation of how the electron's intrinsic spin angular momentum $S' = \pm 1/2\hbar$ and the atomic angular momentum L′, are oriented in space, in a multi-electron system. The resultant produced is due to the interactions, communications, etc., in-between the molecules. This is induced due to the presence of the internal the nature's magnetic field in the brain. In each little volume (voxel) in the brain there is a resultant angular momentum J′ due to all the local spins present. Due to the local nuclear magnetic field spins try to align themselves along the internal Z (order—direction). It is called as the internal local order direction. In MRI this internal order is suppressed by the external static magnetic filed, which is applied along the laboratory, Z-direction. A suitable sequence of RF pulses is applied along X and Y directions to excite the spins for imaging. The J′ = L′ + S′ interaction is commonly used in chemical shift imaging in the conventional MRI. The quantum energy correlations between the nuclei in molecules are excited by the magnetic field gradient-pulsed radiation and the excited multi-quantum correlations in particular then form the basis of multi-quantum imaging. The multi-quantum order is detected on a micron to mm region scale. This is what makes the multi-quantum QMRI (MQMRI)

interaction, does not allow $\mu_J'' = \mu_T$(total) $= \mu_l + \mu_s = (-\mu_b/\hbar)[L' + 2S']$ to be exactly aligned in opposition to the J'. This is the result of dual character of S′. This internal misalignment is suppressed in MRI by the externally applied static magnetic field. The overlapping space in between the voxels, become the source of continuity, in the overall global image of the brain. There is naturally present, for the electrons, intrinsic (up and down two states), degeneracy in angular (spin) momentum = 2S′. It leads to an offset in the line of action of L′ and S′ (Fig. 9.9). The result is that the two do not follow the same precessional quantum structure. There is no technology yet possible to handle that level of quantum precession.
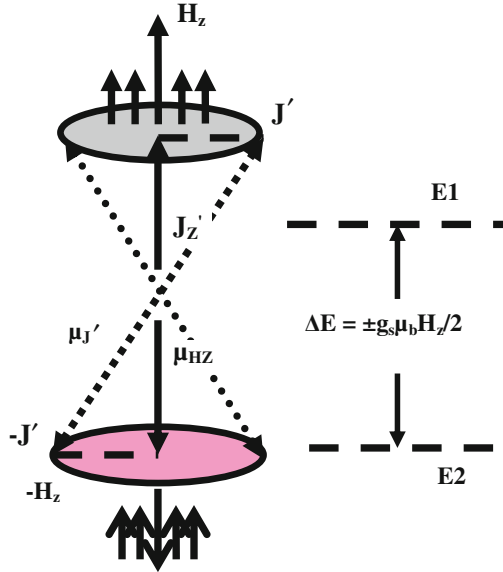
Fig. 9.9   In the presence of an externally applied field H_Z, there is an overall average effect, in a voxel. The measurement is that of a macroscopic average which is close to but not exactly equal to the internal (atomic-nuclear level) magnetic moment $\mu_J{}'$ (the resultant due to many particles). This is what is observed. It is realized through what is created (inside the brain) the μ_{Hz} by external means surviving in a measurable time. For the particular case of a single electron (Hydrogen atom the simplest example) the intrinsic electron spin S will produce for each energy level corresponding to l (the orbital quantum number) of the atom a doublet-split (because, $g_s = 2$) as shown above. In a multi-electron-multi-atom molecule multiple splitting for the orbital quantum number l will be observed. It will be due to the effect of the angular momentum quantum numbers $lz = \pm(0, 1, 2\ldots,)$. Each lz will involve each main orbit n = 1, 2, ….. But one should remember it is the outermost n and l that matter. So the result is not as complex as one may think. One can find a close enough correlation between what is observed and what is inside the brain

   The present MRI technology suppresses this internal effect by the application the externally applied static magnetic field (say ∼3 T) much grater that the internally (natural) present field of around 1 T. Thus what exactly happens in the brain is not exactly the same thing, what we measure in laboratory (MRI). The magnetic moment is supposed to be an exact (though reverse in action) replica of the angular momentum, but it is not. One should note, in passing here, that the conventional MRI does not take much notice of the intermolecular quantum level interactions. They are treated as if they were scalar J-couplings, producing the desired effect, in imaging. In MQMRI, the quantum interactions are encouraged by applying, suitable magnetic field gradients of the order of mT/m (milli Tesl per meter), in x, y, z-directions. These gradients tend to concentrate (localize) molecular spins, in one direction, more than the other, thus producing localization of the molecules, in a desired quantum interaction state. The concept of the two relaxation times and the echo still remains the same, as in the conventional MRI. But the reason for relaxation is different for the MQMRI. Here one selects zero

quantum coherence (ZQC), double quantum coherence (DQC), etc., as the source of analysis in a particular voxel and inter-voxel correlations.

9.2.4.2 The Nuclear Magnetic Dipole Moment

When we go deeper into the nuclear environment the behavior of protons and neutrons becomes very important in knowledge gathering. Proton as a part of the water molecule is present everywhere in the brain. Proton magnetic resonance spectroscopy (PMRS) plays a very crucial role in determining the science of the metabolism in our brain. There is, no technology yet available which can exactly work out the arrangement of the order due to internal magnetic field, around a nucleus in a molecule and how it influences the nature's intricacies of the brain functions. But the overall atomic-nuclear interactions in the presence of the external field, do provide a good enough information through spectroscopy and imaging, for the brain. The conventional MRI tries to, impose an order of its own by external imposition of a static magnetic field followed by the RF radiation on the brain and find out whatever it can. Figure 9.9 is a rough depiction of an average measurable resultant, magnetic moment μ_H, created by the external static, field applied in the z-direction. The right side of the Fig. 9.9 shows as an example the degenerate quantum split (ΔE) in energy for the single intrinsic, electron spin. This simplest case of the electron spin in the Hydrogen atom exemplified here is only the tip of the iceberg. In a real brain situation there will be many atoms, nuclei and molecules making their contribution. The observed molecular imaging in a voxel would have signatures of all the molecules and, their interaction imprints. The spectroscopy of the voxel, along with the imaging is now becoming a common practice to see the brain activates in real time in as narrow a region as possible.

The reader is reminded that what we discussed is a brief summary of the quantum theory, of the energy structure of an atom normally included in the physics teaching curriculum at the secondary school level science education with addition of some angular momentum algebra. Each main orbit n = 1, 2, 3,..of an electron around the nucleus has quantized energy = $-(K/n^2)$ (where K is a constant). Further each of the main orbit n is subdivided into sub shells called as s, p, d, f,.., corresponding to l = 0, 1, 2, 3,..etc. These are the degenerate levels of the main orbit n. The multi-nuclear ensemble like the brain produces a complex RF spectrum. It can be a rich source of information gathering about a tumor in the brain. Over a small region when there is no externally applied magnetic field the internal magnetic field creates an order of its own. We know that due to the degeneracy of, $g_s = 2$, of the electron's intrinsic angular momentum, $S_z = \pm 1/2\hbar$), the multi-particle resultant is $J' = L' + 2S'$ and not $J' = L' + S'$. Thus the magnetic moment μ_J' does not follow exactly, $J' = L' + S'$, but instead follows $J'' = L' + 2S'$. Accordingly the total magnetic moment, μ_H (also referred to as μ_T) = $\mu L + \mu_S$ is not exactly oppositely directed to J' i.e. it is not along $-J'$. By applying an external field H_Z the offset between the total multi-particle angular momentum J' and the total magnetic moment μ_J' is removed. They then follow each other (though they

are not directed in opposite directions internally on the molecular level) close enough and make the analysis simpler. The Z component of the total magnetic moment μ_{HZ} on the application of the RF radiation can now be easily manipulated with little modulations from the internal nuclear magnetic field.

The quantum correlations between the spins within a voxel become a source of detailed RF spectroscopy. For the total spectroscopic effect of the electrons, protons, nuclei, etc., the total spectroscopic splitting factor due to all the interactions, $g_J' = g_l' + g_s'$, will be used. In the Fig. 9.9 is shown as an illustration a doublet split of single energy level of an electron in an orbit like in a Hydrogen atom. This is the ideal lowest possible splitting. This doublet split will be present in the each orbit n for different levels corresponding to different sub-shells of an orbit in a more complex atom. The quantum numbers corresponding to the main orbit are, $n = 0, 1, 2,$ ….For each main total quantum number n there are, the familiar spectroscopic sub-shells, s.p.d, …corresponding to the sub-orbital quantum numbers $l = 0, 1, 2, 3$ …. These angular momentum sub-shells, accommodate the number of electrons as, $n_l = 2, 6, 10,$..according to, the quantum selection rule, $2(2l + 1)$ …,in each sub-shell. The total quantum number n can be written as $n = 1 + l + s$, where the spin quantum number, s, of the electron, produces doublet. This is referred to as the multiplet-structure in spectroscopy due to the l sub-shell and the electron s degeneracy. The internal atomic-nuclear magnetic field produces dynamic interactions among the atoms and molecules. The various brain activities happening all the time inside are part of the internal events dynamics. The overall resultant multi-particle-effect will split the quantum energy sub-shells. This is, called as the hyperfine-splitting.

A detailed spectroscopy of a voxel will show the signatures of, what exactly is happening in a small volume called as the voxel. This information is commonly collected by using the technique called as the proton magnetic resonance spectroscopy (PMRS). For a voxel PMRS is done at the same time when the image scan is performed. In the single electron spin only case the spectroscopic splitting factor is referred to by the symbol, g_s. This will be the case e.g. for the electron in the simplest atom hydrogen. Here the spectroscopic splitting factor, is given by, $g = g_s = 2$. This is an ideal situation when there are no interactions among the nuclei, atoms and molecules. As if they are isolated atoms with no interactions. It is not a real situation. Is it?. The reader is reminded inside the nucleus the forces are much stronger. In the nuclear case L's and S's combine first to form the J's. The $J_1, J_2,$ …etc. then combine to make, $J = J_1 + J_2$….., etc. The overall spectrum observed in a voxel however is not as complex as one may think. One should remember it is the unpaired electron in the outermost orbit of the atom which is chemically active and produces correlations with its neighbors. The electrons in the deeper orbits do not contribute.

9.2.4.3   Various Quantum States of the Nuclear Magnetic Dipole Moment

A nucleus contains protons and neutrons. The number of protons is called as the atomic number Z of an element. The sum of the total number of neutrons N and the
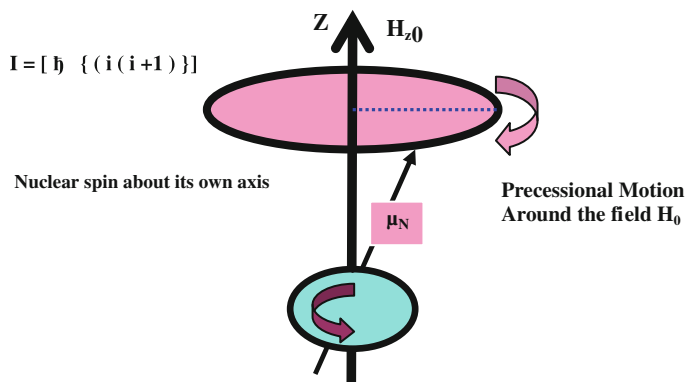
$$I = [\hbar \{(i(i+1))\}]$$

Nuclear spin about its own axis

Precessional Motion Around the field H_0

μ_N

Fig. 9.10 The precessional frequency Ω of the nuclear magnetic moment around the applied static magnetic field H_0 is given as $\Omega = \gamma_N H_0$

protons Z is called as, the mass number, $A = Z + N$ of the atom. The protons and neutrons called as the nucleons have an associated magnetic moment. In a nucleus overall the resultant magnetic moment depends on whether the total number of nucleons is even or odd. Some nuclei have even and others odd number of nucleons. Due to the nuclear forces between them the even pairs have resultant zero magnetic moment. The unpaired (left over) single nucleons produce a resultant magnetic moment. This nuclear magnetic moment call it as μ_N is the result of circulating currents of the nucleons. The circulating motion has associated with it the angular momentum of the motion I. Analogous to the atomic case the nuclear angular momentum (see Fig. 9.10) due to the quantum mechanical principles can occupy only quantized positions give by $I = \hbar [(\sqrt{(i(i + i))}]$. Here $\hbar$ is the angular Planck's constant and $= h/2\pi$ where h is the linear Planck's constant. The quantum number, i, depending upon whether mass number and the atomic number of the nucleus is even or odd can have values $i = 0, 1/2, 1, 3/2, 5/2…$etc. One can split the nuclei into three categories. If the mass number of the nucleus (total mass of the protons and the neutrons) is odd then whether the atomic number (the total number of protons which is also equal to the total number of electrons in the atom) is even or odd the nuclear spin can have values $1/2, 3/2, …$etc. On the other hand if the mass number is even and the atomic number is odd then the nuclear spin can have the integer values, $1, 2, 3,…$etc. And the last when the mass number and the atomic number are both even the nuclear spin is 0.

Consider now a static magnetic field is applied in the Z-direction. The result is that the plane of the circular motion now lies in the X–Y plane. The spin vector which is perpendicular to the orbital plane is now pointing along the z-direction instead of being anywhere in space. But the I_z component is restricted with selected quantized values $I_z = m_z \hbar$. Here $m_z = 0, \pm1, \pm2, …$The nuclear magnetic moment is givens as $\mu_N = (e\hbar/2 m_p)$. Here e is the proton or the electron charge and m_p the mass of the proton. The nuclear magnetic moment has the similar kind of properties as does the atomic one. The only difference is that, the magnitude of the nuclear

magnetic moment is thousand times smaller as the proton is thousand times heavier than an electron. The ratio of the nuclear dipole magnetic moment μ_N to its angular momentum I, is called as the nuclear gyromagnetic ratio $\gamma_N = NGMR = \mu_N/I$. There is an interaction energy associated between the nuclear magnetic moment and the atomic one. It is approximately including the possible interactions written as

$$\Delta E = C \; [\; f \; (f + 1) \text{-} \; i \; (i + 1) \text{ - } j \; (j + 1)].$$

Here f, i and j, are the quantum numbers corresponding to the various angular momentum as follows. f = grand total angular momentum quantum number (atom + nucleus); i = total nuclear angular momentum; j = total atomic angular momentum. The constant C is proportional to the magnitude of the nuclear magnetic dipole moment μ_N. The $\mu_N = (e\hbar/m_p) = 0.505 \times 10^{-28}$ amp-m$^2 \approx 10^{-3} \; \mu_b$ (m_p is the mass of the proton and μ_b, the Bohr magneton, as in the atomic case). Measurement of the hyperfine (Zeeman) splitting, ΔE, can be related to the multiplicity energy structure as expected by the above equation. It is seen that the sign of the nuclear magnetic dipole moment arises due to the relative orientation of the magnetic dipole moment vector and the angular momentum vector of the nucleus. It can be positive as well as negative. The following quantum rules are important to remember. (1) the total nuclear angular quantum number i, often called as the nuclear spin, is obtained by counting the multiplicity of the split nuclear energy level. (2) if the multiplicity is associated with, j > i, then f can have (2i + 1) values, and thus (2i + 1) energy levels. (3) i is an integer for nuclei of even A, with i = 0 if Z is also even. (4) i is a half-integer for nuclei of odd A. (5) the nuclei with integral spin angular momentum (nuclei of even A) are of symmetric type (called as bosons) while the nuclei with half-integral i (nuclei of odd A) are called as fermions. (6) the neutron precisely has the same intrinsic spin angular momentum and symmetry character, as proton, i.e. s = 1/2 and anti-symmetric.

The reader may have noticed by now that the atomic and nuclear spin properties methodically look exactly identical except for the magnitudes. Put it in another way the phenomenological mathematics has been developed by the PCM experts in such a way to make them look mathematically identical. It is very important to have a system mathematically logical and consistent. This is to be able to add further developments in a logical and professional manner. The nature chooses to be methodical, logical and consistent. why can't we?

9.3 Electric Quadrupole and Magnetic Dipole Interaction System

9.3.1 Na Magnetic (Spin 3/2): Electric Quadrupole System

Anisotropic nuclear charge distribution of a nucleus can be broken as a sum of Mono-Pole (centrally symmetric) + Di-Pole (positive and negative centers
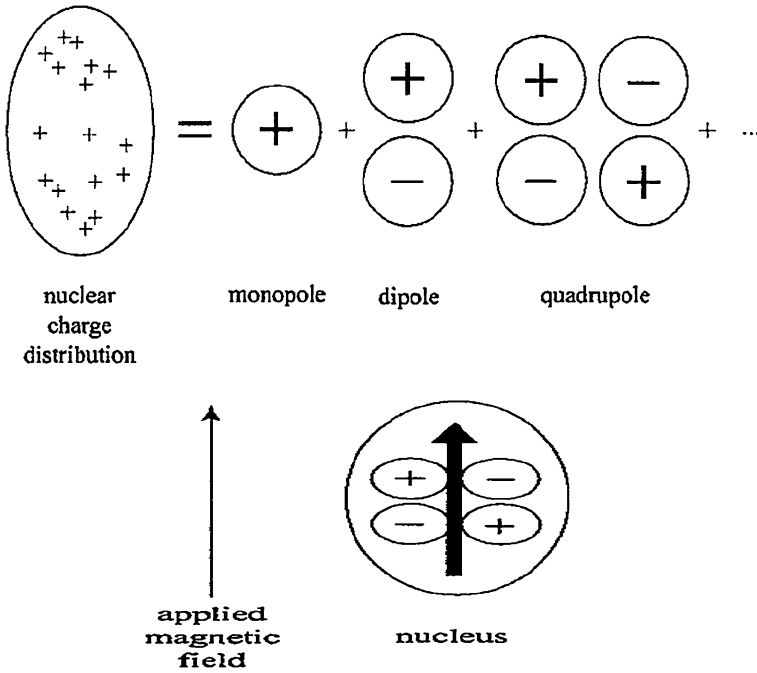
Fig. 9.11 Schematic illustration of the description of a charge distribution as a sum of multipole terms. The electric dipole term effect is always zero for a nuclear charge distribution; if it were not, there would be a net force from the electric field arising for the dipole moment

displaced) + Quadrupole (asymmetric charge distribution with four poles) + higher orders The Figs. 9.11 and 9.12 [4] are an approximate pictorial representation of the breaking of the charge asymmetry into different types of orders. One should notice a quadrupole nucleus e.g. Na (I = 3/2) under the influence of a static magnetic field in MRI aligns itself so that the magnetic dipole moment axis is oriented along the external magnetic field applied. This becomes like a reference axis around which the associated electric quadrupole moment, of Na displays its electric–magnetic interaction properties. As an example in an ischemic situation there is an electric field gradient in the tissue across the membrane where there are Na^+ nuclei present. The sodium concentration gradient maintains an electric field in the tissue and across the membrane for the routine metabolic activities in a healthy tissue. The situation changes when there is a diseased portion in the tissue. Now the concentration inside the tissue and outside are not the same as would have been in a healthy person. The relaxation times (T_1 and T_2), inside and outside of the tissue are also now the different ones with fast and slow characters. The changed relaxation times now become the source of the changed MRI of the region resulting in the diagnostics of the ischemia.
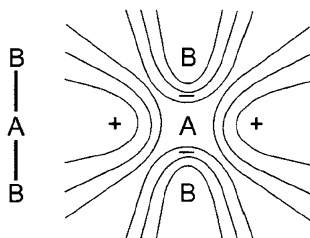
Fig. 9.12 In the high field limit the magnetic dipole moment represented by the *bold arrow* (see Fig. 9.11) is oriented by the applied magnetic field in an NMR experiment. The nuclear electric quadrupole moment associated with the nucleus is thus also oriented with respect to the applied magnetic field, although it has no direct interaction with it. An, example molecule (AB_2/B-A-B) with bonds in the geometry shown on the *left* will give rise to an electric field gradient of the form shown on the *right* by virtue of the electron bond distribution. There will also be an electric field gradient arising from the core electrons of all the atoms. Such an electric field gradient will interact with any nuclear electric quadrupole moment

9.3.2 The Electric–Magnetic Interaction Energy: Simple Concepts

The quadrupole nuclei (i.e. those with $I > 1/2$) possess an electric quadrupole moment in addition to the magnetic dipole moment. All NMR-active nuclei must have that. Electric quadrupole moment, Interacts with the electric field gradient which in turn arises from a particular distribution of electrons and other charges around the nuclei. The nuclear electric quadrupole moment-electric field gradient interaction can be rather large. In the heterogeneous nuclear situation in our brain one can assume medium, as amorphous but still containing some orderly distribution of spins. The size of nuclear electric–magnetic interaction depends on the size of the nuclear electric quadrupole moment. The magnitude of a nuclear quadrupole moment for various nuclei has been worked out and one can see them in a standard text (see Appendices A, for a summary) on NMR spectroscopy. The size of the electric field gradient is determined by the molecular and the electronic structure around the nucleus. In a simplified mathematical expression format one can write the interaction energy between the magnetic dipole and the electric quadrupole as $\sim[(eQ)/\{6I(2I-1)\hbar\}] [(\partial E/\partial x]$. Here (eQ) is called as the electric-quadrupole moment and $[(\partial E/\partial x]$ is the electric field gradient at a point x, and I, is the nuclear magnetic moment (normally referred to as nuclear spin). The electric field will be anisotropic in distribution when represented in the Cartesian or spherical frame of reference. Other technical symbols that often appear in the literature of the quadrupole MRI, are, $eq = [(\partial E/\partial r]$, the electric field gradient along the principal axis of, the gradient in the charge concentration and, $\lambda_Q = [(V_{xx}-V_{yy})/V_{zz}]$, the magnitude of asymmetry in the x–y direction with respect to the principal, axis z of symmetry, etc.

In a large magnetic filed the Zeeman (magnetic splitting) interaction involving nuclear magnetic dipole-electric quadrupole moment is the dominant interaction. The applied magnetic field in such a case acts as the quantization axis for the nuclear spins. Thus the magnetic dipole moment is oriented by the applied magnetic field and with it (because it is part of the same nucleus) the nuclear electric quadrupole moment. This is despite the latter has no direct interaction with the applied field. The electric filed gradient components are merely determined by the molecular structure around the nucleus. It thus has an orientation that is fixed with respect to a molecular frame of reference. The interaction between the nuclear electric quadrupole moments then depends on their orientation with respect to the molecule which in turn is determined by the direction of the applied static magnetic field. How strong the interaction is depends upon the magnetic field applied. In an another interpretation the size of the electric–magnetic interaction is expressed by comparison of the size of the quadrupole coupling interaction relative to the Zeeman interaction.

One can work out the transition frequencies ($\Delta\omega_Q$) expected for a quadrupolar spin I between levels m → m + 1. Here m denotes the magnetic quantum number. Approximately one can write, $\Delta\omega_Q \sim \{[(3\ e^2qQ)/[4I(2I-1)]]\}(2m + 1)$. There are two other mathematical terms frequently used in the case of quadrupole nuclei. The first is the quadrupolar constant $C_Q = [(e^2qQ)/h]$ measured in the units of Hertz (Hz). The second is the quantity $\chi = [(e^2qQ)/\hbar]$ measured in units of radians/s. Here $\hbar$ and h are respectively the angular and the linear Planck' constants respectively. Quadrupole coupling constants are often of the order of megahertz for quadrupolar spins in sites of non-cubic symmetry. One can work out from the above equation as follows. For half integer spins the central transition $+1/2 \to -1/2$ has a transition frequency that to a first order is independent of the molecular orientation. Thus to a first order approximation the transition is not broadened by the quadruple coupling. The second order contribution to the transition frequencies has an isotropic component. This will feature in the NMR spectrum of the nucleus in addition to any isotropic chemical shift that may be present.

9.4 ^{23}Na Electric-Quadrupole Magnetic-Dipole Systems: Practical Examples

9.4.1 Quadrupole Electric-Dipole Magnetic Spin 3/2 System (Molecular Structure-Quantum Energy Diagrams)

We known that the multi-quantum NMR signals arising from quadrupole atomic nuclei with the spin quantum number I = 3/2 can be measured but with some difficulty. The important nuclei in this electric–magnetic system are ^{23}Na, ^{35}Cl and ^{39}K etc. A tissue in the brain is complicated on both the macroscopic and molecular spatial scales. The Na and Cl ions are seen mostly extra-cellular. The
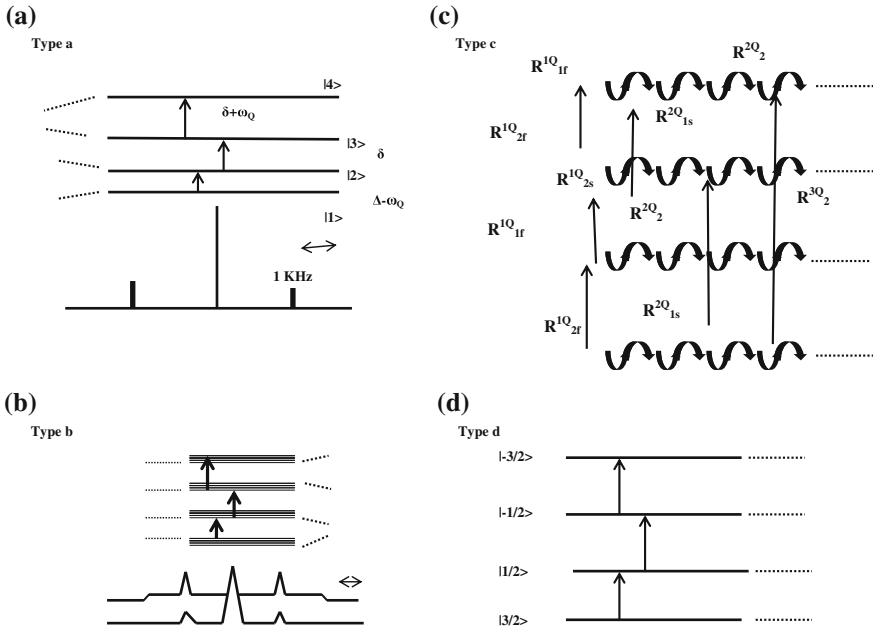
Fig. 9.13 a–d Rotating frame energy level diagrams for isolated I = 3/2 systems. Four types of motionally narrowed 1D1Q (one dimensional one quantum) spectra are possible (**a**, **b**, **c** and **d**). Representative ^{23}Na spectra are shown in each of the energy level diagrams

^{23}Na MR images, appear to show an intriguing correlation with tumor pathology. There are four distinct types of single quantum (conventional MRI) spectrum [5] which can arise depending on the motional characteristics of the nuclear environment. The type a (Fig. 9.13a) [5] is the single crystal-like spectrum. The type b (Fig. 9.13b) [5] is the inhomogeneous 'powder' spectrum. The type c (Fig. 9.13c) [5] is the homogeneous 'biexponential' spectrum. The type d (Fig. 9.13d) [5] is the homogeneous 'extreme narrowed' spectrum. In the molecular environment of the spin 3/2 nucleus the relative energies of the four nuclear spin states (3/2, 1/2, −1/2, −3/2) are modulated by electric field gradient (EFG) effects which fluctuate in time due to thermal motions. One can express the fluctuations of the quadrupolar interactions in term of the quadrupole frequency ω_Q. It is also referred to as the spectroscopic splitting factor sensed by a test nucleus (Na) in different environments. The sodium concentration in a tissue has a dynamic equilibrium with its environment. This concentration fluctuates due to thermal and electrostatic field reasons in a region.

One can measure the fluctuation through the rate at which it changes called as the transition rate R. The inverse of this transition rate $1/R = \omega_Q$ is the frequency of variation of the dynamic processes happening. The dynamic processes are between the electric quadrupole of the sodium nucleus and the environment. The environment is of the electric field gradient between a tissue and the surrounding

region through a cell membrane. The significance of ω_Q arises due to the fluctuating electric field gradient EFG (eq) in the molecular environment. The time averaged value of ω_Q can be approximately represented as $\sim < \omega_Q > = [(4 \text{ h})^{-1}\text{eQ}$ (eq($3 \cos^2 \theta - 1$))]. Here eQ is the electric quadrupole moment of the nucleus (around 10^{-25} $C^2 cm^2$ for ^{23}Na), h is the Planck's constant, e, is the electron charge., θ, is the angle, between the electric field gradient eq and the applied magnetic field in the z direction. Figure 9.13 [5] describes the quantum energy structure of the electric quadrupole in the presence of an electric field gradient for the four different types of molecular structures of the environments in which the quadrupole is present. A summary of the meaning of the four different types of environments is also included.

   The type a (Single Crystal): The type a, 1D lQ ^{23}Na, spectrum, was obtained, from a ternary mesophase of composition 37 % sodium dodecylsulfate, 11 % n-decyl alcohol and 52 % ^2H_2O. The resonance frequencies of the satellites are ± 17 kHz. The acquisition parameters of the spectrum are the following: 90°, t_p (pulse time) = 17.5 µs, SW (signal width) = 33.3 kHz, d (delay) = 35 µs, T = 22 °C, final value of t_5 (signal time) was 30.72 ms; 200 ms was inserted at the end of every t_5 period. Since 256 scans were averaged the total time to acquire this spectrum was 1 min. **The type b (Inhomogeneous Powder)**: **(conventional MRI)**: The type b spectrum was obtained from a ternary mesophase of composition 38 % sodium dodecylsulfate, 8 % n-decyl alcohol and 54 % 'H_2O. The acquisition parameters of the RT (room temperature) spectrum were as follows: 5,000 scans with t_p (pulse width) = 10 µs (51° nutation angle), the final value of t_5 (time after 5th pulse applied) was 40.96 ms, d = 20 µs, and SW (signal width) = ± 5 0 kHz. No inter pulse delay was used, so the total time to acquire this spectrum was 205 s. **The type c (homogenous-biexponential)**: **(conventional MRI)** The type c spectrum is that of Na^+ in an aqueous solution which has a high concentration of micelle-solubilized gramicidin channels. **The type d (Single Crystal)** **(conventional MRI):** The type d spectrum is that of NaCl in H_2O. The type b and type a spectra are of Na^+ in aqueous suspensions of un-oriented and oriented dodecylsulfate micelles, respectively.

9.4.2 Spectroscopy (Simple Theory) Quadrupolar Interactions Dispersion versus Absorption Plots (DISPA)

The longitudinal and transverse relaxation time experiments are commonly used to study spectral features of the nuclei specifically their line shapes and the frequency [the second order dynamic shifts (SODFS)] [6]. It is known that the SODFS can make significant changes to the lineshape as compared to the standard Lorentzian shape. A conventional (single quantum) spectrum of an I = 3/2 (sodium) system can be represented as a superposition of two components a broadened component

and a narrowed component. In the extreme narrowing condition i.e. $\omega_0\tau_c \ll 1$, where ω_0 is the Larmor frequency and τ_c, is the correlation time between different interactions the narrow and broad components are degenerate in both width and absorption frequency. On the other hand when $\omega_0\tau_c > 1$ the extreme narrowing condition does not hold and these degeneracies do not result. This book is not the right place to go into detailed mathematical, treatment to work out the intensity equations for the narrow and broad components. Those readers who are keen to know the details they are refereed to the cross references listed, in the Ref. [6]. For others the following simple extract of equations should prove useful. The equations are as follows.

The Transverse Magnetization:

$$<I_+^n(t)> \; \sim \sin\theta <I_Z^T> [\exp[\{-(J_1+J_2)t\}][\exp\{-i(\omega_0+Q_1-Q_2)t\}]$$

$$<I_+^b(t)> \; \sim \sin\theta <I_Z^T> [\exp[\{-(J_0+J_1)t\}][\exp\{-i(\omega_0-Q_1)t\}]$$

The Longitudinal Magnetization:

$$<I_Z^n>(t)> \; \sim (\cos\theta - 1) \; <I_Z^T> [\{2\exp(-2J_2t)\}-\exp\{-2J_1t)\}]$$

$$<I_Z^b>(t)> \; \sim (\cos\theta - 1) \; <I_Z^T> [\exp\{-2J_1t)\}]$$

In the above equations, I^n and I^b, are the intensities of the narrowed and broad components respectively and I_Z^T is the thermal equilibrium value. The enclosing symbols $<>$ mean an average value. The angle θ in the above equations has its origin in the flip angle present in the duration time of the pulse and $\tau = [\theta/(\gamma B_1)]$. Here γ is the gyromagnetic ratio and B_1 the amplitude of the RF (radio frequency) pulse applied. J_0, J_1 an J_2, above are the spectral densities of zero, 1st and 2nd order arising as a result of the pulse and the Qi are the SODFS. It is known that the SODFS do not directly affect the spin density relaxation characteristics but a synergistic relationship between the (time dependent) lineshape characteristics and the ability to correctly monitor the time-dependent features of the longitudinal magnetization does exist. It is important to note that in longitudinal case the broad component decays as a single exponential whereas the narrow component decays nonexponentially. Figure 9.14 is presented as a simple mathematical-analytic representation for the case $\omega_0\tau_c = 2$.

The Fig. 9.14 shows the theoretical absorption lineshape for an $I = 3/2$ spin system. An isotropic modulation of the quadripolar interaction is assumed. The correlation time, $\tau_c = 2/\omega_0$. From the figure it is obvious that the spectral lineshaspe is skewed and perhaps non-Lorentzian. However if one were unaware of the intrinsic asymmetry of this absorption bandshape a (incorrect) compensating adjustment of phasing would undoubtedly conceal or obscure this inherent asymmetry. Also any incorrect phasing could result in erroneous determinations of the characteristic time constants. The DISA plots thus can provide means in the recognition and isolation of various relaxation parameters.
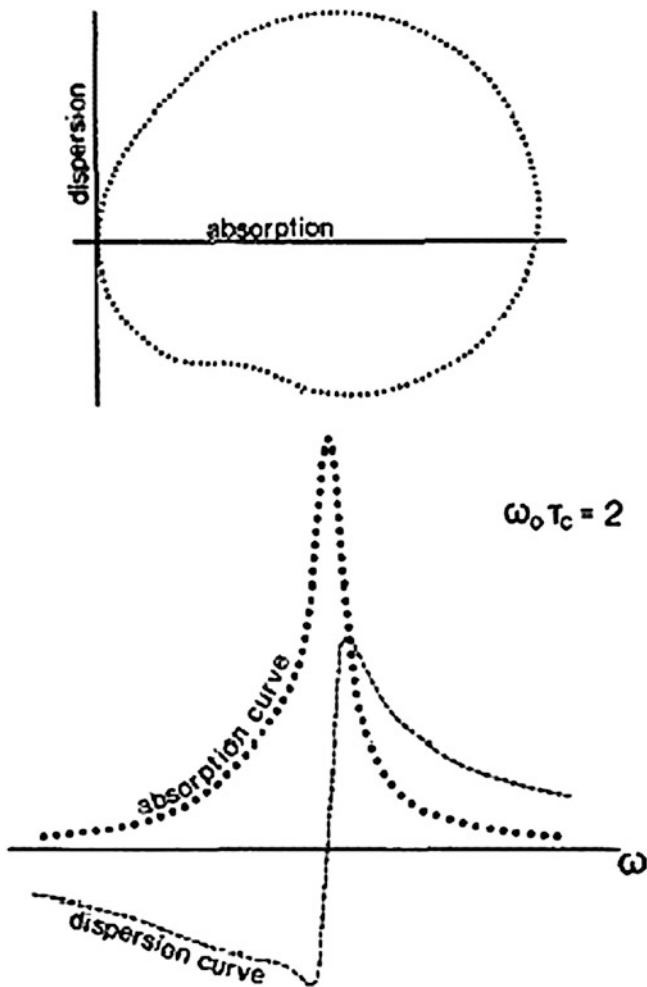
Fig. 9.14 Idealized absorption spectrum for the Z = 3/2 spin system assuming isotropic modulation ($\tau_c = 2/\omega_0$) of the quadrupolar interaction. Also shown is the dispersion representation of this system and the dispersion versus absorption (DISPA) plot

9.4.3 Electric–Magnetic (Double Quantum) Resonance Spectroscopy (Theory) Spin 3/2 System (Cl⁻)

Chlorine is the eighth most abundant element in the human body. It is present almost exclusively as the chlorine ion and is distributed mostly in the extra cellular aqueous spaces. The ^{35}Cl nuclide [7] has a very short longitudinal relaxation time T_1 and gives a very broad signal and thus not easy to observe in vivo situation in the human model. The 2D-2Q experiments are used to perform this kind of
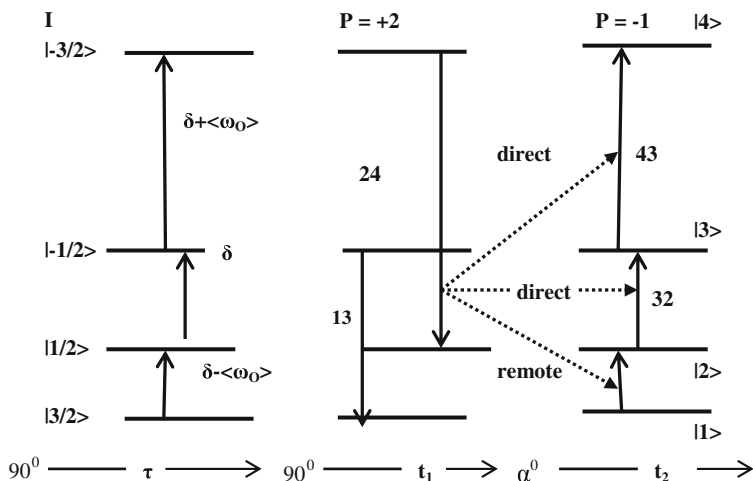
Fig. 9.15 The rotating-frame energy level diagram for a system of isolated spin-2 nuclei in the presence of nonzero averaged electric field gradient magnitude-orientation products. Coherences and coherence transfers are indicated. For the coherences (*solid arrows*) the arrow directions have relative importance

analysis. The Fig. 9.15 [7] depicts a rough sketch of the energy level diagram for an isolated I = 3/2 nucleus in the presence of a non-zero averaged electric field gradient. (EFG) orientation. One can define an average frequency of interaction as $< \omega_Q > = (e^2qQ)[\{(3 \cos^2\theta - 1)/4\hbar\}]$. Here $< \omega_Q >$ is an average nuclear quadrupolar-magnetic moment resonance frequency, eQ is the electric quadrupole moment of the nucleus, eq is the averaged value of the major element of the EFG tensor (presumed axial), θ is the angle between the principal axis of the EFG tensor and, the Zeeman magnetic field direction, e is the electron charge, and $\hbar$, the angular Planck's constant. The Fig. 9.15 is drawn for inherently positive values of $< \omega_Q >$ and γ, the gyromagnetic ratio. The pulse sequence used is the standard for the 2D-2Q system and is $90° (\phi_1) - \tau/2 - 180° (\phi_2) - \tau/2 - 90° (\phi_3) - t_1 - \alpha_0 (\phi_4) - t_2 (\phi_5)$. Here α_o is the flip angle of the read pulse.

If the viscous forces are small compared to the torque created by the interaction of the static magnetic field and the anisotropic diamagnetic susceptibility of the phase, the liquid crystalline domains in the sample, can become oriented with respect to the field. The orientation, in the sample increases with time in the magnetic field and a single crystalline spectral behavior is asymptotically approached. The spectroscopy experiment used the ^{35}Cl resonant frequency of 29.4 MHz. The two-dimensional, experiments were performed with quadrature phase detection enabled during the T_2 acquisition period. The quadrature phase detection was not used in the T_1 time domain. Thus both, the positive and negative 2Q, coherences survive and are present in the processed spectra. The order separation is achieved in experiments in which a transmitter offset ($\delta \neq 0$) is used
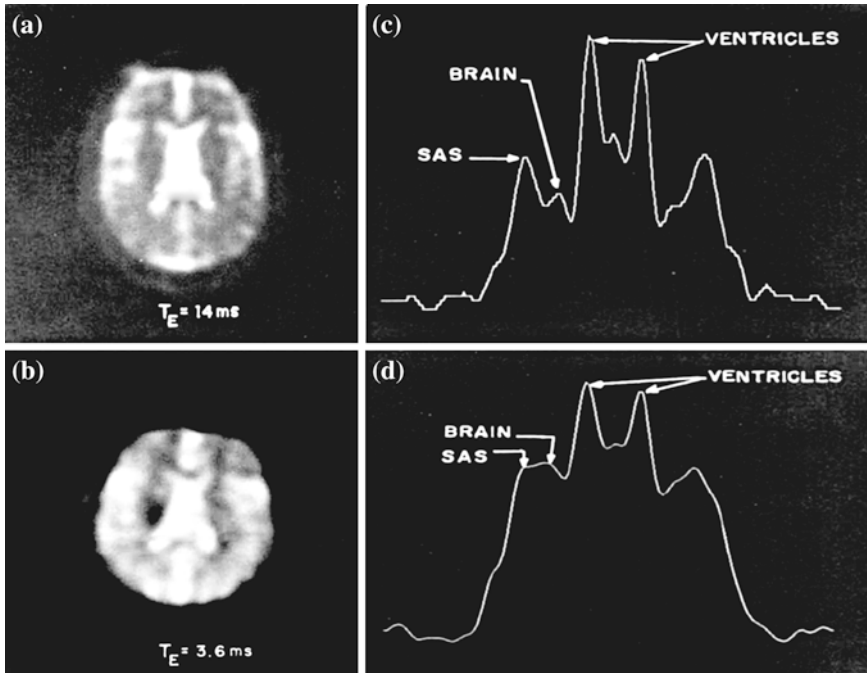
Fig. 9.16 The comparison between **a** 14-ms and **b** 3.6-ms echo images. The transverse plots show the difference in the relative ratios between the CSF (cerebrospinal fluid) and the brain regions containing extra- and intracellular sodium components, respectively. The second set of images (**c**) and (**d**) are the spectrum details corresponding to the first set of images (**a**) and (**b**). In the short echo time (3.6 ms) image there is a pronounced increase in the intraparenchymal sodium signal when compared to the conventional (T_E = 14 ms) case. The long echo time image emphasizes the sodium in the cerebral ventricles and subarachnoid spaces (SAS). The spectrum shows the increased visibility of the short T_2 (T_E = 3.6 ms) in the brain

shifting each manifold by pδ, where p, is the signed order of the coherence. However, when δ = 0, the positive and negative 2Q coherences overlap.

9.4.4 NMRI (Nuclear Magnetic Resonance Imaging) Short T_2 Component (Human Model), Sodium ^{23}Na (3/2 Spin System)

In a living tissues it is observed that sodium has at least two transverse relaxation time (T_2) constants[8]. A short one ~1 ms and a long one ~20 ms. One also sees that the measured T_2 of intracellular sodium is shorter than that of the extra cellular sodium. In pure aqueous solutions sodium is seen to relax monoexponentially with long T_2 around 40 ms. In the intracellular space one finds the electrostatic field gradients are present around cell membranes. The

macromolecular quadrupolar interactions are believed to control the sodium relaxation mechanism of the two T_2 components. The nuclear quadrupole-magnetic dipole interaction splits the magnetic spectrum into three lines. There is a central unshifted spectral line. It reflects the transition between the energy levels characterized by the magnetic quantum numbers m = ±1/2. There are in addition a pair of satellite transitions reflecting the interactions between the energy levels characterized by m = 3/2 to 1/2 and by m = −1/2 to m = −3/2. These satellite lines are equally displaced about the central line. It is commonly observed, that only 40 % of the sodium electrical signal arises from the central transition. The two satellite lines contain the 60 % of the sodium signal. In aqueous solutions the satellite lines are much broader than the central line and have a shorter T_2.

It is now commonly seen that the intracellular sodium has a multi-exponential T_2 decay. It is assumed to be the consequence of the electrostatic field gradient imposed on the Na^+ ion in the complex intracellular environment. The extra cellular space seems to have a less complex environment. The consequence of this discrimination provides the potential of separation of imaging of the short and the long relaxation fractions (Fig. 9.16). One can thus establish insight into the various types of brain edemas. There are for example those associated with the expansion of the extra-cellular space (vasogenic edema) and the edema associated with the expansion of the intra-cellular space (cytotoxic edema). One also observes that the intra-cellular sodium increases roughly threefold in malignant cells. Thus an index of intracellular sodium can provide a worth while tool for useful clinical means to evaluate seriousness of malignancy. Below is presented a practical example of short component T_2 relaxation time using conventional (single-quantum) NMRI.

9.4.5 NMR Spectroscopy (Animal model): Double Quantum Intracellular Sodium Coherence Transfer

One can use a double quantum filter to block signal from sodium which belongs to relaxation as a mono-exponential one. In a cell suspension in which the intracellular sodium relaxes bi-exponentially the selective detection of the intracellular sodium can be accomplished [9]. It is known that bi-exponential relaxation occurs when the −3/2 to −1/2 and the 1/2 to 3/2 transitions of spin −3/2, sodium nuclei, relax much faster than the central −1/2 to 1/2 transition. The interactions between the electric quadrupole moment of the sodium nucleus and the fluctuating electric field gradients at sodium binding sites cause sodium to relax bi-exponentially. This is despite only a small fraction may actually be bound. The sodium which relaxes bi-exponentially can be passed through a state of double-quantum coherence. The reader would find it illustrative to see the following practical (Fig. 9.17 [9]) example which clearly demonstrates the filtering out the bi-exponential signal for detection or imaging.
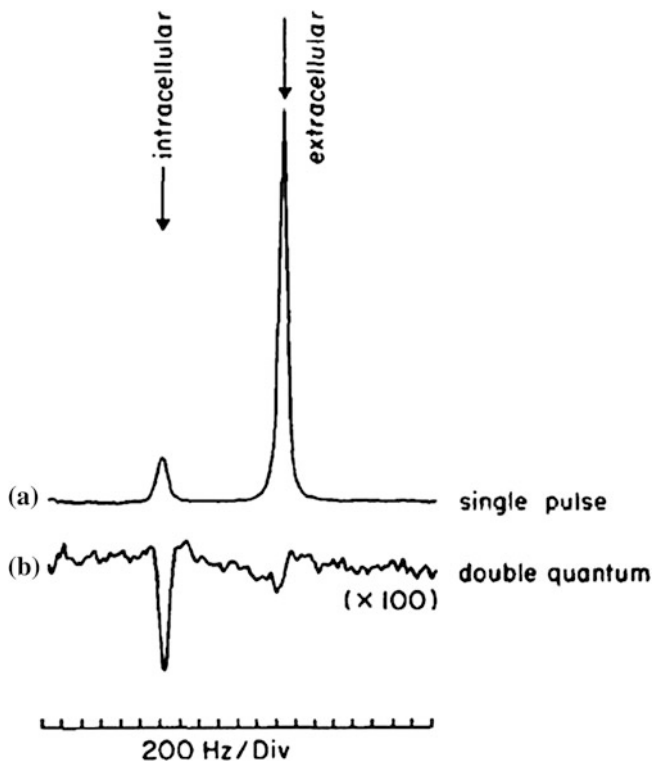
Fig. 9.17 Sodium-^{23}NMR spectra of dog red cells suspended in isotonic medium containing 12 mM $[Dy(P3 \sim O_{10})_2]7^-$. **a** Conventional spectrum; phased Fourier transform of averaged free precession signals following single 90° RF pulses, 64 acquisitions in about 20 s. **b** Double quantum filtered spectrum; phased Fourier transform of averaged free precession signals using phase-cycled pulse sequence, 3200 acquisitions in about 17 min. (Vertical scale corrected for different number of acquisitions; intensity represents signal per scan)

9.4.6 Triple Quantum Filtered (MRI) Sodium Ion Imaging (Animal Model)

In our body normal cells maintain the concentration of intracellular sodium ion $(Na)_i$ at 10–I5 mM against an extra cellular $(Na)_e$ concentration of 150 mM. This gradient is lost in damaged cells. In certain tumor cells and observation of abnormal levels of Na_i in vivo has great diagnostic potential. NMR detection of, Na_i is complicated by the chemical-shift insensitivity of sodium-23. There is a short relaxation times of Na_i. The extra cellular sodium ion Na_e from edema normally accompanies tissue damage or tumor growth and, the chemical-shift overlap of signals from Na_i and Na_e. In all in vivo environments the sodium nucleus experiences electric field gradients at macromolecular binding sites. Coupling of the quadrupolar moment of the sodium nucleus to these gradients
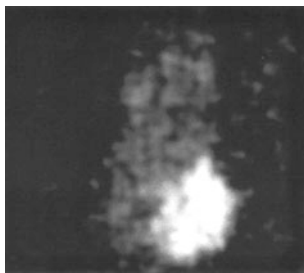
Fig. 9.18 TQC-filtered image of a nude rat with a CG (canine glioma) tumor. A total of 120 scans were acquired per block of a I28 × 256 point data matrix. The field of view was 156 by 156 mm. The echo time and TQC generation times were 4.0 ms, and the repetition time was 250 ms. The receiver gain was increased by a factor of 8 and the data are presented with an eightfold increase in the image scaling factor. The echo in each dimension was treated with 500 Hz of double exponential broadening

induces differential relaxation among the three possible nuclear transitions. When the correlation time of the sodium nucleus is short these effects do not alter the Zeeman splitting among the four possible spin (magnetic) states. Further increases in the effective correlation time leads to shifts in the relative energy levels. The multi-exponential relaxation observed for Na_i is one result of this condition. In addition there is magnetization from those sodium ions with the appropriate correlation time, $\geq \omega_L^{-1}$, where, ω_L, is the inverse angular Larmor frequency. It can evolve into multiquantum coherence (MQC). This result is in fact common to many quadrupolar nuclei with $I > 1$ and is a function of the correlation time the order of the spatial environment and the quadrupole moment.

The triple-quantum coherence (TQC) [10] of quadrupolar nuclei between the $m = -3/2$ and the $m = 3/2$ spin states has unique NMR properties. The TQC is unaffected by the electric field gradients and is expected to have a longer relaxation time than the double-quantum coherence. A TQC filter can be used to image selectively a unique class of sodium ions in the absence of shift reagents. The sodium NMR signal from this subset of ions can be detected using the short echo times normally required to observe the signal from intracellular sodium ions. TQC-filtered images can be obtained in reasonable periods of time and allow altered distributions of sodium ions which generate TQC to be detected in diseased tissues such as, growing tumors. A, TQC-filtered projection image of the sodium ions within a rat is presented in the Fig. 9.18 (Fig. 9.7 [10]). The experimental parameters were as the standard in using the TQC-filtered imaging pulse sequence. The region of the tumor is observed as an area of hyper intense signal within the region of edema observed.

Analysis of the histogram of the image shows that the intensity of signal from TQC-filtered sodium ions in the area around the growing margin of the tumor is 2.0–2.5 times greater than the signal from the surrounding tissues. This observation of greater TQC-filtered signal intensity has been observed, in six rats with tumors of volumes ranging from, 1 to > 27 cc ($P < 0.05$). The conventional sodium

image of a rat has regions of hyperintense signal where the concentration of extra cellular sodium is high: the kidneys, blood in the heart and urine in the bladder. The TQC-filtered image has uniform signal intensity, consistent with a uniform concentration of sodium ions which generate TQC in all tissues. The signal may arise from any tissue compartment where the sodium ions experience a local correlation time which allows creation of TQC such as intracellular sodium ions, interstitial sodium ions or possibly extra cellular sodium ions.

References

1. Giancoli, D.C.: Physics for Scientist and Engineers, with Modern Physics. Prentice Hall, USA (recent edition)
2. Eisberg, R., Resnick, R.: Quantum Physics of Atoms, Molecules, Solids, Nuclei, and Particles. Wiley, USA (recent edition)
3. Goswami, A.: Quantum Mechanics. Wm. C. Brown Publishers, USA (recent edition)
4. Ashbrook, S.E., Duer, M.J.: Structural information from quadrupolar nuclei in solid state NMR. Concepts Magn. Reson. **28**(3), 183–248 (2006)
5. Rooney, W.D., Springer C.S. Jr.: A Comprehensive approach to the analysis and interpretation of the resonances of spins 3/2 from- living systems. NMR Biomed. **4**, 209–226 (1991)
6. Werbelow, L.G. Jr.: The NMR of spin-3/Z nuclei: the effect of second-order dynamic frequency shifts. Magn. Reson. **43**, 443–448 (1981)
7. Xu, Y., Barbara, T.M., Rooney W.d., Springer, C. s. Jr.: Two-dimensional multiple-quantum NMR spectroscopy of isolated half-integer spin systems. II. 35Cl Examples *. J. Magn. Reson. **83**, 219–298 (1989)
8. Ra, J.B., Hilal, s.K., Cho, z.H.: A method for in vivo MR imaging of the short T2 component of sodium-23*. Magn. Reson. Med. **3**, 296–302 (1986)
9. Pekar, J., Renshaw, P.F., John s.J. Jr.: Selective detection of intracellular sodium by coherence-transfer NMR. J. Magn. Reson. **72**, 159–l61 (1987)
10. Griffey, R.H., Griffey, B.Ev., Matwiyoff, N.A.: Triple-quantum-coherence-filtered imaging of sodium ions in vivo at 4.7 tesla. Magn. Reson. Med. **13**, 305–3I3 (1990)
11. Forsfin, S., Drakenbergj, T., Wennerstrom, H.: NMR studies of ion binding in biological systems. Q. Rev. Biophys. **19**(1/2), 83–114 (1987)
12. Tanase, C., Boada, F.E.: Algebraic description of spin 3/2 dynamics in NMR experiments. J. Magn. Reson. **173**, 236–253 (2005)
13. Choy, J., Ling, W., Jerschow, A.: Selective detection of ordered sodium signals via the central transition. J. Magn. Reson. **180**, 105–109 (2006)
14. Shinar, H., Navon, G.: NMR relaxation studies of intracellular Na+ in red blood cells. Biophys. Chem. **20**, 275–283 (1984)
15. Viswanathan Seshan, A., Sherry D., Bansal, N.: Evaluation of triple quantum-filtered 23Na NMR spectroscopy in the in sifu rat liver. Magn. Reson. Med. **38**, 821–827 (1997)
16. Turski, P.A., Perman, W.H., Hald, J.K., Houston, LW., Strother, C.M., Sackett, J.F.: Clinical and experimental vasogenic edema: in vivo sodium MR imaging. Radiology **160**, 821–825 (1986)
17. Thulborn, K.R., Gindin, T.S., Davis, D., Patricia Erb, R.N.: Comprehensive MR imaging protocol for stroke management: tissue sodium concentration as a measure of tissue viability in nonhuman primate studies and in clinical studies. Radiology **213**, 156s–166s (1999)
18. Stobbe, R., Beaulieu, C.: In vivo sodium magnetic resonance imaging of the human brain using soft inversion recovery fluid attenuation. Magn. Reson. Med **54**, 1305–1310 (2005)
19. Bull, T.E.: Nuclear magnetic relaxation of spin-3/2 nuclei involved in chemical exchange J. Magn. Reson. **8**, 344–353 (1972)

20. Pear, J., Legion, J.S.: Detection of biexponential relaxation in sodium-23 facilitated by double-quantum filtering. J. Magn. Reson. **69**, 582–584 (1986)
21. Hancu, I., Boada, F.E., Shen, G.X.: Three-dimensional triple-quantum–filtered 23Na imaging of in vivo human brain. Magn. Reson. Med. **42**, 1146–1154 (1999)
22. Fleysher, R., Fleysher, L., Gonen, O.: The optimal MR acquisition strategy for exponential decay constants estimation. Magn. Reson. Imaging **26**, 433–435 (2008)
23. Chung, C.-W., Wimperis, S.: Optimal detection of spin-3/2 biexponential relaxation using multiple-quantum filtration technique. J. Magn. Reson. **88**, 440–447 (1990)
24. Reddy, R., Shinnar, M., Wang, Z., Leigh, J.S.: Multiple-quantum filters of spin-3/2 pulses of arbitrary flip nagle. J. Magn. Reson. **B 104**, 148–152 (1994)
25. Kemp-Happer, R., Styles, P., Wimpers, S.: Three–dimensional triple-quantum filtration 23Na NMR Imaging. J. Magn. Reson. **B 108**, 280–284 (1995)
26. Hubbard, P.S.: Nonexponential nuclaer magnetic relaxation by quadrupole interactions. J. Chem. Phys. **51**, 985–987 (1970)
27. Marshall, A.G., Bruce, R.E.: Dispersion versus absorption (DISPA) lineshape analysis. Adjacent peaks and simultaneous distribution in peak width and position. J. Magn. Reson. **39**, 47–54 (1980)
28. Augath, M., Heiler, P., Kirsch, S., Schad, L.R.: In vivo 39K, 23Na and 1H MR imaging using a triple resonant RF coil setup. J. Magn. Reson. **200**, 134–136 (2009)
29. Matthies, C., Nagel, A.M., Schad, L.R., Bachert, P.: Reduction of B0 inhomogeneity effects in triple-quantum filtered sodium imaging. J. Magn. Reson. **202**, 239–244 (2010)
30. Boada, F.E., Gillen, J.S., Shen, G.X., Chang, S.Y., Thulborn, K.R.: Fast three dimensional sodium imaging. Magn. Reson. Med. **37**, 706–715 (1997)
31. Bodenhausen, G., Vold, R.L., and Vold, R.R.: Multiple quantum spin-echo spectroscopy. J. Magn. Reson. **37**, 93–106 (1980)
32. Werbelow, L., Pouzard, G.: Quadrupolar relaxation. The multiquantum coherences. J. Phys. Chem. **85**, 3887–3891 (1981)
33. Lu, A., Atkinson, I.C., Claiborne, T.C., Damen, F.C., Thulborn, K.R.: Quantitative sodium imaging with a flexible twisted projection pulse sequence. Magn. Reson. Med. **63**, 1583–1593 (2010)
34. Jaccard, G., Wimperis, S., Bodenhausen, G.: Multiple-quantum NMR spectroscopy of I=3/2 spins in isotropic phase: a new probe for multiexponential relaxation. J. Chem. Phys. **85**, 6282–6293 (1986)
35. Borthakur, A., Hancu, I., Boada, F.E., Shen,G.X., Shapiro, E.M., Reddy, R .:In vivo triple quantum filtered twisted projection sodium MRI of human articular cartilage. J. Magn. Reson. **141**, 286–290 (1999)
36. Hancu, I., van der Maarel, J.R.C., Boada, F.E.: A model for the dynamics of spins 3/2 in biological media: signal loss during radiofrequency excitation in triple-quantum-filtered sodium MRI. J. Magn. Reson. **147**, 179–191 (2000)
37. Yang W., Weixing H., Perez-Trepichio, A.D., Ng, T.C., Furlan, A.J., Majors, A.W., Jones, S. C.: Brain tissue sodium is a ticking clock telling time after arterial occlusion in rat focal cerebral ischemia. Stroke **31**, 1386–1392 (2000)
38. Ellegood, J., Hanstock, C.C., Beaulieu, C.: Trace apparent diffusion coefficients of metabolites in human brain using diffusion weighted magnetic resonance spectroscopy. Magn. Reson. Med. **53**, 1025–1032 (2005)
39. MlynÃrik, V., Gruber, S., Moser, E.: Proton T1 and T2 relaxation times of human brain metabolites. NMR Biomed. **14**, 325–331 (2001)
40. de Bazelaire, C.M.J., Duhamel, G.D., Rofsky, N.M., Alson, D.C.: MR imaging relaxation times of abdominal and pelvic tissues measured in vivo at 3.0 T: preliminary results1, Radiology **230**, 652–659 (2004)
41. Tráber, F., Block, W., Lamerichs, R., Gieseke, J., Schild, H.H.: 1H metabolite relaxation times at 3.0 tesla: measurements of T1 and T2 values in normal brain and determination of regional differences in transverse relaxation. J. Magn. Reson. Im. **19**, 537–545 (2004)

42. Ouwerkerk, R., Bleich, K.B., Gillen, J.S., Pomper, M.G., Bottomley, P.A.: Tissue sodium concentration in human brain tumors as measured with 23Na MR imaging. Radiology **227**, 529–537 (2003)

43. Constantinides, C.D., Kraitchman, D.L., O'Brien, K.O., Boada F.E., Gillen, J., Bottomley, P.A.: Noninvasive quantification of total sodium concentrations in acute reperfused myocardialinfarction using 23Na MRI. Magn. Reson. Med. **46**, 1144–1151 (2001)

44. Wimperis, S., Wood, B.: Triple-quantum sodium imaging. J. Magn. Reson. **95**, 428–436 (1991)

45. Wimperis, S., Cole, P., styles, P.: Triple-quantum-filtration NMR imaging of 200 mM sodium at 1.9 tesla. J. Magn. Reson. **98**, 628–636 (1992)

46. Cockman, M.D., Jelinski, LW.: Double-quantum-filtered sodium imaging. J. Magn. Reson. **90**, 9–18 (1990)

47. Brink, H.F., Buschmann, M.D., Rosen, B.R.: NMR chemical shift imaging computerized medical imaging and graphics. Comp. Med. Im. Graph. **13**, 93–104 (1989)

48. Branca, R.T., Chen, Y.M., Mouraviev, V., Galiana, G., Jenista, E.R., Kumar, C., Leuschner, C., Warren, W.S.: iDQC anisotropy map imaging for tumor tissue characterization in vivo. Magn. Reson. Med. **61**, 937–943 (2009)

49. Jenista, E.R., Galiana, G., Branca, R.T., Yarmolenko, P.S., Stokes a, A.M., Dewhirst, M.W., Warren, W.S.: Application of mixed spin iMQCs for temperature and chemical-selective imaging. J. Magn. Reson. **204**, 208–218 (2010)

50. Kaila, M.M., Kaila, R.: Quantum magnetic resonance imaging diagnostics of human brain disorders. Book: http://www.elsevier.com/2010. ISBN: 978-0-12-384711-9/2010

51. Duce, J.A., Tsatsanis, A., Cater, M.A., James, S.A., Robb, E., Wikhe, K., Leong, S.L., Perez, K., Johanssen, T., Greenough, M.A,. Cho. H.-H., Galatis, D., Moir, R.D., Masters, C.L., McLean, C., Tanzi, R.E., Cappai, R., Barnham, K.J., Ciccotosto, G.D., Rogers, J.T., Bush, A.I.: Iron-export ferroxidase activity of β-amyloid precursor protein is inhibited by zinc in Alzheimer's disease. Cell **142**, 857–867 (2010)

52. Crouch, P.J., Harding, S.-M.E., White, A.R., Camakaris c, J., Bushd, A.I., Masters, C.L.: Mechanisms of a β mediated neurodegeneration in Alzheimer's disease. Int. J. Biochem. Cell Biol. **40**, 181–198 (2008)

53. Jenista, E.R., Branca, R.T., Warren, W.S.: Hyperpolarized carbon–carbon intermolecular multiple quantum coherences. J. Magn. Reson. **196**, 74–77 (2009)

54. Lee, J.-S., Regatt, R.R., Jerschow, A.: Optimal control NMR differentiation between fast and slow sodium. Chem. Phys. Lett. **494**, 331–336 (2010)

55. Laustsen, C., Ringgaard, S., Pedersen, M., Nielsen, N.C.: Quadrupolar-coupling-specific binomial pulse sequences for in vivo 23Na NMR and MRI. J. Magn. Reson. **206**, 139–146 (2010)

56. Hubbard, P.S.: Some properties of correlation functions of irreducible tensor operators. Phys. Rev. **180**, 319–326 (1969)

57. Boada, F.E., LaVerde, G., Jungreis, C., Nemoto, E., Tanase, C., Hancu, I.: Loss of cell ion homeostasis and cell viability in the brain: what sodium MRI can tell us. Curr. Top. Dev. Biol. **70**, 77–101 (2005)

58. Harrris, RK., Mann, B.E. (Eds.): NMR and the periodic table. Academic Press, (London) Ltd. ISBN: 0-12.327650-0 (1978)

59. Evans, J.N.S.: Biomolecular NMR spectroscopy. Oxford University Press, Oxford. ISBN: 0-19 854766 8 (1995)

60. Kentgens, A.P.M.: A practical guide to solid-state NMR of half-integer quadrupolar nuclei with some applications to disordered systems. GEODERMA **80**, 271–306 (1997)

61. Cohen, M.H., Reif, F.: Quadrupole effects in nuclear magnetic resonance studies of solids. Solid State Phys. **5**, 321–438 (1957)

Chapter 10
Biomedical Diamagnetic Spin and Electric-Qudrupole Interaction Systems

10.1 Sodium–Potassium Ion Binding: Biological Systems

It seems nature has evolved as an interplay between a great many organic and inorganic compounds. The result is there is a considerable number of elements essential for higher life forms i.e. animals and humans. Many elements are cofactors of rather integrated parts of, enzyme and of proteins involved in electron transfer and oxygen transport. The physiological processes commonly involve an electrolyte solution containing as the major ions Na^+, K^+, Mg^{2+}, Ca^{2+}, and Cl^-. Many important biopolymers like DNA, RNA and ionic mucopolysaccharides and also the aggregates of charged monomers like biological membranes, are highly charged and interact strongly with these ions. in higher organisms. Most of these are also unevenly distributed between intracellular and extra cellular spaces with the concentration gradients maintained through energy consuming active transport. Temporary changes in these ion gradients are used in nature as means of signal transmission. All essential elements in biological systems have at least one potentially valuable magnetic isotope. In NMR a relatively small group of magnetic nuclei, ^1H, ^2H, ^{13}C, ^{15}N and ^{31}P have been routinely used as a source of diagnostics and imaging. In an axially symmetric complex undergoing isotopic rotation the chemical shift anisotropy (CSA) contribution to the relaxation rates R_1 ($=1/T_1$) and R_2 ($=1/T_2$) can be approximately written as [1]

$$R_1 = (1/15)[\gamma^2 B_0^2 (\Delta\sigma)^2][(2\tau_c)/(1 + \omega^2 \tau_c^2)]$$

and

$$R_2 = (1/90)[\gamma^2 B_0^2 (\Delta\sigma)^2][(8\tau_c) + 6\tau_c/(1 + \omega^2 \tau_c^2)]$$

Here $\Delta\sigma = \sigma_\parallel$ (parallel component) $\sigma_\perp$ (perpendicular component) = CSA in regard to the two major axis, parallel and perpendicular to the major orientation of a macromolecule, B_0 = the static magnetic field applied in the standard z-direction in

the laboratory, τ_c = the correlation time between the interactions under analysis, ω = the resonance frequency of the macromolecule $\approx \gamma B_0$, γ = the gyromagnetic ratio of the macromolecule. For the case of CSA, R_1 will increase with B_0, for small fields. For $\omega\tau_c > 1$ the second set of terms within the brackets [ ] for R_1, will amount to $\sim (1/(\omega^2\tau_c))$. Since $\omega = \gamma B_0$, R_1 will decrease as $\sim (1/\tau_c)$ meaning less rapid pulsing. Eventually as $\omega\tau_c \gg 1$, R_1 will become independent of B_0. R_2 on the other hand shows somewhat different behavior. For $\omega \tau_c \gg 1$ (large fields) the term within the second set of brackets [ ] becomes $(8\tau_c + 6/\tau_c)$. Thus R_2 increases with τ_c.

The experimental unfavorable situation, $R_1/R_2 < 1$ is reached, whenever, $\omega\tau_c > 1$, for the I = 1/2 nuclei. For quadrupolar nuclei (I > 1/2) evaluation of the experimental situation at hand is slightly more complicated than for I = 1 nuclei, due to several factors, notably the occurrence of non-exponential relaxation and second-order frequency shifts. Quadrupolar relaxation is caused by the interaction of a nuclear electric quadrupole moment, eQ, with fluctuating electric field gradients, eq, at the place of the nucleus. Electric field gradients are system-dependent properties and may be regarded as either intramolecular or intermolecular in origin. In isotropic systems and when $\omega\tau_c \ll 1$(extremely narrowing condition) the nuclear magnetization will decay with a single exponent and we have [1],

$$R_1 = R_2 = \left(3\pi^2/10\right)[(2I + 3)/(2I - 1)][(\chi^2/I^2)][(1 + \eta^2/3)(\tau_c)]$$

Here $\chi = (e^2 q_{zz} Q/h)$ is the-nuclear quadrupole coupling constant (in Hertz) and q_{zz} (see η) is the largest component of the electric field gradient and η is the asymmetry parameter for the same gradients. $\eta = (q_{xx} - q_{yy})/q_{zz}$. As η is rarely much larger than 0.5, it will thus have a negligible influence on the relaxation rate. In biological systems the true extreme narrowing ($\omega\tau_c \ll 1$) situation is usually encountered only in the case of free' hydrated ions in solution or in the case of low-molecular weight complexes. More common is the situation when $\omega\tau_c > 1$. In this case the decay of the longitudinal (M_1) and transverse (M_2) magnetizations for quadrupolar nuclei with spins I > 1 is no longer exponential but may be written for half integer spins as a weighted sum of (I + 1/2) exponentials as [1]

$$M_1(t) = M_1(\infty)1 - k \sum\nolimits^{I+1/2}{}_{i=1}[C_{1i}\exp(-R_{1i}t)]$$

$$M_2(t) = M_2(0) \sum\nolimits^{I+1/2}{}_{i=1}[C_{2i}\exp(-R_{2i}t)]$$

where

$$\sum\nolimits^{I+1/2}{}_{i=1}C_{ji} = I \text{ and } k = 2, \text{ for an inversion experiment}$$

t is known in the second-order dynamic frequency shifts the resonance frequencies of the various components will not in general be the same. Furthermore although the above equation is valid for the total magnetization, the decays of the individual components, will normally not be exponential and will also depend on the length of the monitoring pulse. In studies of metal ion nuclei in biological systems we frequently encounter situations when $\omega\tau_c \approx 1$.

It is known that for $I = 3/2$ nuclei, decays of the magnetization M_1 and M_2 will be very nearly exponential up to $\omega\tau_c \approx 1.5$ and useful expressions for the apparent relaxation rates $<R_1>$ and $<R_2>$ can be derived to for the $I = 3/2$, $I = 5/2$, $I = 7/2$, etc. nuclei. To a first order the longitudinal and transverse relaxation rates are given by [1]

$$<R_1> = (3\pi^2/10)(\chi^2)[(2I+3)/\{\Gamma^2(2I-1)\}][0.2J_1 + 0.8J_2]$$

$$<R_2> = (3\pi^2/10)(\chi^2)[(2I+3)/\{\Gamma^2(2I-1)\}][0.3J_0 + 0.5J_2 + 0.2J_2],$$

where J_K are spectral densities that may be taken as

$$J_K = [(\tau_c)/[I + (K\omega_0\tau_c)^2]]$$

These equations may be used in a slightly modified form to cover also the experimental situation when a quadrupolar nucleus is exchanging rapidly between two or more sites. Figure 10.1 (Fig. 1 [1]) is a simple depiction of the various physical quantities involved. The above two equations may be used in a slightly modified form to cover also the experimental situation when a quadrupolar nucleus is exchanging rapidly between two or more sites. For a case when the nucleus is rapidly exchanging between a bound state (B) and a 'free' state (F) we may write the effective spectral density as a weighted average as follows [1].

$$J_q = p_F J_q^F + p_B J_q^B$$

Here p_F and p_B are the relative populations of the two states, free and bound. J_q^F may be taken simply as J_0^F and for isotropic motion J_q^B can be written as [1]

$$J_q^B = [(0.1)(q_{zz})^2(\tau_{cB})/[1 + (q\omega\tau_{cB})^2]$$

By using the above equations, one can derive expressions for the reduced' relaxation rates defined as [1]

$$<R_1>/(p_F R_F) \text{ and } <R_2>/(p_F R_F)$$

Here R_F refers to the relaxation rate of the 'free' state. The spectral densities, J's, and Q's, can be approximately written as follows. For the general case

$$J(\omega) = \int_0^\infty v_0(0)v_0(r)\cos(\omega\tau)d\tau \rightarrow 0.3v_{zz}^2[(\tau_c)/(1 + \omega^2\tau_c^2)]$$

and for the special cases

In addition to non-exponential relaxation for quadrupolar nuclei under conditions of non-extreme narrowing the NMR signal will also be modified by dynamic frequency shift changes that have been termed as 'second-order dynamic frequency shifts (SODFS)'. These shifts were long neglected because they were always smaller than the signal line width. It took some time to be appreciated that though the dynamic shifts were always smaller than the width of the broadest

(a) Slow Motion Limit

$J(0) \geq J(\omega) \geq (2\omega)$

$m = \frac{1}{2} \rightarrow m = -1/2$
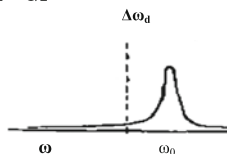
$I = 5/2$

$\Delta\omega_d \sim -(eQ/\hbar)^2(1/25)[\, Q(\omega_0) - Q(2\omega_0)] \sim 6\times10^{-3} \,(\,\chi^2/\omega_0)$

$I = 7/2$

$\Delta\omega_d \sim -(eQ/\hbar)^2(10/585)[\, Q(\omega_0) - Q(2\omega_0)] \sim 2.5\times10^{-3} \,(\,\chi^2/\omega_0)$

(b) Near Extreme Narrowing Condition

$J(0) > J(\omega_0), J(2\omega_0)$
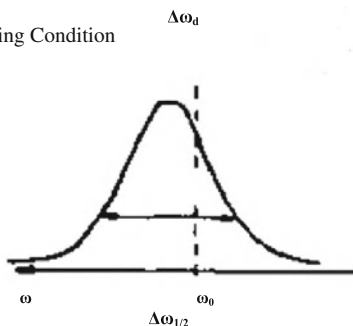
$I = 5/2$

$\Delta\omega_{d\,=}\; (eQ/\hbar)^2 \,(1/125)\, [\, Q(\omega_0) + 2Q(2\omega_0)\,]$

$I = 7/2$

$\Delta\omega_{d\,=}\; (eQ/\hbar)^2 \,(1/125)\, [\, Q(\omega_0) + 2Q(2\omega_0)\,]$

$(\Delta\omega_d/\Delta\omega_{1/2}) = (\,\omega_0\tau_c/2\,)[\, (\, J(\omega_0) + 2J(2\omega_0)\,)]/[\, (\,3J(0) + 5J(\omega_0) + 2J(2\omega_0)\,)\,]$

(c) Extreme narrowing Condition

$\omega_0 \ll 1$
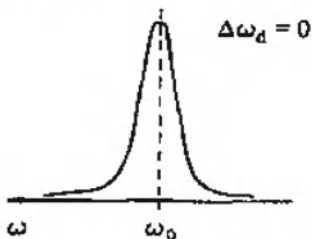
Fig. 10.1 Some general characteristics of dynamic frequency shifts

component of a resonance they may well be larger than the most narrow component and thus be clearly observable in the spectrum. The effects of second-order frequency shifts for the I = 3/2 case is well known now. Under non-extreme ($\omega \tau < 1$) narrowing conditions the two transverse relaxation components will differ in resonance frequencies as well as in relaxation rates. The NMR signal will thus appear asymmetric. A further complication is that the longitudinal relaxation of the two components will in general be non-exponential and the apparent rates dependent on the length of the monitoring (normally 90°) pulse. The magnitude of the second order effects are dependent on the ratio ($\chi^2/\omega o$) and will thus be particularly important in situations of large quadrupole coupling constants and low observing frequency.

The expressions for the NMR band shape for I = 5/2 and / = 7/2 nuclei—both in the presence and absence of chemical exchange are schematically summarized in the Fig. 10.1 [1]. In the limit $\omega\tau_c \gg 1$, the m =/2 to m = −/2 component will dominate the spectrum because it is much narrower than the other components. The intensity of this component relative to the total intensity will be 40 % for I = 3/2, 26 % for I = 5/2 and 19 % for I = 7/2. The narrow signal will be shifted towards lower frequency with a value proportional to ($\chi2/\omega_0$). Between the two limits the resonance will be more or less asymmetric with an apparent shift either to high or low frequencies depending on the values of ω_0, τ_c and χ. The ratio of the dynamic shift to line width will in this region depend only on ω_0 and τ_c. One should note that the temperature dependence of the apparent line width in a chemically exchanging system may deviate considerably from that observed in spin I = 1/2 systems. Considerable care must therefore be exercised when exchange rates are deduced from variable temperature studies of quadrupolar nuclei.

10.2 Spin 3/2 Dynamics Density Matrix Approach NMR Experiments

The NMR behavior of the spin 3/2 systems is particularly interesting in the context of biological systems because of the dependence of their NMR signal on the electrical and structural properties of the biological microenvironment. This dependence has been exploited in the context of multiple quantum-filtered (MQF) sodium NMR experiments for the study of ion fluxes during ischemia experiments and for the identification of neoplastic changes in human tissue. Imaging extensions of the NMR techniques although highly desirable are not as common in the literature because of the low concentration of sodium ions in human tissue and the inherent challenges involved in the fast spatial encoding of the sodium NMR signal. Fortunately the development of efficient spatial encoding techniques in MRI has allowed the generation of sodium images in times that are adequate for practical use in humans (data acquisition time less than 10 min). Extensions of

these techniques have also been used to provide the first demonstration of in vivo MQF sodium MRI techniques in humans. The routine application of MQF techniques for the non-invasive diagnosis and monitoring of pathology in humans, however requires a more thorough understanding of the dependence of this novel image contrast on hard-to-control spatial variations in experimental parameters such as the B_1 field and the B_0 field. Such understanding can only be attained through a proper description of the behavior of the spin system for arbitrary values of the aforementioned experimental parameters. The standard theoretical approach for describing the spin dynamics in the presence of non-negligible relaxation behavior is based on the Redfeld equations. Analytic solutions for the Redfield equations can be obtained by reducing the Redfield equations to a system of linear differential equations in a suitably chosen basis of quantum mechanical operators. These approaches however do not reveal inherent factorizations of the solution. Such factorizations are attractive for practical use because of the natural separation they provide for the effects of the experimental parameters on the signal.

It can be shown [2] that by using the superoperator formalism the solution to the Redfield equations can be reduced to a purely algebraic calculation in which the coherence pathways leading to the measured signal can be easily identified. This approach offers two additional advantages. First, each pathway contribution can be expressed as a product of simple terms representing the succession of RF pulses and RF-free evolutions that is typical of pulsed MQF experiments. Second the associated expressions are constructed in a basis-free form. One starts by reviewing many of the relevant properties of a spin 3/2 system in the super space representation. The super space formulation of the Redfield equations is then presented and used to construct the propagator for the spin system's evolution in the absence of the RF field. This is followed by a description of the RF excitation in the super operator space. The super space formalism is then used to derive the expressions for the time dependence of the NMR signal for the classical one-, two-, and three-pulse NMR experiments. These expressions are then used to model the experimentally acquired signals from agar gels phantoms because such gels offer the isotropic slow fluctuating environment necessary for bi-exponential relaxation behavior of sodium.

The quantum mechanical description of isolated 3/2 spins is constructed in the Hilbert space H, associated with the $j = 3/2$ irreducible representation of the rotation group. In this space of dimension $N = 4$, the natural basis is the angular momentum basis $\{|jm>\}$ with $j = 3/2$, and $m = -3/2,\ldots,3/2$. In the Hilbert space description the pure states are described as four dimensional vectors while the mixed states are described by matrices. The Liouville representation of quantum mechanics (QM) is introduced to treat both types of states in a common fashion. In this representation the states (pure or mixed) are described as self-adjoint positively-defined operators with unit trace. Due to the finite dimensionality of H both the state space and the observable space (the space of bounded operators acting on H) can be embedded in the linear space of $N \times N$ matrices. This N^2 dimensional space is called as the super space (or Liouville space) and is denoted by S. The elements of S are sometimes referred to as super vectors. In super space
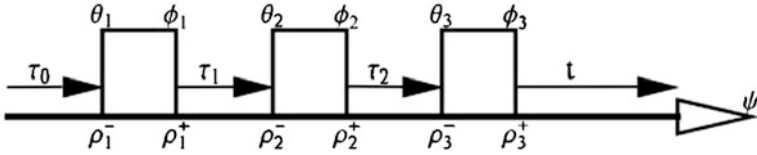
Fig. 10.2 Schematic representation of the three-pulse NMR experiment. A hard (frequency selective) pulse with the flip angle θ_3 and phase angle φ_3 is applied τ_2 s after an initial two-pulse excitation has taken place (with flip angles θ_2 and θ_1 and phases φ_2 and φ_1, respectively). Data collection takes place at time t. When the echo forms at the measurement moment, $t = \tau_1 + 3\tau_2$, the filtering function f(t), in the absence of quadrupolar interaction, is written as [2] follows

the double ''ket'' $|O \gg$ and double ''bra'' $\ll O|$ denote the N^2 dimensional vectors describing the operator 'O' and its hermitic conjugate 'O†'s, respectively. The Liouville space becomes an unitary space when it is equipped with the natural inner product $\ll A/B \gg \equiv \mathrm{Tr}\{A^\dagger B)$.

The linear operators acting on S are called super operators. A special class of super operators is defined by the operation of taking the commutator. The derivation with respect to O, is denoted using the corresponding bold face **O:S** to **S**, and is acting on arbitrary operators B as the commutator **O**$| B \gg = |C \gg$ with $C = | O, B|$. For the particular case of the Hamiltonian the associated commutator super operator is the Liouvillian which is denoted by **L**. From an algebraic point of view the super space is associated with the direct product of two $j = 3/2$ representations of the rotation group. The product reduces to a direct sum of representations labeled with principal quantum numbers $l = 0,1,2,3$. Therefore the quantum mechanical operators can be expanded in terms of the normalized spherical irreducible tensor (**SIT**) operators, T_{lm}, $l = 0,1,2,3$, $m = -1,\dots,l$. For the sake of simplicity the notations $| lm \gg \equiv | T_{lm} \gg$, $\ll lm| = \ll T_{lm}^\dagger|$ are used. In order to have full comprehension of the quantum mechanical algebra involved one need to refer to the Ref. [2]. The main results relevant to sodium MRI however can be summarized as follow. Firstly one employs a three pulse sequence to excite the intracellular sodium group of nuclei. An abstract representation of the sequence of pulses which can be used typically can be represented as shown in the Fig. 10.2

$$= a[\exp\{-(t - 3\tau_2)/T_s\} - \exp\{-(t - 3\tau_2)/T_F\}]$$

$$\mathrm{x}[\exp\{-(t)/T_s\} - \exp\{-(t)/T_F\}]$$

Similarly for the case $\tau_1 = 3\tau_2$, the fit function becomes

$$a[[\{\exp(-3\tau_2/T_S)\} - \{\exp(-3\tau_2/T_F)\}][\exp(-\tau_2/T_S)]$$

The following presentation in the Fig. 10.3 (2), is a practical illustration in regard to the first case, above. T_S and T_F are the slow and fast relaxation times respectively.
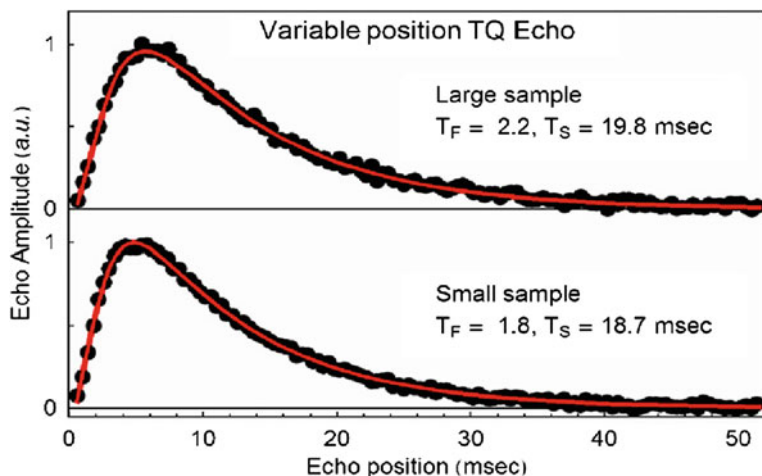
Fig. 10.3 Dependence of the NMR signal from a three pulse experiment on the TQ evolution time, for the small agar phantom (*lower part*) and large agar phantom (*upper part*). Each data point corresponds to the time integral of the corresponding FID (field induction decay) (TR = 217–282 ms, 10 averages). The solid line indicates the fit to the signal envelope

10.3 Sodium Signals: Via Central Transition

The large abundance of ^{23}Na in living tissues especially in areas of brain and cartilage offers promising prospect for ^{23}Na-MRI as a powerful diagnostic method for cartilage pathologies as well as for studying brain tumors [3]. While both free and ordered (bound) sodium are prevalent throughout the body, monitoring the levels of the latter is of particular interest due to the anticipated strong correlation between the changes in the ordered sodium concentration and the early symptoms of most cartilage disorders. For instance proteoglycan depletion which often accompanies the onset of bone and cartilage diseases such as arthritis is consistent with a decrease in ordered sodium levels. In addition sodium plays a direct role in regulating cell mitosis and proliferation and there is an increase of about 350 % in sodium concentration in malignant tumor cells in comparison to normal cells. This discrepancy renders ^{23}Na-MRI an excellent candidate for examining tumors.

Frequently the signal from free sodium overlaps with the central transition of ordered sodium. Selective observation of signals arising from ordered sodium makes exact measurements of the preferred signal from ordered sodium difficult. Methods that make possible the selective observation of signals arising from ordered sodium can therefore greatly enhance the potential for ^{23}Na-MRI in studying living tissues. Techniques that have already been developed to selectively detect sodium signals from ordered environments mostly depend on the evolution properties of the magnetization components under the action of the quadrupolar coupling. For example one can exploit the influence of the quadrupolar interaction

on the evolution of the system by performing double-quantum filter experiments to detect the double-quantum coherence terms ($T^2_{\pm 2}$ in spherical tensor operator representation), which are created from transverse magnetization operators $T^1_{\pm 1}$ under the action of the quadrupolar coupling).

Multiple-quantum coherences may also be created through relaxation induced evolution which may lead to complications when a clean selection of ordered sodium is desired. Alternatively the Jeener–Broeckaert experiment relies on the rotational properties of the tensors of different ranks for this selection. Both the double-quantum filter and the Jeener–Broeckaert methods were later adapted to detecting the filtered signals via the central transition thus providing higher signal-to-noise ratios as well as, higher resolution. In recent developments the idea is to provide another approach to minimize the signal from free sodium thus allowing for the selective detection of the central transition of ordered sodium. Here, we take advantage of the fact that spin-3/2 nuclei (i.e., the ordered ^{23}Na) having a non-vanishing quadrupolar interaction term in the Hamiltonian evolve directly in the presence of radiofrequency (RF) fields expending on the ratio between the mutation frequency (ω_{RF}) and the quadrupolar coupling constant (ω_Q).

Free ^{23}Na, meanwhile is located in isotropic environments and therefore is central transition thus providing higher signal-to-noise ratios as well as, higher resolution. not subject to influence by the quadrupolar interaction. We demonstrate this selection using a liquid crystalline environment as well as a cartilage sample where we selectively detect the central transition of the ordered ^{23}Na NMR signal from a mixture of free and ordered environments. The advantage of this method lies in its simplicity which makes it particularly easy to be incorporated into existing imaging protocols. The experiments on a cartilage sample also show a significant robustness to B_0 inhomogeneity effects. The quadrupolar interaction arises from the electrostatic interactions between nuclear and electric-charge distributions The orientational dependence of this interaction arises as a consequence of the truncation by the Zeeman interaction. In this case the interaction can be written as $H_Q = A_Q/2[I_z^2 - I(I+1)/3]$ with the time-averaged quadrupolar coupling constant A_Q given (in units of angular frequency) by

$$A_Q = [\{P_2(\cos \beta) + (\eta/2)(\cos 2\alpha) \sin^2 \beta\} 3\omega_Q\}]$$

where $\omega_Q = (e^2qQ)/[2I[I-1\}]$. The eq and eQ, respectively represent the zz-components of the electric field gradient and the nuclear electric quadrupole moment, η denotes the anisotropy parameter and is assumed to be zero if the system is cylindrically symmetric. The Euler angles α, β, γ relate the principal axis frame to the laboratory axis frame. The Hamiltonian on-resonance in the rotating frame becomes $H_{total} = H_Q + H_{RF}$. In the regime where $\omega_{RF} \gg A_Q$, we may neglect H_Q. A 90° pulse is obtained when $\omega_{RF} \tau_p = \pi/2$, where τ_p is the pulse duration. In the regime where $\omega_{RF} \ll A_Q$, the first maximum of the central transition signal appears at $\omega_{RF} \tau_p = \pi/4$, apparently under the action of a doubled electric RF field. For higher half-integer spins one can show that the effective RF field acting selectively on the central transition, is enhanced by a factor of

$[(I + 1/)2]$. These effects form the basis of nutation spectroscopy. In the Fig. 10.4 (Fig. 3 [3]) is a practical illustration in a laboratory experiment situation.

The 1D images obtained in the liquid crystalline experiments are displayed in Fig. 10.4 [3]. Four sets of peaks are seen, the central transition and the two satellite images arising from the SDS compartment, and the single image from the NaCl compartment. The two central images are shifted in opposite directions by the magnetic field gradient because the two compartments are separated along the z dimension (as shown in the schematic in Fig. 10.4 [3]. The QFN sequence was used throughout, and only the pulse duration of the soft pulse was varied between 50 and 450 μs to show the approach of the optimal suppression condition for the free sodium signal. Along with the decrease of the free sodium signal the intensity of the ordered sodium peak increases in accordance with the approach to a perfect inversion of the central transition populations by the soft pulse. As shown in Fig. 10.4 [3] a very good suppression of the free sodium signal can be obtained. Figure 10.5 [3] shows a comparison between a hard pulse spectrum and a CPS (central peak suppression) spectrum of the cartilage plug. The sample showed a quadrupolar splitting, centered at approximately $A_Q = 375$ Hz. For the 1D images the sample shown in Fig. 10.5 [3] was used. Figure 10.5 [3] shows a hard pulse gradient spin echo image and the Fig. 10.5 [3] shows the QFN image. A very clean suppression of the free sodium signal is achieved in this case even though sizeable inhomogeneity effects may be expected at the phase boundaries (Shigemi plug–cartilage, cartilage–fluorinert, fluorinert–water, water–air).

10.4 Intracellular Na^+ Red Blood Cells Animal Model

The existence of a Na^+/K^+ concentration gradient across the cell membrane is a well known fact. While human erythrocytes contain relatively low concentrations of Na^+, cat and dog erythrocytes have a high Na^+ content. One can use dysprosium shift reagents (SRs) [4] as complexes with the EDTA or with TPP (tripolyphosphate) to monitor the intracellular Na^+ concentration, and relaxation times, in the animal model, e.g., dog (high-Na^+) and human (high-K^+) erythrocytes. In the human model, the use of SRs is not recommended due to their invasive character. A typical SRs is dysprosium(III) (tripolyphos-phate)$_2^7$ – (DY(TTP))$_2^7$. As an example ^{23}Na-NMR spectra obtained from a suspension of dog and human erythrocytes in solution ions of Dy-EDTA and Dy-TPP shift reagents are shown in Fig. 10.6 (4). The intracellular Na^+ peak (assigned an arbitrary zero frequency) has about the same position as in aqueous NaCl solution. The extra cellular Na^+ resonance which is shifted to low field in the presence of Dy-EDTA, is shifted to high field in the presence of Dy-TPP. The high Na^+ content of dog erythrocytes and the low Na^+ content of human erythrocytes is visible from the figure. In order to determine the molality of the internal Na^+ from the integral of the Na_i peak, one needs to know the volume of the intracellular fluid.

Fig. 10.4 Liquid crystalline test system. **a** Schematic of the sample used. Two capillaries containing a NaCl solution and a liquid crystalline environment are used to separate the two compartments along the z direction. **b–e** one-dimensional images obtained using the QFN (quadrupolar filter by nutation) sequence. **b** 50 **c** 200 **d** 300, and **e** 450°, μs, soft pulse duration. The signal of free sodium is optimally suppressed in (**e**)
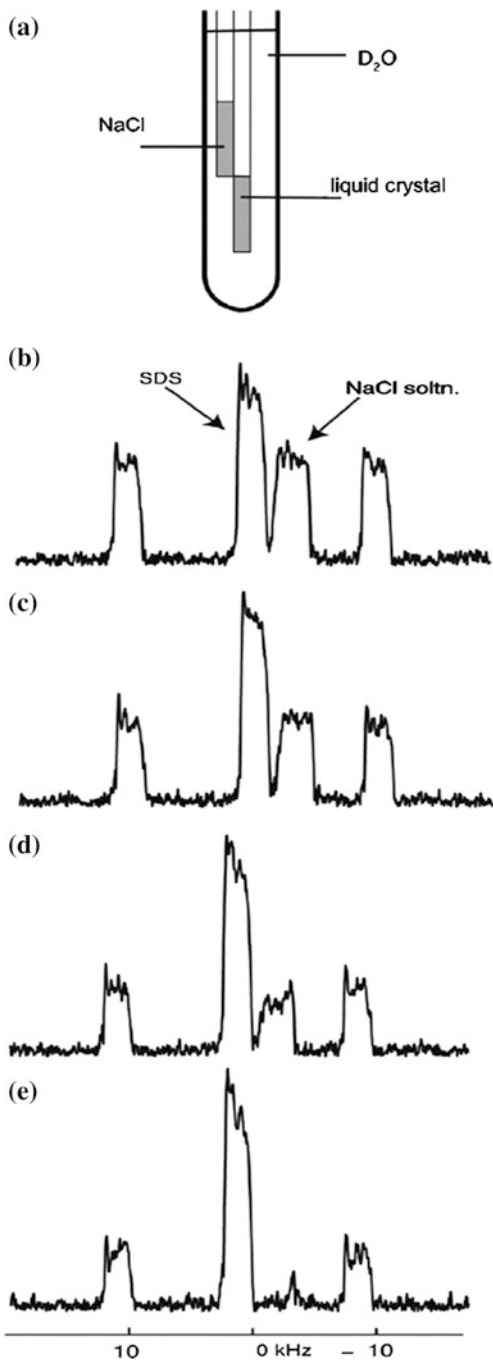
Fig. 10.5 a Cartilage/saline
sample. **b** Hard pulse gradient
spin echo experiment, both
cartilage sodium and saline
sodium are visible. **c, d** QFN
(quadrupolar filter by
nutation) experiment. The
saline signals are suppressed
in this experiment. One
capillary tube contains a
liquid crystal solution
(38.8 % sodium decyl sulfate
(SDS), 6.7 % decanol and
54.5 % water) and the other
was filled with 1 M NaCl
solution, representing sodium
in ordered and free
environment

(a)

(b)

(c)
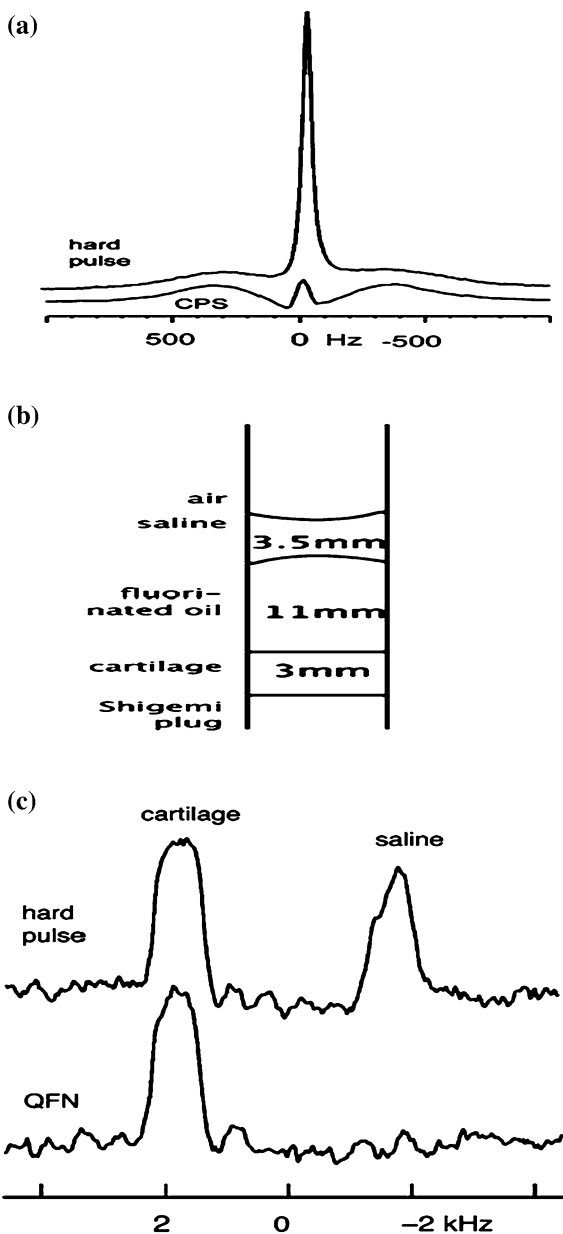
The volume occupied by the cells is traditionally determined by the use of
macromolecules such as insulin or serum albumin labeled with radioactive isotopes.
Here it is calibrated from the volume of the cells by ^{59}Co-NMR. The $Co(CN)_6^{3-}$
experiment is performed on the same sample tube in the same probe as for the

Fig. 10.6 Typical
^{23}Na-NMR spectra obtained
of human (**a**) and dog
(**b**) erythrocytes in a solution
of 0.02 M DyCl$_3$, 0.056 M
Na$_2$ H$_2$ EDTA. 0.028 M
NaCl, 0.01 M glucose.
0.002 M K$_3$Co(CN)$_6$ (pH 7.5)
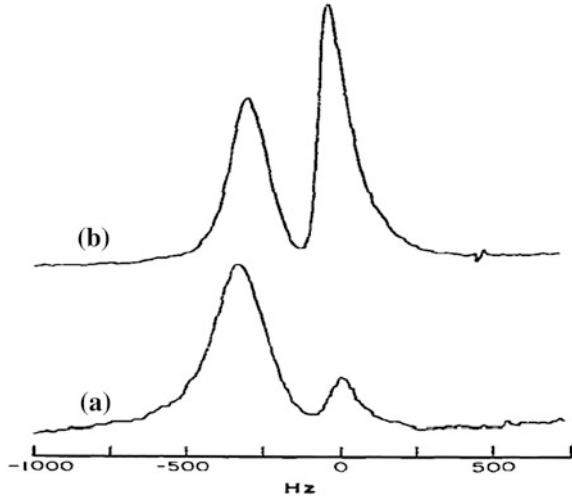
^{23}Na-NMR experiment. In estimating the free volume in the cell suspension from the
^{23}Na signal intensity of the outer solution one assumes that the outer Na$^+$ concen-
tration does not change during the experiment. This assumption is not always valid.
since the Na$^+$ concentration gradient across the membrane is maintained by an active
process which is sensitive to the experimental conditions. Since the increase of
intracellular Na$^+$ is accompanied by a parallel decrease of K$^+$ the lack of change of
relaxation time indicates binding of Na$^+$ and K$^+$ with the same affinity so that the
fraction of bound Na$^+$ is independent of the Na$^+$/K$^+$ ratio. The longitudinal and
transverse relaxation of ^{23}Na nuclei are described by sums of two exponentials. The
general expression for the decay of the longitudinal magnetization is given by,

$$M_z(t) - Mz(0) = [(M_z(t) - Mz(0))][\{0.2\exp(\exp(-t/T_1^f)\} + \{0.8\exp(-t/T_1^s)\}]$$

and that for and for the transverse magnetization it is,

$$M_x(t) = [M_x(0)][\{0.6\exp\left(-t/T_2^f\right) + \{0.4\exp\left(-t/T_2^s\right)\}]$$

In the case of, an exchange between, bulk Na$^+$

$$(1/T_{B2}^f) = [(0.\pi^2)(\chi^2)\{J(0) + J(\omega_0)\}]$$

$$(1/T_{B2}^f) = [(0.\pi^2)(\chi^2)\{J(0) + J(\omega_0)\}]$$

and small fractions (P$_i$) of bound Na$^+$, with relaxation times T$_B$, and exchange
lifetimes, τex, c the decay times, are given by

$$(1/T_1^f) = [(1/T_1(0))] + \Sigma_i\{[(P_i/(T_{B1}^f + \tau_{exc})\}]$$

There are similar expressions for T_1^s, T_2^f and T_2^s. Here $T_1(0)$ is the relaxation time of Na^+ in the bulk solution. The relaxation rates of the bound Na^+ are,

$$(1/T_{B1}^f) = [(0.4\pi^2)(\chi^2)\{J(\omega_0)\}]$$
$$(1/T_{B1}^s) = [(0.4\pi^2)(\chi^2)\{(2\omega_0)\}]$$
$$(1/T_{B2}^f) = [(0.\pi^2)(\chi^2)\{(0) + J(\omega_0)\}]$$
$$(1/T_{B2}^s) = [(0.2)\pi^2(\chi^2)\{J(\omega_0) + J(2\omega_0)\}]$$
$$J(\omega) = [\{\tau_c/\{1 + (\omega^2\tau^2)\}\}]$$

Here $\chi = (e^2qQ/h)$ is the quadrupolar coupling constant in Hz. For the interpretation of the relaxation rates of intracellular Na^+ it is convenient to divide the various contributing factors into three groups: (a) effect of viscosity on the rotational correlation time; (b) binding to small molecules: (c) binding to macromolecules and membranes. Within the frequency range used, the condition (ω_0 τ_c) << 1 is expected to hold for the first two groups but not for the third. Since the rotational correlation times of hydrated ions and their complexes with small molecules in aqueous solutions are in the range of $\sim 10^{-11}$ s, it is only when τ_c changes by a factor of ~ 100 that (ω_0 τ_c) becomes equal to 1.

In the case of the third group of possible contributions to the relaxation rates i.e., binding of Na^+ to macromolecules or membranes, the longitudinal relaxation time is expected to be dependent on the frequency. Measurements of T_1 of intracellular Na^+ in the case of canine and human erythrocytes shows no such dependence at $\omega_0/2\pi$; = 95.26. 79.38 and 23.81 MHz. These results indicate that T_1 of intracellular Na^+ is not affected by binding to macromolecules, but is determined by the viscosity of the intracellular medium or by binding to small molecules. However if this were the only effect one would expect T_1, to be equal to T_2, The fact that the measured T_2, of intracellular Na^+ is significantly shorter than T_1 clearly indicates an effect of Na^+ binding to macromolecules or membranes on T_2.

On examination of the above equations one can see that in cases where T_2 is significantly shorter than T_1 there are contributions from terms with (ω_0 τ_c) > 1 and therefore the two components of T_2, should be significantly different and easily separable. It was noted T_1, is not easily separable because its two components may differ by less than a factor of 4 and the fast relaxing component accounts for only 20 % of the total intensity. However, in our system, an alternative explanation is probably applicable. Since for the bound Na^+. (ω_0 τ_c >> 1), both $J(\omega_0)$ and $J(2\omega_0)$ are very small and the effect of bound Na^+ on T_1 is negligible, i.e., $T_1^f = T_1^s = T_1(0)$.

10.5 Triple Quantum Filtered NMR Animal Model

There is growing trend in research and development efforts to distinguish Na^+ in different tissue compartments by the use of multiple-quantum (MQ) filters [5]. ^{23}Na has a spin quantum number $I = 3/2$ and hence has four possible spin
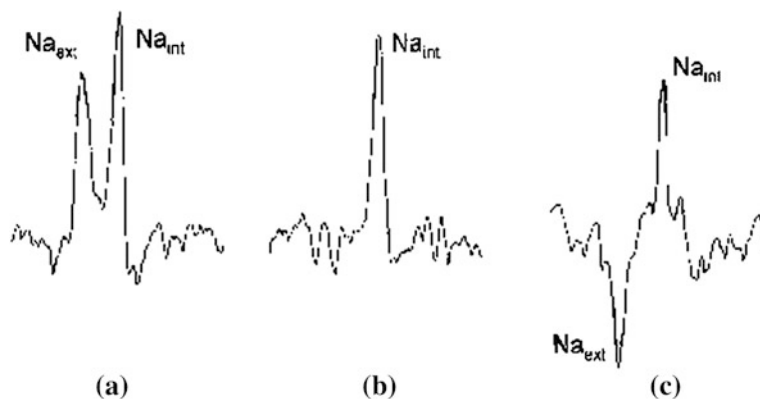
Fig. 10.7 TQ-filtered ^{23}Na spectra from the in vivo rat liver, collected using **a** 3-µs **b** 315-µs, and **c** 630-µs evolution times. The modulation of the Na$_e^+$ signal (5 ppm off resonance) indicates that it is a true TQ-filtered signal (5 ppm). N$_{ex}$ = external sodium, N$_{int}$ = internal sodium

orientations. This results in three possible single quantum (SQ) transitions, one, inner $-1/2$ to $1/2$ transition and two outer $-3/2$ to $-1/2$ and $+1/2$ to $3/2$ transitions. ^{23}Na is transiently bound to macromolecules. The electric field gradients created at those sites act as an effective relaxation mechanism and the outer transitions relax more quickly than the inner transition. It has been shown that, when Na$^+$ has two distinct relaxation rates for the inner and outer transitions, the coherence transfer selection rule, can be violated and, MQ transitions, become possible. Thus it was suggested that the MQ-filtered signal should have large contribution from Na$_i$ compared to Na$_e$. It has been demonstrated that the following studies are very useful. (1) to measure the contributions of Na$_i^+$ and Na$_e^+$ to the triple quantum (TQ) ^{23}Na signal from the in vivo rat liver, using TmDOTP^5 (shift reagent) to lift the degeneracy between the two signals, and (2) to compare changes in SQ (single quantum) versus TQ (triple quantum) ^{23}Na signals, during ischemia, produced by sacrificing the animals. SQ ^{23}Na spectra, were collected using, a simple one pulse sequence with a 30 µs excitation pulse and a 10 µs spectrometer dead time, before acquisition.

TQ-filtered spectra were collected using the pulse sequence given as $(\theta)_{\varphi} - \tau/2 - ((\theta)_{\varphi} - (2\theta)_{\varphi+\pi/2} - \theta)_{\varphi}) - \tau/2 - (\theta)_{\varphi+\pi/2} - \delta - (\theta)_{\pi/2} - (t_{acq})_{\pm}$. Here θ is a nominal 90° pulse, τ is MQ preparation time, δ is MQ evolution time, and t_{acq} is acquisition time. A 48-step phase cycling scheme was used. The basic phase cycling scheme for selective detection of TQ coherence consisted of six steps in which the phase $\varphi = n\pi/3$, where n was cycled through 0,1,2,3,4, and 5. The FIDs resulting from this pulse sequence were alternately added to and subtracted. Modulation of the TQ-filtered Na,$^+$ signal, from liver, can be expressed, as a function of evolution time δ, as $I = I_0[\cos(6\pi v\delta][\exp-\{(\delta/T_{TQ})\}]$. Here I = amplitude of the modulated signal, I_0 = the amplitude of the same signal when $\delta = 0$, v is the frequency offset in Hz, and T_{TQ} is the TQ transverse

relaxation time. Thus, a true TQ-filtered signal would be modulated, such that it would have maximum positive intensity at $\delta = 0$, be null at $\delta = (12v)^{-1}$ and have maximum negative intensity at $S = (6v)^{-1}$.

The intensity of TQ-filtered signal depends upon the slow and fast transverse relaxation times. It is given as $I = A[\{\exp(-\tau/T_{2f})\} - \{\exp(-\tau/T_{2s})\}]$ Here T_{2s} is the slow transverse relaxation time, T_{2f} is the fast transverse relaxation time, and A is a constant related to the number of nuclei, that produce the TQ-filtered, Na^+ signal and the line shape. The Fig. 10.7 (s[5]), presents illustration, of the usefulness of the TQ filter technique, in separation of internal (Na_{int}/Na_i) and external (Na_{ext}/Na_e) sodium signals, in a non invasive manner. It shows that, the Na_e resonance, is modulating, as a function of, δ. There is positive maximum, in intensity, at $\delta = 3$ μs, zero intensity at $\delta = 315$ μs, and a negative maximum at $\delta = 630$ μs. Therefore, the external sodium signal, can be manipulated, independent, of the internal sodium. The two signals appear at different resonance frequencies. Once separated, the fast (internal) and slow (external) relaxation time analysis can be accurately performed. It is also seen, that the overall intensity, of the intra and extra cellular, Na^+, resonances, decrease with increasing δ. It is, due to, the TQ/T_2 relaxation, during the δ delay.

References

1. Forsfin, S., Drakenbergj, T., Wennerstrom, H.: NMR studies of ion binding in biological systems. Q. Rev. Biophys. **19**(1/2), 83–114 (1987)
2. Tanase, C., Boada, F.E.: Algebraic description of spin 3/2 dynamics in NMR experiments. J. Magn. Reson. **173**, 236–253 (2005)
3. Choy, J., Ling, W., Jerschow, A.: Selective detection of ordered sodium signals via the central transition. J. Magn. Reson. **180**, 105–109 (2006)
4. Shinar, H., Navon, G.: NMR relaxation studies of intracellular Na^+ in red blood cells. Biophys. Chem. **20**, 275–283 (1984)
5. Seshan, V., Sherry, A.D., Bansal, N.: Evaluation of triple quantum-filtered ^{23}Na NMR spectroscopy in the in Sifu rat liver. Magn. Reson. Med. **38**, 821–827 (1997)

Chapter 11
Practical Illustrations Sodium Spectroscopy and Imaging: Clinical Applications

11.1 Vasogenic Edema: Experimental Canine/Human Model

A valid distinction between cytotoxic and vasogenic edema [1] is based mainly on the differences in blood–brain barmier permeability. Vasogenic edema fluid develops in association with a variety of pathologic conditions such as brain tumors, brain abscesses hypertension or areas of infarction. In cases of brain tumor edema fluid leaks from the tumor vessels and spreads into the surrounding white matter. Similarly, cryogenic injury of the cerebral cortex causes a transient breakdown of the blood–brain barrier in the zone bordering the necrotic region allowing edema fluid to spread into the white matter. The regions in which the blood–brain barrier is defective and those in which the edema accumulates do not necessarily correspond. MRI has a proved to be a valuable and sensitive method by which to detect vasogenic edema. Multinuclear MR imaging (proton and sodium) permits in vivo assessment of the relative distributions of water and sodium within the brain. One can define the sodium signal associated with edema fluid as well as investigate the relaxation characteristics of extra-cellular sodium, for properties that may be specific to sodium in the extra-cellular compartment. A model of vasogenic edema can thus be developed. Previously models have relied on local injury to the brain by either cold or chemical insult. The resulting region of necrotic brain has a defective blood–brain barrier and vasogenic edema forms adjacent to the injured tissue. One can avoid a mixture of necrotic and edematous brain tissue by the use of a non traumatic mode of vasogenic edema in mongrel dogs.

A major technical obstacle is catheterization of the internal carotid artery without inducing spasm. This was accomplished by gently placing the catheter tip into the infundibulum of the internal carotid artery and making a test injection. The major arterial supply to the canine brain is through the anastomotic ramus that originates from the internal maxillary artery and joins the internal carotid artery. Therefore occlusion of the internal carotid artery by the catheter tip does not produce ischemia. However spasm of the internal carotid artery results in adequate delivery of osmotic

agents to the cerebral hemisphere and failure to disrupt the blood–brain barrier. The proton images of the two patients (chronic/human) with vasogenic edema secondary to well-circumscribed meningiomas revealed reduced signal intensity on the multiple saturation recovery images at TRs of 150 and 300 ms. The calculated T_1 images gave poor definition of the region of edema. On the third- and fourth-echo MSE (multi-spin echo) images as well as the calculated T_2 images the areas of vasogenic edema were well circumscribed and easily discernible. The sodium images of these patients revealed an increased sodium signal from the regions of vasogenic edema. The sodium signal was very intense and easily identified. In the normal brain electron microscopy demonstrates substantial variation in the extra-cellular compartment. In the gray matter the cellular membranes are in a regular pattern and are separated by only 100–200 angstroms (~ 10 nm) whereas in the white matter the intracellular spaces are irregular and may be oven 800 (~ 80 nm) angstroms wide. In the white matter, edema causes widening of the extra-cellular spaces and swelling of astro-cystic processes. In vasogenic edema the excess extra-cellular fluid is related to increased permeability of the blood–brain barrier such as occurs in the vicinity of brain tumors traumatic lesions and inflammatory foci. The increased vascular permeability allows indiscriminate escape of plasma components including serum proteins, electrolytes, and water.

The events that lead to the formation of vasogenic edema are not simultaneous. When the blood–brain barrier is opened through acute injury water and electrolytes first enter the extra-cellular space. The sodium content of vasogenic edema fluid induced by cryogenic injury increases. The spread of extravasated plasma contents (water, sodium and plasma proteins) is much more extensive in the white matter than in the gray matter. Also the osmotic pressure of the edema fluid colloid is elevated in accordance with its high protein content. The force that propagates vasogenic edema appears to be the mean arterial blood pressure which subsequently is influenced by the state of cerebral vasomotor autoregulation. Increased blood–brain barriers permeability effectively makes edematous brain tissue part of the extracerebral systemic extnacellu!ar space and therefore liable to expansion and nonosmotic hyperhydration. Similarly, the defective blood–brain barrier allows rapid penetration of osmotic agents into the affected areas. This accounts for the poor response of vasogenic edema to systemically administered osmotic agents. The characterization of sodium in the extracellular compartment by MR imaging is complicated by the quadrupolar nature of the sodium nucleus. The quadnupolar relaxation of a spin 3/2 nucleus decays as a weighted sum of two exponentials. The result is a two-component T_2 relaxation. Vasogenic edema fluid corresponds best to a two-site exchange model. In such a model the sodium ion exchanges between a solvated free state and a bound site on a serum macromolecule. Sodium ions tightly bound to serum proteins will not contribute to the total intensity of the sodium signal.

It is demonstrated that approximately 1 % of serum sodium is bound and that it is in constant fast exchange between potential binding sites on serum macromolecules and aqueous solution. It is seen there is shortened T_2 values for serum sodium compared with those of sodium bromide solutions. This effect was not attributed to protein binding but rather to the presence in serum of polyelectrolytes

that are surrounded by ordered shells of water molecules, a configuration that increases the reorientation time of both water molecules and hydrated ions. In vivo sodium MR imaging provides an opportunity to study the electrolyte composition of edema fluid. Current imaging techniques enable in vivo measurement of the two major components of edema fluid: water and sodium. Water content is assessed by investigation of the proton density, T_1, and T_2. Sodium content is assessed by signal intensity and T_2 relaxation characteristics. One hopes in the near future to be able to quantitate the sodium signal and thus provide an opportunity to investigate tissue osmolality. Sodium MR imaging offers the potential for providing new insights into the management of patients with vasogenic edema and may also permit in vivo estimation of the abnormalities, in extra cellular space associated with cerebral neoplasm. In the Fig. 11.1 are presented clinical results in the human model.

11.2   Tissue Sodium Concentration Tissue Viability (Stroke): Human Model (Conventional MRI)

It is imporatnat in some situations to know the role of sodium MR imaging in a comprehensive MR imaging protocol for monitoring tissue viability [2] in stroke. One can use for this purpose TSC (tissue sodium concentration) as measured by sodium MR imaging with apparent diffusion coefficient (ADC) and blood pool parameters derived from proton MR imaging. It can be done in a nonhuman primate model of acute embolic stroke and in patients with acute or nonacute stroke. The TSC parameter was evaluated in the setting of stroke along with the diffusion and perfusion parameters. Representative images and maps for a 62-year-old man with a 1-day-old stroke are presented in Fig. 11.2 [4]. It demonstrates the results from the comprehensive MR imaging protocol. In the area of stroke the thrombus caused the bolus of contrast material to have a prolonged TTT (tissue transit time) and delayed TA (arival time). These were displayed as bright voxels. Conventional ^{1}H MR imaging is insensitive for the detection of acute stroke. Diffusion-weighted imaging and its quantitative counterpart of ADC mapping are very sensitive in the early detection of ischemia. ADC and diffusion-weighted imaging show changes well before the thresholds of irreversible tissue injury related to water and ion homeostasis. The ADC and diffusion-weighted imaging are sensitive for detection of ischemia but do not provide a complete description of pathophysiologic conditions due to stroke in the primate brain. For any particular set of MR images to be useful in a clinical setting, particularly in a medically urgent situation such as acute stroke the technical success rate for yielding useful information must be considered.

Sodium MR imaging has long been proposed as a useful method to assess pathologic changes in the brain but medical applications have not developed because of the lack of an acceptable clinical implementation. The potential benefits of this
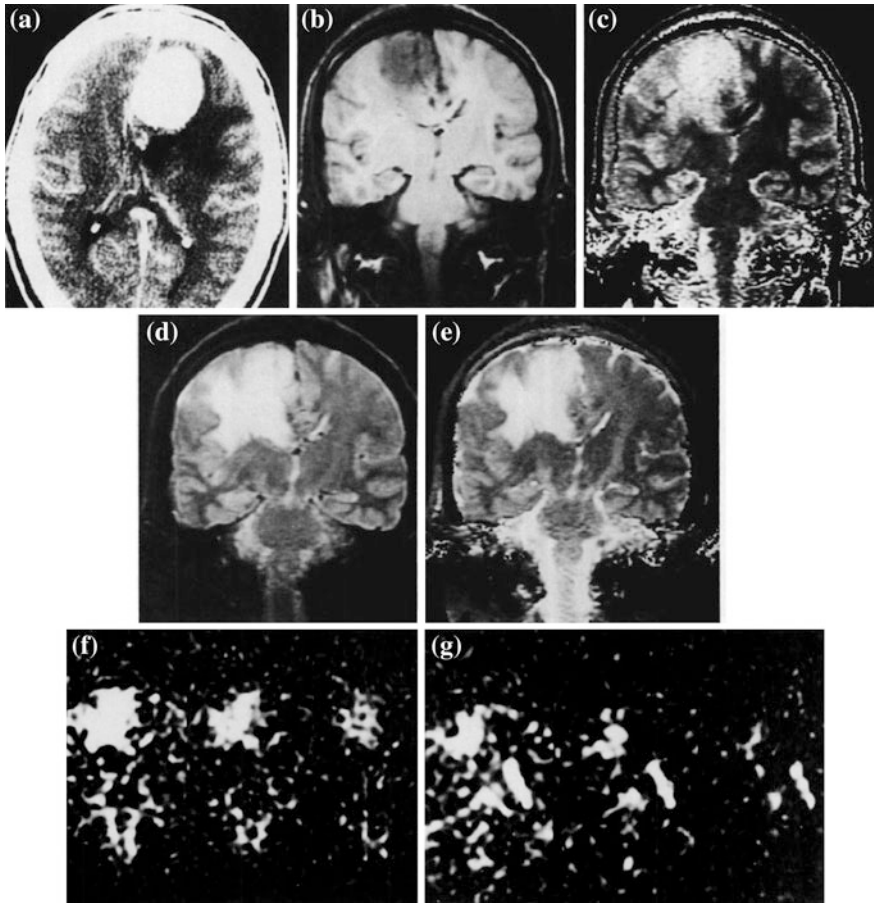
Fig. 11.1 **a** Contrast-enhanced axial CT scan of a patient with a flax meningioma. **b** Coronal MSE image (TR 600 ms) obtained along the posterior margin of the meningioma. The vasogenic edema is inconspicuous. **c** Calculated T_1 image (long T_1 represented as high intensity) poorly defines the edematous region. **d** Coronal image obtained with a MSE sequence (TE 100 ms, TR = 2,000). The edematous area is well delineated. **e** Calculated T_2 image also demonstrates the edematous white matter clearly **f**, **g** Coronal sodium MR images at TE 13, 26, and 39 ms. The sodium signal intensity is markedly elevated in the region of vasogenic edema. **g** Coronal sodium images (TE 13, 26, and 39 ms) that include areas of normal brain tissue, vasogenic edema, and cerebrospinal fluid (CSF) in the occipital horn. The sodium signal in the edema fluid appears to have a slightly shortened T_2 than in the CSF

method in stroke have been overshadowed by the newer proton-based methods of diffusion and perfusion imaging. Whereas the ADC parameter was useful in detecting the stroke very rapidly after embolization it was less informative over the critical first 6 h as it remained relatively stable. In marked contrast TSC (tissue sodium concentration) showed a linear increase over 6 h characterized by a rate of increase of about 5.7 mmol/L/h and approached 70 mmol/L at 6 h by which time the
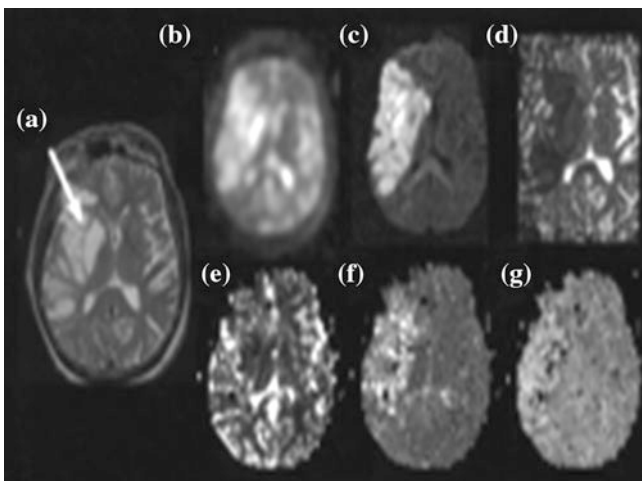
Fig. 11.2 Representative MR images in a 62-year-old man who presented with left-sided paralysis that lasted 24 h. **a** T2-weighted spin-echo ^{1}H image (2,500/102) through a stroke lesion (*arrow*). **b** ^{23}Na image (80/0.4). **C** Diffusion-weighted ^{1}H image (6,000/152). **d** ADC map. **e** Relative CBV map. **f** TTT map. **g** TA map. Parameter values for the lesion and the contralateral normal region respectively are as follows: TSC, 78 and 46 mmol/L; ADC, 0.21×10^{-3} and 0.64×10^{-3} mm^2/sec; TTT (tissue transit time), 37 and 14 s; and TA, 16 and 11 s. The relative CBV (cerebral blood volume) of the lesion was just less than half that of the contralateral homologous region

Table 11.1   Vasucular Compartment (3 % Na)

Vascular Compartment (3 % Na) = 140 mM	
Intra-cellular Compartment	Extra-cellular Comprtment
(85 %)	(12 %)
Na = 10 mM	Na = 140 mM

tissue was shown at histologic examination to be infarcted. The progression of stroke to infarction is dependent on both perfusion level and duration of reduced flow. The steadily increasing TSC level marked the changing metabolic status of the lesion. As shown in the treated animal, thrombolytic therapy after 150 min when TSC was still be (low 55 mmo/L) markedly decreased the volume of the infarct as compared with the result with no intervention.

As new neuroprotective agents enter clinical practice as alternatives to thrombolysis triaging patients to undergo appropriate therapies may be helped by this comprehensive MR imaging assessment of the tissue physiologic condition and viability. The model of TSC for assessing hyperacute stroke physiology is described approximately as follows. Table 11.1 [2] shows the scheme that summarizes the relationship between TSC and loss of tissue viability for a two-compartment model in which the vascular and extracellular compartments are

Table 11.2 Vasucualr Compartment (4 %)

Vascular Compartment (4 % Na) = 140 mM		
Intra-cellular Compartment (Intact) [Na] = 10 mM	Intra-cellular Compartment (loss of ion homeostasis) [Na]> 10 mM	Extracellular Compartment [Expanding] [Na] = 140 mM

considered as one compartment. For an intracellular compartment volume V_i and sodium concentration C_i and an extracellular compartment volume V_e, and sodium concentration C_e, the conservation of mass gives the following: TSC $(V_i + V_e) = V_e C_e + V_i C_i$. For a voxel of volume V, $V = V_i + V_e$ or $V_e = V - V_i$, which allows, TSC to be expressed in terms of the intracellular volume fraction V_i/V, as follows: TSC $= C_e + (C_i - C_e) (V_i/V)$. Thus for a fixed volume fraction increasing intracellular sodium concentration C_i increases TSC. Alternatively as the intracellular volume fraction decreases with loss of cell integrity TSC approaches C_e. It is important to realize this model is not just a redistribution of sodium within a voxel. The extracellular compartment is buffered with even minimal perfusion and the high diffusibility of sodium ions from the space of the entire body which is regulated systemically at a constant value of C_e.

It represents diagram of the two-compartment model of TSC. The vascular compartment is a part of the extracellular compartment as the extracellular sodium concentration (in millimoles per liter) is always maintained because of the rapid diffusion of sodium ions from the vascular compartment that is buffered by the rest of the body. In normal brain tissue the large intracellular compartment maintains a low sodium concentration against a high sodium concentration in the small extracellular compartment. During stroke the normal intracellular space decreases and the extracellular compartment expands with loss of ion homeostasis as the cell integrity is lost. As the extracellular sodium concentration is maintained through the vascular compartment even at low levels of perfusion, TSC must increase, which is a direct measure of the loss of cell integrity. Percentages in parentheses are percentages of voxel volume (Table 11.2) [4].

It represents diagram of the two-compartment model of TSC. The vascular compartment is a part of the extracellular compartment as the extracellular sodium concentration (in millimoles per liter) is always maintained because of the rapid diffusion of sodium ions from the vascular compartment that is buffered by the rest.

11.3 Human Brain In-vivo Sodium MRI: Soft Inversion Recovery (Conventional Versus Quantum MRI)

The ability to assess intracellular sodium concentrations [Na_{in}] may greatly facilitate the diagnosis of diseased tissue in the human brain [3]. [Na_{in}] appears to directly correlate with the rate of cell proliferation and monitoring [Na_{in}] may be

useful in the analysis of neoplasms and their response to chemotherapy. The ability to assess [Na$_{in}$] may also be useful in the setting of acute stroke as dramatically increased [Na$_{in}$] levels associated with anoxic depolarization and the subsequent relatively slow diffusion of sodium ions from other parts of the brain into the ischemic core appear to be directly linked to cell damage during ischemia. The valuable information pertaining to the diseased state of tissue can be obtained with sodium MRI techniques that facilitate quantification of bulk tissue sodium concentrations; strongly intracellular weighted imaging techniques that limit the signal contribution from the more highly concentrated extra-cellular space (ECS) (140 mM vs. 10–15 mM intracellular) may provide an improved means to characterize [Na$_{in}$] in some cases. There is an approach to use of multiple-quantum filtering techniques. However, the signal intensity following a multiple-quantum spin sequence is a small fraction of the signal intensity following a single ideal 90° excitation pulse (10 % has been given as a typical in vivo value). There is an another approach that uses. an inversion recovery (IR) Technique. A considerable T$_1$ relaxation differences exist between two environments. IR can be used to eliminate the signal contribution from either environment. Although it is well understood that the ECS (extra-cellular space) in the brain contains many different types of proteoglycans most attached to the cell membranes little is known about the density of these molecules.

It has been suggested that the density of this extra-cellular matrix is quite sparse allowing volume transmission through the ECS. Because T$_1$ measurements have been shown to correlate with matrix density, sodium T$_1$ relaxation in the ECS may be significantly longer than in the intracellular space (ICS). Shift reagent aided experiments using an implanted gliosarcoma in rats also suggest this to be the case. Minimal sodium exchange is expected between the ICS and ECS on the relevant sodium NMR timescale. If the sodium T$_1$ in the ECS is significantly longer than in the ICS an IR sequence may be used to eliminate the ECS signal contribution from a sodium image. When the relaxation constants T$_1$ and T$_2$ are much longer than an RF pulse the effects of relaxation during the pulse can essentially be ignored. The calculation of flip angle is simple and is directly related to pulse power and length. While this is usually the case for the uncoupled ^{1}H nuclide this is not the case for the quadrupolar sodium nucleus. An IR technique labeled soft inversion recovery fluid attenuation (SIRFLA) is proposed for sodium imaging of in vivo human brain. The efficacy of this technique is demonstrated through the minimization of sodium signal from the cerebrospinal fluid (CSF) brain images acquired at a static magnetic field strength of 4.7 T. The effectiveness of soft inversion pulses to separate sodium longitudinal magnetization in different environments has been shown analyzed along with the resultant benefit in the SIRFLA sequence. This separation is the direct result of the large quadrupole interaction experienced by the sodium nucleus and is not possible in conventional ^{1}H NMR. It is because the inversion pulse length has a dramatic impact on signal acquired from the non-nulled environment.

The IR sequence implemented with long RF inversion pulses has been given the new designation SIRFLA. Considering the relaxation parameters the SIRFLA sequence may offer an SNR benefit over triple quantum filters (TQF) for

intracellular imaging. The TQF sequence is also limited by SAR as three hard 90° RF pulses are required and increasing the RF pulse length decreases acquired signal intensity. A TQF sequence with three 1-ms 90° RF pulses and the same TR repetition time) presented for the SIRFLA sequence would dissipate twice the power of the SIRFLA sequence. The SIRFLA sequence can also theoretically facilitate "full elimination" of the ECS signal contribution. In vivo TQF studies suggest a 40 % residual contribution from the ECS. Several marked artifactual hyper intensities can be seen in Fig. 11.3a [3] that are not apparent in Fig. 11.3b [3]. The most significant affect begins above the sphenoid sinus and extends into the frontal lobe. Two other less pronounced artifacts exist on the outer edges of the parietal lobes. Susceptibility induced B_0 inhomogeneities are well known to exist in these areas, a product of the surrounding sinuses and bone. Artifacts caused by these B_0 inhomogeneities are apparent in other imaging modalities such as single-shot EPI. These artifacts Fig. 11.3 a [3] are the result of the narrow bandwidth associated with the long inversion pulse and are minimized by the wider bandwidth of the short inversion pulse in Fig. 11.3 b [3].

11.4 Statistically Optimal MRI Acquisition (General)

An exponentially decaying signal can be described by two parameters, its amplitude ρ and decay rate λ, given as [4] $S(t) = [\rho \, (e^{-\lambda t})]$. Here t is the user-controlled encoding parameter (diffusion weighting or echo time). At least two measurements with different encodings e.g. t_1 and $t_2 > t_1$, are needed to estimate λ. It has been shown that within all such 'two point' schemes the imaging time is used most efficiently when $(t_2 - t_1)$ is chosen to be about $1.29/\lambda$. One can examine whether multipoint acquisitions with several (more than two) encodings may be more efficient than two-point schemes in the same total measurement duration. One routinely uses the χ^2-statistical fitting procedure as a measure of the precision of the decay rate estimation. It demonstrates that the most efficient multipoint scheme in fact approaches that of the two-point method. The optimal acquisition strategy is specified by a set of t_i's yielding the highest precision in the determination of the decay rate. It is naturally with the smallest σ_λ^2 i.e., the variance. The expression in general for the variance A_i, in terms of the optimum variance σ_0, can be written as $A_i = (1/\sigma_0)[(e_i^{-\lambda t}) - t_i\rho(e_i^{-\lambda t})]$. One performs this optimization in the vicinity of the expected decay value, $\lambda = \lambda_{\text{tune}}$, and then evaluate σ_λ at arbitrary λ's. If the actual value of λ deviates from λ_{tune}, the precision degrades as shown in Fig. 11.4 [5]. The precision loss seen is only 15 % over a wide range $\lambda \sim (0.6, 1.5) \, \lambda_{\text{tune}}$. If the decay constants to be measured are expected to vary by much more than a factor of $1.5/0.6 = 2.5$ the two-point method will be inefficient at the edges of the range of λ's.

Measurement of exponential relaxation constants for which the two-point method is found to be the most efficient should not to be confused with the validation of the model of exponential signal decay. The latter is characterized by
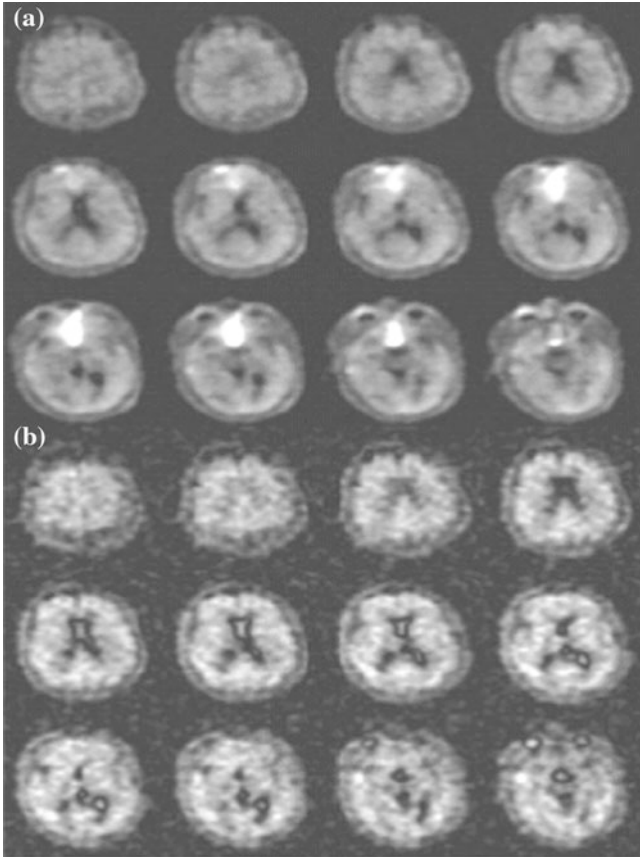
Fig. 11.3 a SIRFLA images acquired in healthy volunteer (inversion pulse length of 10 ms). SNR in the CSF is 4 and SNR in the brain tissue is 17. **b** Sodium IR images acquired with a much shorter inversion pulse length of 1 ms and a TR of 334 ms. SAR and voxel size are equivalent to **a** and the image duration was 10.7 min (or ~25 s shorter than (**a**)). SNR in the CSF is 2.5 and SNR in the brain tissue is 10. The SNR is 70 % greater in (a) with the longer inversion pulse than in (**b**). One disadvantage of the longer inversion pulse is its narrow bandwidth which results in an artifactual hyper intensity in the known areas of susceptibility **a** that is not seen in **b**. The images in (**a**) and (**b**) are not globally scaled

the goodness of the fit and requires acquisitions at multiple distinct encodings t_i. Being optimal the two-point scheme lends itself admirably to applications relying on measurement of the change in the relaxation constants such as micro vessel density estimation. Indeed images acquired before and after the relaxation constant. is altered say by administration of a contrast agent naturally constitute the two points. Image intensity of the first point is given by $[\rho\{e_0^{(-\lambda t)}\}]$ while of the second by $[\rho e_0^{(-\lambda t)}][\rho\{e^{(-\Delta \lambda t)}\}]$. Since modification of the encoding parameter t between the points introduces unwanted sensitivity to the unknown "resting" tissue relaxation constant, λ_0, t has to be common to both acquisitions.
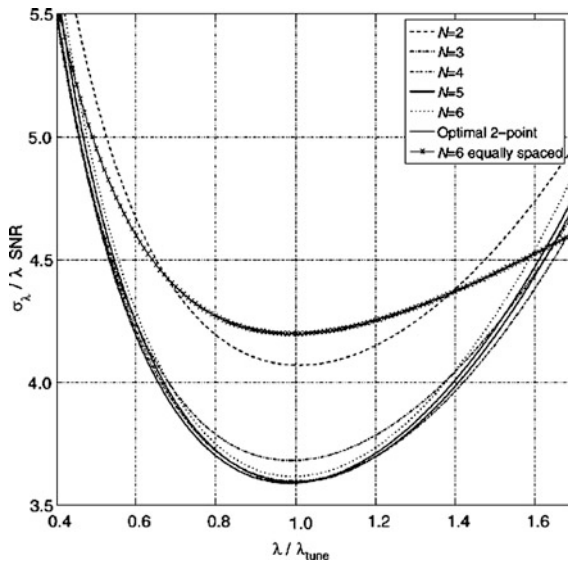
Fig. 11.4 Precision as a function of λ for several N-point protocols tuned for λ_{tune}. Here the SNR is the signal-to-noise ratio of the average of N images with minimal exponential weighting and in general, is a function of λ, if the minimal weighting, is not zero. Note that the precision of protocols with $N \geq 3$ is already very close to optimal. Since the convexity of the curves is very small the precision stays within. 15 % of the best over a broad interval $(0.6, 1.5)$ λ_{tune}. As an example of a commonly used scheme the precision for optimal 6-equally-spaced-point protocol is superposed

The optimal acquisition strategy consists of choosing the value of t to yield the highest precision of $\Delta\lambda$. Interpreting $[\rho\{e_0^{(-\lambda t)}\}]$ as the amplitude of the decay ρ and $\Delta\lambda$ as decay constant, λ casts the problem, in terms of the relaxation constant estimation considered with one exception; ρ depends on the user selectable parameter t. However, in applications such as microvasculature imaging, requiring high doses of contrast agents λ_0 is much smaller than $\Delta\lambda$. Therefore, for optimization purposes in the vicinity of $\Delta\lambda$ the t dependence of ρ can be neglected. Thus, optimal exponential weighting, t as well as relaxation constant alternation are found by replacing λ_{tune} with $\Delta\lambda$. Figure 11.4 [4] represents summary of the graphical picture of the analysis.

11.5 Spin 3/2 Bi-Exponential Relaxation Multi-Quantum Filtration Technique (^{23}Na Spectroscopy)

It is known that metal ions play a vital mediating role in many important biological processes. As a result of their relatively favorable properties NMR studies of the spin-3/2 nuclei, ^{7}Li, ^{39}K, ^{87}Rb, and, most frequently ^{23}Na have proved popular. The two main areas of interest [5] have been the study of these nuclei in

intracellular environments and of their binding to biological molecules in solution. In both cases the spin-3/2 nuclei are likely to be tumbling in the slow-motion regime i.e. possessing a rotational correlation time τ comparable to the inverse of the Larmor frequency ω_o and it is known that under these conditions both the transverse and the longitudinal quadrupolar relaxation are biexponential. Often, however biexponential relaxation is difficult to distinguish from simple exponential relaxation using conventional NMR methods. Recently it has been shown that biexponentially relaxing spin-3/2 nuclei can be filtered through a state of multiple-quantum coherence. Multiple-quantum filtration techniques can therefore provide unambiguous evidence of the presence of biexponential relaxation. In this fashion intracellular and extra cellular metal ions can be distinguished since the latter are almost always in the fast-motion regime (where they exhibit simple exponential relaxation) and the NMR signal from these ions will not pass the filter. The lineshape resulting from multiple-quantum filtration consists of the difference of two Lorentzians and analysis of this highly characteristic line shape in binding studies can indicate the motional and exchange behavior of the metal ions. In all studies of this type sensitivity is usually a prime concern because of the low concentration of metal ions in the slow-motion regime.

It has been demonstrated that a double-quantum filtration experiment for the detection of biexponential transverse relaxation in spin-3/2 nuclei works well. Some workers have apparently without exception adopted the double-quantum filtration techniques. Others also used a triple-quantum filtration experiment for the detection of bi-exponential longitudinal relaxation. It can all be done with greater sensitivity using triple-quantum filtration than using double-quantum filtration techniques. The signal amplitudes produced by the double- and triple-quantum filtration techniques for spin-3/2 nuclei are conveniently calculated using an irreducible tensor operator formalism. The density operator $\sigma(t)$ for an isolated spin of quantum number S is expanded in the form $\sigma(t) = \Sigma_{l=0 \text{ to } 2s} \Sigma_{p=-1 \text{ to } l} C_{lp}(t) T_{lp}$, Here T_{lp} is an irreducible tensor operator of rank l and coherence order p. The matrix representations for S = 3/2 can be found in the MRI literature.

The transformation of an operator T_{lp} under a radiofrequency pulse of flip angle β, and phase φ, is given in the familiar "arrow notation" by $T_{lp} - \beta (I_y \cos \varphi - I_x \sin \varphi) \rightarrow \Sigma_{p'} T_{lp'} dl'_{pp'}(\beta) \exp\{-i \Delta p \varphi)\}$, where p' is the new coherence order, and $Ap = p' - p$ is the change in coherence order under the pulse. The amplitude of the transfer T_{ip} to $T_{ip'}$, is given by the reduced rotation matrix element $d^l p' p(\beta)$. By convention the $d^l p' p(\beta)$ are defined so that the phase φ represents a positive excursion with respect to the rotating frame y axis (i.e., $\varphi = 0$ for a y pulse, $\varphi = 90°$ for a –x pulse, and so on). The rank 1 of a tensor may change under free precession or relaxation but this evolution is the same in both double and triple-quantum filtration experiments and has been calculated in detail. The pulse sequence and coherence transfer pathway diagram for multiple-quantum filtration of spin-3/2 nuclei exhibiting biexponential transverse relaxation are shown in Fig. 11.5 [5]. Significant transverse relaxation takes place during the evolution period τ_e and the acquisition period t_2 but not during τ_m. The phase angle φ' is 0° for excitation of double-quantum coherence (dotted coherence transfer pathways)
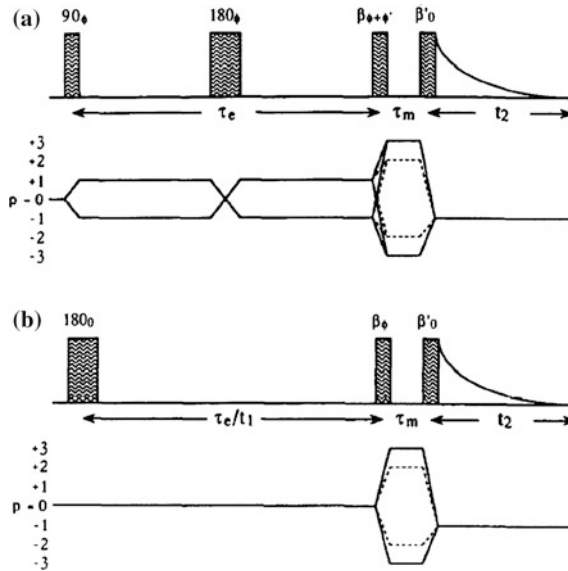
Fig. 11.5 Pulse sequences and coherence transfer pathway diagrams for multiple quantum filtration of spin-3/2 nuclei. The "transverse experiment" (**a**) is used to study biexponential transverse relaxation and the "longitudinal experiment" (**b**) is used to study longitudinal relaxation. The phase φ in (**a**) and (**b**) is stepped through the values $0°$, $90°$, $180°$, and $270°$ for double-quantum filtration (dotted coherence transfer pathways) and through $30°$, $90°$, $150°$, $2\,10°$, $270°$ and $330°$ for triple-quantum filtration (solid pathways), while the receiver phase is alternated between $0°$ and $180°$

and 90° for triple-quantum coherence (solid pathways) while the phase φ and the receiver are phase cycled to select the desired pathway.

The phase φ' in (a) is $0°$ for double quantum and $90°$ for triple quantum filtration. Maximum sensitivity is achieved with flip angles $\beta = \beta' = 90°$, except for the double quantum filtration version of (b) where $\beta = 54.7°$. To study biexponential longitudinal relaxation a variable evolution period t must be used in (b) rather than a fixed evolution period τ_e. The period τ_m, is typically a few microseconds to allow for phase shifting of the pulses. From the form of the third-rank reduced rotation matrix elements $d^3p'p(\beta)$ it can be shown that the signal amplitude from both techniques is maximum if the flip angles β and β' of the two pulses in the filter are both $90°$. With $\beta' = 90°$ the amplitude of coherence transfer through $p = +2$ (or +3) is the same as that through $p = -2$ (or -3). Using the optimum phase cycling of the phase φ and the receiver the relative signal amplitudes from the double- and triple quantum filtration experiments can be determined from $S^{TQF}/S^{DQF} \sim 1.5$ (mono-exponential case), ~ 1.3 (bi-exponential case). One can mathematically calculate relative signal amplitudes produced by the transverse and longitudinal experiments as function of $\omega_0\tau_c$ (ω_0 = Larmor Frequency, τ_c = correlation constant and is plotted in Fig. 11.6 [5].
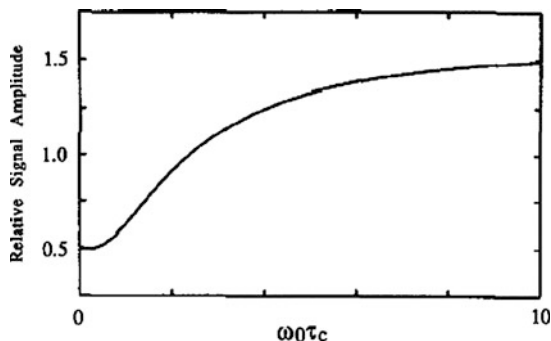
Fig. 11.6 Ratio of the signal amplitude from the optimized transverse experiment to that from the longitudinal experiment as a function of $\omega_0 \tau_c$ (ω_0 = Larmor Frequency, τ_c = correlation constant) for pure quadrupolar relaxation. The optimum fixed evolution periods τ_e have been used at each value of $\omega_0 \tau_c$. The signal amplitude from the transverse triple-quantum filtration experiment is half that from the longitudinal experiment for $\omega_0 \tau_c$ but is 1.59 times greater in the limit of infinitely large $\omega_0 \tau_c$

11.6 Sodium Twisted Projection Imaging (TPI)/Conventional MRI (ADC Maps) Human Model

Regulation of sodium homeostasis through counter-balancing low intracellular and high extra cellular sodium ion concentrations with potassium ions is of vital importance for cellular function [6] These ion gradients across the cell membrane provide the potential energy for many important cellular transport processes. Action potentials intracellular pH regulation and many membrane transport processes are all directly dependent on the sodium ion gradient across the cell membrane. Damage to brain cell integrity and disruption of cell packing produce local increases in tissue sodium concentration (TSC). TSC determined by quantitative MRI has been shown to have a potential role in monitoring tissue viability in humans with diseases such as stroke and in monitoring treatment of brain tumors. Despite these potential medical applications described more than two decades ago quantitative sodium imaging has been slow to evolve.

   The sodium MR signal has a detection sensitivity of four orders of magnitude lower than that of the proton signal. It exhibits biexponential relaxation behavior with fast and slow transverse relaxation characteristics (T_2^{fast}, 1–3 ms and T_2^{slow}, 12–25 ms, respectively) in biologic tissues. Therefore, sodium imaging requires an imaging sequence with a short excitation radiofrequency (RF) pulse and a short echo time (TE) to reduce signal loss from the rapid decay of the transverse magnetization. Twisted projection imaging (TPI) is a three-dimensional (3D) projection reconstruction sequence–based approach that can achieve short TE values and high acquisition efficiency.

   When performed at long pulse repetition times to allow full T_1 relaxation quantification of TSC is possible. However the generation of TPI [6] gradient
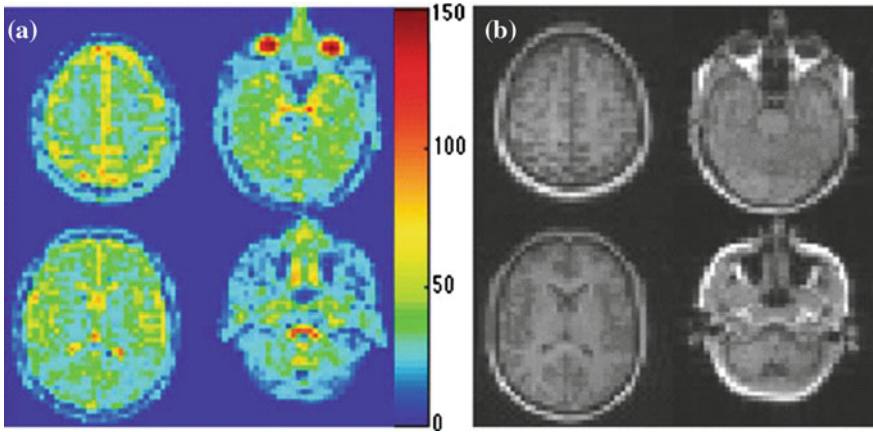
Fig. 11.7 Representative TSC maps **a** obtained on a healthy volunteer (unit: millimoles/liter tissue). The corresponding T_1-weighted proton images are also shown **b** as anatomic references. The TSC images shown are before water fraction correction. The WM (*white* matter) is predominantly shown and also the GM (*Grey* matter) is recognized between cerebrospinal fluid (partial-volume effects with brain parenchyma) and WM

waveforms is often limited by the hardware slew rate constraint especially when starting twisting at low k-space radius is desired to reduce the number of projections needed to sample k-space at the Nyquist rate. Besides being potentially harmful to the subject and the gradient system violations of the slew rate constraint can also cause uncertainty in the k-space trajectory. The slew rate constraint can be met by using low gradient amplitude or numerical smoothing. However, these approaches result in either a long readout time that ultimately limits the achievable spatial resolution due to T_2 relaxation, or k-space trajectory deviations that degrade the point-spread function (PSF) of the sequence. Meanwhile, the high data acquisition efficiency of TPI stems from its ability to sample more k-space locations in each repetition, with a relatively long readout window. This renders TPI sensitive to static field (B_0) inhomogeneity even at the relatively low sodium resonance frequency. These B_0 inhomogeneities must be corrected to avoid significant image blurring and distortion. In the Fig. 11.7 [6] and 11.8 [6] one would find a practical illustration of the results obtained by the TPI technique.

11.7 Human Brain: Diffusion Weighted Magnetic Resonance Spectroscopy (MRS) And Imaging (Conventional MRI)

Magnetic resonance is well established for measuring the diffusion properties of water in the human brain and it has been proven to be useful in numerous neurological disorders. Diffusion-weighted imaging (DWI) of tissue water includes contributions from exchanging intra- and extra cellular water, which makes
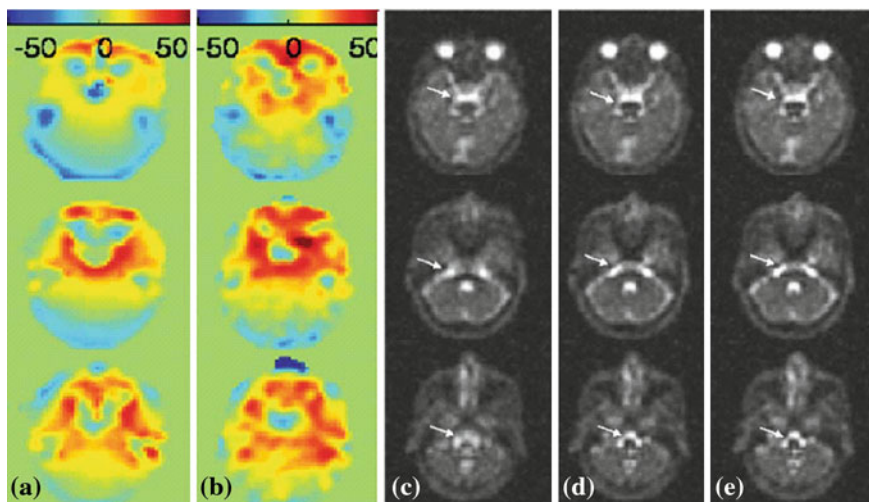
Fig. 11.8 Axial B_0 field maps are shown for a normal volunteer using **a** sodium imaging in 4 min and **b** proton imaging in less than 2 min. These B_0 maps were applied to **c** the uncorrected images to derive **d** human images corrected using sodium B_0 field maps, and **e** human images corrected using proton B_0 field maps. The improvements appreciated in the brainstem (*white arrows*) are similar for both sodium and proton

compartment-specific interpretation of diffusion characteristics rather complex. The diffusion characteristics of intracellular metabolites can be measured by incorporating diffusion sensitizing gradients with spatial localization in a spectroscopy pulse sequence, i.e., diffusion-weighted magnetic resonance spectroscopy (DW-MRS) [7]. The main research focus of DW-MRS thus far has been on animal models of cerebral ischemia in which the apparent diffusion coefficients (ADCs) of the singlet metabolites are reduced significantly in the acute phase of cerebral ischemia, similar to the ADC reduction of water. These studies indicate that diffusion changes of metabolites may be useful in probing the effect of stroke and other pathologies on the intracellular environment. There have been some studies on the diffusion characteristics of the metabolites *N*-acetyl aspartate (NAA), creatine and phosphocreatine (tCr), and choline (Cho) in the human brain.

There are problems with measuring the ADC (apparent diffusion coefficient) of the metabolites, including low concentration, small ADCs, and macroscopic motion due to involuntary subject movements, respiration, and cerebrospinal fluid related brain pulsations. These motion errors cause a decrease in the signal intensity of the metabolite peaks which in turn results in an apparent increase in the measured ADC. It was proposed a phase error correction method using the residual water peak as well as cardiac gating for correction of the motion-induced errors. These methods were applied and reported that the ADCs of NAA, tCr, and Cho were found to decrease in acute stroke and increase in the peripheral region of a tumor including edema. It was suggested that since NAA is a neuronal marker the ADC differences are an indication of neuronal cell viscosity changes as a result

Fig. 11.9 Spectra at low and high **b** (apparent diffusion coefficient) values with the diffusion gradient applied in the *Y* (anterior–posterior) direction in **a** subcortical white matter (SWM) **b** occipital gray matter (OGM), and (**c**) frontal gray matter (FGM). The signal intensity of the NAA peak dropped 17, 20, and 24 % at higher *b* values in the SWM, OGM, and FGM regions, respectively
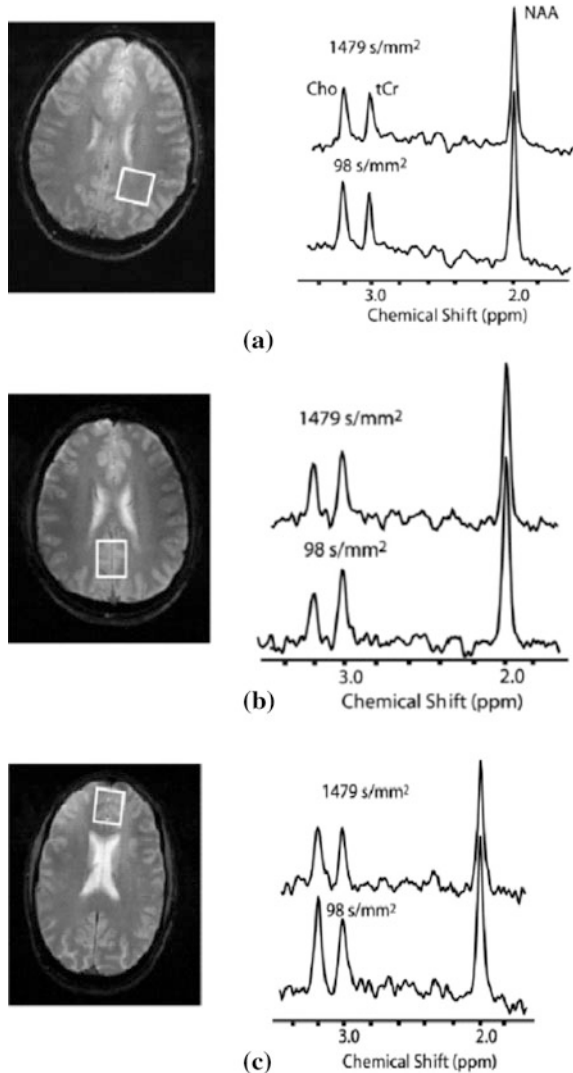
of the pathologic status of the tissue. The micro structural organization of white matter in brain tissue leads to directional dependence (i.e., anisotropy) of the ADC of water, and presumably of the metabolites as well. However, the trace/3 (X, Y, Z), ADC provides a rotationally invariant measure of molecular diffusion in tissue. Some previous human studies examined the ADC of NAA, tCr, and Cho in subcortical white matter of human brain but the diffusion was only measured in one arbitrary direction. Therefore the purpose of this study is to quantify the rotationally invariant trace/3 ADC values of the metabolites NAA, tCr, and Cho in various regions of the healthy human brain. A new phase correction method is proposed for processing the diffusion-weighted spectra. The Fig. 11.9 [7], and the

Table 11.3 An Intra- versus Inter-subject Comparison (Mean ± SD) of the Trace/3 Apparent Diffusion Coefficients of NAA, tCr, and Cho in the Subcortical White Matter (SWM) Region Using the NAA Phase Correction Method

Subcortical White matter region	NAA/ Trace/3 ADC $(10^{-3}mm^2/s)$	tCr/ Trace/3 ADC $(10^{-3}mm^2/s)$	Cho Trace/3 ADC $(10^{-3}mm^2/s)$
Inter-subject t (N = 6)	0.14 ± 0.02	0.19 ± 0.04	0.18 ± 0.06
Intra-subject			
Subject 1 (N = 3)	0.14 ± 0.03	0.20 ± 0.03	0.13 ± 0.02
Subject 2 (N = 3)	0.13 ± 0.02	0.18 ± 0.04	0.18 ± 0.02
Subject 3 (N = 3)	0.13 ± 0.02	0.15 ± 0.03	0.13 ± 0.04

Table [7] present details about a practical illustration of diffusion weighted MRI of tissue structure in human brain (Table 11.3) [7].

11.8   Human Brain Metabolites: Proton T_1 and T_2 Relaxation Times (Conventional MRI)

Reasonable estimates of relaxation times of brain metabolites are important for accurate quantitation of MR spectra, for optimizing measurement protocols, for absolute quantitation in single voxel MR spectroscopy and in quantitative spectroscopic imaging. Relaxation times of metabolites in proton MR spectra of human brain in vivo have been the subject of studies for 3T(Tesla) [8]. Both longitudinal and transverse relaxation times of brain metabolites should follow relaxation dispersion of water protons, experiencing similar longitudinal relaxation mechanisms. Correspondingly, the T_1 values should increase and the T_2 values should decrease with increasing static magnetic field B_0. The decrease in T_2 for N-acetylaspartate, creatine and choline compared to the lower field data has already been reported at 4.1 and at 4T. Accuracy of the obtained relaxation times is affected by several factors. A proton spectrum of the brain in vivo represents a superposition of a large number of spectral lines belonging to various metabolites. Due to the heavy overlap of these lines, reliable quantitative separation of all individual components is almost impossible. Furthermore, broad signals with relatively short T_1 and T_2 are present as a baseline underlying the sharper spectral lines of the metabolites. These signals probably belong to large molecular-weight compounds which were also found in the spectra of brain extracts.

Another factor complicating determination of the T_2 relaxation times is the evolution of spectral multiplets during the echo time. Many spectral lines show complex coupling patterns due to spin–spin coupling with adjacent protons. Evolution of such multiplets combined with a rather large linewidth results in a substantial decrease of signal intensities at longer echo times The factors mentioned above represent potential sources of errors of the measured relaxation times. In practice, they are manifested through the nonexponential behavior of

magnetization amplitudes in both T_1 and T_2 measurements. Here, T_1 and T_2 relaxation times at 3 T are reported for proton resonances of several brain metabolites. Book Table 11.4 [8] and Table 11.5 [8], show the T_1 and T_2 relaxation times, for important brain metabolites.

11.9   Relaxation Times: Human Abdominal and Pelvic Tissue (Conventional MRI)

In pursuit of a higher signal-to-noise ratio, faster imaging and new forms of contrast enhancement the imaging community has been installing an increasing number of magnetic resonance (MR) imagers that operate with field strengths of 3.0 T and higher. Initially motivated by specialized research applications such as functional neuro-imaging many of these MR imagers are now being equipped with body transmit coils and surface coil arrays that enable the development of body imaging applications. Optimization of body imaging protocols at 3.0 T [10] requires an appreciation of the changes in T_1 and T_2 relaxation times, which accompany the change in field strength. These relaxation times help determine the contrast in MR images and they can also affect both the spatial resolution and the signal-to-noise ratio. Furthermore relaxation times directly affect the selection of image pulse sequence timing parameters which affect the total imaging times and consequently patient throughput. T_1 and T_2 are known to change substantially with field strength but the change is determined with water mobility and other tissue properties in such a way that it cannot be predicted accurately with a theoretical calculation.

The accurate determination of proton relaxation times with high-field-strength MR imaging is an essential first step in exploring the capabilities of high-field-strength MR imagers. A large number of techniques for measuring T_1 and T_2 relaxation times in tissues have been reported. These methods, however often require very long imaging times which makes them susceptible to imaging artifacts caused by patient motion. Thus relaxation parameters in the human abdomen have been determined only rarely. The purpose of this study was to measure T_1 and T_2 relaxation times of normal human abdominal, and pelvic tissues [9], and lumbar vertebral bone marrow at 3.0 T. The Fig. 11.10 [9], the Table 11.6 [9] and the Table 11.7 [9] are the practical illustrations of the accurate (after applying suitable statistical correction) determination of the T_1 and T_2, in various tissues of the human body. The following equations are normally used to obtain the important parameters from the signal intensity SI.

$$SI = \left[\sqrt{(S^2 + C_n^2)} \right]$$
$$= \sqrt{\left[\{ (S_0 - 2 . S_0 . \{ \exp - (TI/T_1) \} + S_0 . \exp - (T_{sat}/T_1) \} + C_n^2 \right]}$$

Table 11.4 Mean value of proton T_1 relaxations times (in seconds ± SD) of some metabolite resonances in occipital Grey and White Matter (n = 5) compared to published data (see the cross references number listed in Ref. [9], in column 1), at 1.5, 2 and 4.1T respectively

Location, B_o	NAA (2.01)	Glu (2.35)	Cr (3.03)	Cho (3.22)	Ins (3.57)	Ins (3.66)	Glx (3.75)	Cr (3.92)
Occ GM, 3T, this work	1.47 ± 0.06	1.27 ± 0.10[a]	1.46 ±0.07	1.30 ±0.06	1.23 ±0.09	1.19 ± 0.07[b]	1.20 ± 0.10	0.97 ±0.07[c]
Occ WM, 3T, this work	1.35 ± 0.12	1.27 ± 0.08[a]	1.24 ± 0.10	1.08 ± 0.06	1.01 ± 0.09	0.93 ± 0.11	0.96 ± 0.20	0.83 ± 0.11[c]
Insl GM, 1.5 T	1.65		1.75	1.10	1.35			1.75
Occ WM 1.5 T	1.45		1.55	1.15	0.90			1.05
Occ WM 1.5	1.63		1.67	1.56				
Occ GM 1.5 T	1.29 ±0.09		1.20 ±0.07	1.39 ±0.12	1.10 ±0.17			
Occ lobe 1.5 T	1.5 ±0.1		1.3 ±0.1	1.5 ±0.2				
Hip 2 T	1.41 ±0.07		1.55 ±0.09	1.44 ±0.11	1.73 ±0.15			
Par GM 4.1 T	1.27 ±0.04		1.49 ±0.04	1.11 ±0.04				
Par WM 4.1 T	1.26 ±0.04		1.43 ±0.06	1.07 ±0.04				

Maean Value of Proton T_1 Relaxtion Times in Grey and White Matter. Note: Occ = Occipital, Hip = Hippocmpus; Insl = Insular; Par = Parietal; GM = grey matter, WM = white matters; a: n = 4; b: this line was not always clearly resolved, n = 2, c: the values for Cr(3.92) were calculated from signal intensities measured with TI(inversion time) from 1.53 to 800 ms. Using all TI (inversion time) values, T_1 = 1.8 and 1.05 s were obtained for grey and white matter, respectively

Table 11.5 Mean Values of proton T_2 relaxation times (ms $\pm$ SE (standard error)) measured in occipital grey (GM) and white matter (WM)

Location B_0 (Magnetic Field)	NAA (2.01)	Cr (3.03)	Cho (3.22)	Cr (3.92)
Occipital GM 3T (Tesla)	247 ± 19	152 ± 7	207 ± 16	116 ± 9
Occipital WM 3T (Tesla)	295 ± 29	156 ± 20	187 ± 20	141 ± 16
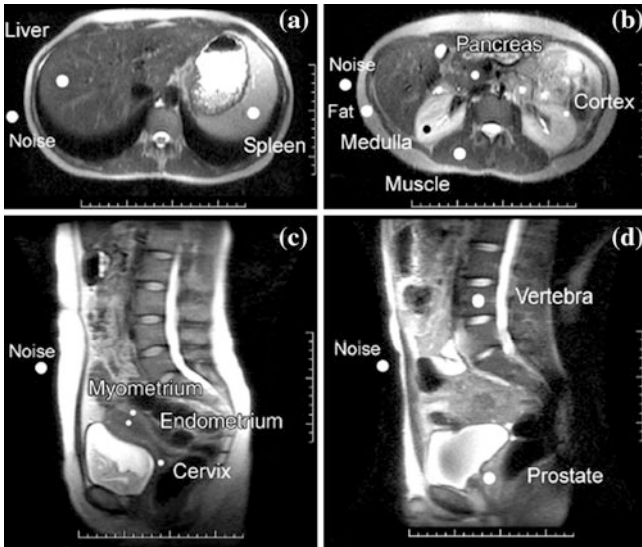
Fig. 11.10 MR images obtained at 3.0 T with a half-Fourier acquisition single-shot fast SE sequence combined with inversion recovery (repetition time [TR], 5,000 ms; inversion time [T_1], 150 ms; field of view, 360 × 252 mm; section thickness, 5 mm; acquisition matrix, 256 × 160; effective TE, 60 ms). Transverse sections through **a**, the liver and the spleen and **b**, the level of the kidney. Sagittal sections through **C**, the uterus, and **d**, the prostate and vertebra were used to generate the regions of interest (ROIs) which are indicated by white circles and labels. The scale is in centimeters

In the above equations, SI is the measured signal intensity when averaged over time or an ROI, S is the true signal intensity (in the absence of noise) from tissue, and Cn is a noise related constant.

The T_{sat} is saturation time and is not equal to TR (repetition time). In the SE (spin echo) prepared images the signal intensity follows a mono-exponential decay as follows

$$SI = [\sqrt{\{S_0 . \exp - (TE/T_2)^2 + C_n^2\}}]$$

Table 11.6   Average T_1 Relaxation Times at 1.5 and 3.0T

Tissue	1.5T	1.5T	3.0T	3.0T	Difference
	T_1 Relaxation Time (msec)*	R^2 Value (%)	T_1 Relaxation Time (msec)*	R^2 Value (%)	(%)
Kidney					
Cortex	966 ± 58	0.999	$1{,}412 \pm 154$	0.990	18[§]
Medulla	$1{,}412 \pm 58$	0.997	$1{,}545 \pm 142$	0.999	9
Liver	586 ± 39	0.995	809 ± 71	0.987	38[§]
Spleen	$1{,}057 \pm 42$	0.998	$1{,}328 \pm 31$	0.998	26[§]
Pancreas	584 ± 14	0.982	725 ± 71	0.976	24
Paravertebral muscle	856 ± 61	0.988	898 ± 33	0.988	5
Bone marrow (L4 Vertebra)	549 ± 52	0.991	586 ± 73	0.994	7
Subcutaneous Fat	343 ± 37	0.997	382 ± 13	0.999	11
Uterus					
Myometrium	$1{,}309 \pm 35$	0.998	$1{,}514 \pm 156$	0.999	16
Endometrium	$1{,}274 \pm 64$	0.997	$1{,}453 \pm 123$	0.998	14
Cervix	$1{,}135 \pm 154$	0.998	$1{,}616 \pm 61$	0.998	42
Prostate	$1{,}317 \pm 85$	0.998	$1{,}597 \pm 42$	0.998	21

*Data are mean value $\pm$ SD, [§] Difference is significant ($P < 0.05$), R^2 inter-subject variation

Table 11.7 T_2 Relaxation Times at 1.5 and 3.0 T [10]

Tissue	1.5T	1.5T	3.0T	3.0T	Difference
	T_2 Relaxation Time (msec)*	R^2 Value (%)	T_2 Relaxation Time (msec)*	R^2 Value (%)	(%)
Medulla	85 ± 11	0.992	81 ± 8	0.996	$-$ 5
Liver	46 ± 6	0.992	34 ± 4	0.984	$-$ 26[§]
Spleen	79 ± 15	0.998	61 ± 9	0.996	$-$ 23[§]
Pancreas	46 ± 6	0.989	43 ± 7	0.977	$-$ 7
Paravertebral muscle	27 ± 8	0.925	29 ± 4	0.867	7
Bone marrow (L4 Vertebra)	49 ± 8	0.997	49 ± 4	0.994	1
Subcutaneous Fat	58 ± 4	0.995	68 ± 4	0.999	17[§]
Uterus					
Myometrium	117 ± 14	0.985	79 ± 10	0.993	$-$ 33
Endometrium	101 ± 21	0.987	59 ± 1	0.999	$-$ 42
Cervix	58 ± 20	0.993	83 ± 7	0.992	43
Prostate	88 ± 0	0.997	74 ± 9	0.995	$-$ 16

11.10 Human Brain: T_1 And T_2 Relaxation Times Regional Differences (Conventional MRI)

Several MR studies performed at magnetic fields of 3 T or higher have shown that longitudinal relaxation times T_1 of water protons in human brain tissue are prolonged at increasing field strength, whereas T_2 of water is progressively reduced. However, until now, only a few reports on the measurement of proton T_1 and T_2 relaxation times of brain metabolites in vivo at magnetic fields beyond the 2 T thresholds have been published. Accurate values for ^{1}H metabolite relaxation times are required for reliable and reproducible determination of absolute metabolite concentrations in cerebral tissue by MR spectroscopy (MRS). Analogous to the observed field dependence of water T_2 relaxation times, the high field MRS studies available up to now indicate a steady decrease of ^{1}H metabolite T_2 values of N-acetyl aspartate (NAA), total creatine (tCr), and choline compounds (Cho) when progressing from 1.5–3 T and up to 7 T. While these data reveal a consistent trend, detailed information at 3 T, particularly regarding variations of metabolite T_2 in different cerebral areas, is still incomplete. One can measure [10] [1]H metabolite T_2 in an extended set of brain regions covering a broad range of different mixtures of white matter (WM) and gray matter (GM) and with an adequate number of samples for each localization. High field measurements of ^{1}H metabolite T_1 have been performed at 3.0 T, 4.0 T, and 4.1 T.

A question often raised in clinical applications of MRS is whether differences in absolute metabolite signals or ratios between patients and normal controls are really due to altered tissue concentrations or rather might be attributed to changes in metabolite relaxation times. Metabolite signals were quantified by time-domain fitting, using the standard software package. The four investigated singlets of NAA, tCr-CH3, Cho, and tCr-CH2 were fitted with Gaussian line shapes, and signal contributions from adjacent resonances of spin-coupled multiplets, could be neglected at least for TE $\geq$ 50 ms. Finally, from the plot of the line areas S (TE), the transverse relaxation times of the respective metabolite resonances were calculated mono-exponentially using a two-parameter least-squares fit to T_2 and S, in light of the equations

$$S'(TE) = S(TE)/f(T_1, TR, TE) = S_0 \exp[-TE/T_2];$$
$$f(T_1, TR, TE) = 1 - 2 \exp[-(TR - TE/2)/T_1 + \exp(-TR/T_1)$$

The slightly TE-dependent correction factor $f(T_1, TR, TE)$ for partial T_1 saturation (differing between shortest and longest TE by 5 % at maximum for TR = 2500 ms was applied to the measured values, prior to the to fit to provide linear proportionality between $S'(TE)$ and the relaxation rate $1/T_2$. Figures 11.11 Fig. 9.1 [10] and Fig. 11.12 [10] and Table 11.8 [10] and 11.9 [10] are practical illustrations about T_2 and T_1 regional variations (Table 11.9) [10].
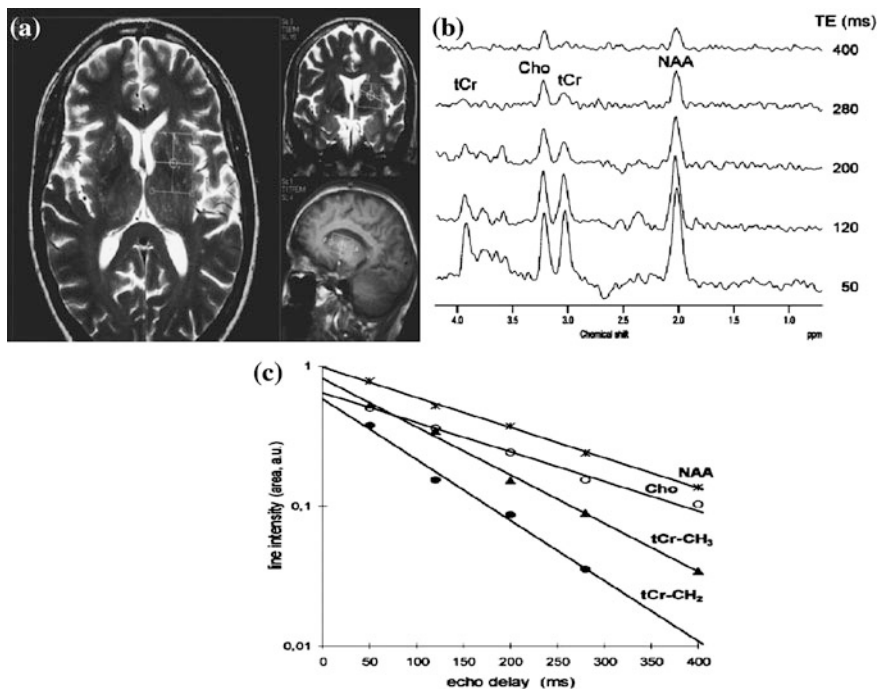
Fig. 11.11 Metabolite T_2 measurement in a $3 \times 2.5 \times 2$ cm (anterior-posterior/*left–right*/cranial-caudal) volume located in the basal ganglia of a healthy volunteer. **a** Display of image-guided VOI selection on transverse and coronal T_2-weighted turbo spin echo (TSE) and on sagittal T_1-weighted turbo field echo (TFE) sequences. **b** Series of SE spectra from selected VOIs obtained with TR 2400 ms and TE = 50/120/200/280/400 ms. **c** Mono-exponential fit of the metabolite line areas as determined by versus echo delay TE. Linear regression curves in semi-logarithmic display correspond to T_2 values ($\pm$ fit errors) of 202 ± 5 ms for NAA, 126 ± 4 ms for tCr-CH3, 195 ± 5 ms for Cho, and 101 ± 7 ms for tCr-CH2
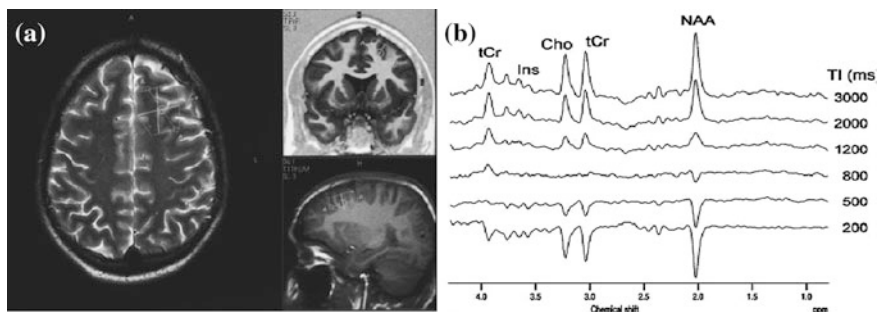
Fig. 11.12 Metabolite T1 measurement in a 15-mL VOI located in the fronto-lateral region **a** Display of selected volume comprising left frontal WM and cortical GM on transverse TSE, coronal IR-TSE, and sagittal TFE images. **b** IR series of localized spectra obtained with TR/TE = 4000/50 ms and TI = 200/500/800/1200/2000/3000 ms

Table 11.8 MRS results for ^{1}H Metabolite Relaxation Times T_2 (ms) in different regions of the brain

Metabolite Component Chemical Shift (ppm)	N	NAA 2.02	tCr-CH$_3$ 3.03	Cho 3.21	tCr-CH$_2$ 3.93
3.0T[a]					
Occipital WM	10	301(18)	178(9)	222(17)	127(13)
Motor Cortex GM	10	247(13)	162(16)	222(15)	121(13)
Cingulate gyrus GM	6	254(15)	161(10)	265(29)	128(11)
Fronto-lat. WM/GM	7	279(16)	169(9)	242(37)	137(7)
Basal ganglia	8	221(18)	143(13)	201(16)	112(14)
Cerebellum	5	287(14)	178(13)	276(13)	132(16)
1.5 T[b]					
Occipital WM	15	361(39)	215(15)	330(44)	
Motor cortex GM	8	317(25)	208(14)	300(33)	
Fronto-lat WM/GM	5	367(26)	216(14)	332(26)	

Data are mean $\pm$ SD (Standard Deviation), N = number of samples. Within brackets () are the cross references in the Ref. [11]

Table 11.9 MRS (magnetic resonance spectroscopy results) for cerebral ^{1}H (proton) Relaxation Times T1 (s)

Metabolite Component Chemical Shift (ppm)	Metabolite Component Chemical Shift (ppm)	NAA 2.02	tCr-CH^3 3.03	Ch0 3.21	Ins 3.54/3.63	tCr-CH$_3$ 3.93
3.0 T[b]						
IR	N = 8	1.34 (0.08)	1.11 (0.11)	1.14 (0.07)	0.98 (0.16)	0.76 (0.13)
PS	N = 8	1.39 (0.03)	1.47 (0.07)	1.15 (0.04)	1.36 (0.25)	1.02 (0.13)
1.5T[c]						
IR	N = 10	1.41 (0.14)	1.19 (0.18)	1.16 (0.16)	0.8 − 1.1 (N = 4)	

Data are Mean $\pm$ SD (Standard Deviation). T_1 results at 3T are pooled mean values averaged over VOI (volume of interest) localization in occipital WM (N = 4), motor cortex GM (N = 5), and fronto-lateral WM/GM (N = 3). 3T results were obtained from inversion-recovery (IR) series and by progressive situation in spin-echo series (PS). 1.5T values were measured by IR parietal WM/GM including the motor cortex (Ref 21 in [10]), sample enlarged by unpublished own work)

11.11 Tissue Sodium Concentration: Human Brain Tumors (Conventional MRI)

Tissue sodium concentration [11] is sensitive to disease, as an indicator of cellular and metabolic integrity and ion homeostasis. Angiogenesis and cellular proliferation are important indicators of tumor malignancy. Changes in sodium/hydrogen (Na$^+$/H$^+$) exchange kinetics are part of the signaling mechanism that initiates cell

division. Cell division and the acidic extra cellular microenvironment of tumor cells are both associated with and increase in intracellular Na^+ concentration ($[Na^+]_{in}$). Increased $[Na^+]in$, increased Na^+/H^+ transporter activity, and altered (Na^+/K^+)-adenosine triphosphatase activity, have all been linked to the tumor malignancy. The observed tissue sodium concentration is composed of given is the weighted average of extra cellular sodium content ($[Na^+]_{ex}$) and $[Na^+]_{in}$, in the tissue being examined. $[Na^+]_{ex}$ at 140 mmol/L is typically much higher than is $[Na^+]_{in}$, which is about 10–15 mmol/L.

Arguably, the more physiologically relevant information is in the intracellular component, reflecting the ability of the cell to pump out sodium ions, whereas $[Na+]_{ex}$ will remain virtually constant as long as there is adequate perfusion to the tissue. When the relative contribution of the $[Na^+]_{in}$ to the tissue sodium concentration is large, as it is in brain tumors, the sodium concentration provides a measure of metabolic changes affecting $[Na+]_{in}$. Estimates for the extra cellular volume fraction in the brain vary from 6 to 20 %. When one considers that the tissue perfusion fixes the extra cellular concentration at about 140 mmol/L, assuming a normal intracellular concentration of 12 mmol/L, it can be calculated that the contribution of $[Na^+]in$ normal tissue is between 26 and 57 %. More than half of the combined ^{23}Na signal is due to intracellular ^{23}Na when the partial volume of the extra cellular compartment is less than 7 %. Thus, despite the inability to resolve intra and extra cellular components of the ^{23}Na signal, the measurement of sodium concentration is a sensitivity measure of $[Na^+]$ in. The Table 11.10 [12] and the Fig. 11.13 [11], show a practical illustration of recent developments in the area of Sodium MRI.

11.12 Tissue sodium Concentration: Myocardial Infarction Human Model (Conventional MRI)

The transport of sodium and potassium between the intra and extra cellular pools, and the maintenance of ionic concentration [12] gradients are basic to cell function and integrity. In particular, the sodium–potassium pump on the cytoplasmic membrane is responsible for the regulation of the excitation–contraction process of heart myocytes. The pump, in concert with exchangers, channels, and transporters, maintains a transmembrane concentration gradient with an intracellular sodium concentration of about 10–15 mM against a concentration of approximately 145 mM in the extra cellular space. During periods of ischemia, the function of the sodium ion pump is compromised by declining energy reserves, such as adenosine triphosphate (ATP), resulting in increased intracellular sodium levels. Although the presence of energetically compromised, nonviable myocardium can be inferred by the use of a variety of clinical techniques, including blood pool serum enzyme assays, echocardiographic, or other invasive nuclear medicine techniques, it has been suggested that loss of cell membrane integrity, as assessed by the dissipation

Table 11.10 Sodium concentration in tumors, hyperintense unenhanced tissues, and normal tissues in patients with brain tumors

N	Dns/Gr	LA LO	Ag	Sx	SI	SI	Na	Na	Na	Na	Na	Na	Na	Na
					Tm	FHN	GM	WM	CSF	Tm	Con	FHN	RVH	LVH
					n20	n12	n20	n20	n = 19	n20	n18	N12	n20	n19
1	Oli/II	L TL	54	F	42	NA	51	63	128	88	62	NA	91	94
2	–	L BL	26	M	48	32	65	75	122	113	76	100	110	108
3	Ast II	R TL	13	F	66	NA	64	68	127	106	94	NA	109	112
4	–	L TL	55	F	45	23	67	73	144	108	74	91	118	118
5	–	L PFL	28	M	40	NA	76	97	160	108	77	NA	124	121
6	–	CC	39	F	26†	NA	75	86	142	39	NA	NA	127	119
7	Ast III	L PL	51	M	66	43	56	57	146	94	56	81	134	135
8	–	R FL	46	M	49	67	53	64	122	88	59	99	95	113
9	Ast III	8 PL	35	M	31	43	69	83	145	98	75	107	114	119
10	–	R FL	41	M	25	NA	54	67	126	78	62	NA	107	109
11	–	L FL	41	M	63	51	78	95	182	155	103	102	124	NA
12	–	L FL	39	F	80	102	51	64	136	117	65	63	90	96
13	–	R FL	37	F	65†	NA	73	96	130	120	NA	NA	107	99
14	Oli IV	F IFL	67	F	27	NA	71	88	140	105	83	NA	128	119
15	Ast IV	R TL	39	F	35	39	67	71	144	102	75	104	136	136
16	Ast IV	R PTL	40	M	58	42	78	110	NA	148	133	94	106	101
17	Ast IV	R FL	25	M	63	73	57	69	152	113	69	120	141	139
18	Ast IV	L OL	65	M	43	NA	62	68	137	97	68	NA	98	90
19	Ast IV	R OL	29	M	74	53	63	72	121	113	65	99	119	114
20	Ast IV	L FL	39	M	77	42	48	53	128	104	59	83	102	94
M					51 ± 18	51 ± 21	64 ± 10	76 ± 15	139 ± 15	105 ± 24	75 ± 19	95 ± 14	114 ± 15	112 ± 14

N = patient number; Dns. = Diagnosis; Ag. = Age; LA = Lesion; Location; L = Left; R = right; LTL = Temporal Lobe; RTL = Right Temporal Lobe; LBL = Basal Ganglia; LPFL = Left Posterior Frontal Lobe; CC = Corpus Callosum; LFL = Left Frontal lobe; RFL = Right Frontal lobe; RIFL = Right Inferior Frontal lobe; RPTL = Right Parietotemporal Lobe; LOL = Left Occipitoparietal Lobe; ROL = Left Occipitoparietal Lobe; Sx = Sex; SI = Sodium Increase (%)*; Na = ^{23}Na Concentration (mmol/kg wet weight); Tm = Tumor; M = Mean ± SD (Standard Deviation); Con = contra lateral uninvolved tissue; FHN = FLAIR; (fluid attenuation inversion recovery) hyper intense nonenhanced tissue; GBM = glioblastoma, L = left, NA = not applicable; R = right, VH = vitreous humor (in right and left eyes); * ^{23}Na = increase in tumor relative to GM; †
^{23}Na = increase in tumor relative to GM; Oli = oligodendroglioma; Ast = Astrocytoma

Fig. 11.13 ^{1}H and ^{23}Na MR images in a 39-year-old woman with glioblastoma multiforme in the right temporal lobe. **a, b** Transverse FLAIR (fluid attenuation inversion recovery) MR images with level contours in *yellow* and contours from the matching contrast-enhanced images **c** and **d** superimposed in *red*. **c, d** Contrast-enhanced T1-weighted MR images with level contours in *yellow* and FLAIR contours superimposed in red. **e, f** ^{23}Na MR images with FLAIR and contrast-enhanced contours superimposed in *blue*
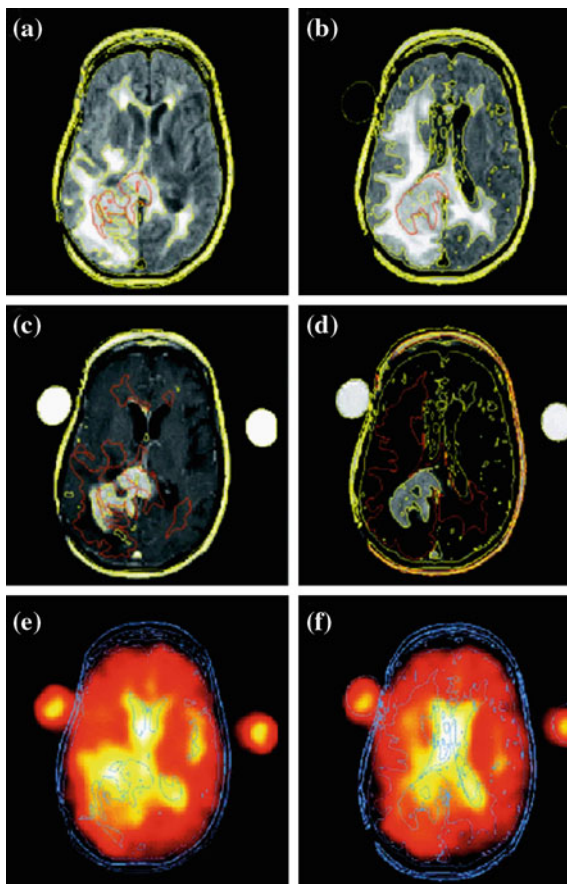
of the trans-membrane ionic gradients, may be a better indicator of cell viability. Sodium (^{23}Na) MRI is uniquely capable of depicting endogenous, naturally abundant sodium.

Initial ^{23}Na MRI studies of myocardial infarction (MI) were performed at 2.7 Tesla (T) on excised canine hearts in reperfused infarction after 1 h of occlusion of the left anterior descending coronary artery (LAD), and after 1 h of circumflex occlusion and reperfusion. The ratio of ^{23}Na MRI signal intensities in MI regions to those in non-MI regions was about twofold, an elevation that was consistent with flame photometric assays of sodium concentration measured in tissue biopsied from the same region.

Recently, MI in isolated and intact rabbit hearts and in intact canine hearts was studied by in vivo ^{23}Na MR spectroscopy (MRS) and MRI in a 4.7T animal system.

The results showed up to twofold elevations of ^{23}Na image signal intensity following acute reperfused infarction, consistent with a twofold increase in sodium concentration measured in biopsies sampled from viable and nonviable
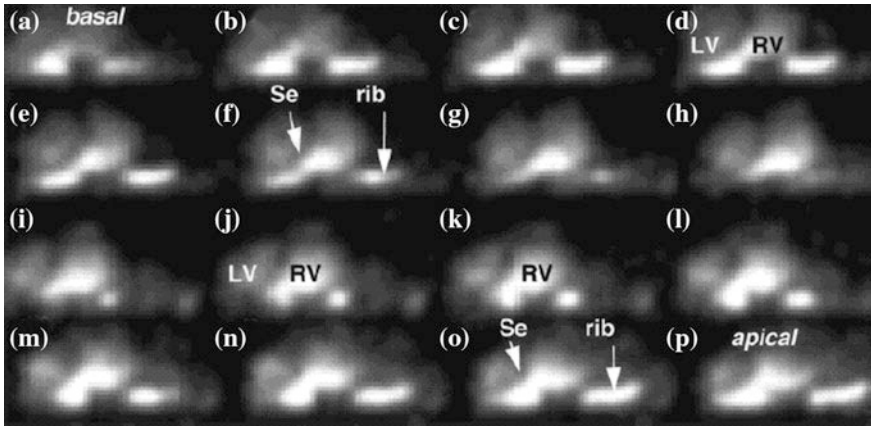
Fig. 11.14 Typical series of sodium images acquired from a normal human volunteer lying prone on a surface coil with TE = 0.37 ms, TR = 55 ms, and NEX = 2 in 16 min. Images are 6-mm-thick contiguous transaxial slices with 6-mm isotropic resolution from the base **a** to the apex **p** of the myocardium (anterior wall at the bottom). The RV, LV, and the ribs where they intersect the sections appear bright, separated by the Se

myocardium. Such work established a link between elevated ^{23}Na MR image signal intensity and myocardial viability, and confirmed the close correlation of the elevated signals with histochemical measurements of infarct size, an important prognostic indicator of reperfused MI. While ^{23}Na MRI of the human heart has been possible at 1.5T, the ability to detect altered sodium levels and, moreover, to noninvasively quantify tissue sodium concentrations in nonviable, infarcted myocardium by in vivo ^{23}Na MRI, has not been demonstrated on clinical systems. Because the in vivo ^{23}Na MRI signal can possess multiple T_2 components with values as short as 1–2 ms that constitute 30–40 % of the signal, the use of ultra short echo times (TEs) are imperative for accurate ^{23}Na MRI quantification, to ensure that all of the ^{23}Na signal is "MRI visible". Concentration estimates were obtained directly from the images by calculating the mean signal intensity, S_{Na}, in rectangular regions of interest in the myocardium, avoiding the pixels closest to the left ventricular (LV) chamber/wall interface. The absolute [Na] was calculated by comparing S_{Na} to the mean signal intensity of a reference, SNa_{ref}, of known sodium concentration, $[Na]_{ref}$, from the equation [13]:

$$[Na]_{tissue}^{mmol/kg} = [S_{Na,\,tissue}/\,S_{Na,\,ref}][Na]_{ref}^{mmol/kg}$$

Typical axial ^{23}Na images from the heart of a human normal volunteer are shown in Book Fig. 11.14 [12]. The observed sodium concentrations are reflective of total tissue sodium, the value of which can be calculated by assuming a simple, two-compartment model, characterizing the intra and extra cellular pools, respectively, by using the following [12] equation.

$$[Na]_{tissue}^{mm/kg} = \{V_{in}[V_{in}^{mM} + V_{out}[Na]_{out}^{mM}\}.\, W^{1/kg}$$

where $[Na]_{in}\, mM$, and $[Na]$ out mM represent the intra- and extra cellular sodium concentrations (typically 10–15 mM and 140–145 mM, respectively). V_{in} and V_{out} are the corresponding relative myocardial tissue volume fractions such that $V_{out} = 1–V_{in}$ and $W^{\,1/kg}$ is the water content of the tissue. In ischemia, intracellular sodium accumulation plays a role in the occurrence of reperfusion-induced Ca^{2+} overload via reverse Na^+–$Ca^{\,2+}$ exchange.

References

1. Patrick, A.T., William, H.P., John, K.H., Lanning, W.H., Charles, M.S., Joseph, F.S.: Clinical and experimental vasogenic edema: in vivo sodium MR imaging Radiology **160**, 821–825 (1986)
2. Kelth, R.T., Tatyana, S.G., BS, Denise Davis, B.S., Patricia E.R.B.: Comprehensive MR imaging protocol for stroke management: tissue sodium concentration as a measure of tissue viability in nonhuman primate studies and in clinical studies. Radiology **213**, 156–166s (1999)
3. Robert, S., Christian, B.: In vivo sodium magnetic resonance imaging of the human brain using soft inversion recovery fluid attenuation. Magn. Reson. Med. **54**, 1305–1310 (2005)
4. Fleysher, R., Fleysher, L., Gonen, O.: The optimal MR acquisition strategy for exponential decay constants estimation. Magn. Reson. Imag. **26**, 433–435 (2008)
5. Chung, C-W., Wimperis, S.: Optimal detection of spin-3/2 biexponential relaxation using multiple-quantum filtration technique. J. Magn. Reson. **88**, 440–447 (1990)
6. Lu, Atkinson, I.C., Claiborne, T.C., Damen, F.C., Thulborn K.R.: Quantitative sodium imaging with a flexible twisted projection pulse sequence aiming. Magn. Reson. Med. **63**, 1583–1593 (2010)
7. Ellegood, J., Hanstock, C.C., Beaulieu, C.: Trace Apparent Diffusion Coef.cients of Metabolites in Human Brain Using Diffusion Weighted Magnetic Resonance Spectroscopy. Magn. Reson. Med. **53**, 1025–1032 (2005)
8. Mlynárik, V., Gruber, S., Moser, E.: Proton T_1 and T_2 Relaxation Times of Human brain Metabolites NMR Biomed. **14**, 325–331 (2001)
9. Cedric M. J. de Bazelaire, Duhamel, G.D., Rofsky, N.M., Alson, D.C.: MR imaging relaxation times of abdominal and pelvic tissues measured in vivo at 3.0 T: preliminary results1. Radiology **230**, 652–659 (2004)
10. Frank Träber, Lamerichs, R., Jürgen Gieseke, Schild, H.H.: 1H metabolite relaxation times at 3.0 Tesla: measurements of T1 and T2 values in normal brain and determination of regional differences in transverse relaxation. J. Magn. Reson. Im. **19**, 537–545 (2004)
11. Ouwerkerk, R., Bleich, K.B., Gillen, J.S., Pomper, M.G., Bottomley, P.A.: Tissue sodium concentration in human brain tumors as measured with 23Na MR imaging. Radiology **227**, 529–537 (2003)
12. Constantinides, C.D., Kraitchman, D.L., O'Brien, K.O., Gillen, B.J., Bottomley P.A.: Noninvasive quantification of total sodium concentrations in acute reperfused myocardial infarction using 23Na MRI. Magn. Reson. Med. **46**, 1144–1151 (2001)

Chapter 12
Summary and Discussion

How and when life started on earth is not known. But its evolution is still going on. There are means available now i.e., intelligent manpower, technologies, nature-science interactions happening-rapidly provoking us round the clock, to guide us into the future. To sit back and think that, we have got what we wanted, why bother any more, is a blitz of ignorance.

Animal and plant life to some extent is replica of the life inside earth itself. Earth lives and so do we. Inside earth's crust there are elements like iron, copper, silicon, sodium, magnesium, uranium, etc., etc. in the form of stable and not so stable compounds. We mine them, process them and use them, in various technologies, including nuclear energy for peaceful, and sometimes not so peaceful purposes. There are circulating molten solid currents, due to high pressures and temperatures, inside earth's crust, which give rise to the magnetism inside and outside earth. We are quite familiar with the N–S poles of the giant magnet, in the core of the earth. It provided the source of navigation and discovery of unknown places on the surface of earth, for centuries, to some clever people. The N–S magnetic axis of the earth is not along the geographic N–S poles of the earth. The N–S magnetic axis of the earth is not fixed in time either. It reorients itself on daily, monthly and yearly basis. Why it does so? One scientific reason we know of is that the earth is bombarded by heavy mass of charged particles, on regular basis, from Sun. The mother nature's magnetic field on the surface of earth which is of the order of only milli to micro Tesla, protects our body from harmful effects of the radiation, we receive on earth on daily basis from the surrounding universe. The radiation e.g., the solar radiation, provides us life on earth, as well, on daily basis. The magnetic field on the surface of earth, changes in a systematic manner, with distance. One can see magnetic field gradient present on the earth and it varies slowly, and is stronger in one direction than the other. Our body is exposed to it all the time. Is it shear coincidence that we use magnetic field gradients of the order mT/meter, close to present on earth, to produce MRI pictures in human body? May be. May be not. Some researchers have used earth's field as the source of magnetic field to perform MRI experiments. This curiosity has produced some interesting

results. That is how the development of the MRI technology we use today was stated half a century ago and is still evolving. This applies to every science-based technology we use.

There are number of elements that are essential for higher life forms such as animal and human. They are part of, enzymes and of the proteins. The electrons are involved in the charge and oxygen transport between the neighboring macromolecules. Various charge, magnetic dipole and electric quadrupole activities are often present at the centre of action and are directly involved in the biological transformations [1–8]. Many physiological processes take place in electrolyte solution present in the medium around the cells, tissue, etc. It involves simple ions like, Na^+, K^+, Mg^{2+}, Ca^{2+}, Cl^-, etc. There are important biopolymers like DNA, RNA and ionic mucopolysaccharides. One also encounters aggregates and monomers, like biological membranes, which interact strongly, through their own charge, with the ions. One finds that the ions are unevenly distributed, between intracellular and extra cellular spaces. The physical energy conservation requirements maintain concentration gradients. These are maintained through energy consuming transport e.g. metabolism. The local dipole magnetic-electric qudrupole dynamic activities create changes in the ion gradients. They become the source of the means of signal transmission. All essential elements in biological systems have at least one potentially valuable magnetic isotope. The examples are ^1H, ^2H, ^{13}C, ^{15}N, ^{19}F, and ^{31}P. One should remember that deep down at atomic and molecular level, there are multi-quantum interactions happening. But they are very difficult to observe with any technology currently available.

It is easy to observe the chemical shift anisotropy (CSA) effects which happen on the mm to cm scale. This is a much broader effect involving the electron clouds, belonging to local macromolecules. The electron clouds tend to smear out, over larger distance the deeper dynamic activities. They mask the magnetic-electric qudrupole interactions. In the simplest local axially asymmetric electric field environment in the medium, which has little influence on the macroscopic environment, one can approximately work out, for the I = 3/2 electric quadruple/ magnetic dipole case, the longitudinal $R_1 = 1/T_1$ and the transverse $R_2 = T_2$ relaxation rates of energy transition, from a higher energy state, to the lower energy state, as follows. It is seen, that for the wider macromolecule situation, one can approximately write as, $R_1 \sim \gamma^2 H_0^2[2\tau_c/(1 + \omega^2 \tau_c^2)]$ and $R_2 \sim \gamma^2 H_0^2 [8\tau_c + \{6 \tau_c/(1 + \omega^2 \tau_c^2)\}]$, respectively. Here γ is the gyromagnetic ratio, H_0 the static magnetic field applied and ω is the frequency of the incident RF radiation. The correlation time τ_c is a measure at the core of all quantum mechanical interactions between macromolecules. When $\omega\tau_c > 1$, R_1 decreases with ω and as $\omega\tau_c \gg 1$(very fast motion of nuclei) it becomes independent of H_0, since $\omega = \gamma H_0$. This situation is more of a representative of the free motion of ions in electrolytes. This is the region where magnetic dipole character of the nuclei dominates, the region of NMR.

The nuclei bound in a tissue, present a situation, which is quite different. Here the nuclei are surrounded by a non-uniform distribution of charges. This is the distribution of bound charges in the form of electric dipoles (one positive and one

negative charge bound together) and quadrupoles (two negative and two positive charges bound together). In the quadrupole nuclei ($I > 1/2$), the situation is more complex. In a local region, the magnetic character of the nuclei is modulated by their overwhelming electric behavior. Now there is non-exponential relaxation of the spins, when excited by the RF pulses. And also there are second order frequency shifts in the received signals. The quadrupole relaxation is caused by the interaction of a nuclear electric quadrupole moment eQ, with the fluctuating electric field gradient, eq, at the position of the nucleus. In isotropic systems, when $\omega\tau_c \ll 1$ (called as the extreme narrow condition, the nuclear magnetization will decay with a single exponent, and one can write, $R_1 = R_2 \sim [\{(2I + 3)\}/\{I^2(2I - 1)\}]$ $[\{\chi^2\}\{(1 + \eta^2/3)\}\tau_c][11]$. Here $\chi = (e^2 q_{zz} Q/h)$ is the nuclear quadrupole coupling constant and $\eta = [(q_{xx} - q_{yy})/q_{zz}]$, is the asymmetry parameter. Here q_{xx}, q_{yy}, and q_{zz} are the axial components of the electric field gradients in the x, y, and the z directions. In the biological systems, the true extreme narrowing ($\omega\tau_c \ll 1$) situation is usually encountered only in the case of free hydrated ions in solution or in the case of low-molecular weight complexes.

One commonly encounters the situation where $\omega\tau_c > 1$. In this case the decay of the longitudinal (M_z) and transverse magnetization ($M_{x,y}$) for quadrupolar nuclei with spins $I > 1$ is no longer exponential. In metal ion nuclei we have $\omega\tau_c \approx 1$ and also holds for the $I = 3/2$ quadrupolar nuclei. The decay of M_z and $M_{x,y}$ will be nearly not exactly exponential. In addition to non-exponential relaxation for quadrupolar nuclei under conditions of non- extreme narrowing, the NMR signal will also be modified by the chemical shift (the smearing electron cloud around nuclei) changes, termed as 'second-order dynamic frequency shifts'. In the limit $\omega\tau_c \gg 1$, the m = 1/2 to m = −1/2 magnetic component will dominate the spectrum because it is much narrower than the other components. The intensity of this component relative to the total intensity will be 40 % for the $I = 3/2$ (Na) case. One can in the lowest approximation consider a tissue, containing Na as a metabolic agent, in the brain, as a single quantum (all spins being identical) ensemble of nuclei. This means basically there is no multi-quantum correlation (interaction) between the $I = 3/2$, sodium nuclei. They act as independent entities, just adding up to the total signal, as absorption and dispersion of energy, in the neighboring environment. A small region of interest (ROI) behaves like a dispersive medium, different sections contribute to imaging character, through different echo time (TEs). This is an oversimplified model, nevertheless a useful one to start with. In the sense of the spectroscopy of the, $I = 3/2$, spin ensemble, one should expect, a superposition of two components, a broadband and a narrowed component [1].

In the extreme narrowing condition, these components are degenerate in both width and absorption frequency. In the other extreme, when here is no extreme narrowing condition, this degeneracy does not result. The broad and narrow (precise) transverse magnetizations can be created by applying a resonant RF field of magnitude (amplitude) H_1 and duration = $(\theta/\gamma H_1)$. Here θ is the flip angle and γ the gyromagnetic ratio (GMR) of the nucleus. The relaxation of the spins after irradiation with RF radiation is considered to be due to the interaction between the electric quadrupole moment of the nucleus and the motionally modulated electric

field gradients, around the nucleus. If the interactions are of random field approximation (RFA) type, the narrow and broad components are not distinguishable. But if both the reorientational correlation time τ_c and the random field correlation time are much larger than the inverse of the Larmor (resonance) frequency, the time dependent character of the transverse magnetization, may be dominated by random field interaction. This may be so even if the qudrupole moment (e^2qQ) of the nucleus is much larger than the magnitude of fluctuations in the local random field. Here eq is the electric field gradient and eQ the qudrupole moment of a macro-molecule.

One can use inversion recovery (application of 180° pulse) RF magnetization technique, to obtain different relaxation rates for the longitudinal M_z and transverse, $M_{x,y}$ magnetizations. We notice through detailed theoretical analysis that in the longitudinal magnetization, the broad component of the spectrum decays as a single exponential, whereas the narrow component decays, nonexponetially, dominated by bi-exponential behavior. It is common knowledge in the MRI literature [6] now that the T_2 (transverse relaxation time) of the intracellular sodium is shorter (~ 4 ms) than that of the extra cellular (~ 20 ms) sodium. In pure aqueous solutions on the other hand Na relaxes monoexponentially with a much longer (~ 50 ms) T_2. It is observed [2] that in the brain tissue situation, there are electrostatic field gradients (EFGs) present around the cell membranes and the macromolecules. EFGs interaction with the nuclear quadrupole moment, results in creation of the two T_2 components.

The central unshifted line reflects the transition between the energy levels characterized by the magnetic quantum number m = $\pm 1/2$. But a pair of satellite transitions, reflecting the transitions, m = 3/2 to 1/2 and m = $-1/2$ to $-3/2$, also exist. These additional lines are equally displaced about the centre line. It is important to note here, that only 40 % of the signal arises from the central line and the two satellite lines contain 60 % of the sodium signal. One can separate imaging of the short and long T_2 fractions. Thus there is possibility of distinction between various types of brain edemas, e.g., those associated with the expansion of the extra cellular space (vascogenic edema) and the edema associated with the expansion of the intracellular space (cytogenic edema). It is also noticed that the intracellular sodium increase manifold, in a malignant cell. There are developments now to extend multi-quantum coherence imaging (MQCI) to the area of sodium imaging. One can determine tissue distribution of sodium ions via triple-quantum coherence (TQC) imaging. Technology has now been developed which allows filtering of the conventional (single quantum) MRI into TQ(triple)MRI. We know that the normal cells maintain the concentration of intracellular sodium ions at 10–15 mM and that of extra cellular sodium at ~ 150 mM.

The electric field gradient (EFG) naturally maintained, gets damaged, in tumor cells. The determination of resulting abnormal levels of Na, in vivo, has a great potential, in the diagnostics of tumors. When the correlation time (τ_c) of the nucleus is short the Zeeman splitting (magnetic dipole effect) among the four possible spin states remains unaffected. As τ_c, increases, it leads to a shift in the energy levels. The multi-exponential relaxation observed, is a natural

consequence, of the electric–magnetic behavior of nuclei in, tissue-surrounding fluid environment, present throughout our body. Also what one observes is, that, the sodium ions, with $\tau_c \geq (1/\omega_L)$, where ω_L is the Larmor (resonance) frequency, specific to a nucleus, the ensemble (Na ions) evolve into mutiquantum coherences(MQCs). The TQC of quadrupole nuclei among the m = $-3/2$ and m = $3/2$ spin states, seems to have a unique behavior. It is unaffected by the EFGs. It has a longer relaxation time than the double quantum coherence (DQC). Tumors, as have increased levels of sodium ions, lend themselves for generation e.g. of TQCs because of altered correlation times. It is seen connected to the metabolic abnormalities such as membrane leakiness or increased synthesis of macromolecules, within the aberrant tissue.

The group of nuclei, e.g. ^{7}Li, ^{23}Na, ^{35}Cl, ^{37}Cl, ^{79}Br, ^{81}Br, ^{79} Br, ^{87} Rb, etc. can be very useful probes [6] for studying the chemical environment in biological tissues. The free ions of these nuclei can be in chemical exchange with large molecules, where these nuclei are in the bound state with the molecule. The sodium nucleus which is of particular interest here has a spin of 3/2. There are 3 magnetic quantum number $\Delta m = 1$, allowed transitions in the Zeeman (magnetic) splitting level structure. These are $-3/2 \rightarrow -//2$, $1/2 \rightarrow 3/2$ and $-1/2 \rightarrow 1/2$. The first two are called as the satellite transitions and the last one the central transition. Other than in the extreme narrowing (small frequency band) condition, it is seen that the satellite transitions decay at a rate s_1, faster than the central transition, at the rate s_2 This is a result of the interaction between the nuclear electric quadrupole moment and the fluctuating electric field gradients, around the nucleus. What one observes experimentally is that the FID (field induction decay) curve in this situation has more than one exponential decay times. The division in two times is considered as an appropriate diagnostic tool, to separate the effects of the chemical exchange between the free and the bound ions, and among the free ions. In a simple mathematical language, one can express the projected transverse magnetization in a sample, in the x–y plane as [6]

$$M(t) \sim \left[\left\{e^{(-s_2\,\tau)} - e^{(-s_1\,\tau)}\right\}\right]\left[\left\{\cos(2\Delta\omega\delta)e^{(-s_{dq}{}^\delta)}\right\}\right]x$$
$$[\{(e^{-s_2\,t} - e^{-s_1\,t})\}][\cos(\Delta\omega t)]$$

Here s_1 and s_2 are the two (biexponential) relaxation rates, τ is the creation (preparation) time, δ is the double-quantum evolution time, $\Delta\omega$ the resonance offset, t the time following the detection pulse and S_{dq} is the double quantum (DQ) relaxation rate. In Fig. 12.1 (Fig. 2 [6]) is presented a typical practical example to illustrate, the basic concepts here, in the operation, in an ensemble of sodium nuclei. A standard sequence of pulses applied along the x-direction, e.g. $(\pi/2)_x - \tau/2 - (\pi)_x - \tau/2 - (\pi/2)_x - \delta - (\pi/2)_x -$ acquire (at time t), leads to the creation of response as shown. Initially (after the $(\pi/2)_x$) pulse, there is a sharp rise of the signal in around a microsecond time τ, called as the preparation time. This is followed by an inversion pulse $(\pi)_x$. It refocuses the pulse in the X–Y plane to enhance the signal strength. After waiting for a time $\tau/2$, the application of $(\pi/2)_x$

Fig. 12.1 Peak height vs creation (preparation time, τ) time using double quantum filter on a sample [(50 % (w/w) solution of bovine serum albumin (sigma) in 2 M NaCl]; acquisitions were at each creation time, using double quantum filter with 10 μs as evolution time
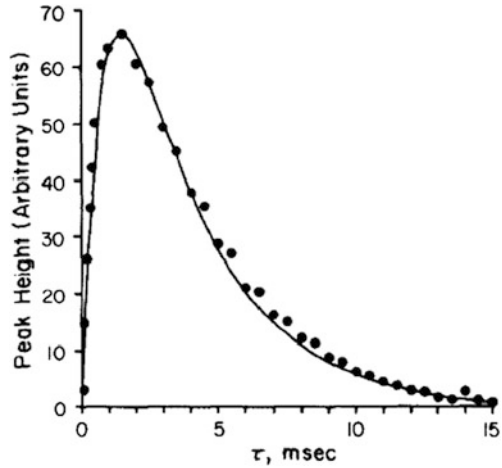
pulse is repeated and so is the projection of spins in the X–Y plane. It now gives chance to the spins in the X–Y plane which were in the process of field induction decay(FID) initially to have coherent interaction with the newly created spins by the 2nd $(\pi/2)_x$ pulse.

The result is a double quantum interference in the spins and is represented by the term $\left[\left\{\cos(2\Delta\omega\,\delta)e^{\left(-S_{dq}\,\delta\right)}\right\}\right]$. It decays with the transition rate S_{dq}. It corresponds to the double quantum transverse relaxation T_2. The final signal M_x (t) is collected, at a time t, starting from the zero time when first time the $(\pi/2)_x$ was applied. A reader is reminded, it is not essential to know the details, about the function of the various pulses applied. All one need to note here is that the ensemble of sodium nuclei (electric-quadrupole in nature) e.g. in a tissue once excited decays with a bi-exponential (see the decay character in Fig. 12.1 [6]) behavior. What it means is that if one plotted amplitude of the signal vs Log $(1/\tau)$ there will be two distinct straight lines with two different slopes. This is in contrast to purely magnetic dipole character e.g. in a proton (Hydrogen nucleus) in a solution where the FID is purely mono-exponential.

In the area of human brain imaging and diagnostics of disorders, using Na imaging (the sodium MRI) [7] is considered, as a versatile tool. It is a compliment to the routine proton MRI. There are several pathological conditions that are associated with abnormal sodium ion homeostasis. We now know that, during cerebral ischemia the reduction in tissue perfusion leads to compromised intra cellular energy metabolism. This leads to a disturbance in the equilibrium of the life giving Sodium (Na)–Potassium (K) ion pump. The increased concentration overall and in particular, the increased sodium intracellular concentration (SIC), in the ischemic tissue, produces changes, to the natural dynamic equilibrium in the healthy tissue. The increased bulk tissue sodium concentration (TSC), is the cause of the concern. This can be detected by Na MRI non-invasively, without the help of chemical shift reagents.

Magnetic dipole (also called as the Zeeman) spectroscopy and the multi-quantum (electric–magnetic) coherences among the sodium nuclei, provides the non-invasive imaging of the SIC. It can provide a direct method to estimate, the degree of cellular impairment. The word electric refers to the electric field created by the concentration gradient of the sodium ions, from outside to the inside of the tissue. The selection of the magnetic quantum number $\Delta m = \pm 1$, provides the coherence between the states, in the transverse magnetization, due to the applied static magnetic field. If $\Delta m = p$ ($p \neq \pm 1$), the pth quantum coherence does not lead to observable magnetization. It has to be detected indirectly, i.e., through a filter which will convert the multi-quantum signal (MQS) into a single quantum signal (SQC). It is known that the bound Na^+ ion, in the tissue, has two distinct transverse relaxation rates [7]. A MQF (multi quantum filter) can be designed (which basically means a suitable arrangement of 90° pulse in sequence with addition of some inversion/refocusing 180° pulses, if required), to select preferentially the signal coming, from nuclear sites, with biexponential transverse relaxation. Book Fig. 12.2 (Fig. 3 [7]) is a pictorial representation, highlighting the biexponential behavior exhibited in a triple quantum (TQ), experiment.

One should realize three is intensive research in progress, in the standardization processes involved in the quantification of the fast and slow relation times, in the area of quantum sodium imaging. The above examples chosen are for education about the various concepts involved in Na MRI, rather than about the exact magnitudes involved. The following is a brief summary of the concepts involved. The composite FIDs (CFID)- the 6 FIDS, corresponding to the six phases ($\varphi = \pi/6$, $\pi/2$ $5\pi/6$, $-5\pi/6$, $-\pi2$, $-\pi/6$) of the RFs added/subtracted together were used to determine the optimum preparation time τ_{opt}. It may be helpful here to remind, that the word phase means the angle with respect to a chosen axis (say Y), along which a 90° pulse is cycled. These RF pulse are applied in the X–Y plane, while the static magnetic field remains fixed along the Z-direction. The magnitude (intensity I) of the received back electrical signal was fitted to

$$I\left[R_1^{(1)},\, R_2^{(1)}\right] \sim \left[e^{\{R_2^{(1)}\, t\}} - e^{\{R_1^{(1)}\, t\}}\right]$$

Here $R_1^{(1)}$ and $R_2^{(1)}$ are the fast and slow SQ (single quantum) relaxation rates.

The optimum preparation time τ_{opt} is determined from the fitted relaxation rates as follows

$$\tau_{opt} = \ln\left[R_2^{(1)}/R_1^{(1)}\right]/\left[R_1^{(1)} - R_2^{(1)}\right]$$

Here τ is the preparation time for the triple-quantum coherence. The Book Fig. 12.2 [7] demonstrate the existence of the bi-exponential behavior in a phantom perspective, in a triple quantum signal analysis. One need to be reminded that the multi-quantum coherence- in vivo brain imaging is the way of the future. In particular the triple-quantum-electric-qudrupole imaging, is of special interest. It provides, vital information at the atomic and molecular level, of the function of Na^+ ion in metabolic and other functional activities in a tissue. But because the

Fig. 12.2 TQ signal time dependency [(Phantom Experiment/3 M NaCl, 10 % agarose gel)] and fit. The *circles* represent experimental data (198 CFIDs (composite FIDs) added together, TE/TR = 0.4/ 130 ms, τ = 5 3 ms), and the solid line represents the theoretical fit. Despite the low SNR attainable because of the small sample size, the nonlinear fit can provides good estimates of the relaxation times (T_2s (slow) 8.6 ms, T_{2f} (fast) 1.5 ms)
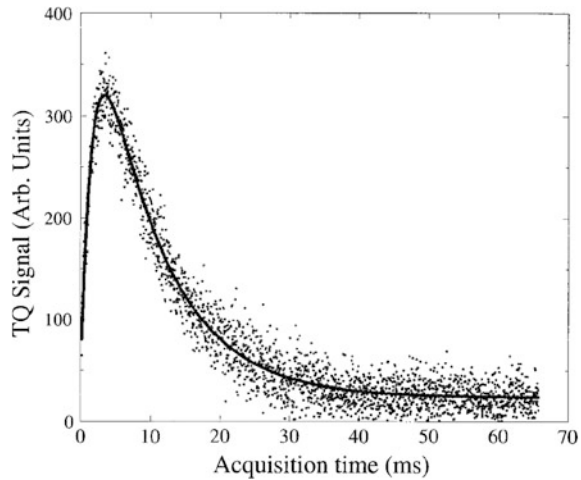
magnitude of the electrical signal received in the MQ (multi-quantum) coherence situation, can be million times weaker than in the SQ (present technology), the uncertainties created by the local static magnetic field and the RF field in-homogeneities, pose a great challenge. This basically requires further research and development efforts to design and test and redesign and retest the structures of RF pulses to get the best result. As, the research, remains, in progress, this book presents, a suitable platform, in the form of a simplified exposure for the clinician and the scientist alike, to participate, and create a much broader horizon in education about the secrets of the science of the human brain. It is very educational referring to the Fig. 12.3 [7] for quality of images under different circumstances. The lack of TQ signal from the cerebrospinal fluid and from the vitreous humor (media characterized by an extremely short coherence time and therefore, by a single transverse relaxation time) demonstrates that the SQ signal leakage into the TQ image is negligible.

One should remember that although there is trend today to make use of the multi-quantum coherences in imaging still at the end the data is converted and collected in the single quantum format for analysis. The receiver of the signal is tuned to a specific resonance single-quantum frequency with the added modulations due to multi-quantum coherences. The spins follow through the routes of different orders of coherences but when they come to the final stage of collection, they are in the form of a single quantum signal but modulated energy state. It, brings with it, the signatures of the multi-quantum molecular level interference effects. In the end the final presentation of the results is carried out, following the well established protocols of statistics. It is a routine practice in MRI technology, to take advantage of the concept of longitudinal (T_1) and or transverse (T_2) relaxation times of the spin echoes. These are the major source of weighting imaging parameters, depicting various physical and chemical properties, in the object scene. This basically assumes that the decay rate λ, behind physical or
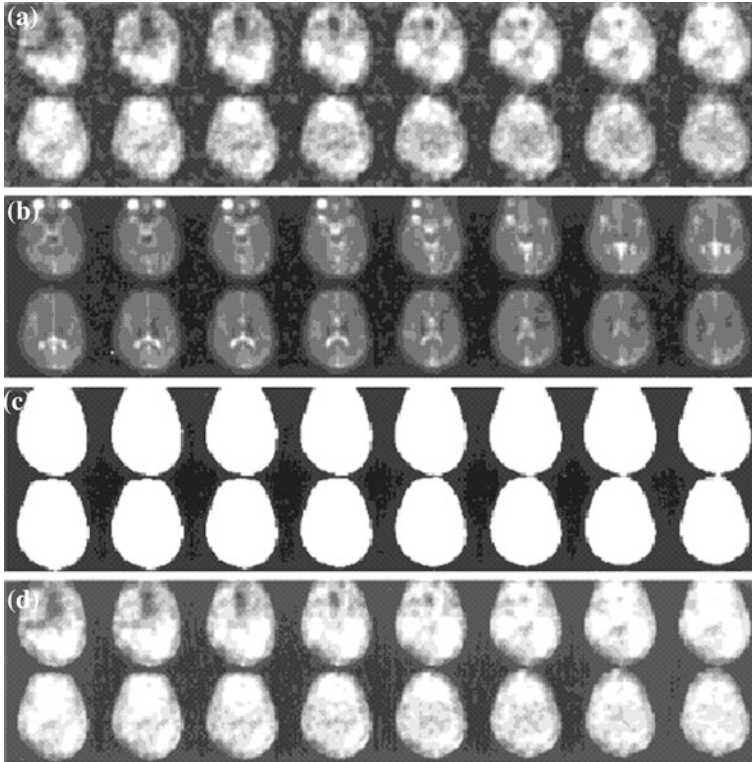
Fig. 12.3 Selected partitions from 3D sodium images from a healthy human brain. **a** Three-pulse TQ image (TE/TR55.5/130 ms, t 5 5.5 ms, n projections 5 214, number of TQ averages 57). **b** High resolution SQ image (TE/TR50.4/100 ms, n projections 5 1596, 4 averages). **c** B1 map obtained from eight SQ images of varying RF amplitude (TE/TR50.4/100 ms, n (number of) projections 5398, 1 average/image). **d** Three-pulse corrected TQ image obtained through pixel-by-pixel division of Fig. 2.1 by the correction factor (magnetic field in-homogeneity)

chemical processes, which correspond to T_1 or T_2, remains the same throughout the process of, spin echo excitations (creation time) and their measurement. But this is not true in many instances. One can represent signal strength, S(t), received in the receiver at any instant of time as $S(t) = [\rho\{e^{-\lambda t}\}]$ [8]. Here ρ is the amplitude, and λ the relaxation rate or say decay constant for a particular imaging process under investigation.

Typical MRI technologies routinely in use where single λ in principle is used are e.g., tensor imaging, fractional volume anisotropy, etc. But one should remember, that static magnetic field and RF magnetic field inhomogeneities are common place in experiments to make λ erroneously space and time dependent. The required corrections are commonly applied for these abnormalities. One optimally needs two time encodings t_1 and $t_2 > t_1$, to evaluate λ. But λ can depart from its single value assumed and encodings employed, can be more than two. This book has focused on the technology, in development, where two decay

(multi-exponential) rates, in a selected region, can be made use of, in imaging. A good example is the sodium ion imaging. Here using triple quantum sodium (magnetic dipole)−(electric quadrupole), interactions, one can distinguish the effects of image contrast produced, as a result of over a micron (10^{-6}) size variations in space. This is due to the bound sodium inside the tissue cell and the free sodium ion outside the cell. In order to understand the depth of sodium ion imaging, one need to take help of the algebraic analysis of the properties of the Spin 3/2 system [3] to which the Na belongs. The medical professionals (MPs) need not really learn the algebra of matrices involved. The variation in regional specific physical and chemical properties and their coordination involved towards imaging may be of interest to some. Several cases, both clinical and experimental have been covered throughout, in this the book, for the continuous education purpose, in which some readers may be interested. Those readers, who can afford to learn the spin-3/2 system algebra, are encouraged to see a standard text book written on the subject. Some mathematical results and their use in the context of the Na MRI are explained in more details, in the appendices (A, B, and A1) added at the end of the book.

Physical and chemical properties of the Na$^+$ ions in the context of the human brain imaging would be of particular interest to the clinicians, in writing the diagnostic report. How multi-quantum types of NMR signals, are related to the biological micro-environment can be seen through the visualization illustrations, presented throughout the book. The multi-quantum (MQ) Na imaging technique, has been found of immense value for study of the ion fluxes, during ischemia experiments, and for the identification of neoplastic changes in the human brain tissue. It is seen, that the low concentration of sodium ions in the brain is an impediment, in developing fast spatial encoding of the sodium-nuclear MRI. The developments in conventional MRI technologies will continue. Research in a suitable design in sequence of pulses, can bring out wonderful results. Soft Inversion Recovery Fluid Attenuation (SIRFLA) is one such example [5]. Intra-cellular weighting with cerebrospinal fluid (CSF) suppression is a natural way of coding in conventional imaging In this technique (see Sect. 3.3 for details), one adds a long e.g. a 10-ms nonselective (flat rectangular band width in frequency) inversion pulse in front of the standard 3D gradient echo pulse, as an improvement in the design, of the sequence of pulses. One should note that use of the shortest excitation pulse length possible, limits the loss, of transverse magnetization, during the excitation. One sees an effectiveness in separating sodium longitudinal magnetization, in different environments. This separation is the direct result of the large quadrupole interaction, experienced, by the sodium nucleus, and is not possible to observe in the routine ^{1}HNMR (proton nuclear magnetic resonance). It is related to the fact that the inversion pulse length has a dramatic impact on the signal acquired from the non nulled (CSF) environment.

The SIRFLA technique offers SNR (signal to noise ratio) benefit over TQF imaging. The TQF sequence of pulses is limited by the SAR (specific absorption) of the RF radiation. There are 3, 90° RF, 1 ms pulses used, and twice the power dissipated. The SIRFLA sequence theoretically allows full elimination of the ECS (extra cellular

space) signal. In TQF case there is 40 % residual contribution from ECS. One finds there is a substantial (35 %) increase in sodium concentration in malignant tumor cells in comparison to the normal; cells. So ^{23}Na-MRI is a good practical tool, for examining tumors, in various portions of the human body. It is known that the signal from the free sodium ($-3/2 \to 1/2$) overlaps with the central transition ($-12 \to 1/2$), corresponding to the ordered (bound) sodium. Selective detection of central (ordered) transition, through MRI is a valuable tool in diagnostics of tumors. One can use double quantum filter in order to perform quantum coherence imaging. Although progress in this direction is steady, a qudrupolar filter by nutaion (QFN) method has also been suggested in the MRI literature [4]. The key of the matter is that, one should be able to work out correlation, between the concentrations of ^{23}Na nuclei when it is in the ordered state as compared to the disordered-tissue state. We know there is relatively larger abundance of ^{23}Na in the areas of brain and cartilage.

One can use the case of cartilage as a route to explore the basic science of sodium function in the tissue-extra cellular environment. It can then be applied to the brain situation in the diagnostics of disorders. The idea here is to produce central peak (bound sodium in tissue) enhancement (CPA) over the free (extra-cellular) sodium signal. In the spin 3/2 nuclei (sodium) there is a non vanishing quadrupolar interaction energy, in the total energy of the system called as the Hamiltonian of the system. The qudrupolar contribution evolves in a different manner in the presence of the RF (radio frequency) field, depending upon the ratio of the nutation frequency ω_{rf} to the quadrupolar coupling constant ω_Q. A selected cartilage (bovine cartilage) sample, provides an excellent example where one can effectively detect the central transition of the ordered sodium from a mixture of free and bound sodium environments. The ratio ω_{rf}/ω_Q provides a guiding parameter for the selection of the RF pulses that can be used in the analysis.

References

1. Lawrence, G.W. Jr.: The NMR of Spin-3/2 Nuclei: the effect of second-order dynamic frequency shifts. Magn. Reson. **43**, 443–448 (1981)
2. Ra, J.B., HILAL, s.K., Cho, zH.: A method for in vivo MR imaging of the short T2 component of sodium-23. Magn. Reson. Med. **3**, 296–302 (1986)
3. Tanase, C., Boada, F.E.: Algebraic description of spin 3/2 dynamics in NMR experiments. J. Magn. Reson. **173**, 236–253 (2005)
4. Choy, J., Ling, W., Jerschow, A.: Selective detection of ordered sodium signals via the central transition. J. Magn. Reson. **180**, 105–109 (2006)
5. Stobbe, R., Beaulieu, C.: In vivo sodium magnetic resonance imaging of the human brain using soft inversion recovery fluid attenuation. Magn. Reson. Med. **54**, 1305–1310 (2005)
6. Pear, J., Legion J.S.: Detection of biexponential relaxation in sodium-23 facilitated by double-quantum filtering. J. Magn. Reson. **69**, 582–584 (1986)
7. Hancu, I., Boada F.E., Shen, G.X.: Three-dimensional triple-quantum–filtered 23 Na imaging of in vivo human brain. Magn. Reson. Med. **42**, 1146–1154 (1999)
8. Fleysher, R., Fleysher, L., Gonen, O.: The optimal MR acquisition strategy for exponential decay constants estimation. Magn. Reson. Imag. **26**, 433–435 (2008)

Chapter 13
Conclusion and Future Horizons

Nuclear magnetic resonance (NMR) phenomena
started, as a curiosity research,
more than half a century ago.
It translated into a routine MRI tool,
attending the diagnostics of brain disorders,
only recently.
Where it will go, towards the end of this century,
depends on the investment, in the research and development,
and the education about it world wide.
Health is an area, where there is, less commercial gain.
It can also serve, in, the security
of the society at large.
May be the MRI research, will be lucky,
and get the timely attention of the leaders.

The resonance phenomenae are in common use in many technologies, we enjoy today. Use of RF (radio frequency) electromagnetic radiation, magnetic resonance of molecules, for the human body, to produce an image, deserves special recognition. MRI is a non invasive application of science, to the diagnostics of various diseases and disorders in human body and is particularly challenging, in the human brain arena. The renounce phenomena used in MRI is little different in principle from other applications. The well known applications are the radio broadcast, the production of television picture, Lases, etc. The subtle difference lies in the selection of the frequency band of radiation, out of the very wide electromagnetic radiation band. TV broadcast uses the visible (light) part of the electromagnetic, radiation spectrum, to produce pictures, and the microwaves are used, to carry it and broadcast over large distances. On the receiving end, electrical resonance phenomena, in the electrical circuits, is used to produce the picture. This picture is about the movement of the external parts of an object or of a living body. The TV picture is clearly visible to the naked eye. MRI uses the dark (invisible) RF radiation. It brings out the behavior of internal molecular movements which are not visible to the naked eye.

The internal topological structure in the brain on a macroscopic (mm-cm) scale is made visible to the naked eye through a photographic pictur produced, through a computer on the screen after the scanning process. It is then printed as a hard copy on a cellulose film, which acts as tool of diagnostics of disorders, if any for the doctor. One can also view the picture in real time on the computer. In the radio broadcast, we use the RF (radio frequency) and the microwaves as carriers of message. These are dark (invisible) radiations. They carry the electrical signals over long distances which are converted into sound, in the radio at the receiver end, e.g. in a car. The differences in various applications of the resonance phenomena, being used in many technologies, also arise, in the different forms of matter being resonated by the incident radiation to produce the desired result. The medium may be e.g., the gas or solid-state in the case of lasers it is liquid crystal display in a Lap Top computer, etc., etc. It can be a biological medium of magnetic spins e.g. in the human brain (The MRI), etc.

The soft-condensed matter, tissues, cells, etc., used as a medium of imaging in the MRI are of specific interest, for analysis in MRI. One need to be careful for the high risk involved about the dose, of the irradiated medium. Here a human i.e., a patient is the subject of investigation. MRI is considered as a non-invasive tool, for all practical purposes, but in fact is not totally invasive. However standard practices and procedures are in place in MRI radiology practice to take care of the risks involved. The word resonance in MRI basically means RF (radio frequency) energy absorption, in tune with the binding energy of the electrons, atoms and nuclei (the micro-particles) as part of the quantum energy structure, of a group of molecules, which may be a part of a cell, tissue, etc. One may ask a question, why particularly RF radiation is used in the case of human body? The answer is simplified as follows. Our body is made of tissues, cells, very many organic, inorganic molecules, macro-molecules, chemicals, various fluids, and above all, the most important ingredient, the water. There is an intrinsic quantum (atomic-nuclear) potential energy stored inside, in various macromolecules, the building block of our body It is due to the chemical and physical bonding structure produced by the electrons, atoms and molecules, and is called, as the biding energy.

The atoms and molecules which are the lowest level building blocks of our body, inherit with them, the micro-particles i.e. the electrons in an atom, protons and neutrons in the nucleus, etc. When spread over a broader perspective of macromolecules, which forms the dynamics of action, in our body, the binding energy is seen to be in the RF part of the electro-magnetic radiation spectrum. The RF radiation used in MRI, is basically used to excite (break the binding energy of) the molecules, in a local small volume (called a voxel). The energy of interaction (breaking the biding energy) involved is around meV (milli electron volt). The returned back electrical signal, has the signatures, of the local medium, in which the magnetic spins (tiny molecular magnets) reside and function. The repetition of this process voxel-to-voxel and coordination in space and time of the electrical signals received over the whole brain results into the picture (the MRI) the doctors use for diagnostics of diseases.

A few decades back nobody thought of being able to see the internal picture of our brain. The X-rays routinely used in imaging bone skeleton, would be very dangerous for the brain, because the energies involved are too high and in the X-ray band of the electromagnetic radiation. They are in the MeV (million electron volt) range. The phenomena of magnetic resonance, in molecules, in general, and in the molecular resonance spectroscopy field, in biological environment, has been well developed, since long. But this knowledge has been translated into in vivo imaging of the brain very recently. Why is it so? Were there not intelligent enough people to work out what to do in the past? The answer is no. The reason is that the education about the basic sciences (PCM) and the useful technologies, existing at that time were not exposed enough to reach the masses. There could have been untapped potential of many scientists deprived of participation to make their point. This has delayed the catch up between the technology and science and the science and the technology.

Have things improved for the future? Unfortunately the answer is no. In order to reinvent, one needs to invent first. One needs feedback from the knowledge of the basic science concepts (PCM), which have to be redeveloped continuously. There has to be a much wider intellectual education base, about the use of technology, and make the best of it. It will enable us to expose more about the basics, and thus encourage new investment, in a new technology. Once this is sorted out better technologies can be developed. Otherwise we have to put up with what we have. This breeds a perpetual source, of wealth from the obsolute technology, for the elite. The fullest possible human potential has not been exploited over decades to alleviate the problems in this direction. There are brains, on a wider demographic scale, available. The situation is not going to get, any better, in future. The slow progress comes from, the slow expansion of the technology, in its full intelligent potential. It tends to limit generation of further wealth, in some localized hands only. There is not enough properly directed investment, in the future of the people or broadly speaking in the very existence of the human race which in some corners of the world is degrading, at a very fast rate.

The present MRI machine is a wonderful tool and does wonderful things i.e., the non invasive diagnostics, of the human brain disorders. It is in fact now being used as a diagnostic tool for any organ of the human body. No other wonderful breakthrough has taken place over the last decade or so. The idea of multi-quantum coherence imaging (MQCI) is now making it mark. This new concept enables quantum physics and chemistry of the events happening in the brain, at the natural molecular level, and in real time, clearly borne out. This capability is not present in the presently developed single-quantum-interaction, brain space map-imaging, the MRI. The use of multi-quantum spectroscopy of molecules in the field of developmental-pharmaceutical medicine is fairly old. Spectroscopic technique has been used over many decades to find the structure of very many bio-medi-chemicals of vital importance to the human body. The transition from multi-quantum spectroscopy to multi-quantum imaging is a new and a slow process. It is not that the progress can not be accelerated.

The wealth generated, by the use of the technology is little feedback into, further research, and the education of the people. It is only education and research in science, on mass scale, which can be a reliable source of the maintenance of the existing technologies and creation of the new ones. The idea of intermolecular quantum coherence imaging (iMQI) is a very basic one. It has been widely reported world wide through research in the field of MRI, very recently. This is the outcome of the basic curiosity research. Recently, it has been published through the work in several research centers world wide. Not long ago it was suspected by intuition to be present, in the conventional MRI pictures, but no concrete conclusion was realized, over quite sometime. One could not recognize its exact potential, location, and even a suitable explanation, of some of the result observed, about it. The scientists who first reported it as a multi-quantum coherence phenomena about a decade ago deserve all the praise, on this earth. But for these scientists, with great intuition, the world of MRI would be a bleak place, today. The quantum theory of free atoms and molecules was put forward more than a century ago. It is now able to predict and explain what is experimentally observed in biological ensembles like our body. This is a typical example how curiosity often neglected as a waste of money can deliver wonderful results. Curiosity research is essential to produce wealthy and healthy future minds for our well being.

One should realize that it is not only the basics of the MRI research but also the basic MRI machine infra-structure itself, which requires further development. The infra-structure needs basic research, in the materials used, in the construction of the machine. Redesigning of the machine e.g. reducing its size needs another look. The parallel imaging concept, with variable-receiver-sensitivity based imaging, is a new emerging direction. Here sensors can be multiple sensors fixed in space on the brain instead of the single mobile coil as a sensor to cover three dimensional space. The superconducting coils, which carry large electrical currents, to produce the large static magnetic fields required, for the MRI machine operation, need to be cooled to liquid helium temperatures. The presently used superconducting coils are the low temperature superconductors, which operate by dipping into liquid helium with boiling temperature, of 4 K. There has been a breakthrough recently in the discovery of high temperature superconductors (HTSCs) which operate at liquid nitrogen boiling point, of 77 K. But being brittle (ceramic) materials with little ductility, they can not be drawn, into flexible wires to carry large electrical currents at present. In the basic research, we yet do not understand, what causes superconductivity and why it is so intimately connected, to the lowering of the temperatures and how far the critical temperature can be raised.

Superconducting quantum interference devices (SQUIDS) are very sensitive sensors and can easily detect very weak magnetic signal in the brain imaging situation. They have been used in brain mapping, detecting weak signals, in the presence of the very weak earth's magnetic fields of micro-Tesla. There is a drive that we should be able to image the human brain, in the nature's own that is the earth's magnetic field. This is a novel idea, and worth the efforts. The slow variation provided by the earth on its surface, of the magnetic-field-gradient, is a

worth while tool for research and development. It can enable the localization process of spins, in our brain, in any desired (x-y) direction on the surface of earth and help achieve the imaging. It is a dream worth the trial. After all, we are the nature's product, living in nature's (earth) magnetic field, and doing natural things, in a day to day life. We know that the gravity is the controlling force for the dynamics of the planets, stars, galaxies, etc. What exactly is the mechanism of the dynamics of the orbiting and the interacting micro-particles in our body? Is it merely a result of coulomb (charge) and nuclear forces? And if so, why it is so? In quantum theory of atoms and molecules, we assume, the angular momentum of the electrons around the nucleus (and of the protons and neutrons in the nucleus) is the driving force, and is quantized, and conserved, in the molecular level events.

The postulates of the quantum mechanics (QM) are able to predict, the quantum energy structure of all the atoms and molecules we know of in the free pace. The results have been experimentally verified by the spectroscopy techniques. In fact the classification of the atoms in the familiar 'Periodic Table' is a direct product of the quantum theory of matter. It is surprising that quantum science education over masses (secondary and tertiary education system) has been not done. There is limited awareness about research and education, about applications of quantum science world wide? Is there something hidden we do not know, about the quantum science education, being prevented from spreading world wide? Can we work it out? May be deeper knowledge about the brain quantum science, through the MRI technology, will provide us with the missing links, and the encouragement needed to achieve the desired goal. A biomedical quantum computer is an interesting area in this respect to investigate. The development of the use of the multi-quantum spin coherence in MRI (the MQMRI) as a research tool to understand brain science is progressing fast. It still has to overcome lot of hurdles particularly in making of the in vivo studies in the human brain. The MQMRI can be broadly broken into three spatial imaging regions in the brain science arena. It is the nm (nanometer), μm (micrometer also called as a micron) and the mm to cm region. The mm–cm region is the conventional MRI region.

The nm–μm is the region where the macromolecules in a tissue, with their resultant magnetically oriented spins (in a particular direction) interact in a quantum mechanical (QMcal) manner. This interaction is with other neighboring macromolecules (which may be oriented in a slightly different direction). These interactions can be constructive or destructive in producing the final result. It means the electrical signal received from a small region can be enhanced (producing bright image) or reduced (producing dark image). This source of improved spatial image quality, may be directly associated with the contrast required, to distinguish, or example, necrotic cells from viable cancer cells, in a tissue. This is basically going in the direction of developing MRI microscopy. The development of that precise technology is still far away to examine a tumor in vivo in the human model. But efforts in that direction are in progress (see the Appendices A and, B, providing recent developments in applications and trace back the basic PCM involved, for education and rediscovery).

There are efforts now to produce nm scale images. There has been reported use of the nano particles called as the SPIONS (the super-paramagnetic nano-iron oxide-articles/Fe_3O_4) in the human brain arena with little danger. This is not in the true non-invasive spirit of the MRI. The particles were perfused in the tumor tissue region, in an animal-model study situation. The good contrast produced in the iDQC (intermolecular double quantum coherence)-MRI, paves the way for the future human-model brain studies. Among the applications of multi quantum coherence (MQC) techniques used in MRI, the intermolecular zero quantum coherence imaging, has some special significance. It has a robust strong bound character of two spins, stuck together, in opposite direction, resulting, in zero spin in total. It can thus move around in a multi-nuclear ensemble of spins like brain with its own magnetic character and little influenced by double, triple, etc. multi-particle, quantum coherences. The unique zero spin coherence between spins can extend over larger distances, rather than being in coherence between the two closest neighbors.

The distant (micron to mm) dipole–dipole interaction leads to frequency resonance broadening of the sharp resonance of the single iZQC dipole. The broadening due to the chemical shift spread of nuclei in a multi-nuclear environment, if it can be isolated, from other sources of contaminations e.g. local magnetic susceptibility variations, magnetic field inhomogeneities, etc., can be used to create temperature dependent MRI map of the brain. In certain body disorders where hyper-thermic treatment, by using RF and ultrasound radiation is used a simultaneous temperature MRI map [1] acquisition, can be very useful in monitoring the progress of the treatment. In epileptic patients this can be versatile tool to find the exact spot of the electrical burst which causes epilepsy. This would not require patient to wait for a epileptic fit to happen and also the treatment can be monitored after medication using the temperature QMRI map.

Reference

1. Jenista, E.R., Galiana, G., Branca, R.T., Yarmolenko, P.S., Stokes, A.M., Dewhirst, M.W., Warren, W.S.: Application of mixed spin iMQCs for temperature and chemical-selective imaging. J. Magn. Reson. **204**, 208–218 (2010)

Chapter 14
Appendices

14.1 Appendices A

The Appendices A, B and A1 [1–35] included here cover a brief exposition of the basic physics principles and the relevant terminologies arising in MRI.

14.1.1 An Electric Current in a Straight Copper Wire Generates a Magnetic Field Around it and a Magnetic Field Created in Space Generates Electric Current in a Copper Coil Placed in the Field

A magnetic field will be experienced in a sensor placed at the centre of the copper coil carrying electric current and the space around the coil. It is important to explain here the relevance of the above simple physics principle to the MRI. In a copper wire the moving electrons are responsible for the electrical current generated. In an ensemble like our brain the circulating charges in the atoms due to the electrons around nuclei (protons and neutrons) and the molecules etc. create a dipole-magnet in the space where they live and function. The movements of these magnets creates electrical currents in the space around them which in turn produces magnetic field around. The electric currents and magnetic field created by atoms and molecules are reversible in nature. They form the key source of communication and energy regulation (renewal, metabolism, etc.) among the cells and tissues for the life to go on. There are also some atoms molecules as ions in free state floating around in the body. They perform certain functions of their own. In an MRI situation we apply external static and RF magnetic fields to interact with the internal fields and provide us with the information we want through the electrical signals which we measure.
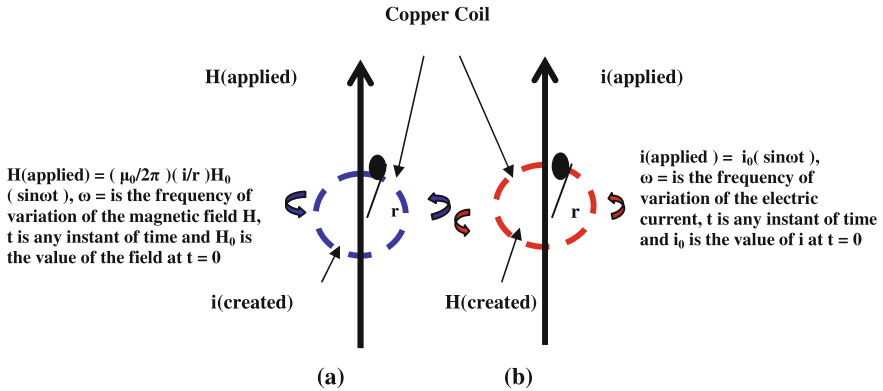
Fig. 14.1 One can experience an electric current i in a copper coil present in a magnetic field $H = (\mu_0/2\pi)(i/r)$ and a magnetic field H within space in a copper coil carrying an electric current i. When i, H are allowed to oscillate or vary transiently in time the corresponding effect is induced in the space around the coil. Thus when electric current i (transient or oscillatory) is flowing through a copper coil it produces a magnetic field H along the axis of the coil and the space around it. In the figure r is the radius of the coil (in meters), H is the magnetic field in Tesla (T) and μ_0 = the permeability of the free space. The value of μ_0 in vacuum is $4\pi \times 10^{-7}$ Tesla m/A. **a** Magnetic field (time varying) is present in space. Electric current will be experienced in a copper coil placed in space enclosing parts of the field. **b** A copper coil carrying electrical current (time varying) creates magnetic field in space

The static magnetic field applied externally to the brain in MRI interacts with the naturally occurring current carrying molecular spins (tiny magnets) and orients them along its own direction. The RF radiation subsequently applied to the brain oscillates the magnetic spins which create their associated oscillating magnetic field. These oscillating magnetic fields produce electrical signals in a nearby preset copper coil. It become the source of imaging in MRI (Fig. 14.1).

14.1.2　The Atomic Magnetic Dipole Moment

An electric current basically originates from an electron in motion whether it moves in a straight line (when it is free to move, e.g., in a copper wire with the application of a voltage difference between the two ends of the wire) or in a circle (when it is bound e.g. to the nucleus in orbital motion). In electron's orbital motion around the nucleus there is an enclosed area say, = A, of the circle generated by the electric current i. When it is placed in an external magnetic field H_{ext} the orbit experiences a torque (twist) by the applied field as to make the plane of the orbit, perpendicular to the applied field. The torque is given by $\tau = (i\ A)\ H$, in Newton mater (Nm). The quantity $\mu = i\ A$ (Amp m^2) is called as the **magnetic dipole moment**. Dipole because the two sides of the atomic disc behave as if they are the two (North–South) sides of a disc shaped magnet. The Fig. 14.2 is a pictorial depiction of the meaning of the magnetic dipole moment for an electron orbiting around the nucleus.
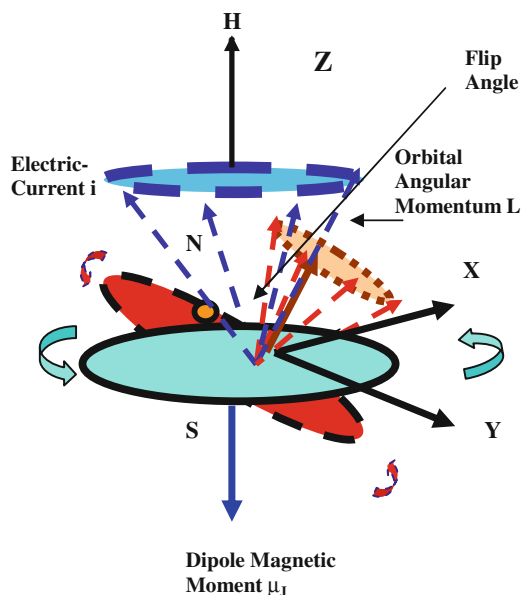
Fig. 14.2 A representative molecular disc-shaped magnet. The preecsion of a group of spins is presented. The system corresponds to a small volume. A group of spins in a small region can be represented by a single equivalent rotating vector rotating around the applied magnetic field. This vector tries to align itself along the Z-axis in the presence of an external static magnetic. It ends up in equilibrium in a precessional motion around the z-axis. One can flip the spins using suitably designed RF pulse to a desired angle with respect to the applied static magnetic field. This angle is called as the flip angle. Normally one flips the spins by 90°, in the X–Y plane for collection of signals in the plane. The reader is reminded here this is a simplified qualitative picture of the of spins. For an exact quantitative picture a reader should refer to, text book in quantum physics, or MRI

One should observe that the resultant spin vector in a voxel situation is not fixed in space. It tries to align itself, along the Z-axis but instead precesses around the Z-axis. The constant source of energy supplied by the static magnetic field, has to be spent somewhere. The spin can not arbitrarily hang in one direction and stay static instead it precesses around the Z-axis in random manner in time at an angle to the Z-axis. It could be pointing in any direction in x–y,z space at any instant of time. The angle at which it will precess around the Z-axis is determined by the gyromagnetic ratio (GMR) = μ_J/J. Here μ_J is the total magnetic moment due to all the neighboring spins in a voxel at a point in the brain and J is the corresponding total angular momentum. The internal resultant J is created by the internal magnetic field due to the effective large equivalent macromolecular nucleus. Inter-macro-molecular interactions are part of some sort of a resultant effect over a voxel. The application of the external static magnetic field suppresses this internal local magnetic order direction and tries to align spins along its own direction. One applies a small additional oscillating magnetic field through an RF pulse along say the x-axis. Monetarily it will move the precession away from the z-axis as if there is a torque

towards the Y-axis around X-axis. The Torque, τ, around the X-Axis results in the precession of the spin around y-axis momentarily. Soon it disperses in the X–Y plane. Thus in the MRI situation the precession of spins directed towards the Z-axis is projected along X and Y directions to make measurements of the electrical signals generated by the oscillating spins in the X–Y plane. The fields applied in the X and Y directions are the RF pulse fields. These fields allow excitation of the spins to allow space and time imaging of the brain.

14.1.3 The Nuclear Magnetic Dipole Moment

A nucleus contains protons and neutrons. The number of protons is called as the atomic number of an element. The sum of the total number of neutrons N and the protons Z is expressed as the mass number, $A = Z + N$ of the nucleus. Each of the protons and neutrons called as the nucleons has a magnetic moment. Some nuclei have even and others odd number of nucleons. Due to the nuclear forces between them the even pairs have resultant zero magnetic moment. The unpaired (left over) single nucleons produce a resultant magnetic moment. This nuclear magnetic moment call it as μ_N is the result of circulating currents of the nucleons. The circulating motion has associated with it the angular momentum of the motion I. Analogous to the atomic case the nuclear angular momentum due to the quantum mechanical principles, can occupy only quantized positions in space give by, $I = \hbar$ $[(\sqrt{(i(i + i))}]$. Here $\hbar$ is the angular Planck's constant and is $= h/2\pi$, where h is the linear Planck's constant, and, i is a nuclear quantum number, with values, $i = 0, 1/2, 3/2, \ldots$ Consider now a static magnetic field is applied in the Z-direction. The result is that the plane of the circular motion is projected in the X–Y plane and the projected I_z component has only the selected quantized values $I_z = m_z\hbar$. Here $m_z = 0, \pm 1, \pm 2, \ldots$ The nuclear magnetic moment is givens as $\mu_N = (e\hbar/2m_p)$. Here e is the proton or the electron charge and m_p the mass of the proton. The nuclear magnetic moment has the same kind of properties as does the atomic one. The only difference is that the magnitude of the nuclear magnetic moment is thousand times smaller as the proton is thousand times heavier than an electron.

14.1.4 The Nuclear Gyromagnetic Ratio (NGMR or γ_N)

The ratio of the nuclear dipole magnetic moment μ_N to its angular momentum I is called as the nuclear gyromagnetic ratio $\gamma_N = NGMR = \mu_N/I$. There is an interaction energy associated with the nuclear magnetic moment and the atomic electrons. It is written as $\Delta E = C [f (f + 1) - i (i + 1) - J (J + 1)]$. Here f, i and j, are the corresponding quantum numbers, according to the various angular momentum, as follows. f = grand total angular momentum quantum number (atom + nucleus); i = total nuclear angular momentum quantum number; j = total atomic angular
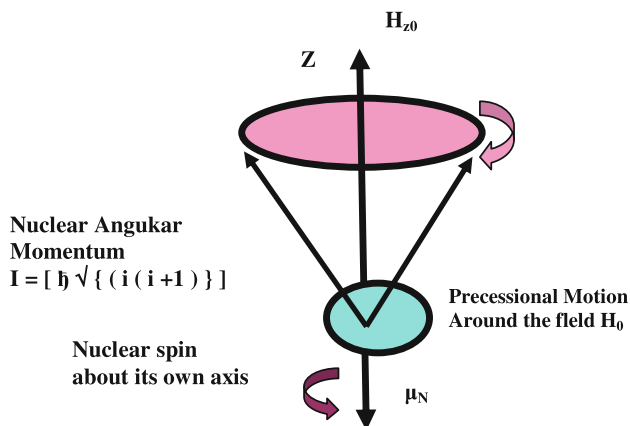
Fig. 14.3 The precessional frequency Ω of the nuclear magnetic moment around the applied static magnetic field H_0 is given as, $\Omega = \gamma_N H z_0$

momentum. The constant C is proportional to the magnitude of the nuclear magnetic dipole moment μ_N. The $\mu_N = (e\hbar/m_p) = 0.505 \times 10^{-28}$ amp$-m^2 \approx 10^{-3}$ μ_b (m_p is the mass of the proton and μ_b, the Bohr magneton, used in atomic case). Measurement of the hyperfine (Zeeman) splitting, ΔE can be related to the multiplicity energy structure as expected by the above equation. It is seen that the sign of the nuclear magnetic dipole moment arises due to the relative orientation of the magnetic dipole moment vector and the angular momentum vector of the nucleus. It can be positive as well as negative. The following quantum rules are important to remember in the nuclear case. (1) The total angular quantum number i, often called as the nuclear spin is obtained by counting the multiplicity of the split nuclear energy level. (2) If the multiplicity is associated with, j > i, then f can have (2i + 1) values and thus (2i + 1) energy levels. (3) i is an integer for nuclei of even A, with i = 0 if Z is also even. (4) i is a half-integer for nuclei of odd A. (5) The nuclei with integral spin angular momentum (nuclei of even A) are of symmetric type (called as bosons) while the nuclei with half-integral i (nuclei of odd A) are called as fermions. (6) The neutron precisely has the same intrinsic spin angular momentum and symmetry character as a proton, i.e. s = 1/2 and anti-symmetric (Figs. 14.3, 14.4).

14.1.5 The Precessional Frequency of the Nuclear Magnetic Moment, with the Applied Magnetic Field

Refer Fig. 14.3.
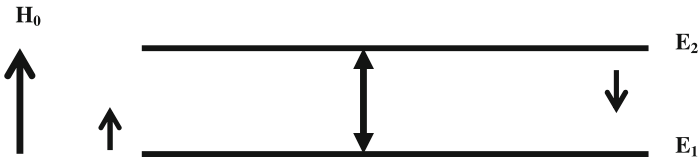
Fig. 14.4 Here E_1 = lower energy state, E_2 = higher energy state and $\Delta E = E_2 - E_1$ = split in an energy level E in an atom due to double (up and down) degeneracy of the intrinsic electron spin of $\pm(1/2)\hbar$ in the presence of an external magnetic field H_0

14.1.6 Energy Split in the Spins (Dipole Magnetic Moments) in a Magnetic Field

Refer Fig. 14.4.

14.1.7 Spin Echo

A spin is a tiny magnet around the size of a nano-meter (10^{-9}m). These tiny magnets when move produce electrical signal around them. Suppose one applies an oscillatory magnetic field to the spin which changes direction from up (+Z) to down (−Z) and back at a certain frequency. The result will be an electrical signal generated. It may have ideally the same frequency but its amplitude will be modulated according to the local metabolic and other activities happening in the surrounding region where the spins are located. This results in the generation of the spin echo. In between the echo times the signal will decay exponentially at a certain characteristic rate as a result of the externally applied RF signal. This time is called as the field induction decay (FID) time. There are two types of FID times.

14.1.8 The Longitudinal Relaxation Time T_1

It is also referred to in the MRI literature as the **spin–lattice lattice relaxation time**. The origin of this time lies in the interaction of the spins with environment in which they are present. The spins are reversed form the +Z direction into –Z direction and then allowed to comeback to +z direction. The time taken to relax is called as the longitudinal or the lattice relaxation time T_1.

14.1.9 The Transverse Relaxation Time T_2

The origin of this time lies in the spin–spin interactions in the local environment in which the spins are present. This relaxation arise due to fact that instead of spins being made to dissociate along +Z and −Z directions they are made to dissocate, along +X and –X or along +Y and –Y directions, in the X, Y plane. In this case the spins after projection in the X or Y-direction decay in the X–Y plane. They generate the corresponding relaxation time in the transverse (X–Y) plane. This is the characteristic relaxation time T_2. In order to create the transverse relaxation time a 90° pulse is applied along the X-direction to the sample in vivo. This rotates the spins in the +Y-direction in the X–Y plane. The spins then dissociates away from the +Y-direction. This process is reversed by applying 180° (reversal) pulse along the X-direction. It results into an echo signal and its decay with time results into, the characteristic time T_2. The transverse relaxation time is also referred to in the MRI literature as the spin–spin relaxation time. The above two relaxation times are commonly used as the source of weighting (a regional statistical average) in producing images in MRI.

14.1.10 The Gradient Echo

The electrons, protons, etc. spins are aligned along the applied uniform static magnetic field, applied along the Z direction, of strength of around 3 Tesla. It is assumed that the spins are uniformly distributed (in the X, Y, Z space) pointing along the z-direction. But the spins distribution can be made non uniform along a particular chosen direction. This is achieved by applying an additional gradient magnetic field of a small magnitude $\sim$ mT/m (milli Tesla per meter) in a chosen direction. What this gradient means is the field increases in strength linearly along one direction. The result of the gradient is that the molecules experience a small translational, directed (superimposed on the static aligned force in the Z direction), force, in the chosen direction. This is a kind of localization of the spin achieved over a selected area, in one direction of the sample. One can create the localization of the spins over small area in any of the three X, Y, Z directions. We can make the gradients as reversible in time or say oscillatory in nature. The result is that one gets echoes from the localized spins created by the field gradients. The above source of echoes is called as the gradient echo. The diagram below, gives a rough picture of the technique. The RF radiation field is allowed to interfere with the externally generated gradient echoes. One can say this is a phenomenon analogous to the interference and diffraction of waves. But in the spins case there is a difference. Here it is created in the time–space. One can choose by resonance selection a desired group of nuclei for analysis (Fig. 14.5).

The information from voxel to voxel all over the brain is coordinated for the map imaging of the brain. The result of the new superimposed lines of force acting on spins due to the magnetic field gradient can be written as follows. It results in a gradient force which along x, is, $F_X = \pm\mu_N (\partial H_Z/\partial x) = \pm\mu_N G_X$; along y, is,
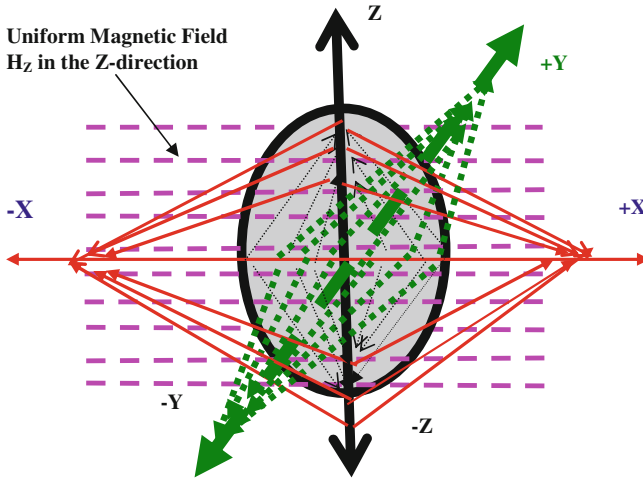
Fig. 14.5 In the sketch the projection of the brain is shown in Z–X Plane. Y-Axis is perpendicular to the plane of the paper. The magnetic lines of force due to the static magnetic field are uniformly spaced along the z-direction. One can theoretically apply along the, +z, −z, +x and −x, and, +y and −y directions, a small magnetic field gradient, of order $\sim$ mT/m. A fraction of the uniformly aligned spins in the z-direction can be partially focused in a chosen direction. This is the result of superimposing small magnetic field gradients on the uniform magnetic field along the z-direction. It is as if the spins are physically translated preferably, in the chosen direction. Normally the field gradient is applied one at a time in a preferred direction with a time gap in-between. The pulsed field gradients create echo waves. These waves are allowed to interfere with the carefully designed and applied RF pulses. The receiver then extracts the desired information from the various interactions happening in the brain

$F_y = \pm\mu_N(\partial H_Z/\partial y) = \pm\mu_N G_Y$; and along z, is, $F_z = \pm\mu_N (\partial H_Z/\partial z) = \pm\mu_N G_z$. The gradient magnetic fields exert a translational force on the spins in the direction of the gradient where the fields become stronger. On can choose slice selection in the Z-direction as, $\Delta Z_Z = [\Delta\omega/(\gamma G_Z)]$; $G_Z = [(\partial H_Z/\partial z)]$; γ = Gyro Magnetic Ratio (GMR) and $\Delta\omega$ = Frequency Bandwidth of the RF radiation. The linear magnetic field along the X-direction can be expressed as $H_Z (X) = H_{Z0} \pm x\, G_X$; $G_X = [\partial H_Z/\partial x]$ and along the Y-direction is $H_Z(Y) = H_{Z0} \pm y\, G_y$; $G_y = [\partial H_Z/\partial y]$. The gradients in space can be made vibratory in nature. This will allow induced signals from either side of the centre of a region to be recognized simultaneously in time–space and manipulated for imaging. One normally chooses application of one magnetic field gradient at a time, in a particular direction.

14.1.11 Spin Encoding in the Brain Using Radio Frequency (RF) Radiation

One needs to first excite the spins in the brain. This is done using an RF pulse which has its amplitude modulated with a selected bandwidth of frequencies
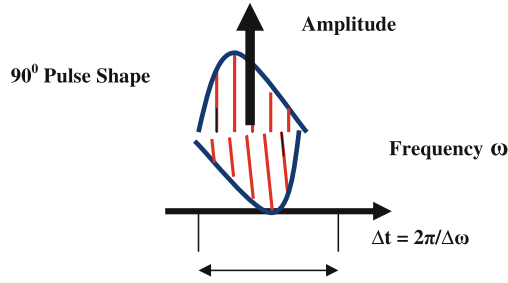
Fig. 14.6 Above is shown a shaped 90° (has a specific frequency content) Gaussian RF pulse. A slice selection is made in the Z-direction by using $\Delta Z = [\Delta\omega/(\gamma\, G_Z)]$. Here $\Delta\omega$ is the bandwidth of frequencies present in the shaped RF pulse, γ the GMR (gyro magnetic ratio) and G_Z the field gradient sin the Z-direction, $G_Z = [\partial H_o/\partial Z]$

around a central frequency ω_0. This is close to the resonance frequency of absorption of due to a group of nuclei present in a selected region of the brain. The pulse used is called as the shaped 90° frequency selective Gaussian pulse and is pictorially depicted below (Fig. 14.6).

The 90° pulse applied in the X-direction allows spins to be projected in the X–Y plane. The spins in the Y-direction very soon start getting out of phase (moving away from the +Y direction). The application and repeated reversal of the y-gradient allows the spins to reinforce them to stay in phase i.e. to stay in coherence, with each other. In between the period between Y-gradients the gradient G_X in the X-direction, is used to pick up or say label the spins according to a particular band of selection of resonance frequencies, corresponding to the local group of nuclei. The spins while they are in the X–Y plane become frequency encoded because of the local events and are picked up by the X-gradient selection. Then a y-gradient, with higher amplitude along the +y direction is applied allowing increased area of collection of spins. This delays the next X-frequency encoding but brings in the new phase encoding from the Y-direction. Now the spins have changed their phase encoding i.e. they have changed their orientation and magnitude with respect to (wrt) the original reference where the spins were initially directed (+y direction).

By redoing this process with different amplitudes of Y-gradient field different M (magnetization or susceptibility) values corresponding to different phase angles φ_Y are recorded. Here $\varphi_Y = [\gamma\, y\, G_Y\, t_Y]$, y is the location of a spin in y direction, G_Y is the gradient field in the Y-direction and t_Y is an instant of time in the Y-direction. The phase encoding process is repeated each time for a new frequency encoding (N) step. The data is digitized. The result is a creation of MxN matrix of data set. One normally uses 256 ± 256 data matrix. The k-space is an inverse of wavelength (λ) space. The wavelength λ is related to k, the wave number, as, $k = 1/\lambda$. The wavelength corresponds to the frequency bandwidth of the RF radiation. Once the data is collected in k-space it is converted into an image in real space i.e. the brain space. This is done by using the mathematical technique called as the Fourier Transform.

Please see Chap. 6 for pictorial representation of the gradient echo technique. For details on Fourier Transform Technique (FTT) the reader should refer to a standard text, e.g. [1].

14.1.12 The Brain: A Complex Ensemble of Spins

Echo Planar Imaging (EPI) is a k-space imaging technique commonly employed in MRI. The symbol k stand for the wave number and $k = 1/\lambda$. Here λ is the wavelength of the RF radiation employed for imaging. It basically reflects a broad picture of the brain on a planar section. Brain science is an intricate, quantum science not precisely accessible by the presently available MRI or any other technology. The conventional MRI uses the well known single-quantum (approximate identical spins model, electronically mediated through chemical shift, broad angular momentum resultant, etc.) spin coherence technique in the brain imaging. It reveals little about the atomic level changes in the chemistry of the events happening, in the brain. EPI uses the echoes received back in the scanner due to the radio frequency (RF) irradiation of the brain. Conventional MRI provides resolution on the scale of mms to cms in the brain space and milli seconds (ms) to seconds in the time–space. A comparison of the scan performed with that of a healthy brain helps a clinical doctor to make a diagnostic decision. The phenomena of communication between various sections of the brain, e.g. the metabolic events delivering the energy for specific actions, neuro-transmission-inhibition, etc., take place at a much faster speed, than recorded in conventional MRI and are quantum correlated. The events happen over nm to micrometer to mm space. The time scale is over micro second (μs) to ms and may be even faster. A conventional image misses on the finer dynamic details, happening on the hundreds of (macromolecules) nano meter scale.

The quantum-detailed events are the result of the atomic level quantum inter-actions, between the brain's soft matter and the surrounding molecules e.g., mobile fluids, blood flow, etc. The molecules in and around the soft condensed matter of the brain are of tens and hundreds of nm (10^{-9}m) in size. They have loose and flexible volume with a bound surface. The electrons on the surface are loose electronic charges corresponding to the outermost electrons in orbits. These charges are superposed on the deep-stable-bound charges inside the molecules. The electrons orbiting in the outer orbits of the atoms and molecules contribute to the magnetic dipole moment associated with the macromolecules. These are sometimes loosely referred to as molecular spins. Deep down there is entangle-ment of angular momentum of electrons around its on axis, around the nucleus, and that of the protons and neutrons, inside the nucleus. These interactions will decide the resultant angular momentum. In a situation e.g. a voxel, the measured resultant dipole magnetic moment is what can be measured through the electrical signal it produces.

The reader is reminded that the angular momentum of electrons, atoms, multi, molecules, etc., can not be measured directly in a laboratory. The resultant precessing magnetic moment of a group of molecules in a voxel situation around the static magnetic field applied is measured through the magnetic resonance frequency of the dipole magnet. In the presence of the static magnetic field applied in a specific direction in the brain called as the z-direction in MRI spins acquire an oriented equilibrium magnetization in the Z-direction. The brain is then said to be magnetized in that direction. On impinging of the RF radiation to the brain along a perpendicular direction wrt (with respect to) to the static magnetic field say in the X-direction the spins vibrate under resonance and produce electrical signals which are recorded in a scan in the X–Y and or Y–Z planes. This is done in space and time. The atomic spins form the key source of quantum information collected in a brain scan. A nano magnetic resonance imaging will be based on the quantum magnetic resonance at the molecular level. This we refer to as quantum magnetic resonance imaging (QMRI) in the book though it refers to multi-quantum phenomena. One can image the events happening due to the quantum-chemistry in time span of nano seconds to milli seconds. The real time events at the multi-quantum level which form part of the collected data can be studied after the QMRI scan data has been completed at a convenient time later. One can thus explore the real-time secrets of the human brain science. This present exposition (the book) is about communicating education about the human brain science at a wider scientific community level. Detailed information at microsecond to milli second (ms) intervals about the chemistry of events happening in the brain can be stored during the QMRI scan. This stored data can be later examined to develop the exact brain science in operation.

14.1.13 Distant Dipole Field

In the liquid state NMR we first have the application of the static magnetic field in the z-direction. It creates inside the sample a screening (reaction) field trying to oppose the applied field. The field inside is modulated by the internally created local dipolar field (due to the magnetic dipoles of the atoms, molecules, etc., located at a distance) and is localized. It stimulates magnetically active local centers. DDF is related to the various quantum orders of the spins present in a region [2]. Although this field in space is present in regions of nm (nm = 10^{-9}) in dimensions a large number of atoms group together in the form of macro-molecules making the field experienced rather on the scale of micrometer (10^{-6}m) i.e. the micron and mm level. This makes the overall continuous spin dynamics in the sample superimposed, by a non-linear (discrete) component. It leads to addition of harmonics to the fundamental character, of the evolution of the spins. This means addition of a fine structure in the evolution of spins. Short range (less than a micron) magnetic dipole–dipole (macromolecule) interactions cancel out due to rotation diffusion etc. of spins. But the long range (micron to mm) interactions in fact enhance each other

due to the quantum correlations, among them. If a sample is spherical in shape and has inside homo-nuclear spins, with no interactions, the spins due to their random distribution in direction will all cancel out each other. But if this were a cylinder with large height with respect (wrt) to its diameter then this becomes an anisotropic structure. It results in producing a resultant which is not zero.

The anisotropy in a local structure e.g. a tumor in the brain leads to interaction between the spins to produce a finite result. In an ensemble of atoms and molecules like in our brain in a confined space the artifacts are anisotropic in their magnetic character. Thus the over all result in a small region the sub-voxel selected for examination makes a contribution, about the abnormality of the region. Conventional MRI machine can not easily see the quantum order or disorder or say it can not handle it in a precise manner. One has to create an MRI technology with microscopic accessibility about the events happening in a sub-voxel structure. The application of RF radiation to a voxel in our brain which can be selective by resonance frequency to a particular nucleus e.g. Na excites the atoms (and the group of atoms within a bandwidth of frequency) for quantum–quantum correlations (communication) between them. The coherences can be of multi-quantum character, e.g., the zero quantum (two spins coupled with the spins opposing each other in direction) the double quantum (two spins coupled with spins acting together in the same direction) triple quantum (three spins coupled with spins acting together the in the same direction) and so on. The quantum interactions can be stronger if locally the symmetry of the applied static magnetic field can be broken. This is achieved by applying a fine gradient magnetic field in a selected region in a particular direction. The gradient is approximately of a strength mill Tesla/meter (mT/m). This is like adding a fine mesh externally for a microscopic examination. The magnetic gradient applies a directed force on the spins. It is like stretching a spring in the length direction. It is an artificially created anisotropy. It becomes the source of quantum correlations between molecules.

In MQMRI the desired anisotropy is created by a technique called as the correlation spectroscopy (COSY) revamped by asymmetric z-gradient echo detection (CRAZED) technique. The reader is reminded that our earth has a magnetic field of around a micro-mill Tesla on the ground and a fairly uniform gradient of micro-Tesla/meter. Is our brain a part of the nature's variation of the earth's magnetic field felt on the surface of earth? We do not know the exact answer to this question yet. But successful experiments have been done to measure the effects. In MQMRI an initial RF pulse followed by a magnetic field gradient pulse generates phase-encoded (different nuclei react over different times) intermolecular quantum coherence (iQMC). The molecular coherences can be transferred into an observable magnetization which can be of single or multiple quantum coherence (MQC) character. The MQC needs to be reinforced by applying more than one RF and gradient pulses in succession. The brain having being magnetized in the z-direction by the static magnetic field H_z, can be spatially modulated by the application of a gradient field of strength G_z, in the any direction, e.g., in the z-direction. This is done by use of a gradient pulse of duration τ.

The modulated static magnetic field also modulates the DDF. A nuclear spin is automatically exposed to this DDF (distant dipole field). This field is determined by the DDFmagnetization experienced from a distance, $d = (\pi/\gamma\ G_z\ \tau)$, due to a distant spin. Here γ = the gyromagnetic ratio (GMR) and G_z the magnetic field gradient in the z direction. The physical property γ, is unique, for every nucleus, and is the source of MQC. One should remember that in an artifact like e.g. a tumor tissue a small volume of the fluid in the brain has a large group of atoms and molecules. This group is usually referred to as a macro-molecule with several nuclei being part of it. A macro-molecule also has a unique resultant (average) γ. Using the conventional MRI technology one can create multiple-spin echo (MSE) experiment to excite MQCs, to image the brain. The technique is as follows. First a 90°_x (the flip angle for the spins is chosen as 90° wrt to the z-direction) pulse is applied in the x-direction and then a second one. The two pulses are separated in time, by τ. First echo appears at time τ, from the first pulse, at frequency ω. After the second pulse a second echo appears at $t = 2\tau$ at twice the fundamental frequency ω of the incident RF radiation.

In the following evolution time of τ after the second pulse there is interaction between the second order component of M_y (the y-direction magnetization produced by the 90°_x pulse) with the DDF. The result is a creation of third order echo at 3τ with modulation frequency of 3ω and so on. It is the application of the magnetic field gradient pulses in between the RF excitation pulses that quantizes or say expose the discrete character of the nuclei locally present. Below is included a practical illustration of the distant dipolar field (DDF) computed for water enclosed in spherical and cylindrical samples under different strengths of gradient fields. Figure 14.7a–k [2]) presents illustrations how one can view DDF field as a diffraction phenomena like the one commonly observed in diffraction of radiation in crystals and molecules.

14.2 Appendices B

An overview of the density matrix concept

14.2.1 Single Spin Rotation in Space and Time

The density matrix ρ of the single spin system [3] is a matrix where the elements in rows and columns quantify the relative population of spins energy levels of an ensemble of atoms and molecules like the one we have in our brain. If all the spins corresponding to the molecules are identical we call it a single spin system. The ρ of this ideal system is represents by a 2×2 spin matrix. The energy levels populations are expressed as the elements of the matrix normalized with respect to that of the thermal (room temperature) energy level of the molecules in the ensemble. The thermal energy, $= kT$. Here k is the Boltzmann constant (k = 1.381×10^{-23} J/K) and
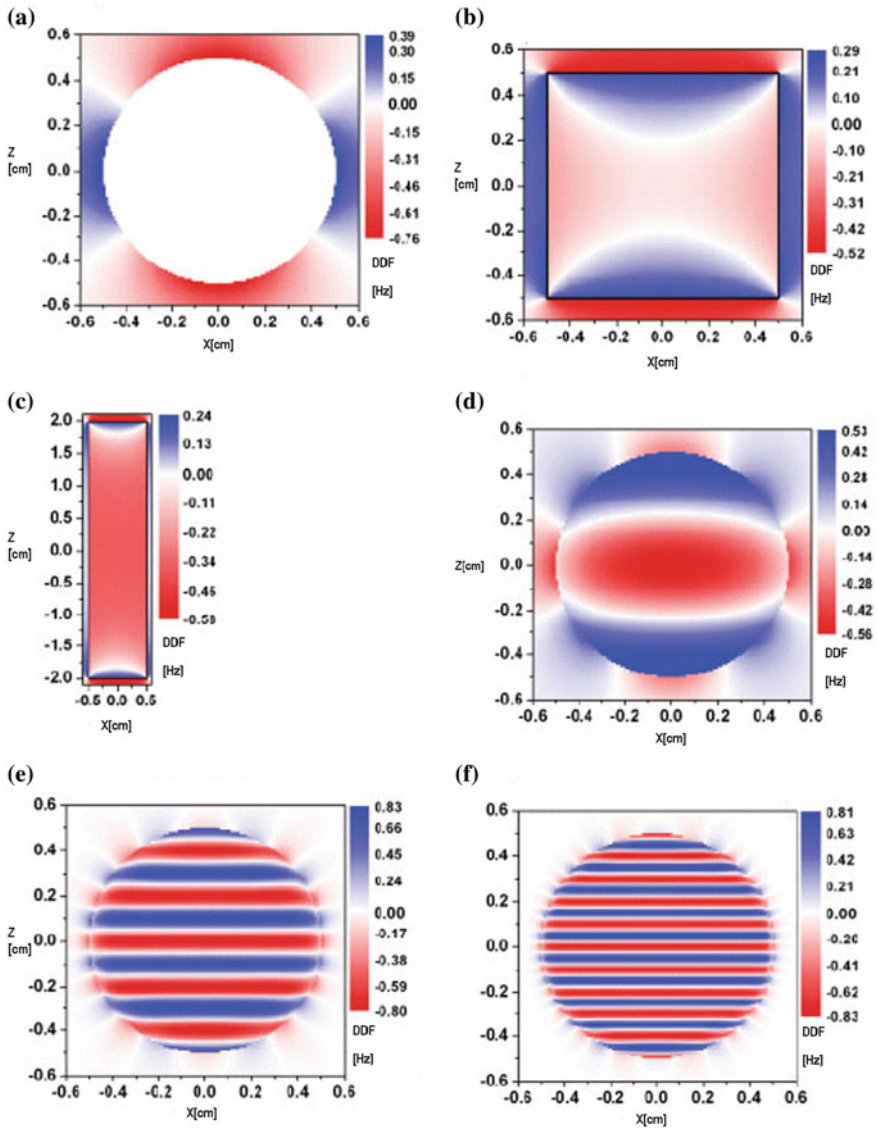
Fig. 14.7 Frequency offset $\Delta\nu_{DDF}$ (x, z) due to the distant dipole field (DDF) for a homogeneously magnetized sphere with diameter (Ds) of 1 cm (**a**), cylinder with diameter and height of 1 cm (**b**), and cylinder with diameter of 1 cm and height of 4 cm (**c**). **d**–**f** $\Delta\nu_{DDF}$ (x, z) is in the case of a spatial magnetization distribution generated by correlation spectroscopy (COSY) revamped by asymmetric z-gradient echo detection (CRAZED). The wavelength of the magnetization helix λ_m, was, λ_m = Ds (**d**), λ_m = (1/5) Ds (**e**) and λ_m = (1/10) Ds (**f**). **g**–**i** The same preparation as in **d**–**f** except that the gradient is applied along the ''magic angle'' (the flip angle where the resultant magnetization becomes zero) (**k**). Gradient of the DDF dBd,z(r')/dr' experienced by a nuclear spin at the center of the sphere (r = 0) with Ds = 1 cm. Note, that for r = 0 the gradient of the DDF is only a function of r ' = (x', z'). The wavelength of the magnetization helix λm was λ_m = (1/5) Ds (**k**). Profile of the gradient $dB_{d,z}(r')/dr'$ along the dashed line z' = 0 in (**k**)
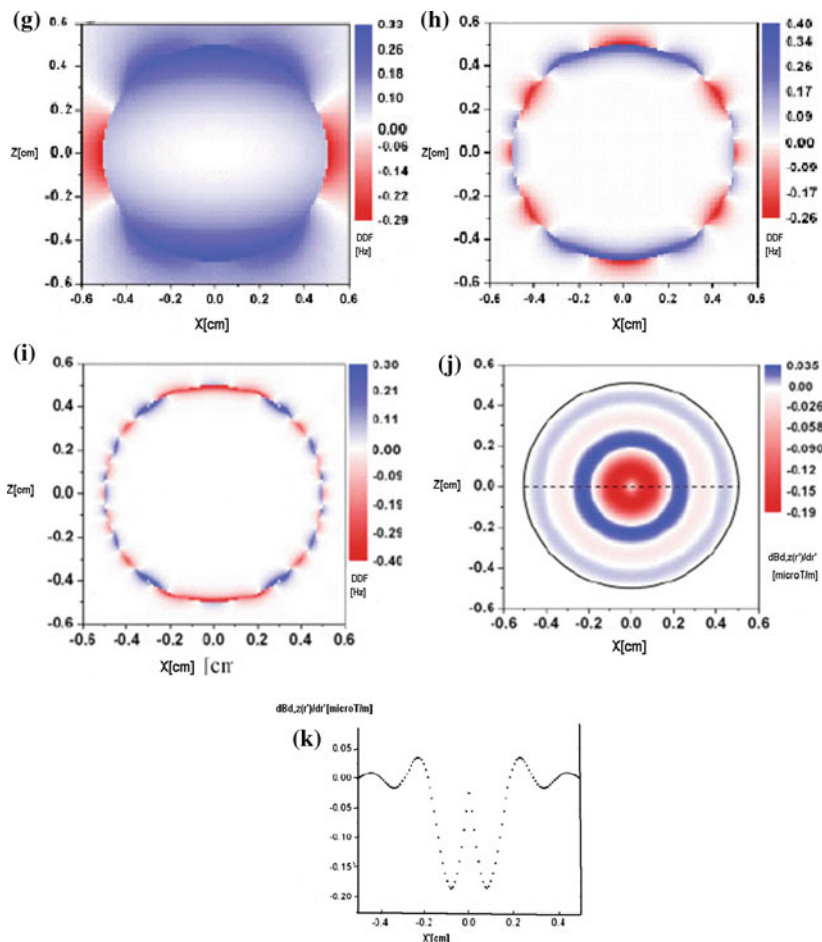
Fig. 14.7 (continued)

T is the temperature of the ensemble in degrees Kelvin (K). The one spin system in the presence of an externally applied static magnetic field, Hz_0 consists of two energy states +1 and −1 oriented along the +Z and –Z direction. The density matrix for the 1-spin (I_z) system is expressed in terms of the probability p of spin being in one of the two spin states ±1/2 and is given by

$$\rho = 1/2\begin{pmatrix} 1+p/2 & 0 \\ 0 & 1-p/2 \end{pmatrix} = 1/2\begin{pmatrix} 1 & 0 \\ 0 & 1 \end{pmatrix} + p/4\begin{pmatrix} 1 & 0 \\ 0 & -1 \end{pmatrix}$$
$$= p/4\begin{pmatrix} 1 & 0 \\ 0 & -1 \end{pmatrix}$$

The first matrix on the extreme rhs (right hand side) is called as the unity matrix or an identity matrix. It is time independent and reflects the original or say the

Fig. 14.8 A 90° pulse along X-direction produces rotation of the spins (density matrix) along Y-direction. It is important to point here that the product of a rotation matrix by its own inverse gives an identity matrix I (all the elements along the diagonal of the matrix being = 1). This is by definition, and holds, for any matrix, of any size

Applied Static Magnetic Field H$_{z0}$

Z

The Signal Out Along Y-Direction

Y

The 90^{0}Pulse

X
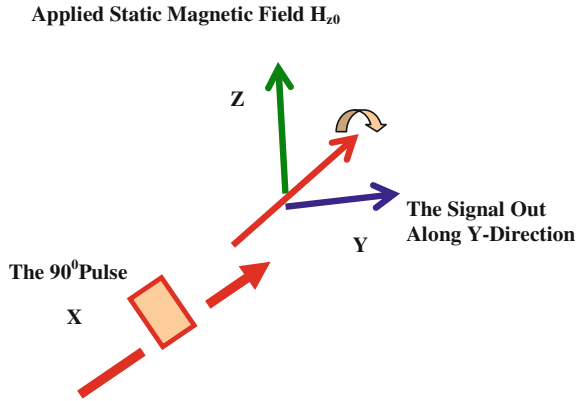
unperturbed state of the system. Thus it is neglected for subsequent analysis. The final result in the system retains changes through p. The magnitude of p is expressed as a ratio between the energy of the spin being, in a magnetic energy level as compared to the spin distribution in thermal equilibrium in the background. The ratio becomes a number with maximum value = 1. The probability of occupation, of the magnetic states, is between 0 and 1. One can write, $p = (\hbar \gamma Hz_0/kT)$. The p is the fraction of the spins occupying a higher energy level through application of the static magnetic field H_{Z0} along the Z-direction. The term $\hbar$ is the familiar angular Planck's constant and γ = the gyromagnetic ratio(GMR). The rotational operation, by 90°, about X-axis is performed by applying a 90° RF pulse, along the X-direction. The rotation is done to ρ representing the static equilibrium of spins along the Z-direction created by the static magnetic field. Mathematically the rotation can be performed by using a rotation matrix U_{90x} and its inverse U_{90x}^{-1}. The operation is as follows.

$$U_{\times 90^\circ(ROT)} = U_{90x}(\rho)U_{90x}{}^{-1} = (p/4)\begin{pmatrix} 1 & i \\ i & 1 \end{pmatrix}\begin{pmatrix} 1 & 0 \\ 0 & -1 \end{pmatrix}\begin{pmatrix} 1 & -i \\ -i & 1 \end{pmatrix} = (p/2)\begin{pmatrix} 0 & -i \\ i & 0 \end{pmatrix}$$

$$= (p/2)\sigma_y.$$

The reader with no background in matrix mechanics (MM) need not really learn the technique of this operation. It is the final result that is important here. The first (U_{90x}) matrix around (ρ) in the equation on the left hand side (lhs, first step) is the 90° rotation operator around the x-direction and the second one multiplying the middle (ρ) matrix on the right hand side (rhs) is the inverse of it. The final result is shown on the rhs in the third step. It is worth pointing out here that the general rotation operators performing rotations by an angle φ about X and Y directions can b expressed as standard operators as $U_{\varphi X}$ and $U_{\varphi}y$ respectively. Their matrix representations are as follows.

$$U_{\varphi X} = \begin{pmatrix} c & -is \\ -is & c \end{pmatrix} \quad \text{and} \quad U_{\varphi}y = \begin{pmatrix} c & -s \\ s & c \end{pmatrix}$$

Here c = cos (φ/2) and s = sin (φ/2) and φ is the pulse (flip) angle.

When φ = 90°, c = s = (1/√2) and $U_{\varphi X} = \begin{pmatrix} c & -is \\ -is & c \end{pmatrix} = (1/\sqrt{2}) \begin{pmatrix} 1 & -i \\ -i & 1 \end{pmatrix}$

and $U_{\varphi} y = (1/\sqrt{2}) \begin{pmatrix} 1 & -1 \\ 1 & 1 \end{pmatrix}$.

The main result to note here is that result of rotation on ρ as shown changes the I_Z density matrix ρ into Y-oriented spin matrix, (p/2) σ_y which can be measured in the laboratory. Pictorially this rotation is illustrated by the Fig. 14.8. One should note here that the rotation matrices will change their sign according to whether the rotation is clockwise or anticlockwise (in the above demonstrated example). The conventional details on the sign (direction clock wise or anti-clockwise) of rotation does not form part of the demonstrated examples here. The main thing here is that the density matrix concept for those who can learn is an important concept to understand about the mathematical details for the design of RF pulses for a specific task used in MRI. This is the area rather of more interest to the readers who have a good background, in quantum physics and mathematics. The readers should refer to a standard text book on quantum mechanics, e.g. [4] particularly dealing with angular momentum and matrix mechanics for details.

Now we next apply to the result (p/2) σ_y, a **time evolution operation**, using the operator $U_H = \exp\{-(H/\hbar)t\}$. Here H is the Hamiltonian (energy) operator of the system and for the simplest case considered of the ensemble of identical z-spins it is $= -\hbar\omega I_z = (-1/2\ \hbar\omega)$ for a single spin system. The negative sign chosen need not really bother. It is the concept involved which is considered important here. One chooses negative sign to represent a bound energy state of the spin, along, the applied static magnetic field in the z-direction. The matrix representation for this operator is

$$U_H = \begin{pmatrix} \exp i\omega t/2 & \\ & \exp -i\omega t/2 \end{pmatrix}$$

The time evolution operation is performed in steps identical to the space evolution as shown before. Here ω is the natural frequency of resonance of the spins and t is any instant of time. Once the spins are transferred in the Y-direction in space by rotation they dissipate in the X–Y plane providing a spin I_{xy} at any instant of time. Performing the time evolution operation U_H (ρ) U_H^{-1} identical in steps to the rotation in space on the density matrix ρ one gets

$$\rho(t) = p/2 \begin{pmatrix} 0 & -\exp i\omega t \\ \exp -i\omega t & 0 \end{pmatrix}$$

One should note here that the time evolution operation transfers, the elements in the density matrix from the diagonal to the off-diagonal side. The measured quantity M(t) in MRI is the magnetization i.e. the magnetic moment per unit volume. One is interested in the measurement of the time variation of the resultant magnetization in particular the projected value in the X–Y plane. It results from the interaction of the spins in the X–Y plane and is proportional to $I_{xy} = (I_x + i\ I_y)$. Here i is the complex number √−1. Its origin lies in the 'complex trigonometry'

branch of mathematics. Its (i's) inclusion in the mathematical treatment provides simplified mathematics for the time varying systems like we have here. In the matrix form one can write the magnetization component in the x, y plane, $M_{x,y}$, as

$$M_{xy} = (N_0\hbar\gamma)(I_x + iI_y) = (N_0\hbar\gamma)\left[\tfrac{1}{2}\begin{pmatrix} 0 & 1 \\ 1 & 0 \end{pmatrix} + i/2\begin{pmatrix} 0 & -i \\ i & 0 \end{pmatrix}\right]$$
$$= (N_0\hbar\gamma)\begin{pmatrix} 0 & 1 \\ 0 & 0 \end{pmatrix}$$

The calculation of the expectation (most probable) value of M(t) is performed as $<M(t)> = [p/2(N_0\hbar\gamma)]Tr[(I_x + i I_y) \rho]$. The product operation of the two matrices $[(I_x + I_y)]$ and $[\rho]$ is done by the standard multiplication rule of matrices row by column. The symbol Tr means adding the diagonal elements of the resultant matrix after the product and is called as the Trace Operation. The final result including intermediate steps is as below.

$$<M(t)> = (p/2)(N_0\hbar\gamma)Tr\left[\begin{pmatrix} 0 & 1 \\ 0 & 0 \end{pmatrix}\begin{pmatrix} 0 & -\exp i\omega t \\ \exp -i\omega t & 0 \end{pmatrix}\right]$$
$$= (p/2)(N_0\hbar\gamma)\begin{pmatrix} i\exp(-i\omega t) & 0 \\ 0 & 0 \end{pmatrix}$$
$$= (ip/2)(N_0\hbar\gamma)(\cos\omega t - i\ \sin\omega t)$$
$$= (p/2)(N_0\hbar\gamma)[i\ \cos\omega t + \sin\omega t].$$

Here ω is the Larmor frequency or the frequency of natural precession of the electron or a proton, depending upon the type of imaging that is under consideration. The above steps have been performed just to demonstrate the usefulness of the concept of the density matrix. It allows one to see the status of the spins in the ensemble at any particular instant of time t. One sees here that the trace of the product, $(M\rho)$, the Tr $(M\rho)$, tells us about the magnitude of the magnetization at any point in time and as to where among the four quadrants in the x–y plane the spin is present. The trace basically means, the sum of the diagonal elements of the resultant matrix. One should note here that at t = 0, $<M(t)> = i(p)/2$. This is positive and purely imaginary (i) number. It means that $<M(t)>$ lies along the y-axis. At time t = (π/ω), $<M(t)> = -1$ a negative real number. That means, $<M(t)>$ lies along the negative x-axis and so on.

14.2.2 Two Spin System

The above demonstration may seem to contain lot of mathematics for a learner to understand. Actually one need not despair. Today all this mathematics is handled by the computer programs which are easily available. A person just inputs the values e.g. the number (say $1/2, 3/2$, etc for the spin in question), the type of spins involved, the gyro-magnetic ratio, the density matrix, etc., into the computer

program. It is very educational to understand what various terms stand for and what are their values in specific situations. In a two spin (α, β) case there are 4-energy states that are possible i.e. ($\alpha\beta$, $\beta\alpha$, $\alpha\alpha$, $\beta\beta$). So the density matrix now will be a 4×4, matrix; $\rho = (p/4)(\sigma_{Iz} + \sigma_{Sz})$, where σ_{Iz} and σ_{Sz} are the 4×4 spin matrices for the two spins I and S. The process as shown before for the one spin (2×2 matrices) case can now be repeated for the two spin case. All these spin operators and the matrices for the one and two spin cases have been described and tabulated in text books; we include only a summary in tabular form in this work. See Appendices B for the corresponding tables. This work is simply to present a first hand knowledge about what goes on behind the scene in the methodology of imaging and how it can be used in the diagnostics of the tumors and disorders of the brain. A person working in an area like clinical medicine need not really learn the mathematics from the roots. Nevertheless the awareness is worth the education required. Getting used to the terms which are required to be input in a computer program in image modeling of the brain can be very useful. Those with adventurous bent of mind can learn how to find at a particular point in space and time what spins were involved and how they evolved. This exposure would also be very useful for those who may have some background of quantum mechanics (QM) but may not be directly involved in the field of applications of MRI in medicine.

14.2.3 Two Spin System: The Density Matrix

This work intends to simplify the knowledge about the spin dynamics involved in the real time imaging. It helps to the least to gather basic knowledge about the science behind and the technology involved, in MRI. The study of 2-spin case is considered very fundamental in understanding the more complex multinuclear systems [5]. A sequence of RF excitation pulses can be represented by the wave function ψ_i. The imaging process in MRI, involves spins of various flip angles, $\theta = \gamma H_1 t$, with respect to (wrt) the direction of the static magnetic field H_{z0}. Here γ is the gyromagnetic ratio, H_1 the amplitude of the RF pulse, and t, an instant of time. The phases φ of the incident waves, can be chosen to be, $\varphi = 0$ (along +x), $\pi/2$ (along +y), $3\pi/2$ (along –x), etc. The phase cycling can be used in order to enhance certain kinds of coherences and eliminate others. The sum of the interference of waves in an echo can be written as, $\psi_i = \Sigma_{j,\,i}\, c_{j*}\, c_i\, \psi_j$. Two symbols i and j are used to include various permutations of coupling between different degrees of freedom e.g. the chemical shift, j-coupling, etc. The echo waves would have the changes in coefficients c's in time. In the case of several spins the coefficients c_i would have a structure of a single column matrix with information from various interactions. One can draw an analogy of column matrix to the components of a vector in the Cartesian space. Let the coefficients c_i* be from the corresponding Hermitian row matrix the single row of components. The meaning of Hermitian row matrix is explained as follows. What c_i* matrix mean is that, it is Hermitian conjugate (changing rows into columns and columns into rows and i into –i, and –i

into i) of c_i. One can write the vector representation, of the magnetization in the z-direction in the 2-spin case as

$$M_z = N_0\gamma\hbar[\text{row vector } c_i*, c_2*, c_3*, c_4*].I_z[\text{column vector } c_1, c_2, c_3, c_4]$$

The descriptive meaning of this equation is that depending upon the structure of, I_Z, the product of the matrices (right to left, in steps) would produce column of the components of the magnetization, in the z-direction. In the case considered here, I_z is the z-spin matrix for the 2-spins, i.e. a 4×4 matrix. The matrices would have only 16 elements (rows and columns) in total. The result of this product of the three matrices (from right to left, row by column) can be written as $M_z = N_0\gamma\hbar\, I_z^{nn}\, C_n^* C_n$. Here $C_n^* C_n$ is defined as the density matrix I_z^{nn}. The I_z^{nn} is a square matrix of size 4×4 with 16 elements, given as, $I_z^{11}, I_z^{12}, I_z^{13}\, I_z^{14}, I_z^{21}, I_z^{31}, \ldots I^{41}\, I_z^{44}$ etc. A 4×4 matrix would have four 2×2 blocks in it. There will be two diagonal and two reverse diagonal blocks. The 2×2 blocks, matrices here are the same as the fundamental 2×2 Pauli single-spin matrices. This approach allows to keep the 4×4 matrix orthogonalized. All the changes that occur in the system in time as a result of the precession, relaxation, J-coupling, etc. are pursued through a density matrix. There is one to one correspondence between what evolves in the density matrix in time and what is observed in the laboratory. The changes in the image can be predicted through the analysis of the density matrix by performing the operations of rotation, time evolution, etc. The advantage of the density matrix approach is that one can find the magnitude of a desired quantity e.g. the magnetization M_y at any instant of time. One just evaluates the trace relation $M_y = (N_0\gamma\hbar)[\text{Tr}\,\{i(M_x + M_y)\{\rho\}]$ at any instant of time.

There are two types of the products of matrices. One is the **simple matrix product** of two matrices like the one above. In this product, the final output, is the result of the, row by column, product of matrices. What it means is that you start with the first column of the right matrix multiply it with the first row of the left matrix element by element and then add the result to produce, the first element of the first row of the new matrix. Then repeat this process to construct the rest of the elements of the first row of the new matrix, using first row of the left matrix and 2nd, 3rd,… columns of the 2nd matrix. Now do the same thing to construct the 2nd row of the new matrix, using second row of the left matrix, and all the columns of the right matrix. This way all the rows and columns of the new matrix are constructed. The other matrix product is called as **direct matrix product** of the two matrices. It is represented by placing the symbol $\otimes$ in between the two matrices. This product is used to construct a higher order matrix from a lower order one. Say for example, you are building, a 4×4 matrix, from the basic known, 2×2 matrix. Consider the simplest example, to construct, the 4×4 matrix for the I_z (z-component of the 2-spin system). You simply place, on the right side of each element, of the old 2×2 matrix, of the I_z, the basic (2×2), the σ_0 (identity matrix). Then use **simple matrix product**, as above, to get the 2×2 blocks, in the new 4×4 matrix. Below is an example of, a **direct** matrix **product** process. Multiply (see below) each element, of the old 2×2 matrix, on the left, with the right placed (σ_0 block), of the 2×2 matrix. The result is a new 2×2 block matrix,

at the place of the each element of, the old 2×2 matrix. One thus constructs the new 4×4 matrix. Some of the 2×2 blocks in new matrix, may have all the elements, as zero. This is because there was zero at the left of 2×2 matrix block at that position. The illustration below is a typical, for the I_z case.

$$I_Z = \begin{pmatrix} 1 & 0 \\ 0 & -1 \end{pmatrix} \otimes (\sigma_0) = \begin{pmatrix} 1\sigma_0 & 0\sigma_0 \\ 0\sigma_0 & -1\sigma_0 \end{pmatrix}$$

$$= \begin{pmatrix} 1 & 0 & 0 & 0 \\ 0 & 1 & 0 & 0 \\ 0 & 0 & -1 & 0 \\ 0 & 0 & 0 & -1 \end{pmatrix} \quad here(\sigma_0) = \begin{pmatrix} 1 & 0 \\ 0 & 1 \end{pmatrix}$$

Detailed construction of the 4×4 matrices, with basic multiplications steps explained, for two spin, I and S system, has already been done. One can get details from a physics text book, devoted to MRI or quantum mechanics (QM). In the case when you add and subtract matrices (of the same order) you just add and subtract the corresponding elements. It is not very important for many readers, to know, how to handle, the algebra of the matrices. They can see how they help to get the results we want. The example above illustrates the simplicity of a quantum algebra process. Fortunately we are at a stage, in the field of MRI now, where all the algebra of one and two-spin matrices, has actually been done and tabulated (refer Appendices B.6 and B.7). The exposition in this work creates just an awareness as to what goes on behind the MRI scene. In computer modeling of the MRI, of the brain, the MRI literature equips one, with the knowledge, of the input data format, for a computer program. This is a kind of training to see how the actual image is obtained. Human brain is a hetero-nuclear ensemble of atoms, nuclei, etc. That is what makes the MRI of the brain, too involved and difficult, to understand, but is so intriguing, at the same time. Higher order matrices can be broken down into smaller dimensions. This is done keeping in mind, as to what type of imaging one is interested in, i.e. J-coupling, quantum coherence etc.

Energy level diagram for a Two-Spin, one I (resonance frequency ν_I), and the other S (resonance frequency ν_S), spin 1/2 system, is shown in the Fig. 5.1. The first character of the wave function (α) indicates the state of the I-Spin (α) and the second character (β) shows that of the S spin. The zero-energy level is defined as the energy of the $\beta\alpha$ state. The populations of the four levels are P_1, P_2, P_{13}, P_4 and are assumed to be all equal to p = ($N_0 \hbar \gamma H_0 / kT$), initially. N_0 = density of spins per mole, $\hbar$ = Planck's constant, γ = gyromagnetic ratio, H_0 = applied static magnetic field, k = Boltzmann constant and T = the temperature of the ensemble. The population of all the levels is expressed wrt to P_2. It is taken as the reference level. Ideally without an external disturbance, e.g. the applied static magnetic field, the population of all the levels, should be equally probable. That is ¥ of the total 1. But on the application of the static magnetic filed, the population of P_1, is lowered (excitation of spin) by ¥, and that of P_4 increased (absorption of spin) by the same amount, conserving the total population, as one. It is like pouring spins, more in

one state, compared with the other. The density matrix (DM) of the system $\rho(0)$ at equilibrium for two-spin system at a particular temperature for the two spins I_Z and S_z, system can be written as

$$\rho(0) = (p/4)\begin{pmatrix} 1 & 0 & 0 & 0 \\ 0 & 0 & 0 & 0 \\ 0 & 0 & 0 & 0 \\ 0 & 0 & 0 & -1 \end{pmatrix} = (p/4)(1/2)\begin{pmatrix} 1 & 0 & 0 & 0 \\ 0 & 1 & 0 & 0 \\ 0 & 0 & -1 & 0 \\ 0 & 0 & 0 & -1 \end{pmatrix}$$

$$+ (p/4)(1/2)\begin{pmatrix} 1 & 0 & 0 & 0 \\ 0 & -1 & 0 & 0 \\ 0 & 0 & 1 & 0 \\ 0 & 0 & 0 & -1 \end{pmatrix}$$

$$= p/4(I_z + S_z)$$

Now we perform two 90° rotation operations. This will be one 90° for each I (frequency v_I and S (frequency v_S) spin I and S matrices respectively. This is done in succession and is applied round the x-direction. One thus gets the new density matrix

$$\rho(2) \text{ as, } \rho(2) = \begin{pmatrix} 0 & i & i & 0 \\ -i & 0 & 0 & i \\ -i & 0 & 0 & i \\ 0 & -i & -i & 0 \end{pmatrix}. \text{ In its equivalent form, it can be rear-}$$

ranged, as below.

$$= -p/4(1/2)\begin{pmatrix} 0 & 0 & -i & 0 \\ 0 & 0 & 0 & -i \\ i & 0 & 0 & 0 \\ 0 & i & 0 & 0 \end{pmatrix} - (1/2)p/4\begin{pmatrix} 0 & -i & 0 & 0 \\ i & 0 & 0 & 0 \\ 0 & 0 & 0 & -i \\ 0 & 0 & i & 0 \end{pmatrix}$$

$$= (p/4)[-I_y - S_y]$$

The two rotation operations result finally in having no z-magnetization, and only; the I_y and S_y spins. One should note here the result obtained is exactly identical to that obtained for the one-spin case. These two spins are measured by the receiver as a free induction decay (FID). The creation of the y-magnetization results from transforming a collection of z-spins, precessing about the z-axis with random phase at thermal equilibrium. Now we have a collection of spins, with coherence, in the x–y plane, and a resultant net magnetization along the y-axis. The single 90° pulses applied (frequency selective) have each created a net transverse magnetization, that can be observed, as FID. The off diagonal elements d_{12}, d_{13}, d_{21}, d_{24}, d_{31},d_{34}, d_{42} and d_{43}, in the first matrix, in the steps, in $\rho(2)$, indicate that the application of the 90° pulses, applied to the I_z and S_z spins, has created the single quantum transitions, I_y and S_y.

The d_{12} indicates $\alpha\alpha \rightarrow \beta\alpha$ and the d_{21} indicates $\beta\alpha \rightarrow \alpha\alpha$. The coherent 'superposition of independent spin states', is called as the single quantum
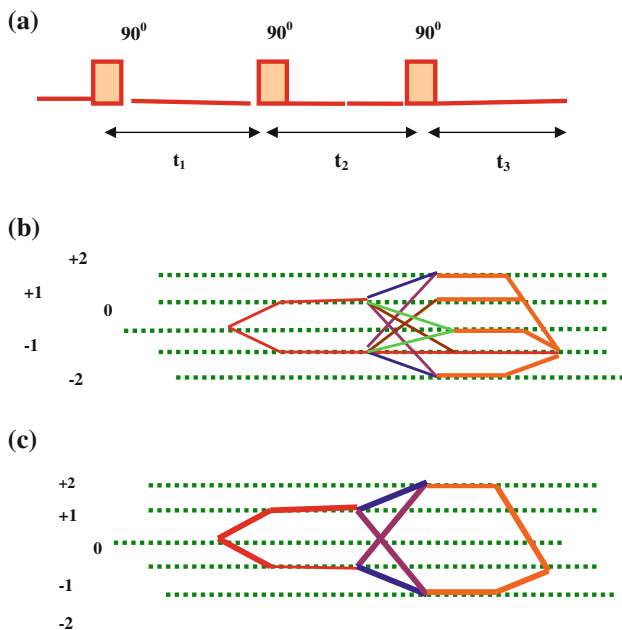
Fig. 14.9 a Pulse sequence for the 2D NMR correlation spectroscopy (COSY) experiment.
b Several coherence Transfer Pathways (CTPs) possible for a two Spin 1/2 system, indicating
coherence orders from −2 to +2. **c** The desired pathways are selected, by the phase cycling
process. There can be more than one CTPs for the same coherence order. Phase cycling technique
is used to enhance the desired ones and eliminate the others

Table 14.1

Single quantum coherences	Mixed zero and double quantum coherences
I_x, I_y, I_z, S_x, S_y	$2I_xS_x, 2I_xS_y, 2I_xS_z, 2I_yS_x, 2I_yS_y, 2I_yS_z, 2I_zS_x, 2I_zS_y$

Table 14.2

Pure double quantum coherence	Pure zero quantum coherence
$1/2(2I_xS_x - 2I_yS_y)$ and $1/2(2I_xS_y + 2I_yS_x)$	$1/2(2I_xS_x + 2I_yS_y)$ and $1/2(2I_yS_x - 2I_xS_y)$

coherences, which is observable as FID. It is possible, with further pulses applied,
to cause the d_{14} and d_{41} elements to become non zero. Therefore the double
quantum coherence can also be created. The elements d_{23}, d_{32} represent zero-
quantum coherence. Neither zero nor double quantum coherence is directly
observable. It has to be measured indirectly following different coherence transfer
paths (CTPs). All CTPs end up in path −1, where the measurement is done. See
Fig. 14.9, and Tables 14.1 and 14.2, for the pulse sequence used for a two spin
system and the coherence pathways expected. The Tables 14.3–14.43 list Matrices,
Operators, etc., corresponding to the cartesian coordinate system (CCS) and the
spherical basis system (SBS).

14.2.4 Multiple-Quantum Correlations: Two Spin System

In the complex biological systems like brain the region of interest based metabolic spectroscopy [6], is an important tool of analysis. Mullti-quantum [5–7] spectroscopy has been used over decades in the field of pharmaceutical medicine. But its translation in MRI has been a very recent approach. Various nuclei present in a small voxel selected for analysis, produce a resultant coherent spectra over different quantum orders depending upon the interactions between the molecules. Collection of such data across a voxel in the brain becomes a versatile complementary tool for the MRI diagnostics of the human brain disorders. This work in its scope does not include any details of spectroscopy techniques used in MRI. Some illustrative examples of imaging in this respect have been included in this work. They explain the basic theoretical concepts involved in MQMRI. A brief pictorial representation in the Fig. 14.9, depicting various orders of coherences (+2, +1,...,−2) and various coherence transfer pathways (CTPs) should be informative for the reader. It would be useful to point out here that when atoms get together in an ensemble like situation, e.g. our brain, the large macromolecules have a resultant (multi-quantum) energy structure. One can find more educational exposure of multiple coherence and the CTPs in Appendices B. The Fig. 14.9 represents simplified picture of the double-quantum coherence pathways, as a result of three $9\bar{0}$ pulses, used in the in the QMRI of brain.

Precession and J-coupling, over the time interval t_2, results in the following, operator terms of coherences. These terms are of the type, $2I_xS_x$, $2I_xS_y$, etc. They contain zero and double quantum coherences. There can be two, an even more j-coupled spins, in a real situation. The Tables 14.1 and 14.2 list the product operators, corresponding to, single quantum and double quantum coherences only for the sake of illustration. The zero and double quantum coherences are not directly observable. These can be obtained only, when multi-quantum coherences, is converted, to single quantum coherences, in MRI which can be measured directly.

$$DQC(Pure) = (1/2)\{2(I_xS_x - IS_y)\} = (1/2)\begin{pmatrix} 0 & 0 & 0 & 1 \\ 0 & 0 & 0 & 0 \\ 0 & 0 & 0 & 0 \\ 1 & 0 & 0 & 0 \end{pmatrix};$$

$$(1/2)\{2(I_xS_y + I_yS_x)\} = (i/2)\begin{pmatrix} 0 & 0 & 0 & -1 \\ 0 & 0 & 0 & 0 \\ 0 & 0 & 0 & 0 \\ 1 & 0 & 0 & 0 \end{pmatrix}.$$
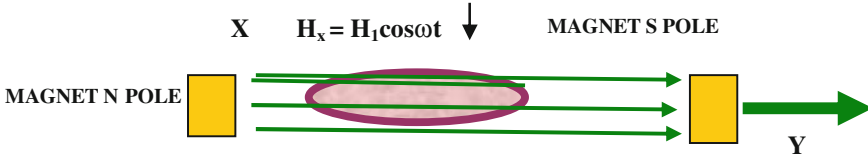
Fig. 14.10 A typical experimental arrangement in MRI. The Z and Y axis are in the plane of the paper. The axis X, is perpendicular, to the plane of the paper

$$ZQC(Pure) = (1/2)\{2(I_xS_x - IS_y)\} = (1/2)\begin{pmatrix} 0 & 0 & 0 & 1 \\ 0 & 0 & 0 & 0 \\ 0 & 0 & 0 & 0 \\ 1 & 0 & 0 & 0 \end{pmatrix};$$

$$(1/2)\{2(I_yS_x + I_xS_y)\} = (i/2)\begin{pmatrix} 0 & 0 & 0 & -1 \\ 0 & 0 & 0 & 0 \\ 0 & 0 & 0 & 0 \\ 1 & 0 & 0 & 0 \end{pmatrix}.$$

The I_x, S_y, etc. are the 4×4 matrices representing spins. The products I_xS_x, I_yS_x, …are called as the product operators. ZQC and DQC cannot be created with a single pulse applied to an equilibrium spin system. Their creation requires at least two pulses. Application of second 90° pulse converts the spins to the product operators that contains single quantum coherences which are converted electrically into observable magnetization if they are allowed to precess with J coupling. The above glimpse of demonstration, about multiple quantum coherences, gives first hand information, about what the multiple quantum coherence, really means. The ground zero mathematics, presented here, will allow some readers, hopefully, to learn, the meaning of multiple-quantum coherences, through symbols, which will last in memory much longer. As they say once you have seen something, in a tangible form it becomes part of your own imagination system to let you imagine more.

14.2.5 MRI: A Single Proton System

Assume a static magnetic field H_z is applied in the z-direction. The Hamiltonian H_{HAMIL} (total energy operator) of this ideal system of identical spins, in a solution, in terms of the standard, Pauli matrix notation depicting the two energy states, (+1 and −1), of the spin can be written as

$$H_{HAMIL} = (-\mu_p H_z)\sigma_z = (-\mu_p H_z)\begin{pmatrix} 1 & 0 \\ 0 & -1 \end{pmatrix}$$

Table 14.3 CCS

(a) A general 4 æ 4 (2-spin system) matrix with 16 elements can be written as

$$\begin{bmatrix} d_{11} & d_{12} & d_{13} & d_{14} \\ d_{21} & d_{22} & d_{23} & d_{24} \\ d_{31} & d_{32} & d_{33} & d_{34} \\ d_{41} & d_{42} & d_{43} & d_{44} \end{bmatrix}$$

(b)

1
$$\begin{bmatrix} 1 & 0 & 0 & 0 \\ 0 & 1 & 0 & 0 \\ 0 & 0 & 1 & 0 \\ 0 & 0 & 0 & 1 \end{bmatrix}$$
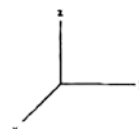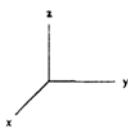
Note First column (spin type), second column (matrix), third and fourth columns (spin directions, spin I and S)

The negative sign means it is the maximum negative binding potential energy between proton spin and the applied static magnetic field. Any excitation of the proton would add a positive (absorption) excitation energy component to this value creating a relatively small population in the next higher energy state of the protons. Here μ_p is the dipole magnetic moment of the proton. $\mu_p = e\gamma\hbar/4m_p = 2.79$ nuclear magneton, γ (the gyromagnetic ratio) = 5.58, e = the charge of the proton (same as that of an electron) and m_p its mass. Application of a small RF (radio frequency) electromagnetic field, $H_x = (H_1 \cos\omega t)$ along the X-direction, creates an additional, time dependent, energy component $H_x = (-\mu_p H_x \sigma_x) = -\mu_p H_1 (1/2)$ [exp $(i\omega t)$ + exp $(-i\omega t)$] σ_x, where H_1 is the amplitude of the RF field. One should remember that we have from complex trigonometry, the relation, $\cos\theta = \{(1/2) (e^{i\theta} + e^{-i\theta})$, $\theta = \omega t$. Here ω is the resonance frequency of the prcession of the proton spins around the static magnetic field applied in the z-direction.

$$H_{HAMIL} = H_{HAMILz} + H_{HAMILx} = \left[(-\mu_p H_z) \begin{pmatrix} 1 & 0 \\ 0 & -1 \end{pmatrix} + (-\mu_p H_x) \begin{pmatrix} 0 & 1 \\ 1 & 0 \end{pmatrix} \right]$$
$$= \begin{pmatrix} \mu p\, H_z & -\mu p\, H_1(1/2)(\exp i\omega t + \exp -i\omega t) \\ -\mu p\, H_1(1/2)(\exp i\omega t + \exp -i\omega t) & -\mu p\, H_z \end{pmatrix}$$

If the resonance condition, $\hbar\omega = 2\mu_p H_z$ is satisfied, there will be a transition between the two spin energy states (up and down), $+\mu_p H_z$ and $-\mu_p H_z$. The population of protons in the two states will not be the same. The higher energy state $+(\mu_p H_z)$ will have population a fraction of that of the ground state There are about 10^{23} spins in a mole of a substance. The excited number of protons would be small. But even a small fraction of 10^{23} would nevertheless have a large absolute value. The static magnetic field H_z makes the spins precess randomly in time around z-axis. The x-direction applied pulsed RF field on the other hand will momentarily tend to rotate the spins along the y direction. The Fig. 14.10 gives a rough idea about the precession of the spins around the z-axis in a laboratory situation. The precession of the spins is due to the static magnetic field applied along the z-axis. They are projected in the x–y plane by applying RF-pulse along

Table 14.4 CCS

I_x	$\begin{bmatrix} 0 & 0 & 1 & 0 \\ 0 & 0 & 0 & 1 \\ 1 & 0 & 0 & 0 \\ 0 & 1 & 0 & 0 \end{bmatrix}$	

Table 14.5 CCS
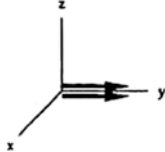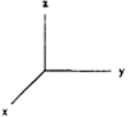
I_y	$\dfrac{i}{2}\begin{bmatrix} 0 & 0 & -1 & 0 \\ 0 & 0 & 0 & -1 \\ 1 & 0 & 0 & 0 \\ 0 & 1 & 0 & 0 \end{bmatrix}$	

Table 14.6 CCS
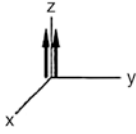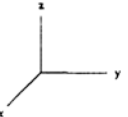
I_z	$\dfrac{1}{2}\begin{bmatrix} 1 & 0 & 0 & 0 \\ 0 & 1 & 0 & 0 \\ 0 & 0 & -1 & 0 \\ 0 & 0 & 0 & -1 \end{bmatrix}$	

Table 14.7 CCS
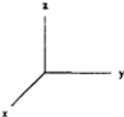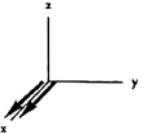
S_x	$\dfrac{1}{2}\begin{bmatrix} 0 & 1 & 0 & 0 \\ 1 & 0 & 0 & 0 \\ 0 & 0 & 0 & 1 \\ 0 & 0 & 1 & 0 \end{bmatrix}$	

Table 14.8 CCS
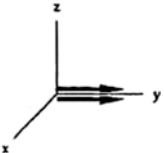
S_y	$\dfrac{i}{2}\begin{bmatrix} 0 & -1 & 0 & 0 \\ 1 & 0 & 0 & 0 \\ 0 & 0 & 0 & -1 \\ 0 & 0 & 1 & 0 \end{bmatrix}$	

Table 14.9 CCS
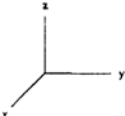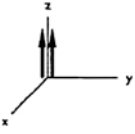
S_z	$\dfrac{1}{2}\begin{bmatrix} 1 & 0 & 0 & 0 \\ 0 & -1 & 0 & 0 \\ 0 & 0 & 1 & 0 \\ 0 & 0 & 0 & -1 \end{bmatrix}$	

Table 14.10 CCS

I_y			
	S_z	$i/4$	$\begin{bmatrix} 0 & 0 & -1 & 0 \\ 0 & 0 & 0 & 1 \\ 1 & 0 & 0 & 0 \\ 0 & -1 & 0 & 0 \end{bmatrix}$

Table 14.11 CCS

I_z			
	S_x	$i/4$	$\begin{bmatrix} 0 & 1 & 0 & 0 \\ 1 & 0 & 0 & 0 \\ 0 & 0 & 0 & -1 \\ 0 & 0 & -1 & 0 \end{bmatrix}$

Table 14.12 CCS

I_z			
	S_z	$i/4$	$\begin{bmatrix} 1 & 0 & 0 & 0 \\ 0 & -1 & 0 & 0 \\ 0 & 0 & -1 & 0 \\ 0 & 0 & 0 & 1 \end{bmatrix}$

Table 14.13 CCS

I_z			
	S_y	$i/4$	$\begin{bmatrix} 0 & -1 & 0 & 0 \\ 1 & 0 & 0 & 0 \\ 0 & 0 & 0 & 1 \\ 0 & 0 & -1 & 0 \end{bmatrix}$

Table 14.14 CCS

I_x			
	S_x	$i/4$	$\begin{bmatrix} 0 & 0 & 0 & 1 \\ 0 & 0 & 1 & 0 \\ 0 & 1 & 0 & 0 \\ 1 & 0 & 0 & 0 \end{bmatrix}$

Table 14.15 CCS

I_y			
	S_y	$i/4$	$\begin{bmatrix} 0 & 0 & 0 & -1 \\ 0 & 0 & 1 & 0 \\ 0 & -1 & 0 & 0 \\ 1 & 0 & 0 & 0 \end{bmatrix}$

Table 14.16 CCS

I_x
  S_y
  $i/4$ $\begin{bmatrix} 0 & 0 & 0 & -1 \\ 0 & 0 & 1 & 0 \\ 0 & -1 & 0 & 0 \\ 1 & 0 & 0 & 0 \end{bmatrix}$

Table 14.17 CCS

I_x
  S_z
  $i/4$ $\begin{bmatrix} 0 & 0 & 1 & 0 \\ 0 & 0 & 0 & -1 \\ 1 & 0 & 0 & 0 \\ 0 & -1 & 0 & 0 \end{bmatrix}$

Table 14.18 CCS

I_y
  S_x
  $i/4$ $\begin{bmatrix} 0 & 0 & 0 & -1 \\ 0 & 0 & -1 & 0 \\ 0 & 1 & 0 & 0 \\ 1 & 0 & 0 & 0 \end{bmatrix}$

Table 14.19 The 9 product operator matrices are

	S_x	S_y	S_z
I_x	I_xS_x	I_xS_y	I_xS_z
I_y	I_yS_x	I_yS_x	I_yS_x
I_z	I_zS_x	I_zS_y	I_zS_z

Table 14.20

(1) Pulses along the y-axis rotating spins through an angle $\theta = \gamma H_1 t$		Transformation
	I_x	$I_x \cos\theta - I_z \sin\theta$
	I_y	I_y
(2) Pulses along the x-axis rotating spins through an angle $\theta = \gamma H_1 t$		The transformation
	I_x	I_x
	I_y	$I_y \cos\theta + I_z \sin\theta$
	I_z	$I_z \cos\theta - I_y \sin\theta$
(3) Precession about the z-axis with frequency ω		Transformation
	I_x	$I_x \cos\omega t + I_y \sin\omega t$
	I_y	$I_y \cos\omega t - I_x \sin\omega t$
	I_z	I_z
J coupling with $\lambda = 1/2\ Jt$	I_x	$I_x \cos\lambda + 2 I_yS_z \sin\lambda$
	I_y	$I_y \cos\lambda - 2 I_xS_z \sin\lambda$
	I_z	I_z

Table 14.21 Immediate application of a 90° pulse ($t_2 = 0$) along the y-axis, is followed by precession and J-coupling

$-I_z$	$\cos(\pi J t_1)$	$\cos(\omega I t_1)$
$-2I_x S_y$	$\sin(\pi J t_1)$	$\cos(\omega I t)$
$+I_x$	$\cos(\pi J t_1)$	$\sin(\omega I t_1)$
$-2I_z S_y$	$\sin(\pi J t_1)$	$\sin(\omega I t)$

Table 14.22 The result from Table 14.21

$2 I_z S_y$	$\sin(\pi J t_1)$	$\cos(\omega I t_1)$	$\cos(\pi J t_3)$	$\cos(\omega S t_3)$
$-S_x$	$\sin(\pi J t_1)$	$\cos(\omega I t_1)$	$\cos(\pi J t_3)$	$\sin(\omega S t_3)$
$-2I_z S_x$	$\sin(\pi J t_1)$	$\cos(\omega I t_1)$	$\cos(\pi J t_3)$	$\cos(\omega S t_3)$
$-S_y$	$\sin(\pi J t_1)$	$\cos(\omega I t_1)$	$\sin(\pi J t_3)$	$\sin(\omega S t_3)$

Table 14.23 Result from Table 14.22 single quantum coherences

$2I_z$	$\cos(\omega I t_1)$	$\sin(\pi J t_1)$	$\sin(\omega I t_3)$	$\cos(\pi J t_3)$
$-2I_x$	$\cos(\omega S t_1)$	$\sin(\pi I t_1)$	$\sin(\omega I t_3)$	$\sin(\pi J t_3)$
$2S_x$	$\cos(\omega S t_1)$	$\sin(\pi I t_1)$	$\sin(\omega s t_3)$	$\sin(\pi J t_3)$
$-2S_y$	$\cos(\omega I t_1)$	$\sin(\pi J t_1)$	$\sin(\omega s t_3)$	$\sin(\pi J t_3)$

Table 14.24 The single operators and the product operators in the spherical basis

1 (unity matrix)			
	S_+	S_0	S_+
I_+	I_+S_+	I_+S_0	$I_+ S_-$
I_0	I_0S_+	I_0S_0	$I_0 S_-$
I_-	I_-S_+	$I_- S_0$	I_-S_-

Table 14.25 SBS

1	$-$	$\begin{bmatrix} 1 & 0 & 0 & 0 \\ 0 & 1 & 0 & 0 \\ 0 & 0 & 1 & 0 \\ 0 & 0 & 0 & 1 \end{bmatrix}$

Table 14.26 SBS

I_0	$-$	$1/2$	$\begin{bmatrix} 1 & 0 & 0 & 0 \\ 0 & 1 & 0 & 0 \\ 0 & 0 & -1 & 0 \\ 0 & 0 & 0 & -1 \end{bmatrix}$

Table 14.27 SBS

I	−1	1/√2
		$\begin{bmatrix} 0 & 0 & 0 & 0 \\ 0 & 0 & 0 & 0 \\ 1 & 0 & 0 & 0 \\ 0 & 1 & 0 & 0 \end{bmatrix}$

Table 14.28 SBS

I_+	+1	1/√2
		$\begin{bmatrix} 0 & 0 & -1 & 0 \\ 0 & 0 & 0 & -1 \\ 0 & 0 & 0 & 0 \\ 0 & 0 & 0 & 0 \end{bmatrix}$

Table 14.29 SBS

S_0	−	1/√2
		$\begin{bmatrix} 1 & 0 & 0 & 0 \\ 0 & -1 & 0 & 0 \\ 0 & 0 & 1 & 0 \\ 0 & 0 & 0 & -1 \end{bmatrix}$

Table 14.30 SBS

S_+	+1	1/√2
		$\begin{bmatrix} 0 & -1 & 0 & 0 \\ 0 & 0 & 0 & 0 \\ 0 & 0 & 0 & -1 \\ 0 & 0 & 0 & 0 \end{bmatrix}$

Table 14.31 SBS

S_-	−1	1/√2
		$\begin{bmatrix} 0 & 0 & 0 & 0 \\ 1 & 0 & 0 & 0 \\ 0 & 0 & 0 & 0 \\ 0 & 0 & 1 & 0 \end{bmatrix}$

Table 14.32 SBS

I_0S_+	+1	1/2√2
		$\begin{bmatrix} 0 & -1 & 0 & 0 \\ 0 & 0 & 0 & 0 \\ 0 & 0 & 0 & 1 \\ 0 & 0 & 0 & 0 \end{bmatrix}$

Table 14.33 SBS

I_0S_-	$_-1$	$1/2\sqrt{2}$

$$\begin{bmatrix} 0 & 0 & 0 & 0 \\ 1 & 0 & 0 & 0 \\ 0 & 0 & 0 & 0 \\ 0 & 0 & -1 & 0 \end{bmatrix}$$

Table 14.34 SBS

I_+S_0	$+1$	$1/2\sqrt{2}$

$$\begin{bmatrix} 0 & 0 & -1 & 0 \\ 0 & 0 & 0 & 1 \\ 0 & 0 & 0 & 0 \\ 0 & 0 & 0 & 0 \end{bmatrix}$$

Table 14.35 SBS

I_-S_0	-1	$1/2\sqrt{2}$

$$\begin{bmatrix} 0 & 0 & 0 & 0 \\ 0 & 0 & 0 & 0 \\ 1 & 0 & 0 & 0 \\ 0 & -1 & 0 & 0 \end{bmatrix}$$

Table 14.36 SBS

I_+S_+	$+21$	$1/2$

$$\begin{bmatrix} 0 & 0 & 0 & 1 \\ 0 & 0 & 0 & 0 \\ 0 & 0 & 0 & 0 \\ 0 & 0 & 0 & 0 \end{bmatrix}$$

Table 14.37 SBS

I_-S_-	-2	$1/2$

$$\begin{bmatrix} 0 & 0 & 0 & 0 \\ 0 & 0 & 0 & 0 \\ 0 & 0 & 0 & 0 \\ 1 & 0 & 0 & 0 \end{bmatrix}$$

Table 14.38 SBS

I_+S_-	0	$1/2$

$$\begin{bmatrix} 0 & 0 & 0 & 0 \\ 0 & 0 & -1 & 0 \\ 0 & 0 & 0 & 0 \\ 0 & 0 & 0 & 0 \end{bmatrix}$$

Table 14.39 SBS

$I_0 S_0$	–	1/4

$$\begin{bmatrix} 1 & 0 & 0 & 0 \\ 0 & -1 & 0 & 0 \\ 0 & 0 & -1 & 0 \\ 0 & 0 & 0 & 1 \end{bmatrix}$$

Table 14.40 SBS

I_-S_+	0	1/2

$$\begin{bmatrix} 0 & 0 & 0 & 0 \\ 0 & 0 & 0 & 0 \\ o & -1 & 0 & 0 \\ 0 & 0 & 0 & 0 \end{bmatrix}$$

Table 14.41 SBS

1. $I_0 \rightarrow [I_0 \cos\theta] - [(i/\sqrt{2}) I_+ \sin\theta \exp(-i\Phi)] - [(i\sqrt{2}) I_- \sin\theta \exp(i\Phi)]$; $I_+ \rightarrow [(1/2) I_+ \cos(\theta)] - [(i/\sqrt{2}) I_0 \sin\theta \exp(i\Phi)] + [(1/2) I_- \cos(\theta) \exp(2i\Phi)]$; $I_- \rightarrow [1/2 I_- \cos(\theta)] - [(/i\sqrt{2}) I_0 \sin\theta \exp(-i\Phi)] + [1/2 I_- \cos(\theta) \exp(-2i\Phi)]$

Only precession about the z-axis with frequency ω

2. $I_+ \rightarrow I_+ \exp(-i\omega t)$; $I_- \rightarrow I_- \exp(i\omega t)$; $I_0 \rightarrow I_z$

Only J coupling

3. $I_+ \rightarrow I_+ \cos\lambda - i\, 2I_+S_0 \sin\lambda$; $I_- \rightarrow I_- \cos\lambda + i\, 2I_-S_0 \sin\lambda$; $I_0 \rightarrow Iz$

Constant, $\lambda = 1/2\, J\, t$, one gets, *Note* $\Phi =$ is the axis about which the pulse field is applied, it is 0 for the x-axis, $\pi/2$ for the y-axis, π for the $-x$ axis, and $3\pi/2$ for the $-y$ axis

Table 14.42 SBS

1	$-0.5\, I_0 \cos(\pi Jt) \exp[-i(-\phi_1 + \phi_2)]$
2	$-0.5\, I_0 \cos(\pi J t) \exp[-i(\phi_1 - \phi_2)]$
3	$-0.354\, i\, I_- \cos(\pi Jt) \exp[-i(-\phi_1)]$
4	$+0.354\, i\, I_- \cos(\pi Jt) \exp[-i(\phi_1 - 2\phi_2)]$
5	$-0.354\, I_+ \cos(\pi Jt) \exp[-i(\phi_1)]$
6	$+0.354\, I_+ \cos(\pi J t) \exp[-i(-\phi_1 + 2\phi_2)]$
7	$-0.707\, I_0 S_- \sin(\pi Jt) \exp[-i(\phi_1)]$
8	$+0.707\, I_0 S_- \sin(\pi Jt) \exp[-i(\phi_1 - 2\phi_2)]$
9	$+0.707\, I_0 S_+ \sin(\pi Jt) \exp[-i(\phi_1)]$
10	$+0.707\, I_0 S_+ \sin(\pi Jt) \exp[-i(\phi_1 + 2\phi_2)]$
11	$+0.5\, i\, I_- S_- \sin(\pi Jt) \exp[-i(\phi_1 - \phi_2)]$
12	$-0.5\, I_- S_- \sin(\pi Jt) \exp[-i(\phi_1 - 3\phi_2)]$
13	$+0.5\, I_+ S_- \sin(\pi J t) \exp[-i(-\phi_1 + \phi_2)]$
14	$+0.5\, I_+ S_- \sin(\pi Jt) \exp[-i(\phi_1 - \phi_2)]$
15	$-0.5\, I_- S_+ \sin(\pi Jt) \exp[-I(-\phi_1 + \phi_2)]$
16	$-0.5\, I_- S_+ \sin(\pi Jt) \exp[-i(\phi_1 - \phi_2)]$
17	$+0.5\, I_+ S_+ \sin(\pi Jt) \exp[-i(-\phi_1 + 3\phi_2)]$
18	$+0.5\, I_+ S_+ \sin(\pi Jt) \exp[-i(\phi_1 + \phi_2)]$

the x-direction. One can work out the status of the spins at any time t by applying to the brain (mathematically to the Hamiltonian, H) the rotation and time evolution operators.

14.2.6   Sixteen Spin Matrices of the Two Spins (I and S) System: Cartesian Coordinate System (CCS)

This section is written for those readers who wish to learn more about the use of mathematical description of the density matrix concept. The description here is however restricted to a symbolic mathematics only. Suppose the ensemble of spins (two spins I and S here) is irradiated with RF 90° pulses in transverse direction. This means the RF pulses are applied in perpendicular (i.e. in the x or y) directions with respect to (wrt) to the Z-direction. The equilibrium of the Z-spins is now partially projected on the X–Y plane. This net transverse magnetization is subsequently observed as a field induction decay (FID), i.e. the decay of the spins in the X–Y plane, and ultimately back to their original equilibrium position, in the Z-direction. A density matrix for a two spin system is a 4×4 matrix, whose elements describe the state of the system at any instant of time (see Table 14.3a). The existence of non-zero off diagonal elements d_{12}, d_{21}, d_{24}, d_{42}, d_{13}, d_{31}, d_{34}, and d_{43}, means that the application of the 90° pulses has induced multi-quantum transitions. As an example, the d_{12} indicates, the transition $\alpha\alpha \rightarrow \beta\beta$, and d_{21}, indicates $\beta\alpha \rightarrow \alpha\alpha$ The creation of the y-magnetization, is a result of transforming, the collection of spins precessing about the Z-axis, with random phase, at thermal equilibrium, by a rotation through 90° degree. This now becomes (in the X–Y plane), a collection of spins with coherence in the X–Y plane .

   A resultant net magnetization along the Y-axis is consequentially exhibited by this new system. The above "coherent superposition" of states is called as 'single quantum coherence'. This is what is used as an FID, in the form of, e.g., the T_2 (transverse) relaxation, weighted image, in the conventional MRI. It is possible with more subsequent pulses, to cause the off diagonal elements, d_{14} and d_{41}, d_{23} and d_{32}, etc., in the density matrix, to become nonzero. It will create paths for a double quantum coherence (DQC) or a zero quantum coherence (ZQC). The non-zero matrix elements at positions d_{23} and d_{32} will represent ZQC, whereas the elements at d_{14} and d_{41}, the DQC. Neither the ZQC nor the DQC can be observed directly. What rotations of spins will cause ZQC and DQC to become observable, can be worked out, mathematically. There are 6 basic single Cartesian angular momentum operators I_x, I_y, I_z, S_x, S_y, S_z for the two spin I and S. They represent observable single quantum magnetization. Then there are, the 9 **product operators**, constructed from these 6 basic operators. These are (I_xS_x, I_xS_y, I_xS_z); (I_yS_x, I_yS_y, I_yS_z); (I_zS_x, I_zS_y, I_zS_z). One should also count the identity operator for completeness sake. (1) The function of the **identity operator** is that any operator (matrix) when multiplied with it, just remains the same. There are thus 16 matrix

Table 14.43 DQF J-coupling and precession neglected

1	$0.177I_- \cos(\pi Jt_1) \cos(\pi Jt_3) \exp[-i(\phi_1 - 2\phi_2)] \exp[-i(\omega It_1 - \omega It_3)$
2	$0.354I_- \cos(\pi Jt_1) \cos(\pi Jt_3) \exp[-i(\phi_1 - \phi_2 - \phi_3)] \exp[-i(\omega It_1 - \omega It_3)]$
3	$0.177I_- \cos(\pi Jt_1) \cos(\pi Jt_3) \exp[-i(\phi_1 - 2\phi_3)] \exp[-i(\omega It_1 - \omega It_3)]$
4	$-0.177I_- \cos(\pi Jt_1) \cos(\pi Jt_3) \exp[-i(-\phi_1)] \exp[-i(-\omega It_1 - \omega It_3)]$
5	$0.354 I_- \cos(\pi Jt_1) \cos(\pi Jt_3) \exp[-I(-\phi + \phi - \phi_3)] \exp[-i(-\omega I t_1 - \omega I t_3)]$
6	$-0.177I_- \cos(\pi Jt_1) \cos(\pi Jt_3) \exp[-i(-\phi_1 + 2\phi_2 - 2\phi_3)] \exp[-I(-\omega It_1 - \omega It_3)]$
7	$-0.177I_- \sin(\pi Jt_1) \sin(\pi Jt_3) \exp[-i(\phi_1 - 2\phi_2)] \exp[-i(\omega It_1 - \omega It_3)]$
8	$-0.088I_- \sin(\pi Jt_1) \sin(\pi Jt_3) \exp[-i(\phi_1 - 3\phi_2 + \phi_3)] \exp[-i(\omega It_1 - \omega It_3)]$
9	$-0.177 I_- \sin(\pi Jt_1) \sin(\pi Jt_3) \exp[-i(\phi_1 - \phi_2 - \phi_3)] \exp[-i(\omega It_1 - \omega It_3)]$
10	$-0.177I_- \sin(\pi Jt_1) \sin(\pi Jt_3) \exp[-i(\phi_1 - 2\phi_2)] \exp[-i(\omega It_1 - \omega It_3)]$
11	$-0.088I_- \sin(\pi Jt_1) \sin(\pi t_3) \exp[-i(\phi_1 + \phi_2 - 3\phi_3)] \exp[-i(\omega It_1 - \omega It_3)]$
12	$0.177I_- \sin(\pi Jt_1) \sin(\pi Jt_3) \exp[-i(-\phi_1)] \exp[-i(-\omega It_1 - \omega It_3)]$
13	$-0.088I_- \sin(\pi Jt_1) \sin(\pi Jt_3) \exp[-i(-\phi_1 - \phi_2 + \phi_3)] \exp[-i(\omega It_1 - \omega It_3)]$
14	$-0.177I_- \sin(\pi Jt_1) \sin(\pi J t_3) \exp[-i(-\phi_1 + \phi_2 - \phi_3)] \exp[-i(-\omega It_1 - \omega I t_3)]$
15	$0.177 I_- \sin(\pi J t_1) \sin(\pi Jt_3) \exp[-i(-\phi_1 + 2\phi_2 - 2\phi_3)] \exp[-i(-\omega It_1 - \omega It_3)]$
16	$-0.088I_- \sin(\pi Jt_1) \sin(\pi Jt_3) \exp[-i(\phi_1 + 3\phi_2 - 3\phi_3)] \exp[-i(-\omega It_1 - \omega It_3)]$

spin operators to describe the 2-spin (I, S) system. and are tabulated in Tables 14.3b.

The individual operators (spins) I_x, S_x, etc., on the application of a RF pulse, give rise to single quantum coherences and form the basis of conventional MRI. But a sequence of pulses, precession, J-interaction, create in addition, product operators I_xS_x, I_yS_x, …etc. These give rise to multi-quantum coherences (MQCs) i.e. ZQCs, DQCs.etc. These coherences were suspected present in conventional MRI for long time in MRI. But they were considered as unexplainable nuisance and were ignored. It is only very recently that their origin has been fully understood, and now forms the basis of a new independent imaging technique, the QMRI. This work tries to illustrate, in a simple language, the meaning of the MQCs and the QMRI. The origin of QMRI lies in the interaction of spins at atomic and molecular level. Under the application of RF pulses, the spins interact and produce in space and time, an ordered structure of pathways, the coherence transfer pathways (CTPs) along which paths the selective constructive interference takes place. These interferences lead to unique signals, with information on molecular level. One should note that first single RF pulse, only excite the individual spins. It is only during, the interval in-between the subsequent pulses (the relaxation time) when the spins have time to precess and perform J-coupling, that the MQCs emerge. The brain is like a heterogeneous mixture or say a reactor of spins. When RF radiation is applied, spins go into excited states, and interact. It is through these interactions, and the receiver being tuned, to the selected coherences, that a data, in space and time, about quantum coherence imaging, can be created. One should note here the **product operators** are simple mathematical representations of cross-coherences, between spins. It would be very instructive to work out, what is physically operative behind these coherences, at every step of time.

The **product operator formalism** is fully developed now. One can pictorially work out, intermediate steps, by using actions of rotation, precession, J-interaction, etc. The reader should refer to a standard text book on MRI, for more illustrations. The pictorial representations, can depict, how the spins rotate under RF pulses, in different directions, to produce the final result. It is simple to demonstrate how each of the product operators behaves under the action of an arbitrary pulse sequence as a result of precession and J-coupling. The product operator technique makes it easier to visualize progress in the behavior of spins under the effect of different kinds of operations. It is a more or less standardized and an easier to follow procedure. The equations have been summarized, following a set of quantum angular momentum algebraic rules. Tables 14.1–14.43 (in Appendix B) list a brief summary of the algebraic results, important in the spin 2-system for the possible multi-quantum coherences, in Cartesian and spherical coordinate reference systems. It is important to mention here that each spin single, double, triple et., are assigned a matrix with unique placement of various angular momentum of spins in the elements of the matrix. In the MRI, they interfere, and produce, multi-quantum, orders. Theoretically the structure of the orders and their contribution towards MRI can be predicted, by manipulation of product operators of different orders. The Cartesian coordinate system (CCS) of handling matrices and their products, in the prediction of results, provides a visual picture of every step in progress. The spherical basis system (SBS) is also discussed here. It reduces the volume of computations, and is more efficient, in handling, mathematically. But it lacks in pictorial depiction of the results, as the multi-quantum coherence progresses.

Together with the unit matrix 1(identity matrix), the 6 single spin matrix operators I_x, I_y, I_z, S_x, S_y, S_z, and the above 9 product operators, make a total of 16 operators. A two spin system can be used to analyze most of multi-spin system. This is because higher order systems can be broken down into a 2-spin system. The I_x, I_y, I_z, S_x, S_y, S_z represent the 6 directly observable single quantum magnetizations. The 9 product operators tabulated above can not be observed directly. They have a mixture of zero and double quantum coherences.

The effect of application of pulses, rotation, precession and J coupling, in Cartesian product operators can be tabulated as follows.

The RF pulses applied in the system are applied with an amplitude = H_1. Other teems that are important in the system, are γ = gyro magnetic ratio, t = the time of the pulse, ω the precession frequency of the spin, and J represents the J-coupling among the spins. The product operators containing product of two or more angular momentum operators, contain antiphase (x, y, z) magnetization for the two I, S, spins. These hidden antiphase magnetizations do not become clear directly. They become apparent mathematically, through the effects of precession and J-coupling.

14.2.7 *Two Dimensional Homonulcear correlation spectroscopy (COSY): Cartesian Coordinate System (CCS)*

Homonuclear COSY: One, first applies, a 90° pulse along x-axis, to the I and S spins (these are initially aligned along z-direction) at t = 0. Then there is a relaxation period of time t_1. During the t_1 period, there will be precession and J-coupling among the spins. It is followed by a second 90° to I, S, spin pulses, along x-axis, applied at the end of t_1. Final precession and J-coupling takes place over the second interval of time t_2. The reader is referred to the Fig. 2.12, for the pictorial representation of the pulse sequence, and the resulting, quantum coherences. In a symbolic mathematics formulation, one can write the steps of the operations as follows. To start with there are single quantum coherences (SQC) = $[I_x, I_y, I_z, S_x, S_y]$. After the period of time t_2, there is a mixture of the, Zero and DQCs. Their presence is hidden inside the combination operators, $[2 I_x S_x, 2 I_x S_y, 2 I_x S_z]$; $[2 I_y S_x, 2 I_y S_y, 2 I_y S_z]$; $[2 I_z S_x, 2 I_z S_y]$. These are 13 term in all. The $I_z S_z$ matrix is not included. We now see that with two pulses and two precession periods, we have a mixture of single, zero and double quantum coherences. If this were a correlation spectroscopy (COSY) experiment alone, the receiver is turned on after the second pulse, to collect the MQCs data. We place the detector along the y axis.

Double Quantum Filter (**DQF**): One needs to be concerned finally only with the I_y and S_y terms. In the detected signal we will have the diagonal peaks at ωI, ωI, ωS, ωS and the off diagonal peaks, at ωI, ωS, ωS, ωI, called as the correlation peaks. The J-coupling produces multiplets, with the diagonal peaks 90° out of phase with respect to the cross peaks. One can show mathematically that the operator terms $(I_x S_x)$, $(I_y S_y)$, $(I_x S_y)$ and $(I_y S_x)$, contain zero and double quantum coherences. It is possible to work out, what rotation operations, will produce, the nonzero multi-quantum coherence, elements, d_{14}, d_{41}, d_{23} and d_{32}, in the density matrix. They can not be referred to as pure zero and pure double quantum coherences. In order to obtain pure zero (ZQC) and pure double quantum coherences (DQC) one need to perform the following linear combinations.

$$\text{Pure DQC} : 1/2(2I_xS_x - 2I_yS_y) = 1/2 \begin{bmatrix} 0 & 0 & 0 & 1 \\ 0 & 0 & 0 & 0 \\ 0 & 0 & 0 & 0 \\ 1 & 0 & 0 & 0 \end{bmatrix};$$

$$\text{Pure DQC} : 1/2(2I_xS_y - 2I_yS_x) = i/2 \begin{bmatrix} 0 & 0 & 0 & -1 \\ 0 & 0 & 0 & 0 \\ 0 & 0 & 0 & 0 \\ 1 & 0 & 0 & 0 \end{bmatrix}$$

$$\text{Pure ZQC}: 1/2(2I_xS_x - 2I_yS_y) = 1/2 \begin{bmatrix} 0 & 0 & 0 & 1 \\ 0 & 0 & 0 & 0 \\ 0 & 0 & 0 & 0 \\ 1 & 0 & 0 & 0 \end{bmatrix};$$

$$\text{Pure ZQC}: 1/2(2I_yS_x - 2I_xS_y) = i/2 \begin{bmatrix} 0 & 0 & 0 & -1 \\ 0 & 0 & 0 & 0 \\ 0 & 0 & 0 & 0 \\ 1 & 0 & 0 & 0 \end{bmatrix}$$

These are however not directly observable. They can be detected only when there are two or more J-coupled spins. Their creation requires at lest two pulses. Application of the second 90° pulse, converts the above operators, to product operators that contain single-quantum coherences, which are converted into observable magnetization, if they are allowed to precess with J-coupling. At the end of the second pulse in a COSY experiment, before precession and J-coupling, the product operator expression for spin I, (and for S spin replaced I with S) is as in Table 14.21.

It converts the double quantum coherence containing term $2I_xS_y$. The result that follows, is shown in Table 14.22.

This contains an observable signal. It is possible to construct a double quantum filter such that the only signal that survives from the magnetization, is by passing through the double quantum filter (DQF). This is done by four separate phase cycling experiments, by sending pulses, along x, y, −x, −y, directions respectively. Then each time, with a separate setting for the receiver, along x, −y, −x, y, directions, an FID (field induction decay) signal is recorded. The FIDs are then summed for the final result. The complete signal is as follows. The diagonal, 1st and 3rd terms, and the cross peaks, 2nd and 4th terms, have the same phase.

14.2.8 Spherical Basis System (SBS) for Two Spins (I and S)

It is seen that spherical basis for the expansion of the density matrix is much better suited for the analysis of phase cycling, and design of a pulse sequence, for a desired purpose. In this system each product operator is associated with a single coherence level or order. Its disadvantage lies in its inability to provide vector diagrams to visualize the vector representation. The I and S spins are now written as the linear combinations, as below. $I_+ = (-1/\sqrt{2}(I_x + i\,I_y)$; $I_0 = I_z$; $I_- = (-1/\sqrt{2}(I_x - I_y)$; $S_+ = (-1/\sqrt{2}(S_x + S_y)$; $S_0 = S_z$; $S_- = (-1/\sqrt{2}(S_x - S_y)$. The 15 basic operators including the product operators I_+S_+, etc., in this spherical basis (coordinate) system are tabulated in the Table 14.24. It can be seen that the pure double-quantum coherencies is now represented by I_+S_+ and I–S_. The pure zero-quantum coherence is represented by I_+S_- and I–S_+ and the single quantum coherence is represented by

terms such as I_+, I_-, $I_0 S_+$ and $I_0 S_-$ The coherence order is given by the sum of the indices. One immediate benefit of the spherical representation is the ability to use a single operator to obtain the phase sensitive quadrature signal from the density operator, rather than simply I_x or I_y. If the real part of the quadrature signal is along the y-axis and the imaginary part is along the x-axis, then a pure absorption signal is obtained from $I_y + i\, I_x = i\, \sqrt{2}\, I_0$ ($I_0 = I_z$).

The 16 (including the unit matrix) operators and their matrices in spherical basis are presented in the following Tables 14.25–14.40: Spherical Basis System (SBS) for two spins (I and S) O = operator (1st column); C – coherence (2nd column); M = Matrix (3rd column).

One should note in this system the structure of the product operators has information about the coherence level. For example the pure double quantum coherence (DQC) is represented by $I_+ S_+$ and $I_- S_-$. The pure zero quantum coherence (ZQC) on the other hand is represented by $I_+ S_-$ and $I_+ S_-$. It is clear that the coherence order is given by sum of the two indices on the product operators. This table below lists the effect of application of pulses, precession, and J-coupling on spherical operators. Pulse is applied along the Φ axis (e.g. x, y, −x, −y), through an angle $\theta = \gamma\, H_1\, t$ (e.g. $\theta = \pi/2$). Here γ = gyro-magnetic ratio, H_1 = static magnetic field applied along Z-direction, and t is the time of the pulse.

Following is the effect of application of a pulse to a single spin system. One obtains the following transformations for the spins. We term Φ axis in general as an axis in the X–Y plane along any direction, from 0 to 360°. Its direction at a particular angle is wrt (with respect to) to the = +X-axis. Pulse along the general Φ axis leads to the following representative expressions.

Pulse along the general Φ axis leads to the following representative expressions.

14.2.9 Spherical Basis: Effect of Application of a Pulse Along a General φ Axis, Precession About z Axis and the J-Coupling

A simple Illustration: correlation spectroscopy (COSY): Consider application of 90° pulse along the x-axis ($\phi_1 = 0$) to the I spins of a two spin (I, S) system. By using Table 14.41, for the case I_0, and the case of rotation only, with no precession and no J-coupling, at equilibrium, converts I_0, to [0.707 i {exp(−i ϕ_1)}I_-] − [−0.707i {exp−(i ϕ_1)} I_+]. The symbol ϕ_1, has been retained in the final result. It is jut to emphasize that in the spherical coordinate system, the phase of the system appears in the final result, which is 0, i.e. along the x-axis, in this case. The result is in equal parts of I_+ and I_-. This means that the zero quantum coherence (ZQC) has been converted into equal parts of +1 and −1 coherence. Precession under the influence of chemical shift can be ignored. It does not affect the coherence level. But it does multiply the coherence by an additional phase factor.

The J-coupling also does not affect the coherence level. But it does create a new two-spin product-operator term necessary for movement to a coherence level other
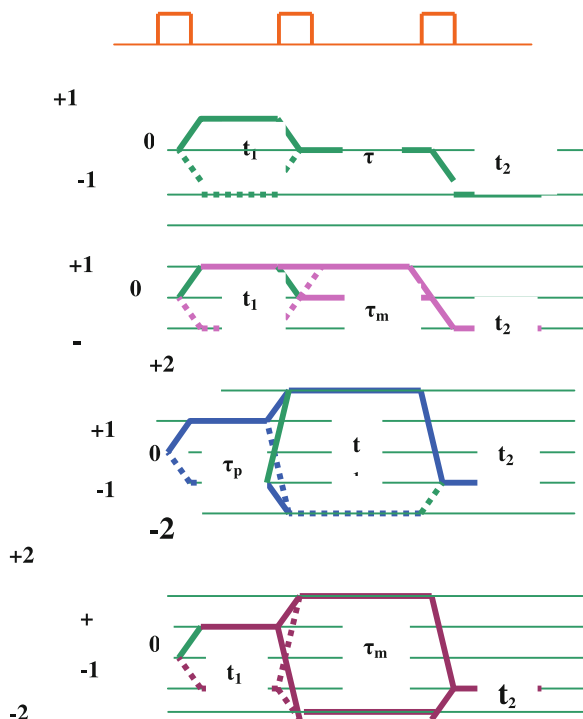
Fig. 14.11 It shows coherence-transfer maps (CT maps) for various 2D experiments involving three pulses. Solid lines indicate pathways that involve a single-order p in the evolution period. If pure phase lineshapes are not essential (e.g., if composite lineshapes or absolute-value plots are acceptable), it is sufficient to select the pathways, shown by solid lines. Mirror image pathways with −p, in t_1, are indicated, by dashed lines. For pure phase spectra (i.e. pure 2D absorption lineshapes), both solid and dashed pathways must be retained. There are shown, four experimental schemes. The above result can be interpreted as follows. **a** 2D exchange spectroscopy (NOESY = Nuclear Overhuser Exchange Spectroscopy), **b** relayed correlation spectroscopy (pathways shown for fixed mixing interval τ), **c** double-quantum spectroscopy and **d** 2D correlation spectroscopy with double quantum filter ($\tau_m = 0$)

than +1, 0, −1, with the application of another pulse. Continuing with the single pulse applied to I_0, as shown above, and including the J-coupling, one observes that new coherence levels of −1 (I_-S_0) and +1 (I_+S_0) are created, but no additional coherence transfer pathway(CTP) is seen, as shown. The J-coupling leads to −0.707 i [cos (π J t)] exp−(− i ϕ_1) I_- −; 0.707 i [cos (π J t)] exp−(− i ϕ_1) I_+ +; 1.41 (I_-S_0) sin (π J t) exp − (− i ϕ_1)} −; 1.41 (I_+S_0) sin (π J t) exp −(−i ϕ_1). All the four terms are the single quantum coherences (SQCs) and the CTP is only −1 (the coefficient of i ϕ_1). It is the application of the second 90° pulse, that creates, additional CTPs, for the same coherence level. This is exemplified in B10 below.

14.2.10 Spherical Basis COSY: Effect of Application of Two 90° Pulses Along x Axis to the I Spins of a Two Spins (I and S) System

In the simple case of correlation spectroscopy (COSY) as in B9, the first, $\theta = \pi/2$ pulse with phase ϕ_1 was applied to the I_0 spin. No spin and no precession, but J-coupling was included. Now we apply a second $\pi/2$ pulse, and then applying J-coupling, neglecting precession, at the moment. One ends up with 18 term as shown in the Table 14.42. We can notice the existence of the coherence levels, from −2 to +2, including zero, single and double-quantum coherences. An important feature to observe is that, each term contains, not only the coherence level (e.g. for $I_+S_+ = 2$), it also gives information, about the coherence transfer pathway (CTP) that is followed. As a typical example in the entry 1, the coherence level is zero (I_0), whereas the CTP is −1 to +1, i.e. the coefficients of ϕ_1 and ϕ_2 respectively (see Table 14.42).

The advantage of retaining the pulse phase factors ϕ can now be seen. Each term contains not only the coherence level in the product operator (e.g. a typical $I_+ S_+$), but also the coherence transfer pathways are also indicated in the exponent, that contains the pulse phases. For example **entry** 18, above, has a coherence level of +2 (indicated by $I_+ S_+$). This was arrived at with a, +1 coherence transition, with the first pulse, indicated by +1, in the coefficient for ϕ_1. Also there is a, +1 coherence transition with the second pulse, indicated by + 1coefficient for ϕ_2. In contrast the entry 17, has a coherence level of +2 (I_+S_+), but its coherence transfer pathway is −1 for the first pulse and +3 for the second pulse (see Table 14.42 [3]).

14.2.11 Spherical Basis: Double Quantum Filter (DQF): Correlation Spectroscopy (COSY) Two Spin System/ Coherence Pathway Selection by Phase Cycling

Analysis of the DQF COSY experiment, see Fig. 14.9, using the spherical basis with a two spin system. The analysis is briefly represented by the Table 14.43 [3]. Here t_2.is assumed to be so brief, and the J-coupling and precession are neglected, during t_2.

The four underlined terms represent the I_- single quantum coherences (in time t_3) that existed as double quantum coherence between the second and the third pulses. The coherence transfer pathways (CTPs) for these 4 items are diagramed in Fig. 14.11. One needs to design a phase cycle to selectively accumulate only the coherences that pass though the desired pathways. We need to carry out several experiments, in order to, select a particular coherence pathway, and eliminate others. Selection of a particular coherence pathway of interest is accomplished by setting the receiver accordingly. In the above selected, term 11, one chooses the +1, +1, −3 pathway (or say phases). It requires setting the receiver such that, $e^{rec} = e^{-i(\Phi_1 + \Phi_2 - 3\Phi_3)}$. Thus the detector

phase is, $\Phi_{rec} = -(1.\Phi_1 + 1.\Phi_2 - 3.\Phi_3)$. The Φ_1, Φ_2 and Φ_3 are the phases of the three pulses. The selectivity of the phase cycle that is required for a given pulse is determined by the size of the desired coherence step. In the above example, the transfer steps that one wants to retain, with the third pulse, in a DQF COSY, experiment are, +1 and −3. We need to eliminate all other transfer steps, between +1 and −3, for this electivity. The selectivity required therefore is 4. The phase increment $\Delta\Phi$ for the phase cycle is, $\Delta\Phi = 2\pi/N$. Here N = 4 is the selectivity, for the particular case chosen. The phase of the third pulse, needs to be incremented, through the cycle, 0 (x), $\pi/2$ (y), π (−x) and $3\pi/2$ (−y). The receiver phase will be set at x, −y, −x, y.

14.2.12 Multiple Coherence Transfer Pathways: Selection Rules

In an ensemble of the spins, like in our brain, there are nuclei with different identities. These can be nuclei, with different atomic numbers, i.e. different numbers of protons in the nucleus, or mass numbers (equal to total mass of the proton an neutrons inside the nucleus). When they are present near to each other, they affect each other, due to the proximity. This group of atoms and nuclei, in a molecule, establish an equilibrium, quantum energy structure, within the molecule. On the other hand interaction between the neighboring molecules establishes a kind of a bigger multi-quantum energy structure we call it a macromolecule structure. It is representative of the nearby groups of molecules, a resultant quantum structure [26, p. 116]. Suppose we now apply a 90° non selective pulse (normally a rectangular pulse with wide band) to this group. What non selective means is that the frequency band width selected for the pulse, is wide enough, to excite a much wider group of atoms and molecules, rather than just a specific atom or a molecule. The atoms and molecules are then allowed to relax, over a period of time τ. A second pulse, which can be of 90°, and may be with a flip angle say β, is subsequently applied. The spins of nearby electrons and atoms have a chance to work together (behave coherently) now. Their energy levels behave as if were of the group (macromolecule). In this group there can be interaction between the atoms and molecules, quantum mechanically. This interaction can be a constructive one or a destructive one. The group follows some selected coherence transfer paths, allowed by quantum selection rules, for the resultant angular momentum of the group. This is expected to have +1, 0, −1 quantum numbers. Immediately after the second pulse, application of a third 90° pulse, would generate coherence transfer pathways (CTPs) with possible quantum numbers +2, +1, 0, −1, −2.

One should note here in normal voxel (of size ≥ 1 mm^3) used in conventional MRI, there would, several macromolecules, allowing there influence, spawning on distance scale, from 1μ (10^{-6} m) to 1 mm. Multi-quantum CTPs can only be experienced within this kind of distance scale. In voxel of size cm ^{3} and larger, one can only get a map imaging of the brain, with no microscopic details. One can keep on applying further (one number higher than the order of quantum coherence

required) pulses to generate higher and higher order of quantum coherences. This in principle seems simple to achieve. But in actual practice a lot more care is required. Firstly the receiver of the signals has to be fine tuned to the order desired, and rejection of others. Secondly one needs to follow the procedure of phase encoding and cycling to keep alive the desired CTPs and annul others. Phase encoding is performed by applying magnetic field gradient pulses, normally in the Y-direction. For each phase nodding then phase cycling s performed. What it means is that we direct the pulses on the spins, over four different quadrant angles $0, \pi/2, \pi, 3\pi/2$, of the X–Y plane, and keep on repeating this process, to allow build up of the desired coherences and elimination of the others. One should note that coherence is created by transverse magnetization i.e. by projection of the spins in the X–Y plane. Suppose there are a pair of eigen- states i.e. energy states with an arbitrary difference in quantum numbers $p_{rs} = M_r - M_s$. The transverse magnetization corresponds to a particular class of coherence associated with a change in quantum number p. The coherences can be described as a coherent superposition of the two eigen-states as $\Psi_{rs} = a_r | r > + a_s | s >$. The bra and ket are symbols, commonly used, in the field of quantum mechanic (QM), and refer to the two different energy states of a single or a group of atoms. The behavior of an ensemble of spins in a confined space is analyzed through the treatment of the density matrix operator concept.

This work would be out of place to go into the details of the quantum mechanics of the density matrix. The reader is referred to a standard text on quantum mechanics on this subject. A brief description in the present context is as follows. In terms of the density operator σ, a coherence between the states, is expressed by the existence of non-zero density matrix elements. These elements, indicate a transition in progress between two connected states. Each transition is associated with two opposing coherences σ_{rs} and σ_{sr}, with coherence orders of opposite sign. The coherence σ_{rs} conserves its quantum number p_{rs} in the course of free precession. RF (radio frequency) pulses induce a transfer between coherences σ_{rs} and σ_{tu}, a process that may change the coherence order. One can write the various terms of the density operator according to the coherence order of p, $\sigma_t = \sum_p \sigma_t{}^P(t)$. For a system of K-spins 1/2, p extendsfrom –K to K. The characteristic properties of coherence of order p, are determined by the transformation, under rotations, about the z-axis; $[\exp\{-i\psi F_z\}\sigma^P \exp\{i \psi F_z\}] = [\sigma^P \exp\{-i p\psi\}]$, where $F_z = \sum_{k=1}^{N} I_{kz}$ is the total number of spins aligned along the z-direction. It is common in MRI literature, to represent the sequence of events, in an experiment, by the so called 'coherence transfer map'.

A pictorial representation in the Fig. 14.10, of the CTPS, is a typical example, for illustration. The free precession proceeds within the levels of the CTP, while pulses may induce transitions between orders. The route of a particular component of the coherence is, according to the CTP, for the coherence. There are four common techniques in practice involving three consecutive CTPs. Apart from the incrementation of the intervals in the course of the experimental sequence these methods merely differ in the selection of CTPS. A single pathway suffices if absolute value spectra or phase-sensitive spectra with composite (phase twisted) lineshapes are acceptable. The 'mirror image' pathways (dashed lines) must be retained
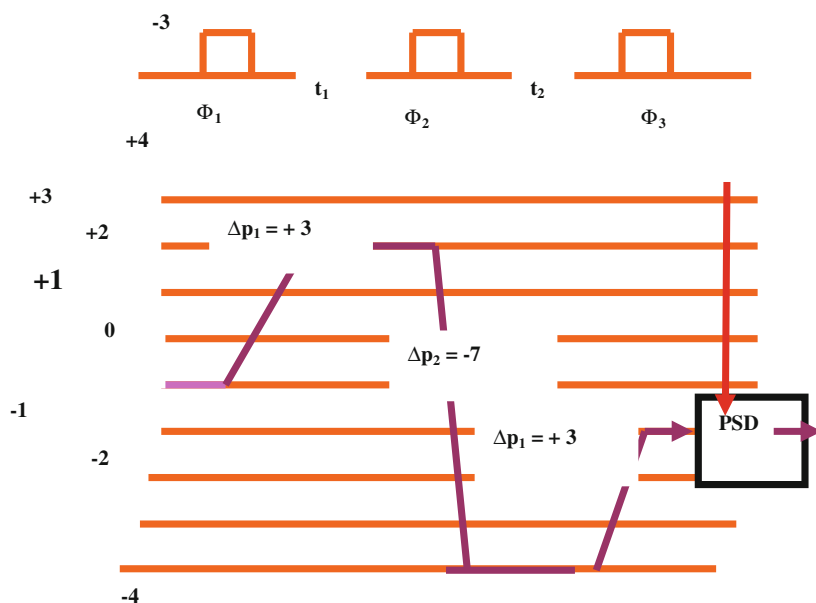
Fig. 14.12 $\Delta p = \Delta p_f$ (**final**) $- \Delta p_i$ (**initial**). The selection of a coherence transfer pathway, is characterized, in the above hypothetical example, by the changes in coherence order $\Delta p_1 = +3$, $\Delta p_2 = -7$, and $\Delta p_3 = +3$. It can be achieved by cycling the phases of the three coherence transfer pulses and by shifting the phase of the reference channel of the phase sensitive detector (**PSD**). The dynamic processes within a molecule or in an intermolecular situation are determined by more than one processes. The most dominant ones can be the molecular relaxation, molecular diffusion, the chemical exchange, and the magnetization exchange, by cross-relaxation, leading to nuclear Overhauser (NOE), processes. These processes are governed by very similar principles

simultaneously if pure phase spectra (i.e. pure 2D absorption lineshapes) are essential. It is important to note that the order $p = 0$ may contain Zeeman polarization (I_{kz}), longitudinal scalar or dipolar spin order ($I_{kz}I_{lz}$) and zero-quantum coherence ($I_k^+I_l^-$). This is particularly relevant for 2D exchange spectroscopy Fig. 14.11a [26, p. 116]. In the case of delayed magnetization transfer Fig. 14.11b [26, p. 116], the delay τ can be kept constant, in which case the sign of the coherence in τ is irrelevant and the two CTPs can be allowed simultaneously. It is also possible to vary τ, in concert with t_1 (duration of the first pulse), in which case, the pathway selection determines, whether the ω_1 (one frequency selection) domain will contain sums or differences of the chemical shifts.

14.2.13 Multi-Quantum Spectroscopy

In multi-quantum spectroscopy refer to (Fig. 14.11a–d) [26, p. 116] it is shown that one has the option of observing both +p and –p coherences in the evolution period,

or one may restrict the transfer as shown by the solid lines. In correlation spectroscopy with multi-quantum filters [7], it is not necessary to select the sign of the coherence order in the τ_m interval. One has the option of selecting only $p = + 1$ coherences in the evolution period.

In general a complete coherence pathway is specified by a vector, $\Delta p = [\Delta p_1, \Delta p_2, \Delta p_3, \ldots]$. Here $\Delta p_i = p'(t_i^+) - p(t_i^-)$; and $p(t_i^-) =$ coherence immediately before the pulse and $p'(t_i^+)$, immediately after the pulse. The output signal S(t) consists of all possible contributions of all pathways Δp. A non vanishing signal happens when $\Delta p'(\text{receiver}) = \Delta p$ (transmitter). However, since the selectivity is determined by the number N_i of phase increments, there are a manifold of pathways that survive the selection process. Because the maximum order of coherences $p_{max} <= K$ (a system with K spins 1/2) and because the amplitude of coherence transfer into very high orders is small, it is usually possible to retain a unique pathway by relatively small increment number N_i. One adopts shifting of the phase of the receiver channel. Figure 14.12 (Fig. 4) is a rough pictorial representation of the typical case discussed above. All pathways must begin with $p = 0$ and are assumed to end with $p = -1$, to be observable. The sum of the components is fixed. This is given as $\sum_i \Delta p_i = -1$ (the observable path). Figure 14.12, is a typical example with order $p = 4$.

The straightforward analysis of 2D exchange spectra is possible only in the absence of spin–spin interactions. These interactions can also lead to additional cross-peaks in a 2D exchange spectrum. These are the J-cross peaks. The J-cross peaks arise from a coherent magnetization transfer via a quantum–mechanical coupling network, whereas the chemical exchange and the cross-relaxation or NOE cross-peaks reflect incoherent transfer processes. The J-cross peaks therefore have characteristic different from those of the exchange cross peaks. These features enable one to design procedures for their distinction and selective suppression. There is a close analogy to the cross-peaks, well known from the 2D auto-correlated spectroscopy. The pulse sequence technique is commonly used now to study quantum coherence processes. The various components, created initially by the first pulse, during the preparation period, create transverse spin magnetization. They are frequency labeled by letting them precess at their characteristic resonance frequencies. It happens, during the evolution period (t_1). The exchange processes, take pace, during the following mixing period (τ). Finally the exchange magnetization components are measured by letting them precess at their new resonance frequencies and by recording the induced signal as a function of the time variable t_2. In 2D ($t_1 - t_2$) spectroscopy, the experiment is repeated, for a number of equally spaced values of the evolution time periods. This result in a data matrix (t_1, t_2). The double Fourier Transform (FT), gives the desired spectrum S (ω_1, ω_2). The appearance of an off-diagonal peak at frequencies ω_1, ω_2, indicates an exchange process during the mixing period, has transferred magnetization components, of precession frequency, ω_1 to ω_2.

When the experiment is performed for a sufficiently short mixing time, the resulting 2D spectrum can be considered as a quantitative map of the kinetic matrix describing the exchange process. It is of particular importance, for
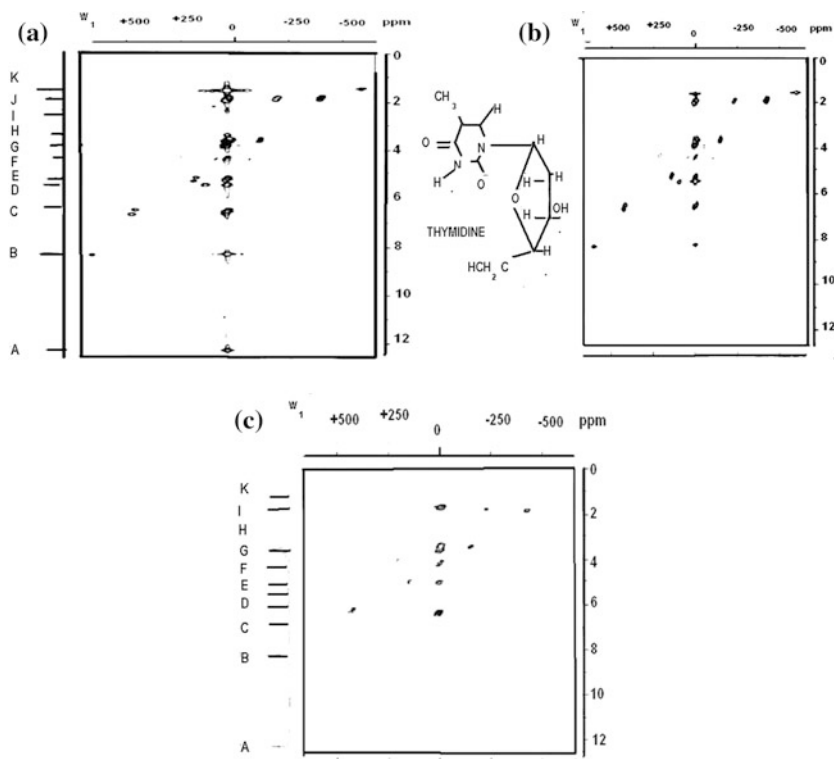
Fig. 14.13 Homonuclear 2D correlation spectra of thymidine. **a** Conventional spectrum with delayed acquisition (SECY—spin echo correlation Spectroscopy). **b** Double quantum filtered SECSY (= echo correlation spectroscopy) spectrum with the sequence $\pi/2 - t_1 - \pi/2 - \pi/2 - t_1 -$ acquisition. It is done with selection of the pathways $p = 0 - +1 \overset{\pm}{-} 2 - 1$. One should note, the elimination of the singlet of the proton A, and the attenuation of the ridge at $\omega_1 = 0$

elucidation of the complex exchange networks. The transverse magnetization is created during the preparation period by a nonselective 90° pulse. After evolution for a time τ, the x-component of the precessing magnetization, is selected and rotated a bout the z-axis by a second 90° pulse, which is applied along the y-axis. The z-components, which form the initial state for the mixing or exchange processes, appear now modulated by the precession angles acquired during the evolution period. It provides the desired frequency labeling of the magnetization components. After exchange, the resulting distribution of longitudinal magnetization component is again converted into observable transverse magnetization by a third 90° pulse. It enables the detection of the final state of the system. The information necessary to determine the original state before exchange is obtained by a systematic variation of t_1 from experiment to experiment. The use of a magnetic filed gradient pulse to destroy transverse magnetization is often undesirable. It is because of the disturbance of the field frequency lock system.

An alternative approach is provided by sequences involving phase-shifted RF pulses, for the comparison of transverse magnetization. A major complication in coupled spin systems arises from the additional creation of zero, single, double, and higher order quantum coherence by the second $(\pi/2)_y$ pulse, which is also transformed into observable magnetization, by the third pulse. This coherence is responsible for the J-cross peaks. Figure 14.13 [26, p. 116] is a practical example of the spectroscopy (the CTPs) for the molecule Thymidine.

14.2.14 NMR Multi-Quantum Spectroscopy and Brain Science/Practical Illustration

In the Fig. 14.13 is presented multi-quantum spectroscopy results (MQS) through an experiment performed on a typical chemical, the **thymidine**, in a laboratory situation. There is a close relationship between MQS of a molecule and how it can be translated into imaging in a multiple assembly of molecules. MQS has been practiced over decades to find the chemical structure of important pharmaceutical drugs. Now it is being incorporated as part of imaging in the MRI, particularly in the QMRI. The reader should notice that MQS in a single free molecule is easy to perform. In an ensemble like the brain, the neighboring (multi-species) molecules interact, through angular momentum, e.g. the L-S (spin orbit interaction), J-J (stronger inter-nuclear interactions), etc. These interactions originate from the basic life giving energy processes e.g., energy delivery, in metabolism. There are also other energy delivery processes, e.g. the neurotransmission, all over the body. The new approach to the imaging i.e. the multi-quantum coherence imaging (MQCI) is a new advancement to MRI. It will reveal the mysteries of the brain science operative in performing various functions of our mind.

Triple-quantum filtered spin echo correlation spectroscopy (SECY) spectrum obtained with the same sequence but with selection of $p = \pm 3$. Nuclei with less than two coupling partners are eliminated altogether (resonances A, B, C, D and K), while a pair of coupled nuclei must have at least additional coupling parameter to give rise to cross-peaks (e.g. cross-peaks between C and I with common coupling parameter J). The spectra were obtained at 90 MHz with a solution of 1 mol/liter at 300 K, 256 $\pm$ 1024 data matrices, contour levels at 5, 8, 16, and 25 % of the highest peak and without digital filtering. Figure 14.13 presents a typical example of a multi-quantum spectroscopy in an experiment in the laboratory situation.

14.3   Appendix A1

14.3.1 Relaxation Rates: Chemical Exchange

The phenomena of nuclear magnetic resonance (NMR) was discovered as a process of curiosity to find out the dipole-magnetic moment of a proton and a neutron the main constituents of a nucleus. It all happened, like many other curiosity driven discoveries, during the middle of the twentieth century. At that time, the physicists, were after verifying, the basic quantum electric structure of nuclei, atoms and molecules, through the NMR, atomic optical, etc., spectroscopy results. Today we are able to use the technology of NMR spectroscopy, as an imaging tool, the so called MRI. One must not forget, that all the technologies, we enjoy toddy, are the result of the competence, in the basic knowledge of, the PCM involved, achieved, and applied the technologies. One need to rear and comprehend the PCM of the NMR, in depth, to really understand, the MRI and its applications. The reader is advised to follow standard texts in the area.

This work is more of an abridgement effort in the PCM advancements, applied to the MRI. In a simple mathematical language, the phenomena of nuclear magnetic resonance (NMR) induction, in a sample, is analyzed through a set of mathematical differential equations. These equations equate the rate of change of the magnetic moment per unit volume, M, in small volume say a voxel, to the original value, dived by the relaxation time (longitudinal T_1 and transverse T_2, in the simplest model) of the magnetization relaxation, once a sample is irradiated with the RF radiation. This is called as the relaxation time approximation, and is seen prevalent as a mathematical tool of analysis, in the solidstate branch of physics. In the most simple (rudimentary) form the relaxation for the induced magnetization, by the RF radiation, applied to a ample, equation can be expressed as

$$(dM_z/dt) \sim -M(1/T_1); (dM_{x,y}/dt) \sim -M(1/T_2)$$

This is called as the simplest form of the Bloch equation which was invented by the physicist Bloch half century ago. Since then this equation has been used in various situations, MRI is only a typical case. If one performs an integration assuming T_1 and T_2 as two characteristic constants on gets

$$M_z = M_0 \; e^{-t/T1} \;\; \text{and} \;\; M_{x,y} = M_0 \; e^{-t/T2}, \text{respectively},$$

where M_0 is the magnetization at the initial time t = 0 and t is the time at any instant. Some researchers still prefer to apply a modified form of this equation, suiting to various situations. It simply leads to adding more terms on the right hand side (RHS) of the equation and re-finding, the required solution of the equation. But the progress towards multi-quantum coherence imaging (MQCI) over the recent years demands a more comprehensive approach. This is the approach, using the quantum mechanics (QM) mathematical discipline developed over the last several decades. The Bloch equation, has its limitations, when one is interested in

the multi-quantum MRI (MQMRI). In this specific situation one need to adopt a quantum algebraic approach. The quantum approach is more intuitive, as it allows, to visualize, mathematically, the progress, of the spins (dipole-magnets), in an imaging situation.

A reader who is interested in the quantum mathematics approach is referred to he Appendices, A10 and A30, and the references provided, in this work, for guidance. Here we present simple Bloch equation results, in some special circumstances, as an example. There are a large number of nuclei, with electric–magnetic character e.g., ^{7}Li, ^{23}Na. ^{35}Cl, ^{37}Cl, ^{79}Br, ^{81} Br, etc. which serve as important probing agents in MRI. These nuclei have Spin 3/2, as compared to the atom, Hydrogen, ^{1}H (proton) which is purely magnetic, and possess, spin 1/2. The proton in the nucleus has a spin of 1/2. The Bloch equations most often used [8] in describing the effects of chemical exchange are the following modified Bloch equations. These for the two site (A and B) chemical exchange [8], are written in the following form

$$d(\Delta M_{ZA})/dt = [-\Delta M_{ZA}(1/T_{1A} + 1/\tau_A) + \Delta M_{ZB}/\tau_B]$$
$$d(\Delta M_{ZB})/dt = [-\Delta M_{ZB}(1/T_{1B} + 1/\tau_B) + \Delta M_{ZA}/\tau_A]$$
$$d(M_{+A})/dt = [-M_{+A}\{(1/T_{2A} + 1/\tau_A) - i(\omega_A - \omega)\} + M_{+B}/\tau_B]$$
$$d(M_{+B})/dt = [-M_{+B}\{(1/T_{2B} + 1/\tau_B) - i(\omega_A - \omega)\} + M_{+A}/\tau_A]$$

Here τ_A and τ_B are the lifetimes (time to interact with its neighbor) of the species at sites A and B, respectively. T_{1A} and T_{1B} are the longitudinal relaxation times at sites A and B, respectively, in the absence of exchange; T_{2A} and T_{2B} are the corresponding transverse relaxation times in the absence of exchange; ω_A and ω_B are, the resonance frequencies of sites A and B; ω is the reference frequency. The symbol M refers to the magnetization. The subscript z means magnetization in the z direction and + refer to magnetization in the x, y (directions) plane, i.e. the transverse magnetization. The changes in magnetization ΔM are

$$\Delta M_{Zj} = M_{Zj} - M^0{}_{Zj}$$
$$M_{+j} = M_{Xj} + i\, M^0{}_{Yj}$$
$$j = A, B$$

M_{xj}, M_{yj}, M_{zj} are the x, y, z components of the magnetization at site j, $M^0{}_{zj}$ is the equilibrium magnetization in the z direction (assumed to be parallel to the main static field) at site j; and $i = \sqrt{-1}$. In approximation, one can write, the modified Bloch equations as for chemical exchange between two nuclei A and B, with individual character (correlation through τ_{AB}) of magnetizations. On solving above equations one gets

$$M_A(t) = a_1 e^{(\lambda_+ t)} + a_2 e^{(\lambda_- t)}$$

$$M_B(t) = b_1 e^{(\lambda_+ t)} + b_2 e^{(\lambda_- t)}$$

$$\lambda_\pm = (1/2)[\{(-1/T_A) + (-1/T_B)\}$$

$$\pm \sqrt{\{(1/T_B - 1/T_A)^2 + \{(4/\tau_A \tau_B)\}\}}]$$

$$b_1 = \beta_+ a_1,$$

$$b_2 = \beta_- a_2$$

$$\beta\pm = \tau_B[\lambda_\pm + (1/T_A)]$$

$$\lambda_+ \approx [(-1/T_A) + (T_B/\tau_A \tau_B)]$$

where, for longitudinal relaxation

$$\lambda_+ \approx [-(1/T_{1A}) - (P_B/P_A)\{(1/(T_{1B} + \tau_B)\}]$$

and for transverse relaxation,

$$\lambda_+ = [[-(1/T_{2A}) - (P_B/P_A/\tau_B)$$

$$\{(1/T_{2B})(1/T_{2B} + 1/\tau_B) + \Delta\omega^2\}/$$

$$\{(1/T_{2B} + 1/\tau_B)^2 + \Delta\omega^2\}]]$$

The symbols λ are the transition rates, inverse of the relaxation times. Here Δw is the chemical shift difference between sites A and B, P_A and P_B are the probabilities, at sites A and B, respectively, and the other symbols have their usual meanings. Also, use has been made of the fact that $P_B/P_A = \tau_B/\tau_A$. Furthermore, it can be shown that to the 0th order in τ_B and T_B, $a_1 = M_A(O)$ and $a_2 = b_1 = b_2 = 0$. This means that, in this limit, the relaxation is described by a single relaxation time, with the amplitude of the decay, independent of the magnitude of the decay constant, and, the, exchange time. In the case of Quadrupolar spin-3/2 nuclei, the mathematical relations are as follows. The isotropic reorientation gives for the longitudinal magnetization (rate of transition)

$$r_1 = [\{(1/10)(1 + (1/3)\eta^2)\}\{\{(e^2 qQ/\hbar)^2 \{\tau_c/(1 + \omega^2 \tau^2)\}\}]$$

$$r_2 = [\{(1/10)(1 + (1/3)\eta^2)\}\{\{(e^2 qQ/\hbar)^2\}\{\tau_c/(1 + 4\omega^2 \tau_c^2)\}\}]$$

Here $(e^2 qQ/\hbar)$ is the quadrupole coupling constant, τ_c, is the correlation time, ω is the resonant frequency, and η is the asymmetry parameter for the electric field gradient.

Manipulation of the relaxation matrices for transverse relaxation yields

$$(<I_x(t)> + i<I_y(t)>) = [(<I_x(0)> + i<I_y(0))]$$

$$[\{(\exp -i\omega t)(3/5 \exp -s_1 t + 2/5 \exp -s_2 t)\}]]$$

Here I_x, and I_y, represent the x and y components of the nuclear spin operators, respectively and

$$s_1 = [\{(1/20)(1 + (1/3)\eta^2)\{\{(e^2qQ/\hbar)^2\}\{\tau_c + (\tau_c/(1 + \omega^2\tau_c^2))\}\}]$$
$$s_2 = [\{(1/10)(1 + (1/3)\eta^2)\{\{(e^2qQ/\hbar)^2\}\{\tau_c/(1 + 4\omega^2\tau_c^2) + \tau_c/(1 + 4\omega^2\tau_c^2)\}\}]$$

Now the symbols s_1 and s_2 have been used for the transition rates. One of the implicit assumptions made in deriving the effect of chemical exchange on the nuclear relaxation is that the relaxation is exponential at both sites, in the absence of chemical exchange. This seems to be generally valid for quadrupolar relaxation under conditions of extreme narrowing ($\omega\tau << 1$). However, as we have seen, if the spin of the exchanging nucleus is greater than one and if at least one of the exchange sites is not under conditions of extreme narrowing, then the original equations are no longer valid. If one assumes, that the actual process of the nuclear transfer is "instantaneous," i.e. there is no relaxation during the exchange process, then the exchange couples χ_{Ai} (susceptibility A) only with χ_{Bi} (susceptibility B). That is for our case if a nucleus is in a particular nuclear state just before the transfer process, it will be in the same nuclear state at the other site after the transfer.

A completely analogous derivation results in the time dependence of the transverse magnetization. Thus, in general, it can be seen that the relaxation of an exchanging spin-3/2 nucleus is the sum of four exponentials if one or both sites are not under conditions of extreme narrowing and that the coefficient of each exponential is dependent upon the value of the relaxation times and exchange times. Furthermore, this procedure for reducing the complexity of the problem can be applied mutatis mutandis to any pair of exchanging sites, regardless of the type of relaxation at each site. The case of particular interest, however, is where the relaxation times and exchange time at one site (site B) are much less than at the other site. In this limit, we have single exponentials, the coefficients of which are independent of the relaxation times and exchange times, to the 0th order in the relaxation times, and exchange times at site B. Consequently, the z magnetization may be approximately written as

$$(<I_z(t)> - <I_z^0>) = [(<I_{AZ}(t)> - <I_{AZ}^0>)]$$
$$= [[(<I_{AZ}(0)> - <I_{AZ}^0>)][\{(1/5\exp-c_1t + 4/5\exp-c_2t)\}]]$$

where

$$c_i = [r_{Ai} + \{(P_B/P_A)(1/(1/r_{Bi} + \tau_B))\}]$$

Here r_i correspond to the site at i, and other meanings are, as before. Now by the same procedure, the transverse magnetization can be approximated with the results,

$$<I_x(t)> + i<I_y(t)> = <I_{Ax}(t)> + i<I_{AY}(t)>$$
$$= (<I_{Ax}(0)> + i<I_{AY}(0)>)$$
$$(\exp-i\omega_At)(3/5\exp-d_1t + 2/5\exp-d_2t)$$

where

$$d_i = [[S_{Ai} + (P_B/P_A/\tau_B)\{S_{Bi}(S_{Bi} + 1/\tau_B) + \Delta\omega^2\}/$$
$$(S_{Bi} + 1/\tau_B) + \Delta\omega^2\}/]]$$

A typical experiment would involve the addition of small amounts of a large molecule (site B) to an aqueous solution (site A) of the ion being studied. In this case, site A would most probably be under conditions of extreme narrowing and, consequently, $r_{Al} = r_{A2} = l/T_{1A} = s_{Al} = s_{A2} = l/T_{2A}$. In order to obtain the relaxation times, the logarithms of the difference of the magnetizations from their equilibrium values would be plotted as a function of time. Ideally, the nonlinearity of such a plot would enable one to extract both time constants for the longitudinal and for the transverse relaxation. However, it indicates that if the two time constants differ by less than a factor of about two, visually the plot appears to be linear within the experimentally accessible region. If there is a significant noise in the measurement, the accessible time region decreases, the error in each point increases and one's ability to distinguish two time constants diminishes. One can make a rough approximation by expanding the logarithms, in infinite series and retaining only those terms which are linear, in time, one then obtains approximations as,

$$1/T_1 \approx 0.2\,c_1 + 0.8\,c_2$$
$$1/T_2 \approx 0.6\,d_1 + 0.8\,d_2$$

Here l/T_1, and l/T_2, are the slopes of the longitudinal and transverse relaxation plots, respectively, c_1 and c_2, and d_l and d_2 are as above. For the typical experiment, where site A is under the conditions of extreme narrowing, one can write

$$1/T_1 \approx 1/T_{1A} + (P_B/P_A)\{(0.2/(1/r_{B1} + \tau_B) + 0.8/(1/r_{B2} + \tau_B)\}]$$
$$1/T_2 \approx [[1/T_{2A} + (P_B/P_A)[(0.6/\tau_B)\{\{S_{B1}(S_{B1} + 1/\tau_B) + \Delta\omega^2\}/$$
$$(S_{B1} + 1/\tau_B)^2 + \Delta\omega^2)\}\} + \{(0.4/\tau_B\}$$
$$\{S_{B2}(S_{B2} + 1/\tau_B) + \Delta\omega^2\}/$$
$$\{(S_{B2} + 1/\tau_B)^2 + \Delta\omega^2\}]]$$

The r_{Bi} and s_{Bi} are the r_i and s_i defined as above, respectively, for the site B, and $T_{1A} = T_{2A}$ and P_A and P_B are the longitudinal and transverse relaxation times respectively, for the site A in the absence of exchange ($T_{1A} = T_{2A}$), and P_A and P_B are the probability of sites A and B, respectively, $\Delta\omega$ is the chemical shift difference between the two sites and τ_B is the exchange time for site B.
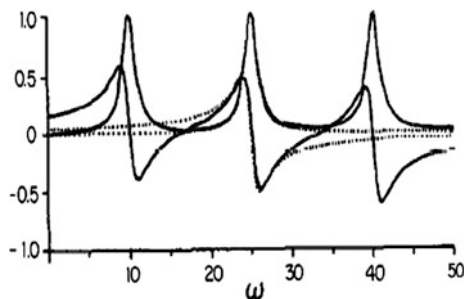
Fig. 14.14 Absorption and dispersion spectra for a single Lorentzian line (*dotted curves*) and for the same Lorentzian line in the presence of equally intense Lorentzian peaks of same width located at frequencies 7.5 linewidths on either side of the original peak (*solid curves*). The leftmost and rightmost dispersion signals partly cancel at frequencies near the central peak position

Fig. 14.15 Courtesy.
DISPA plots for the *central solid curve*, of the Fig. 14.14, for the ratio of peak separation of either pair of adjacent peaks) to peak width. The effect of adjacent peaks is much less than that for the previous example
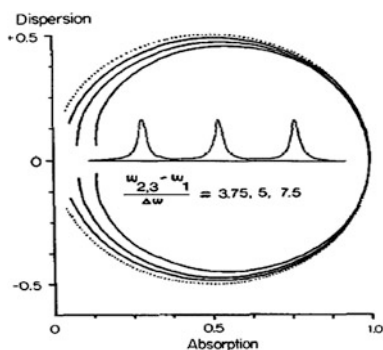
14.3.2 Dispersion Verses Absorption (DISPA) NMR Spectrum-Dynamic Frequency Shifts

For a single Lorentzian line, a plot [9] of dispersion versus absorption (DISPA), gives a circle tangent to the y-axis, centered on the positive abscissa. The direction and magnitude of the displacement of an experimental DISPA plot from its reference circle (diameter equal to maximum absorption peak height) are highly sensitive to deviations from Lorentzian lineshape, as has been demonstrated by examples from NMR spectroscopy. In particular a symmetrical distribution in Lorentzian peak position displaces a DISPA curve outside its reference circle while any distribution in Lorentzian peak width displaces the DISPA curve inside its reference circle. One can extend DISPA analysis to a simultaneous distribution, in both peak position (ω) and width (Δ). DISPA examples have normally been based on data from a single peak, well separated from, other nearby peaks. It is clearly necessary to establish the magnitude of DISPA plot distortion of data from a given peak produced by partial overlap from one or more adjacent peaks. Below

are given typical mathematical expressions for the absorption and dispersion line shapes for Lorentzian lines of equal widths weighted by a Gaussian distribution, in resonant frequency (i.e. line position). The absorption and dispersion have each been normalized by dividing each absorption or dispersion value by the maximum absorption peak height in the equations. A larger value of σ_A (distribution breadth parameters) corresponds to a broader distribution, in peak position.

$$A(\omega) = [1/(2\pi\sigma\Delta)]\int_{-\infty \text{ to } +\infty}[\tau/[1 + (\omega_0 - \omega)^2\tau^2]\exp[-\Delta^2/(2\sigma^2)]d\Delta,$$

$$D(\omega) = [[1/(2\pi\sigma\Delta)]\int_{-\infty \ +\infty}[\{(\omega_0 - \omega + \Delta)\tau^2\}/$$
$$\{1 + (\omega_0 - \omega)\tau\}^2]\exp[-\Delta^2/(2\sigma^2)d\Delta]],$$

$$A(\omega_0) = [1/(2\pi\sigma\Delta)]\int_{-\infty \ +\infty}[\tau/[1 + \Delta^2\tau^2]\exp[-\Delta^2/(2\sigma^2)]d\Delta,$$

Above $A(\omega_0)$, is the maximum $(\omega = \omega_0)$ absorption peak. The equations below give the normalized absorption and dispersion lineshapes, for Lorentzian lines, of equal resonant frequencies, weighted by a log-Gaussian distribution, in (transverse) relaxation time. Each has been normalized by dividing by the maximum absorption peak height (denominator in the equations).

$$A(\omega) = [\int_{-\infty \text{ to } +\infty}[\exp(x + y)]/[(1 + (\omega_0 - \omega)^2 \exp 2(x + y)]$$
$$[\exp(-x^2/2\sigma^2\tau)dx]/$$
$$\int_{-\infty \text{ to } +\infty}\{\exp(x + y)\exp[-\Delta^2/(2\sigma^2\tau)dx]$$

$$D(\omega) = [\int_{-\infty \text{ to } +\infty}[\{(\omega_0 - \omega)\exp\{2(x + y)\}]/[(1 + (\omega_0 - \omega)^2 \exp\{2(x + y)\}]$$
$$[\exp(-x^2/2\sigma^2\tau)dx]/$$
$$\int_{-\infty \text{ to } +\infty}\{\exp(x + y)\exp[-\Delta^2/(2\sigma^2\tau)dx]$$

The absorption and dispersion lineshapes for a simultaneous Gaussian distribution in resonant frequency and log-Gaussian distribution, in relaxation time is obtained from the above equations. The result is shown in Fig. 14.14 [9]. The absorption and dispersion expressions are normalized by dividing by the maximum absorption peak height given. Here $x = \log e (\tau/\tau_0)$, $y = \log (\tau_0)$, $x + y = \log e(\tau)$.

$$A(\omega) = [\int_{-\infty \text{ to } +\infty}[\exp(x + y)]/[(1 + (\omega_0 - \omega + \Delta)^2 \exp 2(x + y)]$$
$$[\exp(-\Delta^2/2\sigma^2\Delta)][\exp(-\chi^2/2\nu^2\tau)]\,d\Delta\,dx]$$

$$D(\omega) = [\int_{-\infty \text{ to } +\infty}[(\omega_0 - \omega + \Delta)\exp 2(x + y)]/[(1 + (\omega_0 - \omega + \Delta)^2 \exp 2(x + y)]$$
$$[\exp(-\Delta^2/2\sigma^2\Delta)][\exp(-x^2/2\sigma^2\tau)]\,d\Delta\,dx]$$

$$A(\omega_0) = [\int_{-\infty \text{ to } +\infty}[\exp(x + y)]/[(1 + (\Delta)^2 \exp 2(x + y)]$$
$$[\exp(-\Delta^2/2\sigma^2\Delta)][\exp(-x^2/2\sigma^2\tau)]\,d\Delta\,dx]$$
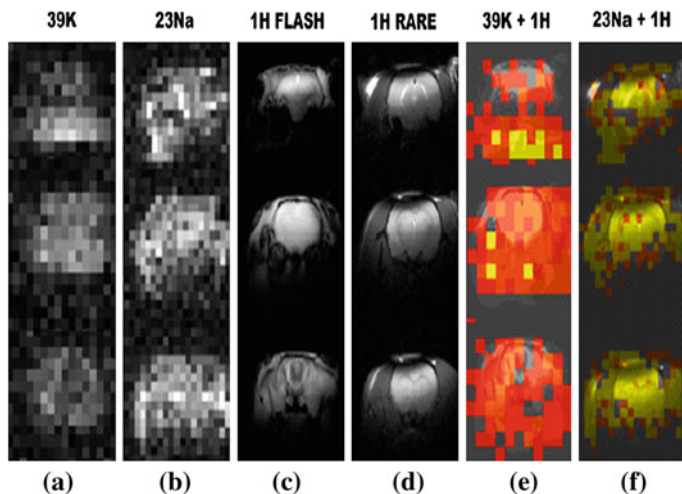
Fig. 14.16 Three raw unprocessed ^{39}K (**a**) and ^{23}Na (**b**) MR images of a rat head. ^{1}H images with a FLASH (**c**) and a RARE (**d**) sequence. Overlay of the thresholded and cropped ^{39}K images with the coronal ^{1}H FLASH images (**e**). Overlay of the thresholded and cropped ^{23}Na images with the coronal ^{1}H RARE images (f)

The Fig. 14.15 [9] shows absorption and dispersion spectra for a single Lorentzian line (dotted curves) and for a symmetrical triplet of Lorentzian lines of equal widths. The dispersion curves overlap, even though the absorption signals do not. One can see, the DISPA curves corresponding to various separations, between the component lines of the triplet based on the central component line. In NMR, continuous-wave spectroscopy the steady-state solution of the Bloch equations in a frame, rotating at the frequency, ω, of the applied oscillating magnetic field, $H_1 \cos$ (ωt) is given by

$$A(\omega) = (M_0)[[\gamma H_1 T_2]/[\{1 + T_2^2(\omega_0 - \omega)^2\} + \gamma^2 H_1^2 T_1 T_2]$$
$$D(\omega) = (M_0)[[(\omega_0 - \omega)\gamma H_1 T_2^2]/[\{1 + T_2^2(\omega_0 - \omega)^2\} + \gamma^2 H^2 T_1 T_2]$$

Here M_0 is the equilibrium z magnetization in the absence of oscillating applied fields, γ is the magnetogyric ratio, ω_0 is the Larmor frequency, and T_1 and T_2 are the longitudinal and transverse relaxation times. One observes that the direction and magnitude of the displacement of an experimental DISPA curve from its reference circle is more strongly determined by a distribution in peak position ("chemical shift" in NMR) than by a distribution in linewidth. If experimental DISPA data, are displaced inside, the reference circle, we can be quite sure, that there is a pronounced distribution in (transverse) relaxation times for that spectrum. However, even a relatively narrow spread in Larmor frequency, can evidently compensate (as far as DISPA behavior is concerned) for quite a broad distribution in linewidth. Figure 14.15 [9] showed DISPA plots for the central line of a symmetrical triplet. In this case, the dispersion overlap largely cancels out,
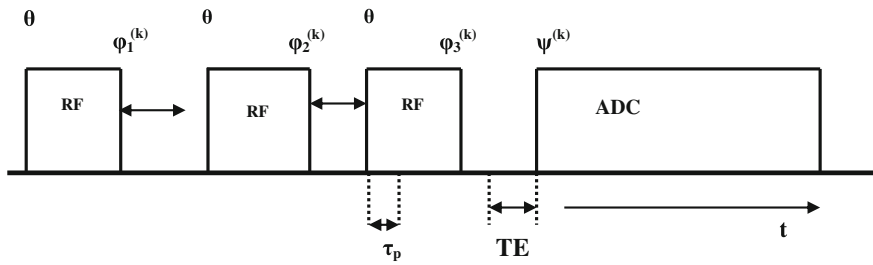
Fig. 14.17 Sequence employed for ^{23}Na TQ filtering experiments: three RF pulses with flip angle θ, phases φ_i (i = 1, 2, 3) and width τ_P., delay times between pulses: preparation time τ_1 and evolution time τ_2, typically $\tau_2 << \tau_1$. Signal acquisition (duration: t) starts after echo time TE with receiver (ADC—apparent diffusion coefficient) phase set to $\psi^{(k)}$, TE = echo time

because the dispersion signals (near the central peak) from the left, and rightmost peaks, are nearly equal and opposite. Thus, the distortion-free DISPA plots, for the central line, can result from peak separations, as small as about eight linewidths. This condition may be satisfied, for the m = 0 transition, of nitro-oxide permitting DISPA analysis of these spectra in the limit of relatively rapid motional, tumbling rates. Finally, the dispersion overlap problem, can be overcome in another way, by using only the (resolved) absorption spectrum, and then generating the dispersion spectrum by a Hilbert transform. This technique yields undistorted DISPA plots for doublet separations as small, as about five line widths. The DISPA plot is not only sensitive to small deviations from Lorentzian lineshape, but is also sensitive to any asymmetry, in the spectrum. Finally, since, the magnitude of displacement, for any given line-broadening is automatically scaled in units of the width, of a single unperturbed Lorentzian component, it should be possible to use, the DISPA plot quantitatively, to determine, the value of the line-broadening mechanism parameter, of interest (e.g., chemical exchange rate) from the data from a single spectrum.

14.3.3 Potassium Imaging Versus Sodium Imaging

The most abundant natural isotopes ^{23}Na and ^{39}K [6] have a nuclear spin of 3/2 and therefore exhibit an electrical nuclear quadrupole moment. Compared to the well established MRI of water protons (^{1}H), MRI of quadrupolar nuclei, suffers from a low sensitivity caused by the intrinsic gyromagnetic ratio and from a high quadrupolar relaxation rates. Typical reported relaxation times of the spin–lattice relaxation T_1 are 23 ms at 8.4 T for ^{23}Na and 14 ms at 7 T for ^{39}K. The relaxation constants of the biexponential transverse signal decay TI $_2$ and TII $_2$ are reported as 2 ms and 17 ms at 8.4 T for 23Na in the frog heart and as 2.4 ms and 12.9 ms at 7 T for 39 K in the rat brain. Na$^+$ and K$^+$ are the most important ions for the normal cell function in the mammal organism. The maintenance of a specific gradient of

Fig. 14.18 An illustration of the k-space sampling scheme in conventional three dimensional projection imaging. The surface of a sphere of radius K_{max}, is divided in an even number of circles of latitude separated by a distance equal to the inverse of the image field of view. Projections are then placed on each ring so that the separation between adjacent projections also equals the inverse of the image FOV
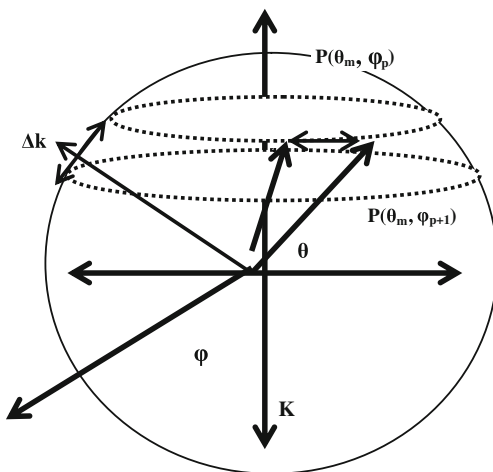
Fig. 14.19 Constant azimuthal angle constant sample density k-space trajectories. The trajectories lie on the surface of a disk perpendicular to the $K_x - K_y$, plane. The normal to the plane makes an angle $\pi/2 - \varphi_o$ with the K, axis
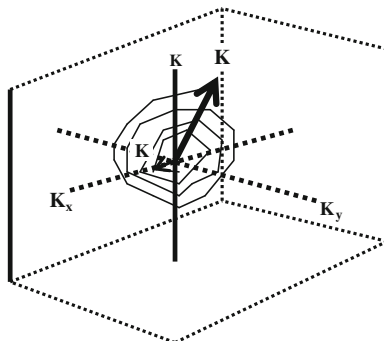
these ions across the cell membrane by the active Na/K pump is very crucial. In addition to the fast relaxation the in vivo concentration of ^{23}Na and K is much lower compared to water protons, resulting in MR signals which are 20,000 times (^{23}Na) and 2.1 million times (^{39}K) lower than ^{1}H signals, see Fig. 14.16 [6], for experimental results.

14.3.4 Triple Quantum Filtered Sodium Imaging

Trans membrane sodium–potassium pumps generate a permanent gradient between the extra cellular (Na^+_{ex}) and intracellular (Na^+_{in}) sodium concentration. A breakdown of this gradient indicates severe functional disorders in living tissue. An MR technique for selective imaging of intracellular sodium is therefore desirable. It has been shown that, compared to a four-pulse sequence including a 180° refocusing pulse, a three-pulse sequence has advantages for TQ filtered

$$G = [\, (\, 1/\{(\, 2\gamma T_2^c(\text{effective time})\Delta x\}) \,] \,)[(\, 1 + 2 \, p^3 \,)/3p^2 \,]$$
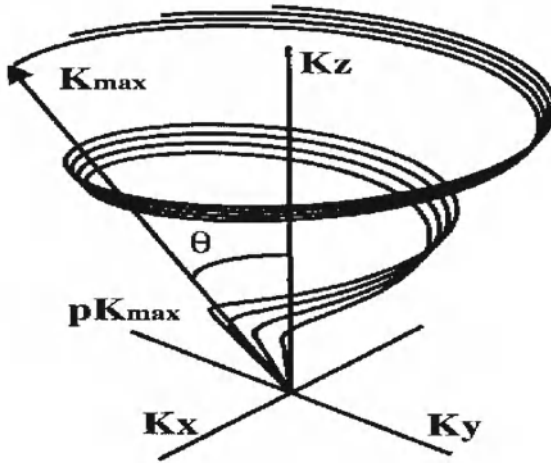
Fig. 14.20 An illustration of the k-space sampling scheme in TPI. The sampling scheme is obtained as a modification of conventional PI in which the twist of the k-space trajectories is adjusted so that critical sample density is maintained between K_o and K_{max}

sodium imaging in humans due to less specific absorption rate (SAR) and a B_1 (RF magnetic field) dependence more amenable to subsequent corrections. A non-invasive approach utilizes differences of relaxation rates in different physiological compartments for selective signal suppression via inversion recovery. In this case, only one type of environment with one specific decay rate of the ^{23}Na transversal magnetization can be suppressed at once and regions with similar decay rates might be unintentionally suppressed. An alternative non invasive method uses a triple quantum (TQ) filter selective for sodium ions, that are restricted in their mobility. This happens because of, the interaction with macromolecular structures, within the intracellular compartment. A standard triple quantum (TQ) coherence filtering sequence is made of three RF pulse with a flip angle θ. The phases φ^k of the pulses are, φ^1, φ^2, φ^3 (where k specifies the choice of the pulse phases in the k-th cycle) and delay times τ_1 and τ_2 for preparation and evolution of TQ coherences, respectively. $\psi^{(k)}$ is the relative phase of the receiver.

The three standard TQ coherences pulses (Fig. 14.17) create coherences of the order $m_1 = -1$ and $m_1 = +1$ (besides possibly remaining longitudinal magnetization of order 0), which the second pulse converts into coherences between orders $m_2 = -3$ and up to $m_2 = +3$. The third pulse is applied to transform TQ coherence into detectable transverse magnetization. The altogether 21 possible coherence pathways are uniquely determined by m_1 and m_2. One is are interested in the effect of static magnetic field B_0 inhomogeneities on the signal intensity of the experiment. To quantify the inhomogeneity in a particular voxel, one uses the frequency offset δ of the applied RF frequency ω from the Larmor frequency $\omega_0 = \gamma B_0$ in the

voxel; $\delta = \omega - \omega_0 = \gamma (B - B_0)$. The signal, obtained from that voxel is a superposition of the partial signals from different coherence pathways passed through in the course of the sequence.

14.3.5 Three Dimensional Fast K-Space Sodium Imaging

It is known that constant sampling density trajectories in 3D, provide a fast and reliable means, to obtain sodium images, of acceptable signal to noise ratio (SNR) [10]. This is done by removing the non-uniform sample density that results from uniform sampling in time, along radial lines, in k-space. One need to understand (refer to Figs. 14.18, 14.19, 14.20) [10], the modifications required, in the angular distribution of projections, used for conventional projection imaging (PI). In order to achieve constant sampling density, what is done is, that, we make the surface corresponding to a sphere, of maximum wave number, radius K_{max}, as the modulus of the largest spatial frequency vector. This is used during image reconstruction, divided into an even number N_R of rings. Each circle is a circle of latitude defined by the polar angle, $\theta_n = (n/N_R)\pi$ (Fig. 14.18 [10]) and separated by a distance equal to the inverse of the required field of view (FOV). Here n is the number corresponding to the specific polar angle and N_R, the total number of rings. In order to improve the efficiency of PI, the k-space trajectories, can be modified, so that the twist in the trajectories, preserves the sample density $(1/k^2)$. Since the noise variance is minimized when the sample density is uniform throughout the k-space three dimensional constant sampling density sampling trajectories, with spherical symmetry, represent a desirable choice for improving the SNR efficiency, of PI. In three dimensions the sample density for a spherically symmetric distribution of trajectories will be constant if the number of samples inside a thin spherical shell is proportional to the volume of the cell. It is important to point out here that a complete mathematical analysis of the technique would be out place in this book. Here one can learn about important technical terms that commonly appear in the area of k-space imaging. Theses are referred to as the imaging technical parameters.

It is worth elaborating them here as follows. These are as follows: k = the wave number = $1/\lambda$, λ being the wavelength of the RF radiation = the spatial frequency vector, $k_0 = k$ (when t = 0) $\neq 0$, G = magnetic field gradient strength, γ = gyromagnetic ratio divided by 2π, θ = the polar angle, φ = the azimuthal angle. The constant polar angle generates the sampling geometry (Fig. 14.20) of the conventional PI (in which k-space is sampled uniformly in solid angle along radial lines on the surface of concentric cones). This property makes it ideally suited for developing efficient extensions of PI. The constant azimuthal angle solution φ, on the other hand, requires sampling on disks perpendicular to the K_x–K_y plane (Fig. 14.19). The constant polar angle solution is considered as a suitable technique, due to some technical (mathematical) simplicity. This method corresponds to 'helix-like' trajectories, on the surface of the cone $\theta = \theta_m$ (Figs. 14.18–14.20).

The acceleration along these trajectories decreases as one moves away from the origin ($k = k_0$) of the k-space.

The constant polar angle solution is preferred, to develop a 'twisted' projection imaging (TPI). On each cone the k-space trajectory departs from the origin of k-space along a radial line up to a fraction p (p < 1) of K_{max} (so $k_o = pK_{max}$). At that point k(t) and φ(t) start evolving, so that the critical sample density is maintained until K_{max} is obtained. The choice of p is limited by the gradient capabilities of the scanning system. Because the distance between neighboring projections increases linearly with k(t) particular choice of p decreases the number of projections on each cone by a factor of p and therefore amounts to a saving of (1 − p), in data acquisition time (DAT). One can work out that the maximum gradient slew rate required will not exceed $S_{max} = (\gamma \, G^2 L/p)$. Here L is the desired image field of view (FOV). One should note, that the equation does not depend on the resolution, but rather on the degrees of DAT (data acquisition time due to p) reduction required. This is not surprising, since an increase in spatial resolution requires, narrowing the innermost cone by the same amount so that the K_{max} is decreased which keeps the demonstrator in the equation, constant.

One should note that the above equation about S_{max}, does not include the slew rate required to make the transition from a radial line to the constant sample density k-space trajectory. Sodium imaging involves spatial encoding of weak MR signals. So, it is important to use a gradient strength that does not compromise the signal to noise ratio (SNR) of the reconstructed images. The time required to reach K_{max} along a twisted projection imaging (TPI) trajectory is

$$T_{Read} = [(K_{max}/(\gamma G)]s[(1 + 2p^3)/3p^2]$$

The relationship between the gradient strength, G, required for desired spatial resolution (Δx) and trajectory twist (p) is given as

$$G = [(1/\{(2\gamma T_2^e(\text{effective time})\Delta x\})])][(1 + 2p^3)/3p^2]$$

Sodium images of much improved spatial resolution can be acquired at a clinical field strength (1.5 Tesla) in DATs comparable with those used for proton MRI. These developments have been possible through the use of efficient strategies for sampling the spatial frequency data and optimized RF probes. Four aspects of the TPI acquisition scheme make it well suited for sodium imaging. First, the lower gyromagnetic ratio of sodium reduces the amount of spin dephasing that takes place because of the main magnetic field (B_0) inhomogeneities. This feature decreases blurring in the images due to the off resonance effects. Second, the behavior of the trajectories near the origin of k-space is ideally suited for the acquisition of MRI signals from short T_2 species, since the low spatial frequency components are sampled before significant T_2 weighting occurs. Third since the percent twist on each cone is identical, the point spread function (PSF) is isotropic. This last feature is relatively important since varying the percent twist to match the maximum slew rate on each cone (which would further decrease the DAT) could introduce severe changes in the PSF due to sodium's fast transverse

relaxation rate. Fourth, the uniform sample density for the high spatial frequency values, produces noise, that is more spatially uncorrelated.

14.3.6 Double Quantum Filter Single Spin I = 1 (Deuterium System)

Standard techniques for measuring spin–lattice (R_1) and spin–spin (R_2) relaxation rates in coupled systems are, not always sufficient to determine a complete set of spectral density parameters. This situation is particularly common for anisotropic liquid crystalline systems [11] where the complicated motional spectrum spans a wide range of frequencies. In this context, recent developments in two-dimensional Fourier Transform techniques and multiple quantum spectroscopy present, exciting opportunities for gathering novel information about relaxation mechanisms and molecular motion. The utility of double and zero quantum coherence decay rates has been demonstrated in a study of a weakly coupled proton AB spin system subject to relaxation by paramagnetic agents. Studies of relaxation in partially ordered deuteron spin systems have demonstrated the feasibility of using double quantum line widths and have shown the need for such measurements on multispin systems if a complete analysis of motional parameters is desired. So far, experimental studies have been confined to systems where the natural multiple quantum line width is a significant fraction of the total line width. In many cases of practical interest, this pleasant situation does not occur, because n quantum line widths are broadened by n times the normal field inhomogeneity. Furthermore, multiple quantum lineshapes can be distorted by coherence transfer echoes. Both these limitations can be overcome by using refocusing techniques and monitoring multiple quantum echoes or by multiple quantum spin-locking procedures. Here we are concerned specifically with accurate measurements of double quantum decay rates of deuterium in partially ordered fluid phases. Procedures for excitation and detection of double quantum echoes are discussed, including phase cycled pulse sequences designed to cancel artifacts arising from unwanted single quantum coherence and imperfect pulses. The effect of a single refocusing pulse applied in the middle of the evolution period is considered in detail. Selective detection schemes developed are extended to account for the phase of the refocusing pulse and a phase-cycled pulse sequence capable of providing accurate double quantum spin-echo linewidths is presented.

Multiple quantum coherence exists in a spin system if the density matrix possesses nonzero off -diagonal elements between eigenstates differing in magnetic quantum number by $\Delta m = \pm 1$. Such coherent states can be established by a variety of techniques including a weak "double quantum" pulse applied to an equilibrium system or a strong $\pi/2$ or weak pulse applied to a spin system in a non equilibrium state of either the first or the second kind. For excitation of deuterium double quantum coherence in solids or liquid crystals any of these methods may be
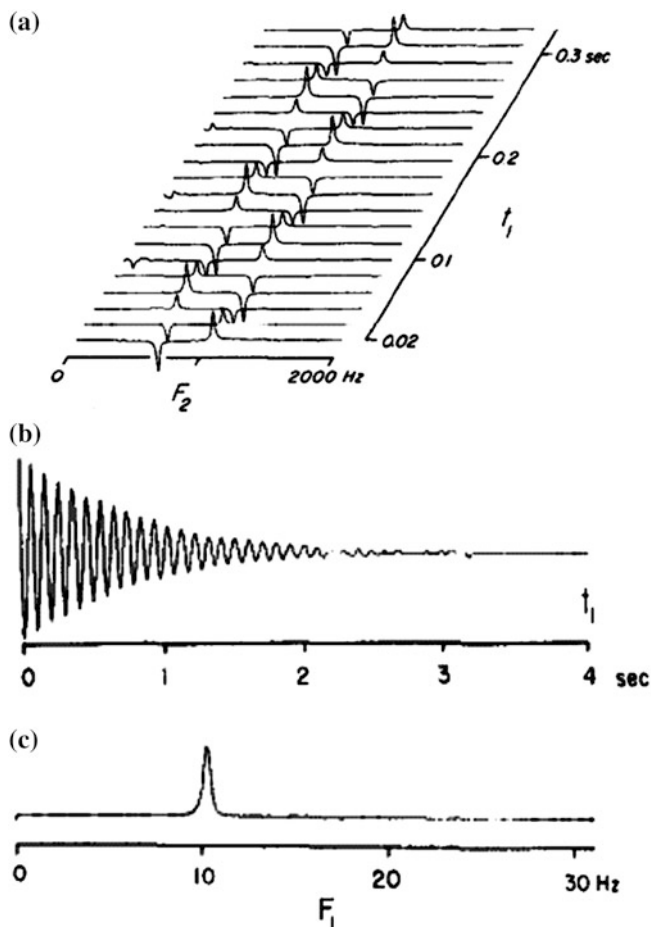
Fig. 14.21 Double quantum echo experiment with phase advancement. Excitation and detection of the double quantum echo were performed using the hexcycle sequence. In addition, the phase of both excitation pulses was advanced by 30° for each value of t_1. The resulting amplitude modulation is shown in **a**. In **b**, the result of sampling the top of the right-hand resonance is shown. This is the double quantum echo decay, which in the absence of phase advancement would appear as a simple unmodulated exponential. Fourier transformation of **b** yields the spectrum in **c**, where the double quantum coherence occurs at one-third the spectral width. The linewidth yields a rate $R_{1313} = 1.33$ s^{-1} for the transverse relaxation of the double quantum coherence of 10 % (w/w) PBLG in CDCl$_3$ (chemical solution in deuterochloroform representing liquid crystalline system of spin I = 1 system [11])

used. In this section we confine our attention to excitation by means of strong pulses, which may be represented by simple rotation operators in closed analytical form. In general, the time evolution of the spin density operator $\sigma(t)$ is given by $\sigma(t) = \exp(-i \, Ht) \, \sigma \, (O) \exp(i \, Ht)$ where H is the effective Hamiltonian operating in the time interval 0 to t and is time independent in an appropriate rotating frame.

Our restriction to strong pulses permits the above to be simplified: $\sigma(t^+) = R(\alpha, \varphi)$ $\sigma(t^-) R^{-1}(\alpha, \varphi)$. Here t^- and t^+ are instants of time just before and after the pulse of flip angle α. The phase φ is referred to the x axis of the rotating frame. In the eigenstate representation of the static Hamiltonian H_0, individual density matrix elements σ_{pq} correspond either to eigenstate populations (p = q) or to coherence between such states (p ≠ q). Utilizing the unitary property of the rotation operator $R^{-1}(\alpha, \phi) = R^*_{qs}(\alpha, \phi)$ we may write $\sigma_{pq}(t^+) = \sum_{rs} R_{pr}(\alpha, \phi) \sigma_{rs}(t^-) R^*_{qs}(\alpha, \phi)$. This equation represents the transfer of coherence from $\sigma_{rs}(t^-)$, before the pulse to, $\sigma_{pq}(t^+)$ after the pulse, and the probability of coherence transfer is given by the magnitude of $R_{pr} R^*_{qs}$.

By examining the individual terms (or elements of the supermatrix $R \otimes R$) in the Liouville representation, detailed pathways of coherence transfer can be discerned. Thus, the transfer equation is a powerful tool in multiple quantum spectroscopy, especially if an analytical expression for R $(\alpha\phi)$ is available. Other workers have avoided the matrix element evaluations implicit by expanding above equations in fictitious spin or single transition operator representations and using commutator algebra, but for the systems considered here the direct evaluation is straightforward. Moreover, extensions to situations where numerical methods are needed to evaluate R $(\alpha\phi)$ are conceptually simple. Now we consider the three-level system of a single spin I = l, the simplest case for which double quantum coherence can occur. It is desirable to obtain an explicit expression for R $(\alpha\phi)$ in the eigenstate basis of the static Hamiltonian $H_0 = -\Delta\omega\, I_Z$, + 1/3 ω_Q (3 I_Z^2 – I.I). Here $\Delta\omega = (\omega_0 -\omega)$ is the offset of the pulse carrier frequency from exact resonance, and $\Delta\omega$ is the residual quadrupolar splitting observed, in a partially ordered medium. The rotation operator is given by R $(\alpha, \phi) = \exp\{i\, \alpha\, (I_X \cos\phi + I_X \sin\phi)\} = \exp(-i\, \phi\, I_Z;)$ $\exp(i\, \alpha\, I_X) \exp(i\, \phi I_Z)$.

For a single spin I = 1, the angular momentum operators are represented by 2×2 Matrices. The phase shift 4ϕ experienced by a double quantum coherence upon ideal refocusing is unique and sets this type of transfer apart from all other non ideal forms of coherence transfer. Thus, advancing the phase of the refocusing pulse by 45° causes the double quantum echo to reverse in phase, while all other transfer processes experience phase shifts of 0, 45°, 90°, or 135°. An experiment which cancels all forms of undesirable coherence transfer in systems with one or two deuterons consisting of a sequence of 16 transients (hexadeca-cycle). The phase of both excitation pulses is maintained at zero for the first eight transients, and shifted to 180° for the last eight. The phase of the refocusing pulse is advanced in regular increments 0, 45°, 90°, 135°,…, 315°, while the monitoring pulse alternates between 0 and 180°. This sequence achieves cancellation of the single quantum artifacts, as well as echoes arising from coherences of all odd orders and even orders, = 4p, p = 1,2,3,…. In general, it is unfortunate that the refocusing pulse suppresses double quantum precession, because the resulting two-dimensional double quantum spin-echo spectrum yields peaks at $F_1 = 0$. Experience with two-dimensional spectroscopy has shown that modulated interferograms yield spectra which are more suitable for accurate linewidth measurements in the F1

domain. Furthermore, it may be desirable to separate multiple quantum echoes of higher order which occur in more complicated spin systems.

A simple device, which solves both problems at once, in effect forces all echoes to be modulated. This scheme requires the transmitter phase to be advanced as it is incremented and should not be confused with the phase-cycling techniques, which differentiate between subsequent transients recorded for a given t_l. By advancing the phase of both excitation and refocusing pulses for the kth, t_l value, by $k\pi/l$, where 1 is an arbitrary integer, the phase of an n-quantum echo signal is advanced by nrk/l. For example, with l = 6, the phase of the double quantum echo advances through 60° for each t_l increment. This leads to modulated echoes as shown in Fig. 14.21 ([11]), with subsequent Fourier trans-formation giving a peak displaced from $F_1 = 0$ by a fraction n/l (e.g., 2/6) of the spectral width. For a single deuteron the double quantum coherence decays exponentially with a rate constant given by the Redfield relaxation matrix element R_{1313}. If the dominant relaxation mechanism is of quadrupolar origin, one obtains

$$R_{1313} = (3\pi^2/2)[(e2qQ/h)^2\{(J_1(\omega_0) + 2J_2(2\omega_0)\}]$$

Here (e^2qQ/h) is the deuterium quadrupole coupling constant and $J_1(\omega_0)$ and $J_2(\omega_0)$ are spectral density functions, normalized such that in the White Spectrum limit, it is for an isotropic medium, $Ji(\omega_0) = J_2(2\omega_0) = 1/5\ (\tau_R)$, where τ_R is the rotational correlation time. From repeated measurements of the double quantum spin-echo linewidth, we obtain $R_{1313} = 1.33 \pm 0.06\ s^{-1}$ for our liquid crystalline solution of l0 % (w/w) PBLG in deuterochloroform at 35°C. It is of interest to compare this decay rate with the spin–lattice relaxation rate $R_1 = 1.17 \pm 0.01\ s^{-1}$, which we determined by inversion recovery using nonselective pulses. For quadrupolar relaxation, R_1 is given as

$$R_1 = (3\pi^2/2)[(e2qQ/h)^2\{(J_1(\omega_0) + 4J_2(2\omega_0)\}]$$

Here $J_1(\omega_O)$ and $J_2(2\ \omega o)$ are necessarily positive, and therefore, R_{1313}/R_1 must be less than or equal to unity. The observed double quantum decay rate is greater than R_1 by a factor of 1.14 ± 0.05.

The analysis presented here for a single spin I = 1, can be extended in straight-forward fashion to multi-spin systems. When applied to a system of N deuterons in a partially ordered mesophase, the $90° - \tau - 90°$ excitation sequence will generate all orders of multiple quantum coherence up to and including 2 N. It is convenient to classify the coherence on the basis of subsequent precession frequency: Class 1 consists of all coherences (off-diagonal density matrix elements) with precession frequencies dependent only on the resonance offset. The class 2 is comprised of coherences with precession determined by resonance offset and $^2H–^2H$ dipolar interactions, while class 3 coherences precess at rates determined, at least in part, by quadrupolar interactions. Classes 2 and 3 are unique to systems of two or more spins. For example, in the two-deuteron system there are six double quantum coherences (two of each class), two class 3 triple quantum coherences, and one class 1 four-quantum coherence. Multiple quantum coherences of different classes can be

operationally distinguished on the basis of their "resonance" frequencies in a two-dimensional spin-echo experiment. Since Zeeman interactions are refocused by the 180° pulse while dipolar and quadrupolar interactions are not, class 1 coherences give rise to signals at $F_1 = 0$ (unless phase advancement is used). For deuteron systems, in which dipolar interactions are typically less than a few hundred Hertz, while quadrupolar interactions are normally several kilohertz, class 3 coherences will usually be aliased in the F_1 domain while class 1 coherences are not.

More fundamentally, there is a one-to-one correspondence between eigenstates which define class 1 coherence and eigenstates which are inter-converted by spin inversion. For purposes of spin-echo studies of multiple quantum relaxation it is advisable to avoid exciting class 3 coherence. A small fractional inhomogeneity in liquid crystal-line order (e.g., resulting from minor thermal gradients) leads to a large dispersion of quadrupolar precession frequencies. Since this is not refocused by the 180° pulse, class 3 coherence will give rise to spuriously wide lines. Analogous dispersion of class 2 coherence is much smaller since dipolar interactions are small. In cases where the relaxation information inherent in class 3 coherence is needed, refocusing may be achieved with 90° pulses. However, a 90° refocusing pulse will produce a variety of unwanted coherence transfer phenomena which would have to be suppressed by appropriate phase-cycling schemes. In multi-spin systems it is likely that several multiple quantum coherences may precess at a common frequency. In perfect analogy with degenerate transverse magnetizations in scalar coupled systems, cross-relaxation then gives rise to multiple exponential decays. This feature, as well as the averaging effect of the 180° refocusing pulse, must be considered when analyzing the spin-echo lineshapes.

14.3.7 *Quadrupolar Relaxation Rates: The Multi-Quantum Coherences*

The study of intensive processes which are responsible for the loss of multi-quantum coherence [12] provides an important complement to conventional relaxation studies. For example (Figs. 14.22, 14.23) certain spin correlations which do not affect the observable quantities in conventional T_I and T_2 studies, do indeed affect the relaxation behavior of the multi-quantum coherences. Likewise, the measurement of the loss of single quantum coherence (lQC), double quantum coherence (2QC), and the n quantum coherence (nQC), often provides linearly independent combinations of spectral density terms. This can greatly aid in the isolation and identification of the large assortment of factors responsible for effecting nuclear spin thermalisation. Below we examine the simplest of spin systems that exhibit multi-quantum coherence- the isolated multipolar nucleus relaxed by quadrupolar interactions. Of course, for systems at thermal equilibrium all coherences of all order vanish. However, we shall assume that multiquantum coherence can be produced and monitored (e.g., with a $90° - \tau - 90° - \tau_1 -$ "look" pulse-digitize (τ_2) pulse sequence).

Table 14.44 Half width at half height and dynamic frequency shift of the narrowed components for, I = 1, 3/2 and 5/2[a]

I	1QC	3QC	5QC	2QC
		a. Half-width at half-height		
3/2	$8/3(J_1 + J_2)$	$8/3(J_1 + J_2)$		
5/2	$16/25(J_1 + 7/2J_2)$	$4/25(14J_1 + 9J_2)$	$20/25(2J_1 + J_2)$	
1				$4(J_1 + J_2)$
		b. Dynamic frequency		
3/2	$8/3(Q_2 - Q_1)$	$8/3(Q_1 + Q_2)$		
5/2	$16/25(Q_2 - Q_1)$	$12/25(3Q_2 - 2Q_1)$	$20/25 (2Q_1 + 2Q_2)$	
1				$4(Q_1 + 2Q_2)$

[a] In this table, the notational abbreviates, $J_k \equiv J_k(k\omega_0)$ and $Q_k \equiv Q_k(k\omega_0)$ have been employed. 1QC denotes component $|1/2> \rightarrow |-1/>$, 3QC $|3/2> \rightarrow |-3/2>$, 5QC$|5/2 \rightarrow |-5/2>$, and 2QC$|(1) \rightarrow |-1>$

Our immediate interest is the quantification of the disappearance of coherence subsequent to creation.

We will consider only the case where the anisotropic quadrupolar Hamiltonian is averaged (not necessarily to zero) in a time short compared to the reciprocal rigid lattice, quadrupolar splitting (motional narrowing), and the case where the anisotropic quadrupolar Hamiltonian is averaged in a time short compared to the reciprocal, Zeeman splitting ($\tau \varphi \, l/\omega_0$), the extreme narrowing. The theory necessary for this development can be summarized quite briefly. If we assume that the motional narrowing limit obtains, then the quantitative characterization of the quadrupolar relaxation, can be derived from a truncated perturbative expansion of the quantum mechanical Liouville equations. In this density operator theory of relaxation, the phase coherence between states $|a>$ and $|a'>$ can be identified as the, α-', the element of the spin density operator, $<\alpha|\sigma(t)|\alpha'>$. These states will be labeled with their $I_Z(m)$ projection. The explicit form of the time evolution of the coherence $|\alpha) \rightarrow |\alpha')$ is described by the Redfield expression

$$(-d/dt)\sigma_{\alpha\alpha'} = -i\omega_{\alpha\alpha'}\sigma_{\alpha\alpha'} + \Sigma_{\alpha''}\Sigma_{\alpha'''}R_{\alpha\alpha'\alpha''\alpha'''}\sigma_{\alpha''\alpha'''}.$$

Where

$$\omega_{\alpha\alpha'} = [(E\alpha - E\alpha')/\hbar]$$

and $R_{\alpha\alpha'\cdot\alpha''\cdot\alpha'''}$ is defined as the first order rate transition constant. Here $\hbar$ is the familiar angular Planck' constant. A detailed quantum mechanical treatment of the above equation leads to the following important results. The summation noted in equation above extends over only those terms for which $\omega_{\alpha\alpha'} = \omega_{\alpha''\alpha'''}$. The spin functions, T_2^k, and the spectral density function, $G_k(\omega)$, are defined as follows:

Fig. 14.22 The coherence level diagrams for multi-quantum filters (MQ). The P represent the pulses in the pulse sequence. **a** double quantum filter (DQF), **b** for triple quantum filter (TQF)
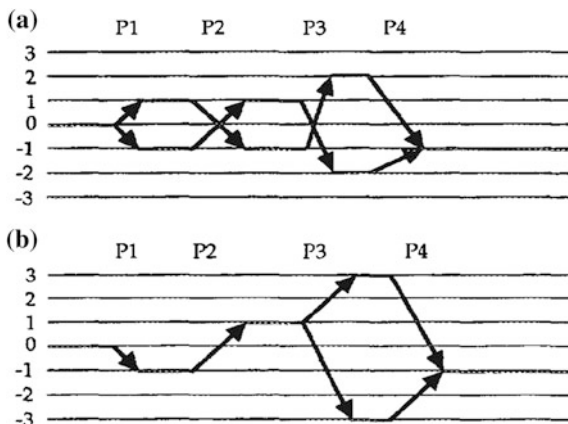
$$T^0{}_2 = (-2/\sqrt{6})\left[\left(3I_z{}^2 - I^2\right)\right]$$

$$T_2{}^{\pm 1} = \pm\left[(I_Z I_\pm + I_\pm I_Z)\right]$$

$$T_2{}^{\pm 2} = -I_\pm{}^2$$

$$Gk(\omega) = J_k(\omega) + i\,Q_k(\omega)$$

$$J_k(\omega)\}\left[(3\pi/40)\left(e^2 qQ/\hbar\right)\left(1 + \eta^2/3\right)Q_k(\omega)\right.$$

$$\{\text{Real/Imaginary}\}\int_0^\infty <Y_2^k(\Omega(t))Y_2^{-k}(\Omega(0) >)\exp(-\omega t)dt.$$

The interaction parameters q, η, and Q are the principal component of the field gradient tensor the field asymmetry parameter and the nuclear quadrupole moment respectively. The time-dependent angular argument of the spherical harmonic (Y) appearing in the above equation positions the principal axis of the electric field gradient, in the laboratory frame. It is well-known, that if the extreme narrowing limit obtains, and the discussion is restricted to isotropic or nonordered environments, then the free evolution of the single quantum coherence, behaves is a simple exponentially damped oscillation even though the observable coherence is a weighted superposition of $2I$ components. If extreme narrowing does not obtain, the kinetic behavior is multi-exponential, except for the simplest of systems (i.e. $I = 1$). These two quite general characteristics can be further generalized, to describe a nQC of any order. It can further be shown that if the extreme narrowing limit obtains and discussion is restricted to isotropic environments free evolution of the n quantum coherence, (I^n-) can be described by an exponentially damped oscillation,

$$<I^n{}_i(\sigma) > \ = \ <I^n{}_-(0) > \exp(in\omega_0 t)\exp(-t/T_2)$$

Fig. 14.23 The experimental flip-angle dependences of three pulse filters. **a** Triple-Quantum filters and **b** double-quantum filters. *Solid-line* envelopes represent the theoretical results. Experimental spectra obtained with 90° flip angle are shown in *upper right* hand corners
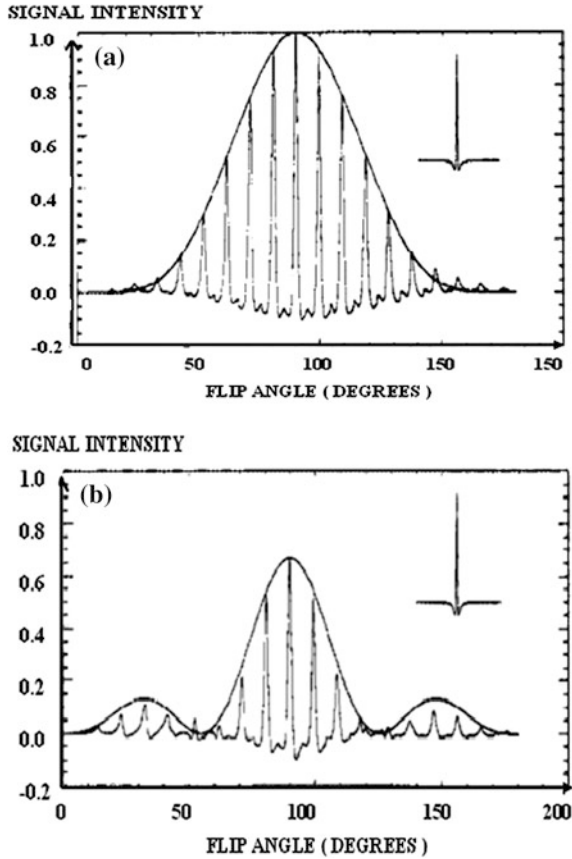
where

$$(1/T_2)_n = [\{2n(n+1)\}\{(4I(I+1)\} - n(n+1) + 1\}$$
$$\{I(2I-1\}^{-2}J]$$

Since extreme narrowing and spatial isotropy is implicit, both the projection and frequency dependency of $J_k(\omega)$ are superfluous and have been omitted. For the simple single quantum (n = 1) coherence, the time constant appearing in the above equation reduces to the well-known result

$$(1/T_2) = \left[4(2I+3)(2I-1)^{-1}I^{-2}J\right]$$

Although these multi-quantum coherences are 21 + 1 − n-fold degenerate, each of these components are coupled together in a way, such that, for an arbitrary *I* and n, the total coherence decays, as a single exponential. If the (Real) spectral density J, is frequency dependent (extreme narrowing does not obtain; Ji(0) ≠ Ji(ω_0) ≠ Ji (2ω_0)), then, the n, quantum coherence, will decay, as a sum of (21 + 2 − n)/2 or

$(2l + 1 - n)/2)$ exponentials, depending upon whether $(2l - n)$ is even or odd, respectively. The isolated spin, does not provide, the investigator, with a convenient handle, to create, nor to observe, these multi-quantum coherences. However, if the spin is oriented by an anisotropic environment, the situation becomes quite different. For the quadrupolar spin, situated, in a spatially anisotropic (ordered), environment, the energy separation, to first order, between any two states, $|m>$ nd $|m' = m - n>$, is given by the expression

$$\hbar\omega_{mm'} = \hbar(m - m')(\omega_0 + (m + m')\omega_Q) = \hbar n(\omega_0 + (2m - n)\omega_Q)$$

In this expression, ω_Q is the residual quadrupolar splitting. We shall assume that $\omega_Q \varphi \omega_0$. It is illustrative to note that whenever $2m = n$, the energy separation is independent of the quadrupolar splitting. The above equation demonstrates that the spectral degeneracy of the $2l + 1 - n$ components of the n quantum coherence, is lifted, whenever $\omega_Q \neq 0$. This assumes that the spin is located at a molecular site with a nonvanishing field gradient. The quantitative description of the relaxation characteristics of these components is extremely simple since each component of the nQC evolves independently from all other components. The explicit widths of a selected narrowed components are given in the Table 14.44 [12].

14.3.8 Multi-Quantum Filters Spin 3/2 Nuclei

We known that multi-quantum filter (MQF) sequence for the analysis of spin-3/2 nuclei has intrinsic localization [13]. It is also known that the triple quantum filter (TQF) is more sensitive than the double quantum filter (DQF). A simplified density matrix approach to the description of bi-exponential behavior of spin-3/2 nuclei can be summarized as follows. The initial reduced thermal equilibrium density matrix $\rho(0)$ is expressed through the Zeeman order T_0^1. The evolution of different tensor operators under the influence of an RF pulse of flip angle β and phase φ is give in terms of the conventional arrow representation. See Figs. 14.22 and 14.23 [13] for expected theoretical and experimental results. The following simplified mathematical expressions should be helpful to some readers.

$$T_p^1 \xrightarrow{\hspace{3cm}} \beta(I_y \cos\varphi - I_x \sin\varphi)$$

$$\sum_{p' = -l}^{l} T_{p'}^1 \, d_{p'p}^1(\beta) \exp(-i\Delta p \, \varphi)$$

Here p' is the new (above thermal) coherence order, and $\Delta p = p' - p$, is the change in the coherence order, under the influence of the RF pulse. See Figs. 14.22 (Fig. 3 in [13]) and 14.23 (Fig. 4 in [13]) for theoretical and experimental results.
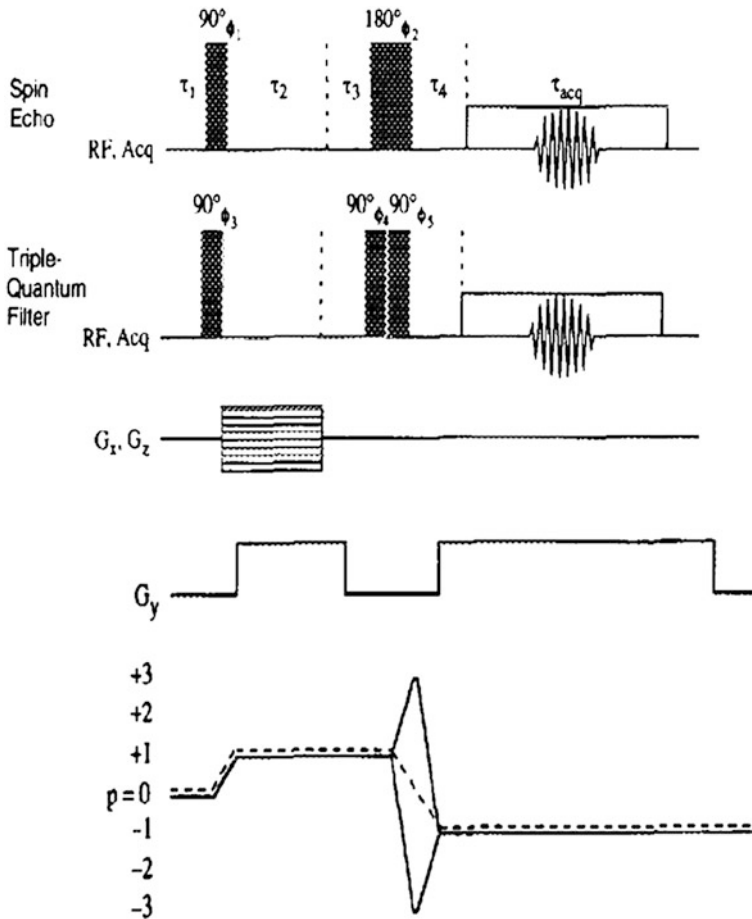
Fig. 14.24 Pulse and gradient sequences and coherence transfer pathway diagrams for three dimensional spin-echo (SE) and triple-quantum filtration (TQF) ^{23}Na imaging. The coherence pathway for the SE and TQF experiments are shown as *dashed solid lines*, respectively. The pulse phases ϕ_1 an ϕ_2 and the receiver phase in the SE experiment are cycled through 16 steps (CYCLOPS + Exorcycle), while the pulse phases ϕ_3 an ϕ_4 and ϕ_5 and the receiver phase in the TQF experiment are cycled through 18 steps

$d^1_{p'p}(\beta)$ are the reduced rotation-matrix elements. The evolution under the influence of RF interaction (with short RF pulses) changes the order and retains the rank.

The evolution of tensor operators under the quadrupolar relaxation changes the rank and conserves the order. For example, under the influence of transverse relaxation T^1l and T^3l evolve as
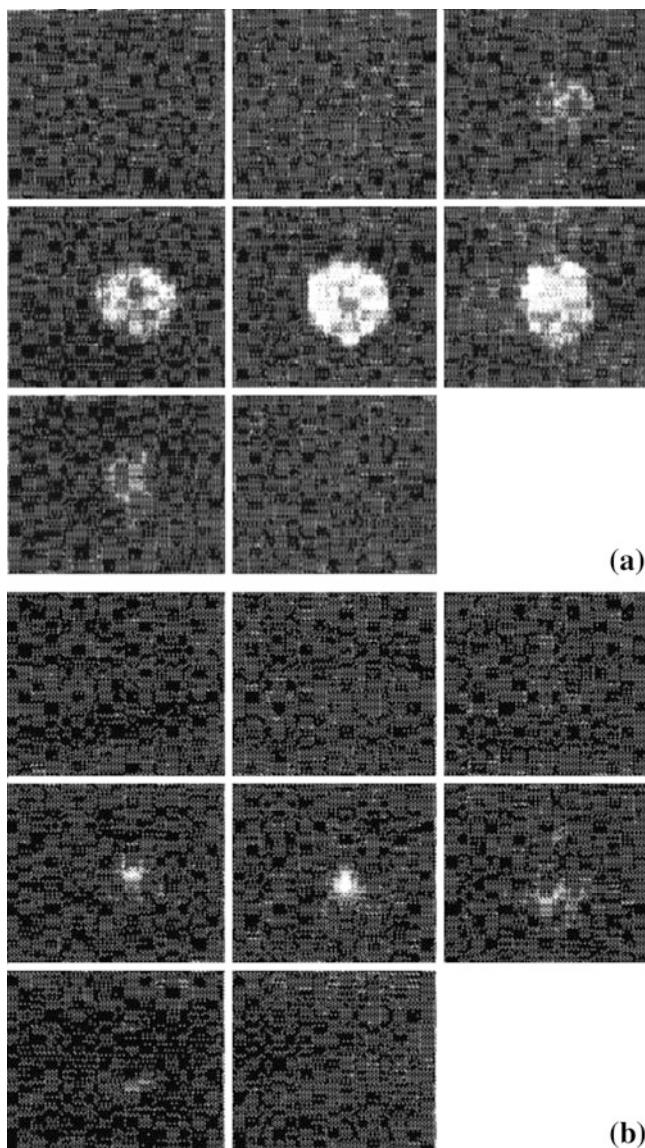
Fig. 14.25 Three dimensional image of a live mussel (Mytilus edulis). The conventional SE ^{23}Na image is shown in (**a**), while (**b**) shows the TQF ^{23}Na image. Note that the *darker area* in the SE image correspond precisely to the *brighter areas* in the TQF image, indicating that these represent concentration of slowly tumbling sodium ions. Imaging parameters used in both SE and TQF experiments: 46 μs 90° pulse length; 33,333 Hz spectral width; 32 complex points in acquisition period τ_{acq} = 9.6 ms; duration of G_x an G_z phase encoding gradients τ_2 = 4.5 ms; gradient stabilization interval τ_3 = 0.5 ms in (**a**) pre-acquisition period τ_4 = 0.2 ms; approximate filed of view 60(x) æ 40(y) æ 40(z) mm. The relaxation delay after acquisition was, τ_1 = 80 ms in (**a**) τ_1 = 140 ms in (**b**). The image in (**a**) represents 16 acquisitions for each of $8G_x$ and $32G_z$, phase encoding steps, while that in (**b**) represents 270 acquisitions for each of $8G_x$ and $32G_z$, phase encoding steps. The total imaging time for (**a**) was 6 min, while for (**b**) 173 min. A Gaussian weighting factor was applied in the y and z dimensions to the data (**b**)

$T^1_1 = \text{Relaxation}$

$T^3_1 = = \text{Relaxation}$ $\quad f^{(1)}{}_{11}(1)T^1_1 + f^{(1)}{}_{31}(1)T^3_1$

$\qquad\qquad\qquad\qquad f^{(1)}{}_{13}(1)T^1_1 + f^{(1)}{}_{33}(1)T^3_1$

The functions f in the above equations are given by

$$f^{(1)}{}_{11}(t) = (1/5)[3\,\exp\left(R^{(1)}{}_1 t\right) + 2\,\exp(R^{(1)}{}_2 t)]$$

$$f^{(1)}{}_{31}(t) = f^{(1)}{}_{13}(t) = (\sqrt{6}/5)[\exp\left(R^{(1)}{}_1 t\right) - \exp(R^{(1)}{}_2 t)]$$

$$f^{(1)}{}_{33}(t) = (1/5)[R^{(1)}{}_1 t + 2\,\exp(R^{(1)}{}_2 t)]$$

Here $R^{(1)}_1$ and $R^{(1)}_2$ are fast and slow relaxation rates respectively.

14.3.9 Triple Quantum Filtering: Sodium NMRI

One can demonstrate the effectiveness of a simple pulse sequence of three dimensional triple quantum filter (TQF) ^{23}Na imaging [14]. Three-dimensional images of a small phantom containing 50 mM Nacl, in an agarose gel and of a blue mussel (Mytilus edulis) are considered. The optimum values of the three precession and gradient intervals are different in the spin echo (SE) and triple quantum filter (TQF) imaging experiments. In the SE experiment, the NMR signal starts decaying immediately, immediately after the initial 90° pulse, due to transverse relaxation. Thus, the sensitivity of the experiment, is optimized, by keeping the half-echo time $1/2\ T_E = \tau_2 + \tau_3 = \tau_4 + 1/2\ \tau_{acq}$, as short as possible. This is consistent with the requirements of the pulse encoding and readout gradients. In the TQF experiment, in contrast, the bi-exponential transverse relaxation of the slowly tumbling sodium ions, must be allowed to produce double anti-phase single quantum coherence. See Figs. 14.24, 14.25 [14] for theoretical and experimental results.

14.3.10 Quadrupole Interactions: Quantum Biexponential Relaxation

The spin relaxation of a nucleus having an electric quadrupole moment (spin $I \geq 1$) is usually due mainly to the interaction of the quadrupole moment with electric field gradients present at the position of the nucleus. Previous calculations predict that both the longitudinal and transverse spin relaxation produced by a quadrupole interaction are simple exponential decays if (1) the nucleus has spin 1 = 1, or (2)

the electric field gradients fluctuate much more rapidly than the Larmor period of the nucleus, a situation referred to as a short correlation time, or extreme narrowing case. If neither of the above conditions is satisfied, both the longitudinal and transverse relaxations produced by a quadrupole interaction are the sums of two or more decaying exponentials [15]. While this fact must surely have been apparent to previous investigators, the author [15] is not aware of a treatment of this situation in the literature. Consider a nucleus with spin $I \geq 1$, gyromagnetic ratio γ, and quadrupole moment Q, located in one of the molecules of a sample which is exposed to a magnetic field H_{ok}.

The spin interacts with its molecular surroundings through a quadrupole coupling. It is assumed that the average of the quadrupole coupling is zero, as is appropriate for a nucleus in a molecule of a liquid or gas. The spin can be described by a reduced density operator $\sigma(t)$ in the sense that the expectation values of the components of the spin I, averaged over an ensemble of identical systems, are given by $<I> = Tr[s\sigma(t)I]$. The matrix elements of $\sigma(t)$ can be evaluated by use of the density operator theory of relaxation, which provides a first-order linear differential equation for $\sigma(t)$. The initial condition of the spin system is taken to be the result of the application to the system in thermal equilibrium of a "θ-degree pulse;" i.e. the application of a magnetic field H_1 (i cos ω_ot− j sin ω_ot) for a time $t_\theta = \theta/\gamma H_I$ short compared to a time in which appreciable relaxation occurs. $\omega_o = '\gamma H_o$ is the Larmor frequency of the nucleus in the magnetic field H_{ok}. For details about useful mathematical expressions, see Appendix A.30.

14.3.11 Multiple-Quantum Spectroscopy 3/2 Spins-Isotropic Phase

In isotropic phase, the longitudinal and transverse relaxation of quadrupolar nuclei with spin quantum numbers $S > 3/2$ can only be described by single exponential decays if the extreme narrowing approximation is fulfilled, i.e. if the correlation time is much shorter than the inverse of the Larmor frequency, '$\omega_c << \omega_{o-1}$. If the nuclei under investigation are associated with macromolecules, clusters or slowly tumbling complexes, the relaxation is multiexponential [16]. This behavior has been the subject of intensive studies, particularly for quadrupolar nuclei such as ^7Li, ^{23}Na, ^{35}CI, ^{37}CI, ^{39}K (S = 3/2) or ^{17}O, ^{25}Mg, ^{27}AI, ^{67}Zn (S = 5/2) or ^{43}Ca (S = 7/2), which frequently occur in systems that feature rapid exchange with binding sites of (biological) macromolecules. Under such circumstances, the bound species is usually not observable, but the line shape and longitudinal relaxation of the free species is again multiexponential. The deviations from simple exponential behavior tend to be more pronounced for transverse relaxation, but appear difficult to measure by conventional one-dimensional spectroscopy.

The detection of triple-quantum coherence in S = 3/2 spins provides a straightforward measure of the deviation from simple exponential behavior of both transverse and longitudinal relaxation. Transverse Relaxation: It has long been recognized that transverse relaxation of coherences of degenerate transitions

cannot in general be described by a single relaxation time T_2 For S = 3/2 spins in isotropic solution, where the quadrupole interaction is averaged to zero, $(\omega_Q) = 0$, there are three degenerate single-quantum transitions. The density operator may be expanded in terms of single-element operators, as below.

$$\sigma(t) = \sum \sigma_{rs}(t)|r> <s.|$$

The coefficients σ_{rs} of the operators $|r> <s|$ are equivalent to elements of the matrix representation of the density operator in the eigenbase of the free preces­sion Hamiltonian. If the eigenstates are numbered $|1> = |M = 3/2>$, $|2> = |M = 1/2>$, $|3> = |M = -1/2>$, and $|4> = |M = -3/2>$, the decay of the three degenerate single-quantum elements σ_{rs} is described by a coupled set of differential equations

$$\begin{pmatrix} d/dt(\sigma_{12}(t)) \\ d/dt(\sigma_{23}(t)) \\ d/dt(\sigma_{34}(t)) \end{pmatrix} = \begin{pmatrix} R^{(1)}_{1212} & R^{(1)}_{1223} & R^{(1)}_{1234} \\ R^{(1)}_{2312} & R^{(1)}_{2323} & R^{(1)}_{2334} \\ R^{(1)}_{3412} & R^{(1)}_{3423} & R^{(1)}_{3434} \end{pmatrix} \begin{pmatrix} (\sigma_{12}(t)) \\ (\sigma_{23}(t)) \\ (\sigma_{34}(t)) \end{pmatrix}$$

The Redfield matrix $R^{(1)}$ for pure quadrupolar relaxation [the superscript (1)] stands for relaxation among the $|p| = + 1$ quantum coherences]:

$$R^{(1)} = C \begin{pmatrix} -(J_0 + J_1 + J_2) & 0 & J_2 \\ 0 & -(J_1 + J_2) & 0 \\ J_2 & 0 & -(J_0 + J_1 + J_2) \end{pmatrix}$$

with the spectral densities for isotropic motion:

$$Jn = (2\tau_c)/\left[1 + (n\omega_0\tau_c)^2\right]$$

And the constant for s = 3/2, is

$$C = (1/40)\left[(e2qQ/\hbar)^2(1 + \eta^2/3)\right]$$

In order to describe the time dependence of the coefficients $\sigma_{rs}(t)$, the matrix $R^{(1)}$ can be diagonalized:

$$R_{diag} = U([R^{(1)}]U^{-1}$$

With

$$U = (1/2)^{1/2} \begin{pmatrix} 1 & 0 & 1 \\ 0 & 2^{1/2} & 0 \\ 1 & 0 & -1 \end{pmatrix}$$

This leads to a decoupled set of differential equations. The single-quantum eigenvectors $\sigma i^{(1)}$ (t) are labeled with a single subscript i, to distinguish, to distinguish them from the σ_{rs} coefficients, as below.

$$
\begin{pmatrix} d/dt(\sigma_{12}(t)) \\ d/dt(\sigma_{23}(t)) \\ d/dt(\sigma_{34}(t)) \end{pmatrix} = U \begin{pmatrix} d/dt(\sigma_{12}(t)) \\ d/dt(\sigma_{23}(t)) \\ d/dt(\sigma_{34}(t)) \end{pmatrix} = R_{diag} \begin{pmatrix} \sigma^{(1)}{}_1(t) \\ \sigma^{(1)}{}_2(t) \\ \sigma^{(1)}{}_3(t) \end{pmatrix}
$$

with

$$
R_{diag} = \begin{pmatrix} R_1^{(1)} & 0 & 0 \\ 0 & R_2^{(1)} & 0 \\ 0 & 0 & R_3^{(1)} \end{pmatrix}
$$

The eigenvectors decay exponentially (the elements $R_i^{(1)}$ of R_{diag} are negative) as follows.

$$
\sigma_i^{(1)}(t) = \sigma_i^{(1)}(0)\exp\left\{R_i^{(1)}t\right\}
$$

with the following eigenvalues and eigenvectors:

$$
R_1^{(1)} = -C(J_0 + J_1), \sigma_1^{(1)} = (1/2)^{1/2}(\sigma_{12} + \sigma_{34}),
$$
$$
R_2^{(1)} = -C(J_1 + J_2), \sigma_2^{(1)} = \sigma_{23},
$$
$$
R_3^{(1)} = -C(J_0 + J_1 + 2J_2),
$$
$$
\sigma_3^{(1)} = (1/2)^{1/2}(\sigma_{12-}\sigma_{34})
$$

Thus the sum of the "outer" components of the three degenerate single-quantum coherences of the spin $S = 3/2$, in isotropic phase, decays with in the fast motion limit (extreme narrowing). Iin the case of isotropic motion, one has $J_o = J_1 = J_2 = J = 2\tau_c$, and all the components decay with the same rate. The equation, which describes the net effect of transverse relaxation, is summed up symbolically, as follows.

Transverse Magnetization

$$
R^{(1)}
$$
$$
T_{1,+1} \rightarrow T_{1,+1}f^{(1)}{}_{11}(t) + T_{3,+1}f^{(1)}{}_{31}(t)
$$
$$
f^{(1)}{}_{11}(t) = (1/5)\left\{3\ \exp R^{(1)}{}_1 t + 2\exp R^{(1)}{}_2 t\right\}
$$
$$
f^{(1)}{}_{31}(t) = \left(6^{1/2}/5\right)\left\{\exp R^{(1)}{}_1 t - \exp R^{(1)}{}_2 t\right\}
$$

The functions $f_{l',l(t)}$ describe the change in rank from l to l' due to transverse relaxation among the $p = \pm 1$ (single quantum) coherences. The sequences of indices is chosen to be consistent with those appearing for the Wigner rotation elements $d_{p'p}$, which represent change in coherence produced from p to p' under radio frequency (RF) pulses. The functions $f^{(1)}{}_{l'l}$ are both biexponential. In the simplest case of, the fast motion, one gets

$$f^{(1)}{}_{11} = \exp(-t/T_2)$$

$$f^{(1)}{}_{31}(t) = 0$$

Here $T_2 = (2CJ)^{-1}$. In the case of longitudinal magnetization, similarly, the final result can be summarized as below.

Longitudinal Magnetization:

$$R^1$$

$$T_{1,+0} \rightarrow T_{1,0}f^{(0)}{}_{11}(t) + T_{3,0}f^{(1)}{}_{31}(t)$$

$$f^{(0)}{}_{11}(t) = (1/5)\left\{4\,\exp R_3{}^{(0)}{}_1 t + \exp(R^{(1)}{}_4 t)\right\}$$

$$f^{(1)}{}_{31}(t) = (2/5)\left\{-\exp R^{(1)}{}_3 t - \exp(R^{(1)}{}_4 t)\right\}$$

In the fast limit (extreme narrowing) case, on obtains, $R3^{(0)} = R4^{(0)} = -2CJ) = -4C\tau c$, And we obtain as expected,

$$f^{(0)}{}_{11} = \exp(-2CJ) = \exp(-t/T_1)$$

$$f^{(1)}{}_{31}(t) = 0$$

with the single time constant $T_1 = (2CJ)^{-1} = (s4C\tau_c)^{-1} = T_2$.

14.3.12 Triple Quantum Filtered Sodium MRI

In the human skeletal system, cartilage performs the important function of facilitating joint movement and distributing mechanical load. Osteoarthritis (OA) a progressive disease of cartilage, can cause severe disability by impeding normal joint function. It is estimated that over 40 million people suffer from this debilitating disease in the United States alone. While therapeutic modalities exist, they are generally useful in the early stages of the disease. Early diagnosis would allow efficient therapeutic intervention to halt the progress of the disease. The major components of the extracellular matrix of cartilage are proteoglycans (PG), collagen, and water. The early stage of OA is primarily associated with a loss of PG and changes in water content. Although conventional proton MRI provides high-resolution images of cartilage, it is not sensitive to early changes in cartilage degeneration. Recently, sodium MR has been shown to be useful in measuring PG changes in cartilage. Furthermore sodium in cartilage is under the influence of a nonisotropically or incompletely averaged quadrupolar interaction which leads to biexponential relaxation rates and the generation of multiple quantum coherences. Several workers have studied sodium in biological tissues using multiple quantum filtered (MQF) NMR. MQF NMR signal is more sensitive to the macromolecular content and arrangement in the extracellular matrix. Therefore was employed to obtain single quantum sodium MR images. Sodium images were compared with
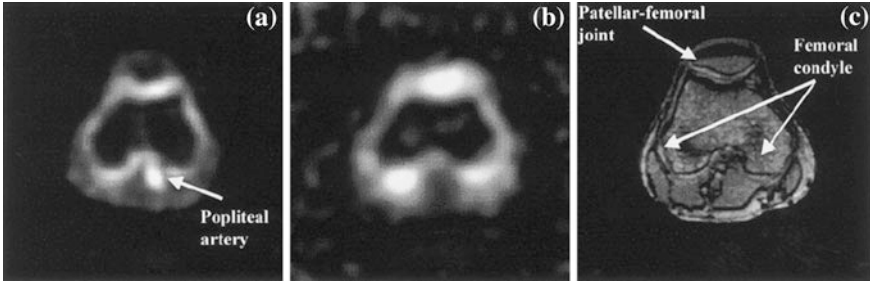
Fig. 14.26 In vivo sodium (**a**) single quantum and **b** TQF axial MR images across the human knee of a healthy 27-year-old male volunteer. **c** is the corresponding proton image of the same location. In the single quantum image (**a**), the arrow indicates an artery, which is not visible in the TQF image (**b**)

reference proton images obtained with a standard spoiled gradient-echo imaging sequence.

One can also determine sodium transverse relaxation times from the biexponential fit of the TQF [7] time domain signal. Further optimizations to improve signal-to-noise ratio and image resolution are discussed. We have developed the theory as to how incomplete averaging of a quadrupole Hamiltonian over the relevant time scales leads to multiple quantum coherences and multi-exponential relaxation for spin-3/2 nuclei.

Here we briefly review some of the relevant concepts of biexponential transverse relaxation of sodium nuclei in the presence of quadrupolar interaction. In the case of sodium ions undergoing fast isotropic motion, the quadrupolar interaction is averaged to zero and the three single quantum transitions are degenerate. Sodium nuclei exhibit biexponential relaxation rates in biological tissues: $R_f^{(1)}$ is the relaxation rate associated with the two outer transitions and $Rs^{(1)}$ is the rate for the inner transition. In the extreme narrowing condition $\omega\tau_c \ll 1$, where τ_c is the correlation time describing isotropic motion and ω is the Larmor precesion frequency, the two decay rates are equal. The correlation time reflects the rotational motion modified by the chemical exchange that the sodium ions experience in cartilage. But if the motion is slow ($\omega\tau_c \gg 1$), as is the case of sodium nuclei, in the presence of large PG and collagen macromolecules in cartilage, the two rates will be different. In this regime, NMR relaxation creates multiple quantum coherences that can be detected by using the appropriate multiple quantum filter. Triple quantum filtered NMR provides information about sodium in cartilage undergoing slow motions. The TQF signal intensity for a single spin-3/2 system as a function of preparation time (τ) and detection time (t) is given by

$$S(\tau, t) \sim \left[\left\{ \left(\exp\left(-R^{(1)}{}_f \, \tau \right) \cos\left(\omega_q \tau \right) - \exp - \left(R^{(1)}s \, \tau \right) \right\} \right.$$
$$\left. \times \left\{ \left(\exp\left(-R^{(1)}{}_f t \right) \cos\left(\omega_q \, \tau \right) - \exp - \left(R^{(1)}s t \right) \right\} \left\{ \left(\exp - R^{(3)}{}_i \delta \right) \right\} \right]$$

Here, R_f and R_s are the fast and slow components of the transverse relaxation rate, respectively. The relative contribution of $R_1^{(3)}$ (longitudinal), the triple quantum coherence relaxation rate, is kept small by choosing a very short evolution time (δ). The quadrupolar interaction frequency, ω_q, is

$$\omega_q = \omega^1 q\left[(3\cos^2\theta_{1d} - 1)/2\right]$$

where ω^1_q is the quadrupolar coupling constant in the local director frame and θ_{ld} is the angle between the local director and the static magnetic field (B_0). The above equations, show that the quadrupolar interaction frequency affects the fast relaxation component of the NMR signal. Therefore, to compute relaxation rates accurately, one must determine ω_q in cartilage. This poses an intractable problem during in vivo imaging. Cartilage, like most biological tissues, is heterogeneous in nature and therefore the orientation of the local directors can assume different values. This is also true if the entire cartilage is molecularly homogeneous. The net result is an unknown distribution of ω_q values for a given sample of cartilage. In order to overcome this problem, we assume transverse relaxation rates, R_{2rise} and R_{2fall}, which are the residual quadrupolar interaction weighted $R_f^{(1)}$ and $R_s^{(1)}$ rates, respectively. Therefore, for a small evolution time (δ), the signal can be written as

$$S(\tau, t) \sim [\{(\exp(-R_{2rise}\tau) - \exp - (R_{2fall}\tau)\}$$
$$\times \{(\exp(-R_{2rise}t) - \exp - (R_{2fall}^{(1)}t)\}]$$

Thus one can deduce that there will be a value of preparation time (τ) for which a maximum signal amplitude will occur. During imaging, we set the value of τ to this optimum evolution time ($\tau_{optimal}$) which can be determined from the relaxation rates according to the equation

$$\tau_{optimal} = [\{\ln(R_{2rise}/R_{2fall})\}/\{(R_{2rise}/R_{2fall})\}]$$

In the experiment, one calculates the relaxation rates by acquiring a TQF FID for an arbitrary preparation time. One then calculates t he $\tau_{optimal}$ to be used during imaging. Since one calculates the relaxation times from the FID, one actually obtains R^*_2 rise and $R^*_{2\ fall}$, the relaxation rates in the presence of inhomogeneity. The Fig. 14.26 [7] demonstrates the illustration of the above theoretical concept being put into practice, as imaging. One should note that the bright artery at the bottom of image A (indicated by arrow) is not visible in the TQF image. This is because the TQF sequence suppresses signal from the mutationally narrowed sodium in blood. Although the concentration of sodium is lower in blood than in cartilage, the T_2 of sodium in blood is longer and therefore results in an enhanced signal from the artery in the single quantum image. Thus the signal from the artery served as an internal control for evaluating the filtering capability of the TQF sequence. See Fig. 14.26 [7] for practical illustration.

14.3.13 Triple Quantum Filtered Sodium MRI-Spin 3/2 Dynamics

Sodium MRI has been proposed as a means to diagnose and monitor pathology in humans. One of the main thrusts for the pursuit of sodium MRI lies in the large changes in sodium content that are associated with the development of pathology [17]. In the brain, for example, there is a large concentration gradient across the cell membrane. This gradient results from the active maintenance of a relatively low intracellular sodium concentration (~ 10 mM in normal brain cells) against a very large extracellular sodium pool (with an average brain concentration of 140 mM). The large difference in sodium content between these two tissue compartments is of critical importance for the brain's function and, because of its large energetic cost, is highly sensitive to the changes in brain physiology that follow the onset of disease. Because the extracellular sodium content is in equilibrium with the plasma (which has a fixed sodium content of 140 mM), the intracellular compartment can exhibit very large (100 %), and distinctive, changes in sodium concentration during the course of disease. Therefore, a means for monitoring the intracellular sodium content in vivo using MRI could prove to be a very useful tool for the diagnosis and follow-up of disease in humans. Different schemes have been proposed for separating the sodium NMR signal from the intra and extra cellular compartments. Among them, the triple-quantum (TQ) filtered NMR [17] techniques have received considerable attention because of their non-invasive nature and relatively simple implementation.

Although the characteristics of the TQ-filtered sodium NMR signal have been well described in various organ systems using animal models, it is only recently that in vivo TQ-filtered sodium MRI in humans has been demonstrated. This stems from the relatively weak nature of the TQ-filtered sodium NMR signal, which requires the use of efficient imaging schemes in order to produce images of acceptable signal-to-noise ratio, in reasonable imaging times (20 min). As previously demonstrated, the TQ-filtered sodium signal has a strong dependence on the spatial distribution of the radiofrequency (RF) field and, in particular, can be better observed in whole-body scanners if no refocusing pulses are used. The dynamics of the system of spins is described by the evolution of the density operator [17]. All calculations reported here are done in the Larmor frequency rotating frame, indicated by an asterisk. The time evolution of the density matrix under a static Hamiltonian H^*_S (time-independent) and a fluctuating part $H^*_{QF}(t)$ is given by the master equation

$$d\sigma^*/dt = -[H^*_S, \sigma^*] + f(\sigma^*)$$

The relaxation term $f(\sigma^*)$ is expressed as

$$f(\sigma^*) = -\int <[H^*_{QF}(t), [(\exp - iH^*_s\tau)H^*_{QF}(t-\tau)(\exp(iH^*_s\tau), \sigma^*(t)]]d\tau$$
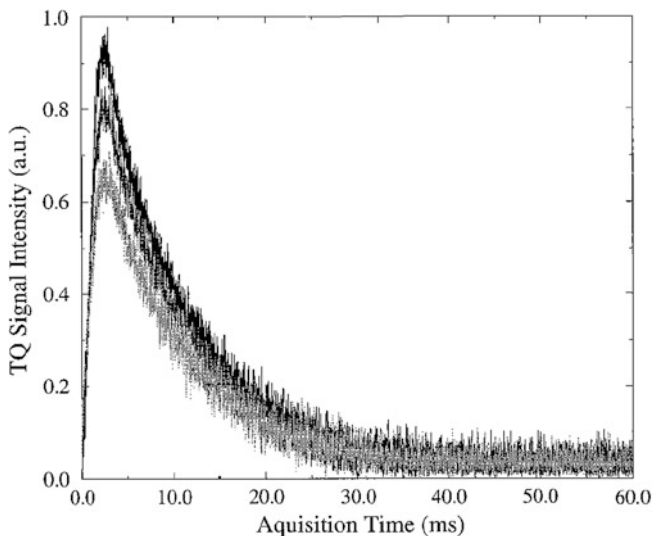
Fig. 14.27 Experimental TQ signal intensity as a function of acquisition time. The three curves shown correspond to RF pulse widths of 0.1 ms (*top*), 0.51 ms (*middle*), and 0.9 ms (*bottom*)

Throughout this work, the density operator and the Hamiltonians are represented in terms of irreducible tensor operators. Symmetric and antisymmetric combinations are defined as

$$T_{lm}(s) = (1/\sqrt{2})(T_{1-m} + T_{lm})$$
$$T_{lm}(a) = (1/\sqrt{2})(T_{1-m} + T_{lm})$$

With respect to the Larmor frequency rotating frame, the Zeeman Hamiltonian ($Hz = \omega_0 I_z = \omega_0 T_{10}$) vanishes. The static Hamiltonian in the master equation is then given by the sum of the static quadrupolar and RF contributions:

$$H^*{}_s = [H^*{}_{QS} + H^*{}_1]$$

Denoting ω_Q as the residual static quadrupolar interaction parameter, the static quadrupolar Hamiltonian is expressed as

$$H^*{}_{QS} = [(1/6)\omega_Q\{3I_x{}^2 - I(I+1)\}]$$
$$\omega_Q[\sqrt{(1/6)}T_{20}] = [\omega_Q T_{20}]$$

the RF field is applied exactly on resonance along the *x*-axis and has the form

$$H^*{}_1 = [\omega_1 I_x] = [\omega_1 T_{11}(\alpha)] = [\sqrt{5}\omega_1 T_{11}(\alpha)]$$

a phase is associated with the hard pulse, this will be reflected in a change of base, not in the form of the RF Hamiltonian. Assuming that a hard pulse of phase ϕ_1 is followed by a hard pulse of phase ϕ_2, the change in base can be expressed as

$$T^{(a)}lm(\alpha) = T^{(b)}lm(\alpha)\cos[m(\varphi_2 - \varphi_1)]$$
$$+ iT^{(b)}lm(s)\sin[m(\varphi_2 - \varphi_1)],$$
$$T^{(a)}lm(s) = T^{(b)}lm(s)\cos[m(\varphi_2 - \varphi_1)]$$
$$+ iT^{(b)}lm(a)\sin[m(\varphi_2 - \varphi_1)],$$

We now, express the static Hamiltonian, and neglecting the relaxation contribution, the master equation becomes

$$d\sigma^*/dt = -i[\omega_Q T_{20} + \sqrt{5}\omega_1 T_{11}(\alpha), \sigma^*]$$

With the commutation relations, the above reduces to two sets of coupled differential equations. One need to go through some more mathematical manipulations [17] to get the final result. Biological systems are intrinsically complicated, with properties varying spatially and temporally. One can model the sample as composed of a multitude of domains; within each domain, the motion of the ions is rapid, contributing to the spectral densities J_0, J_1, and J_2 that determine the conventional transverse relaxation rates T_{2f} and T_{2s}. The exchange between domains is considered negligible on a time scale exceeding the inverse line splittings and/or widths. All nuclei in the domain have the same relaxation times and, for simplicity, we will assume that all of the domains are characterized by the same relaxation times. In each domain, the 3/2-spin sodium nuclei experience a non-zero average EFG due to the anisotropic interaction of these ions with macromolecules and to the nonrandom distribution of these macromolecules within each domain (the fluctuating part induces relaxation).

The residual EFGs are characterized by the principal value $<V_{zz}>$ along the major axis (given by the domain orientation) and by the asymmetry parameter $\eta = [(V_{xx}-V_{yy})/(V_{zz})]$. Therefore, each domain will be characterized by a static quadrupolar coupling ω_0 that depends on the orientation of the domain with respect to the main magnetic field B_0 (defined by the angles θ and ϕ). The final useful result as applied to a biological sample is

$$\omega_Q = (eQ/4\hbar)<V_{zz}>\left[(3\cos^2\theta - 1 + \eta\sin^2\theta\cos2\varphi)\right]$$

In single crystals and macroscopically oriented liquid crystals, all of the domains have the same residual EFGs and are parallel. If the ions/molecules are constrained within the domains and the domains are randomly oriented with respect to B_0 (but having the same residual EFGs and η), the NMR spectrum has the well-known "Pake powder" characteristics. For poorly ordered samples, such as biological tissue, the domains are characterized by a wide distribution of $<V_{zz}>$ & and η values. As can be shown by simulations, the resultant ω_Q distribution in such samples can be approximated as Gaussian. Consequently, we assumed that such a Gaussian distribution is valid for our sample. It is expressed as

$$W(\omega_Q) = (1/\sqrt{2\pi}\sigma)\exp[-(\omega_Q - <\omega_Q>^2)/2\sigma^2]$$
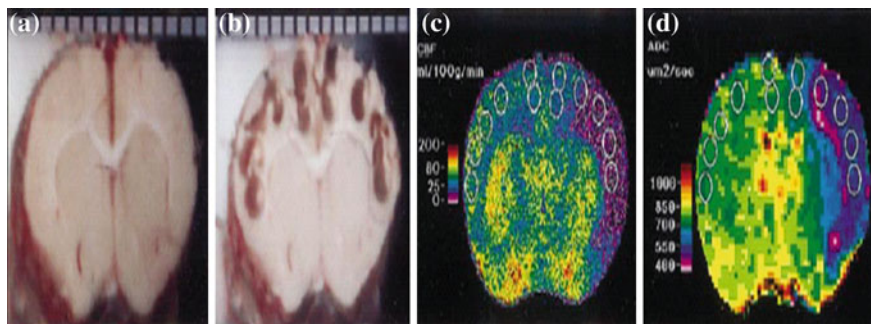
Fig. 14.28 Prepunch (**a**), postpunch (**b**), CBF (**c**), and ADC (**d**) images at the same coronal level. The prepunch image (**a**) shows the cut face of the brain in the cryostat. The prepunch (**a**) and postpunch (**b**) images were photographed in the cryostat with a millimeter scale placed along the dorsal surface. The prepunch image (**a**) was aligned with the ADC image (**d**), and its ventral surface was aligned with the postpunch image (**b**). The CBF image (**c**) was aligned to the ADC image (**d**) by positioning the autoradiographic film before digitization. The locations of the punches in the postpunch image (**b**) were used to locate the regions (*white circles*) selected in the CBF (**c**) and ADC (**d**) images

Here, by ω (within $<\,>)_Q$ we denote the average value of the static quadrupolar interaction parameter, while σ denotes its second moment, $\sigma^2 = [(\omega(\text{within} <\,.>)_Q)]^2$. In an experimental situation one observes as follows. We have assumed the sample to be homogeneously anisotropic, such that the pool of isotropic ions outside the extreme narrowing limit present in the sample was negligible. Therefore, the only ions contributing to both the TQ-filtered and the DQ-MA signal were the ions in anisotropic motion. Since in the presence of a non-zero average electric field gradient (EFG) the relations between transverse relaxation times and spectral density functions are

$$(1/T_{2f}) = [J_0(\omega_0) + J_1(\omega_0) + J_2(2\omega_0)]$$
$$(1/T_{2s}) = [J_1(\omega_0) + J_2(2\omega_0)]$$

and assuming no high-frequency dispersion ($J_1 \approx J_2$), the two relaxation times T_{2s} and T_{2f} completely determine the relevant spectral density functions. The Fig. 14.27 [17], shows the experimental results, in agreement with the simulations carried out.

14.3.14 Brain Tissue Sodium: Focal Cerebral Ischemia—Animal Model

Several thrombolytic treatments have been shown to be efficacious. These treatments require administration during the hyper acute period within 6 h of stroke onset. For example, if intravenous tissue plasminogen activator (tPA) administration is delayed
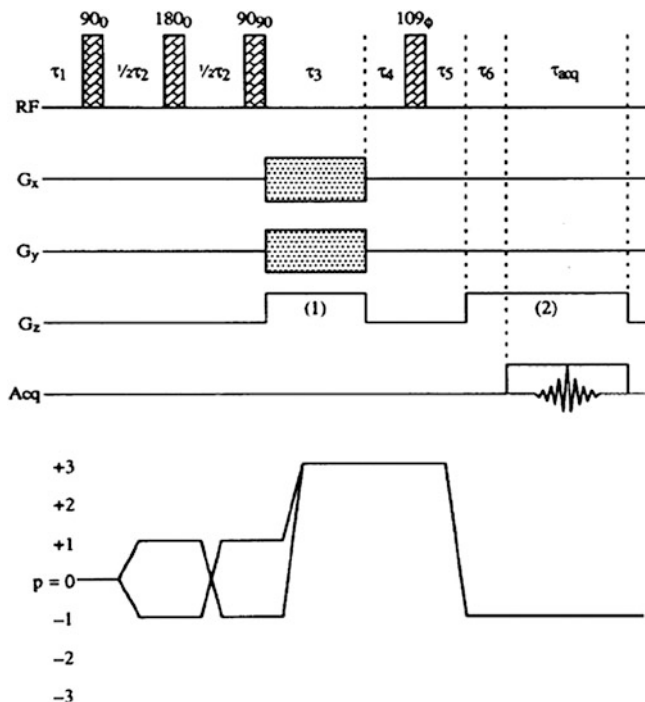
Fig. 14.29 Pulse sequence and coherence transfer pathway diagram for triple-quantum sodium imaging. Pulse flip angles and phases are given in degrees. The sequence for three-dimensional Fourier imaging is shown, but in the experiments described, only one phase-encoding gradient was used since only a two-dimensional projection image was required. The assignment of the gradients G_x, G_y and G_z, is arbitrary

past 3 h, the risk of cerebral hemorrhage outweighs the benefit of thrombolysis. However one-fifth to one half of potential subjects cannot be treated with these agents because they or a family member were not aware or were asleep when the stroke occurred and the time of stroke onset could not be determined accurately or at all. Brain tissue sodium concentration ($[Na^+]$), including intracellular, extracellular, and interstitial concentrations, increases gradually and incessantly during the initial hours of experimental focal cerebral ischemia [18]. MRI Na^+ measurements have been advocated as possessing a threshold that if exceeded, indicates irreversible tissue damage. In contrast to the persistent increase in $[Na^+]$, cerebral blood flow (CBF) and the apparent diffusion coefficient (ADC) of water drop very quickly and remain relatively constant during this same several-hour period. It is seen that by measuring several physiological and biochemical parameters, an objective estimate of the time after onset can be determined.

By using the initial drop in ADC and CBF to select endangered brain tissue, we hypothesize that $[Na^+]$ in these selected regions can be used to estimate the time after arterial occlusion. Although we use an experimental model of ischemic stroke

in the rat and brain tissue sampling, all of the crucial measurements can be made in humans with MRI, which suggests that this scheme for estimation of time after onset could be used to make an inclusion decision for thrombolytic therapy. A sagittal gradient recalled echo image through the midline of the brain was acquired to position the coronal images for the study. In regions with either low or normal ADC, ADC and CBF did not change between 100 and 450 min after arterial occlusion (data not shown). These parameters were used to select those ischemic regions in which [Na$^+$] increased. When both CBF and ADC thresholds were used to select at-risk regions in the subset of animals, Ta (time after occlusion) showed a strong linear correlation with [Na$^+$]. The slow process of Na$^+$ accumulation in ischemic regions is based on residual blood flow that delivers Na$^+$ from plasma and is based primarily on the increase in Na$^+$ influx meditated by the stimulation of Na$^+$, K$^+$-ATPase in ischemic the cortex.

The albuminal location of Na$^+$, K$^+$-ATPase contributes to the lack of Na$^+$ transport from brain to blood. The rates of Na$^+$ increase vary between 0.71 and 1.10 (mEq/kg DW)/min. The determination of ADC with MRI is well established and is considered a surrogate measure of therapeutic effectiveness in clinical trials. However, the MRI methods for determination of CBF and especially [Na$^+$] are still evolving. Perfusion indices are currently monitored with MRI with spin-tag and racking. The lack of quantification and the inaccuracy at low flows could be overcome with the use of the ratio of ischemic to normal cortex. This proposed scheme to estimate time after occlusion is a 2-step process. First, the identification of severely endangered tissue with both CBF and ADC or just ADC is needed to choose only the regions in which brain tissue [Na$^+$] increases. Both CBF and ADC drop quickly after occlusion and stay relatively constant during the initial hours, so they can be used without regard to the time after occlusion. Second, the pattern of slow and constant change in [Na$^+$] is used as a stopwatch that is started at the moment of arterial occlusion. This general scheme has potential for estimation of the time after ischemic onset in humans because all of these parameters, including ADC, CBF, and [Na$^+$], can be estimated with MRI. See Fig. 14.28 [18] for a practical illustration in rat focal cerebral ischemia.

14.3.15 Sodium Imaging; Triple Quantum

Magnetic resonance imaging of sodium is known to be an attractive alternative to proton imaging for detecting certain physiological abnormalities. Relative to the proton however the disadvantages of the ^{23}Na nucleus for medical imaging purposes are (i) its low physiological concentration, (ii) its lower Larmor frequency, and (iii) its very efficient quadrupolar relaxation. Despite being offset to some extent by the fact that ^{23}Na signals can be acquired very rapidly, these three factors all combine to make the sensitivity of sodium imaging rather poor. The unfavorable properties of the ^{23}Na nucleus create two further problems for imaging, first, when compared to proton imaging, the lower Na Larmor frequency means

that larger field gradients are required to achieve the same spatial dispersion of the resonance frequency and, second, the universally fast Na relaxation often makes it difficult to obtain image contrast between tissues on the grounds of Na relaxation rate The original multiple-quantum filtration experiments for NMR spectroscopy of spin-3/2; nuclei were introduced long back.

Multiple-quantum [19] coherences can be excited if the quadrupolar relaxation of the spin-3.2 nuclei is biexponential and this occurs only when the nuclei are in the slow-motion limit (i.e. where the product of their Larmor frequency ω and correlation time τ is comparable to or greater than unity). These filtration experiments can therefore be used to distinguish between slowly and rapidly tumbling spin-3/2 nuclei, since the latter exhibit simple exponential relaxation, and so have their NMR signal canceled by the filtration. Both double and triple quantum filtration experiments have been used to study biexponential transverse relaxation but triple-quantum filtration has been shown to be 50 % more sensitive and is thus the preferred method.

Multiple-quantum filtration imaging of sodium therefore consists simply of appending a conventional gradient-echo or spin-echo imaging sequence to either the double or (preferably) the triple-quantum filtration experiment. The pulse sequence and coherence transfer pathway diagram for triple-quantum sodium imaging are shown in Fig. 14.29 [19]. The first three radio-frequency pulses excite triple-quantum coherence in biexponentially relaxing Na nuclei. The phase-encoding gradient or gradients, as well as the first part of the readout gradient, are then applied for an interval τ_3. These gradients are switched off, and after a short gradient stabilization interval τ_4, a 109° radiofrequency pulse converts the Na triple-quantum coherence back into observable transverse magnetization.

This flip angle is chosen to maximize the amplitude of the transfer of p = +3 coherence into observable p = −1 coherence. After another short interval τ_5, the readout gradient is switched back on and data acquisition commences a further interval τ_6 later. The minimum experiment time in any practical sodium imaging experiment will be determined by the sensitivity so; slice selectivity is best obtained by incrementing two orthogonal phase-encoding gradients and then performing a magnitude-mode three dimensional Fourier transformation. If slice selectivity is not desired, then only one phase-encoding gradient may be used and a magnitude-mode two-dimensional Fourier transformation performed. As in any Fourier imaging experiment the pulse sequence parameters require careful selection. If the gradient echo formed by the combined action of the readout gradient and the 109° pulse is required to fall in the middle of the acquisition period then the condition below,

$$3G_z^{(1)}\tau_3 \approx G_z^{(2)}\left(\tau_6 + \tfrac{1}{2}\tau_{acq}\right)$$

should be satisfied, where G_z^1 and G_z^2 are the strengths of the first and second parts of the readout gradient. The unusual timing of this gradient echo (i.e. the additional factor of 3) is a consequence of the fact that the rate of dephasing or rephasing of a p quantum coherence in a field gradient G is proportional to pG. In addition to the
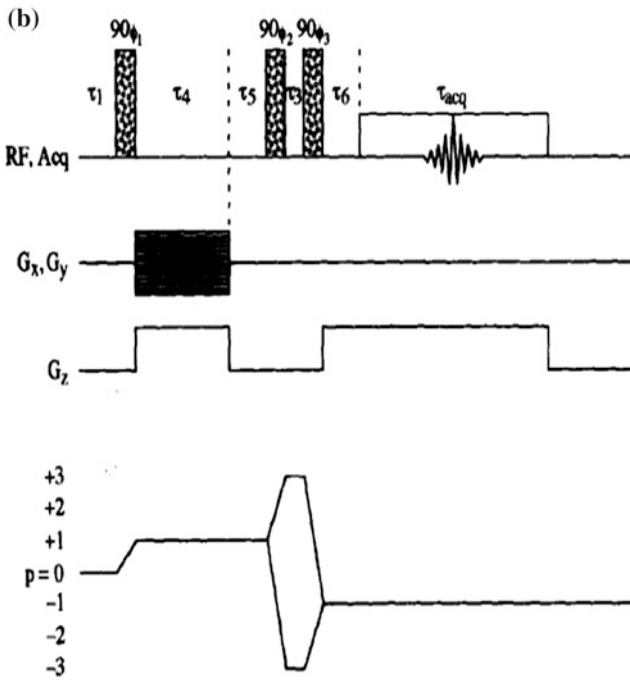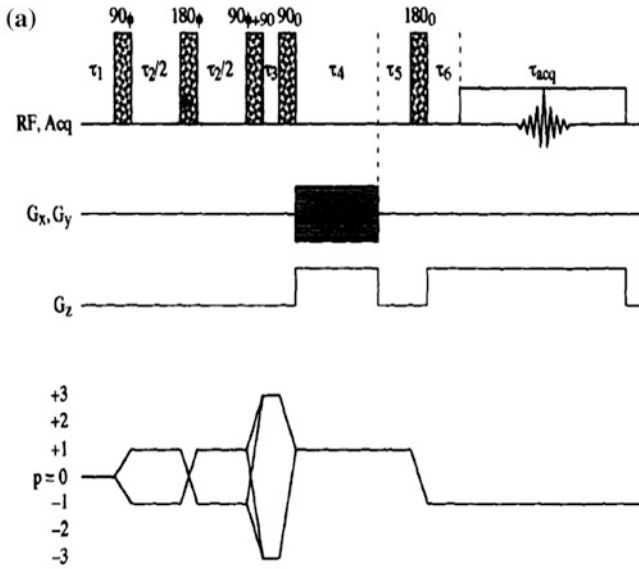
◀ **Fig. 14.30** Pulse sequences and coherence-transfer-pathway diagrams for triple-quantum-filtration imaging of sodium. Pulse flip angles and phases are given in degrees. Two phase-encoding gradients, G_x, and G_y are used for three-dimensional Fourier imaging while only one, G_x suffices for the two-dimensional Fourier imaging experiments. The assignment of the gradients G_x, G_y and G_z, is arbitrary. In (**a**) the "spin-echo" version of the triple-quantum-filtration imaging technique is shown. The duration of the sequence is quite long because of the inclusion of a transverse relaxation interval τ_2 and a phase-encoding interval $\tau_4 + \tau_5$. The novel triple- quantum-filtration imaging technique for sodium is shown in (**b**). The intervals τ_1 and $\tau_4 + \tau_5$ have been combined to produce a much shorter and simpler pulse sequence. The pulse phases φ_1, φ_2, and φ_3 and the receiver phase are cycled as set out in Table 12 [20] to select triple-quantum coherence during the very short interval τ_3 (typically a few microseconds)

Table 14.45 Six step triple-quantum phase cycle

Φ_1	0°	60°	120°	180°	240°	300°
	240°	300°	0°	60°	120°	180°
	120°	180°	240°	300°	0°	180°
Φ_2	0°	60°	120°	180°	240°	300°
	120°	180°	240°	300°	0°	60°
	240°	300°	0°	60°	120°	180°
Φ_3	0°	0°	0°	0°	0°	0°
	120°	120°	120°	120°	120°	120°
	240°	240°	240°	240°	240°	240°
R	0°	180°	0°	180°	0°	180°
	0°	180°	0°	180°	0°	180°

above equation, if the dephasing caused by the inherent spatial inhomogeneity of the static magnetic field, B_0, is required to be similarly rephased at the center of the acquisition period, then the condition

$$3(\tau_3 + \tau_4) \approx (\tau_5 + \tau_6 + \tfrac{1}{2} \tau_{acq})$$

should be satisfied as well. Note, however, that in many experimental situations, it will not be possible, to satisfy this second condition, since it would result, in the overall duration, of the pulse sequence, being unacceptably long. Finally, if the image produced by the triple-quantum experiment, is to have the correct proportions, in each dimension, then the spectral width, in the phase-encoding dimension, or dimensions must be three times greater than that in the readout dimension. Therefore the condition

$$3(\Delta G_{x,y})\tau_3 = \left(G_z^{(2)}\right)/(2f_{nyq})$$

should be satisfied, where ΔG_{xy}, is the increment of the phase-encoding gradient or gradients and $2f_{nyq}$ is the spectral width (i.e. twice the Nyquist frequency) in hertz in the readout dimension. It is the above equation that contains the significant result that either the duration τ_3 of the phase-encoding gradients or the size of their increment ΔG_{xy} need only be one-third of that required for normal or multiple-

quantum filtration sodium imaging. The conditions stated above assume that all gradients in the pulse sequence are rectangular in profile as shown. If gradients with shaped profiles are used instead then the relevant parameter in these equations becomes the integral under the gradient profile, rather than simply the product of the strength of the gradient and its duration. The potentially shorter duration of the phase-encoding interval $\tau_3 + \tau_4$ in triple quantum sodium imaging can be used to advantage only if the relaxation properties of Na triple-quantum coherence are favorable. Fortunately this is the case. The pure quadrupolar relaxation rate of spin 3/2 triple-quantum coherence is given by $R^{(3)} = C(J_1 + J_2)$, where $C = (1/40)$ (e2qQ/ℏ)2 $(1 + \eta^2/3)$ and the spectral densities $J_n = 2\tau_c/(1 + n^2\omega_Q^2 \tau_{c2}^2)$. In contrast, the biexponential relaxation of the spin-3/2 single-quantum coherence, is descri- bed, by the two rates $R1^{(1)} = C(J_0 + J_1)$ and $R2^{(1)} = C(J_1 + J_2)$. Therefore, since $J_0 \geq J_1 \geq J_2$, it can be seen that Na triple-quantum coherence relaxes exponentially with t he same rate as the slower of the two components of the single-quantum coherence.

The triple-quantum imaging experiment thus keeps signal loss during phase encoding to a minimum by (i) ensuring that the phase-encoding interval is as short as possible and (ii) performing the phase encoding upon the slowest relaxing of all spin 3/2 coherences. In principle, the experiment described, requires no phase cycling. The first three pulses in the sequence excite coherences of order p = +3, +1, −1, and −3. As a consequence of their negative signs, the p = −1 and −3 coherences do not give rise to echoes after the 109° pulse, while the pulse sequence parameters can be adjusted so that the echo arising from the p = +1 coherence falls outside the acquisition period. In practice, however, we have found that this single-quantum echo is very intense and, if phase cycling is not used, can still give rise to unwanted signals in the final image. In the alternative imaging experiments, the transfer of p = +3 to −1 coherence by the 109° pulse was exclusively selected by cycling the phase 4 of the 109° pulse through eight steps (i.e. 0°, 450°, 90°, 135°, 180°, 225°, 270°, 315°) while alternating the phase of the receiver (i.e. 0°, 180°, 0°, 180°, 0°, 180°, 0°. 180°). See Fig. 14.29 [19] for the pulse sequence used.

14.3.16 Sodium Imaging: Triple Quantum Filtration

There have been several preliminary demonstrations of the potential of both multiple-quantum filtration and true multiple-quantum techniques for selectively imaging only slowly tumbling sodium nuclei, i.e. those with correlation times τ_c, approximately equal to or longer than the inverse of the Larmor frequency ω_o. These experiments provide a potentially exciting source of image contrast, as the slowly tumbling sodium ions are precisely those which are most difficult to detect in a conventional Fourier image on account of their short transverse relaxation times. From the early investigations, it is already clear that the low sensitivity of multiple quantum filtration and multiple-quantum imaging is the major obstacle to

their be-coming important techniques for biological and clinical imaging of sodium. A triple-quantum filtered [20] sodium spectrum typically has a signal-to-noise ratio an order of magnitude lower than that of a conventional sodium spectrum recorded in the same experiment time. One might automatically conclude that a triple-quantum filtration or triple-quantum sodium image would require two orders of magnitude longer to record than a conventional sodium image with the same signal-to-noise ratio. Here we aim to attempt to dispel some of this pessimism. We present a novel triple-quantum-filtration NMR imaging technique which uses a sequence of pulses much shorter and simpler than those of previously proposed filtration techniques.

Experimental tests of the new technique are performed at the relatively low magnetic field strength of 1.9 T. The Fig. 14.30 [20] shows the pulse sequence and coherence-transfer-pathway diagram for a "spin-echo" version of the triple-quantum-filtration imaging experiment It consists of a conventional spin-echo imaging sequence appended to the standard triple-quantum-filtration experiment for sodium. The overall duration of the sequence is quite long because of the need for an interval τ_2 during which biexponential transverse relaxation occurs (a prerequisite for excitation of triple-quantum coherence in an isolated spin-3/2 nucleus in solution) and an interval $\tau_4 + \tau_5$ during which phase encoding is performed. Our approach to constructing a shorter triple-quantum-filtration imaging sequence is to combine the function of the intervals τ_2 and $\tau_4 + \tau_5$, i.e. to phase encode the sodium magnetization during the transverse relaxation interval. To do this, the first 180° pulse is removed and the interval τ_2 replaced with the phase-encoding interval $\tau_4 + \tau_5$. The pair of 90° pulses that make up the triple-quantum filter may then be used to form an echo under the influence of the readout gradient G_Z. This means that the final 180° pulse may now be removed and the acquisition period brought forward until it immediately follows the final 90° pulse. The resulting pulse sequence and coherence-transfer-path-way diagram are shown in Fig. 14.30.

There is an optimum duration of the transverse relaxation interval τ_2 which results in the maximum amount of triple-quantum coherence being excited. This optimum duration τ_2^{opt} (which should always be measured, where possible) may be as short as 2 or 3 ms for sodium in biological samples. The free-induction decay resulting from a multiple-quantum-filtration experiment is zero immediately after the filter and, in a spatially homogeneous static magnetic field B_o, rises to its maximum amplitude only after a time which is also given by τ_2^{opt}. It means that the center of the echo should be formed at a time τ_2^{ops} after the final 90° pulse, i.e. $\tau_4 + \tau_5 + \tau_6 + (1/2 \ \tau_{acq})$; τ_{acq} should approximately equal τ_2^{opt}. Even with the finest gradient hardware this is a difficult condition to meet if τ_2^{opt} is short. The equivalent condition for the new triple-quantum-filtration imaging experiment in the Fig. 14.30 (Fig. 1b in [20]) is that $\tau_6 + 1/2 \ \tau_{acq}$ should ap-proximately equal τ_2^{opt} and this is considerably easier to satisfy. One further condition applies only to the sequence of Fig. 14.30 (Fig. lb in [20]), in order that the maximum triple-quantum coherence still be excited, the duration of the phase-encoding interval $\tau_4 + \tau_5$ should also be equal to τ_2^{op}.
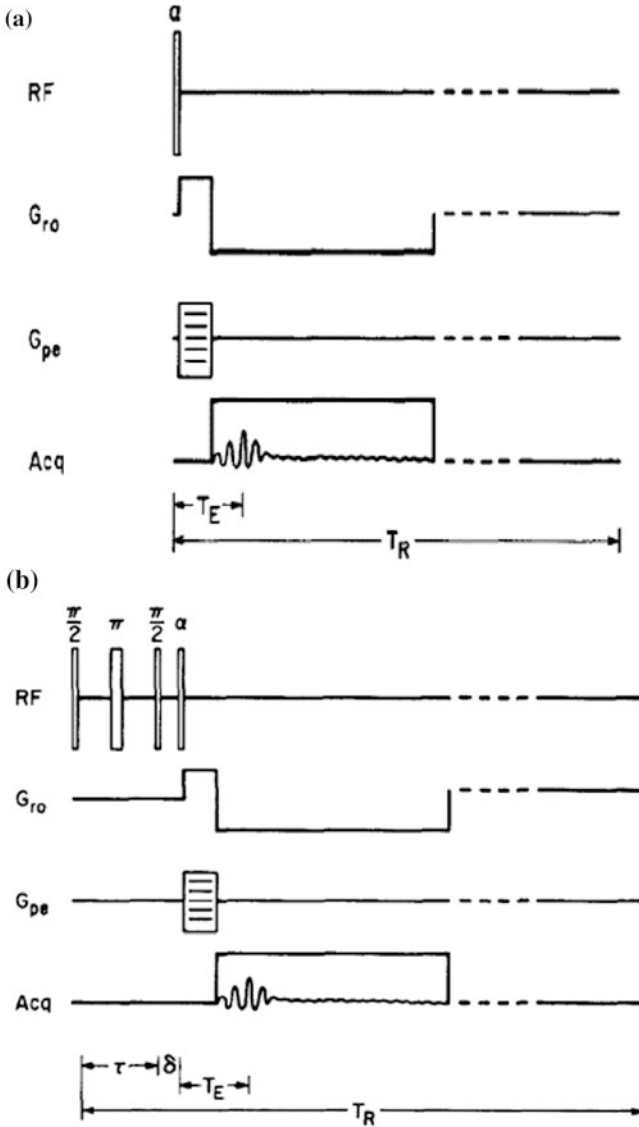
Fig. 14.31 Pulse sequences for gradient-echo sodium imaging. **a** A single-quantum gradient-echo imaging sequence. **b** A double quantum-filtered gradient-echo imaging sequence. The creation time, τ, can be adjusted to optimize the DQ-filtered signal intensity. The evolution period for the DQ magnetization, δ is kept short, to conserve signal. For our experiments, the α pulse was set to π/2 radians, about 37 ± 2 μs for our 16 mm solenoid. T_E echo time; T_R repetition time; RF radiofrequency transmitter; G_{ro} readout gradient; G_{pe} phase-encoding gradient; Acq acquisition window

Fig. 14.32 A plot of the peak height (arbitrary units) versus the creation time, τ, for a 4 % agarose and 145 mM saline gel at 8.4 T (95.26 MHz for 23Na). The peak maximum appears at 24.7 ms
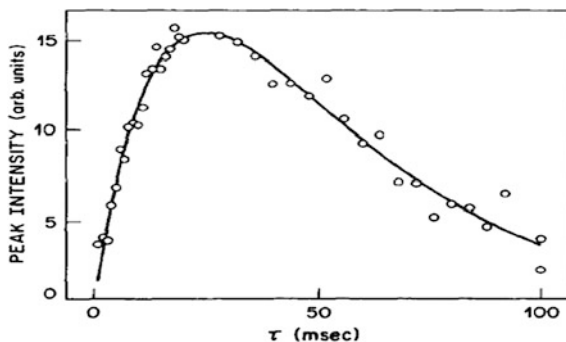
If the phase encoding cannot be carried out within the time τ_2^{opt}, then neither of the experiments in Fig. 14.30 [20], is recommended and the true triple-quantum imaging experiment, becomes the method of choice as it allows the phase encoding to be performed, in a third of the normal time. The pulse and receiver phases in the new imaging experiment must be cycled so that only coherence-transfer pathways that pass through a triple-quantum (p = +3) state during τ_3, contribute to the observed signal. This may be achieved with the standard 6-step phase cycle for triple-quantum filtration which is set out in Table 14.45. If spurious signals still appear in the final image, the most likely cause is that p = -1 coherence precessing during $\tau_4 + \tau_5$ is not being sufficiently dephased by the readout gradient G_z. This unwanted coherence-transfer pathway may be suppressed by cycling the pair of 90° pulses that makes up the triple-quantum filter through an alternative scheme. Since the triple-quantum-filtration phase cycle uses 60° phase shifts, the most straightforward scheme to implement is the 3-step scheme, which uses 120″ phase shifts. See Table 14.45 for phase cycle details.

Pulse cycling for the Triple-Quantum-Filtration Imaging Experiment (Fig. 14.30b) x-step triple-quantum phase cycle plus three step Exorcycle, R = Receiver

14.3.17 Sodium Imaging Double Quantum Filtration

The concentration gradient of sodium across the cell membrane is a fundamental parameter which determines the electrical and contractile behavior of cardiac and other cells. Alterations of this gradient occur in a variety of pathological conditions such as myocardial and hernia or neoplasms of the central nervous system. The potential of NMR spectroscopy and NMR imaging to monitor intracellular and extra cellular sodium in various organs has prompted investigators to develop paramagnetic shift reagents and to examine a variety of approaches for imaging intracellular sodium. Since the shift reagent does not pass through the cell membrane, sodium within the cell does not contact the shift reagent, and the two sodium pools have different NMR resonances. However, the potential toxicity of shift reagents at high concentrations has prompted us to investigate other possible
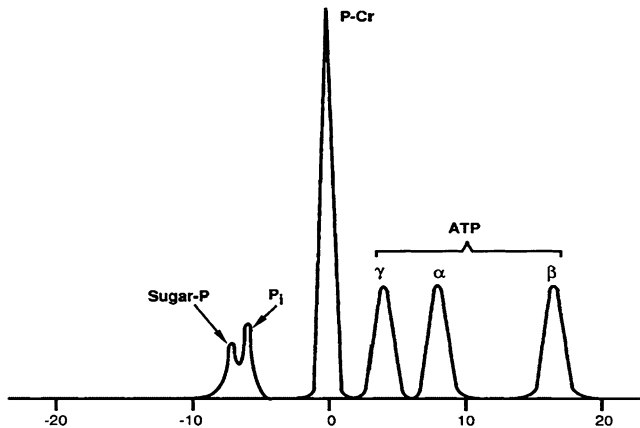
Fig. 14.33 Schematic of a ^{31}P NMR spectrum. Resonances are assigned as alpha-, beta-, and gamma-phosphates of adenosine triphosphate (ATP), phosphocreatine (P–Cr), inorganic phosphates (Pi), and sugar phosphates (Sugar-P)

methods for selectively imaging intra-cellular sodium. It has been shown that the double-quantum (DQ) [21] and triple-quantum (TQ) filters can discriminate isotropically mobile spin-3/2 nuclei from those where motion is restricted, such that the nuclei exhibit, the biexponential relaxation. A multiple-quantum filter causes the NMR signal belonging to isotropically reorienting sodium, to vanish, while the signal from sodium exhibiting biexponential decay survives. However, this discrimination may not be perfect for distinguishing between intracellular and extracellular sodium, since some of the extracellular sodium may also be bound.

One can use a multiple-quantum filter to produce DQ images corresponding to bound or entrapped sodium. Since a DQ filter can discriminate between isotropic and bound states of sodium ions, it could afford another mechanism for introducing contrast into magnetic resonance imaging (MRI) experiments. Because sodium signals decay within milliseconds and most commercially available imaging gradient systems require several milliseconds to encode spatial information, most sodium species undergo, substantial relaxation before their signals, can be acquired. Thus, the contrast between tissues, in many in vivo sodium images, has been the result of differences in sodium concentration, not nuclear relaxation. Fortunately the sodium concentrations of different tissues span a large range. However, the complete suppression of isotropically mobile sodium by a DQ filter and the biexponential behavior, of the DQ response, of sodium, in a more restricted environment, could produce even greater contrast.

If applied to biological systems, this contrast would depend, on the cell characteristics and could possibly be used, to discriminate normal from abnormal tissue much as, T_2 differences are exploited now, in proton imaging, to selectively visualize tumors, in the brain. By adjusting the creation time, τ, of the DQ-filtered imaging sequence, one might "tune" an image to highlight, the distribution of sodium, in a particular environment.

One can highlight DQ-filtered sodium images at 145 mM NaCl concentration and DQ-filtered sodium profiles at 46 and 4.6 mM NaCl concentrations, which discriminate, sodium nuclei entrapped, in agarose gels, from free sodium ions. Results show that, it is possible, to obtain images that discriminate isotropically mobile sodium from sodium, that is entrapped in a gel and therefore displays, biexponential relaxation. These concentrations begin to approach the 12 mM intracellular sodium concentration, reported for slowly dividing, the tissues. The biexponential relaxation of sodium in agarose gels is known and thus these gels are good models for DQ-filtered sodium studies. See Figs. 14.31 and 14.32 [21] for a representative practical illustration.

14.3.18   NMR Chemical Shift Imaging

It is known that the application of a static magnetic B_0 to an ensemble of nuclei, tries to align the nuclei along its field lines. The angular momentum of the nucleus, due to angular momentum conservation laws, prevents the nuclei from readily realigning. From both a classical and quantum mechanical perspective, a simple law can be derived. It relates the strength of the external field B_0, seen by the nucleus, the strength of the nuclear magnetic moment and its angular momentum, and the frequency ω of the precessional motion. This relation called the Larmor equation, states that the resonance or larmor. Frequency, ω, is $\omega = \gamma B_0[1 - \sigma]$. Here γ the gyromagnetic ratio, is a constant and is unique for each type of nucleus. The factor $(1 - \sigma)$ is included to correct for the fact that the applied magnetic field is partially shielded by the electron cloud surrounding all nuclei, and thus the actual magnetic field experienced by the nucleus is slightly different from the applied B_0 field. This shielding constant σ [22], for a nucleus in a specific molecular environment is usually expressed in parts per million (ppm), relative to a reference standard. Of great importance is, this factor, is invariant, of magnetic field strength, and is different for nuclei in different chemical environments. Because this shielding varies with the exact electron configuration, which in turn is influenced by neighboring chemical groups, the amount of resonance frequency offset (the chemical shift) can be correlated with the stereochemistry of the observed compounds.

In order to obtain a measure of what resonance frequencies and hence what chemical shifts are present within a sample, the signal intensity as a function of time measured by an NMR instrument, following perturbation (application of an RF pulse), of the nuclear spin system, is converted, by Fourier transformation, to signal intensity, as a function of frequency. This process will yield a spectrum like the one shown in Fig. 14.33 [22]; in this case following interrogation, of the phosphorus nucleus. Each peak in this spectrum corresponds to the presence, of a distinct, chemical group, within the sample. There is a wealth of information to be obtained from the NMR spectrum of tissues. With the appropriate experimental design, one can, determine, for example, nuclei concentration, metabolic state,

exchange reactions and rates, ion fluxes, and intracellular pH and temperature. Of principle interest to the biologist is the in vivo determination of certain metabolite concentrations, with ^1H, ^{31}P, ^{23}Na, and ^{13}C, as the primary nuclei, under study. Sodium is another NMR-observable nucleus, present, in biological tissue, with a normal distribution of, 160 mM, in the extracellular space, and an intracellular concentration of 12–20 mM.

Following tissue injury or cell death expansion of the extra cellular space or impairment of the sodium pump, will result in an increase in the sodium concentration of the tissue. ^{23}Na NMR imaging has the potential to diagnose edema, neoplasms, infarction, and ischemia. Carbon 13, either with natural abundance study, or with administration of ^{13}C-enhanced compounds, has also been used to study living systems. Metabolism of a ^{13}C-labelled compound can be followed, and individual metabolites, such as glucose, glycogen, and lactate can be identified during active metabolic processes. It is seen, the magnetic field gradients, used to encode information, in space and time, in general modify B_0, to a much greater extent than the chemical shift shielding σ, thus in conventional NMR imaging, the presence of a field gradient, during signal acquisition, results in loss of the chemical shift spectral information. The difference in NMR signal between membrane and stored lipids lies in the mobility of the protons. In membrane lipids the highly ordered lipid bilayers restrict aliphatic chain mobility, resulting in very short T_2 relaxation times, essentially rendering them invisible to standard NMR techniques.

The chemical shift images were thus instrumental in demonstrating that discrimination between gray and white matter seen on conventional NMR images reflects, differences, in the water component relaxation times, rather than direct visualization of myelin lipid protons, as some had hypothesized. Data obtained using 3-D chemical shift imaging have demonstrated the ability to quantitate, as well as simply identify, chemical constituents of tissue. These techniques thus have the potential to detect and monitor diseases characterized by abnormalities of lipid distribution, mobilization, and metabolism, including muscular dystrophy and fatty liver infiltration used to measure, differences in the relaxation times, of each spectral peak. However, several important species besides lactate can also be seen in the proton spectrum, and due to the higher sensitivity of the ^1H nucleus and the favorable relaxation times of proton species, proton imaging times can be substantially shorter, with better spatial resolution, than chemical shift images of other species such as ^{31}P.

The methods discussed above, offer unique challenges, to the imager, as well as special advantages in the study of, certain nuclei, in specific applications. In particular, three-dimensional techniques offer, the opportunity to visualize the chemical shift spectra explicitly, while two-dimensional techniques allow for rapid imaging times, and high spatial resolution. The goals of an imaging experiment, will influence, the choice of methodology implemented, deciding which of the above chemical shift imaging techniques is optimal, may well be answered differently, in different situations. For example, in vivo imaging data, has thus far focused on the two dominant peaks in the proton spectrum: lipids and water. The requirements to image this simple two-line spectrum with proton concentrations in

the molar range are much different than those needed to image the other metabolites visible in the proton or phosphorus spectrum in millimolar concentrations. The ability to map tissue aliphatic and water will allow proton chemical shift imaging, to perform, four primary functions, in a clinical setting.

First, differences, between fatty- and water-predominant tissues, can be used, to enhance the detestability of tissues, of one type, within a milieu of the other. Infiltration of carcinoma into, the surrounding fatty tissue, for example, in the breast, rectum, or prostate, is a primary example. In order to insure maximum sensitivity in detecting small lesions, high spatial resolution, will be required. Second, chemical shift imaging, will be called upon, to characterize, tissues, where signal intensities, in conventional images are ambiguous, for example in distinguishing lipid from hemorrhage (each with high signal on conventional spin-echo images). In these settings resolution may be sacrificed at the expense of sensitivity to tissue type. Third, the ability to quantitate the levels of fatty acids build up in certain tissues, for example, in diseases, such as the muscular dystrophies, and fatty liver syndromes, will enhance efforts to monitor and evaluate, therapeutic interventions, as well as, the natural history of such disorders.

14.3.19 Is MRI A Diffraction Phenomena? NO it is not. But, Yes it is

The internal functional system operative in our body nature has evolved, over the millions of years. In MRI, the investigation of the, life functioning system is done in a gentle way, using the radio frequency (RF) radiation. MRI does not involve breaking the nuclei by using neutrons to produce fission of the nuclei, which would then lead to the production of dangerous nuclear radiations, destructive to our body. This misconception arose in the past due to the lack of populous education about the basics of the science of MRI in particular and science as a whole. In fact on a wider scale the basic infrastructure of the education about science for the new generation of students is on fast decline. On the other hand expansion in financial and bureaucratic fields like accountancy, management, information technology (IT) etc. is fast on the rise. One must not forget that science leads to creation of the necessary literacy about life itself on the one hand and develops practical inventions like MRI which is worth billion dollars of industry today on the other. Unnecessary bureaucracy tends to be destructive to the creation of knowledge based, economy.

Propagating scientific knowledge is the only way to survive today in the world of ignorance, suspicion misconceptions, neglect and insecurity. What useful benefits of science the human civilization, should adopt and leave others, should be decided, based on the proper education about, the existing scientific balance the nature has created on earth. There is no other planet like earth, in our universe. Better protect the one we have than trying to, invent another one which you can not make use of MRI can detect organic matter in addition to the rigid calcite

structure like bones in our body. It thus can be a very useful method of detection, involving security procedures in the aviation industry. We are a scientific civilization. Using science to produce wealth, is a very constructive way of employing young minds. Just shouting about 'climate change' as a 'political word' of power is not going to produce anything. But staring education, at the school level, about the 'science of climate' and the science as a whole, would produce an appropriate scientific manpower for the future to take right decisions. MRI is only one among many visible commercial products from science, working in our day to day life.

The scientific society we have developed ourselves into over centuries can not survive without science. No point in destroying the very foundation of humanity developed, based on science. Nature itself has preferred science in its own evolution. Over time the present civilization has studied the secrets of nature learnt them and used them towards its own benefit. A freely available scientific material produced by research and development work over the world would go a long way towards education of humanity. The authors feel, the work prepared here is a step, in the right direction for the future generations. Pretending that we do not need science is a shear act of ignorance.

Survival of human race today is only on education about science. One should realize plant and animal life is the science of atom and molecules. Deep inside life is the quantum science the nature builds on. It is what the Multi-Quantum QMRI (MQMRI) is based on. It is very much a natural quantum phenomena. It is better to understand it, than, to ignore it. The conventional MRI uses quantum science, as a wholesome i.e. in a broader macroscopic quantum perspective. Assuming molecules, in our brain as an ensemble of independent spins is the crudest model of the brain, and that is what the conventional MRI is about. It is natural, for any technology, to evolve starting from, the very fundamental basics. That is how the development of the MRI technology has evolved. Mind can only start from the simplest, and then find out, the intricacies, step by step. The nature itself has followed that, in the evolution of life. The intricate discrete nature of atoms and molecules does not form the basis, of imaging in the conventional MR we have today. The technology of MRI employs the use of, non-invasive radio frequency (RF) radiation. This is in order to excite the nuclear and atomic magnets, which are an integral part of the biological structure of our brain.

The RF radiation, is chosen because we are only interested in exciting atoms and molecules to their higher energy levels. On returning back to their normal or say zero energy state the RF radiation is transmitted back. The receiver which is tuned to this out coming radiation registers the events happening in a local selected area under investigation. A point by point repetition over the whole brain and coordinating the events over the global brain produces the picture we are so familiar with. It is important to recognize here that the magnitude of the excitation energy involved here is of the order of a few m(10^{-3}) eV. One should compare this with million electron volt (Mev) energy used in the X-ray imaging. We live our, day to day life on earth under solar radiation with full electromagnetic radiation spectrum and under the influence of the magnetic field of earth. Our life exists in earth's magnetic field of around a micro Tesla. This is very small to think about of
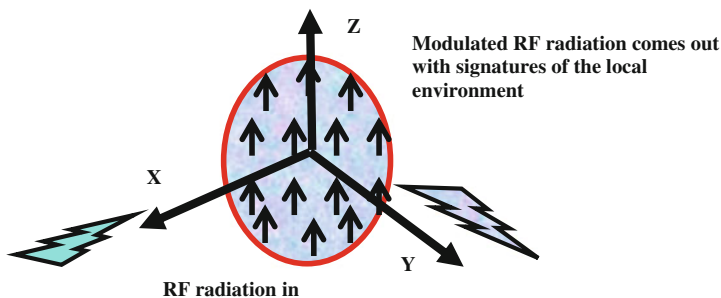
Fig. 14.34 Brief description: The picture is as if the whole brain has all the spins (tiny macromolecular dipole magnets) pointing along the +Z-direction, the direction along which the static magnetic field is applied. The spins are assumed to be identical in nature, though they are not. This is a crudest possible model. But one should remember that in the first approximate stage, we image, the identity of the spins, through their, being present, in different environments, and performing different functions. The functions of spins are recorded in a much broader sense in space and time. The mutual quantum level interactions between macromolecules are neglected, in fact not recorded as the sensor of the machine, and the design of the pulse sequence is not geared to the quantum level of intricacy. In the conventional MRI, the output signal is produced by using a much simpler design of RF radiation pulses. The structure of pulses e.g. frequency content shape, duration, number of pulses, time in-between pulses, etc., is not particularly designed to stimulate quantum level interactions. A 90° pulse is applied along the X-direction. It leads to a rotation of a fraction of the spins, pointing, towards the +Y-direction. Because of the oscillatory nature of the RF radiation applied the output signal is also an alternating current (a.c.) one. The signal, is detected as an output, along the +Y-direction, by a copper coil, or some another form of sensor
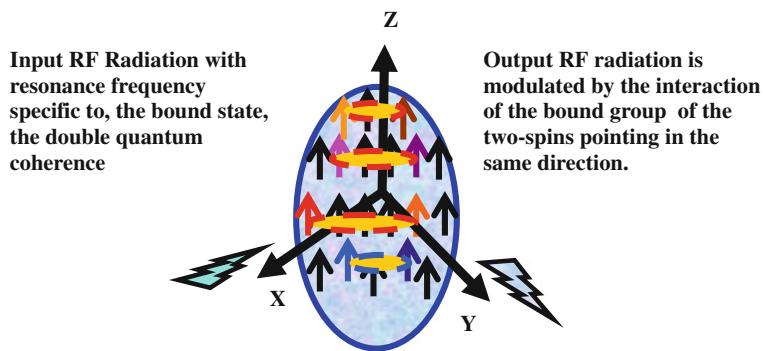
Fig. 14.35 Brief description: In this case the two spins pointing in the same direction are considered, as a group, in action. Normally nearby spins pointing in the same direction would repel each other like two bar magnets with north–south poles pointing in the same direction. But there will be some spins further away, where the magnetic influence of the spins will be attractive on each other. This in other words means, quantum coherence (acting together for a specific activity, say metabolism) in the quantum science language. This correlation or interaction of parallel spins, in a group of two's is called as double quantum coherence. This picture holds, on a scale in the brain, over distances of microns to mms. One needs to see, the in depth picture, of this two-spin state resonance. In a selected region we have to go to distances of the order of a micron (10^{-6} m) and choose a resonance frequency corresponding to this group-of- two-bound spins, pointing in the same direction, for the regional analysis

Input RF radiation tuned is in resonance to the bound-state of the-group of two spins, pointing in the opposite direction

Z

Output RF radiation is modulated by the quantum interactions of the group of two-spins, in the zero-quantum-state, the oppositely directed spins

X   **Y**
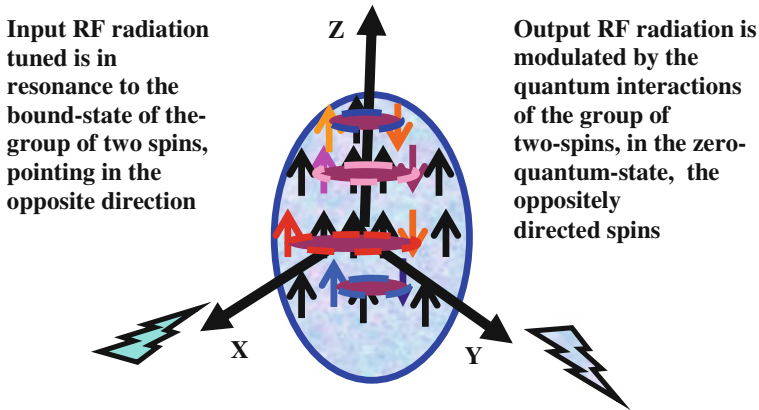
Fig. 14.36 Brief description: This interaction group consists of two spins together but with the two spins pointing in the opposite direction. Two nearest located spins influence each other and try to reverse the spin direction of the other spin nearby as well as at farther distances. This is so because it is the lowest energy state for the two spins. But the applied static magnetic field along the Z direction tries to keep all the spins aligned, along the Z direction. Spins pointing in the same direction is the highest energy state, of the spins. This particular (oppositely aligned) possible binding of the spins, near and farther is called as the ZQC. This will have a unique resonance frequency. It can be excited by externally applied, suitable RF magnetic field pulses like in the case of DQC to the brain. The quantum interactions allow quantum chemistry of nuclei to be observed in space and time. Detection of quantum interactions is very helpful to predict in early stages the onset of a tumor or a disorder in our brain. ZQC being relatively magnetically neutral, is insensitive to magnetic field in-homogeneities. It is considered to bea powerful quantum probing tool in the MQMRI. This is a case of strong binding spin structure and has its own unique quantum energy spectrum. One can control and use this unique quantum structure externally by using suitable RF pulses to stimulate micro quantum level interactions

having any dangerous effect on human body. But inside our brain, things on a similar scale are happening. There is no research to suggest yet that this small magnetic field can control the routine functions happening in our brain. But it would be curious enough for a normal human being to find out what does. MRI just tries to emulate the internal dynamics of the brain through the imaging process. It is important to recognize that a nucleus as part of an atom or of a macromolecule produces a field of about 1 Tesla around it. But this is over a region of nano meter (nm) to micrometer scale. It decays fast over many molecular distances. But as the volume under consideration locally becomes larger the larger is the number of spins (remember a mole of a substance has 10^{23} spins) participating in a particular activity. The result is that the effect of the decay of the field is not as fast as one would think. The distant spins as far as 1 micron to 1 mm distance can influence the local spins, through a small distant dipole (spin)-dipole interaction (spin) field, indirectly created, within by the applied external static field. In the QMRI literature this new field is referred to as the distant dipole field (DDF).

The distant spins produce a de-magnetizing field at a point, locally and generate the intermolecular, quantum phenomena. This is the basis of imaging in the newly
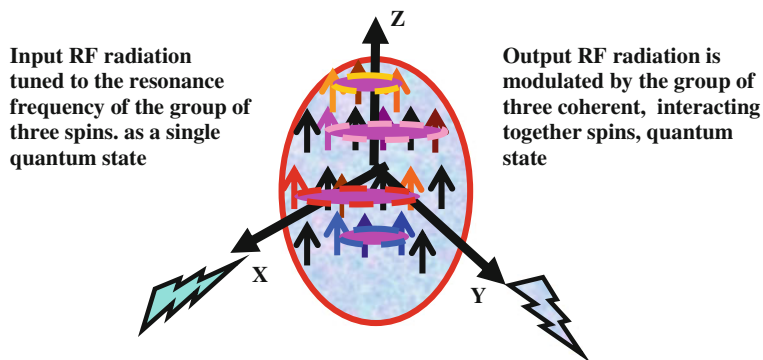
Fig. 14.37 Brief description: One can involve binding of more than two spins e.g. three or even four spins, as a special bound group. This triple bound state will have quantum energy structure of its own. It thus has a unique resonance frequency of its own. One can excite the group of three nuclei and study their interactions, on a microscopic scale, and predict which way, the local quantum chemistry, is heading to, and make an early detection of a cancer in the brain. One should remember that our brain is a hetero-nuclear (multiple species of nuclei) structure. Various nuclei present in macromolecules as part of a tissue fluids etc. are performing, their routine duties of metabolism, neuro-transmission, etc. The influence of interaction extended can be visualized through analyzing, the resonance of the triple quantum coherence (TQC) as a group from voxel to voxel in the brain

emerging Multi-Quantum QMRI (MQMRI). One may wonder if the earth's magnetic field is already doing this in the brain what we are trying, to find out? Wouldn't it be nice to know? The natural dipole–dipole interactions (DDI) in the brain can be studied using the proton magnetic resonance spectroscopy imaging (PMRSI). It is one of the many techniques available. The PMRSI technique utilizes mainly the simplest, the Hydrogen nucleus i.e. the proton spin. In fact the nucleus is part of the overall electron-atom-molecule quantum structure present in the brain. In the conventional concept of imaging e.g. the chemical shift imaging (CSI) the atomic spins, polarized along the direction of the applied static magnetic field are being used as independent entities with no multi-quantum interaction between them, to get the desired result. This is basically the macroscopic effect in the small regions (referred to as a voxel) of the order of mm^3 and above. But in order to see the intricate events happening in the brain in time and space over smaller distances i.e. the atomic distances one need to understand the multi-quantum interactions between atoms and molecules. The effective macro-molecular distances i.e. micron (10^{-6} m) to mm is the region of the 'multi-quantum magnetic resonance imaging (MQMRI)'.

What MQMRI means, is that one takes into account the explicit quantum reactions, between atoms and molecules, as the source of imaging. The collected data, is then more than just the broader map imaging. This means getting close to exactly what nature has created, in our brain. That is, what allows our body functions to continue on moment to moment and day to day basis. We need to understand this nature's atomic level incredible quantum phenomena happening in

our brain to work out the right diagnostics and treatment of diseases which our brain suffers, in our life time. In order to master the intricate quantum science of life one need to start from a standard text book on quantum mechanics (QM). Also the reader should refer to the recent research papers describing the science of life as the quantum science (QS). For the reader however is presented below a simplified conceptual picture. It explains the basics of the multiple quantum coherence (MQC). The MQC exists between molecules in our brain. It is a kind of interaction which allows various fundamental processes like metabolism, neurotransmission, neuro-inhibition, etc., to continue in our brain.

14.3.19.2 Single Quantum Coherence (SQC) (Conventional MRI)

There is evolution of the spins, after applying the RF radiation pulse, in the X–Y plane, as spins start dissipating towards the –Y direction in the X–Y plane. As time progresses, evolution of spins, leads to their dissociation, as a group in the X–Y plane. They are refocused by applying an inverting (180°) pulse, so as to make them switch in the opposite –X, -Y, direction. The inverting pulse reverses the aligned (pointing) structure of a bunch of spins from the +X, +Y quadrant to the –X, –Y quadrant. The back and forth switching of the spins allows them to reinforce. It also allows longer time, to measure and record them. This basically leads to mapping a specific thickness of the brain (choosing a particular slice thickness in the z-direction) in the X–Y plane. The slice thickness (Δz) can be increased in steps to get a deeper picture of the brain. Relaxation time of the spins in the X–Y plane, is called as the characteristic time, T_2 (transverse relaxation time), of decay. In a similar fashion, if the spins are reversed by applying 180° pulse, inverting them towards the -z direction, the spins are switched to –z direction. The spins are then allowed to relax back towards the +z direction. This characteristic time of relaxation is called as the T_1 (longitudinal relaxation time). Both T_1 and T_2 weighted image data, in space an time, is used in producing the final image. Repetition, voxel by voxel, and coordination of the data, over the whole brain produces, the global brain image. This is the basics of the conventional MRI technique. A technique using this principle in MRI is broadly referred to as the eco planar imaging (EPI). Other concepts e.g., correlating the diffusion based anisotropy, of the spins, called as tensor imaging, in a tumor situation, are also prevalent in conventional MRI (Figs. 14.34, 14.35).

14.3.19.2 Double Quantum Coherence (DQC) (the QMRI)

Refer Fig. 14.35.

14.3.19.3   Zero Quantum Coherence(ZQC) (the QMRI)

Refer Fig. 14.36.

14.3.194   Triple Quantum Coherence (TQC)

As a bound group of spins becomes larger one is approaching towards what the conventional imaging does. One may however be interested in the detailed chemistry of the participation of a regional group of nuclei. The chemical identity of nuclei due to their unique electronic structure provides a probe to understand in depth the science of the brain. This opportunity is provided by the multi-quantum coherence imaging. The word coherence means in the literary sense acting (radiation transition) together. In the scientific knowledge it means exciting or stimulating together a group of atoms or nuclei which may be part of a macro-molecule. We then find out as to what activity, they are enhancing (i.e. having a constructive interference) within a specific period of time and the others they are e.g., suppressing (i.e. making a destructive interference) (Figs. 14.36, 14.37).

The unique resonance frequency of a macro-molecule gets smeared out due to its constituent nuclei; the nuclei being of different identities. This group may be interacting with a neighboring group. The group–group interaction is through their common (broader) group-resonance (a wider band of frequencies). This gives rise to multiple quantum coherences. It now is a broader frequency RF band. RF radiation band can be chosen, to include as many widely dispersed nuclei, one is interested in. The quantum coherence imaging (QCI) approach in MRI is a fast advancing area and will one day be able to predict moment to moment events, happening in the brain. It is a common knowledge that the MRI has its origin in using the quantum behavior of the magnetic spins present in the atoms and molecules. But the quantum nature of the MRI is evident explicitly only when one is dealing with ZQC, DQC, etc.

The scientific literature in MRI loosely refers the molecular and atomic magnets as spins. They are atomic size dipole-magnets which are globally present in the brain and due to their random distribution overall neutralize themselves. The atoms and molecules the constituent parts of the tissues, fluids, including the blood cells, etc., are the integral part of the biological and medical activities happening in our brain in equilibrium. The atomic spins are the natural result of circular motion of the electrons around the nucleus in an atom. An electron by itself (due to intrinsic rotation about its own axis) makes an additional contribution of spin to that due to the electron's orbital motion around the nucleus. A nucleus also has its own magnetism. It arises from the circulating electrical currents of neutron and protons inside the nucleus. The relative circular motion of the negative charge of the electron with respect to the positive charge of the nucleus, also produces locally, a magnetic field of about 1 Tesla. The internal magnetic field is strong enough to create a local magnetism in the soft matter in the brain. The local magnetization created is called as the diamagnetism. The result is a local

polarization. There is among the neighborly atomic and molecular spins some sort of local equilibrium due to this internal magnetic field. It controls the local events e.g. metabolism, neurotransmission etc. Nature has cleverly manipulated this order on its own. How clever? One may say that we are still today on the path of slow evolution of life. It is true to say that.

The nature has passed on from generation to generation the secrets of survival of human gene code and keep on mutating it for survival in worse and worse scenario of diseases. It is for us to find out now 'how and why'. The internal magnetic field of approximately 1 Tesla of a nucleus, naturally present in our brain, produces a local magnetic order of atoms and molecules in the brain, on the micrometer scale. The MRI by its externally applied static magnetic field of around 3 Tesla, and sometimes even more (allowed within safe limits) extends this spatial order over larger spaces. The present MRI technology provides us with an easy tool to mimic the nature's operation of the brain system. This can be skillfully observed by the modern day MRI technology. It certainly is a powerful tool to find out how our brain works. The natural internal static magnetic field creates a stable equilibrium, of the spins over regions of the order of nanometers to micro meters to mms. The external magnetic field in MRI on the other hand, produces rough regions of magnetic equilibrium from mms to cms. These are the regions of externally imposed diamagnetic equilibrium.

This created diamagnetism in MRI in the brain is a natural consequence of the reaction of the atoms and molecules to the applied static magnetic and the dynamic RF fields. The reaction to the applied field is to shield or say to save the brain from any damage. How clever of nature?. The diamagnetism due to the internal nuclear magnetic field is basically neutralized locally as well as globally all over the brain. The application of the external magnetic field, as is done in MRI mimics this invisible order over large volumes of order say mm^3 to cm^3, termed as voxels. After the application of the static magnetic field an RF electromagnetic field is subsequently applied to the brain to excite the magnetic spins to their higher order quantum states. The quantum correlations of the neighboring atoms and molecules provides the basis of the advanced technique of multi-quantum magnetic resonance imaging (MQMRI). This become a source of better resolution in imaging as compared to the currently prevalent techniques of chemical shift imaging (CSI), diffusion weighted imaging (DWI), etc.

The intensity variation of the echoes received acts as the sources of the signatures of the activities in the brain, in conventional imaging. In MQMRI it is the fine physical and chemical quantum reactions, in space and time, that is the source of imaging. This way one is approaching the intricate situation, present in the brain. A healthy brain works in a mysterious way. It can think analyze and control body functions in a judicious manner. But when diseased, the functions of the brain are impaired, and it can not perform, in its full analytical capacity. The idea behind writing this work is to implicate the basic principles of physics, chemistry and mathematics (PCM) involved in the science of the human brain. MRI is a humble tool trying to solve the mysteries of the nature. More often than not professionals and the technical workers use MRI in analyzing the human brain
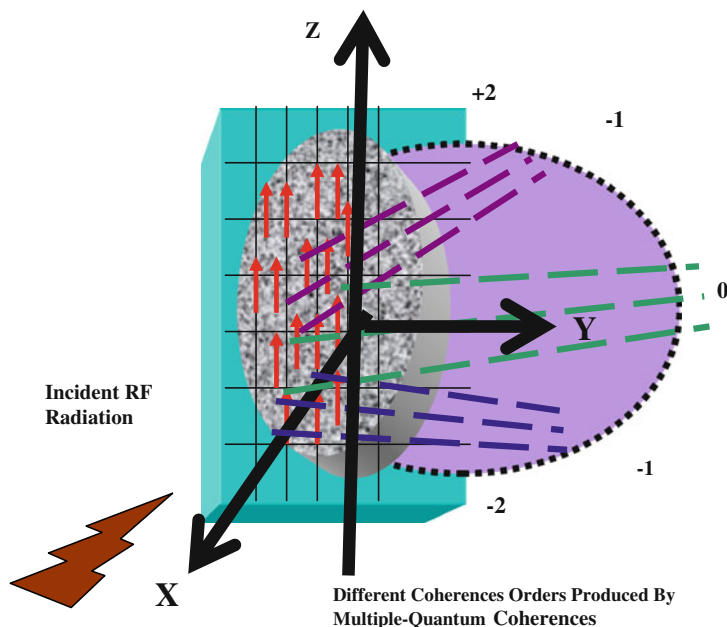
Fig. 14.38 An ensemble of spins in the brain, depicted as, a three dimensional diffraction grating

disorders. MRI is a standard tool used in the diagnostics of tumors. Some professional workers do not really have he strong enough background of the PCM principles, used in producing, an image. So they are not able o make the best of the image produced. In this work, an effort is made, to explain the concepts involved, through pictures, diagrams, etc. Mathematics involved is kept only to a minimum level and at some specific locations e.g. in the Appendices added at the end of the book. This enables those readers with good mathematics background to enhance their own knowledge, and participate in the simplification of it, for the benefit of others. Some simple equations are included, as symbols, representation of, the physical quantities involved. Although MRI is based on the physics of the quantum nature of the soft matter, a detailed relationship to the quantum science is avoided, to keep things simple.

The quantum information science (QIS) is emerging as a new discipline. There, detailed quantum mechanical mathematics is used to study quantum systems. This is not the aim here. In this book the goal is to lay down simple concepts of quantum physics and analyze, their use in imaging, the moment to moment activities, in the brain, etc. So far the imaging has been based on manipulating the maximum magnitude possible of signals, received from the echoes produced by the RF radiation in the brain space. A small region is chosen at a time for examination, called as a voxel. In the present day echo planar imaging (EPI) technique the voxel is macroscopic in size of around mm^3 to cm^3. Recently there is a growing trend in going towards a microscopic imaging. This means moving to
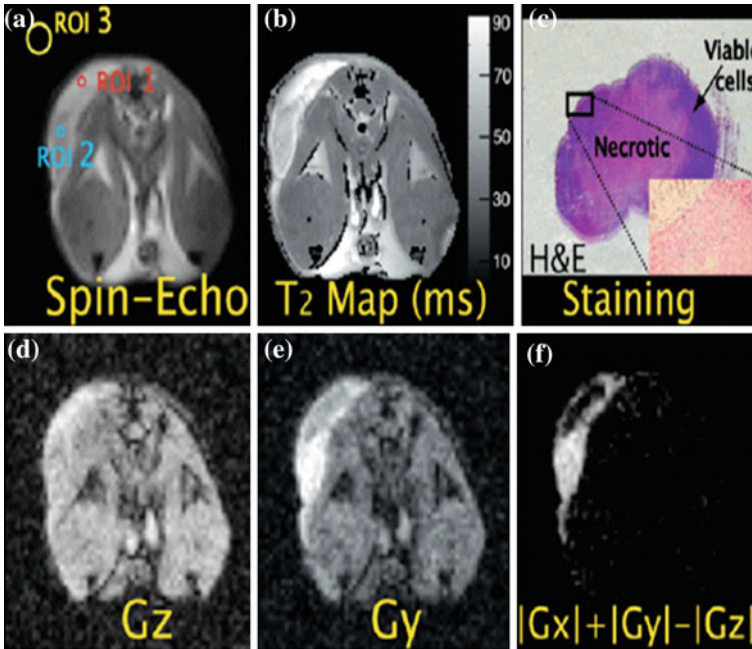
Fig. 14.39 In vivo images of the prostate tumor mouse. The tumor lobe can be seen on the *upper left corner*. **a** Spin-echo image indicating the selected ROI 1, ROI 2, and ROI 3 for the measurements of SNR and contrast to noise ratio (CNR). ROI 1 is placed in the inner region of the tumor (necrotic), ROI 2 is placed in the outer region of the tumor (viable tumor region) and ROI 3 is placed within ghost-free regions of the background, outside the mouse. **b** T_2 map image in milliseconds obtained using a multi-spin-echo sequence: TE = 7 ms, TR = 4 s, NEchoes = 16. **c** Hematoxylin and eosin (H&E)-stained section of the imaged prostate tumor tissue (cation): the inner necrotic area is surrounded by viable cancer cells. The outer area shows iron-positive cells (inset: 10 æ amplification). **d**, **e** In vivo iDQC images with the correlation gradient along the z and y direction (NA = 8, t1 = 2.25 ms, TE = 30 ms, TR = 4 s). f In vivo iDQC anisotropy map image

narrower spacing of less than 1 mm^3, and to close to around a micron size volume (10^{-6} m^3). This brings us in a more rigorous territory of quantum science in operation. The theoretical quantum details are avoided in this work. Instead pictures and diagrams are used for the conceptual expression. The quantum-detailed imaging provides a much better resolution than the conventional broad relaxation-time based imaging. The chemistry of the events also becomes clearer.

The conventional imaging uses as a typical example a simple echo-planar imaging (EPI) method. It is a fast technique but lacks good resolution. The further developments in MRI depend on the continuous education of the professionals who develop it and others who want to use it. This written work, has taken a simplified approach to attract medical professionals to make better use of the science of imaging in their, diagnostic decision making process. This work is also aimed, in achieving a much wider circulation of, the understanding of the basics of the MRI and its application in turn through the knowledge enchanting the

knowledge about the science of the human brain. Interaction of radiation with matter is well studied field in the physics domain. Typical examples are electron waves diffraction in electron microscope optical waves diffraction in optical diffraction gratings, neutron waves diffraction in solids and molecules for structure determination etc., etc.

Now the question is, Is MQRI a diffraction phenomena?. The answer is no. A diffraction is bending of waves of radiation, by an object. This can only be done if the wavelength of the radiation, is of the size of the object, obstructing the radiation. This is not the case here. The wavelength of the radio frequency (RF) electromagnetic radiation used in MRI is around a meter in length may be even longer. The space studied in MRI is of voxel in size of mm^3 to cm^3 in size. It would be further smaller to micron. and nm level, if one were interested, in MQRI. In MRI, one simply excites the macromolecules to their higher energy states by RF pulses and on de-excitation the modulated RF radiation brings back, the signatures, of the space and time events, happening in the brain. In the receiver and the supporting computer imaging system, it is then converted into an image. So it is not the normal diffraction, we are using, here. One can model MRI as a diffraction phenomena.

The atomic and nuclear spins do form some kind of orientational structure but is of a very anisotropic and local in character. There is no regularity, in the patterns as one goes from, one region to the other. In fact there is a chaos over all, in the physical space, in the brain. But there is certainly an order in the time space where the magnetic dipoles influence each other in a coherent manner. If there was not, this happening then how the brain functions in such a coherent and orderly manner. The externally produced order in the brain in the QMRI situation, leads to production of diffraction orders, … +3, +2, +1, 0, −1, −2, −3…etc., and is used in the imaging process in QMRI. One can measure interference between waves in different orders as maximum and minimum in the intensity of electrical signals received, This is in perfect analogy with what is observed in say an optical diffraction grating. Thus indirectly there is a diffraction-interference phenomena happening, in the QMRI situation. The physicists and mathematicians now have the opportunity to explore the brain science to its depth. One can develop models predicting quantum science in action in the brain. The experiments in MRI can be carried out on animals to start with using it as nature's own laboratory to test the models. This approach back and forth between modeling and the experimentation can be extrapolated to the true model of the brain by repetition. The younger minds can be involved in this learning process by the required academic training at earlier level of the education system e.g. the secondary school level of education.

The mathematics of matrices which forms the core of spin dynamics can be handled by using commercially available computer packages, e.g., Mathematica, Matlab, etc. The students need only be exposed to the basic concepts of rotation, inversion etc. of matrices which represent various spin structures, in different situations. The only thing lacking at the moment is the will power on the part of the, decision making, education system leaders. Investment now in the useful
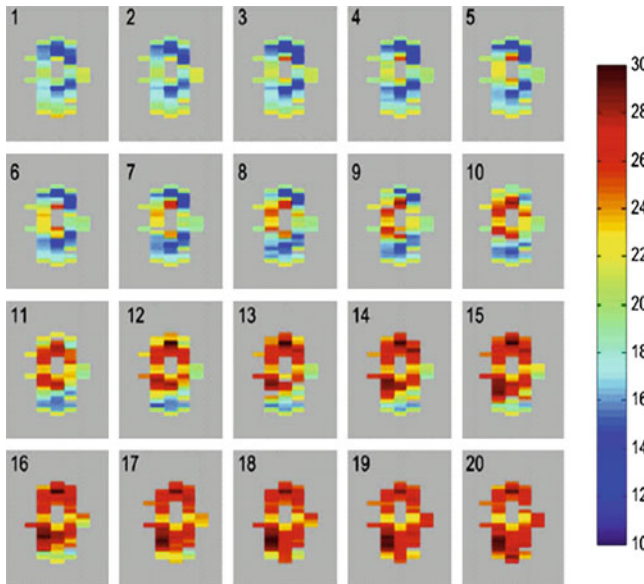
Fig. 14.40 iZQC temperature maps for the heating of porcine adipose tissue acquired every 2 min using the two acquisition pulse sequence. Increasingly hot water was pushed through a tube running through the center of the tissue. The sample was imaged every 2 min using the two-window HOT sequence. Each individual image is numbered to indicate the order of the time course of the images. In these experiments, we initially acquired 10 images typically spanning 10 ms of τ evolution. Once these scans verified iZQC evolution the initial temperature map was made by fitting the phases of images 2 and 7 of the series. Subsequent dynamic thermometry was performed by repeatedly running the scan at the τ equivalent to image 7 and phase changes in each window were related to temperature changes. Temperature near the core was seen to increase from 14 to 36° C as monitored by a temperature probe. FOV = 4 cm; TE = 40 ms; TR = 2 s; mGT = 1 ms*8.4 G/cm; nGT = 1 ms*21 G/cm; correlation distance = 0.0945 mm, t1 = 3 ms; τ = 10.66 ms

engagement of young minds will produce a healthy and secure caring society for the future. Refer to the Fig. 14.30 as simple illustration of the meaning of the diffraction picture of the QMNRI (Fig. 14.38).

14.3.20 Double Quantum Coherence: Superparamagnetic Iron Oxide Nano particles (SPIONS) Animal Model/Prostate—Tumor Mouse

One can create, using suitable pulse sequence, intermolecular double quantum coherences (iDQCs) signals. They basically result from simultaneous transitions of two or more separated spins. The result is production of images that are highly sensitive to sub-voxel (micron scale) structure [23]. One can use superparamagnetic
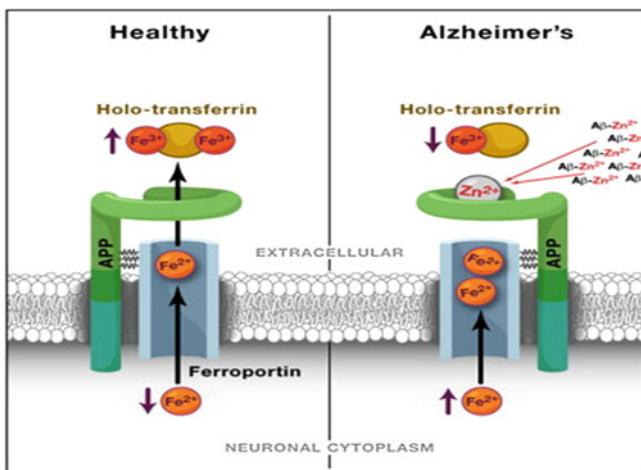
Fig. 14.41 Model for the Role of APP in Cellular Iron export and its inhibition in Alzheimer's Disease. FPN transports Fe^{2+} from the cytosol across the plasma membrane. Fe^{2+} is then converted to Fe^{3+} by a membrane-bound or soluble ferroxidase such as CP or APP (shown). The absence of the ferroxidase results in decreased iron release into the extracellular space, as Fe^{2+} is unable to be converted into Fe^{3+}. APP ferroxidase is inhibited by extracellular Zn^{2+}, which can exchange from $Ab:Zn^{2+}$ aggregates. Free Zn^{2+} is normally buffered by the presence of ligands such as metallothioneins (including metallothionein III in the extracellular space), which are lost in AD. Loss of metallothioneins and other Zn^{2+} buffers may lie upstream in amyloid pathology, APP ferroxidase inhibition, and neuronal iron accumulation in AD

iron oxide nano particles (SPIONs) which are essentially small rust particles of the chemical compound [Fe_3O_4], for imaging diagnostics of a brain tumor. The unique feature of SPIONs is that they create large magnetization that aligns with the bulk field. It creates an anisotropic structure, with a very well-defined spatial distribution. This happens over a short (microns) distance scale. In general, iMQC is very sensitive to local magnetic field gradients. It is particularly so, if there is well defined, spatial anisotropy. The iDQC images can be acquired by selecting the correlation gradient along the three orthogonal gradient directions x, y, and z, with a correlation distance of ~ 100 μm (10^{-6} m). The anisotropy map images can be obtained by a point-by-point subtraction of the three image using, corresponding to the three magnetic field gradients, Gx, Gy, Gz. See Fig. 14.39 [23] for experimental results as an illustration.

14.3.21 MRI Thermal (Temperature) Imaging

Recent research efforts have shown, that non-invasive temperature measurements, in the brain situation, can be very useful, for a variety of applications in medicine [24]. There are developments, in hyperthermia, as an adjunctive cancer therapy. It treats

tumors, through radio frequency (RF) or ultrasound heating. This has resulted, in interests, for developing new methods, in order to do temperature imaging, of the brain. Medical applications of hyperthermia, vary from, treatment of uterine fibroids, to recent research, in the treatment of, the breast cancer. There are also applications, of hyperthermia, in the area of, the study, of the brain tumors. Many magnetic resonance (MR) parameters (relaxation times, diffusion rates, magnetization density) change with temperature. Most parameters are highly heterogeneous, in magnitude or temperature dependence. This has led to a focus on two specific markers, the proton frequency shift (PFS) of water (which changes by ~ 0.01 ppm/°C) and the difference in the chemical shift of water and the fat. The fat resonance frequency, changes relatively little, with temperature, and thus serves as, an internal reference. Since, the absolute resonance frequency, depends, on susceptibility and precise field strength, PFS measurements are done, by subtracting two phase images (one at a reference temperature and one at an elevated temperature), to obtain a relative temperature map. However, the requirement of a baseline image, makes the measurement highly susceptible, to motion. Spectroscopy methods that observe differences between, the water resonance frequency, and a reference peak, can extract absolute temperature, but generally, the voxel size, for such experiments, is quite large, and the inhomogeneities present, within the voxel, cannot be removed.

One can develop a method, for temperature imaging, using intermolecular multiple quantum coherences (iMQCs). A particular type of the iMQC, the intermolecular zero-quantum coherence, iZQC, has been demonstrated, to yield, very sharp, narrow peaks, even in, incredibly inhomogeneous magnetic fields. The iZQCs, represent simultaneous transitions, of two (or more) spins, bound-pointing, in the, opposite direction. The characteristic iZQC resonance frequency, is the difference, in resonance frequency, of the two spins. The two spins, that create, the coherence, are separated by a tunable distance (usually about 100 μm), so the iZQC peaks, are narrow, because all contributions, from magnetic susceptibility variations, and inhomogeneity, are removed, on a distance scale. This is an order of magnitude smaller, than, the typical voxel size. This technique can be applied to temperature imaging, by observing, the iZQC signal, between water and fat spins. It can give a sharp line, even if the fat and water peaks are, individually broadened.

The detected iZQC signal, contains only, the temperature information. While, the iZQC temperature imaging, is superficially, very similar, to the PFS methods, the technique used, to create the signal, isolates changes, in the chemical shift, of water, rather than its absolute resonance frequency. The result, is a temperature map, that circumvents, most artifacts and, can be interpreted, on an absolute scale. In reference to the Fig. 14.40, below, there is described, in its caption, how the iMQC signal, can be used, to measure temperature. It is shown, how, the necessary modifications made, to a standard iZQC pulse sequence, one can obtain, a clean temperature map. One can see the demonstration, about the iMQC temperature imaging method, using phantoms, in different temperature situations (uniform temperature distribution as well as a phantom with a temperature gradient). It is shown, that the iMQCs, provide a clean temperature measurement. See Fig. 14.40 ([24]) as a practical illustration of iZQC-thermal imaging.
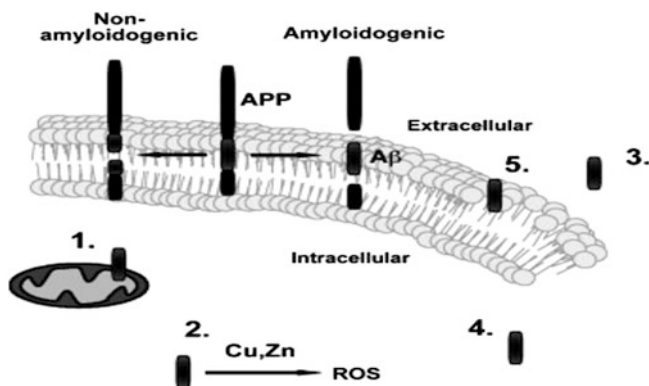
Fig. 14.42 Mechanisms of Aβ mediated neurodegeneration in Alzheimer's disease (AD). Amyloidogenic processing of APP via γ- and β-secretases, produce Aβ with the potential, to generate, neurodegeneration, by inhibiting mitochondrial activity, synaptic transmission and axonal transport, by disrupting membranes, and by generating oxidative stress. *1* Mitochondrial dysfunction. *2* Oxidative stress. *3* Synoptic transmission. *4* Axonal transport. *5* Membrane disruption

14.3.22 Alzheimer Disease (AD) Chemistry Model I

Recent developments have led to a conclusion that Alzheimer's Disease (AD) is complicated by pro-oxidant intraneuronal Fe^{2+} elevation as well as extracellular Zn^{2+} accumulation within amyloid plaque [25]. It is found that the AD β-amyloid protein precursor (APP) possesses ferroxidase activity, mediated by a conserved H-ferritin-like active site, which is inhibited specifically by Zn^{2+}. Like ceruloplasmin, APP catalytically oxidizes Fe^{2+}, loads Fe^{3+} into transferrin, and has a major interaction with ferroportin in HEK293T cells (that lack ceruloplasmin) and in human cortical tissue. Ablation of APP in HEK293T cells and primary neurons induces marked iron retention, whereas increasing APP695 promotes iron export. Unlike normal mice, $APP^{-/-}$ mice, are vulnerable to dietary iron exposure, which causes Fe^{2+} accumulation and oxidative stress in cortical neurons. Paralleling iron accumulation, APP ferroxidase activity in AD postmortem neocortex, is inhibited by endogenous Zn^{2+}, which is demonstrated, can originate from Zn^{2+}-laden amyloid aggregates and correlates with Aβ burden.

Abnormal exchange of cortical zinc may link amyloid pathology with neuronal iron accumulation in AD. Ferroxidases prevent oxidative stress caused by Fenton and Haber–Weiss chemistry by oxidizing Fe^{2+} to Fe^{3+}. Losses of ferroxidase activities cause pathological Fe^{2+} accumulation and neurodegenerative diseases, such as aceruloplasminemia where mutation of the multi copper ferroxidase ceruloplasmin (CP) leads to glial iron accumulation and dementia. Iron-export ferroxidases CP and hephaestin interact with ferroportin and facilitate the removal (e.g., by transferring) of cytoplasmic iron translocated to the surface by ferroportin. Their expression is cell specific (e.g., CP in glia, hephaestin in gut epithelia), but an iron-export ferroxidase
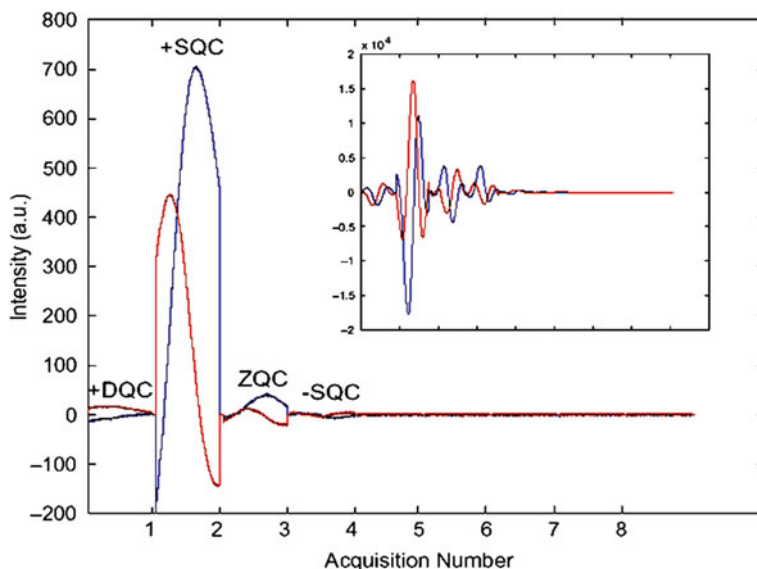
Fig. 14.43 Multi-CRAZED FID of hyperpolarized urea compared to the multi-CRAZED FID of water (*top corner*). It is important to note that this is not one long FID, but a series of consecutive FIDs separated by a gradient pulse

Table 14.46 Signal Intensities for the coherence observed in the multi-CRAZED experiment53

	+DQC	+SQC	ZQC	−SQC
Maximum signal intensity, ^{3}C Urea	25	700	50	10
Percent of +SQC maximum signal intensity, ^{13}C urea (%)	3.59	100	7.14	1.43
Maximum signal intensity, ^{1}H water	1920	16.150	3720	3815
Percent of +SQC maximum signal intensity, 1H water (%)	11.9	100	23.0	23.6

for neocortical neurons is unknown. CP is expressed in GPI-anchored and soluble forms APP, similarly is expressed, in transmembrane and secreted forms. It is explored whether APP is a ferroxidase and in turn has a role in neuronal iron export, an activity, consistent with APP translation, being responsive, to iron levels. It is also tested, whether, in AD, APP ferroxidase activity is altered in a manner, linked to the accumulation of its Aβ derivative, in plaque pathology. See Figs. 14.41, 14.42 [25, 26], for a pictorial representation of the chemical model of the AD.

14.3.23 Alzheimer Disease (AD) Chemistry Model II

Evidence for the relationship between the development of AD and abnormal Aβ production comes from the familial forms of AD [26]. Familial AD (fAD) only accounts for 10 % of all AD cases, but the most significant fAD mutations are all
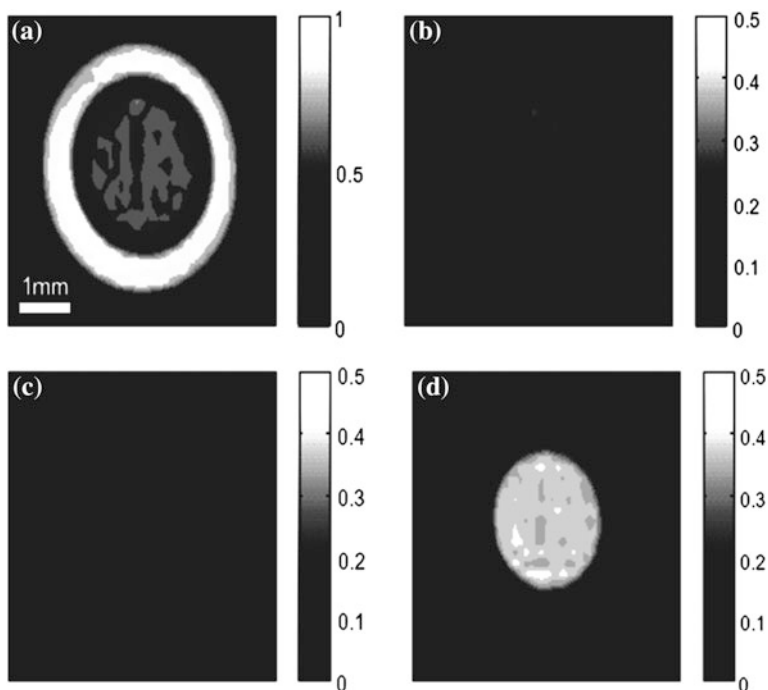
Fig. 14.44 ^{23}Na images of a phantom consisting of an inner 3 mm tube filled with 20 % agarose gel (fast sodium compartment) and an outer 5 mm tube filled with phosphate buffered saline (PBS, slow sodium compartment). The images were recorded by using (**a**) a hard 90 degree pulse, (**b**) inversion recovery with a delay of 35.5 ms, (**c**) spin echo TQF, and (**d**) Pulse I (optimal excitation control excitation sequence). The intensities were scaled with respect to the pixel of the highest intensity from the image (**a**)

associated with APP processing to yield Aβ. Mutations within APP that are adjacent to the α-, γ- and β-secretase cleavage sites, have been identified, and by altering secretase activity, at these sites, the relative Aβ yield from APP is affected. Familial APP mutations increase the relative production of Aβ$_{42}$ compared to Aβ$_{40}$, and this may be an important factor, in the development of, AD, since Aβ$_{42}$ tends to be more toxic and, more amyloidogenic. Familial AD mutations are also associated with, components of the APP secretases, such as presenilin 1, from γ-secretase. It is less clear however, whether these fAD mutations increase Aβ production, or the ratio of Aβ$_{42}$ compared to Aβ$_{40}$. Relative abundance, of the peptide, within the AD brain is central to disease development, but less certain are, the mechanisms of Aβ mediated neurotoxicity.

Amyloidogenesis is common to several proteins associated with degenerative diseases, indicating that the mechanisms of degeneration, may share some commonality with respect to the proteins' amyloidogenic properties, for review. Initial AD research focused on extracellular Aβ fibrils, as the primary toxic Aβ species, due to their abundance, within amyloid plaques, but this has been a contentious

point, since relatively early reports, demonstrated poor correlation between AD severity, and amyloid plaque burden. Soluble Aβ species (monomers, dimers, trimers, etc.) became more intensely studied in AD, once it was shown that Aβ, in the soluble fraction of AD, brain samples correlated best, with AD severity. This has since been further refined to exclude monomeric Aβ after reports demonstrated, that when compared to soluble Aβ oligomers/aggregates, Aβ monomers are relatively non- toxic, for example, it was demonstrated that Aβ oligomer preparations are 40 times, more toxic, towards neuronal cells, grown in culture, compared to unaggregated Aβ preparations, that contained predominantly monomeric Aβ.

The general consensus in AD research at present therefore is that soluble Aβ oligomer intermediates in the Aβ amyloidogenic pathway are the key contributors, to Aβ mediated neurodegeneration and it was recently proposed that the large insoluble Aβ deposits within the AD brain, may even act, as Aβ reservoirs for the formation of toxic soluble oligomeric species. However there is still no consensus on the specific species of Aβ that contributes most to neurodegeneration in AD. See illustration in Fig. 14.42 [26] for pictorial, conceptual information.

14.3.24 Carbon–Carbon (^{13}C–^{13}C) Multi-Quantum Coherence Imaging

^{13}C is a magnetic-dipole nucleus and is present in our body. The gyromagnetic ratio $\gamma = 6.7283 \times 10^7$ radians per second per Tesla, for ^{13}C, is much smaller than that of ^{1}H (proton), $\gamma = 26.7522 \times 10^7$ radians per second per Tesla. This means for the same magnetic field applied in MRI, the signal obtained in the case of ^{13}C, will be much smaller, than that for the proton, in MR situation. We have long way to go, to find out, a suitable way, to make use of the ^{1}3C dipole-magnetic and electrical quadrupole interactions to produce, MR metabolic picture of the brain. The reader is referred to Appendices A.28 and A.29 for a tabular comparison the magnetic-dipole and electric quadrupole properties of various nuclei important to our body. The multi-quantum coherence imaging (MQCI), has fundamentally, different physical an chemical properties of the spins, in action, than does the conventional (single quantum) signal imaging. In particular, it has, an intrinsic sensitivity, to sub-voxel structure. This sensitivity makes MQCI particularly suitable for a wide range of applications, such as the ^{13}C–^{13}C imaging [27].

MQCI experiments in a test tube of water can exhibit strong signals (within a factor of two of the equilibrium magnetization). However, applications to water, in more complex samples, such as tissue, are limited by relaxation effects resulting, in a smaller signal (typically 10–20 % of the conventional MRI signal). For nuclei, e.g. Na, K, etc., the drop is even more dramatic, essentially because the signal scales as the square of the magnetization density. One alleviates the problem using dynamic nuclear polarization (DNP). It transfers the large spin polarization present in the electron spin reservoir, to the nuclei. This transfer is routinely done by microwave irradiation, at or near the electron Larmor frequency, in the presence of
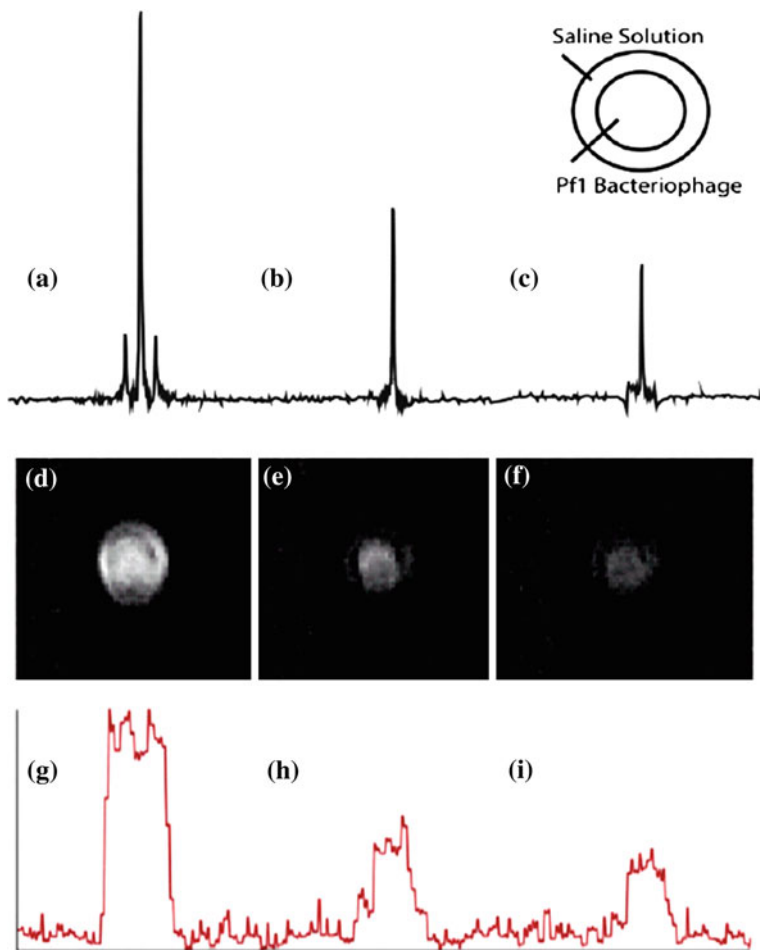
Fig. 14.45 Experimental comparison of single-pulse, (α = 54.7, τ = 1/CQ) binomial, and (α = 58.63, τ = 1/C_Q, C_Q is qudrupolar coupling constant) binomial gradient echo, in experiments for a phantom containing two concentric vials (schematic drawing in *upper-right corner*) containing 77 mM Na$^+$ ions in both vials, with the inner vial containing a 2.7 mL standard phosphate buffered saline (PBS), sow sodium compartment solution and 1.6 mL Pf1 solution while the outer vial contains a saline solution. **a–c** ^{23}Na spectra for the full sample volume and **d–f** ^{23}Na gradient echo images (projected slice, non-selective square pulse) obtained using (**a, d**) 90° single-pulse excitation, (**b, e**) (α = 54.7, τ = 1/C_Q,) binomial excitation, and (**c, f**) (α = 58.63, τ = 1/C_Q) binomial excitation. **g–i** Trace taken through the images in the row above

a large magnetic field. DNP techniques have been used to see tremendous increases, in signal to noise ratio. By using hyperpolarization to enhance the initial magnetization of the sample, it is possible to acquire the multi-correlation spectroscopy revamped by asymmetric z-gradient echo detection (CRAZED) field induction decay (FID) of carbon–carbon coherences. Figure 14.43 [27] and Table 14.46 [27] for recent research and development results.

14.3.25 Separation of Fast Sodium Component

A variety of tissues and organs, including the brain, cartilage, the disc, breast, and kidneys, contain large concentrations of sodium ions. With the advent of high field MRI scanners, high-resolution sodium images [28] can be obtained within clinically acceptable scan times, which makes ^{23}Na MRI, a promising tool, for the diagnosis of some important diseases, such as osteoarthritis (OA), degenerative disc diseases (DDD), breast cancer, and brain tumors. Certain disorders, can show up, as concentration changes, of bound sodium ions. In cartilage tissue, for example, the sodium concentration is particularly high since the ions are attracted to the negative charge of glycosaminoglycans (GAGs). A decrease of GAG concentration, is generally a sign, for the onset of disorder. Hence, the sodium concentration in cartilage can be regarded a direct reporter of degenerative diseases such as OA and DDD. Techniques for modifying ^{23}Na contrast have been developed in order to cleanly separate ordered sodium ions (in cartilage) from free sodium ions (in non-cartilage tissues) on high-resolution ^{23}Na images, both in vivo and ex vivo.

As a result of the attraction of the ions, to large macromolecules, the sodium ion motion is restricted, and ^{23}Na signals, in cartilage, show frequently, a residual quadrupolar interaction, which is visible as a line-splitting. Experiments such as the triple-quantum filtered experiment are able to detect slowly-tumbling sodium, selectively. Intracellular compartments, have significantly higher viscosity than, extra cellular compartments, so that sodium inside the cell, experiences a much decreased, tumbling rate. Experiments such as, triple-quantum filtering, can be used to distinguish intra- from extra cellular sodium signals. One uses, optimal control excitation pulse, sequences, which suppress the signal, from fast sodium ions, and maximizes the signal from slow sodium ions. Figure 14.44 ([28]), shows the images obtained, in selected situations. There is, one recorded by optimal pulse I (optimal excitation control excitation sequence), which clearly demonstrates that, it out-performs, the inversion recovery (IR) and the TQF, in terms of contrast.

14.3.26 Quadrupolar-Coupling ^{23}Na NMR

It is now well known that the sodium concentration gradient plays an important role in the cell metabolism and proliferation [29]. ^{23}Na is the second most abundant NMR-active spin species in vivo; this spin isotope, is 100 % abundant, and it is a spin I = 3/2 quadrupolar nucleus, with a relatively small quadrupole moment, enabling straightforward detection, in both liquid and solid phase. In most biological (cellular) environments, ^{23}Na displays non-vanishing, quadrupolar interactions, with effective quadrupolar coupling constants, in the order of 20–550 Hz, facilitating distinction between intracellular and extra cellular sodium compartments, in vivo, applications. Early studies indicated, that the intracellular sodium ions, were orientationally constrained, leading to isotropic motion, without
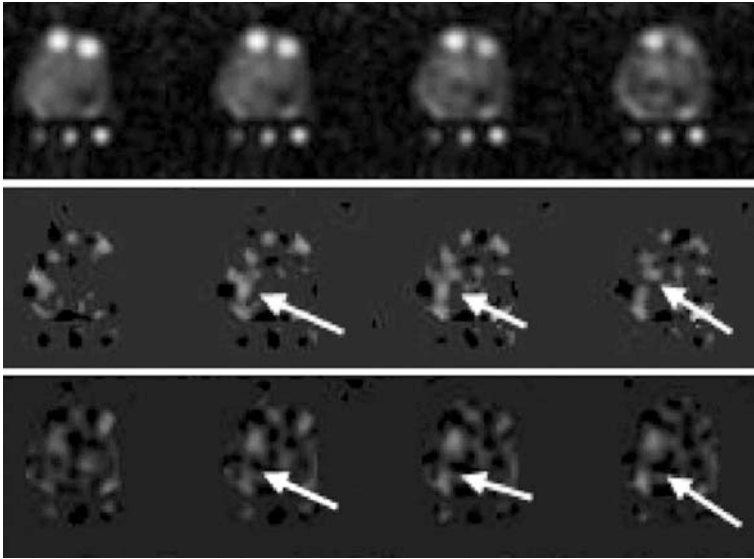
Fig. 14.46 Selected partition of a sodium image and its corresponding slope map before (*middle row*) and after (*bottom row*) reperfusion of the middle cerebral artery (MCA) territory. Changes in the rate of tissue sodium concentration (TSC) accumulation, are clearly observed, in the region corresponding to the MCA (animal/monkey) model (*arrows*). Only pixels with statistically slopes ($P < 0.005$) are presented in these maps
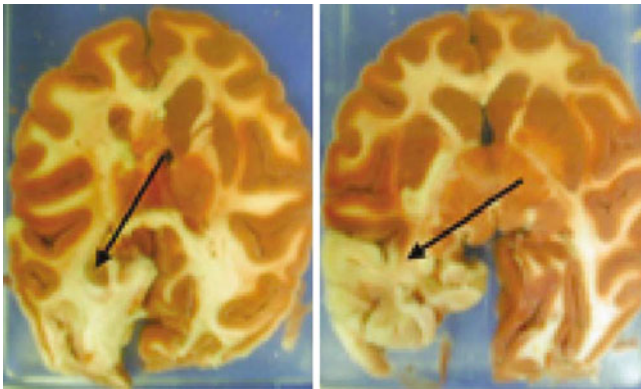
Fig. 14.47 The TTC (2, 3, 5-triphenyltetrazolium chloride) stained sections from the brain of the animal (temporary ischemia model). The images demonstrate ischemic damage to the PCA territory which is the only vascular territory that remained occluded upon removal of the balloon catheter

motional narrowing, but with a dominant quadrupolar interaction. The resulting non-vanishing quadrupolar interaction, was observed in terms, of line broadening, through biexponential relaxation, with unresolved residual quadrupolar splitting,

Table 14.47

Non-metals	^1H	^{13}C	^{15}N	^{19}F	^{29}Si	^{31}P	^{77}Se	^{125,} ^{123}Te	^{129}Xe
Group B metals	115, 117, 119Sn	203, 205Tl	207Pb						
Transition metals	57Fe	89Y	03Rh	109Ag	113Cd	183 W	187Os	195Pt	199Hg
Lanthanides	169Tm	171Yb							

Note The superscript on the left on each element represents the atomic mass of the element. It approximately represents the total number of protons and neutrons, expressed in terms of the proton mass which is very close to the neutron mass

Table 14.48

Magnetic strength	Natural abundance		
	High (>90 %)	Medium	Low (<10 %)
Strong	7Li		
Medium	^9Be, ^{23}Na, ^{27}Al, ^{45}Sc, ^{51}V, ^{55}Mn, ^{59}Co, ^{75}As, ^{93}Nb, ^{115}In, ^{127}I, ^{133}Cs, ^{181}Ta, ^{209}Bi	(^{10}B), ^{11}B, ^{35}Cl, ^{63}Cu, ^{65}Cu, (^{69}Ga), ^{71}Ga, (^{79}Br), ^{81}Br, (^{85}Rb), ^{87}Rb, ^{121}Sb, (^{123}Sb), ^{137}Ba, ^{139}La, (^{185}Re), ^{187}Re	^2H, ^6Li, ^{17}O, ^{21}Ne, (^{113}In), (^{123}Ba)
Weak	^{14}N, ^{39}K	^{35}Mg, ^{37}Cl, ^{83}Kr, ^{93}Mo, ^{131}Xe, 189Os, ^{201}Hg	^{33}S, (^{41}K), ^{43}Ca, ^{47}Ti, ^{49}Ti, ^{53}Cr, ^{67}Zn, ^{73}Ge, ^{87}Sr, (^{97}Mo)

Note The superscript the before the element represents the atomic mass of each element. The less favorable nuclei (where the choice is clear cut) for a given element are enclosed in brackets. The elements more relevant to MRI in human body are expressed in bold

while later studies reported, direct observation of distinct quadrupolar splitting ex vivo. Such residual quadrupolar splitting of sodium ions have been reported, in human and animal tissues, including, muscle, brain, cartilage, and blood. The existence of ^{23}Na ions with different quadrupolar couplings may be of great interest for several applications. Direct excitation or multiple-quantum filtering facilitates distinction of signals in terms of their quadrupolar couplings. Ischemic stroke is an interesting example, where metabolism is disturbed secondary to changes in the Na^+, K^+-ATPase, resulting in, increasing intracellular, sodium content.

The intracellular contribution to the overall ^{23}Na signal is often very small compared to the signal, originating from the extracellular space. To address such problems, it was recently introduced, the so-called quadrupolar jump-and-return (QJR) method, where ^{23}Na spins were excited in a quadrupolar-coupling-specific manner using a pulse sequence bearing resemblance to standard liquid-state NMR binomial solvent suppressions techniques. A pulse sequence with the pulse flip angle adjusted to $\alpha = 54.7°$ (i.e. the magic angle) facilitates suppression of the satellite transitions, while enhancing the amplitude of the central transition,

Table 14.49 Selected nuclei (spin 1/2 and >1/2) of interest in the configuration of the 'Periodic Table' are shown [31]

H ≥ 1/2				Spin1/2	Spin >1/2	Spin ≥ 1/2	
				C 1/2	N ≥1/2	O>1/2	F 1/2
Li >1/2	Be> 1/2			P 1/2	S >1/2	Cl >1/2	
Na >1/2	Mg >1/2			As >1/2	Se 1/2	Br >1/2	
K >1/2	Ca >1/2			Sb >1/2	Te 1/2	I >1/2	
Rb >1/2	Sr >12						
Cs >1/2	Ba >1/2	Mn >1/2	Fe 1/2	CO >1/2	Cu> 1/2		Bi >1/2

Some of the elements of importance to the human

relative to normal 90 excitation, for the selected quadrupolar coupling. In this study, one takes advantage of the analogy between such quadrupolar-coupling specific pulses, and the binomial pulse sequences, used for water suppression, in liquid-state NMR, and introduce a series of more advanced binomial pulse sequences, offering a high degree of flexibility in the discriminative excitation of ^{23}Na spins, with small differences in the effective quadrupolar coupling constants. As an important additional benefit, some of the pulse sequences are significantly more robust towards experimental artifacts, such as the RF field inhomogeneity. Figure 14.45 ([29]) presents an illustration of the results from this new technique.

Table 14.50 Biologically important nuclei [32]

Isotope	Spin	Natural abundance (NA) (%)	Quadrupole moment Q ($10^{-28}m^2$)	Gyromagnetic ratio γ ($10^7 rads^{-1}T^{-1}$)
^{1}H	1/2	99.98	–	26.7522
^{2}H	1	1.5 ± 10^{-2}	2.87 ± 10^{-3}	4.1066
^{3}H	1/2	0	–	28.5350
^{7}Li	3/2	92.58	-3.7 ± 10^{-2}	10.3976
^{11}B	3/2	80.42	4.1 ± 10^{-2}	8.5847
^{13}C	1/2	1.108	–	6.7283
^{14}N	1	99.63	1.67 ± 10^{-2}	1.9388
^{15}N	1/2	0.37	–	-2.7126
^{17}O	5/2	3.7 ± 10^{-2}	-2.6 ± 10^{-2}	-3.6280
^{19}F	1/2	100	–	25.1815
^{23}Na	3/2	100	0.10	7.0704
^{25}Mg	5/2	10.13	0.22	-1.6389
^{31}P	1/2	100	–	10.8394
^{35}Cl	3/2	75.53	-8.2 ± 10^{-2}	2.6242
^{39}K	3/2	93.1	5.5 ± 10^{-2}	1.2499
^{43}Ca	7/2	0.146	-5 ± 10^{-2}	-1.8028
^{51}V	7/2	99.76	2.17 ± 10^3	-5.2 ± 10^{-2}
^{57}Fe	1/2	2.19	–	0.8687
^{75}As	3/2	100	0.29	4.5961
^{77}Se	1/2	7.58	–	5.1214
^{113}Cd	1/2	12.26	–	-5.9609

Note If the Mass Number is odd and the Atomic Number is even or odd, we have I = 1/2, 3/2, 5/2…. If the Mass Number is even and the Atomic number is also even, we have I = 0. If the Mass number is even and the Atomic Number is odd, we have I = 1, 2, 3, …

14.3.27 Loss of Cell Ion Homeostasis and Cell Viability in the Brain

The sodium nucleus yields the second strongest nuclear magnetic resonance (NMR) signal among all biologically relevant NMR active nuclei. The ^{23}Na nucleus has a spin of 3/2 and a gyromagnetic ratio of 1126 Hz/Gauss, leading to an overall NMR sensitivity (relative to water protons) of 0.092. The sodium ion plays a critical role in cell physiology [30] as many physiological conditions lead to large changes in the average concentration of this nucleus in tissue. For example, during brain neoplasia, sustained cell depolarization, a common precursor of cell division, leads to an increase in the intracellular sodium content and a concomitant rise in the average tissue sodium concentration. As these changes in sodium content are directly related to the underlying physiological changes and typically large (>50 %), they represent an ideal means to noninvasively monitor cellular processes associated with the development of pathology in vivo. Magnetic resonance imaging (MR I) has evolved into one of the preferred techniques for noninvasive topographic imaging in vivo.

There have been in the past continued advances in radiofrequency (RF) electronics, computing performance, and high power amplifiers. It has led to a significant improvements in the capabilities of MRI as an imaging technique. Moreover, methodological improvements have changed the role of MRI from a high resolution anatomical imaging tool to that of a functional and anatomical one. Despite the rapid advances in conventional proton MRI, progress in sodium imaging did not follow suit for many years. This was due in part to the stringent constraints imposed by the sodium nucleus on image signal. Fortunately, recent developments in the field have led to imaging schemes that have removed the limitations and allow sodium MRI to be performed with adequate spatial resolution and SNR, in practical imaging times (<10 min). These developments have allowed the study of important physiological conditions such as ischemia and neoplasia in vivo. Figures 14.46 and 14.47 [30] are typical representatives of the problems solved, and progress on the way, in the field of ^{23}NaMRI.

14.3.28 Nuclear Magnetic Dipole (Spin 1/2 Nuclei) and Quadrupolar Nuclei/Courtesy (1)

The Spin 1/2

Some Selected Magnetic Dipole Nuclei: All the nuclei tabled below do not form part of the human body life cycle [31]. They are included for their location in the broad perspective of the 'Periodic Table (Table 14.47 [31])

14.3.29

The Quadrupolar Nuclei (Spin ≥ 3/2) All the nuclei tabulated do not form part of a natural life cycle of our body. Selection is to show their position in the perspective of the 'Periodic Table' (Tables 14.48, 14.49, 14.50 [32]).

14.3.30

Refer Table 14.16.

14.3.31

Refer Table 14.17.

14.3.32 Molecular Qudrupole Moment: Electric Field Gradient Interactions

This appendix would be of particular interest to the readers with fairly good background of mathematics, both classical and that of the quantum mechanic (QM). One should realize without revised and inventive input from mathematicians, no filed of science can progress, MRI is no way an exception. The spin relaxation of a nucleus having an electric quadrupole moment (spin I ≥ 1) is usually due mainly to the interaction of the quadrupole moment with electric field gradients present at the position of the nucleus [15, 33]. Calculations predict that both the longitudinal and transverse spin relaxation produced by a quadrupole interaction are simple exponential decays if (1) the nucleus has spin I = 1 or (2) the electric field gradients fluctuate much more rapidly than the Larmor period of the nucleus, a situation referred to as a short correlation time, or extreme narrowing case. If neither of the above conditions is satisfied, both the longitudinal and transverse relaxations produced by a quadrupole interaction are the sums of two or more decaying exponentials.

Consider a nucleus with spin $I \geq 1$, gyromagnetic ratio γ, and quadrupole moment Q, located in one of the molecules of a sample which is exposed to a magnetic field $H_o k$ [15]. The spin interacts with its molecular surroundings through a quadrupole coupling. It is assumed that the average of the quadrupole coupling is zero, as is appropriate for a nucleus in a molecule of a liquid or gas. The initial condition of the spin system is taken to be the result of the application to the system in thermal equilibrium of a "θ-degree pulse;" i.e. the application of a magnetic field H_1 (i cos $\omega_o t$ − j sin $\omega_o t$) for a time $t_\theta = \theta/\gamma H_1$ short compared toa time in which appreciable relaxation occurs. $\omega_o = \gamma H o$ is the Larmor frequency of the nucleus in the magnetic field $H_0 k$. The effects of the molecular surroundings occur in the relaxation theory through spectral densities

$$J_{lk}(\omega) = (^1\!/_2) \int C_{lk}((t) \exp(i\omega t) dt$$

and of correlation functions.

$$C_{lk}(t) = Tr_b[\rho^T(1/2)(U^l(t)U^k + U^k U(t)]$$

where Tr denotes a trace over the molecular coordinates; $p^T = \exp(-\beta F)/Trb[\exp(-\beta F)J; \beta = \hbar/kT$, where k is the Boltzmann constant and T the temperature of the sample; $\hbar F$ is the Hamiltonian of the molecular system; and $U^l(t) = \exp(iFt) U^l \exp(-Ft)$. The operators Uk, for the case under consideration of relaxation by quadrupole interactions, are given by $U_k = (-l)^k F_{-k}$, where

$$F_0 = (1/2)(V_{zz})$$
$$F_{\pm 1} = \pm(6)^{-1/2}(V_{zz} \pm i\, V_{zy)}$$
$$F_{\pm 2} = (1/2)(6)^{-1/2}(V_{zz} - V_{yy} \pm i\, 2V_{xy})$$

and where V_{ij} represents a second partial derivative, with respect to the laboratory coordinates, of the electric potential V_{ij} at the position of the nucleus. In the solution of the differential equations for the elements of the reduced density operator, only terms containing J_{lk} with $1 = -k$ need be retained because (1) if the relaxation is slow compared to the Larmor frequency, the other terms can be shown to be nonsecular, and hence produce negligible effect, or (2) if the Hamiltonian $\hbar F$ describing the molecular motion is invariant under rotations, then it can be shown that $J_{lk}(\omega) = \delta_{l-k}(-1)^k J_{oo}(\omega)$, as a consequence of the fact that the operators F_k are the elements of an irreducible tensor operator of rank two.

The results for relaxation by quadrupole interactions may now be stated. If the correlation time is not short, the longitudinal and transverse relaxations of a nucleus with spin 1 are different, but each is the sum of I decaying exponentials if 1 is an integer, or the sum of $I + 1/2$, decaying exponentials if I is half an odd integer. For $I = 1$, the longitudinal and transverse relaxations are simple exponential decays. In the present notation, the longitudinal relaxation time T_1 and the transverse relaxation time T_2 are given by $1/T_1 = (3/2)\{eQ/\hbar)2[-J_{-11}(\omega_0) + 4\,J_{-22}(2\omega_0)]$ and $1/T_2 = (3/2)\{eQ/\hbar)^2[3/2J_{00}(0) - 5/2\,J_{-11}(\omega_0) + J_{-22}(2\omega_0)]$.

For $1 = 3/2$, both the longitudinal and the transverse relaxations following a θ-degree pulse are the sums of two decaying exponentials. The longitudinal relaxation is

$$<I_z> - <I_z>^T = <I_z>^T(\cos\theta - 1)[(4/5)\exp(-a_1t + (1/5)\exp(-a_2t)]$$

where

$$a_1 = 2(eQ/\hbar)^2 J_{-22}(2\omega_0); \quad a_2 = -2(eQ/\hbar)^2 J_{-11}(2\omega_0)$$

and $<Iz.>^T$ is the thermal equilibrium value of $<Iz>$. The transverse relaxation is given by

$$<I_x> + i<I_y> = <I_z>^T i\,\exp[-i\omega_0(t+t_0)]\sin\theta[(3/5)\exp(-b_1t) + (2/5)\exp(-b_2t)]$$

where

$$b_1 = (eQ/\hbar)^2[J_\infty(0) - J_{-11}(\omega_0)]$$

and

$$b_2 = (eQ/\hbar)^2[J_{-11}(\omega_0) + J_{-22}(2\omega_0)]$$

For $1 = 2$, the longitudinal and transverse relaxations are also the sums of two exponentials. Since there are no stable nuclei with spin of two, the results in this case are of no importance. The exponents that occur in the expressions for the relaxation are the roots of algebraic equations of degree I, if I is an integer, or degree $1 +1/2$ if 1 is half an odd integer. For $1 > 2$ it is feasible to calculate the roots only if numerical values for the spectral densities are assumed. We have not

carried out such calculations. The spectral densities $J_{kk}(k\omega_0)$ in the above expressions can be replaced by $(-1)^k J_{oo}(k\omega_0)$ if the Hamiltonian governing the molecular motion is invariant under rotations, or by $J_{-kk}(0)$ if the correlation time is short compared to the Larmor period. If both of these conditions are satisfied, J_{-kk} (kwo) can be replaced by $(-1)^k J_{00}(0)$. In this case, both the longitudinal and transverse relaxations are simple exponential decays, with the resulting longitudinal and transverse relaxation times for a given I being equal. For a nucleus of arbitrary spin I, the results in the present notation are

$$1/T_1 = 1/T_2 = (3/2)(eQ/\hbar)^2 \left[(2I+3)/I^2(2I-1) \right] J\infty(0)$$

The second partial derivatives of the electric potential at the position of the nucleus, the quantities V_{ij} occurring are the elements of a real, symmetric tensor of rank two. Hence there exists a Cartesian coordinate system, say S'', in which V_{ij} is diagonal, the only nonzero elements being Vxx, Vyy, and Vzz. The axes of S'' can be labeled so that $V\ zz \geq V\ xx \geq 1\ Vyy$ I. If quantities *eq* and η are defined by eq = Vzz, η = [(Vxx − Vyy)/Vzz], then the elements of the spherical tensor are given in S'' by

$$F''_0 = 1/2 eq; F''_{\pm 1} = 0; F''_{\pm 2} = 1/2 (6)^{-1/2} (\eta eq)$$

If the nucleus under consideration is in a molecule of a liquid or gas, it is usually assumed that the electric field gradients are produced by charges in the molecule that are in effect fixed with respect to the molecule. In this case, the coordinate system S'' is fixed in the molecule, and the quantities *eq* and η are constants. In order to evaluate the correlation functions, it is usually convenient to introduce another coordinate system, S_l, fixed in the molecule in a manner to be specified below. Let $g_l = (\alpha_1 \beta_1 \gamma_1)$ be the Euler angles of S_l with respect to the laboratory coordinate system *S,* and $g'' = (\alpha'' \beta'' \gamma'')$ be the fixed Euler angles of S'' with respect to S_l. There can be a body with rotational diffusion constants D_1, D_2, and D_3, with an arbitrary shape. If the body has axial symmetry, them $D_2 = D_1$. For a spherical body, with D1 = D2 = D3 = D, and $b_{2k} = 6D$, one gets

$$J_{lk}(\omega) = \delta_{l,-k}(-1)^k(1/20)(1 + 1/3\eta^2)(eq)^2 \tau_c \left[1 + \left(\omega \tau_c^2 \right) \right]$$

where $\tau_c = (1/6D)$. There is no doubt that the interest in using quadrupolar nuclei to study molecular structure has received a huge boost from the introduction of the multiple-quantum magic-angle-spinning (MQMAS) method. But there remains the question of why we should wish to use quadrupolar nuclei in any structural study when, despite the high-resolution methods for quadrupolar nuclei, there is no doubt that spin-1/2 nuclei are still much easier to handle. The answer is simple: 75 % of NMR-active nuclei are quadrupolar (and of these, the vast majority are half-integer). Thus, for many materials that we may wish to examine, we have no choice but to use quadrupolar nuclei in our study. Even if there are convenient spin-1/2 nuclei present, we cannot hope to obtain a full structural picture if we ignore all the atomic species that have quadrupolar nuclei. Beyond this, there is the further consideration

that many otherwise useful spin-1/2 nuclei have inconveniently low natural abundances—for example, ^{13}C (1.1 % natural abundance) and ^{15}N (0.37 %). So if we wish to study the structure of a naturally occurring solid protein, we have the option of using these low-abundance nuclei or ^{1}H if we restrict ourselves to using spin-1/2 nuclei.

The strong dipolar couplings within the network of abundant ^{1}H in a solid protein means that ^{1}H NMR spectra consist of broad, featureless lines unless rather sophisticated methods are employed. How much easier life would be if we could use instead the near-100 % abundant ^{14}N quadrupolar ($I = 1$) nucleus in our study. To this end, there have been experiments developed that use ^{14}N overtone spectroscopy and measure the ^{14}N overtone spectrum directly, indirectly, and via cross-polarization, which brings us closer to this goal. The so-called quadrupolar nuclei (i.e. those with $I > 12$) possess an electric quadrupole moment in addition to the magnetic dipole moment that all NMR-active nuclei must have. Electric quadrupole moments interact with electric field gradients, which in turn arise from the particular distribution of electrons and other nuclei around the nucleus in question, unless that nucleus is at a crystallographic site of cubic symmetry. The nuclear electric quadrupole moment and electric field gradient interaction can be rather large, causing powder patterns of megahertz in width for solid samples consisting of large numbers of randomly oriented crystallites (i.e. powders). The size of the interaction depends on the size of the nuclear electric quadrupole moment, a constant, and the size of the electric field gradient, which is determined by the molecular and electronic structure around the nucleus. In a simplified form [33], the nuclear electric quadrupole moment and electric field gradient interaction can be described by the Hamiltonian

$$H_Q = [(eQ)]/[6I(2I-1)\hbar](I.V.I).$$

Here eQ is the nuclear electric quadrupole moment and V is a second-rank Cartesian tensor describing the electric field gradient. Such a tensor can be represented by a 3 ± 3 matrix in which a component $V_{\alpha\beta}$, ($\alpha\,\beta$ = x, y, z), is the α-component of the electric field gradient. The applied magnetic field of the NMR experiment, is in the direction β, of the defining frame of reference.

$$V = \begin{pmatrix} Vxx & Vxy & Vxz \\ Vyx & Vyy & Vzz \\ Vzx & Vzy & Vzz \end{pmatrix}$$

As already implied, such a tensor can be expressed with respect to any Cartesian axis frame. One frame of particular relevance is the principal axis frame (PAF), which is the reference frame in which the tensor is diagonal, with components Vxx, Vyy, and Vzz, which are often expressed as the anisotropy and asymmetry:

$$Eq = V_{zz}^{PAF}; \quad \eta_Q = \left(V_{xx}^{PAF} - V_{yy}^{PAF}\right)/V_{zz}^{PAF}$$

where eq is the anisotropy of the electric field gradient tensor and η_Q its asymmetry. The trace of the electric field gradient tensor is always zero. In a large
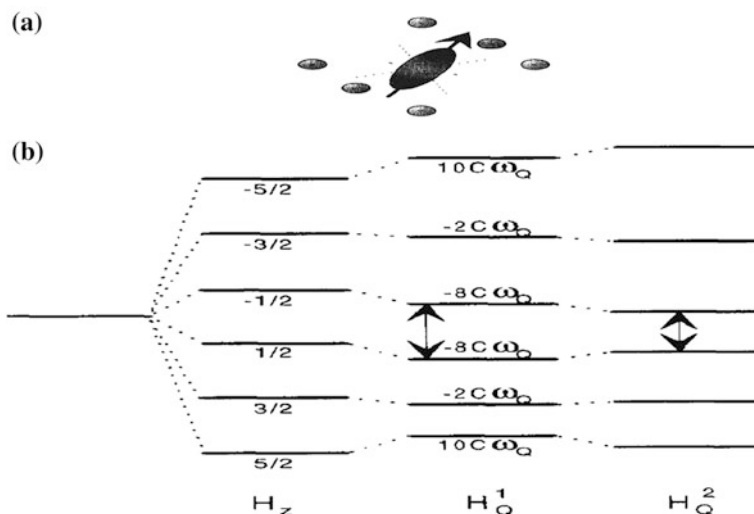
Fig. 14.48 a The charge distribution of a quadrupolar nucleus is not spherically symmetric, therefore it experiences an electrostatic force depending on the charges that surround it. The spin levels are affected by the interaction of the quadrupole moment eQ of the nucleus and the field gradient eq caused by the external charges. **b** Spin energy level diagram for an $1 = 5/2$ nucleus in a strong external magnetic field. The Zeeman interaction splits the levels by an equal amount hv_z, In first-order perturbation theory all levels $1 + m >$ and $1 - m >$ are shifted by the same amount, indicated in the figure, due to the quadrnpolar interaction. Thus there is no effect on the central $I + 1/2 \leftrightarrow - 1/2 >$ interaction. In second-order perturbation theory all transitions are affected

magnetic field, the Zeeman interaction with the nuclear magnetic dipole moment is the dominant interaction, and the applied magnetic field in such a case acts as the quantization axis for the nuclear spins. Thus the magnetic dipole moment is oriented by the applied magnetic field, and with it (because it is part of the same nucleus) the nuclear electric quadrupole moment, even though the latter has no interaction with the applied field. The electric field gradient tensor meanwhile is determined purely by the molecular structure around the nucleus and thus has an orientation that is fixed with respect to a molecular frame of reference. The interaction between the nuclear electric quadrupole moment then depends on its orientation with respect to the molecule, which in turn is determined by the direction of the applied field. In other words, the strength of the nuclear electric quadrupole moment and electric field gradient interaction depends on the orientation of the molecule (or more precisely, the electric field gradient tensor arising from it) with respect to the applied magnetic field, and so is termed anisotropic (i.e. the interaction strength depends on molecular orientation).

The principal axis frame of the electric field gradient tensor is a property of the molecular structure; the orientation of the electric field gradient is generally described by the orientation of its principal axis frame with respect to the applied magnetic field or, equivalently, with respect to a laboratory frame in which, by convention, the applied magnetic field lies along z. The effect of the quadrupole

coupling Hamiltonian can then be approximated in this high field case using average Hamiltonian theory or, equivalently, perturbation theory. Both these approaches express the quadrupole interaction Hamiltonian as a sum of contributions of successively higher order in the applied magnetic field; the level of approximation required for any given case then depends on the size of the quadrupole coupling interaction relative to the Zeeman interaction. The first and second-order contributions to the quadrupole coupling Hamiltonian are given

$$H^{(1)}{}_Q = \{(\sqrt{6})[(e2qQ)]/[4I(2I-1)]\}\{WQ_{20}T^Q{}_{20}\}]$$

$$H^{(2)}{}_Q = -\left[\{(e^2qQ)/(4I(2I-1))\}^2\left[(1/\omega_0)(2/5)\right.\right.$$
$$\times [(-3\sqrt{10})TQ_{30} + TQ_{10}(3-4I(I+1)))V^Q{}_{00}$$
$$+ (-12\sqrt{10})T^Q{}_{30} - T^Q{}_{10}(3-4I(I+1)))V^Q{}_{20}$$
$$+ (-34\sqrt{10})T^Q{}_{30}) + 3T^Q{}_{10}(3-4I(I+1)))V^Q{}_{40}]$$

Here the spherical tensor operators $T^Q{}_{k0}$ are,

$$T_{10}{}^Q = I_z, T^Q{}_{20} = (1/\sqrt{6})[3I^z{}_z - I(I+1)]$$

$$T^Q{}_{30} = I_z, T^Q{}_{20} = \left[(1/\sqrt{6})\left(5I^z - 3I(I+1)+I\right)\right]I_z$$

The $W^Q{}_{k0}$ parameters that contain all the geometrical terms for the first-order term are given by

$$W^Q{}_{20} = \sum D^2_{n0}(\alpha,\beta,\gamma)B_{2n}$$
$$n = 0, \pm 2$$

These equations can be used to derive the transition frequencies expected for a quadrupolar spin I between levels $m \rightarrow m+1$, where m denotes the magnetic quantum number. The first and second order contributions to the transition frequencies so derived are given by

$$\Delta\omega^{(1)}{}_Q = \left[3e^2qQ/4I(2I-1)\right]\left[(2m+1)W^Q{}_{20}\right]$$

$$\Delta\omega^{(2)}{}_Q = -\left[(e^2qQ/4I(2I-1)\right]^2\left[(2/\omega_0)\right]$$
$$\times [I(I+1) - 9m(m+1) - 3)V^Q{}_{00}$$
$$+ 8I(I+1) - 36m(m+1) - 15)V^Q{}_{20}$$
$$+ 3[(6I(I+1) - 34m(m+1) - 13)]V^Q{}_{40}]$$

14.3.33 Quadrupole Nuclei: Disordered Systems

This appendix is included to attract the attention of those readers other than just interested in MRI of human body. There can be other applications of MRI e.g. the design of a solid-state or liquid state quantum computer (QC). The element ^{27}Al has a spin of 5/2, thus is dipolar as well as diamagnetic. This can be a useful dopant in the Si lattice, to design a solid-state QC [34]. There is also discussed an example of ^{23}Na spectroscopy in the solution NaNO$_3$ in the context of the human body situation. Quadrupole nuclei permit the study of the local structure around nuclei in both crystalline and amorphous materials [34]. Nuclei possessing a quadrupole moment are common, some of the most important being ^{27}A1, ^{23}Na and ^{17}0. Contrary to a nucleus with spin 1/2, a quadrupolar nucleus has a non-spherically symmetric charge distribution. As a result a quadrupolar nucleus experiences an interaction with the electric field gradient due to the surrounding charge distribution [Fig. 14.48 ([34])].

The interaction is described by the quadrupole coupling constant QCC = $e2qQ/h,$ where eQ is the nuclear quadrupole moment and eq = Vzz the main principal value of the electric field gradient tensor V. The asymmetry parameter describes the asymmetry of the electric field gradient (i.e. a cylindrical symmetry yields asymmetry = 0). Comparing electric field gradients for different nuclei, one should consider the contributions of the inner closed electron shells to the observed electric field gradient. The originally spherical symmetrical inner shells of electrons are polarized by the external electric field gradient and thus contribute to the gradient actually felt by the nucleus. This is expressed in the Sternheimer (anti-) shielding factor γ_∞. In a purely ionic crystal, the experimental field gradient eq$_{obs}$ = $(1 - \gamma_\infty)$ eq$_{ioni}$c, where eq$_{ionic}$ is the field gradient due to the surrounding ionic charges. In the rare case of perfect cubic symmetry the quadrupolar interaction vanishes; any distortion of the local environment expresses itself in the appearance of a quadrupole interaction.

Nuclei with spin-quantum number I = 1/2, such as ^{1}H, ^{13}C and ^{29}Si, can appear in two spin states, $\left| +1/2 > \right.$ and $\left| -1/2 > \right.$, and can thus undergo one spin transition in the external magnetic field, I + 1/2 $\leftrightarrow$ I − 1/2, associating one spectral frequency with each nucleus. In general a nucleus with spin I has 2I + 1 energy levels, with 2I allowed single quantum transitions, thus the NMR spectrum of a single nucleus will display 2I resonances. The energy level diagram of a spin 5/2 nucleus is given in Fig. 14.48 (Fig. 1 in [34]). Placing the nucleus in an external magnetic field leads to an equal splitting of the energy levels due to the Zeeman interaction (Hz). Here we restrict ourselves to the situation, generally encountered in high fields, were the quadrupole interaction is an order of a magnitude smaller than the Zeeman interaction. In that case all energy levels are perturbed by the quadrupole interaction in first order (H$_Q^1$). We see that every energy level +m is shifted by the same amount. As a result the central transition, I + 1/2 > I − 1/2 >, is not affected in first order. The effect is that a half-integer quadrupole nucleus will have a spectrum consisting of a line at the Zeeman frequency (i.e. the isotropic chemical
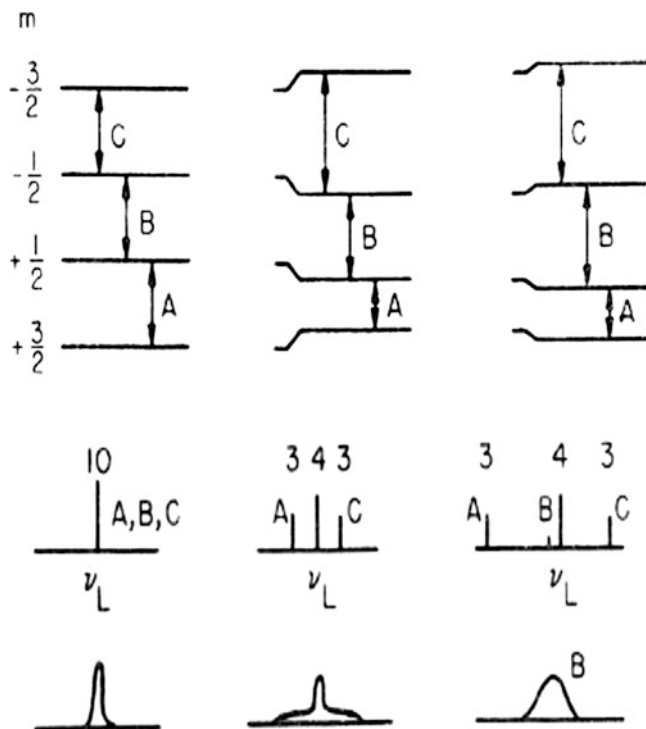
Fig. 14.49 Quadrupole splitting of the magnetic resonance of a nucleus of spin 3/2. *Top* energy levels. *Middle* spectrum of a single nucleus. The numerals indicate relative intensities. *Bottom* line shape in an imperfect crystal. *Left* no quadrupole interaction. *Center* first-order shifting of satellites. *Right* second order splitting of central component. $a_{||}$ = Larmor frequency

shift t) of the central transition, accompanied by a set of lines due to the satellite transitions which are symmetrically displaced away from the central transition by n times (n = ±1 for the 3/2 ↔ 1/2 and −1/2 ↔ − 3/2 transition etc.) the quadrupole frequency ∼ Ω_Q...$\Omega_Q = (\omega_0/2)(3\cos^2\beta − 1 + \eta\,\sin^2\beta\,\cos^2\alpha)$, with $\omega_Q = 3e^2qQ/[2I(2I−1)\hbar]$, and α and β are the angles relating the position of the electric field gradient tensor to the external magnetic field.

If we study a powdered sample we will get a sharp central transition, unaffected by the (anisotropic) quadrupolar interaction, whereas the satellite transitions give broad powder patterns. In $NaNO_3$ the quadrupole coupling constant (QCC) of sodium is exceptionally small (337 kHz). In most cases much larger QCC's (several MHz) are encountered, making the satellite transitions hard to detect. Furthermore, for such large quadrupole interactions it is not sufficient to consider only first-order perturbations of the energy levels. Looking at second-order perturbations it is seen that the central transition is also affected by the quadrupolar interaction which gives rise to a shift of the central resonance. So in practice only a broad powder pattern is observed for the central transition. In principle this powder

Fig. 14.50 Figure illustrating relaxation of the central component (1/2 to −1/2 transition) for a nucleus of spin I = 3/2. The *heavy arrow*, indicates transitions, produced by the applied radio-frequency field; the other *arrows* show the transitions caused by the quadrupolar relaxation mechanism
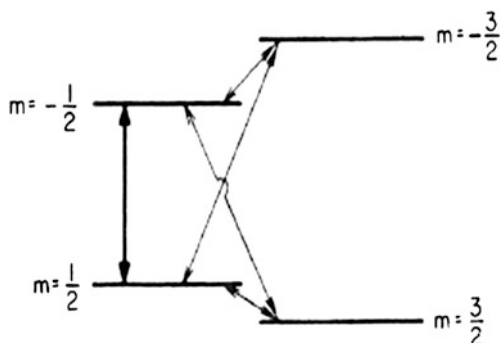
pattern is useful as it contains information about the quadrupole interaction. However, for samples containing several distinct sites, their powder patterns, often overlap rendering the resulting spectra un-interpretable. A well-known strategy to enhance the resolution of powder spectra in NMR is magic-angle spinning (MAS), which is capable of removing the anisotropic contributions of e.g. chemical shift anisotropy and dipolar interactions to the spectra. Obviously MAS has been applied extensively to half-integer quadrupolar nuclei.

14.3.34 The Basics: The Quadrupole Nuclear-Magnetic Dipole Interaction Energy

This appendix covers the conceptual part of the interactions between a quadrupole nucleus with the electric field gradient, surrounding it, as is present in various situations, in the human body organs. The approach is presented starting from the basic simple mathematics. Only the peripheral introductory equations and the final results form part of the exposition. Those readers who have a reasonably background of mathematics can simplify the mathematics further, in the context of human body, which can be useful in the continuous education of medical professionals (MPs). Consider a nucleus of atomic number Z whose total electric charge Ze is distributed over the nuclear volume with a density p(x) at the x. Let V(x) be the electrostatic potential arising from all the charges other than those of the nucleus under considerations. We are interested, in the general problem of computing the electrostatic interaction energy H. of the nucleus, with these charges, constituting its environment. More particularly, we are concerned with finding that part of H, which depends on the orientation of the nucleus, and which thus contributes to the spin dependent effects, involved in the hyperfine structure, or nuclear resonance. The electrostatic interaction H is simply expressed as an integral over the nuclear volume

$$H = \int \rho(x)V(x)d^3x$$

The variation of V(x), over the small but a finite nuclear volume, cannot be neglected entirely. It is natural, therefore, to expand it in a power series, about the nuclear center of mass, the motion of which is unaffected, by any nuclear reorientation. If the three Cartesian components of x, relative to this origin, are denoted by x_i (i = 1, 2, 3), one gets [35]

$$H = \int d^3 x \rho(x)[V_0 + \sum_j (\partial V/\partial xj)_0 x_j + \tfrac{1}{2} \sum_{j,k} (\partial^2 V/\partial x_j \partial x_{k,})_0 x_j x_k + \cdots$$

where the summation over each subscript extends from 1 to 3. The subscript 0, indicates a quantity, which is evaluated, at the center of mass x = 0, and which can, therefore be taken outside the integral sign. Thus one obtains

$$H = (ZeV_0) + \sum_j Pj(\partial V/\partial xj)_0 + \tfrac{1}{2} \sum_{j,k} Q_{jk'}(\partial^2 V/\partial x_j \partial x_{k,})_0 x_j x_k$$

Where

$$\int d^3 x \rho(x) = Ze = \text{nuclear charge}$$

and where we have introduced the definitions

$$\int d^3 x \rho(x) x_j = \text{electric dipole moment,}$$
$$\int d^3 x \rho(x) x_j x_k = Q_{jk'} = \text{electric qudrupoles moment tensor,}$$

The expansion above, is a convenient form, for the electrostatic interaction Hamiltonian H, in both, the classical, and quantum–mechanical description. In the latter case, $\rho(x)$, is an operator $\rho_{op}(x)$, which depends, on the position vectors, r_1, r_2, …r_A, of the, A, nucleons in the nucleus. The first term in H, simply, represents the electrostatic energy of a point nucleus. It is independent, of nuclear size, shape or orientation, and thus of no interest to us. Further, the electric dipole moment, vanishes. It is, by virtue, of the fact, that the nuclear ground state is, except for m (m = 2I + 1 wave functions), nondegenerate, and far below, the excited states. Thus one can write (dipole magnetic moment for the nuclear case, being zero)

$$H = \tfrac{1}{2} \sum_{j,k} Q_{jk'}(\partial^2 V/\partial x_j \partial x_{k,)0} x_j x_k + \text{hexadecapole terms}$$
$$= \tfrac{1}{2} \sum_{j,k} Q_{jk'} x_j x_k + \text{hexadecapole terms}$$
$$V_{jk} = (\partial^2 V/\partial x_j \partial x_{k,})_0$$

Here both $Q_{jk'}$ an V_{jk} are second rank tensors, symmetric by heir definition. Since $V_{jk} = -[\partial(E_k)/\partial x_j]$, where, $E_k = (-V/\partial x_k)$, is the electric field, at the nucleus. One sees that the nuclear electric qudrupole interacts with the gradient of the electric field. See Figs. 14.49, 14.50 [35] for conceptual explanation of energy structure of a qudrupole nucleus.

The motion, of surrounding charges, produces at the nuclear position, field gradient components, which are functions of time. The Hamiltonian H_Q, which couples the nuclear spin, to the surrounding lattice, can lead to transitions, in which the nucleus changes, its quantum number, m by $\Delta m = \pm 1$ or $\Delta m = \pm 2$. On the other hand, if only time dependent magnetic interactions couple, the nuclear spin couple to the lattice, and produce nuclear relaxation; only those spin transitions, in which the quantum number, m, of a given nucleus changes by $\Delta m \pm 1$, are possible. As a result, if the equilibrium populations of the nuclear spin states are disturbed, the manner in which the populations, become readjusted, depends in a characteristic way, on, whether the relaxation mechanism, is magnetic or quadrupolar in origin. In a crystal like $NaNO_3$ for example, the Na line is split into 3 components, by static quadrupole effect. One can then perform a double resonance experiment, in which a strong radio-frequency field, saturates one of the components, while a weak radio-frequency test signal measures, simultaneously, the intensity of one of the other, components. In this way, one obtains information, concerning the distributed population, of nuclear energy levels.

If the equilibrium populations, of the nuclear energy levels, are disturbed, it is not generally true, that the rate at which they return, to their equilibrium values, is governed by a simple exponential law, when quadrupole interactions are involved. This means that a unique relaxation time T_1 can not in general, be defined. The longest time constant, governing the return of the energy level populations, to the equilibrium may then serve, as a measure of a characteristic relaxation time. In specific cases, however, a more careful analysis, can often be made. Consider, for example, the case which is of frequent experimental interest, namely that of a nucleus with spin I = 3/2, and a quadrupole moment. Suppose further, that only, the central component of the resonance line, is observed, the two satellites lying, in somewhat different frequency ranges, are a result of static quadrupole interaction. We wish to examine, how the quadrupolar relaxation processes, affect the behavior of the observed central line. The first peculiarity, to be noted is that, although one observes, the absorption of radio-frequency power, only, in the 1/2 to −1/2 transition, the quadrupole Hamiltonian H_Q responsible, for the relaxation induced, transitions are, between all energy levels, for which $\Delta m = \pm 1, \pm 2$ (see Fig. 14.50 [35]), except between the levels, 1/2 and −1/2, since $<-1/2 \ | H_Q$ (Hamiltonian Quadrupolar $| \ 1/2 > = 0$. The nuclear relaxation, therefore, takes place, in a round about way.

References

1. Giancoli, D.C.: Physics for Scientist and Engineers, with Modern Physics. Prentice Hall, Upper Saddle River
2. Matthies, C., Nagel, A.M., Schad, L.R., Bachert, P.: Reduction of B_0 inhomogeneity effects in triple-quantum filtered sodium imaging. J. Magn. Reson. **202**, 239–244 (2010)
3. Werbelow, L.G.: The NMR of spin-3/Z nuclei: the effect of second-order dynamic frequency shifts. J. Magn. Reson. **43**, 443–448 (1981)

4. Goswami, A.: Quantum Mechanics. Wm. C. Brown Publishers, Dubuque

5. Xu, Y., Barbara, T.M., Rooney, W.D., Springer, C.S. Jr.: Two-dimensional multiple-quantum NMR spectroscopy of isolated half-integer spin systems. II. 35Cl examples. J. Magn. Reson. **83**, 219–298 (1989)

6. Augath, M., Heiler, P., Kirsch, S., Schad, L.R.: In vivo ^{39}K, 23Na and ^{1}H MR imaging using a triple resonant RF coil setup. J. Magn. Reson. **200**, 134–136 (2009)

7. Borthakur, A., Hancu, I., Boada, F.E., Shen, G.X., Shapiro, E.M., Reddy, R.: In Vivo triple quantum filtered twisted projection sodium MRI of human articular cartilage. J. Magn. Reson. **141**, 286–290 (1999)

8. Bull, T.E.: Nuclear magnetic relaxation of spin-3/2 nuclei involved in chemical exchange. J. Magn. Reson. **8**, 344–353 (1972)

9. Marshall, A.G., Bruce, R.E.: Dspersion versus absorption (DISPA) lineshape analysis. Adjacent peaks and simultaneous distribution in paeak width and position. J. Magn. Reson. **39**, 47–54 (1980)

10. Boada, F.E., Gillen, J.S., Shen, G.X., Chang, S.Y., Thulborn, K.R.: Fast three dimensional sodium imaging. Magn. Reson. Med. **37**, 706–715 (1997)

11. Bodenhausen, G., Vold, R.L., Vold, R.R.: Multiple quantum spin-echo spectroscopy. J. Magn. Reson. **37**, 93–106 (1980)

12. Werbelow, L., Pouzard, G.: Quadrupolar relaxation. The multiquantum coherences. J. Phys. Chem. **85**, 3887–3891 (1981)

13. Reddy R., Shinnar, M., Wang, Z., Leigh, J.S.: Multiple-quantum filters of spin-3/2 pulses of arbitrary flip angle. J. Magn. Reson. B **104**, 148–152 (1994)

14. Kemp-Happer, R., Styles, P., Wimpers, S.: Three-dimensional triple-quantum filtration 23Na NMR imaging. J. Magn. Reson. B **108**, 280–284 (1995)

15. Hubbard, P.S.: Nonexponential nuclaer magnetic relaxation by qudrupole interactions. J. Chem. Phys. **51**, 985–987 (1970)

16. Jaccard, G., Wimperis, S., Bodenhausen, G.: Multiple-quantum NMR spectroscopy of I = 3/2 spins in isotropic phase: a new probe for multiexponential relaxation. J. Chem. Phys. **85**, 6282–6293 (1986)

17. Hancu, I., van der Maarel, J.R.C., Boada, F.E.: A model for the dynamics of spins 3/2 in biological media: signal loss during radiofrequency excitation in triple-quantum-filtered sodium MRI. J. Magn. Reson. **147**, 179–191 (2000)

18. Wang, Y., Hu, W., Perez-Trepichio, A.D., Ng, T.C., Furlan, A.J., Majors, A.W., Jones, S.C.: Brain tissue sodium is a ticking clock telling time after arterial occlusion in rat focal cerebral ischemia. Stroke **31**, 1386–1392 (2000)

19. Wimperis, S., Wood, B.: Triple-quantum sodium imaging. J. Magn. Reson. **95**, 428–436 (1991)

20. Wimperis, S., Cole, P., Styles, P.: Triple-quantum-filtration NMR imaging of 200 mM sodium at 1.9 tesla. J. Magn. Reson. **98**, 628–636 (1992)

21. Cockman, M.D., Jelinski, L.W.: Double-quantum-filtered sodium imaging. J. Magn. Reson. **90**, 9–l8 (1990)

22. Brink, H.F., Buschmann, M.D., Rosen, B.R.: NMR chemical shift imaging computerized medical imaging and graphics. Comptzd. Med. Im. Grphcs. **13**, 93–104 (1989)

23. Branca, R.T., Chen, Y.M., Mouraviev, V., Galiana, G., Jenista, E.R., Kumar, C., Leuschner, C., Warren, W.S.: iDQC anisotropy map imaging for tumor tissue characterization in vivo. Magn. Reson. Med. **61**, 937–943 (2009)

24. Jenista, E.R., Galiana, G., Branca, R.T., Yarmolenko, P.S., Stokes A.M., Dewhirst, M.W., Warren, W.S.: Application of mixed spin iMQCs for temperature and chemical-selective imaging. J. Magn. Reson. **204**, 208–218 (2010)

25. Duce, J.A., Tsatsanis, A., Cater, M.A., James, S.A., Robb, E., Wikhe, K., Leong, S.L., Perez, K., Johanssen, T., Greenough, M.A., Cho, H.-H., Galatis, D., Moir, R.D., Masters, C.L., McLean, C., Tanzi, R.E., Cappai, R., Barnham, K.J., Ciccotosto, G.D., Rogers, J.T., Bush, A. I.: Iron-export ferroxidase activity of β-amyloid precursor protein is inhibited by zinc in alzheimer's disease. Cell **142**, 857–867 (2010)

26. Crouch, P.J., Harding, S.E., White, A.R., Camakarisc, J., Bushd, A.I., Masters, C.L.: Mechanisms of Aβ mediated neurodegeneration in Alzheimer's disease. Int. J. Biochem. Cell Biol. **40**, 181–198 (2008)

27. Jenista, E.R., Branca, R.T., Warren, W.S.: Hyperpolarized carbon–carbon intermolecular multiple quantum coherences. J. Magn. Reson. **196**, 74–77 (2009)

28. Lee, J.-S., Regatt, R.R., Jerschow, A.: Optimal control NMR differentiation between fast and slow sodium. Chem. Phys. Lett. **494**, 331–336 (2010)

29. Laustsen, C., Ringgaard, S., Pedersen, M., Nielsen, N.C.: Quadrupolar-coupling-specic binomial pulse sequences for in vivo 23Na NMR and MRI. J. Magn. Reson. **206**, 139–146 (2010)

30. Boada, F.E., LaVerde, G., Jungreis, C., Nemoto, E., Tanase, C., Hancu, I.: Loss of cell ion homeostasis and cell viability in the brain: what sodium MRI can tell us. Curr. Top. Dev. Biol. **70**, 77–101 (2005)

31. Harrris, R.K., Mann, B.E. (eds.): NMR and the Periodic Table. Academic Press, London (1978). ISBN: 0-12.327650-0

32. Evans, J.N.S.: Biomolecular NMR Spectroscopy. Oxford University Press, Oxford (1995). ISBN: 0-198547668

33. Ashbrook, S.E., Duer, M.J.: Structural information from quadrupolar nuclei in solid state NMR. Concepts Magn. Reson. **28**(3), 183–248 (2006)

34. Kentgens, A.P.M.: A practical guide to solid-state NMR of half-integer quadrupolar nuclei with some applications to disordered systems. Geoderma **80**, 271–306 (1997)

35. Cohen, M.H., Reif, F.: Qudrupole effects in nuclear magnetic resonance studies of solids. Solid State Phys. **5**, 321–438 (1957)

Glossary

^{13}C (magnetic dipole)
^{14}N (100 % abundance) quadrupolar (I = 1)
^{23}Na MR images with FLAIR
^{23}Na MRI of the human heart
^{23}Na spectroscopy twisted projection imaging (TPI)
^{23}Na-MRI
^{2}ch$_2$ gaba resonance (2.97) ppm
2D-cosy (two dimensional correlation spectroscopy)
3D ^{31}PMRS (proton magnetic resonance spectroscopy)/CSI (chemical shift imaging)-pri(phospholipids resonance imaging)
3D MPRAGE (three dimensional magnetization prepared acquisition gradient echo)
3-D MPRAGE(three dimensional magnetization prepared rapid acquisition echo)-DTI
3D RARE
βch2 gaba resonances
γch2 gaba resonances

A

Abscess (differentiation from cystic or necrotic tumor)
Adding spins (two particle spin system)
Adiabatic pulse vector representation
ADP(adenosine diphosphate)
AEDS-antiepileptic drugs
ALA: alanine
Alcoholism
Algebraic description of spin 3/2 dynamics
ALS (amiotrophic lateral sclerosis)

Alzheimer disease(AD)
Angular momentum
Angular momentum (atomic)
Angular momentum j = l + s
Animal model
Antiepileptic medication (vigabatrin)
Apparent diffusion coefficients (ADCs)
Astrocytic(AST)
Astrocytomas-high-grade
Asymmetric z gradient echo detection
Atom data register
Atomic dipole magnetic moment
Atomic magnetic moment
Atomic moments
Atomic physics
Atomic spinning top (AST)
Atoms, molecules, electrons
ATP (adenosine triphosphate)
ATPFB (copper binding atpase)
AUTO-SMASH (auto calibrated simultaneous acquisition of spatial harmonics)
ax$_3$ spin system (lactate doublet)
Axon firing-human optic nerve (MRI/SENSE)
Aβ mediated neurodegeneration in Alzheimer's disease

B

B$_0$ in homogeneity effects
Bell's inequalities(BIS)
Biochemistry human brain
Biochemistry-brain tumors
Bio-chemo-medical
Biologically important nuclei
Biomedical diamagnetic spin

Vascular dementia (VD)
Vasogenic edema
VD (variable density)

W
White matter
White matter (wm) lesions

White matter normal appearing (NAWM)
Wilson disease (copper metabolism)

Z
Zero quantum coherence (ZQC)
ZQC (zero quantum coherence)